Experimental Investigations into the Accuracy and Precision of Material Extrusion Additive Manufacturing

Samuel Lewis Massey

Pembroke College

Date of Submission: 09/2022

This thesis is submitted for the degree of Doctor of Philosophy

DECLARATION

This thesis is the result of my own work and includes nothing which is the outcome of work done in collaboration except as declared in the Preface and specified in the text. I further state that no substantial part of my thesis has already been submitted, or, is being concurrently submitted for any such degree, diploma or other qualification at the University of Cambridge or any other University or similar institution except as declared in the Preface and specified in the text. It does not exceed the prescribed word limit for the relevant Degree Committee.

ABSTRACT

Experimental Investigations into the Accuracy and Precision of Material Extrusion Additive Manufacturing

Samuel Lewis Massey

Material Extrusion Additive Manufacturing (ME AM) is one of the most popular AM technologies thanks to its ease of use and ability to produce complex shapes from a range of materials at a comparatively low cost. However, it is commonly characterised by poor quality, including unsatisfactory surface roughness, dimensional and geometrical accuracy, and dimensional precision. As a relatively recent technology, it is common for users have limited familiarity with design implications and process capability. Consequently, many of the purported benefits are negated as components do not conform to specification and trial-and-error approaches are often employed instead. Given these limitations, improvements to the process would help increase the proliferation of the technology and maximise potential benefits.

The existing capability of the ME AM process was first established in this thesis through experimental work involving the production of identical components across multiple prints and machines of differing designs and price points. This highlighted that all axes on all machines exhibited average dimensional error of up to 0.25mm and error variability of approximately ±0.20mm. The Z axis, typically driven by a lead screw rather than belt drive, exhibited lower error and variability. Geometrical inaccuracy was also demonstrated to be prominent, largely due to swelling outwards at corners. Using a standard process capability value of 1.33, these errors suggest a tolerance of 1.2mm is needed such that any component feature aligned with any machine-axis can be assembled with another matching feature. However, with suitable adjustments for average error and by addressing the geometrical inaccuracy, this tolerance may be reduced substantially. A high-level characterisation was then presented to categorise error sources as arising either from machine positional error or from the extrusion and deposition of material itself.

Positional error was determined in terms of fixed backlash and variable scale components. This showed that backlash errors were typically of the order of 0.05mm, and scale errors were undersized by up to 0.6% representing one of the largest error sources. In addition, filament diameter and extrusion lengths were measured and found to contribute a very limited amount to overall error. Extrusion errors were characterised in terms of steady-state filament morphology and the XY plane corner errors identified in the initial performance experimentation. A new cross-sectional morphology model was presented which accounted for volumetric flow rate and the deposited material aspect ratio. This represented the outer boundary of vertical surfaces as a series of arc lengths, which predicted a deposition approximately 0.035mm wider than the standard rectangular model included in

current popular slicing software. XY plane corner errors were investigated for 11 separate angles, alternative perimeter deposition orders and the inclusion or exclusion of a perimeter weld. This showed typical geometric deviations of approximately 0.1mm relative to the straight depositions before and after the corner.

Potential methods of process improvement were discussed, including existing studies which have sought either to avoid the errors, compensate for them or remove them via post-processing techniques. As a result, a new machine and nozzle design were proposed. The novel nozzle incorporated a side piece, which could guide over-extruded material at corners and improve the surface finish of vertical walls. In order to operate in the XY plane, this was combined with a 4-axis machine to allow the rotation of the nozzle. Steady-state experimentation showed that a doubled layer height to 0.4mm was required for controlled morphology with the new nozzle design. For an optimal combination of temperature, extrusion rate and print speed, a comparable surface roughness and improved dimensional error, build time and bonding width were observed compared to the lower layer height standard nozzle. However, application to corners in the XY plane revealed several limitations. First, pauses at the corners associated with the nozzle rotation introduced over-extrusion as residual pressure causes the continued extrusion of molten material. Whilst the side piece was demonstrated to interact with this additional material, some nonetheless flowed beyond it resulting in poor geometrical accuracy. Reducing the effects of the pause through faster rotation speeds, lower temperatures and filament retractions did improve this behaviour, though introduced additional geometrical error inwards from the corner.

Ultimately, it was determined that immediate improvements can be made through adoption of the updated filament model and better positional control of machines, to include scale calibration and limitation of backlash through proper tensioning of belts and gantry arrangements. Whilst the novel nozzle design shows promise, particularly during steady state deposition, the root cause of over-extrusion at corners still requires addressing in popular slicing software. If these issues can be overcome, improved average dimensional error and tolerances of 0.05mm and ±0.10mm respectively are achievable.

PREFACE

I have thoroughly enjoyed investigating the Material Extrusion Additive Manufacturing process, combining and developing a wide range of skills during what has been a fairly broad study. I first used the process as an undergraduate to fabricate components for the major projects in third and fourth years, where I experienced first-hand many of the shortcomings identified early on in this work. Nonetheless, I was fascinated by watching finished parts being built up layer by layer then and remain so after four years of delving into the intricacies in detail. I will hopefully continue to use the technology and will follow future developments with keen interest, perhaps some of which may be in some small part enabled by the work in this thesis.

I would like to thank my Supervisor, Dr James Moultrie, for his guidance throughout my studies and enthusiasm towards all experimental work. I first met James in 2011, so it is great to have first discussed the idea of undertaking a PhD with him and then later completing it within his Design Management Group at the Institute for Manufacturing (IfM). I would also like to thank my Advisor, Professor Ronan Daly, for his valuable input. I would further like to acknowledge the support from the EPSRC, who funded this work and provided additional resources during the COVID-19 pandemic.

Much of the work in this thesis was only made possible with the support of technicians and workshop staff at both the Department of Engineering and Institute for Manufacturing. In particular, I owe many thanks to Chris Jennings of the IfM for his sustained help and in fabricating countless custom components to enable the experimental work.

Finally, I have been lucky to count on the support of friends and family as well as the various groups of fellow students from the department, college and university societies who have all made the entire experience so rewarding.

ACRONYMS

ABS Acrylonitrile Butadiene Styrene

AM Additive Manufacturing

ASTM American Society for Testing and Materials

BAAM Big Area Additive Manufacturing

CAD Computer Aided Design

CC Contour Crafting

CFD Computational Fluid Dynamics

CMM Coordinate Measuring Machine

CNC Computer Numerical Control

DfM Design for Manufacturing

EF Extrusion Factor

FDM Fused Deposition Modelling

FEA Finite Element Analysis

GD&T Geometric Dimensioning and Tolerancing

ISO International Organization for Standardization

LH Layer Height

LSL Lower Service Limit

MAS Manufacturability Analysis System

ME Material Extrusion

PLA Polylactic Acid

RW Road Width

S/N Signal-to-noise

SCF Shrinkage compensation factor

STL Standard Tessellation Language

USL Upper Service Limit

1. INTRODUCTION

This thesis presents a series of experimental investigations into the Material Extrusion (ME) Additive Manufacturing (AM) process. It details the existing performance as outlined in literature and builds upon this with detailed experimental work. The underlying cause of process error is explored through further targeted experimentation and subsequently, a novel machine design solution is developed and tested. The overall purpose is to maximise the potential of this highly accessible and popular technology through the minimisation of current limitations.

1.1. BACKGROUND

There are four main categories of manufacturing process that may be employed to produce a component: subtractive, forming, casting and additive. The first three date back thousands of years, where primitive tools and other items were produced using rudimentary versions of these methods. Over the past 150 years in an industrial context, these processes have been developed and revised, affording a detailed understanding of process capability. The fourth process (AM) is a much more recent technology that has only been made possible through developments such as those in computer-controlled machinery, machine software and materials. The first commercialised AM machine was the Stereolithography Apparatus (SLA1), manufactured in the mid-1980s [1,2]. Since then, the number of technologies has grown and many hundreds of manufacturers now offer machines with a wide variety of capabilities. As a result of its comparatively recent introduction, AM user knowledge is still developing and there is likely scope for further improvements in understanding and process performance.

AM refers to manufacturing processes that involve the joining of materials to make objects from three-dimensional Computer Aided Design (CAD) model data, usually layer upon layer [2]. AM is also commonly referred to as Layered Manufacturing (LM) or 3D Printing (3DP) and is a subset of Rapid Prototyping (RP) or Rapid Manufacturing (RM). Formal definitions vary, but the most obvious distinction is that AM technologies are additive layer-based, whereas RP is a more general term describing the manufacture of 3D objects from CAD data. Berman [3] suggests that additional features of AM are lower costs, increased software integration and ease-of-use. Both RP and AM are typically utilised to lower the time and costs of product development and can be used to verify designs prior to production via higher-volume manufacturing technologies [4].

AM is an umbrella term that encompasses a number of more specific technologies. Each of these varies in the method of material delivery and inter-layer bonding. As a result of these differences, components manufactured by the various AM technologies also vary in terms of their quality and performance characteristics. These technologies are therefore often selected for their performance in specific areas, depending on the properties of the component required.

Although it is often noted that AM technologies are well-suited for initial prototyping or hobbyist use [5], Berman [3] and Mohamed et al.[6] note that AM is increasingly used to create finished goods, particularly for early production runs or test marketing. Wohlers [2] reported that final goods accounted for approximately 50% of AM output in 2020.

1.2. AM TECHNOLOGIES

AM consists of seven distinct technologies [7], which offer many benefits including reduced manufacturing time [8,9] and cost [10,11], complex geometries [12-14], material waste reduction [3,12,15] and compact machine designs [16-18]. However, potential disadvantages of AM include material restrictions [19-21], the need for support structures [12,22,23], warpage or dimensional inaccuracy [12,24,25], component anisotropy [26-28] and the need for post-processing [24,29,30].

The International Organization for Standardization (ISO) classified AM technologies in ISO/ASTM 52900:2015 [31]. This lists the seven AM technologies as: binder jetting, directed energy deposition, material extrusion, material jetting, powder bed fusion, sheet lamination and vat photopolymerization. These vary both in their process (feedstock format, bonding method) and capabilities (resolution, material, quality, mechanical strength and so on) [9]. Kim and Oh [24] conducted a detailed benchmarking study of AM technologies, drawing quantitative comparisons on a variety of performance metrics. They found that vat photopolymerization has the best accuracy, hardness and surface roughness; powder bed fusion performs best for compressive strength and speed; material jetting exhibits the best tensile strength and material extrusion provides the best impact strength.

Wohlers [32] stated that the total global market for AM grew 19.5 percent to USD15.3bn in 2021. Their report discussed specific developments in the 3D printing of food, medicines and electronics and noted that particularly strong growth was evident from AM service providers as opposed to the manufacturers of the systems themselves. In the United Kingdom, Additive Manufacturing UK, supported by the government, have presented a national strategy running to 2025 [33]. This identified a strong High Value Manufacturing (HVM) sector within the UK and stated that the adoption of AM is crucial in maintaining competitiveness. The report predicted that by committing GBP225 million to develop capabilities, the UK's High Value Manufacturing sector can grow to GBP3.5 billion per year and support more than 60,000 jobs by 2025. They particularly identified a lack of expertise with the various AM technologies as a major barrier, where only 17% of UK manufacturing companies reporting experience with AM compared with 37% in Germany and 24% in China.

1.3. Material Extrusion Additive Manufacturing

ME AM, also commonly referred to as Fused Deposition Modelling (FDM) and Fused Filament Fabrication (FFF), is one of the most pervasive AM technologies [12,34,35]. Statista [36] conducted a worldwide survey of AM users and found that 95% used ME AM, far ahead of any other AM technology. ME AM is popular primarily because of its simplicity and low-cost machinery and maintenance. It is predicted that the ME AM combined hardware and materials market will be USD2.2 billion by 2027 [37]. ME AM is therefore well placed to push AM technologies further and unlock their potential benefits. This thesis focuses exclusively on the ME AM process in order to provide a detailed review of the technology and the specific factors that contribute to its current limited performance.

1.3.1. History

ME AM was pioneered by Scott Crump at Stratasys Inc. in 1989 and was patented in 1992 [38], where it was referred to by the protected term *FDM*. The patent for this expired in 2009 [5], which has since allowed for the development of new machines [39]. This has significantly increased both the number of machines available and manufacturers involved [5], and has reduced machine costs [40,41] to as low as USD100. These machines are often generally referred to as '3D printers' and are commonly based on open source designs [42]. In parallel, research interest in the technology has also grown [40,43]. Traditionally, the ME AM process was suitable only for pure thermoplastics [44] and Stratasys machines typically used Acrylonitrile Butadiene Styrene (ABS). However, recent developments have enabled fabrication from materials such as ceramics [45], fibre reinforced composites [46], metals [47] and biomaterials [48]. Today, the technology is popular amongst hobbyists [49] but is also frequently used in production of concept models, functional prototypes and customised end-use components [50,51].

1.3.2. Process

The ME AM process can be characterised by four main steps, as demonstrated in Figure 1.1.

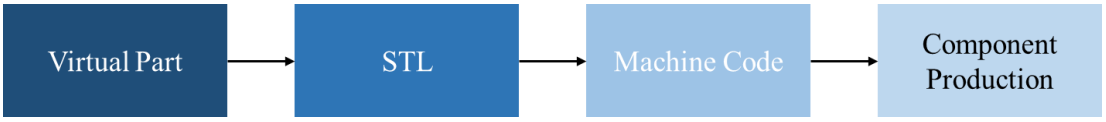

Figure 1.1 *Overview of the ME AM process*

A 3D component is first created in a CAD software package. The design rules that may be employed by the user at this stage are discussed in detail later in Section 7.1.1, just as would be applied to alternative technologies. This virtual part is an idealised representation of the component, which theoretically contains no material error. In some cases, rather than being manually designed and produced this virtual part representation can be generated from scanned data of physical objects. This virtual part must then be saved as a file which determines the outer surface geometry. Hager et al. [52]

noted that Standard Tessellation Language (STL) is the by far the most popular file format. In this, the surface geometry is translated into polygonal approximations with vertex coordinates and normal vectors. Curved geometry must therefore be converted to a series of straight lines, though with a suitable resolution selected in the software errors are minimal [53].

Slicing software (a "slicer") converts the virtual component to machine instructions, usually referred to as G-code. This code is specific to the ME AM process and machine being used. The code is executed by the machine's Central Processing Unit (CPU), with each 'instruction' in the machine code leading to a specific action being taken.

The G-code contains line-by-line instructions, which are executed in order. A typical sample of such code is included below in Figure 1.2.

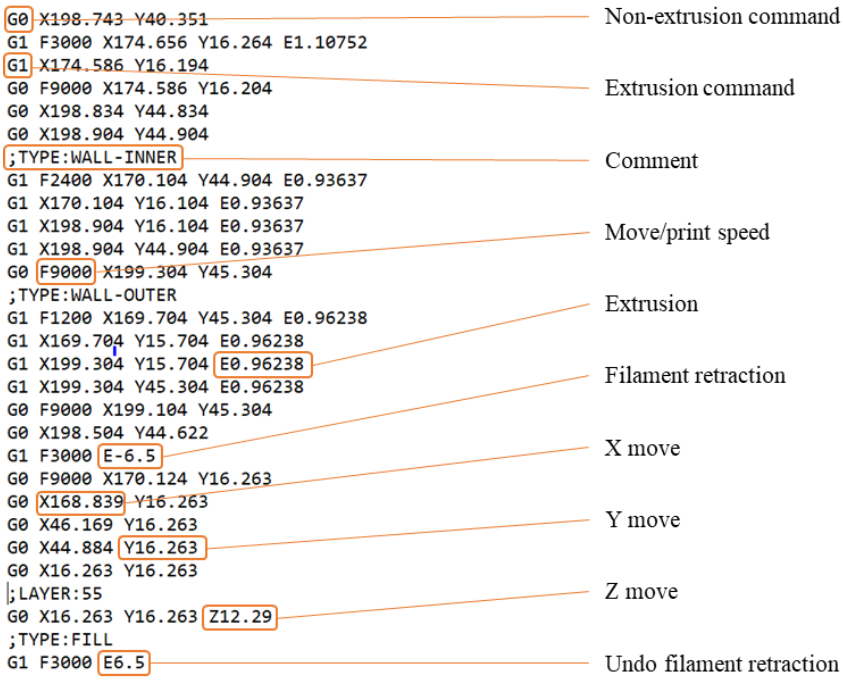

Figure 1.2 *Typical example of ME AM G-code*

Each letter prefix denotes a specific command. In the above example. *X*, *Y* and *Z* correspond to positions in space. These may be relative to the previous position if the *G91* command is used at the beginning of the code, or absolute values as in the figure above. Similarly, *E* commands correspond to an extrusion value for that particular move. This value represents the length of filament fed into the liquefier in that step, since the ME AM process is unique in that the filament acts as both piston and extrudate [54]. The associated volume extruded is calculable via the filament diameter, assuming volume conservation. The other most commonly-used command is the *F* value, which denotes the speed of movement in units of mm per minute.

The final component is built up through the step-by-step execution of the G-code. The nozzle is moved within the XY plane together with extrusion volumes to deposit individual strands at the sub-millimetre scale. A typical layer consists of one or more contour-parallel perimeter depositions and infill. Once the layer is finished, the nozzle is raised in the Z axis by the layer height and begins the next layer. As a result, a "staircase" error on sloped surfaces associated with the layer-by-layer approach is unavoidable [55,56]. The algorithms that control toolpaths and deposition volumes vary by slicer, and can have a significant effect on the properties of the final component [57-59].

1.3.3. ME AM STRENGTHS AND LIMITATIONS

As noted previously, ME AM is one of the most popular AM technologies. ME AM is effectively a combination of two well-understood processes; extrusion and Computer Numerical Control (CNC) positional movement. As such, it is relatively simple and avoids complex components such as lasers [60] and digital light masks. Build volumes are often higher than with other AM technologies [12] [61], as the main restriction on volume is the XYZ motion mechanism. It is also highly cost effective [34,49], with low machine, material and maintenance costs [12], making it particularly well-suited to hobbyists [49]. In addition, as with other AM technologies, complex shapes can be manufactured [62] more quickly than other conventional manufacturing processes [12,24] without the need for tooling [62].

However, ME AM also has a number of limitations. It is commonly characterised as exhibiting poor quality, including dimensional accuracy [49,62-64] and precision [12,63,65], which are key factors in the applicability of the technology [66]. Surface finish is also often inferior to other AM processes [49,63], largely due to the staircase effect on sloped surfaces mentioned previously. Furthermore, ME AM has been demonstrated to be less suitable for producing small-scale features [64] and requires support for overhanging features [67]. Materials are somewhat limited; in particular the highly-crystalline polymers often used in more conventional technologies shrink significantly upon solidification leading to poor print bed adhesion and part warpage [34]. The limitations above reduce technology adoption [12]. Therefore, understanding the nature of these limitations and developing appropriate solutions will allow the full potential of this technology to be realised.

1.4. RESEARCH QUESTIONS AND THESIS STRUCTURE

1.4.1. RESEARCH QUESTIONS

This thesis seeks to experimentally investigate the accuracy and precision performance of the ME AM manufacturing process. In particular, it considers three main aspects;

1) What is the current performance of the ME AM manufacturing process?
    a. What is the level of accuracy and precision that is typically achievable?

   b. Therefore, what tolerance should designers use to ensure components can be assembled?
   c. What is the nature of dimensional error and where are these errors concentrated?
   d. What factors influence these errors?
2) What immediate improvements can be made that will benefit the average user without physical modification to the existing process?
3) What wider changes can be made to the process to improve accuracy and precision?

1.4.2. THESIS STRUCTURE AND APPROACH

Given the research questions highlighted above, this thesis is structured in order to explore the three aspects in turn. Clearly, the current process performance must be sufficiently characterised prior to exploring both immediate improvement and potential subsequent changes to the process itself. This thesis is therefore structured as follows:

Section 2 provides a review of extant ME AM accuracy and precision experimental literature. This summarises all experimental work to date in order to understand the current performance of the process across a wide variety of machines, materials, parameters and component designs. Furthermore, research gaps are identified from this review which form the basis for the subsequent current ME AM performance experimentation.

Section 3 takes the gaps identified in the previous literature review section as the basis for specific experimental work covering the current performance of the ME AM process. This provides error magnitudes, precision data and helps inform the nature of the dimensional errors observed. Following this experimentation and analysis, a framework for the characterisation of errors is developed which then forms the basis for the following three experimental chapters.

Sections 4, 5 and 6 conduct experimental work to explore specific aspects of the achievable performance utilising the current process. The positional accuracy of ME AM machines is first considered. Next, steady state micro-level morphology is explored. Finally, XY plane geometrical inaccuracies at direction changes and joints are experimentally determined.

Following the experimental error characterisation work undertaken in the previous four sections, **Section 7** then considers error improvement. Potential approaches to improve the ME AM process are outlined, and existing studies in each of these areas discussed to understand the improvements made to date. A potential new machine design element is posited as a means of process improvement, to subsequently be explored experimentally.

Sections 8 and 9 utilise the machine modification identified in Section 7 as the basis for targeted experimentation. First, steady-state micro-level morphology is explored with an updated print nozzle design, in a repeat of the experimentation carried out in Section 5. Next, a modified machine

incorporating a fourth (rotational) axis and a novel print nozzle is used to assess XY plane geometrical accuracy in a direct comparison to the current process performance experimentation carried out in Section 6. Any limitations to this new approach are discussed and potential for improvements considered.

Finally, **Section 10** comprises an overarching discussion of the work contained in this thesis. Conclusions are presented and areas of future work suggested.

2. MATERIAL EXTRUSION ADDITIVE MANUFACTURING ACCURACY AND PRECISION

For ME AM to be valued as a reliable prototyping or production process by designers, accuracy and precision are two critical performance aspects that must be optimised and as Haghighi [68] stated, it is therefore important to draw the distinction between these two. Bochmann et al. [69] stated that accuracy is a measure of the deviation of average measurements against their intended value, whilst precision concerns the degree of variability, or repeatability of the process. In their study, precision related to 90% of measurements about the mean but other precision measures are often used instead. In addition to these dimensional metrics, geometrical accuracy is also introduced. This relates to specific geometrical deviations such as circularity, flatness and squareness error. Representations of these are shown in Figure 2.1.

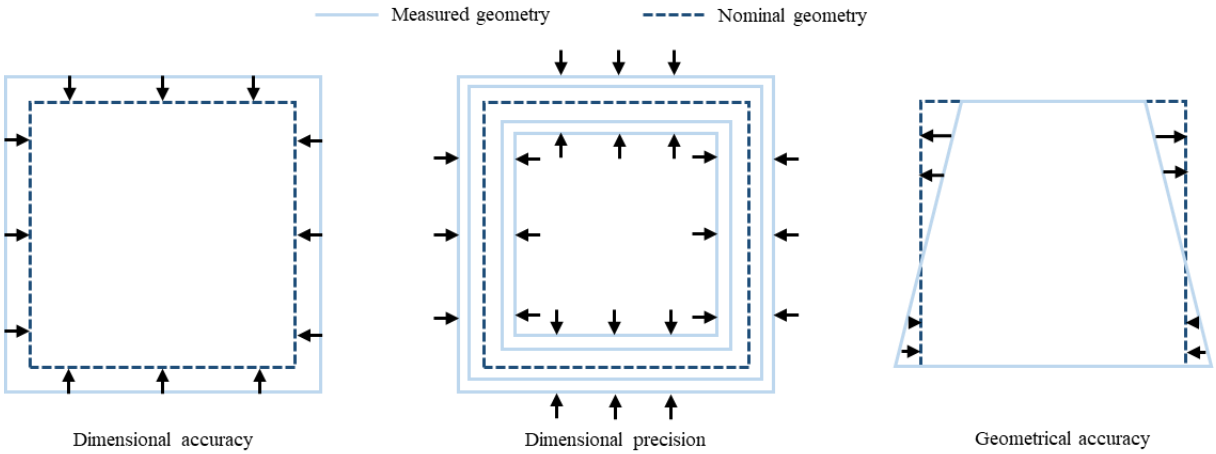

Figure 2.1 *Representations of dimensional accuracy, dimensional precision and geometrical accuracy*

Throughout this thesis, dimensional accuracy data is generated by subtracting the measured dimension from the nominal dimension for both macro component features and later, for individual deposited strands. Where multiple measurements are taken either across the same feature or across different features on the same component, an average (mean) dimensional accuracy figure is generated. This may be an average offset where both the magnitude and sign of all deviations are used. Alternatively, an average error can be calculated where only the magnitude is used. In the former example, two deviations of +0.5mm and -0.5mm respectively average to a value of 0mm, whereas the latter example yields an average error of 0.5mm. As noted above, precision instead considers the variability of measured dimensions. Using the same measured values that inform average dimensional accuracy, a measure of variability can be generated. The magnitude/sign accuracy metric combined with a precision metric is a common combination, as together they capture process error offset (accuracy) and repeatability (precision).

It should be noted that precision can be considered as variability in two main respects. The first is to consider variability of the measured versus nominal dimensions across a component. For a basic component such as a cube or cylinder, this could be the variability of the error for either the face-to-opposite-face dimensions or cylinder diameter measurements. This could equally be applied to more complex components with many varied features. A second measure is the variability between different components of the same design. This can be either components manufactured within the same print, between prints on the same machine, or between prints on different machines.

Stratasys state in their FDM Design Guidelines documentation that the tolerance required (for assemblies not printed in the fully assembled state) is equal to the tolerance of the (FDM) machine itself [70]. As Relvas et al. [71] stated, manufacturers usually provide some basic capability ranges for their machine but this data is usually sparse and poorly defined. In any case, this performance is expected to vary with many other factors including component design and the material used. As a result, it is currently not clear what level of tolerance should be used for assembled components. Similarly, average dimensional accuracy figures are never quoted, perhaps because to recognise an average error could suggest a poorly calibrated machine or process. For a non-zero dimensional error, the tolerance must account both for this and the process variability. However, it is more straightforward to account for average dimensional accuracy error given its predictable nature. In contrast, random factors will always result in some degree of variability.

Ultimately, both accuracy and precision are crucial because they have a direct influence on the usability of manufactured components. This is especially true for assembled components, where the fit of one part with another is critical for their proper function. As was previously noted, there is often a lack of clear information regarding the tolerances that should be used for AM processes, including for desktop ME AM machines. This is in contrast to more traditional processes, where process capabilities have been established in much greater detail. As a result, the ME AM process often leads to users adopting an iterative approach to component production. For example, as demonstrated in Figure 2.2, for the fabrication of a box and lid the user will typically build in some small tolerance for the production of the initial components. This may be based on expectations from alternative processes such as injection moulding or machining. These will often be proven too small after both components are produced, so the user iterates the virtual design until a suitable fit is achieved. With long build times, this iteration is undesirable and is also wasteful of raw material. However, without greater certainty on dimensional accuracy and precision, designers currently have little alternative.

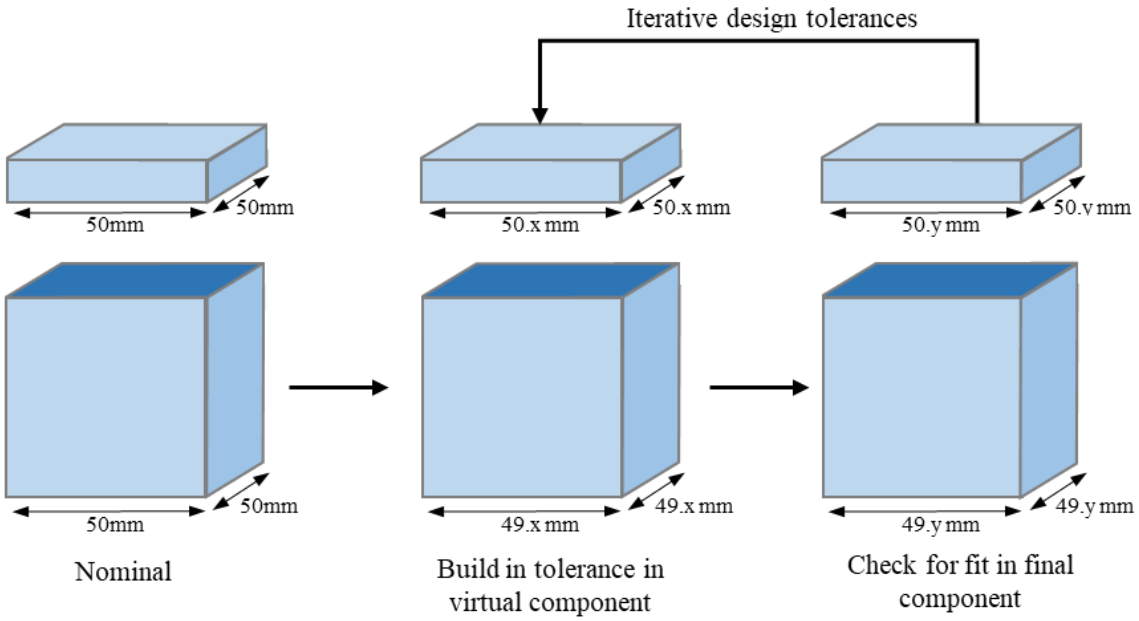

Figure 2.2 *Iterative approach for ME AM component production*

To meet the full potential of the ME AM process, these quality issues must first be characterised in detail before solutions may be implemented. This will ultimately serve to provide a more capable technology which is more likely to see widespread adoption and therefore deliver the greatest benefits possible.

2.1. ME AM Experimental Accuracy and Precision Literature

There is a large body of extant literature that explores the performance of the ME AM process. In this review, only studies that conduct physical experimentation and subsequently measure the fabricated component are included. For clarity, this requires a nominal dimension to have been determined at the component design stage and physical component to be produced, followed by measurement and comparison with the nominal values. Other, more specific literature reviews are included in the relevant experimental sections throughout this thesis.

Collating and analysing the component error studies in this section confers multiple benefits. First, it provides a comprehensive collection of all experimental work in a single location. It also allows macro analysis of the studies including temporal and geographic distribution, study methodologies and materials. Finally, it enables a summary of accuracy and precision findings across all studies.

2.1.1. Literature Search Methodology

In order to comprehensively analyse the extant experimental literature a rigorous review was undertaken. Two separate approaches were taken to capture as much literature as possible. First, a non-systematic scoping study was conducted to assess the subject area and understand the key terms and aspects that should be considered as part of a more detailed search. This initial approach consisted of utilising *Google Scholar* to search the combination of the most common technology terms (i.e.

Fused Deposition Modelling, FDM, Fused Filament Fabrication, FFF and Material Extrusion Additive Manufacturing) with the keywords ‘accuracy’ and ‘precision’. Upon exploring the results, alternative platforms including specific journals and *Mendeley* reference management software provided recommendations for additional studies. Together with the results of the initial searches, these helped inform further areas to be searched. As an example, it became clear that some experimental work captured the accuracy of manufactured ME AM components as a comparison with other technologies in a ‘benchmarking’ study. Such studies would not necessarily be returned as a result of ‘accuracy’ or ‘precision’ searches, but nevertheless contained relevant work.

The second approach comprised a thorough systematic review. This utilised the *Scopus* literature database. Broadly, this took the form of four major stages in line with *PRISMA* principles [72,73]: identification of potentially relevant studies, review, inclusion/analysis and the final collection of studies. This second approach consisted of a more detailed search coupling methodology, again utilising a wide range of terms for the technology in conjunction with key words. For this, the following search terms were used to cover the technology itself: ‘Fused Deposition Modelling’, ‘FDM’, ‘Fused Filament Fabrication’, ‘FFF’, ‘Material Extrusion Additive Manufacturing’, ‘ME AM’, ‘Fused Layer Modelling’, ‘FLM’, ‘3D Printing’, ‘3DP’ and ‘Rapid Prototyping’. These were coupled with key words both as a full search term and with the use of the Boolean operator ‘AND’. The key words used with the technology search terms listed above were; ‘accuracy’, ‘precision’, ‘comparison’, ‘benchmark’, ‘dimensional accuracy’, ‘geometry’, ‘geometrical’, ‘repeatability’, ‘error’, ‘warpage’ and ‘shrinkage’. An initial review of the search results determined the likelihood of relevant material based on the study title. This first categorisation returned approximately 25% of all search results as potentially relevant. As a first stage, the most highly cited papers were reviewed and any papers that were referenced by these or citations of them were collected in a process commonly referred to as ‘snowballing’. Once a full list of potential studies were created, each study was reviewed to assess for experimental accuracy or precision data and if present, the study was included in this review. Further upstream and downstream snowballing was then performed on these papers in order to gain additional studies.

Collectively, these additional searches returned many thousands of results. A total of 306 experimental articles were ultimately deemed directly relevant based on their titles and abstracts and were therefore analysed for this review. 204 of these are directly cited within this thesis, where each study’s findings are referenced in detail. The remaining 102 [74-175] are used to inform the analysis in this section, but are not directly cited otherwise. 231 studies were available in *Web of Science*’s database. Using this allowed analysis through *CitNetExplorer*’s citation network tool which enables a visualisation of the citation and reference links between studies as shown below in Figure 2.3 for the most highly connected publications. This is also included in a larger format Section 12.1 in the Appendix. This software includes an expansion of highly referenced studies in addition to those input.

In this case, these are studies that do not experimentally investigate dimensional accuracy but nevertheless are highly cited by those that do. Using this, the core publications (i.e. those cited most often) that directly perform experimental work are; Ippolito et al., [176] Boschetto et al., [177] Peng et al., [178] Galantucci et al., [19] Nuñez et al., [179] and El-Katatny et al., [66] Mahesh et al., [64] Wang et al., [180] Sood et al., [181] Nanchariah et al., [182] and Tong et al. [183]. As noted, in a small number of cases further highly cited additional studies are identified. The most prominent of these are: Anitha et al., [184] Lee et al., [185] Ahn et al., [186] and Pandey et al., [187]. These additional studies are all examples of pioneering studies for specific aspects of the technology such as influencing parameters [184,185], improvements of the surface finish [187] and the anisotropic nature of the process [186] and are widely cited on that basis.

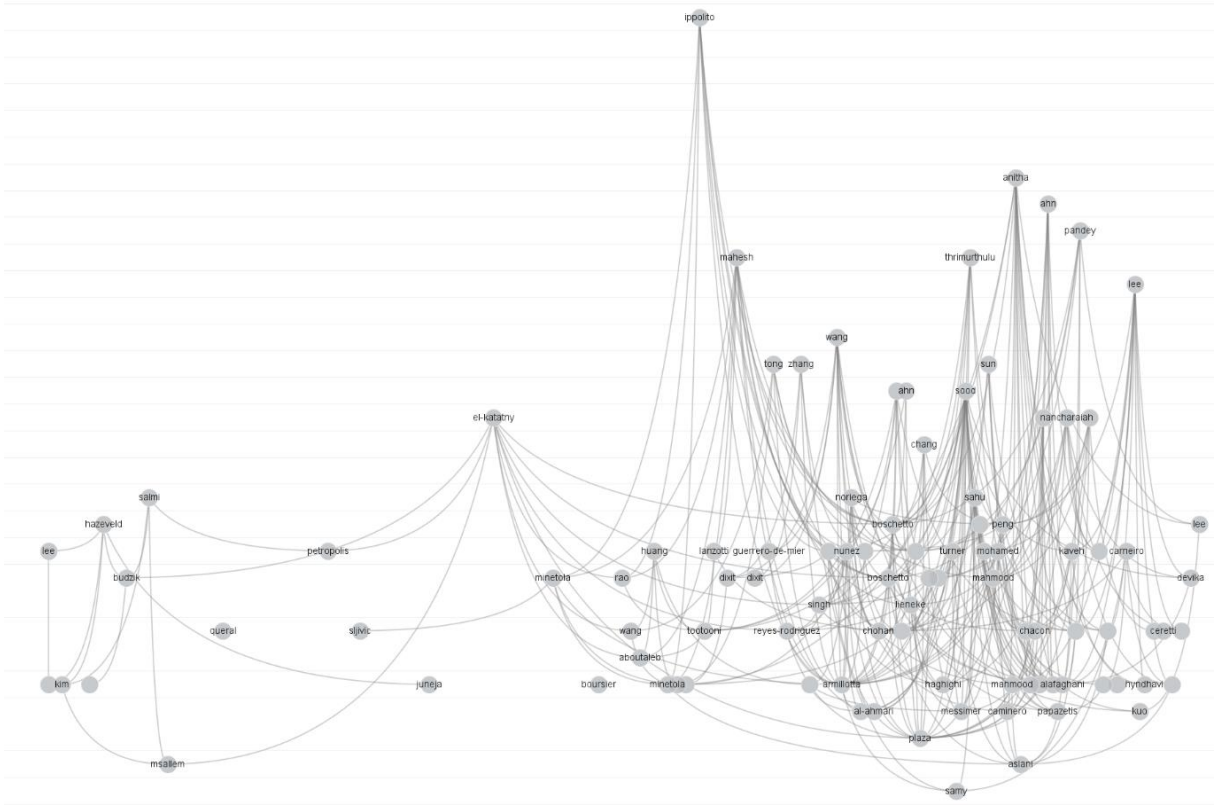

Figure 2.3 *Citation network of key publications*

2.1.2. EXPERIMENTAL STUDY APPROACHES

This section provides summaries of the experimental studies including publications by year, geographic distribution and study materials and methods. This therefore provides a high-level overview of the existing work that has been undertaken as well as informing emerging trends.

2.1.2.1. TEMPORAL DISTRIBUTION

The distribution of studies published over time is presented in Figure 2.4.

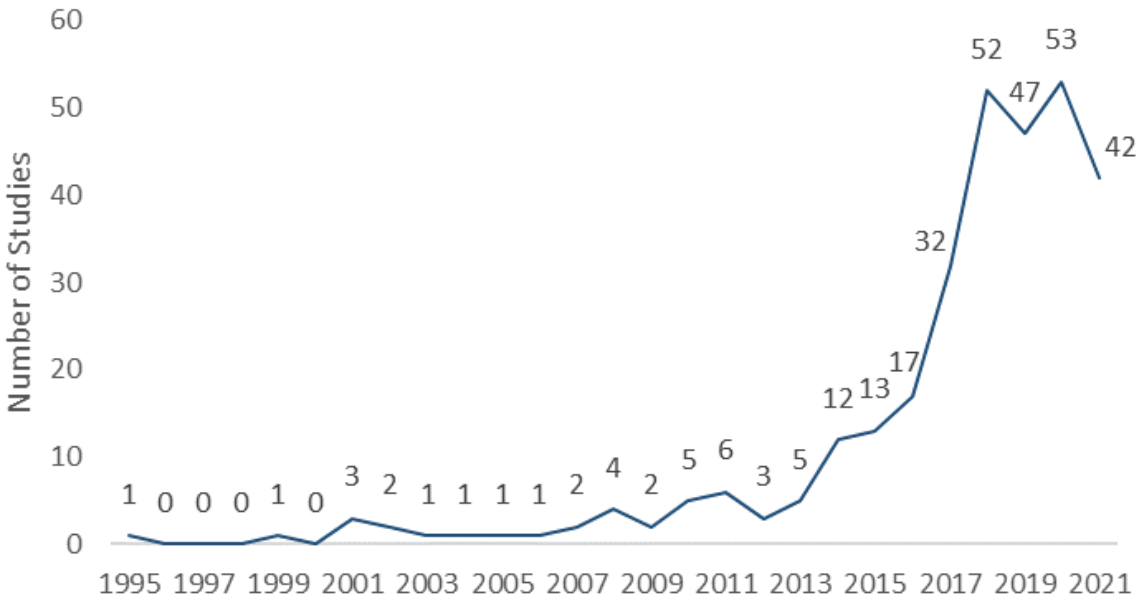

Figure 2.4 *Experimental study temporal distribution*

The first experimental study was published in 1995 by Ippolito et al., [176]. From 1995 to 2008, relatively little attention was paid to ME AM, with no more than three studies published in any one year. In the next six years to 2013, there is evidence of some heightened interest. However, a major increase in the number of published studies occurred in 2014 and sharply grew to a peak of approximately 50 studies per year between 2018 and 2020. This increase broadly coincides with the lapsing of the FDM patent in 2009, accounting for an additional period of alternative machine development and familiarisation by researchers. It also mirrors an increase in the number of studies published that are returned by the *Scopus* database using the search term 'Additive Manufacturing', which shows a similar trend after 2012. The number of studies fell between 2020 and 2021, coinciding with the COVID-19 pandemic and reduced access to laboratory facilities. Research attention was likely directed to non-physical experimentation, given that the number of studies identified for general additive manufacturing (i.e. via the *Scopus* search) does not exhibit this same dip.

2.1.2.2. GEOGRAPHIC DISTRIBUTION

The geographic distribution of experimental studies is shown in Figure 2.5. This represents each study's first author's institution, though in most cases at least one other author is also affiliated with that same institution.

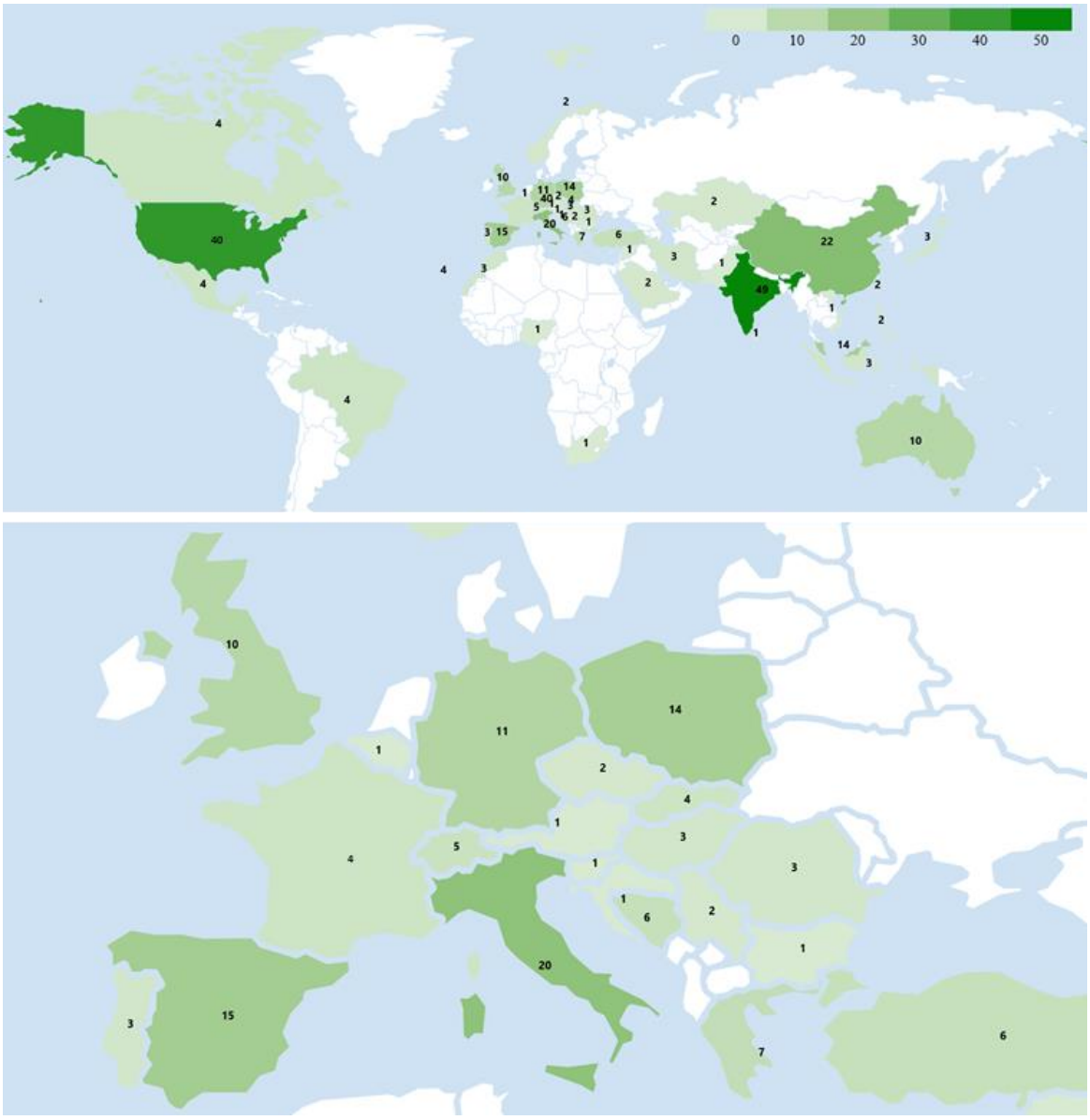

Figure 2.5 *Experimental study geographic distribution*

Both figures are also included in a larger format in Section 12.1 in the Appendix. India, the United States and China represent the three countries with the most studies at 49, 40 and 22 studies respectively. Within these countries, there are a wide variety of authors and institutions represented. For example, in India the 49 studies were conducted at 39 different institutions and by 38 different lead authors. Within Europe, Italy, Spain, Poland, Germany and the United Kingdom account for the majority of studies.

2.1.2.3. STUDY PURPOSE

Experimental studies have been conducted for several purposes. Figure 2.6 presents the number of studies across seven principal categories.

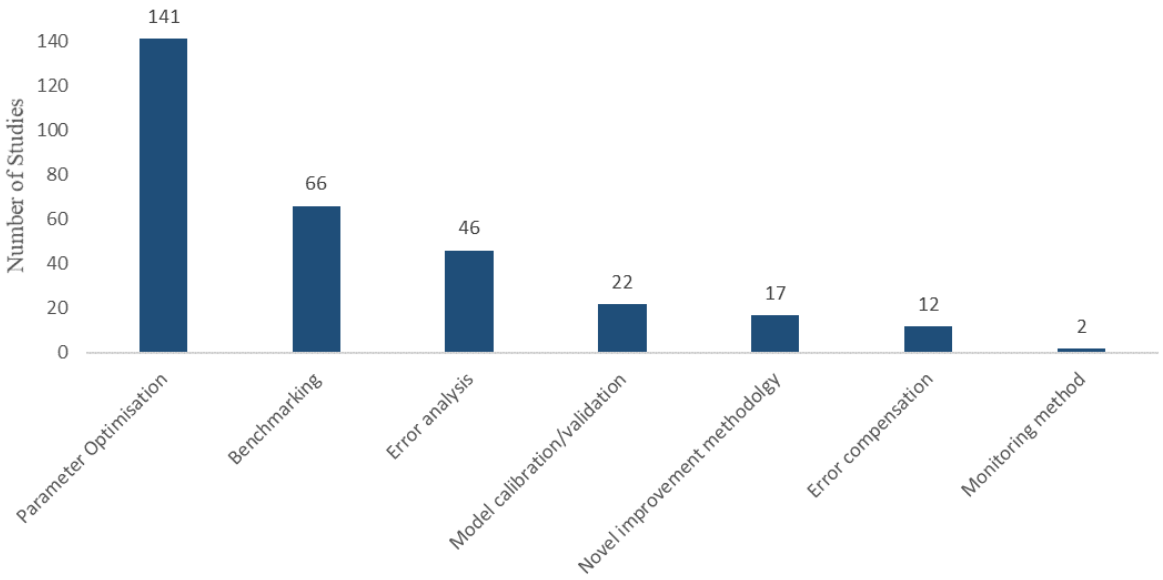

Figure 2.6 *Experimental primary study purpose categorisation*

Existing study purposes are considered in greater detail in Section 7, where particular attention is paid to error improvement studies. In a small number of cases, a single study has multiple purposes. For example, Petropolis et al. [188] conducted a parameter optimisation study where the layer height was varied in conjunction with a benchmarking against the SLS AM technology. In this case, the primary objective is recorded.

Figure 2.6 demonstrates that almost half of all studies are concerned with the optimisation of process parameters to improve performance. There are more than 60 benchmarking studies which compare different ME AM machines and materials as well as the ME AM process against other AM processes and conventional technologies. The 46 error analysis studies purely state the current performance, usually with default printing parameters. There are a smaller number of model validation, novel improvement (e.g. new techniques, post-processes etc.) and error compensation studies. Finally, there are two isolated studies which tests in-situ monitoring to detect errors in the process as they occur.

2.1.2.4. MACHINES

Across the 306 studies, more than 140 unique ME AM machines were utilised. The vast majority of machines were used in three or fewer studies, as demonstrated in Figure 2.7. In addition, 40 studies did not state the machine used at all, though they did state that the ME AM process was used.

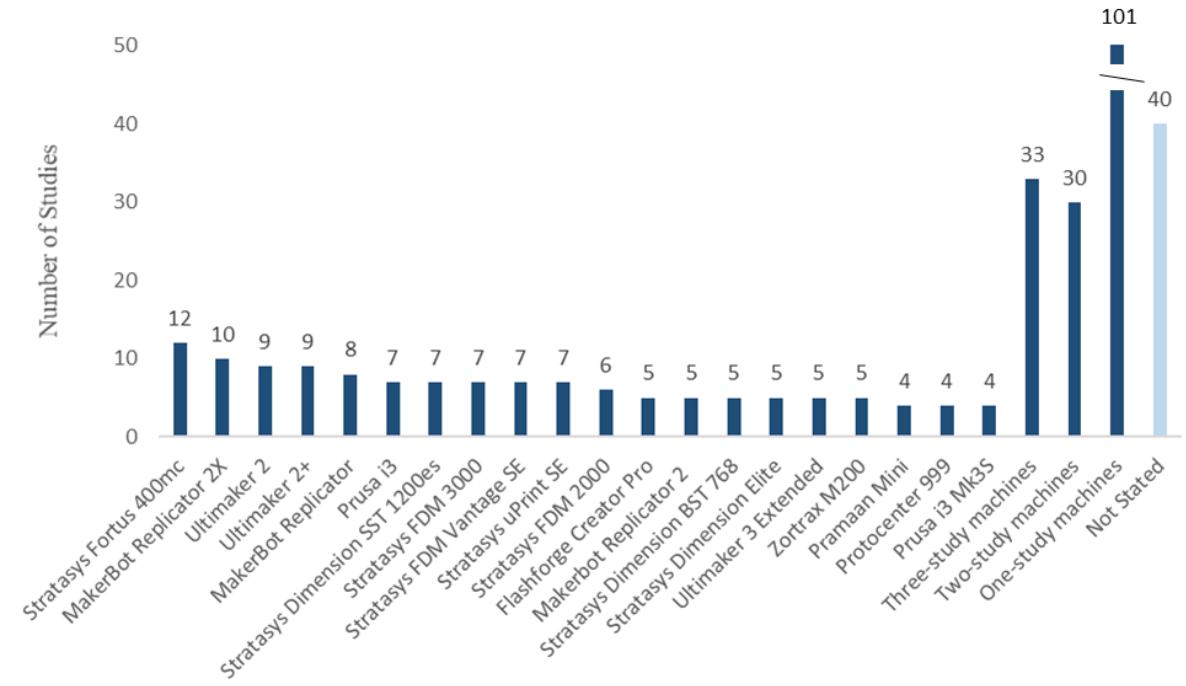

Figure 2.7 *Experimental study machine utilisation*

Prior to the FDM patent expiring in 2009, all studies utilised Stratasys machines. Whilst the use of these has declined heavily since (and were used in just three of the 42 studies in 2021), this nonetheless means that eight of the most popular machines over the entire period were manufactured by Stratasys. Otherwise, MakerBot, Ultimaker and Prusa are the most popular manufacturers. Given that different machines achieve nozzle motion in different ways (see Section 4 for further detail) and with differing levels of precision, the large number of machines used suggests an additional source of variation that is rarely discussed.

2.1.2.5. SLICING SOFTWARE

As Figure 2.8 demonstrates, fewer than half of the studies provide information regarding the slicer used. Certain machine manufacturers produce their own slicer, such as Stratasys with their *Insight* slicer and MakerBot with *MakerBot Print* and *MakerWare*. Whilst other slicers can be used with these machines, it is likely (although not explicitly stated) that studies utilising these machines did use these slicers. Ultimaker's *CURA* software is by far the most popular, with 45 studies using it in their experimentation. The open-source *Slic3r*, free *MakerBot Print* and paid *Simplify3D* are also popular, though represent fewer than ten percent of studies combined. These results are consistent with Šljivic et al. [58], who also identified *CURA*, *Slic3r* and *Simplify3D* as the most popular slicers.

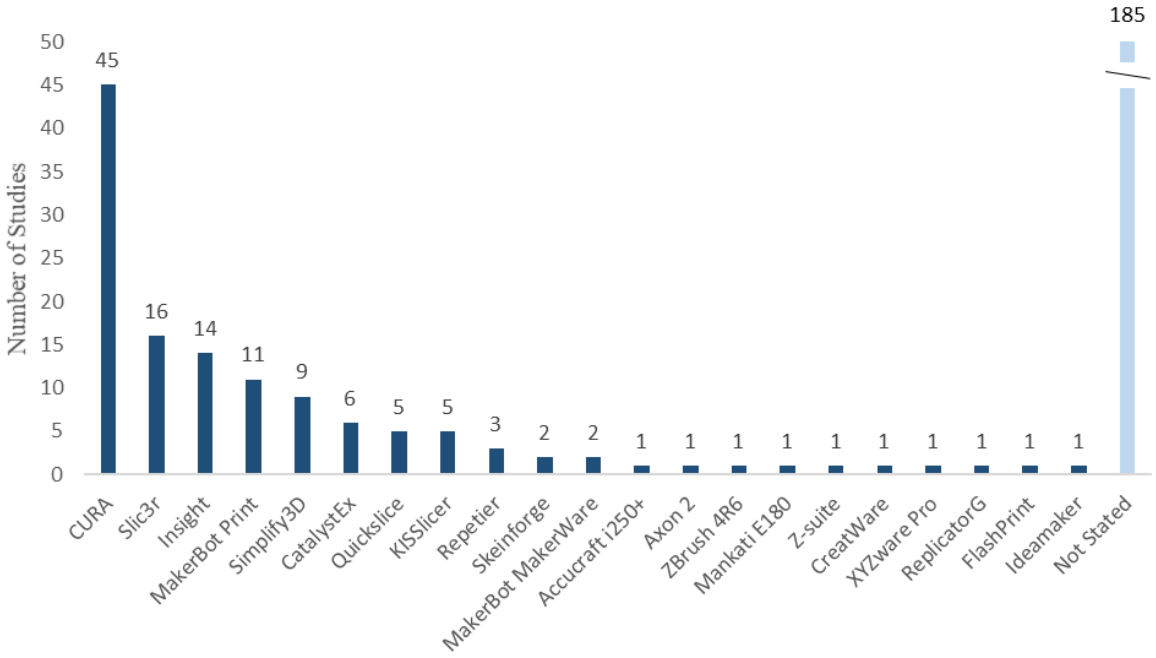

Figure 2.8 *Experimental study slicer utilisation*

2.1.2.6. ARTEFACT

Studies have utilised a wide variety of artefacts. These range from simple cubes and cuboids where the three main face-to-face dimensions are collected, to highly-complex medical replicas of organs or bones. The number of studies for six main categories of artefact are shown in Figure 2.9.

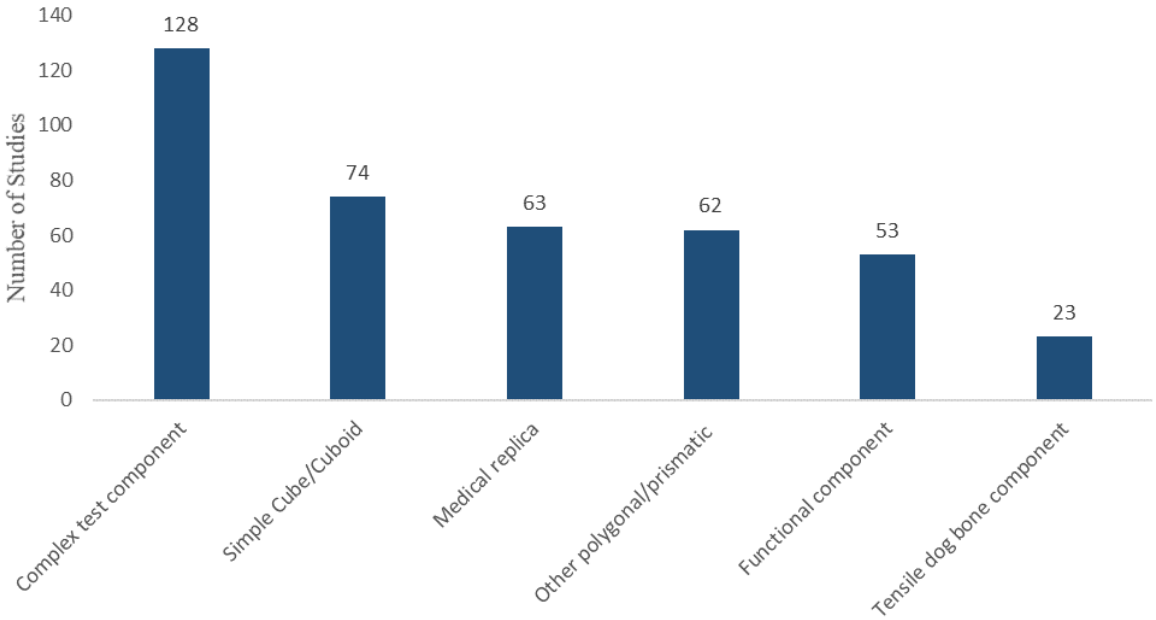

Figure 2.9 *Experimental study artefact designs*

This demonstrates that the most popular artefact is a complex test component consisting of multiple geometries, produced specifically for the purposes of the study. Simple cubes/cuboids, medical

replicas, other polygonal/prismatic designs and functional components each represent approximately one sixth of studies. Tensile 'dog bone' components have been measured in 23 studies, in all cases where that same component was produced for the express purpose of measuring mechanical performance. Of relevance to later experimental work in this thesis, 78% of components contain at least one section of vertical outer wall.

2.1.2.7. *Measurement Method*

Eight main measurement methods were identified across the studies, as shown in Figure 2.10. The use of digital calipers to manually record dimensions was the most popular method and was utilised in 84 studies. Coordinate Measuring Machines (CMMs) and 3D scanners were used in 76 and 68 studies respectively, and give a greater level of dimensional data across surfaces. Micrometers were used in 26 studies, providing a similar level of information to the digital caliper measurements. Microscope measurements were taken in 24 studies, allowing for particularly detailed measurements of smaller features.

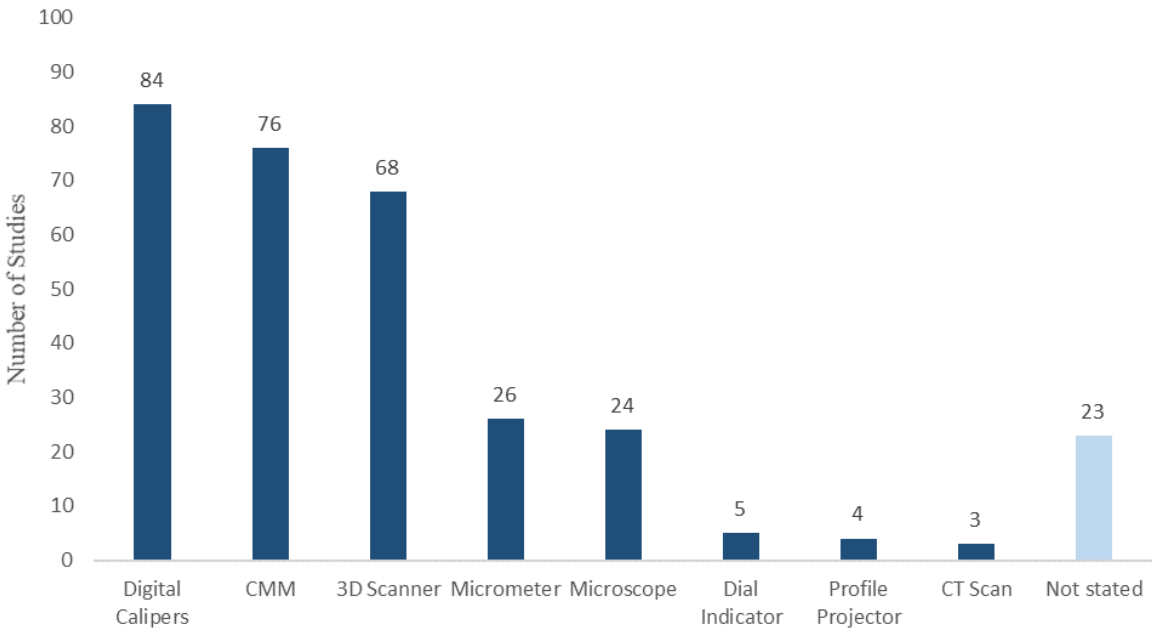

Figure 2.10 *Experimental study measurement methods*

2.1.2.8. *Materials*

ABS and Polylactic Acid (PLA) are by far the two most popular materials used in experimental studies and together account for more than 96% of all materials used as demonstrated in Figure 2.11.

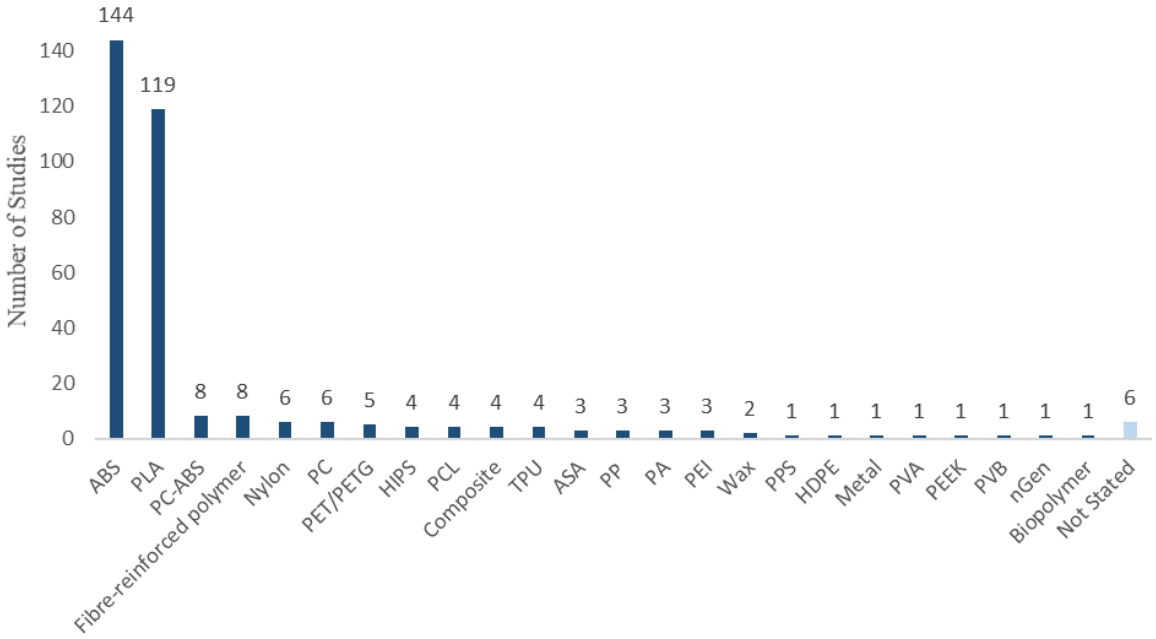

Figure 2.11 *Experimental study material utilisation*

Whilst ABS has been used in more studies than PLA over the period examined, this is largely skewed by its heavy use in earlier studies. In particular, the Stratasys machines used in all studies prior to 2009 exclusively used ABS or, in a small number of cases, ABS blends or other novel materials. In more recent years, PLA has gained in popularity. Since 2017, it has been the most widely used material and in addition, other materials have been also used far more widely as shown in Figure 2.12.

.

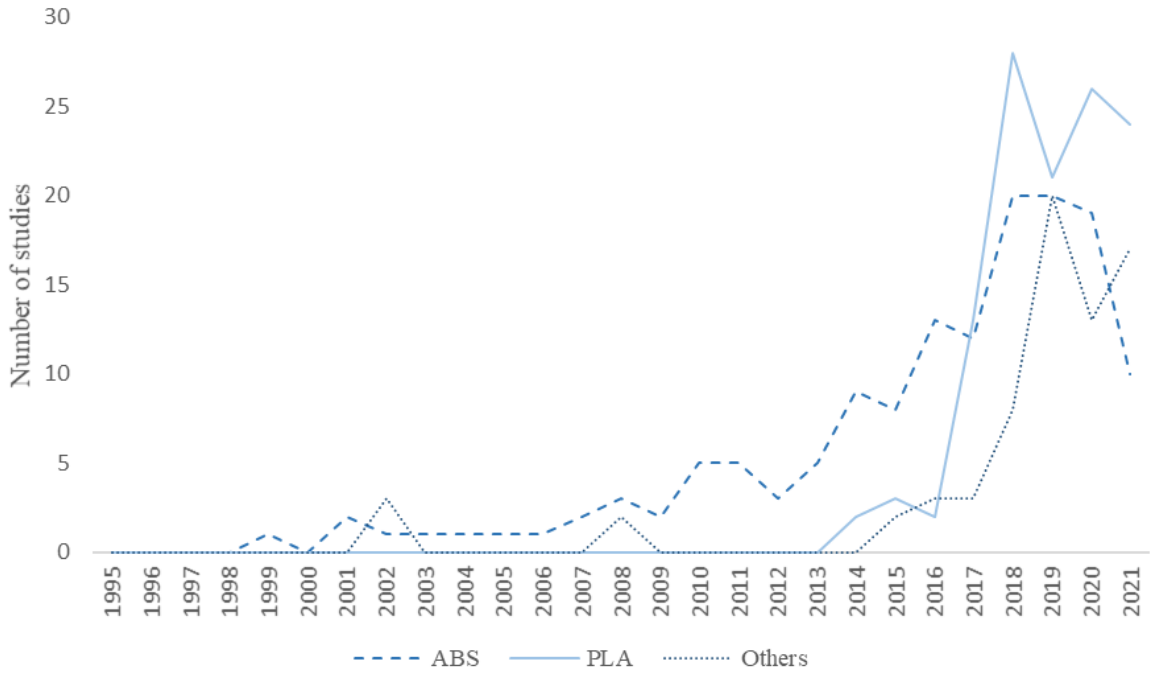

Figure 2.12 *Experimental study material utilisation over time*

2.1.3. EXPERIMENTAL STUDIES OF ACCURACY AND PRECISION

Despite the large number of studies examined, they often differ from one another in key aspects. Whilst some studies have only characterised the process or compared it, others have made efforts to improve performance. In addition, different machines, materials, test artefacts, slicer and print parameters have been employed. The data presented varies significantly between studies with many measures of dimensional error, variability or geometric error presented. As a result, direct comparisons between studies and generalisable findings are challenging. This subsection discusses the key approaches taken by existing experimental studies and provides typical performance figures where possible.

2.1.3.1. DIMENSION ACCURACY

The majority of studies focused on parameter optimisation. In these, a range of parameters are varied to produce the optimal dimensional accuracy. Such solutions therefore typically exhibit very low dimensional error (i.e. of the order of 0.01-0.02mm or lower). Many of the parameter settings do not align with typical values, and therefore the dimensional accuracy error presented by these studies is not fully representative. Similarly, studies that present novel improvement approaches give an unrealistically low error. In addition, improvement studies reduce error only for their experimental setup and so their results cannot be considered fully generalisable.

Benchmarking, error analysis and model calibration/validation studies typically utilise default parameters and so are better suited to represent dimensional error. Typical (average) errors range between 0.1mm to 0.2mm across the majority of studies. However, in certain cases the error is much higher. Both Sudin et al. [189] and Taşdemir [190] demonstrated that curved features produce greater error than square sections, suggesting average dimensional errors of 0.2mm-0.5mm for round and elliptical sections and spherical features. Similarly, macro component shrinkage can yield significantly higher error. As Schumacher et al. [191] note, the ME AM process lacks holding pressure and so generates higher shrinkage error compared to other processes such as injection moulding. The majority of shrinkage studies utilise ABS, which exhibits greater volumetric change on solidification owing to its higher crystallinity [61]. These studies typically calculate shrinkage compensation factors (SCFs) and commonly determine error of 1% or greater [192-196].

A small number of studies have examined dimensional accuracy performance between ME AM machines, different materials and in different axis directions and locations on the build plate. In general, no strong trend has been determined for any of these factors; rather individual studies have identified specific behaviour for each experimental setup. For example, Gulanová et al. [23] compared the performance of four machines and four materials and found all average deviations to be between 0.10 and 0.19mm. Similarly, Sljivic et al. [197] compared two consumer grade machines with a ‘professional’ machine. This showed slightly improved performance for the professional machine,

though only on a highly intricate artefact with very small features. Clemon et al. [198] stated that the quoted machine resolutions, often higher for more expensive machines, has no bearing on actual performance and that all machines have a limit in terms of achievable feature size. Performance across axes has been shown to vary, though results are highly specific to individual studies. A number of studies have reported no clear difference in dimensional accuracy for the X, Y and Z axes [199-204]. Others have reported various combinations; X worse than Y/Z [183], X worse than Y [71], Z worse than X/Y [179,205,206], Y better than X/Z [69], Z better than X/Y [207-210]. Only very few studies have investigated dimensional performance across the build plate. These have typically hypothesised an error resulting from non-uniform heating of an enclosed printing envelope to limit the shrinkage and warpage of ABS, which Pennington et al. [211] showed to be a statistically significant factor. Other studies have found no relationship [212,213], whilst some have found slight differences either with performance being best at the centre of the build plate [69] or at the edges [214,215].

2.1.3.2. DIMENSION PRECISION

As Velineni et al. [216] noted, reproducibility is a major challenge for AM, particularly for interference fit or assembly of components [217]. The original developers of the ME AM process, Stratasys, claim an accuracy of ±0.127mm or 0.04mm per mm, based on a detailed study with multiple components [218]. However, some studies suggest that precision performance is worse than this and can vary with many other factors including machine, material and component design. Existing studies have captured process variability in many different ways. These include: max-to-min ranges [199,219], specific percentile ranges [220], interquartile ranges (IQRs) [221], standard deviation, process capability, repeatability coefficients [222] and International Tolerance (IT) grades. Each of these effectively captures the spread of measured values about a mean, whilst some also account for an average process offset (i.e. average dimensional accuracy error).

Johnson et al. [223] investigated two separate ME AM machines, a high-end *Stratasys SST* and desktop *Cupcake CNC*. They determined the dimensional precision to be superior for the Stratasys, and that most dimensions were within 0.5mm of the nominal value. However, fewer than 80% of data points on the *Cupcake* fell within 0.2mm and approximately 1% of measurements fell outside of this range for the *Stratasys*, despite the claimed precision noted earlier. Other studies have typically reported precision of approximately ±0.1-0.2mm [218,224-231], though as much as ±0.5mm for some more complex artefacts [232,233].

Standard deviation has commonly been determined in experimental studies. A single standard deviation either side of the mean represents approximately 68% of all values, and therefore has a lower value than many other precision metrics. Reported standard deviations have typically been around 0.1mm or lower [226,234-240] or 0.1-0.3% [241,242].

IT grades are used to classify achievable tolerances for a given process. Values are calculated according to the formulae included in the ISO 286-1-2010 [243] standard shown below.

$$T = 10^{0.2(ITG-1)}\left(0.45\sqrt[3]{D} + 0.001D\right)$$

where: T = tolerance, ITG = IT Grade, D = geometric mean dimension

This relates the tolerance, T (often taken as 95th percentile of values [244]) and the mean dimensions of the feature being measured D to an IT Grade value. Many studies have calculated IT grades [14,41,176,202,218,234,244-255], and have found values of between IT5 [254] and IT16 [176]. These are dependent of the feature geometry and size and other factors including machine and material. The majority of studies report a range of approximately five IT grades for the specific experimental setup, demonstrating the highly variable nature of tolerances across different component features.

A further precision metric explored in some studies is process capability (C_{pk}), a measure of the capability of a process to provide output that is within the process specification limits (upper and lower, USL and LSL respectively). The C_{pk} calculation for an offset process is as follows:

$$C_{pk} = \min\left(\frac{USL - \mu}{3\sigma}, \frac{\mu - LSL}{3\sigma}\right)$$

Equation 1: *C_{pk} calculation*

where: USL = upper specification limit, LSL = lower specification limit, μ = mean, σ = standard deviation. This therefore allows either a calculation of C_{pk} for given service limits, or service limits for a given C_{pk}. Singh [254] determined that C_{pk} values for all four measured dimensions were above a critical value of 1.33. Mohamed et al. [6] also determined a C_{pk} value of 3.07 based on USL/LSL error values of 2%. However, Bodur et al. [256] found that the C_{pk} value was significantly too low unless error compensation was applied.

2.1.3.3. GEOMETRICAL ACCURACY

Geometrical accuracy can be defined by many separate measures, collectively referred to as Geometric Dimensioning and Tolerancing (GD&T) and defined in ASME Y14.5 [257] and ISO 1101 [258].

Rupal et al. [8] proposed a generic benchmarking test artefact specific to AM to capture all the major GD&T metrics, which subsequent studies could then utilise. However, the majority of studies have investigated multiple GD&T measures for a specifically designed component. GD&T metrics determine the upper and lower bounds for a given geometry. For example, a circularity measure represents the difference between the smallest and largest circles that contain the measured perimeter.

The following GD&T metrics have been captured in existing literature (definitions available in Section 12.1 of the Appendix): Cylindricity [71,215,232,247,249,259,260-265], Circularity [199,215,247,261-264,266-269], Concentricity/Coaxiality [41,71,199,244,248,262,263], Flatness [41,71,199,215,232,244,259,247-249,262-265,270], Parallelism[41,71,199,244,248,261,265], Straightness [199,269], Perpendicularity [41,71,199,232,248,261,265] and Angle deviation [71,199,269]. Most reported results fall between approximately 0.1mm and 0.2mm. Angle deviations have been reported as lower than 0.5^{o} [71,269]. There is no clear difference in performance between curved versus straight geometries, though coaxiality in particular provided higher levels of error at approximately 0.5mm [71,244]. Whilst flatness errors were often of the order of 0.1mm, Minetola and Galati [41] noted that this error increased significantly if the flat surface was inclined.

Many studies have experimentally investigated warpage, which typically manifests as straightness or flatness error [187,191,236,271-278]. This is caused by shrinkage of the crystalline polymer and non-uniform stress gradients developing within the layered component. For long, thin components with poor bed adherence, this can give errors of many millimetres, far greater than the standard dimensional errors identified previously. However, as was noted previously, ABS is more prone to this phenomenon than the increasingly popular PLA, and measures may be taken to reduce it including improved bed adherence, heated build envelopes and a novel slicing approaches.

2.1.4. Experimental Literature Limitations and Implications for Further Research

Despite the large body of literature that has been presented in this section, limitations remain. There are a wide variety of factors which vary between studies that are known to influence results in addition to print parameters including artefact design, slicer and materials. However, these are rarely consistent between studies and in many cases the values for these are not stated. As a result, individual studies produce isolated results that are therefore not typically used by current users or manufacturers who will likely have an alternative process setup. Direct comparisons between studies are also challenging and it is not clear what tolerances (resulting from a combination of accuracy and precision error) should be used for interoperability of manufactured components between machines or between prints.

It has been identified that the ME AM process is increasingly being utilised for final-use components, including in small batches. In order to do this, multiple prints across multiple machines must be investigated. However, only five of the 306 studies have considered more than two machines [23,198,225,279,280] and even within these, the slicer was never stated and other factors were often changed. To properly compare performance between fabricated components, it would therefore be beneficial to utilise multiple machines for a standard artefact and consistent print settings. As Mohamed et al. [6] stated, there has been a greater focus on dimensional accuracy rather than

repeatability, particularly between prints for the same component. Additionally, as Fahad et al. [259] noted very little attention have been paid to the repeatability of the parts produced by open-source (i.e. lower cost, desktop) machines. Finally, performance across the three principal machine axes and across the build plate has not been adequately addressed, especially for the more popular PLA material.

The findings presented in this section can partially address the research questions 1a to 1d and in particular, 1a and 1b. Although it has been noted that there are specific circumstances where errors are higher, typical accuracy errors are of the order of 0.1-0.2mm and precision errors are ±0.1-0.2mm. However, as has been discussed, comparisons between studies with like-for-like metrics and experimental setups is difficult and so a full assessment of tolerances between prints and machines is not possible. The first contribution of this research is to address this with consistent component, material and slicer but varying machines to understand the level of tolerance required for the guaranteed assembly of fabricated components. In addition, build plate position and axis direction effects can be studied across the same component for multiple machines, which may yield more consistent findings than have been presented thus far. In effect, this first experimental approach may be viewed as multiple studies in parallel which, by virtue of their consistent factors, are more amenable to comparison.

In terms of addressing the nature of errors and factors that influence them, most studies provide only a relatively high-level assessment or none at all. More than half of the studies conducted parameter optimisation. This is covered in greater detail later in this thesis, though it should be noted that these have demonstrated that a wide range of factors can influence performance but do not address the underlying error sources. For example, changing print speed may affect multiple underlying properties including the deposition toolpath, deposition temperature and volumetric flow rate. Parameter optimisation studies typically present only the output of parameter changes rather than this more fundamental behaviour, and, in the absence of slicer information, provide an incomplete picture. Similarly, more detailed discussion regarding the nature of errors is usually not presented. More than 85% of studies perform either a parameter optimisation, benchmarking or an error analysis. As such, in addition to the issues associated with parameter optimisations, these other studies do not seek to understand the underlying sources of error but rather focus on simply presenting the level of error in the existing process. This thesis is therefore structured to answer these more specific questions regarding the nature of errors and their underlying causes. Following this, existing attempts to improve the process can be reviewed and potential methods for further improvement investigated in detail.

3. CURRENT ME AM PERFORMANCE

Despite the large body of existing experimental work identified in the previous section, some limitations in their scope was suggested. This section provides baseline experimentation of the current ME AM process performance for a typical small batch operation. This enables a fuller understanding of the current process capability in terms of both accuracy and precision, as well as informing where errors are concentrated and therefore where improvements can be made.

3.1. METHODOLOGY

This experimentation has been undertaken in order to characterise the capability of current desktop ME AM machines with respect to their X, Y and Z dimensional and geometrical accuracy and precision.

3.1.1. TEST ARTEFACT DESIGN

As identified in the previous section and noted by Noriega et al. [281], existing experimental studies have demonstrated that no emergent test artefact design has gained acceptance as a standard. Instead, ad hoc test artefacts designed specifically for the metrics being explored in that particular study have been used. For this experimental work, a test artefact was designed with multiple dimensions in each of the three axes. Z height dimensions were all set as integer multiples of the layer height (0.2mm) so as to avoid the potential intrinsic error that can arise otherwise. The design is shown below in Figure 3.1.

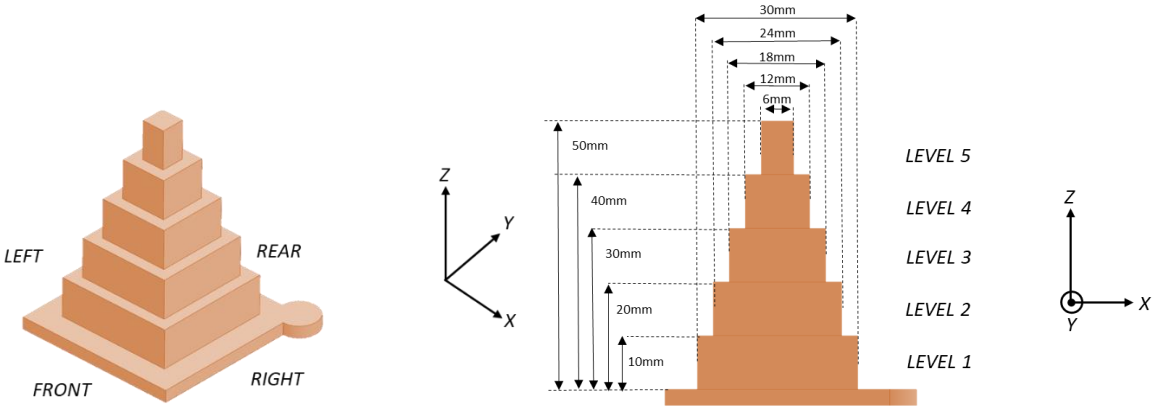

Figure 3.1 *Current ME AM performance experimental test component design*

This allows for external measurement using a CMM on each of the faces, whereas some more complex artefacts with smaller or internal features can only be measured optically [282] or via destructive measurement methods which can be both time consuming and inaccurate. To assess performance across the build plate, test components were produced at the centre and at a randomly selected front corner in each print. The front location was selected as it was expected that there may be greater errors here, since on two of the three machines the Z drive screw was located at the rear leaving the front unsupported.

3.1.2. ME AM DESKTOP MACHINE CHOICE

The three desktop machines were selected to represent a range of price points (for similar build size capabilities), and therefore potential quality differentials. Machine specifications are listed in Table 3.1 for reference and comparison. The resolutions included here represent a minimum theoretical movement for each axis (i.e. a product of minimum step rotation angle on the stepper motor and diameter of the drive wheel) rather than the actual accuracy or precision performance achievable.

	ANet A8	**MakerBot Replicator**	**Ultimaker 3**
X axis movement	Belt drive, nozzle assembly moved	Belt drive, nozzle assembly moved	Belt drive, nozzle assembly moved
Y axis movement	Belt drive, build plate moved	Belt drive, nozzle assembly moved	Belt drive, nozzle assembly moved
Z axis movement	Lead screw, nozzle gantry moved	Lead screw, build plate moved	Lead screw, build plate moved
Filament size	1.75mm	1.75mm	2.85mm
Nozzle diameter	0.4mm	0.4mm	0.4mm
Feed mechanism	Direct	Direct	Bowden
Approximate price	GBP150 (kit)	GBP1500	GBP3500
Build volume	220 x 220 x 240mm	252 x 199 x 150mm	215 x 215 x 200 mm
Heated bed	Yes	No	Yes
X Resolution	0.012 mm	0.011mm	0.0125mm
Y Resolution	0.012 mm	0.011mm	0.0125mm
Z Resolution	0.004 mm	0.0025mm	0.0025mm
Min. layer resolution	0.1mm	0.1mm	0.02mm

Table 3.1 *Desktop ME AM machine specification*

There are some notable differences in the physical design of the selected machines. The Ultimaker uses a larger diameter filament of 2.85mm rather than 1.75mm, although all 3 utilise a 0.4mm nozzle diameter. The machines achieve XYZ motion in various combinations of nozzle and workpiece motion, although the X and Y axes are always belt-driven and the Z axis operated via a lead screw. Both the ANet and Ultimaker utilise a heated print bed, whereas the MakerBot does not. Finally, there is a clear difference in price with the ANet representing the lowest-priced ME AM machine currently available (less than GBP150 in kit form), the MakerBot a mid-range machine at approximately GBP1500 and the Ultimaker a high-end desktop machine costing around GBP3500.

3.1.3. PRINT PARAMETERS

Print parameters were selected in line with default values included in popular slicing software such as *CURA* and *Slic3r,* and similar to those used in previous experimental studies. Test artefacts were fabricated from PLA. PLA is non-toxic and biodegradable with limited shrinkage [61], and as was previously demonstrated has become increasingly popular in recent years. Material was held constant between prints and machines (i.e. manufacturer, colour and batch). The parameters selected for experimentation are shown in Table 3.2.

	ANet A8	MakerBot Replicator	Ultimaker 3
Layer height (mm)	0.2	0.2	0.2
Wall line count	2	2	2
Infill density (%)	10	10	10
Infill pattern	Grid	Diamond	Grid
Printing temperature (ºC)	200	200	200
Bed temperature (ºC)	60	N/A	60
Print speed (mms^{-1})	30	'Default'	30
Travel speed (mms^{-1})	150	150	150
Retraction Distance (mm)	6.5	6.5	6.5
Retraction Speed (mms^{-1})	50	'Default'	50
Roof Thickness (mm)	0.8	0.8	0.8
Floor thickness (mm)	0.8	0.8	0.8

Table 3.2 *Desktop ME AM print parameters*

3.1.4. COMPONENT PRODUCTION AND MEASUREMENT

Ten prints with two components each were fabricated on the three machines, producing a total of 60 components. This provides significantly more examples of nominally identical components at the same orientation than any previous study. Prints were conducted at an ambient temperature of approximately 21ºC, although other environment factors such as humidity were not explicitly noted. In addition, no specific environmental metrics were recorded at the point of measurement though these were likely similar to the point of printing. Theoretically, increased ambient temperature and humidity will lead to increases in measured dimensions, although PLA is less susceptible than some other polymers such as Nylon. Nonetheless, the lack of detailed environmental control is consistent with previous studies, which seldom report such metrics. The prints were conducted in a standard laboratory facility in the University's Engineering Department, and measurements taken in the metrology facilities. Both were out of direct sunlight or sources of moisture and likely represent somewhat typical printing conditions as any user might experience. Nine measurements were then taken on each vertical face using a CMM, a common technique in the metrology of AM parts as demonstrated in previous studies [253,281,283]. All measurements were conducted approximately 2-4 weeks after the fabrication of the specimens, which were stored away from direct sunlight or sources of moisture in the interim. The *Mitotoyo Euro-M 544 CMM* was utilised, which has a stated accuracy of 5+5L/1000µm or 5.25µm for the largest feature size on the artefact being measured (*Status Metrology 2017*).

In addition, eight measurements were taken on each of the horizontal faces (nine on the uppermost face) including the reference flange at the bottom. X and Y measurements represent the distance between matching points on opposite faces, and Z measurements were taken relative to the lower flange (see Figure 3.1). The measured point positions (for level 1 as an example) are shown in Figure 3.2. In total, 221 individual points were collected per component or 131 measured dimensions (45 X, 45 Y and 41 Z measurements).

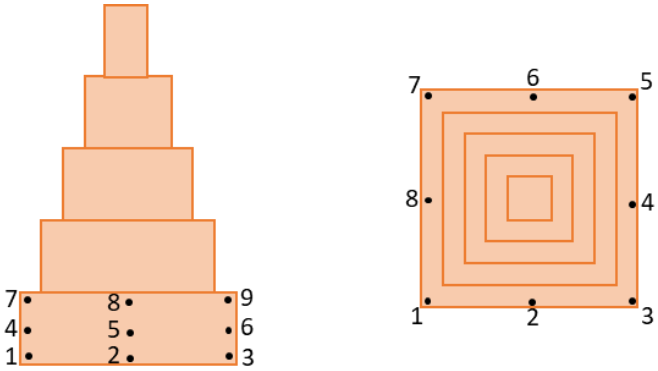

Figure 3.2 *Representative X/Y (left) and Z (right) measurement positions*

Care was taken to ensure measurements were taken as close to the edge of each face and at the centre as possible. The real time CMM position readout was used to ensure an equal spacing between the left, central and right points of measurement on each face.

3.2. RESULTS

In this section, the results of the dimensional measurements are displayed. The appendix contains detailed numerical results for each of the three machines, the mean, maximum and minimum error, as well as standard deviations for the X,Y and Z axes and levels 1-5 for both centre and corner components. The total error distribution for the three axes is presented in this section, where each data point represents a measured dimension minus the nominal. Finally, a geometrical error representation is provided, showing the average measured dimension as a proportion of the nominal across the component's features.

3.2.1. ANET A8

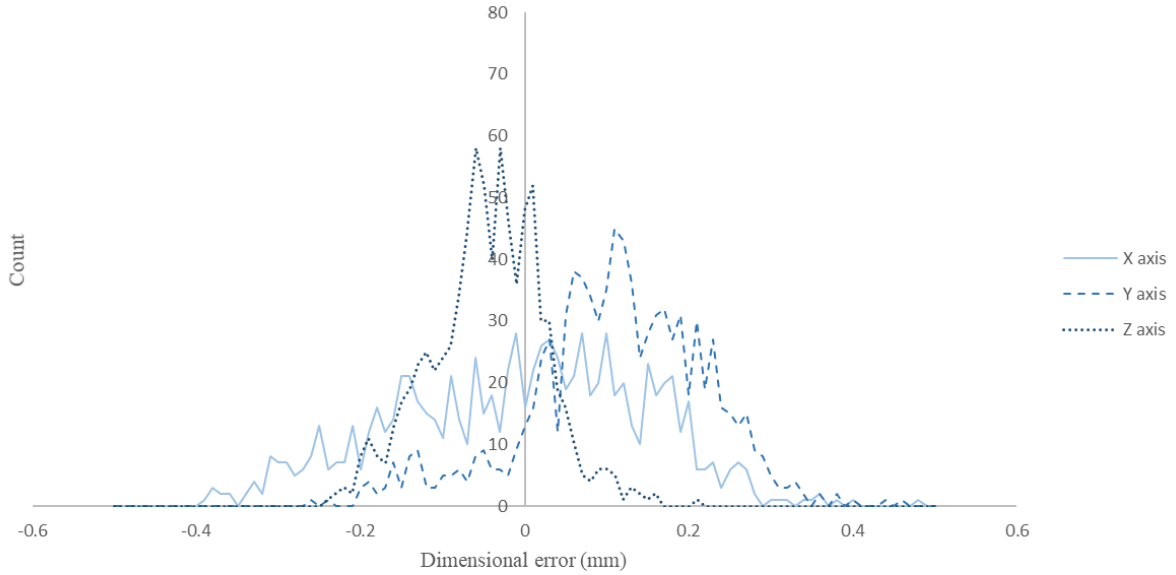

Figure 3.3 *ANet A8 distribution of dimensional error*

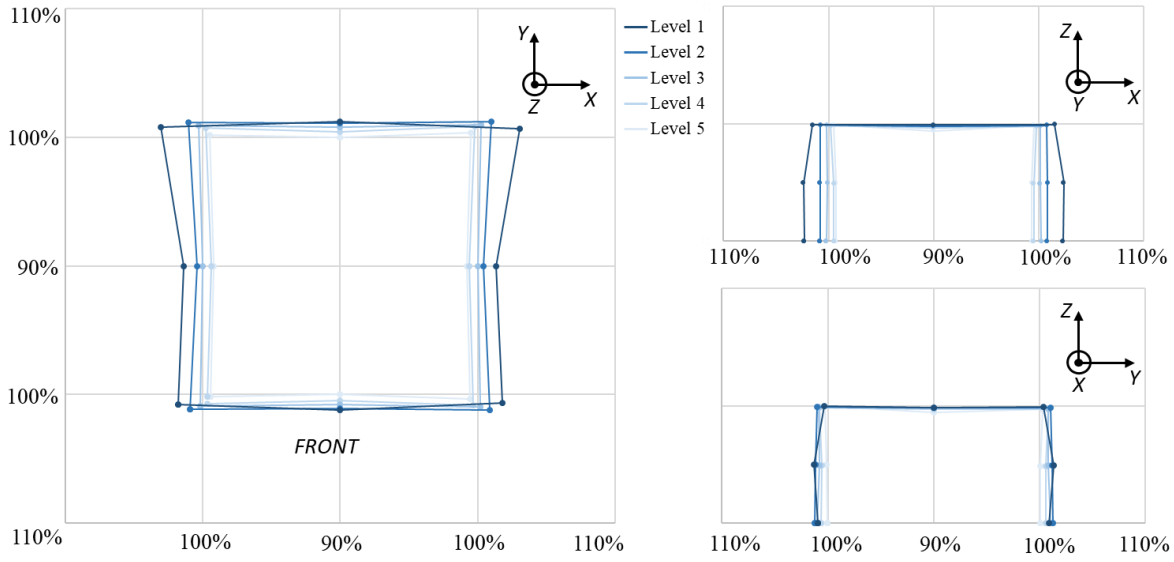

Figure 3.4 *ANet A8 X/Y dimensions as % of nominal (Left: Top view, Top right: Front view, Bottom right: Left view)*

3.2.2. MAKERBOT REPLICATOR

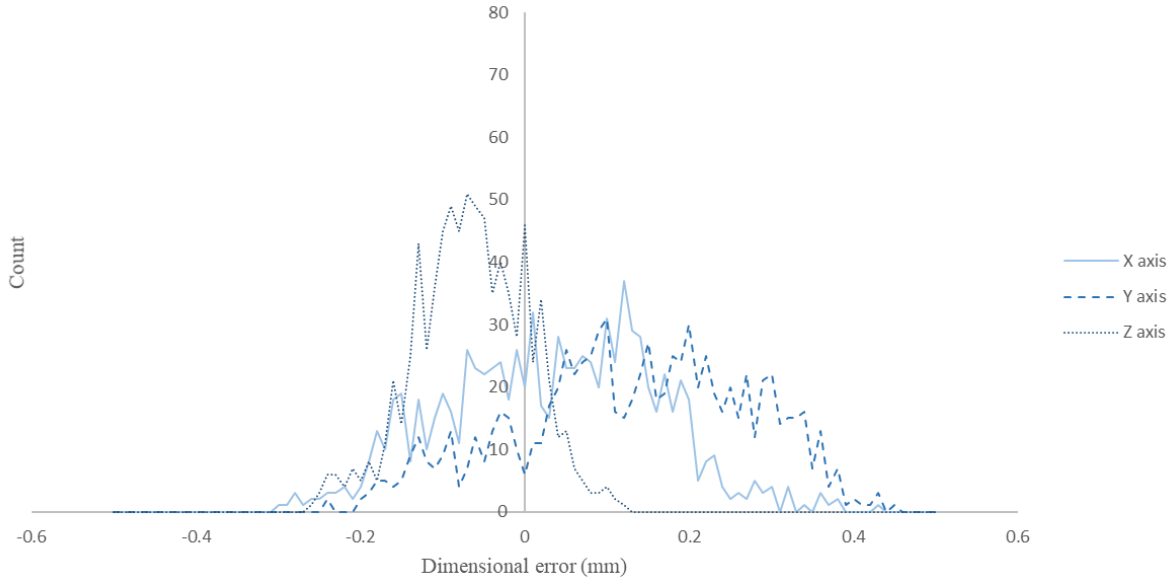

Figure 3.5 *MakerBot Replicator distribution of dimensional error*

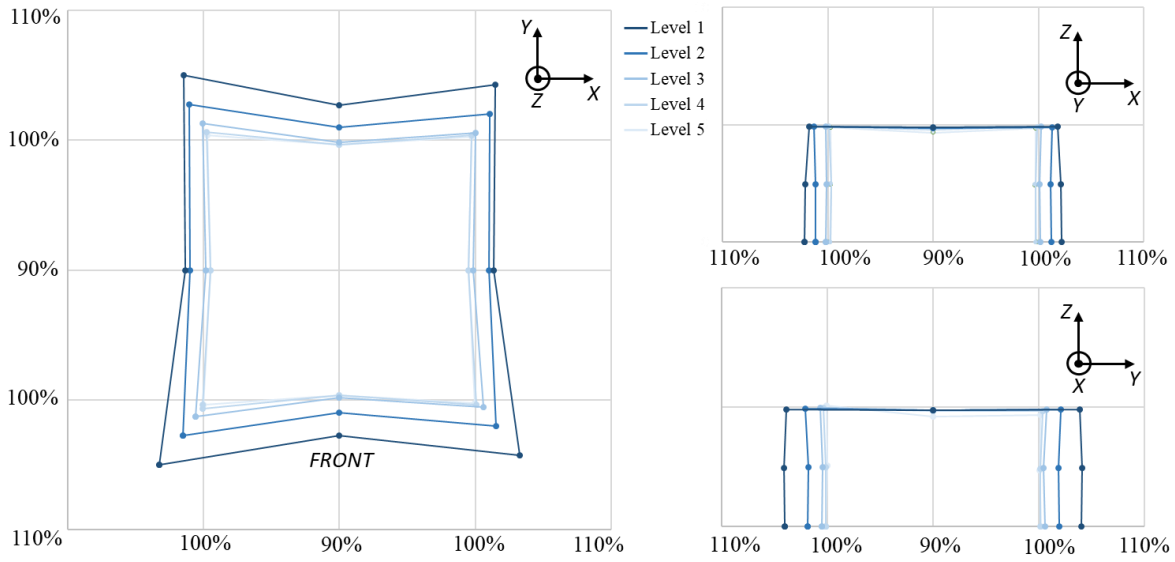

Figure 3.6 *MakerBot Replicator X/Y dimensions as % of nominal (Left: Top view, Top right: Front view, Bottom right: Left view)*

3.2.3. ULTIMAKER 3

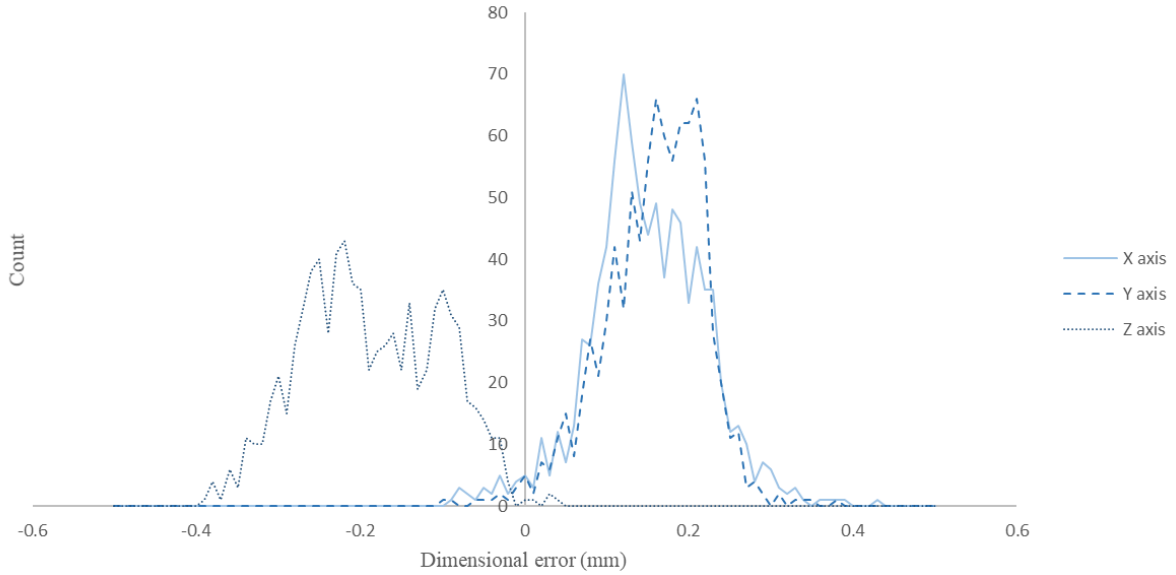

Figure 3.7 *Ultimaker 3 distribution of dimensional error*

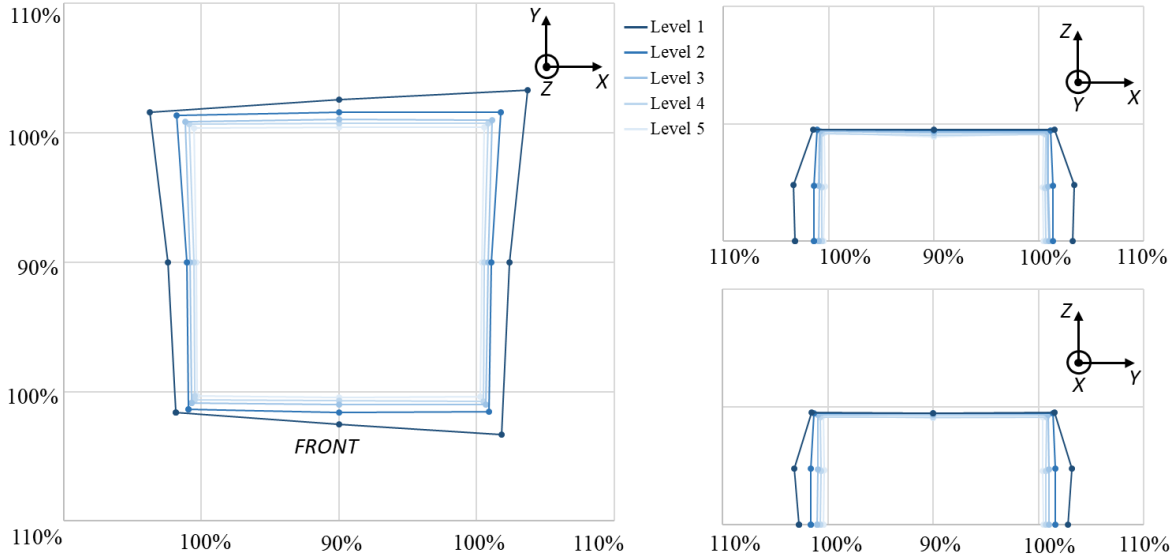

Figure 3.8 *Ultimaker 3 X/Y dimensions as % of nominal (Left: Top view, Top right: Front view, Bottom right: Left view)*

3.2.4. SUMMARY OF RESULTS

	ANet A8	MakerBot Replicator	Ultimaker 3
Dimensional Accuracy			
Average X	-0.01mm (-0.40%)	0.03mm (0.58%)	0.15mm (1.17%)
Average Y	0.11mm (0.74%)	0.13mm (1.37%)	0.16mm (1.21%)
Average Z	-0.05mm (-0.18%)	-0.07mm (-0.24%)	-0.19mm (-0.69%)
Centre vs. Corner components	Corner significantly less accurate for Y axis only	Corner less accurate for Y and Z axes, more accurate for X axis	Little difference
Geometrical Accuracy			
X vertical	Slightly concave for levels 1-3. Convex level 5	Concave for levels 1-4, convex level 5	Slightly concave for levels 1-3. Convex level 5
X horizontal	Concave for levels 1-4, convex level 5	Highly concave for all levels	Flat, but rotated relative to square
Y vertical	Slightly concave for levels 1-4, Highly convex level 5	Slightly concave for levels 1-3. Convex level 5	Slightly concave for levels 1-3. Convex level 5
Y horizontal	Concave for all levels, increasing from 1-5	Concave for all levels, increasing from 1-5	Concave for all levels, increasing from 1-5
Z	Slightly concave for all levels	Slightly concave for all levels	Slightly concave for all levels
Precision			
X Stand. Dev.	0.15mm (1.33%)	0.13mm (1.21%)	0.07mm (1.14%)
Y Stand. Dev.	0.11mm (0.86%)	0.14mm (1.73%)	0.06mm (0.98%)
Z Stand. Dev.	0.07mm (0.37%)	0.07mm (0.36%)	0.08mm (0.32%)
Centre vs. Corner components	Centre Z slightly lower, X slightly higher	Little difference for any axis	Centre Z lower
Other	Poor adherence to bed if not heated. Significant ridges in X, Y and Z directions. Some stringing on most parts.	Poor adherence to bed in Corner components. Significant ridges in X, Y and Z directions. Some stringing on most parts, and some areas of clear over-extrusion.	Poor adherence to bed if not heated. Significant ridges in Z direction, less noticeable but still present in X, Y directions. Minimal stringing or over extrusion errors.

Table 3.3 *Comparison of desktop ME AM machine accuracy and precision*

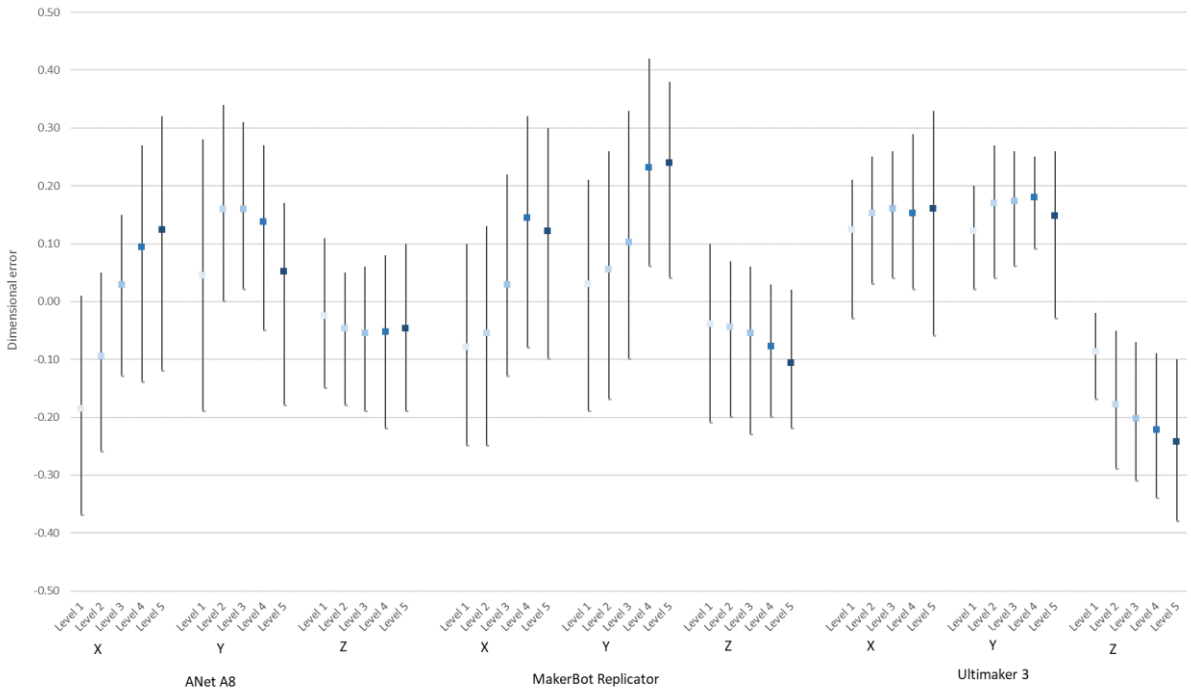

Figure 3.9 *Mean error and upper/lower limits of 95th percentile values*

3.3. DISCUSSION

This experimentation has investigated the dimensional accuracy, dimensional precision and geometrical deviation of the ME AM process. This subsection discusses each of these aspects in turn, and later the potential underlying performance of the ME AM process given the nature and distribution of error. Finally, potential sources of error and a basic model for characterising outer surface error are presented.

3.3.1. DIMENSIONAL ACCURACY

Average dimensional accuracy error is less than 0.25mm for all print directions, component levels and machines as demonstrated in Figures 3.3, 3.5 and 3.7. The most expensive machine exhibits the greatest average error (Figure 3.7) whilst the cheapest has the lowest average dimensional error (Figure 3.3). Although a limited sample size, this suggests that with the current process machine selection is unlikely to be the greatest factor in influencing achievable levels of dimensional accuracy. There is no clear pattern for the achievable dimensional accuracy across different length scales, although dimensional error as a proportion of the nominal dimension does increase as the nominal dimension decreases suggesting the errors consists of both fixed and variable components.

Measured X and Y dimensions are typically larger than the nominal value, except for levels 1 (30mm) and 2 (24mm) on the two cheaper machines. Average Z dimensions are always smaller than required, regardless of the machine or dimension. Whilst on the most basic desktop machines this could be due to a lack of calibration of the build plate, this would typically be accompanied by a flanged lower surface which was not observed in the printed components. In addition, the Ultimaker and MakerBot both utilise auto-levelling and height-adjustment features, and the ANet was manually levelled and first-layer print quality checked. Instead, given this consistent behaviour, it seems likely that a blanket adjustment to the slicer to compensate for this error would prove beneficial. Similarly, given the excess of X and Y dimensions, these would also benefit from adjustment. On average, across all machines and component levels, the following single compensations are suggested: -0.06mm (X axis), -0.13mm (Y axis), +0.10mm (Z axis). Naturally, these would be subject to change depending on the machine selected, material used and component geometry and so should not be considered as equally applicable in all situations. In addition, the Z height is necessarily a multiple of the layer height and so cannot be treated as a continuous variable.

A further observation is that there is no major difference between parts printed at the centre of the build plate and those printed at the corners (i.e. dimensional accuracy is shown to be at a similar level across the build envelope). This suggests that machine deflection leading to positional error arising from the cantilevered print bed or deviations in the print head X-Y position is not a significant factor when considering dimensional accuracy.

3.3.2. DIMENSIONAL PRECISION

The precision performance of the ME AM process is crucial in terms of overall process capability. Mean dimensional error can be improved via virtual part error compensation (either machine/component specific or more general compensation factors as suggested above) but the same approach cannot be used to improve precision.

The Ultimaker exceeds the precision performance of the two cheaper machines (Figure 3.7 versus Figures 3.3 and 3.5). This is likely due to design decisions made in the selection of components and configuration of the axes (e.g. motors, drive belts, lead screws, slideways, chassis materials etc.). This machine also exhibits two major differences when compared to the other two machines tested: an increased filament diameter and a *Bowden* (i.e. off-gantry) filament drive mechanism. It is likely that these machine design aspects produce superior repeatability through lower extrusion variability and reduced kinematic errors owing to the lower gantry mass.

For the two cheaper machines, the Z axis shows superior precision in comparison to the X or Y axes. The Ultimaker maintains a similar level of precision to the other two machines in the Z direction, with significant improvement in the X and Y directions. This suggests that if requiring a high degree of precision for a particular dimension, that dimension should be aligned with the Z axis on either a cheaper ME AM machine or a machine with unknown component quality and tolerances.

Many previous studies have utilised IT grades to present process precision, as was demonstrated in Section 2.1.3.2. Using the same methodology as in these studies with the 95th percentile of the error distribution [244], the IT grades shown in Table 3.4 are calculated.

	ANet A8			**MakerBot**			**Ultimaker**		
	X	**Y**	**Z**	**X**	**Y**	**Z**	**X**	**Y**	**Z**
Level 1	IT 13	IT 12	IT 11	IT 12	IT 11	IT 11	IT 11	IT 11	IT 12
Level 2	IT 13	IT 12	IT 11	IT 11	IT 12	IT 11	IT 12	IT 12	IT 12
Level 3	IT 13	IT 13	IT 11	IT 12	IT 13	IT 11	IT 12	IT 12	IT 12
Level 4	IT 13	IT 12	IT 11	IT 13	IT 13	IT 11	IT 13	IT 12	IT 12
Level 5	IT 14	IT 12	IT 10	IT 13	IT 14	IT 11	IT 14	IT 13	IT 12

Table 3.4 *Measured IT grades*

This shows that the IT grade varies from IT 14 in the worst case (in the X or Y axes, Level 5 and all machines) to IT 10 in the best case (Z axis level 5 for the ANet). The most expensive machine has the most consistent IT grades, and as seen previously is generally superior to the other machines for the X and Y axes. These results are largely consistent with the existing literature, although they are higher than the best cases calculated. This in part is due to the offset (i.e. dimensional accuracy error), which increases the limits required to contain 95% of all error data. Suitable error compensation, such as that suggested previously, would therefore immediately improve the IT grades.

The calculation for C_{pk} for an offset process was presented in Section 2.1.3.2, together with definitions for it and the upper and lower specification limits. As Günay et al. [246] state, in order for a process to be deemed satisfactory a C_{pk} value of at least 1.33 is required such that 99.99% of measured values lie within the specified range. Using this value of 1.33, USL and LSL may be calculated. This gives values of between 0.3 and 0.6mm depending on the machine, print direction and dimensional value. If two printed components (with dimensions in the range of 6mm to 50mm) must be assembled such that 99.99% of components fit regardless of machine or print direction, a tolerance of approximately 1.2mm should be used. This is significantly larger than the level quoted by Stratasys of 0.127mm [284]. Such is the nature of the error distribution, the USL and LSL become much smaller with only modest increases in the acceptable failure rate of components. Using a C_{pk} value of 0.66 (where 95.45% of components are within the limits), the required tolerance reduces from 1.2mm to 0.8mm. The required failure rate depends on the application; for large batch processes a C_{pk} of 1.33 may be sensible, whereas for prototyping a lower C_{pk} may be suitable. Using the value of 0.127mm as the USL and LSL, the calculated C_{pk} values are only greater than 1 for a small number of print direction, dimension and machine combinations, suggesting the process would not be capable if repeatability of the 0.127mm claimed were required. Although the Ultimaker shows improved precision, its inferior accuracy means that there is little difference in the C_{pk} and IT grade values whilst the offset remains. This does, however, suggest that the Ultimaker would benefit to a greater extent from any error compensation.

3.3.3. GEOMETRICAL ACCURACY

Some geometrical errors (i.e. deviation from straight-sided square or rectangular sections) were observed at all levels and directions on every machine. From initial observations, it appears that the curvature of the edges within the XY plane was mostly concentrated towards the vertical edges, suggesting that this error is most likely to be associated with the change in direction at the corner and necessary deceleration/acceleration of both the nozzle and extrusion mechanism rather than a more general curvature error or warpage. A component was produced and the print aborted halfway to obtain a cross-section as presented in Figure 3.10. This clearly demonstrates that geometrical error is concentrated at the corners.

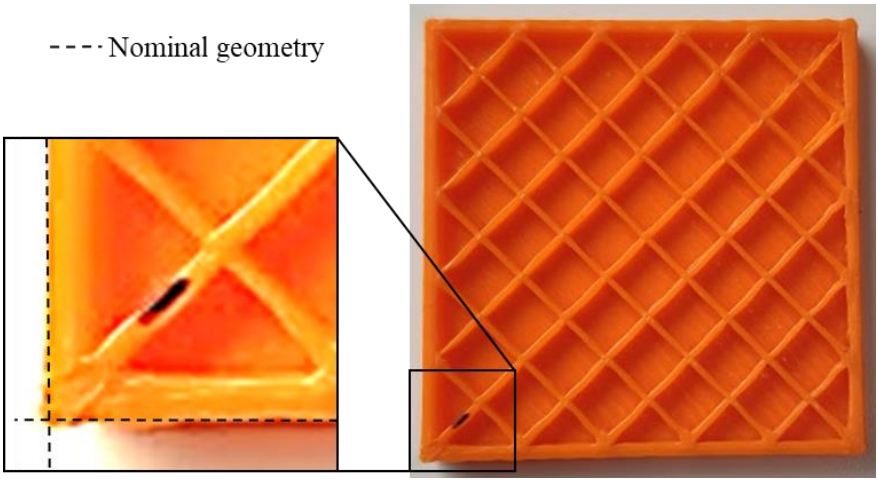

Figure 3.10 *Geometrical error concentrated at corners in the XY plane (side length = 30mm)*

XY plane geometrical error was observed on all three machines. Z geometrical error was less pronounced, though still present, particularly at longer length scales (i.e. on level 1). Across the three machines tested, levels 1 to 3 generally exhibit slight concave surface curvature error. The smaller cross-sectional areas of levels 4 and 5 exhibit much greater geometrical error - and in particular some complex geometrical error was observed on level 5 with a mixture of concave and convex surfaces. This phenomenon was observed on all machines. Unlike with dimensional accuracy, the most expensive Ultimaker machine is by far the most geometrically accurate printer. Whilst these geometrical errors may theoretically be corrected in the same way that dimensional error could be, if the corner related-errors are more fundamental to the process it is preferable to address the cause rather than attempt machine-specific error compensation.

Also observed were horizontal ridges evident on all components, which are inevitable given the layer-based approach. However, vertical ridges were also present on every level. These are most noticeable on the ANet and MakerBot artefacts, but can be seen with all three machines. It is not immediately clear what the source of these is, but as these features did not align with the infill pattern, it is likely that they are the result of a resonance within the system.

Stringing (i.e. fine strands of material) and other over-extrusion artefacts were observed throughout, particularly on the two cheaper machines. This led to some highly localised dimensional or geometrical errors, particularly at the beginning and end (‘Z-weld’) of the external perimeter which is located on one of the 90 degree corners. The stringing is observed to be dependent on the location of a part and the print order for that particular layer. A higher degree of stringing occurs before large movements (i.e. from one component to another) within a layer. This suggests that part error should not be considered solely as a single geometry in isolation, but instead depends to some extent on other surrounding geometries and future toolpaths and extrusions.

3.3.4. UNDERLYING PERFORMANCE

There are three ways in which the variability of the ME AM process can be characterised. The first and simplest is to consider each measured dimensions against its nominal dimension. For example, all nine measurements in the X axis direction on each level have the same nominal dimensions so the error for every measurement is simply relative to this. This is the measure included in in the previous results, which use this absolute deviation for every measurement taken.

An alternative is to take the same measurement location on any given test component and compare it only with the same measurement location on other parts. In this approach, the reference becomes the average of these measurements rather than the nominal dimension. In the third measure of variability, this can be extended to be only the same measured location of parts printed in the same build position on a machine (i.e. as per the second option but only for, say, centrally-printed artefacts). Variability between machines is not considered here, though could potentially be of interest where the same component is being produced in large volumes.

The primary benefit of considering these final two metrics is that they remove the accuracy error of each measurement location and present only the precision component. There will of course be lower variability if each measured dimension location is considered individually. For example if a specific measurement location is always undersized by the same amount, at the individual location level this is an example of low accuracy but high precision. By averaging all results across all positions, this appears as a lack of repeatability, whereas if a suitable error correction was made against the intended dimension this would not be the case. Instead, if each measurement is compared with the average measurement at that given position then an understanding of underlying ME AM process precision can be achieved.

By definition these error distribution curves have a mean of zero. This shows the underlying precision of the ME AM process and is more consistent across the machines (Figures 3.11 to 3.13). This demonstrates that at a minimum, most error is lower than 0.2mm. This also clearly characterises the three machines and shows that underlying precision is gained when moving from the cheapest to the most expensive machine.

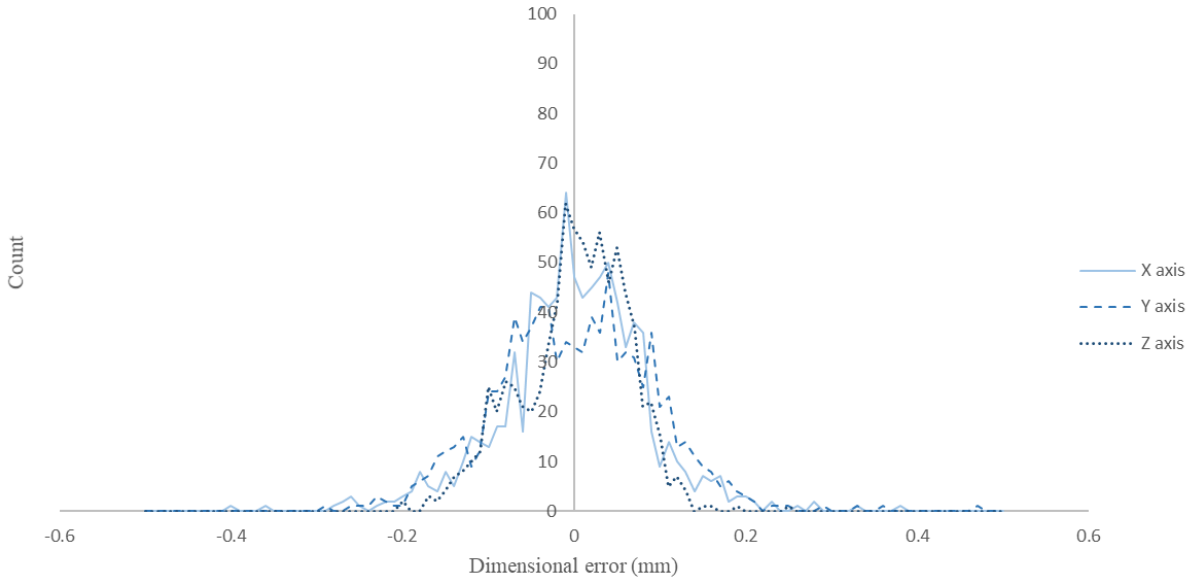

Figure 3.11 *ANet A8 distribution of dimensional error against the average dimension at each measured position*

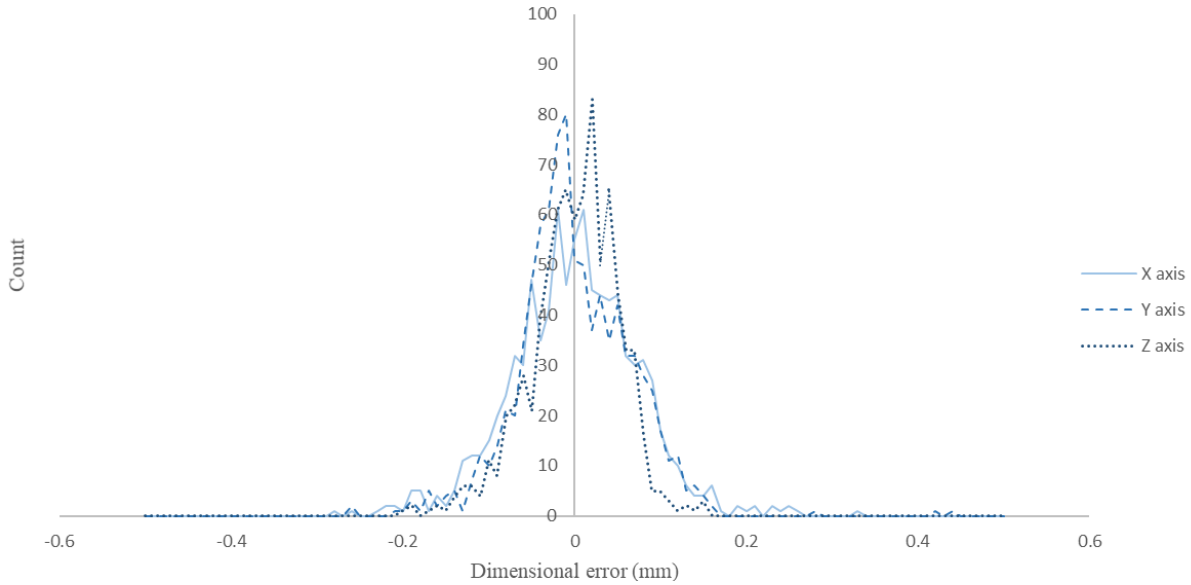

Figure 3.12 *MakerBot Replicator distribution of dimensional error against the average dimension at each measured position*

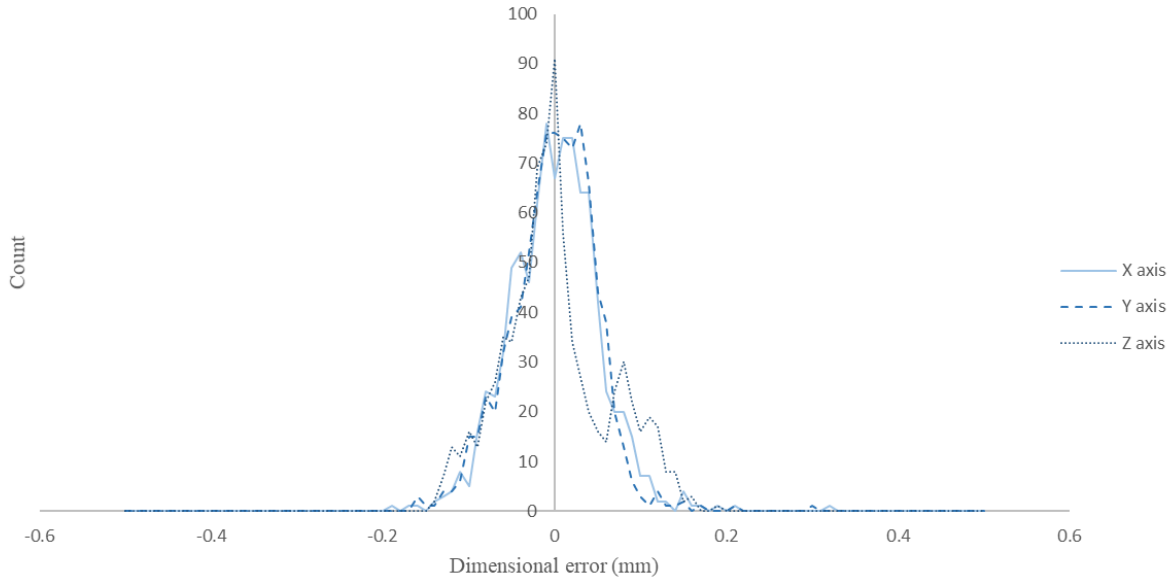

Figure 3.13 *Ultimaker 3 distribution of dimensional error against the average dimension at each measured position*

Each dimension can also be compared with the same measured location on each component, for components only in the same build plate location. This gives an even more specific measure of precision, effectively for the same points in space within the build envelope on any given machine. This therefore provides a best case scenario for precision, beyond which no improvement can be made through error compensation alone and the process would instead require some fundamental alteration. These error distributions also have a mean of zero and a much lower deviation.

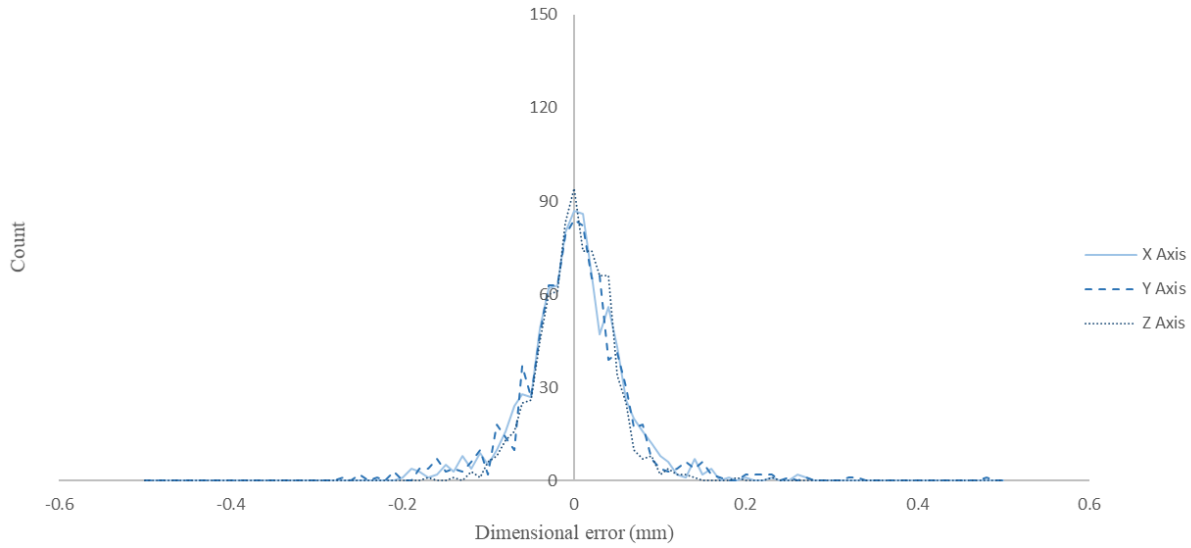

Figure 3.14 *ANet A8 distribution of dimensional error against the average dimension at each measured position for components in the same location*

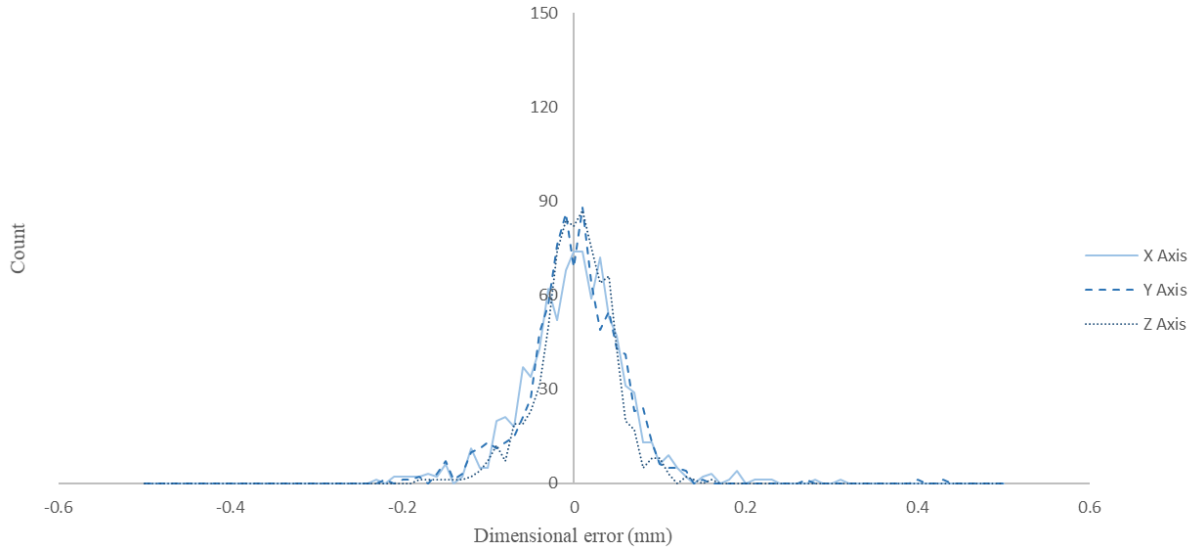

Figure 3.15 *MakerBot Replicator distribution of dimensional error against the average dimension at each measured position for components in the same location*

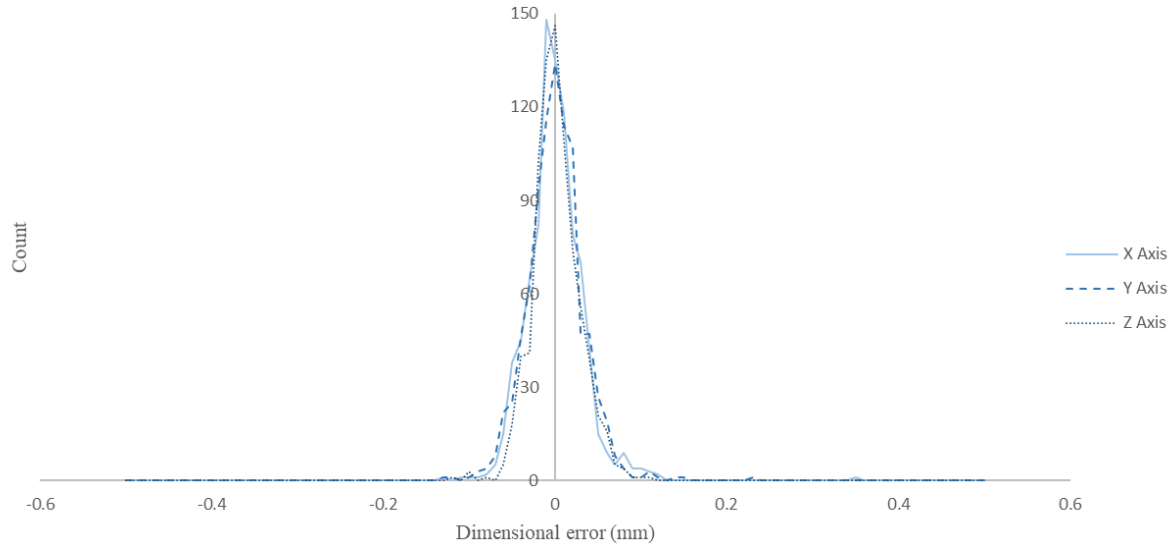

Figure 3.16 *Ultimaker 3 distribution of dimensional error against the average dimension at each measured position for components in the same location*

These error distributions show a clear improvement in precision from the cheapest to the most expensive machine, though this effect is even more significant with this measure of variability. This suggests that there is a greater variation across the build envelope for the cheaper machine than for the more expensive machine. The reduced variability when normalising against position suggests that some of the dimensional error on a component arises from a lack of geometrical calibration (i.e. they are fairly repeatable errors) within the slicer algorithms rather than being inherent to the process itself as a manifestation of poor underlying precision.

Both the IT grade and C_{pk} value have been negatively affected by the presence of accuracy offset errors. As a result, comprehensive error compensation would produce a significant improvement in dimensional performance. However, even if all average dimensions could be adjusted to give perfect average dimensional accuracy (and geometrical accuracy), there would remain the variability demonstrated in Figures 3.14 to 3.16 for each of the machines included in this experimentation. If the accuracy errors were completely removed (i.e. perfect error compensation were applied), the tolerance values fall between 0.1 and 0.4mm, a significant improvement over an uncompensated process (0.3 to 0.6mm). However, if the single compensation values found in the previous subsection were used, there would be little improvement, because the errors have been shown to vary across levels and machines to a large extent and a single adjustment has only a small effect in the largest error cases. Figure 3.9 shows that the Ultimaker may benefit from single adjustments, but that the other two machines would more likely require a linear adjustment ('scale') factor to vary with size. Further research would be required in order to determine whether these findings could be generalised and applied to additional machines, geometries and materials.

In addition, error compensation of ME AM machines is not straightforward because it requires components to be printed and measured with a high degree of accuracy. Even if a user had access to this, any calibration component used would not necessarily produce the correct offsets for a component with different dimensions, component design, parameter settings or material. The most viable approach (and therefore that most often adopted) is a less thorough error compensation amounting to trial and error at the virtual part design stage, though this carries time and cost penalties. The various potential approaches to improving the output of the ME AM process are covered in further detail in Section 7.

3.4. Error Characterisation

The results presented in this section suggest there is error across all three axes on each of the three desktop ME AM machines. Prior to detailed experimentation to understand the nature of these errors, their potential sources and classifications are discussed here.

3.4.1. Sources of error within the ME AM Process

Section 1.3.2 outlined the ME AM process. This showed that there were four main production stages: Virtual part, STL, machine code and component fabrication. The associated sources of error are discussed in greater detail later in Section 7, where existing and potential solutions are also investigated.

At the virtual part production stage, there is theoretically no intrinsic error. However, it may be argued that the inclusion of features that either induce poor performance or outright failure (e.g. very small features, sharp corners) necessarily entail an error in the final component. Where the virtual part is

produced not from first principles but instead from scanned data, this can introduce specific errors [285,286].

The STL conversation requires a virtual component to be approximated to polygonal geometry. For curved geometry this introduces chordal errors. However, CAD software packages allow the selection of STL resolution and provided a suitable level is chosen these errors are small.

A major area of interest in ME AM is the production of G-code. This subject is covered in detail in Section 7, where the options available to minimise errors within the current process framework are discussed. As was noted previously, the G-code provides instructions for toolpath and extrusion. Any error in either of these directly contributes to error in the fabricated component. The assumptions made in this slicing procedure consider the process as predictable and consistent. Therefore whilst adjustments can be made at this stage, they are largely done to correct for errors manifesting in the final stage, component production.

The final stage is the physical production of the component. This requires the nozzle to move in the X, Y and Z directions as indicated by the machine code, and extruded strands to be deposited during each deposition movement. Errors at this stage arise from mismatches between the theoretical geometry as described by the machine code and the physical deposition of material. Using the results presented in this section, it was demonstrated that single axis offsets would produce superior dimensional quality. Final deposition errors such as this can be effectively reduced from direct modification of the machine or through the alteration of the machine code, though in many cases the latter is more straightforward.

3.4.2. ERROR CLASSIFICATION

Macro inaccuracies may be considered as arising from errors in the outer perimeter [287,288,289]. As such, dimensional accuracy and precision error observed for a final component can be reduced to these same errors present in the outermost deposition. In order for this perimeter to differ from the theoretical geometry, either of the deposited road width or toolpath must be the source of the error. Therefore, it can be presented that;

$$Error_{macro} = fn(Error_{position}, Error_{extrusion})$$

The next three experimental sections explore these two sources in turn. First, the positional performance of the machine without the extrusion process is investigated. Next, extrusion errors under steady state print conditions and around corners in the XY plane are quantified.

4. MACHINE POSITIONAL PERFORMANCE

In the previous section it was posited that the measured error in a printed component can be broadly classified as either positional and extrusion error. This section investigates the first of these, measuring the positional performance of two low-cost commercially available ME AM machines.

The vast majority of machines have three axes of movement and are usually based around a Cartesian system [17,290]. The ME AM process effectively combines a small-scale extrusion process with movements in three dimensions. Generating tool motion in this way is of course not limited to ME AM but is also required in other processes such as machining operations, laser etching, cutting and other AM technologies. As such, many robust machine design principles have already been developed in these contexts.

ME AM machines typically vary nozzle position through movement of the X, Y and Z axes independently, though as noted later in Section 7 some alternative designs have been developed. Whilst there is a large body of literature that covers the physical production of ME AM components, there has been little attention given to the decoupling of the motion performance from the overall performance including the extrusion process. Whitney and Moultrie [17] showed that machine motion design has shown little evolution in the 25 years since ME AM machines were first introduced. It is therefore often assumed that the machine motion element has reached a performance plateau, and that research efforts are better focused elsewhere.

Nevertheless, there have been some studies that have specifically addressed machine motion performance. Kun [291] reverse engineered a low-cost desktop ME AM machine. In this, deficiencies identified in a base machine were addressed with proposed new designs. However, this was largely a qualitative study, and the superior performance of the updated design was not fully demonstrated. Cunico and de Carvalho [292,293] investigated the optimisation of the ME AM positioning system using an analytical approach in two separate studies. They described a theoretical model of machine motion to provide an estimation of machine errors and suggested improvements. Belt stiffness, linear bearing tolerances and ball screw accuracies were analysed and found to have a worst case error of approximately 0.07mm. They determined that the largest contributory factors for the X and Y axes were the pulley accuracy, whilst for the Z axis the lead screw was the dominant factor. Through the use of higher quality components and the replacement of a linear bearing with a linear guide, this error was estimated to be reduced by approximately 0.02mm. They also investigated the relationship between the increased cost of higher quality components and dimensional performance. Weiss et al. [294] noted that the presence of belt slop, motor accuracy errors and chassis dynamics mean that large error terms are seen in practice, at least an order of magnitude higher than the resolutions quoted by manufactures such as those included in Table 3.1. Feuerbach at al. [295] determined the performance of three desktop machines. For each printer, they measured the accuracy of individual axes through

the use of a dial gauge at a low speed of 4mms^{-1}. They concluded that whilst belt drives allow faster movement than lead screws, this is at the expense of dimensional accuracy and precision performance. Errors ranged from negligible to more than 0.1mm.

Kłodowski [290] developed a 4-link planar motion system to enable nozzle motion. This was modelled and found to give similar performance to the traditional Cartesian approach although it required more complex control. During their simulations they assumed a best case with nominal stepper motor increments of 0.9^{o} and the use of micro-stepping. Given their machine geometry, this gave theoretical accuracy of approximately 0.02mm, whilst they calculated that traditional Cartesian systems are capable of approximately 0.01mm. Kearney et al. [296] explored kinematic errors of a desktop ME AM machine. They applied methodologies associated with high-precision CNC machining systems such as kinematic error modelling and compensation together with standardised test methods. Applying this approach to an *Ultimaker* machine, they reduced circularity errors by 58% and squareness errors by 90%.

Bochmann et al. [69] stated that ME AM machines have 21 separate error components arising from their three axes. These include scale errors, straightness errors, squareness error and roll, pitch and yaw. They conducted columnar test prints to determine each of these, though in doing so the presented errors represented the combination of machine movement and printing conditions. Similarly, Song et al. [51] printed small cross-shaped components across the build envelope to measure error prior to error compensation. However, this also failed to delineate the machine position performance from the extrusion and deposition aspects but does give an accurate result for the two combined.

Heras et al. [297] designed a plate levelling system to reduce first layer deposition error. This was achieved via the use of an inductive sensor to measure the nozzle to bed distance and automatically adjust to produce a flat build plate. This is a similar approach to the popular *BLTouch* hardware which uses a microswitch to measure height but otherwise operates along the same principles.

Most filament manufacturers provide a stated accuracy and precision level. This is typically ±0.05mm or lower, as is shown in the summary later in Section 4.2.1. The only experimental results of this available were presented by Lee et al. [298], who measured a 3mm ABS filament 30 times and found a standard deviation of 0.014mm and Marchewka and Laska [299], who demonstrated an error of ±0.04mm across 100 measurements. Santana et al. [300] investigated the lengths of filament extruded, and found the actual lengths were smaller than the theoretical values owing to slippage and scale error and that error was increased at higher print speeds.

In summary, extant studies suggest a relatively low theoretical positional error of approximately 0.01-0.02mm. However, very few studies have experimentally investigated this in isolation or determined

the actual level of accuracy. This section therefore provides detailed experimentation of machine positional errors as realised on current ME AM desktop machines.

4.1. METHODOLOGY

The G-code executed by Cartesian ME AM machines include four axes. These are the three movement axes of X, Y and Z and an additional extrusion axis, denoted by *E* commands. To extrude material through the nozzle, solid filament is driven into the top of the liquefier and thus acts as the piston. The *E* command is therefore treated exactly as the X, Y and Z commands, whereby each machine code line denotes a movement (in mm) and a speed. In practice, the movement speed is applied to the X, Y and Z movement and the extrusion movement is adjusted at the machine firmware level to theoretically match this travel. Any error in this extrusion distance therefore directly translates to a volumetric extrusion error through the nozzle and results in filament-level dimensional inaccuracies. Similarly, any deviations in filament cross-sectional area (most easily characterised by the filament diameter, assuming a circular cross-section) will lead to over- or under-extrusion. The first stage of experimentation therefore focuses on both extrusion mechanism filament drive length errors and filament diameter error.

The second area of positional error is that of the X, Y and Z movement axes. Different desktop ME AM machines achieve this movement utilising a variety of mechanisms which may potentially affect the dimensional accuracy and precision that is achieved. This experimentation involved taking multiple direct positional measurements in the three axes via various movement paths in order to understand the nature of positional errors. Combined with the extrusion errors in the first experimental approach, this enables a full determination of the accuracy and precision of current desktop ME AM machines prior to the consideration of the physical extrusion process and component fabrication itself, which will be dealt with in subsequent sections.

4.1.1. MACHINE DESIGN

As was noted previously, different desktop ME AM machines achieve their XYZ movements via different mechanisms. Evans [301] stated that there are three fundamental aspects of an ME AM system. These are machine architecture, electronic hardware and software. The overall performance of a machine is therefore the product of these three aspects. Whitney [12] presented three main areas of machine design consideration as being the build platform, material processing and relative motion. Elshennawy [302] developed a simple way of describing machine motion (i.e. architecture, as defined by Evans). In this, the letter *F* designates a fixed machine foundation and any letters to the left indicates workpiece motion and to the right, tool/probe motion. A completely fixed workpiece would therefore be described as *FXYZ*. There are two main approaches to the filament drive mechanisms. First, the *direct drive* mechanism places the drive motor directly above the liquefier as part of the gantry assembly. Second, a *Bowden* arrangement places the drive motor away from the gantry and

feeds the liquefier via a guide tube. This reduces gantry mass and therefore theoretically allows for improved accelerations and speeds, though performance can be poor for elastic materials given the increased feed distance.

In this experimentation, desktop ME AM machines with two separate movement and extrusion mechanisms were selected. The first machine was an ANet A8, which uses a *direct drive* and *YFXZ* motion, though this was not the exact machine used in the previous experimentation due to a lack of access to the original following a machine failure. The second machine was a Creality Ender-5 Pro. This machine instead used a *Bowden drive* and *ZFXY* motion.

4.1.2. EXPERIMENTAL DESIGN

The first element of experimentation was to determine the accuracy and precision of the extrusion mechanism of desktop ME AM machines. The extrusion mechanism was isolated from the rest of the machine. Solid filament was fed through the extrusion mechanism using the inbuilt *move axis* functionality on each machine. The filament was marked with a fine marker pen at the exit of the filament drive mechanism after 50mm of incremental extrusion, from 0 to 500mm in total extruded length. Each of these lengths was then measured and recorded. This process was repeated three times on the two machines.

To determine the accuracy and precision of the filament feedstock, 50 measurements were taken using a pair of digital Vernier calipers along a randomised one meter length of filaments of different colours, materials, manufacturers and nominal diameters. In addition to this experimental data, a range of manufacturer's claimed tolerances were collected for comparison.

X, Y and Z axis positional data was collected via an analogue dial indicator, which had a stated accuracy of ±0.01mm. This was verified through the use of gauge blocks, which demonstrated an error of less than 0.02mm across the full 25mm of travel. For the X and Y axes, this was mounted to the print bed of the ANet and Creality machines using a custom mount fixed to the bed with adhesive tape. The tip of the dial indicator was aligned with the centre of the print bed (i.e. at X, Y=110mm for the ANet and X, Y=117.5mm for the Creality). The liquefier and hot end were replaced with an aluminium fixture with a 1mm machined cylindrical feature (see Figure 4.1). Similarly, for the Z axis measurements the usual gantry equipment was replaced with the dial gauge, and an identical 1mm cylindrical feature placed on the print bed at the central location.

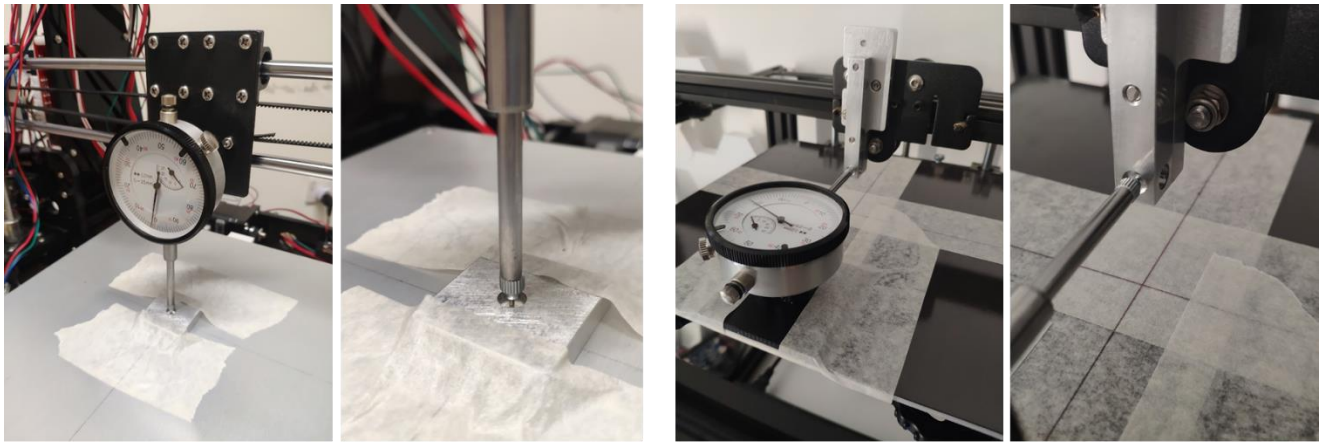

Figure 4.1 *XYZ axes positional error experimental setup; (a) ANet A8 Z axis, (b) Creality Ender-5 Pro Y axis*

Prior to collecting measurements, the full range of the dial indicator was checked to ensure that the tip maintained contact with the top of the cylindrical feature. Given the range of the dial indicator is 25mm, this produces a maximum potential misalignment error of 0.005mm in the extreme case of the tip moving from one edge of the 1mm cylinder to the other during the 25mm of movement. Whilst the initial test movement of 25mm ensured the tip remained in contact with the top surface of the cylindrical piece, and deviation from this during experimental work would quickly be characterised by increased length measurements and therefore would trigger a rerun of that experiment.

In order to record these two error sources and collect precision data, four sets of measurements were taken. For the purposes of this experimentation, the positive direction was considered to be left-to-right for the X axis, rear-to-front for the Y axis and low-to-high for the Z axis.

Schematic diagrams of the four experimental measurements are shown in Figure 4.2. G-code was produced using a bespoke G-code generator produced in *Microsoft Excel*. All movements were at $3600 mm min^{-1}$ and a pause time of 3 seconds at each position was included to enable each position value to be recorded. Experiment (a) shows the main repeatability experiment, consisting of 125 0.2mm movements from 0 to 25mm. Prior to the first measurement, a ‘prime’ movement of 0.2mm in the first (positive) measurement direction was undertaken to ensure all experiments began under the same conditions. This enables both a repeatability of each step (of nominal value 0.2mm) and repeatability of position reached (e.g. after 100 steps, a nominal travel distance of 20mm). This run was repeated three times, giving a total of 850 measurements for each axis on each machine. Backlash measurements are also possible from this experiment by considering the initial 0.2mm movement in either direction. Experiment (b) targets backlash behaviour specifically, moving a distance of 0.2mm in the X, Y or Z axis, switching between the positive and negative direction for each movement. This was repeated five times in each experimental run (i.e. each run contained ten moves) and three repeats were conducted for a total of 30 measurements for each machine-axis. Experiment (c) combines

backlash and scale error experimentation, taking measurements over movements of 5mm, 10mm, 15mm, 20mm and 25mm. After each position is reached there was a return to the origin, such that every move contains both a backlash and scale error in both directions. Each run contained three repeats and the runs were replicated three times for a total of 90 measurements for each axis. Finally, experiment (c) was modified in (d) to add in a backlash-specific move before each major movement. This enabled a verification of (c) by separating the backlash movement from the scale movement. This again consisted of 90 measurements per axis.

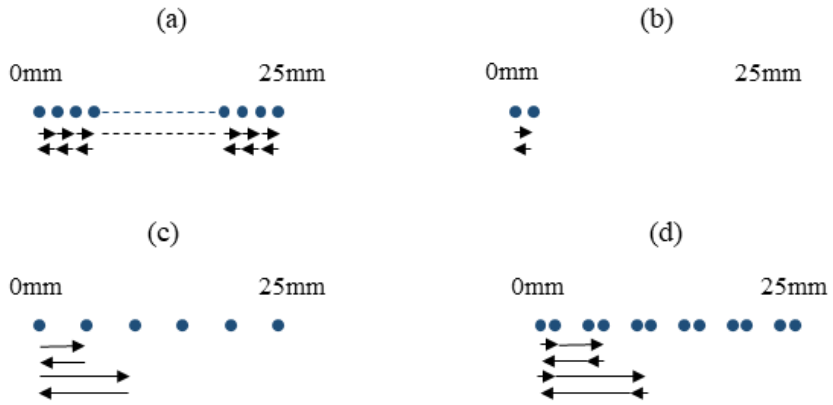

Figure 4.2 *XYZ axes positional error experiments*

4.2. RESULTS

This section contains the experimental data for extrusion lengths, filament diameters and XYZ position error. The full data is available in Section 12.3 in the Appendix.

4.2.1. EXTRUSION MECHANISM

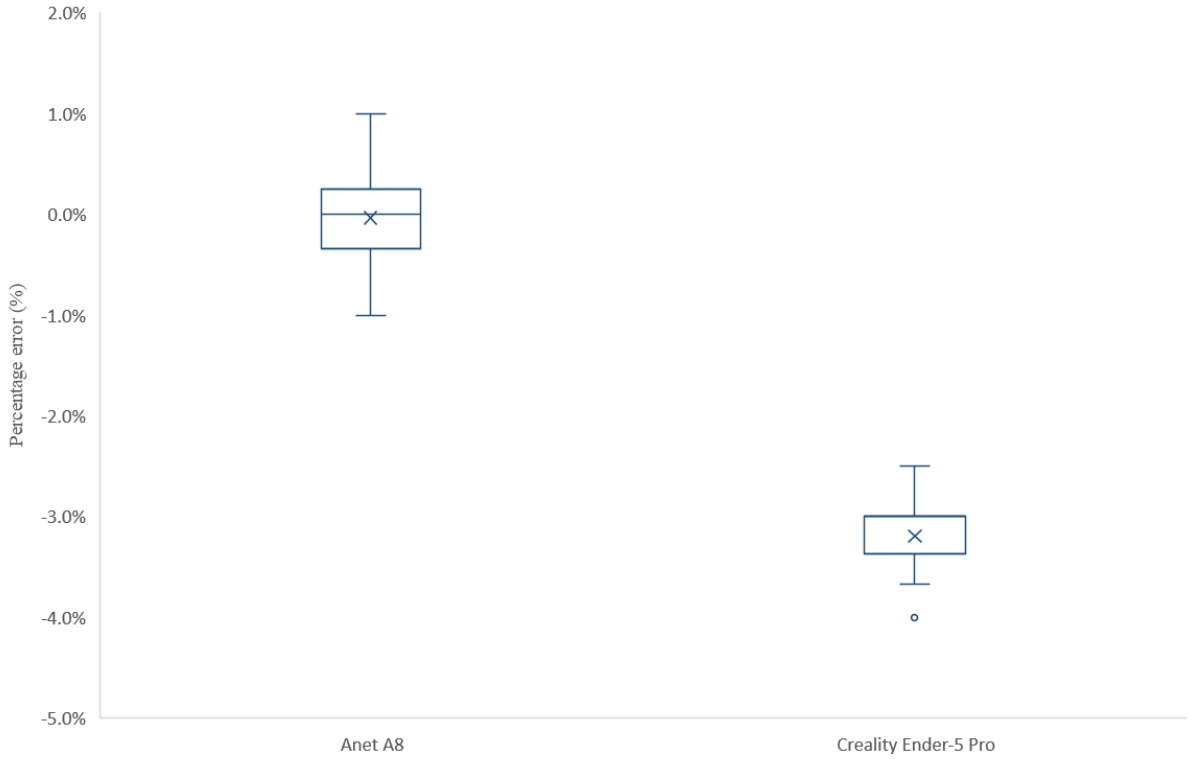

Figure 4.3 *Extrusion mechanism error*

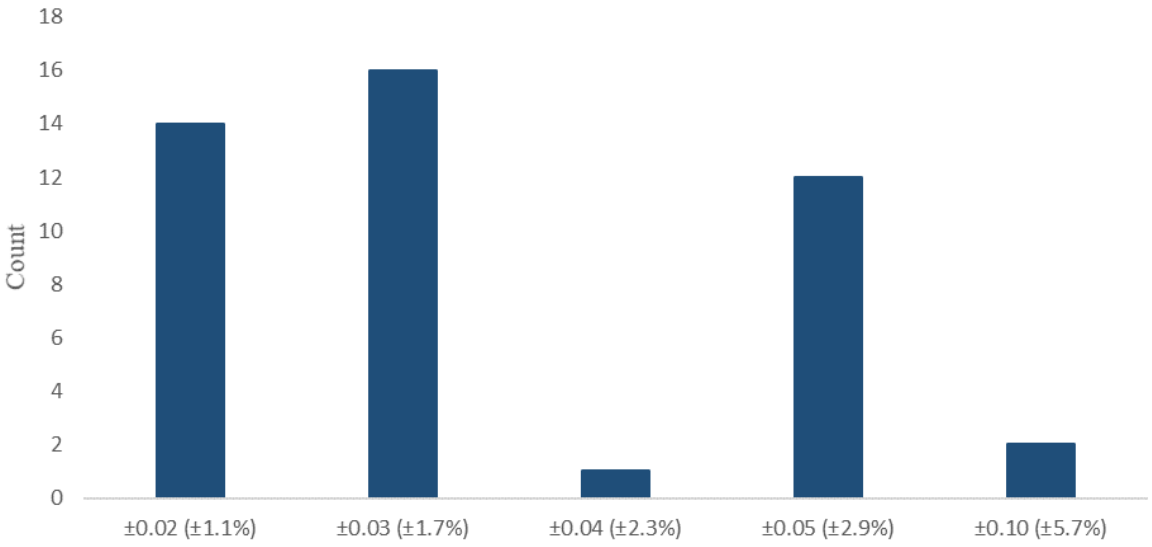

Figure 4.4 *Manufacturer filament accuracy and precision specifications*

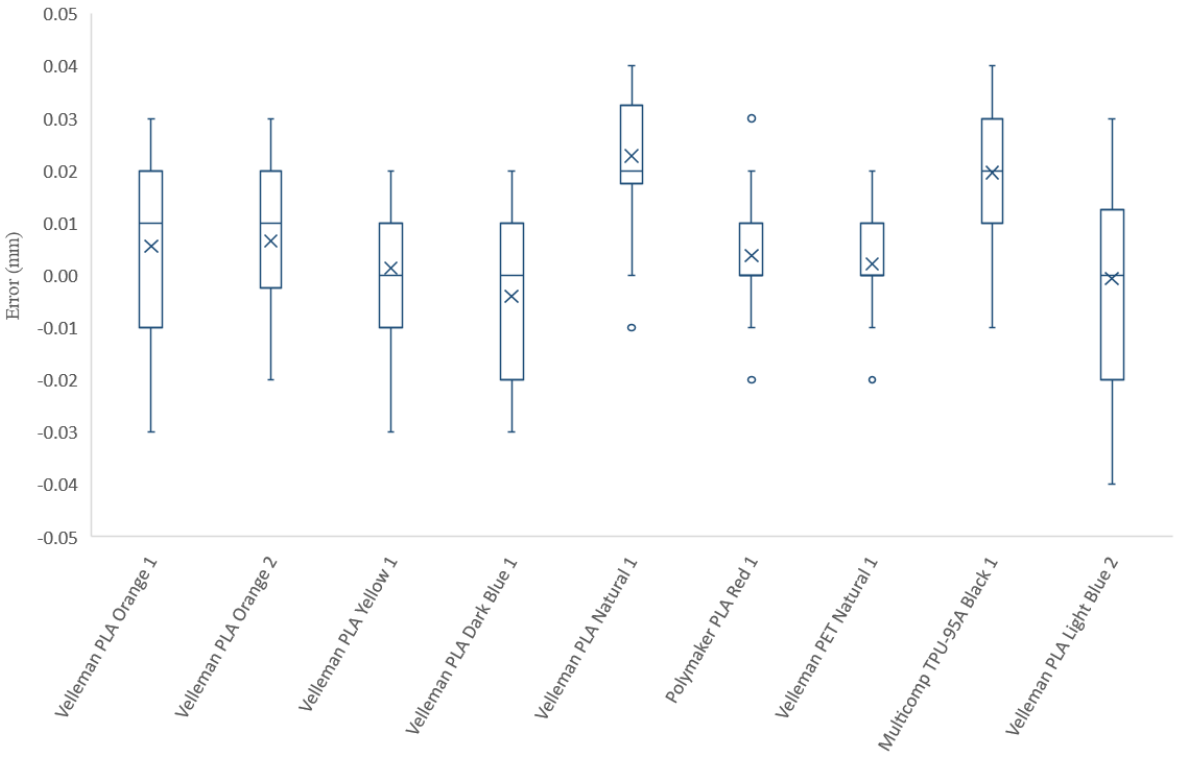

Figure 4.5 *Measured filament diameter dimensional errors*

4.2.2. POSITIONAL PERFORMANCE

4.2.2.1. REPEATABILITY EXPERIMENTATION

This repeatability experimentation consists of three sets of measurements.

In Figures 4.6 and 4.9, the error of each individual 0.2mm step (i.e. the difference between the measured value and the nominal 0.2mm) is plotted.

In Figures 4.7 and 4.10, the variability of each position reached against the other instances of that nominal position is recorded. For instance, in each experimental run in the positive X direction (i.e. left to right) the position of 15mm from the origin is reached 3 times. These figures display the difference between the second two readings and the first, for each of the 250 positions (125 in the positive direction, and 125 in the negative). This is highly representative of the ME AM production process, as when building layers on top of one another the same position is commonly required multiple times to form a vertical wall.

Figures 4.8 and 4.11 shows data from this same approach, but for the 5mm increments between 0 and 25mm from experiment (d) and therefore has a reduced sample size.

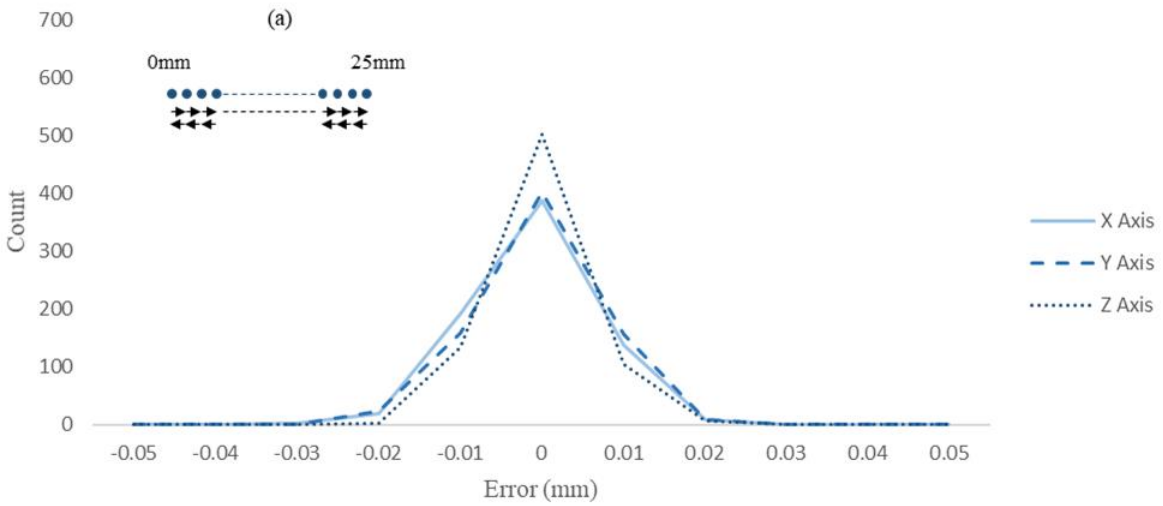

Figure 4.6 *ANet A8 0.2mm increment error distribution*

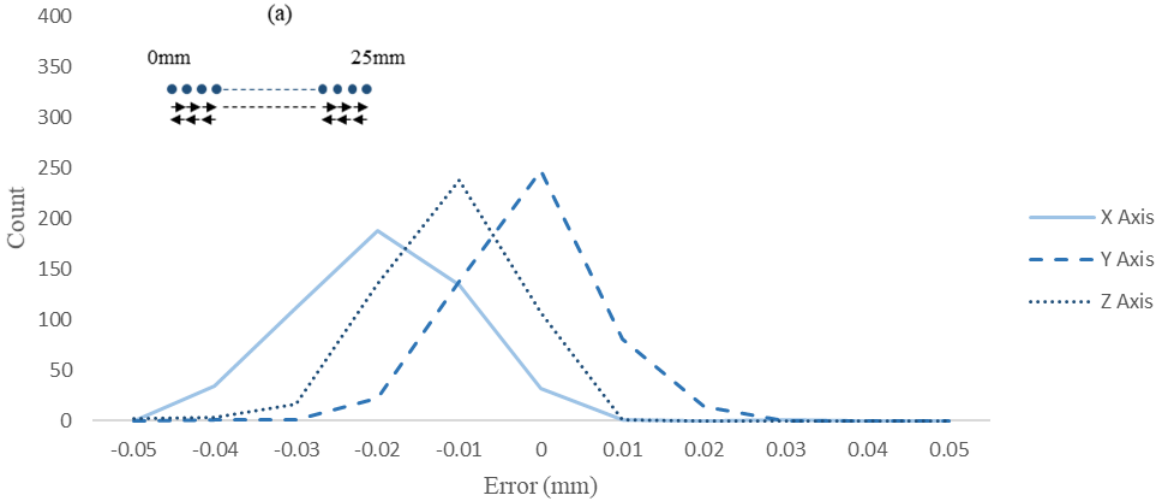

Figure 4.7 *ANet A8 0.2mm positional error distribution*

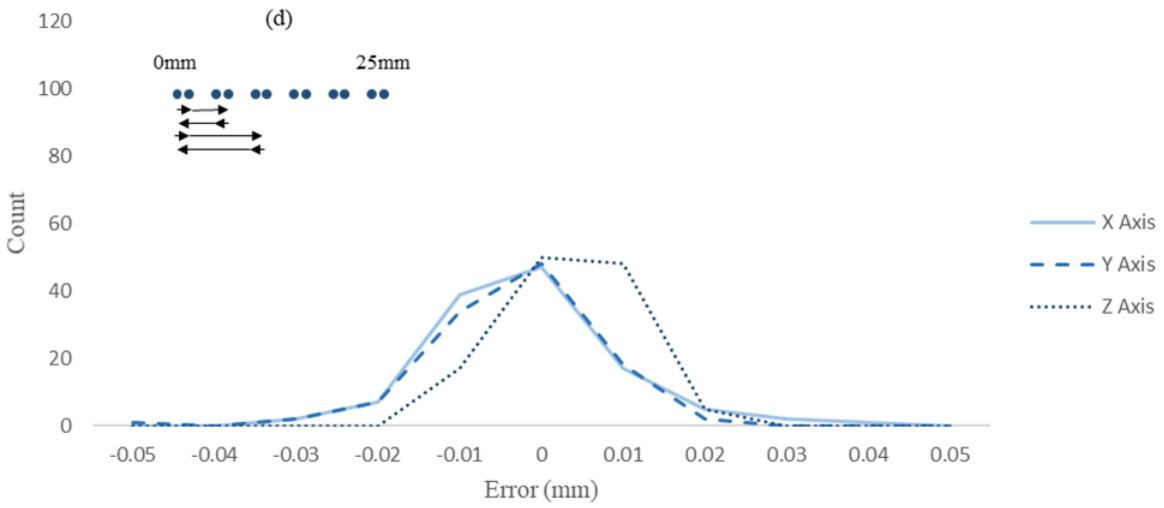

Figure 4.8 *ANet A8 0-25mm positional error distribution*

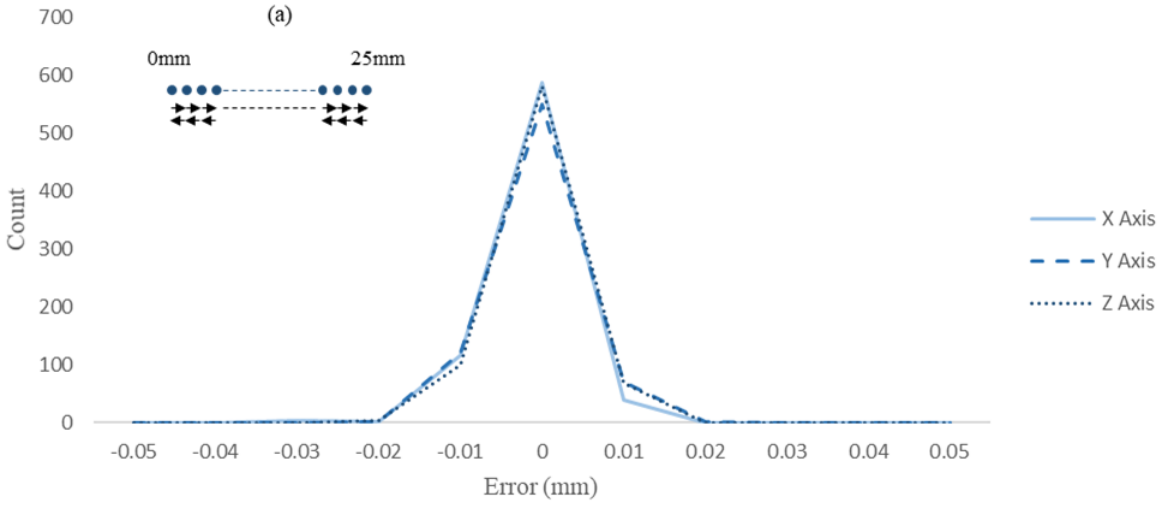

Figure 4.9 *Creality Ender-5 Pro 0.2mm increment error distribution*

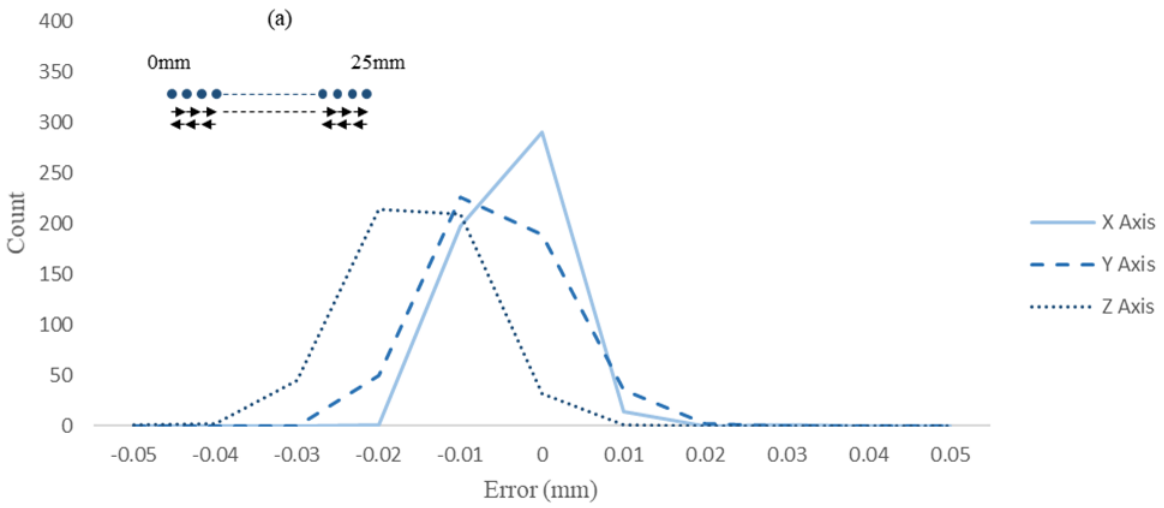

Figure 4.10 *Creality Ender-5 Pro 0.2mm positional error distribution*

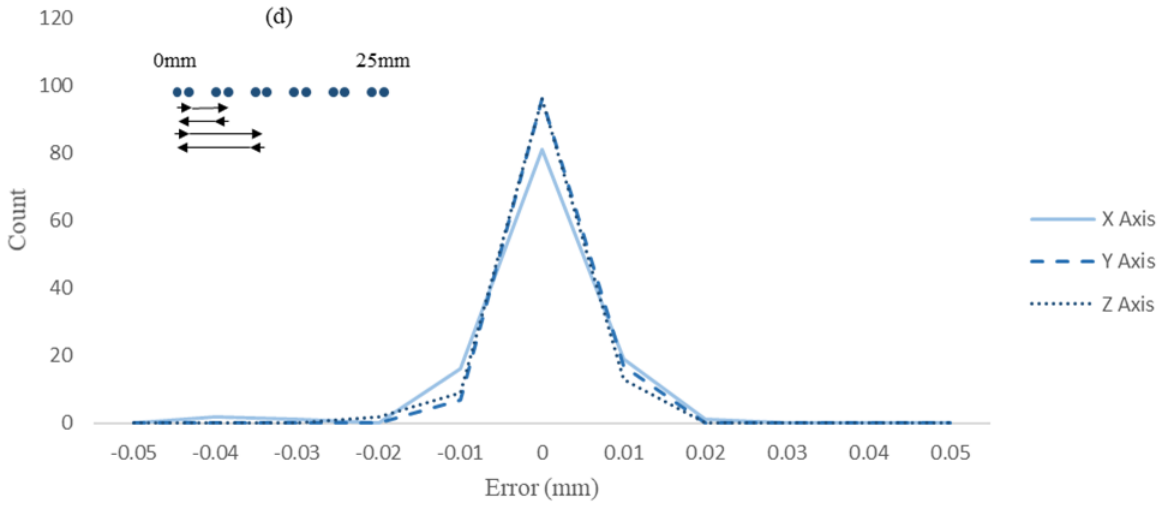

Figure 4.11 *Creality Ender-5 Pro 0-25mm positional error distribution*

4.2.2.1. POSITIONAL ACCURACY EXPERIMENTATION

Figures 4.12 and 4.13 show the results from experiment (c), where each movement contains both backlash and scale errors.

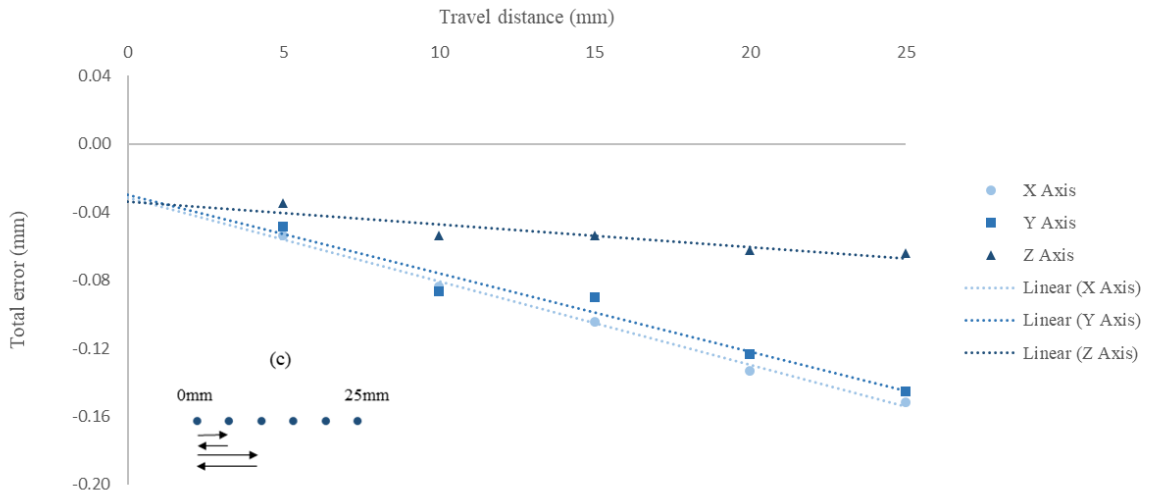

Figure 4.12 *ANet A8 measured error on distance between points for X, Y and Z axes*

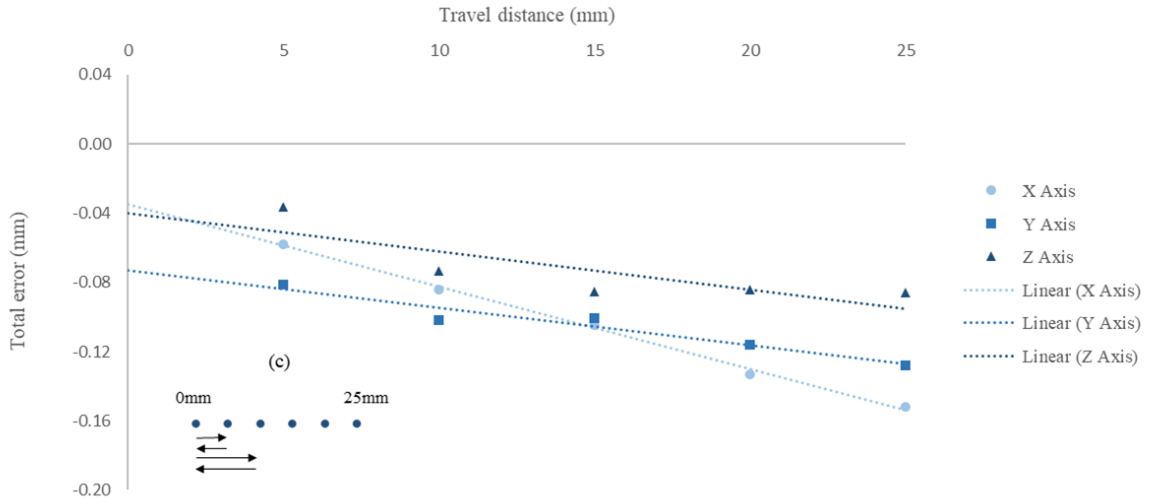

Figure 4.13 *Creality Ender-5 Pro measured error on distance between points for X, Y and Z axes*

Figures 4.14 and 4.15 show the results from experiment (d), which separates the backlash error from the scale error, with only the scale errors shown in these figures.

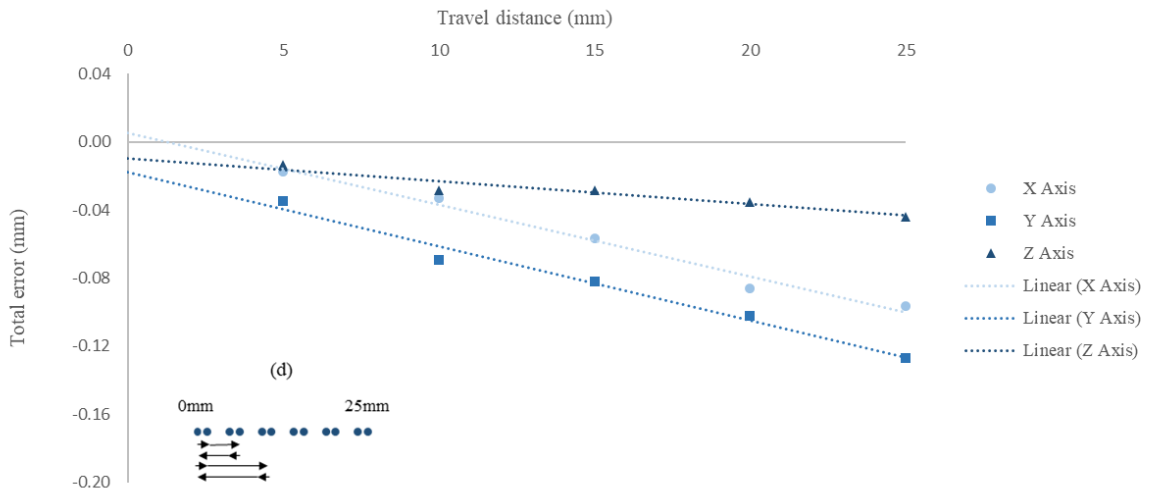

Figure 4.14 *ANet A8 distance between points with backlash removal error distribution*

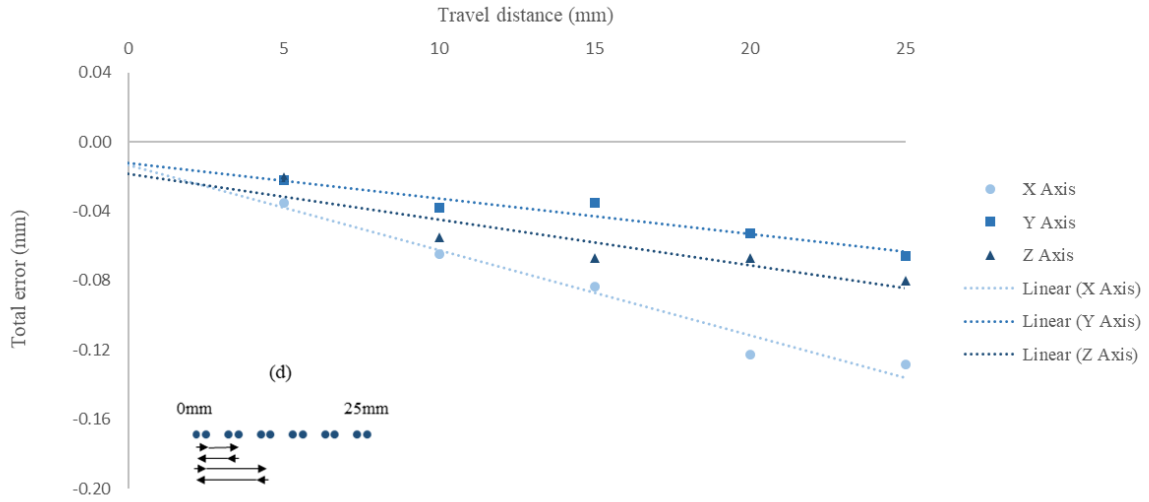

Figure 4.15 *Creality Ender-5 Pro distance between points with backlash removal error distribution*

4.2.2.1. BACKLASH

Figures 4.16 and 4.17 show backlash measurements from the X, Y and Z axes for the Anet A8 and Creality Ender-5 Pro ME AM machines. Eight experimental measurements for each axis are shown; five in the positive and three in the negative direction. Explanations of each of these measurements are given in Table 4.1. The solid bar on each figure represents the mean across these.

Number	Experiment	Measurement direction	Explanation
1	(a)	Positive	Difference between first 0.2mm movement in positive direction (i.e. 0mm to 0.2mm) following prime 0.2mm movement and other two positive initial movements representing a direction change
2	(b)	Positive	Average of backlash experiment (b) in the positive direction
3	(c)	Positive	As **1** for experiment (c)
4	(c)	Positive	Implied backlash error from linear line of best fit using 5mm increment values in experiment (c)
5	(d)	Positive	Average of positive backlash (0.2mm movements) errors in experiment (d)
6	(b)	Negative	As **2** in the negative direction
7	(c)	Negative	As **4** in the negative direction
8	(d)	Negative	As **5** in the negative direction

Table 4.1 *Backlash error measurements*

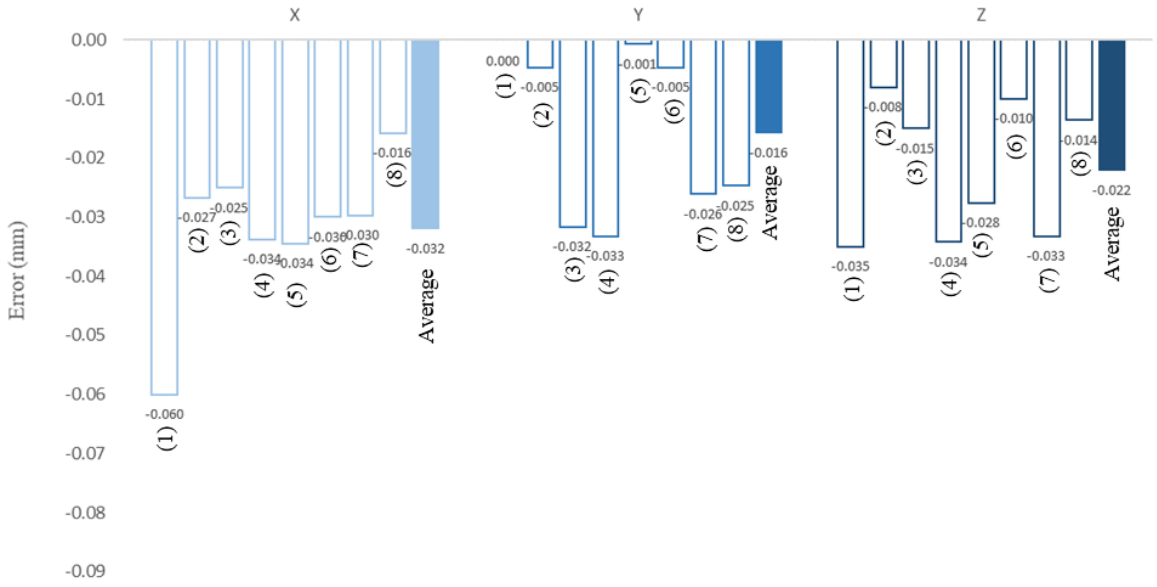

Figure 4.16 *ANet A8 backlash error*

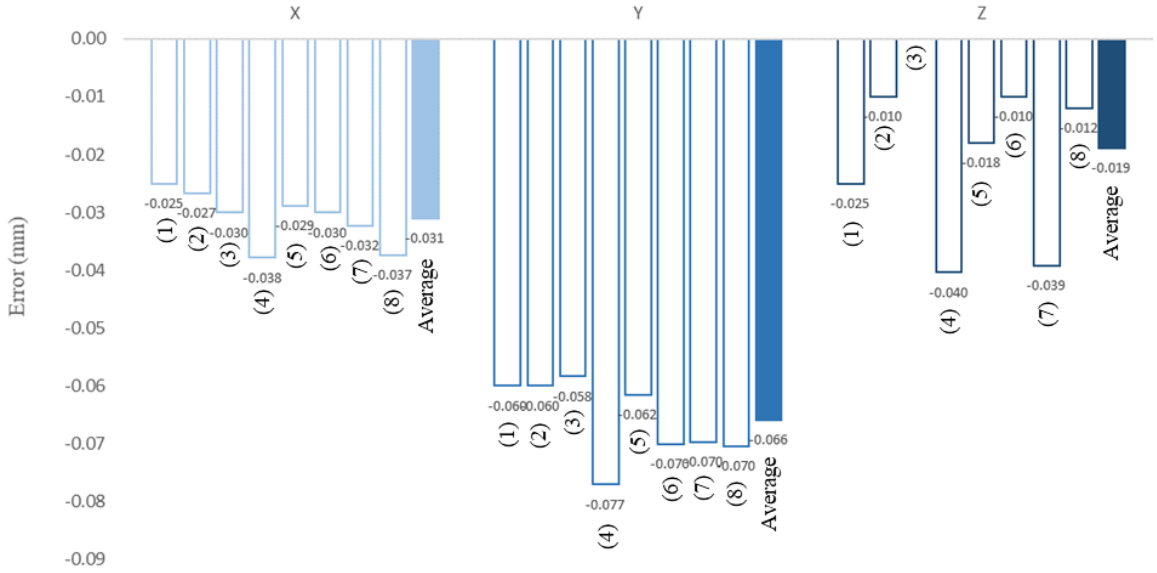

Figure 4.17 *Creality Ender-5 Pro backlash error distribution*

4.2.2.1. SCALE ERROR

Table 4.2 shows the six scale measurements collected across the four experiments conducted. In all cases, the measurement represents an error per mm travelled. The solid bar on each figure again represents the mean.

Number(	Experiment	Measurement direction	Explanation
1	(a)	Positive	Average error in the positive direction between the origin (0mm) and measured locations at 4mm increments (i.e. 6 measurements 4 to 24mm, each consisting of 20 0.2mm steps)
2	(c)	Positive	Implied scale error from linear line of best fit using 5mm increment values in experiment (c)
3	(d)	Positive	Average of positive movements in isolation from 0.2mm backlash movements (e.g. movement from 0.2 to 5.2mm)
4	(a)	Negative	As **1** for the negative direction
5	(c)	Negative	As **2** for the negative direction
6	(d)	Negative	As **3** for the negative direction

Table 4.2 *Scale error measurements*

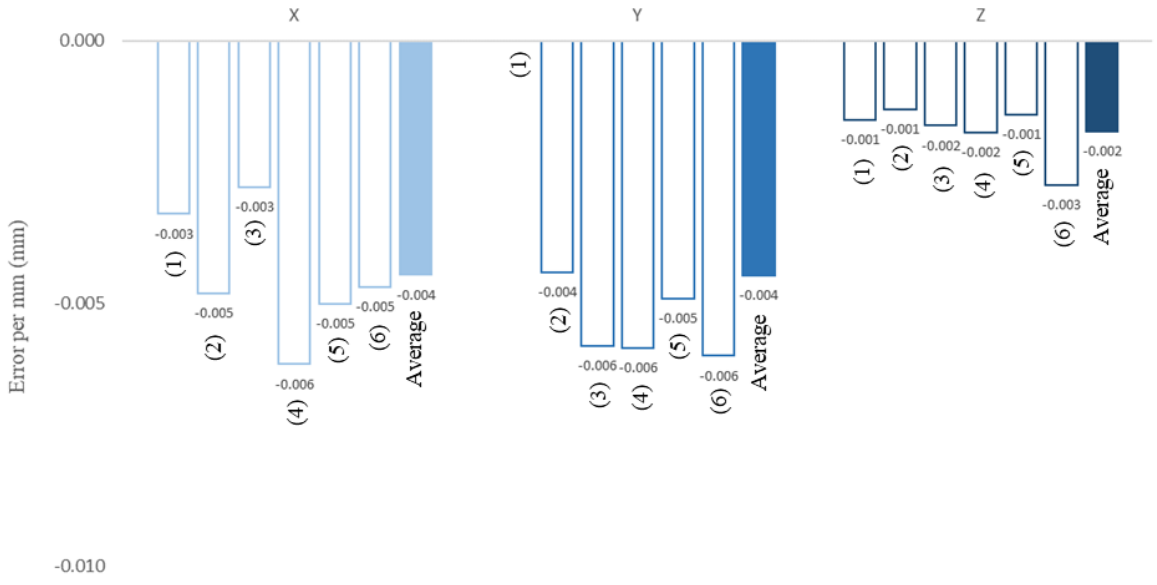

Figure 4.18 *ANet A8 scale error*

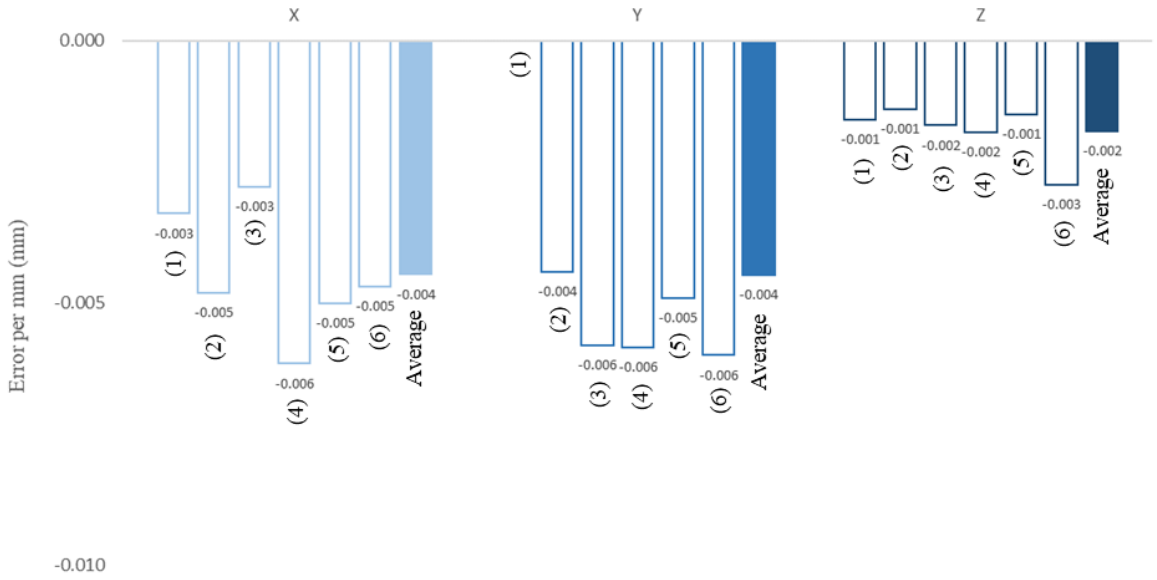

Figure 4.19 *Creality Ender-5 Pro scale error*

4.3. DISCUSSION

4.3.1. EXTRUSION MECHANISM

Extrusion experimentation considered filament dimension errors and errors in the length of filament fed into the liquefier by the drive stepper motor. Figure 4.3 demonstrates that there is very little average error for the ANet, but an under-extrusion of approximately 3% on average for the Creality. The error was observed to be proportional to the extruded length suggesting a consistent scale error. This most likely arises from a mismatch against the software distance calibration from a smaller drive wheel than the software assumes. Some additional degree of filament slippage during extrusion may be present when a pressure component is added pushing against the filament motion, though not in this experimentation with a cold extrude and no nozzle assembly. The precision of the extrusion length is slightly lower for the ANet at approximately ±1% versus ±0.75% for the Creality.

Measured filament diameter errors were typically found to be ±0.02mm for all material types, manufacturer, colour and nominal diameter, as shown in Figure 4.5. The exception was a Velleman light blue PLA filament, though this had a larger nominal diameter of 2.85 making the slight increase lower in percentage terms. These results are in line with manufacturer claimed accuracy and precision levels, which were most commonly ±0.02mm or ±0.03mm as displayed in Figure 4.4.

The combination of these errors gives a volumetric extrusion error. Assuming the conservation of material volume during the deposition process, this therefore directly translates to deposited strand width error. This suggests that an error of no greater than approximately 3%, or 0.012mm on a nominal road width of 0.4mm, would be observed from the extrusion mechanism and filament alone.

4.3.2. POSITIONAL PERFORMANCE

It is predicted that there are two main sources of error for X, Y and Z movement. First is a backlash error, associated with direction changes on any given axis. This arises naturally from play within the movement mechanism, either between the lead screw thread and the threaded piece in the case of both Z axis movement mechanisms, or in reversal of tensile direction and play between the toothed belt and gear as is the case with the X and Y movement mechanisms on both machines The second is a scale error, which is expected to be proportional to the distance travelled. Like the scale error measured in the extrusion distance experimentation discussed above, this arises from dimensional errors in the drive gears or pitch of the lead screws. Both scale and backlash error, in addition to the repeatability of movements (i.e. a precision assessment) are of significant benefit in the context of component production and are therefore worth calibrating for.

4.3.2.1. REPEATABILITY

It is important to note the limitation of measurement resolution. Each 0.2mm step was recorded to the nearest 0.01mm, with a manual reading of the analogue dial. As a result, modest scale errors of a few percent are not properly accounted for in this experimental design. However, it can be accounted for elsewhere and through multiple 0.2mm steps in sequence. In addition, this experimentation does reveal any significant step deviations arising from more serious movement errors.

Repeatability of the 0.2mm increments is slightly superior for the Creality, though is less than 0.02mm for both machines. All three axes are very similar for the Creality, though the Z axis exhibits better repeatability on the ANet. This is likely due to the poorer quality belt mechanisms used to the drive the X and Y axes on the ANet versus the Creality.

Considering repeatability of absolute position from 0 to 25mm, the ANet again exhibits worse repeatability than the Creality. For the ANet, the X axis shows lower repeatability than either the Y or Z axes, as well as an offset mean suggesting greater scale error. This is likely due to higher belt tension in the Y axis, where an additional tensioner was present in the mounting solution. The X axis showed better repeatability on the Creality than for the other two axes. The lower repeatability of the Z axis may arise from the machine design, where the print bed is cantilevered from the rear only. The X axis moves on a rail, which itself moves for Y axis motion. The gantry mounting solution is much wider in the X direction than the Y, as shown in Figure 4.20.

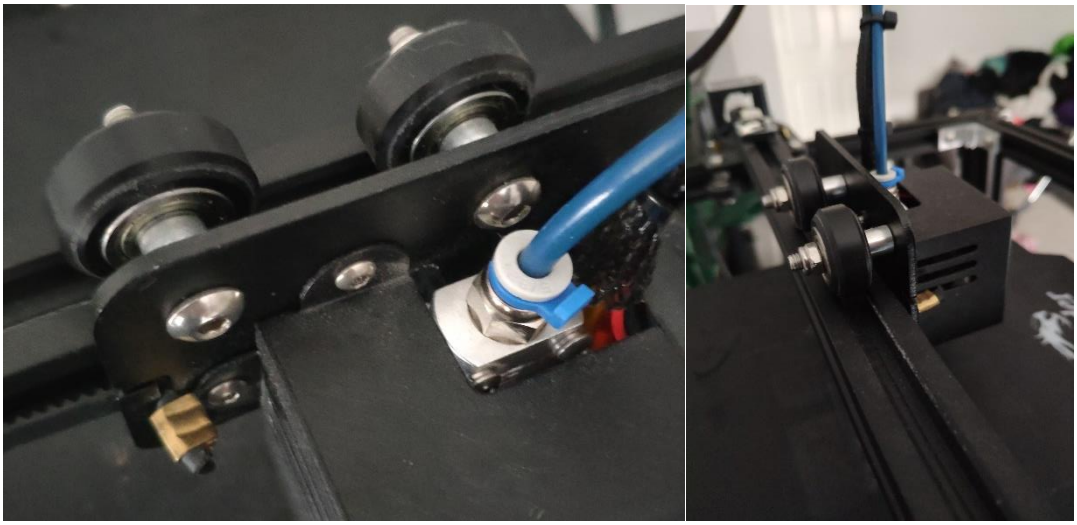

Figure 4.20 *Creality gantry mounting mechanism*

This arrangement allows the entire nozzle assembly to rock slightly in the Y direction but not the X, suggesting greater repeatability. The guide wheels can be adjusted as part of this design, but have been left as assembled by the manufacturer for this experimentation.

The final repeatability experimentation shows the performance of each machine in 5mm incremental movements. This shows that the ANet performs significantly worse than the Creality for all three axes, although almost all measurements fall within 0.03mm of the nominal dimension. It must be noted that these errors are relative to previous positions rather than the nominal value and as such, demonstrate precision only and not accuracy.

4.3.2.1. BACKLASH

Measures of backlash error were possible from all four experimental approaches. Figures 4.16 and 4.17 show these for the ANet and Creality respectively. This demonstrates a maximum error of 0.077mm for the Y axis on the Creality. The X axis displays a larger error than the Y or Z axes on the ANet. This is likely because of the addition of the tensioner on the Y axis compared to the X axis, and the superior quality lead screw mechanism on the Z axis. For the Creality, the Y axis is worse than the X and Z axes. As was discussed in the previous subsection, this is likely due to the gantry mounting setup, where there is greater play in the Y direction than the X. Again, the addition of a lead screw for the Z axis gives improved backlash error. This suggests that the biggest immediate improvements on either machine would be to tension the belt on the X axis on the ANet and tighten the gantry for the Y axis on the Creality.

4.3.2.2. SCALE

Scale errors are presented for movements of 5 to 25mm with and without an initial movement to reduce the backlash impact. In both cases, a linear line of best fit can be generated as shown in Figures 4.12 to 4.15. This shows that all three axes on both machines exhibit a clear linear scale error,

where all movements are slightly smaller than the nominal dimension. The Z axis has a lower error for the ANet, likely due to the superior quality of the lead screw mechanism used to move this axis. The Y and Z axes are both better than the X axis on the Creality. This suggests a simple calibration error in the X axis since the stepper motor and belt are both identical to the Y axis arrangement.

Three scale errors are presented for the positive and negative directions in each of the three axes in Figures 4.18 and 4.19. This also clearly demonstrates a lower Z scale error for the ANet than the X and Y axes, and the Y and Z axes compared to the X on the Creality. Scale errors are shown to be consistent in both directions for every axis, with little difference between the errors determined by the three separate experimental approaches. These are demonstrated to be between 0.001 and 0.006 mm per mm of travel. This suggests that on the largest component direction from the previous section, an error of up to 0.18mm smaller than nominal.

4.3.3. COMPONENT ACCURACY IMPLICATIONS

The positional errors discussed above will have an impact on the accuracy and precision of components produced on an ME AM machine. These errors can be categorised as arising from the extrusion mechanism (extrusion length and filament diameter) and from backlash and scale errors of the XYZ positioning system. Clearly, the X, Y and Z backlash and scale positional errors directly translate to errors in their respective component dimensions. However, the extrusion error must be converted to deposited filament errors in terms of filament X, Y and Z dimensions. The next experimental section explores filament morphology in greater detail. However, for the purposes of this experimentation the extrusion length and filament diameter errors are combined to give a volumetric error assuming conservation of volume, steady material flow and no filament slippage. It is assumed that material volumetric errors do not alter the Z height of the deposited filament, which is restrained by the nozzle itself. Therefore, only the filament width is altered and as a result only the X or Y dimension, depending on the direction of fabrication, are affected. Given this, a 1% error in extrusion volume leads directly to a 1% error in the deposited filament road width and so the X or Y strand dimension depending on the direction of deposition.

Maximum, minimum, mean and the 95^{th} percentile distributions have been calculated for a nominal 15mm square-cross-sectional component on the ANet A8 and Creality Ender-5 Pro ME AM machines. These errors are shown below in Figure 4.21.

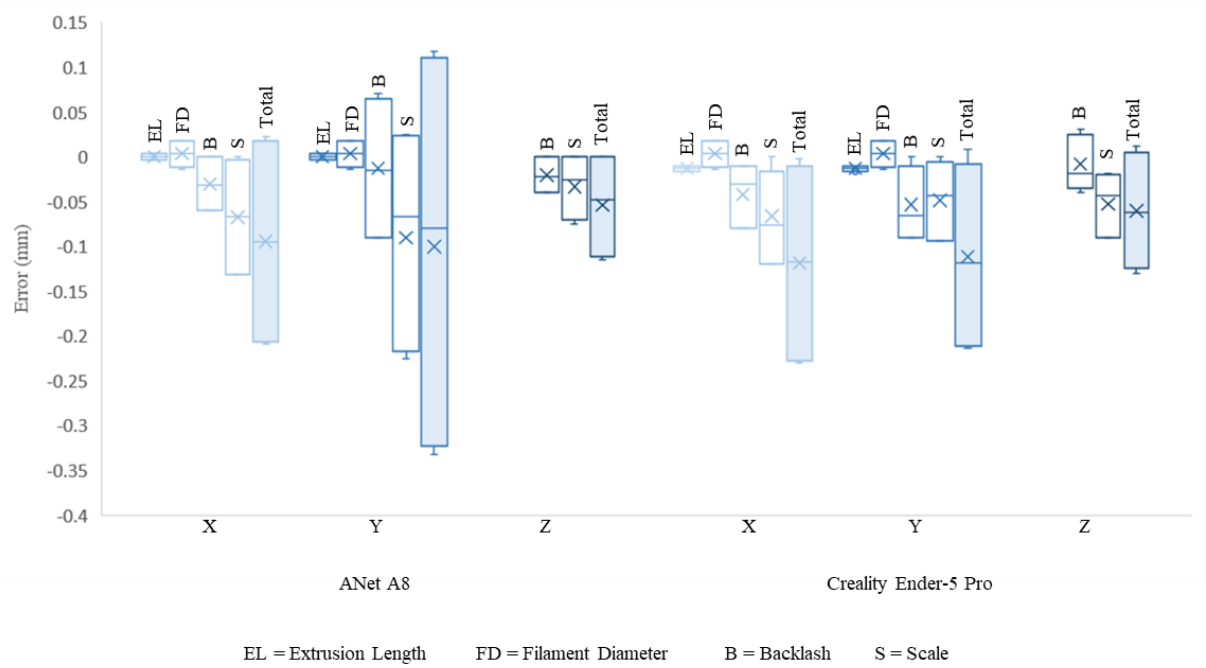

Figure 4.21 *Positional errors of ANet and Creality ME AM machines for a theoretical 15mm cuboid component*

The backlash and scale values have been taken from the most extreme of the eight or six sources outlined in the previous section. As such, these represent a worst-case scenario for positional error. Regardless, the average error when combining the four error sources is between 0.05 and 0.10mm for all axes on both machines. The precision is generally ±0.1mm, though is significantly improved for the Z axis on both machines. This is likely due to the superior precision performance of the lead screw movement mechanism used on both rather than the belt and gear used to move the X and Y axes. The Y axis on the ANet A8 machine shows significantly higher variability than any other axis. This arises specifically from experiment (d) which gave large scale errors for the Y axis on this machine. If compared to the component errors in the previous experimental section, the precision error accounts for approximately half of the values observed in that experimentation. Given accuracy errors are likely machine-specific it is difficult to directly compare though it appears that the scale and backlash errors are either less negative on the machines presented there or other factors counteract this error.

Figure 4.22 shows the percentage contribution of each of the positional error sources, again for a nominal 15mm dimension.

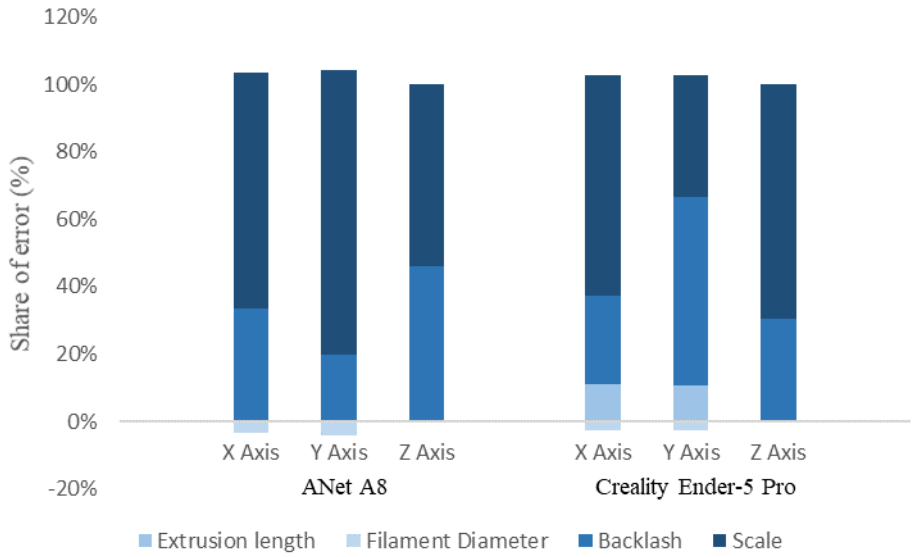

Figure 4.22 *Percentage share of positional errors for a theoretical 15mm cuboid component*

This demonstrates that the error is dominated by the XYZ positional error rather than filament-related error, with these areas representing more than 90% of the total mean error in all cases. Furthermore, of this error the scale error is most significant. Although the Y axis on the ANet A8 has a much larger error range with a 95th percentile range of 0.45mm, the mean error on this axis is no larger. This large range in fact arises from significant errors specific to experiment (d). It is therefore likely that under standard production conditions this error range would be lower. Backlash errors may be reduced through improved tensioning of the belts or use of more precise components. In order to improve the scale error, a compensation factor can immediately be applied directly within the slicer. However, the average user cannot reasonably be expected to conduct the experimentation carried out in this section to reduce the scale error. It would therefore be preferable for the manufacturers to better account for the actual motion of their machines (i.e. account for the scale accuracy error) or utilise higher precision components if the particular machine examples used in this experimentation are not typical.

5. STEADY-STATE FILAMENT MORPHOLOGY

Previous sections have demonstrated that there exists dimensional and geometric inaccuracies in components manufactured via desktop ME AM machines but that the positional performance of these machines does not account for all of these errors.

As was discussed in Section 3.4, macro inaccuracies may be considered as arising from errors in the outer perimeter [287-289], which themselves can be classified as either positional or extrusion-related. The previous section explored the purely positional component of error – that is the positional performance of the ME AM machine nozzle tip in 3D space. This section considers the extrusion element, in particular the morphology of deposited material representing the outer perimeter of a component manufactured via the ME AM process.

The ME AM process was outlined in Section 1.3.2. Here, the production of the final component was described as resulting from the execution of G-code, which is produced by a specialist slicing software package. This effectively determines the nozzle's path in space (i.e. the toolpath, congruous with other CNC processes such as machining, laser etching or other AM techniques) and extrusion volumes for each move. To complete a single layer, one or more perimeters are deposited as well as 'infill'. The exact nature of this infill (e.g. density, pattern) varies between slicers and can usually be selected by the user as required. Low densities typically yield lower component strength and weight [303-305], though clearly also have reduced print times. Similarly, the order of deposition both in terms of infill versus perimeters and outer perimeter versus inner perimeter(s) can vary between slicers as well as the default number of perimeters. Finally, a crucial aspect of difference between the slicers is in their assumptions regarding deposited filament dimensions.

The key values of a deposited filament are its layer height (LH) and road width (RW). The LH is almost always assumed to be equal to the incremental step between layers. In this respect, each deposited layer builds up the component by exactly the layer height in the build direction regardless of extrusion rate and therefore variabilities in this rate affect the road width alone. As a result, the road width dimension is less straightforward. The volumetric flow rate of deposited material can be thought of either with respect to time (often called *printing head velocity* [306], measured in mm^3s^{-1} or simply mms^{-1} if converted to the filament drive speed) or with respect to movement (often called the *velocity ratio, V/U* [306], measured in mm^2 or dimensionless if filament drive speed is instead used). Whilst RW will clearly be a function of the *velocity ratio* – assuming conservation of volume and a fixed layer height – exactly how wide the individual deposited strand is requires some assumptions. This width directly effects the component accuracy and precision. This is because if the actual RW is not properly accounted for in the toolpath (i.e. the outer perimeter toolpath is not offset such that the outside surface of the deposited filament is in line with the nominal geometry) then errors will necessarily arise.

The primary purpose of this section of experimental work is to understand and characterise the relationship between deposition parameters and deposited filament morphology, with a particular focus on the road width and outer perimeter geometry given their direct influence on macro accuracy performance. This data can then be used to inform the toolpath in order to ensure optimal dimensional accuracy.

5.1. EXTRUSION PROCESS MODELLING

This subsection presents an overview of the melting, extrusion and deposition processes. It is important to understand the underlying nature of these in order to characterise the single-filament deposition experiments contained within this section and the remainder of this thesis. First, a review of the thermal processes are presented both during melting and solidification. Next, the morphology of strands is discussed. Finally, extrusion rate limits are explored. Together, these will inform the experimental results presented in this chapter.

5.1.1. THERMAL MODELS

Modelling the thermal behaviour of the ME AM process is important to understand both manufacturing limits and performance characteristics. In particular, the thermal history within the liquefier dictates the exit temperature and therefore initial conditions for solidification, whilst the thermal history during deposition can effect both strand morphology (covered in the next subsection) and inter-filament bonding strength. Existing models focus on these two main areas, with many studies covering liquefier and nozzle dynamics as well as deposition thermal history.

The liquefier is an element of the ME AM machine that melts the solid feed material and extrudes the molten material through a nozzle with a set diameter. There are two main aspects to model within the liquefier; heat flux into the material (and therefore temperature gradients within the chamber) and properties of the material with respect to its temperature at any given location.

Early analytical models of the liquefier typically assumed a constant wall temperature [307,308] or constant heat flux [309]. Bellini et al. [309] presented the following equation for the necessary heat flow, q;

$$q = (T - T_i)\left(\frac{\rho v A c_p}{2\pi\frac{D}{2}L}\right)$$

where; T = temperature at the nozzle exit, T_i = temperature at the entrance to the liquefier, ρ = density of the melt, v = velocity of the melt flow, A = cross-sectional area of the inner liquefier and c_p = specific heat capacity of the melt. The denominator within the brackets on the right represents the wall surface area of the liquefier with length L and diameter D.

Pandey and Prahan [310] noted that the heat capacity of the melt was often considered to be constant (as in Bellini et al's work [309]) but offered their own relationship between heat capacity and temperature depending on whether the material is above or below 300K. The equation above simply represents the mass flow rate $\dot{m}$ multiplied by the temperature delta and specific heat capacity. This dictates how much heat energy in total must flow into the material per unit area per unit of time in order for the desired temperature to be reached by the exit. Failure to reach this temperature may lead to print error or failure, as discussed further in Section 5.1.3.

Yardimci et al. [307] described the heating of filament within the liquefier with a two-dimensional axisymmetric steady-state model with the simplification of plug flow (i.e. no shearing between layers, all fluid assumed to have constant and uniform velocity for any given cross-section). They developed a dimensionless equation that linked temperature to radius and length in a generalised form via the velocity and thermal diffusivity of the material. This enables the calculation of the melting point within the liquefier and the thermal gradient of the cross-section to be estimated.

The behaviour of the material within the liquefier (given the thermal history outlined above) is a relatively complex process to model because properties of the material within the liquefier have a non-linear relationship with temperature and shear rate [310]. The shear rate relationship (and therefore overall governing equation between viscosity and temperature and shear rate) are discussed in the context of rate limits in Section 5.1.3. In addition to the shear rate-viscosity relationship, the temperature-viscosity relationship must also be considered as clearly the material will not be isothermal [311] throughout the deposition process (entering at approximately room temperature and exiting close to the nozzle temperature, a difference of approximately 190°C for PLA and 220°C for ABS). Bellini et al. [309] presented the thermal contribution to viscosity change as an Arrhenius model when considering ABS;

$$H(T) = exp\left[\alpha\left(\frac{1}{T - T_0} - \frac{1}{T_\alpha - T_0}\right)\right]$$

where α is the energy of activation, T_α is a reference temperature for which $H(T)=1$ and $T_0=0$ for temperatures T and T_α. This is combined with the shear rate-viscosity relationship to give an overall viscosity expression, and effectively acts as a non-linear scaling factor with respect to the reference temperature, T_0.

Jerez-Mesa et al. [312] conducted finite element analysis of a ME AM liquefier. In this study, they focused on the convective heat dissipation along the liquefier body during the production of a component. They found that airflow over the liquefier had a significant effect on the temperature above the heating element with a reduction of around 50°C possible at higher airflow velocities. Ouballouch et al. [313] undertook a very similar study with the same findings. Above the melt chamber, low temperatures are preferred to avoid buckling of the filament whilst under compression.

Jerez-Mesa et al. [314] conducted a comparative study of 3 different ME AM liquefiers with varying geometrical designs. This found some small differences in heat dissipation, though not as significant as changes in airflow velocity. Mackay et al. [315] determined the maximum feed velocity of an ME AM machine with a homogenous temperature field at the nozzle exit. In this study, they assumed plug flow in the liquefier, however Peng et al. [316] showed experimentally that this is not the case. In their study, they introduced dye markers to characterise flow through the liquefier, and found highly non-isothermal behaviour. This study was taken further by Pigeonneau et al. [317], who numerically solved mass, momentum and energy conservation equations to visualise the temperature gradient within the liquefier. This work assumed perfect contact between the melt and the liquefier walls, though work undertaken by Serdeczny et al. [318] and Phan et al. [319] suggests that this is not the case since they both observed lower material temperatures at the outlet than the liquefier temperature suggesting the presence of thermal resistance. Serdeczny et al. [320] most recently provided two models of melt flow through the liquefier. As with [317], this work again showed that the more simplified early models of isothermal behaviour did not properly capture the melt flow behaviour. They were able to demonstrate detailed thermal fields across the liquefier for varying feed rates and times since the initial introduction of material. In particular, these modelling approaches were able to capture non-steady flow of material. Similarly, Stewart et al. [321] developed a computational model of temperature variation within the liquefier and validated this via experimental work. This also suggested that modelling external sources of heat is more accurate than the assumption of constant heat flux or wall temperature. Phan et al. [322] developed a numerical simulation of the melting and pressurisation mechanism. These results showed that the incoming material melts axisymmetrically, forming a cone of unmelted material in the centre surrounded by melted material. It also showed that a recirculating vortex of melted polymer is formed at the entrance to the liquefier.

Whilst most modelling approaches assume a relatively large melt pool, Osswald et al. [323] instead modelled only a melt ‘film’ at the very tip of the liquefier. They assessed the feasibility of various nozzle geometries via this modelling and demonstrated the validity of the model through a specially-designed extrusion apparatus. Mostafa et al. [324] developed detailed 2D and 3D numerical analysis of the deposition process through a 90 degree bent tube in a departure from the straight liquefier modelled in all other studies. The main flow parameters of temperature and flow rate were investigated in a finite element approach, and thermal gradients across the liquefier demonstrated and validated with experimentation on a desktop ME AM machine.

Vanaei et al. [325] noted that heat transfer during deposition is a complex problem to model and is influenced by radiation, convection, and conduction. They demonstrated both experimentally and via a computational model that a deposited layer is heated up by each of the next five deposited layers but that the recrystallization temperature is not exceeded for any of these. Similarly, Seppala et al. [326] undertook infrared (IR) thermography of the deposition process. This also showed some reheating of

the two prior layers, for a period of approximately 4 seconds with a print speed of 100mms^{-1}. Wolszczak et al. [327] similarly demonstrated this phenomena through the capture of thermograms of a 0.3mm layer height. In this experimentation, elevated temperatures were again seen in the previous 4 or 5 layers. Xia et al. [328] developed a numerical simulation based on previous fluid flow modelling approaches to model the fluid deposition and solidification process. This gave a detailed approach to predict the thermal history of material following extrusion and cooling but considered the melt chamber as a volume of molten material with the thermal modelling applied only downstream.

Zhou et al. [329] developed a thermal model which noted non-linear behaviour of thermal conductivity. The temperature evolution of the deposited ABS filament was modelled via a finite element analysis method, where a uniform temperature across the filament cross-section was assumed. Zhou et al. [330] conducted both experimental and theoretical modelling work. This showed that PLA materials had the longest thermal diffusion time for high print temperatures, high platform temperatures, low print speeds and high layer thicknesses. Zhou and Tsieh [331] developed a finite element model, supported by IR thermography imaging. This study focused on the temperature history of filament interfaces and their corresponding cooling mechanism. The model demonstrated a good degree of alignment with the experimental data, suggesting it would be applicable to bond formation analysis. Zhou et al. [332] developed a novel voxelisation finite element simulation approach to model the ME AM deposition process. This demonstrated that chamber temperature has a significant effect on warping deformation of ABS components post-deposition.

Costa et al. [333] developed a predictive model of extruded filament surface temperature with varying deposition strategies. This showed that filaments remained at slightly elevated temperatures for longer periods of time where they interacted, but that nonetheless temperature reduced sharply post-deposition. Costa et al. [334] modelled many aspects of the filament deposition process including convection and radiation with the environment, conduction with support and between adjacent strands, radiation between adjacent filaments and convection with entrapped air. Rather than modelling the filament deposition itself, Prajapati et al. [335] modelled the thermal field in the gap between the nozzle and the build plate. This study developed a single parameter combining mass flowrate, heat capacity, filament size and cooling conditions to demonstrate its effect on heat transfer in the gap. Wijnen et al. [61] developed a thermal model of multiple deposited layers to predict the degree of warpage of thin vertical walls fabricated with PLA. D'Amico and Peterson [336] modelled Big Area Additive Manufacturing (BAAM) in addition to the ME AM process covered in other studies. Through the use of finite element models, they showed that small scale ME AM loses heat at a faster rate which decreases interlayer diffusion and weld formation. This modelling also confirmed earlier studies which demonstrated there was significant thermal diffusion into previously-deposited layers.

5.1.2. DEPOSITION MORPHOLOGY MODELS

As was noted previously, slicers contain an implicit deposition morphology model. This coverts the volumetric flow rate with respect to movement (which in turn determines the cross-sectional area) to a deposited filament height and RW. The outer perimeter nozzle path can then be inset from the nominal outer perimeter by a value equal to half of this implicit road width. In practice, it is the road width that can be altered by the user in these software packages, and it is then the volumetric flow rate which is changed to achieve this. There are two main approaches taken in popular slicers. The first, and most simple, considers the deposited filament to have a purely rectangular cross-section, with a height equal to the layer height. Ultimaker's *CURA* slicer uses this model. For this model, the relationship between the cross-sectional area and the road width and layer height are as per Equation 2.

$$RW = \frac{A}{LH}$$

Equation 2: *Relationship between RW, deposited cross-sectional area and LH for the rectangular model*

Whilst this may seem overly simplified, with multiple perimeters and potentially flow rate reductions this may still provide an accurate final component. The second model assumes the filament cross-section to consist of a rectangle with two semi-circular side profiles. Again, the height is considered to be equal to the layer height, but in contrast to the previous model the width is in all cases larger at its widest point. This model is used by the popular *Slic3r* software, on which a number of manufacturer slicers are built such as Prusa's *PrusaSlicer* and Creality's *Creality Slicer*. The relationship between the cross-sectional area and the road width and layer height for this model is shown in Equation 3.

$$RW = LH + \left(\frac{A - \pi \left(\frac{LH}{2} \right)^2}{LH} \right)$$

Equation 3: *Relationship between Road width, cross-sectional area and layer height for the semi-circular model*

There has been a large amount of previous work on the morphology of deposited material (often referred to as a *strand* or *bead* in existing literature) in the ME AM process. Early work focused on aligning layers of a set height with the nominal outer surface to reduce error but more recently, detailed filament-level studies have been undertaken. Various empirical and numerical models have been proposed to capture the shape and dimensions of the strand which enable component surface roughness, dimensional accuracy and internal porosity to be accurately predicted prior to component production.

As has been noted previously, the production of a component by any AM technique requires the building of consecutive layers. As a result, any vertically sloped surface may only be approximated by

the collective outer surfaces of each individual layer. Such an approximation naturally leads to error, often referred to as the staircase effect. As such, a large amount of attention has been given to edge profile modelling, particularly with regards to increasing adherence to the nominal vertical surface and, where possible, reducing build time.

Kulkarni and Dutta [337] described the staircase effect on sloped surfaces and developed an accurate slicing procedure based on the local surface angle and layer cusp height. Adaptive slicing has been an area of significant interest, whereby layer height is reduced in areas with fine features or large angles to the build direction, but is increased in other more vertical areas. For example, Sabourin et al. [338,339] were early developers of adaptive slicing techniques which gave build speed improvements of up to 50% without any loss of dimensional accuracy. Adaptive slicing techniques are covered in greater detail in Section 7.1.2, but these are usually applicable to all AM techniques as they all share the same layer-by-layer build process. The core principle in studies of slicing procedures was the concept of cusp height tolerance, developed by Dolenc and Makela in their 1994 study [340]. This is the normal distance between the nominal surface and the layer boundary at any given point and is minimised in these studies for maximum accuracy and superior surface finish.

As Pandey et al. [341] noted, all of these early studies implicitly assumed that the filament edge profile was rectangular. However, in practice this is not the case and especially so for ME AM compared to other AM technologies. Vasudevarao et al. [342] used a parabolic model for the filament cross-section in a study which investigated the surface roughness of components at varying print temperatures. Here, it was hypothesised that higher temperatures would lead to a more pronounced curve as material flowed outwards under deposition. However, it was instead concluded that print temperature has little effect and layer thickness and part orientation were the main contributory factors. Similarly, Pandey et al. [55] had demonstrated that the edge profile could be approximated to a parabola as part of their study on improving surface finish via hot cutter machining, where the tip of each parabola was removed to improve surface roughness. In this work, the height of parabolic curve representing the filament side profile was shown empirically to be approximately 30-35% of the base following surface profile experimentation. This work enabled the development of a simplified model for the surface roughness of parts manufactured via the ME AM process. Pandey et al. [341] presented a similar semi-empirical model which approximated to outer surface of deposited filament to a parabola in their own study of adaptive slicing.

In two studies by Boschetto et al. [343,344], a filament model was developed which described the component outer surface as a series of circumference arcs of radius r spaced apart by a distance f. Where the outer surface is a vertical wall, the arc radius is assumed to be half the layer height and the distance between arcs equal to the layer height giving a semi-circular cross-sectional morphology. As a result of changing wall angles, the support, or lack of support and interaction with previous layers

changes the value of both r and f enabling a predicted surface profile to be generated. The filament profile could be higher than the layer height at larger angles, where the upper and lower surfaces were not fully constrained by the level above and below. This model was shown to be valid for wall angles of 30 to 150 degrees, but was not accurate outside of this range. Boschetto et al. [177] used these filament models and developed them further to predict the surface error or surfaces at various inclines, which could then be used to compensate for the predicted error. Gharehpapagh et al. [345] also noted a curved side profile described by a width, λ, and a height equal to the layer height Δz in order to calculate total road width as a function of flow rate. It is suggested that λ can be reduced through suitable control of the feed rate conditions. In a slight deviation from the arc approach, Bakrani Balani et al. [346], Ma et al. [347] and Vega et al. [348] all modelled the deposited bead as an elongated oval, with the side profile a semicircle with a radius equal to half the layer height under all conditions. This same approach is taken by the popular *Slic3r*, as noted by Aksoy et al. [349]. McIlroy et al [50] conducted detailed polymer flow simulations, during which they also assumed an oval cross-sectional shape though not elongated in this instance. Dabiri et al. [350] modelled the deposited filament cross-section as almost entirely circular, although the focus in this study is on the thermal history and the solidification process rather than microgeometry. Aksoy et al. [349] developed a detailed multi-layer model of filament geometry based on stacked ellipses with overlaps and varying extrusion rates. This was compared to the less complex model consisting of two semicircles (as used in many of the studies noted above) and was found to be more accurate in predicting strand width.

Vega et al. [348] explored the use of the Volume Conserving (VOLCO) model developed at the University of Nottingham. Gleadall et al. [351] first presented this model, which could be used to predict the geometry of 3D printed microarchitecture, particularly for scaffolds where filaments interact within the build plane. This model involves modelling the extruded material as voxels, and placed material at ever-increasing radii from the nozzle tip centre, excluding voxels which were already accounted for by previously-deposited material (hence a volume conservation model). This approach lead to curved sides on the deposited bead, though the exact geometry depends on other depositions and layer height and flow rate. This model was later updated as VOLCO-X [352], an extended model which allowed for non-uniform extrusion rates and asymmetric depositions. Again, this creates curved-sided filament geometry dependent upon other parameters but was shown to have good correlation with supporting experimental work.

Comminal et al. [353] conducted a detailed study of the strand deposition. In this study, Computational Fluid Dynamics (CFD) was employed to model the molten material as a fluid flow whose dynamics are governed by the conservation of mass and the Cauchy momentum equation. This produced very detailed predicted strand morphologies, which were then compared to idealised models of an ellipse, oblong and cuboid depending on the process parameters selected. It showed that filament morphology was affected by two main dimensionless factors; normalised gap (layer height

divided by nozzle diameter) and velocity ratio (defined as the print speed divided by the speed through the nozzle). Du et al. [354] also used CFD to model multiple layers of a single perimeter, although this focused more on thermal gradients rather than geometry. Serdeczny et al. [355] conducted similar experimentation, again exploring the same two dimensionless variables. This study also showed that strand cross-sections varied from near-circular to high aspect ratio oblongs depending on the print parameters, with curved sides in all cases. Comminal et al. [356] conducted a further study that focused on the effect of nozzle geometry on the deposited strand cross-section. This showed that a square nozzle did not aid the compactness (i.e. vertical and flat nature) of the deposited strand but did increase printing force. This theoretical modelling suggested that a side plate may improve compactness with only a modest increase in printing force for the only straight side profile demonstrated in any detailed study.

Comminal et al. [306] conducted a study of multiple strands both vertically and horizontally. This numerical and experimental study showed that for lower strand spacing (horizontally) there was little effect on the outer surface roughness, but a reduction in horizontal surface roughness and reduction in void volume was observed. Notably, it demonstrated that for lower deposition spacing values, the strand deposited second moulds into the first strand, with the majority of the additional material in the upper half of the printed layer giving highly asymmetric strand morphology. This was also demonstrated by Gleadall et al. in their VOLCO-X study [352] giving rise to triangular rather than diamond void geometry between multiple layers and perimeters. Rodriquez et al. [357] also studied the internal geometry of both overlapping and aligned multilayer deposited strands. They showed that the internal mesostructure could be relatively easily predicted and controlled to drive overall component properties.

Jang et al. [358] investigated the effect of process parameters on filament geometry and inter-filament voids. This showed curved outer geometry, although this was not quantified specifically. The study found that layer height, print speed, extrusion rate and nozzle diameter all had a significant effect on extruded road width and therefore also void volumes. However, only extrusion rate and print speed affected the overall filament cross-sectional area. Similarly, Kaveh et al. [359] varied print parameters including temperature and road spacing to understand the inter-filament void geometry. Golab et al. [360] conducted cross-sectional experimentation on both single and multilayer depositions. This varied the print head velocity and volumetric flow rates to understand their effect on strand shape, though the shape was not modelled specifically.

Whilst it is clear that a large amount of work has been undertaken to understand the deposited filament morphology, there remain some areas that have received little attention. Only recently has inter-perimeter bonding been modelled, and experimental validation remains at the nascent stage. Similarly, the effect of multiple adjacent perimeters on the outer perimeter surface profile remains

poorly understood, despite the fact that most modern slicer use a minimum of two perimeters by default. In addition, an updated and simplified outer perimeter profile as a function of actual print parameters (e.g. actual volumetric flow rate, aspect ratio, layer height) may still prove beneficial, especially if applicable to multiple perimeters.

5.1.3. EXTRUSION RATE LIMITS

Section 5.1.1 showed that the viscosity of the material was related both to temperature and shear rate, where the temperature relationship was discussed in further detail. Bellini et al. [309] noted that because the melt adheres to the liquefier walls, the material is subjected to shear deformation during the flow. Many have stated [307-309,324] that the materials typically used in the ME AM process exhibit shear thinning behaviour – that is that their viscosity decreases with increasing shear rate. The following equation is typically presented;

$$\eta = k(\dot{\gamma})^{n-1}$$

Where η is viscosity, $\dot{\gamma}$ is the shear rate and k and n are consistency/flow parameters.

This can be combined with the viscosity-temperature relationship introduced in Section 5.1.1 to give an overall expression for viscosity;

$$\eta = H(T)n_0(\dot{\gamma})$$

Bellini et al. [309] combined the shear thinning and temperature-related behaviours with momentum flux balance equations on a fluid element as per Michaeli [361] in the liquefier and extruder. To do this, the liquefier and extruder were conceptualised as consisting of 3 regions – a straight-wall inlet section, a conical section and a smaller straight-walled exit section for the nozzle. This provided expressions for the pressure drop in each, which can then be summed to express the overall pressure drop across the liquefier and nozzle assembly. The pressure drop is shown to be dependent on the temperature, velocity and geometry of the three regions.

Pandey and Prahan [310] commented on the validity of the power law approach. They noted that the approach was commonly adopted for its mathematical simplicity, whilst it is accepted that certain aspects are not captured. In particular, they suggested that yield stress is not captured and that the power law assumption may not properly account for large ranges in shear rate (Osswald and Menges [362]). Relatively low shear stress is expected near the entrance to the liquefier, whereas it is much higher at the nozzle exit.

Early systems commonly employed a nozzle diameter or 0.5mm and a nozzle angle of 120º (Yardimci et al. [307]). However, this is no longer representative, with many modern ME AM desktop machines utilising a 0.4mm nozzle as standard with an angle of approximately 85º. Ramanath et al. [308] explored the effects of nozzle diameter and nozzle angle. They tested diameters of 0.25mm, 0.3mm

and 0.4mm and nozzle angles of between 20° and 60°. They found that the pressure drop decreased with increasing nozzle diameter and increasing nozzle angle. As part of their modelling of the pressure drop, Bellini et al. [309] also included nozzle angle in their calculations. This again demonstrated that an increasing cone angle reduced the overall pressure drop. However, this does not account for the possible introduction of flow instabilities and vortices which may form in the corners at high nozzle angles (Liang et al. [363]), potentially placing a limit on the optimum angle. Indeed, Yardimci et al. [307] originally suggested that 120° was the optimal angle. In addition to the theoretical models outlined thus far, Finite Element Analysis (FEA) models have generally shown lower pressure drops (Pandey and Prahan [310]) owing to the mathematical simplifications contained in their formation. FEA shows that the major pressure drop occurs due to the presence of the conical and nozzle sections [311]. Phan et al. [322] suggested the final 0.5mm long nozzle section accounted for almost half of the total pressure drop alone.

Whilst most studies considered the pressure only within the liquefier and nozzle, Percoco et al. [364] developed a model of the extrusion force required as a function of layer height. They found that that whilst the nozzle pressure increased at higher layer heights due to the increased volumetric flow, the flow counter-pressure counteracted this such that the maximum force required was for very low layer heights. However, within the range of normal layer heights (0.1mm to 0.4mm) the force required was shown to increase with an approximately linear relationship for both PLA and ABS materials as a result of increasing flow rates.

The polymer filament is in tension above the feed rollers, which pull the filament from its source and deliver it into the melt chamber. Below the rollers the filament is in compression, pushing against the pressure drop inside the liquefier which was demonstrated above (Bellini et al. [309]). If this pressure drop is known, the compression force (F) required can be calculated as the total change in pressure (P) multiplied by the cross-sectional area of the filament (A);

$$F = \Delta P \times A$$

Bellini et al. [309] calculated the required torque from the filament drive stepper motors, although in their calculation dual motors were assumed. In the ME AM machines used for the purposes of this thesis, a single motor is only ever employed. As such, the torque (T) and power (P) requirements are given by the following;

$$\mathrm{T} = F \times r \qquad \mathrm{P} = \omega \times \mathrm{T}$$

where r = radius and ω = angular velocity of the drive gear.

Go et al. [365] conducted a detailed study of the rate limits of the ME AM process and produced guidelines for a high-throughput system. In this study, three main areas of potential limit were explored; drive force, material heating and nozzle positioning. It found that all of these placed

potential limits on the process. The first two errors pertain directly to the force equation developed above, whereby either insufficient force can be delivered or insufficient heat to produce a full melt (and therefore too high a pressure drop, and too high a force) can be achieved. In their experimental work, they found slippage of the filament drive gear against the filament to be the limitation on force rather than the torque of the stepper motor. Luo et al. [366] developed models to predict the upper bound of feed rates. This work focused on the relationship between the liquefier wall temperature and Péclet number for the solid portion of the incoming filament. However, this considers only the melting behaviour of the polymer rather than the ability of the extrusion mechanism to overcome an increasing pressure drop. Gutowski et al. [367] looked at rate limits for a number of AM technologies. They noted that BAAM has employed a single-barrel melt extruder fed via pellets to increase the melting capacity of machines.

Other studies such as Gilmer et al. [54] and have suggested that filament buckling via Euler buckling may be another failure mode, especially where ceramic materials are used (Venkataraman et al. [311]). In one study, Mackay et al. [315] tested three different materials to empirically determine maximum feed velocities on a desktop ME AM machine. They created master curves of dimensionless feed velocity versus temperature to display the limits of the process for the current machine configuration.

Ultimately, it has been demonstrated that a compressive force is required to overcome the pressure drop across the liquefier and nozzle. The exact nature of this pressure drop is dependent on a number of factors, but increases with lower thermal transfer to the melt, smaller nozzle diameters and unfavourable internal geometric and increased flow rates. Under perfect conditions, an assumption of volume conservation relative to the filament feed velocity is valid. However, where this reaches a critical pressure drop value, the nominal extrusion rate will no longer be satisfied. In the context of the experimentation contained within the remainder of this thesis, when close to the rate limits it is assumed that some degree of filament slippage will occur resulting in a lower extrusion rate than the machine code would suggest.

5.2. METHODOLOGY

The experimental work included in this section aims to aid understanding in a number of ways. First, it will determine the exact nature of a vertical outer surface for varying layer heights, extrusion rates (road widths) and number of adjacent perimeters. Additionally, the difference between the observed and theoretical cross-sectional areas will help establish the rate limiting effects of the ME AM process, particularly for a low cost desktop ME AM machine.

Section 5 described the importance of the outer perimeter in determining the accuracy of the final manufactured component. It is therefore necessary to determine the cross-sectional measurements of deposited material. Whilst the slicers create the outer perimeters as part of any macro component, they

are poorly suited to create these in isolation. For particularly small or thin features, various approximations are often made within the slicer to mitigate errors. A custom G-code generator was therefore produced, with detailed functionality added for the purposes of this experimentation. This custom G-code generator allows, for example, the selection of; layer height, total number of layers, road width, slicer flow rate assumption, print speeds, print temperature and bed temperature. This mirrors the exact outer perimeter of a number of popular slicers, though for the purpose of all perimeter-based experimentation in this thesis Ultimaker's *CURA* software assumptions are adopted. In particular, this informs the default perimeter spacing and material flow rates for a nominal layer height and road width. Prior to the main deposition, a 'prime' loop is deposited for the first layer only (shown towards the left of the build plate represented in Figure 12.4in the Appendix). The deposition begins well in advance of the removable slide (100mm for all experimentation) and ahead of the deposition end (80mm) to ensure that beginning and end effects are removed as far as possible. Yardmci [368] and later Bellini et al. [309] showed that the deposition sequence could be considered to consist of 5 stages, including start and end stages and a middle 'steady state'. This experimental procedure therefore aims to produce results which represent this state away from significant changes in direction or speed. Deposition behaviour around these changes will be investigated in later sections.

Layer height and nominal road width values were selected as shown in Table 5.1. This covers layer heights of between 0.1 and 0.4mm and road widths from 0.2 to 1.2mm. For reference, *CURA* uses a layer height of 0.2mm and a road width of 0.4mm as a default setting. Initial testing showed that road widths of below 0.2mm (for a layer height of 0.1mm) were highly unstable as these required a 0.1mm nozzle, and road widths of over 1.2mm similarly led to print failures. The nozzle diameter was also changed depending on the nominal road width such that the nominal road width was never less than the diameter and never more than twice the diameter. *CURA* also uses a default of F1800 ($mmmin^{-1}$) for outer perimeters and F3600 for inner perimeters. However, initial experimentation showed that for extreme parameter settings (i.e. very low or high cross-sectional areas or low aspect ratios) these print speed settings led to total print failure. The speed was therefore reduced until an experimental specimen could be fabricated. The final print speeds used throughout the experiments in this section are also included in Table 5.1. All prints were carried out at 200^{o}C and perimeter spacing was set to be equal to the nominal road width according to *CURA*'s rectangular filament cross-sectional model. As was discussed in Section 3, environmental conditions are not directly considered in the experimentation in this section or within the remaining experimental work in the following sections, although this is not expected to be a major influencing factor. Similarly, the time between fabrication and measurement was never greater than 4 weeks in any instance, though was not explicitly recorded throughout.

Number	Layer height (mm)	Nominal road width (mm)	Cross-sectional area (mm^2)	Semi-circular model road width (mm)	Inner perimeter(s) print speed ($mmmin^{-1}$)	Outer perimeter(s) print speed ($mmmin^{-1}$)	Nozzle diameter (mm)
1	0.1	0.2	0.020	0.221	900	900	0.2
2	0.1	0.25	0.025	0.271	900	900	0.2
3	0.1	0.3	0.030	0.321	3600	1800	0.3
4	0.1	0.4	0.040	0.421	3600	1800	0.4
5	0.2	0.22	0.044	0.263	900	900	0.2
6	0.2	0.3	0.060	0.343	3600	1800	0.3
7	0.2	0.4	0.080	0.443	3600	1800	0.4
8	0.2	0.5	0.100	0.543	3600	1800	0.4
9	0.2	0.6	0.120	0.643	3600	1800	0.4
10	0.2	0.8	0.160	0.843	3600	1800	0.6
11	0.3	0.33	0.099	0.394	3600	1800	0.3
12	0.3	0.45	0.135	0.514	3600	1800	0.4
13	0.3	0.6	0.180	0.664	3600	1800	0.4
14	0.3	0.75	0.225	0.814	3600	1800	0.4
15	0.3	0.9	0.270	0.964	3600	1800	0.6
16	0.3	1.2	0.360	1.264	3600	1800	0.6
17	0.4	0.6	0.240	0.686	3600	1800	0.4
18	0.4	0.8	0.320	0.886	3600	1800	0.6
19	0.4	1	0.400	1.086	3600	1800	0.6
20	0.4	1.2	0.480	1.286	900	900	0.6

Table 5.1 *Steady-state filament morphology experimental parameters*

Previous studies which have taken cross-sectional images and measurements have typically set individual filaments in resin [177,306,358,360], which is used to support the structure in subsequent cross-sectional preparation (i.e. sanding and polishing). Many other studies do not explicitly state the sectioning and measurement process, though to maintain geometrical integrity it is likely the majority of these also set the sample in resin; evidence of this can often be seen in the included images. Wang et al. [369], Takagishi et al. [370] and Wang et al. [371] used liquid nitrogen in their cross-sectional characterisation, though this typically allowed the observation of fracture surfaces and may have led to morphological changes as part of the measurement preparation process. Wijnen et al. [61], Gurrala et al. [192] and Alafaghani et al. [372] took a similar approach, though did not use liquid nitrogen in order to facilitate fracture. For the experimental procedures in this thesis that require filament cross-sections to be assessed, the resin setting, cutting a polishing approach was taken as a proven method which is relatively straightforward.

A low cost ANet A8 desktop ME AM machine with a v1.7 motherboard running *Marlin* firmware was utilised for the production of steady state filament depositions, as per the machines used in the previous two sections. 1.75mm PLA orange filament manufactured by Velleman was utilised throughout, except where explicitly stated otherwise for multicolour or alternative material tests. The bed was manually levelled in line with manufacturer recommendations, and alignment of the gantry with the print bed checked prior to production of the samples. A bespoke print bed was designed and fabricated from 3mm thick aluminium plate. This was covered with a plastic adhesive print bed material and incorporated a removable acrylic slide. This was held securely in place during the print

and flush with the build plate surface, but could then be removed and replaced between experimental runs. This custom build plate set up is shown in Figure 5.1.

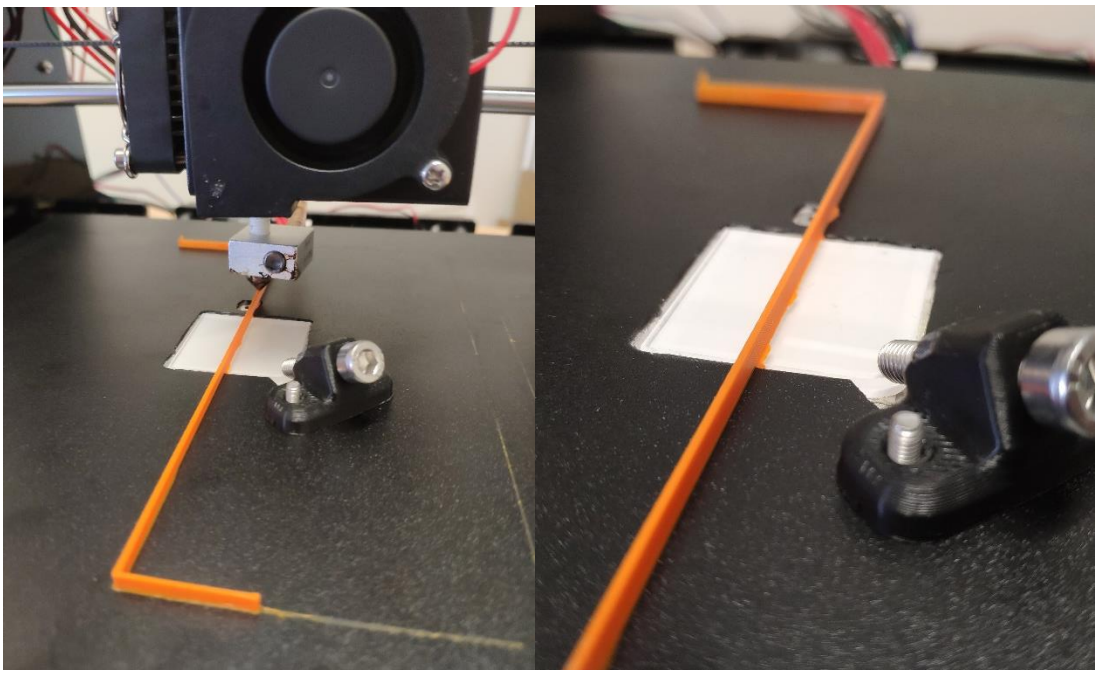

Figure 5.1 *Experimental machine setup utilising a modified print bed with removable slide on ANet A8 ME AM Desktop printer for steady state experimentation*

First layer effects are difficult to properly characterise. In particular, given the manual nature of the bed levelling process on the ANet machine the initial layer height is much harder to verify than subsequent layer heights, which are relative only to the previous layer. As a result, the initial layer extrusion rate was set at three times that of the subsequent layers. This ensured strong adhesion to the acrylic slide and image analysis was then exclusively focused on the higher layers.

After production of the sample, it was cut at either side of the removable slide and the slide was placed in a sacrificial holder. The holder was then filled with *MetPrep EPO-SET* resin (resin and hardener at a ratio of 4:1) and left to harden. The resin holder was then cut 10mm from the bottom of the holder (i.e. approximately 8mm from the rear side of the acrylic slide), sanded and polished to reveal the strand cross-sections as per Figure 5.2. Image analysis of the cross-sections was performed using a *Zeiss Olympus BX51 TRF-6* Optical Microscope with 5x magnification.

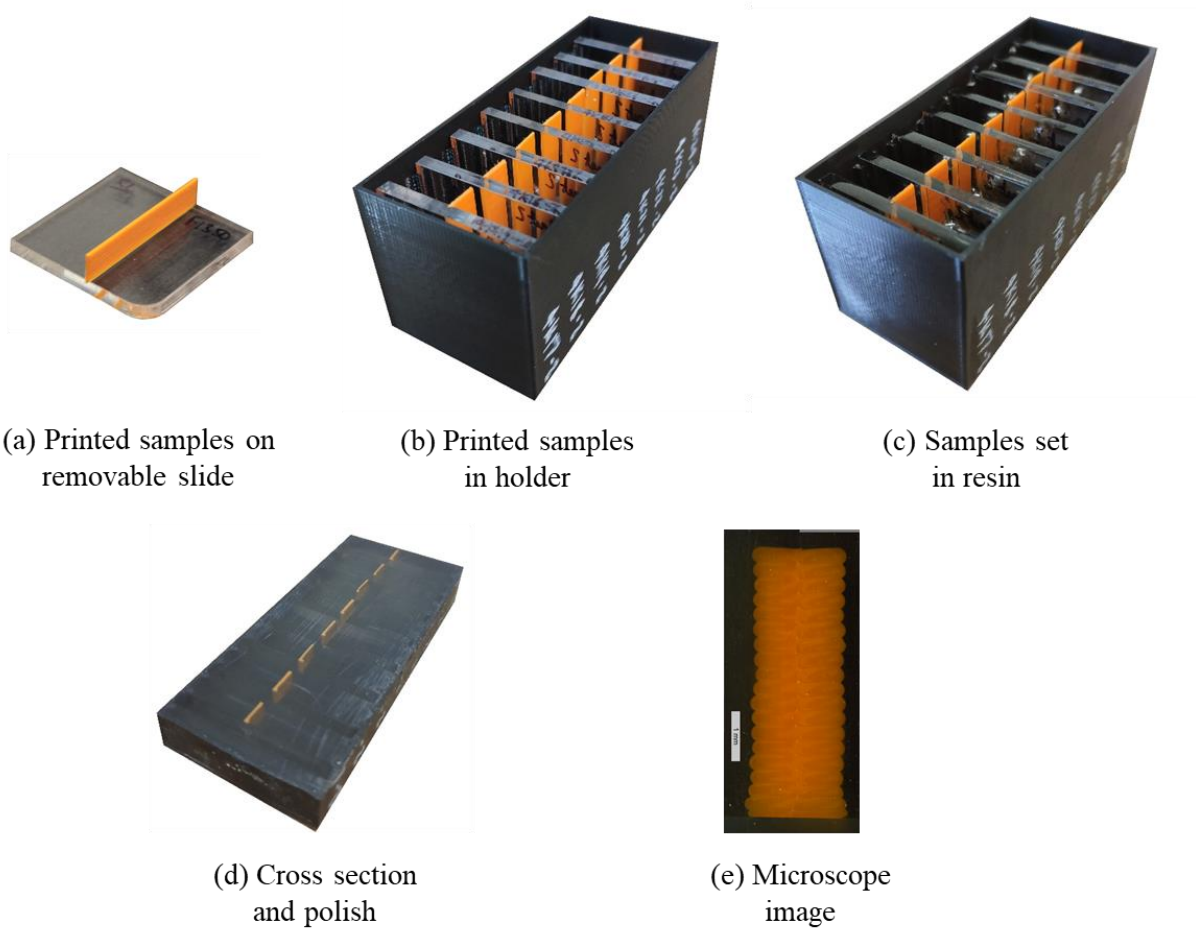

Figure 5.2 *Printed sample preparation process*

Following the capture of a cross-sectional image, analysis was conducted using *ImageJ* and *Microsoft Excel* software. Using *ImageJ*, five layers excluding those affected by the build plate and the uppermost two layers, were selected. These samples show a vertical wall feature, in line with what was previously demonstrated in Section 2 where 78% of components used in experimental studies exhibited such geometry. The vertical reference was established using the bond areas between layers given the symmetrical nature of the perimeters. Once the filament boundaries were identified, a number of quality metrics were established. First, the total cross-sectional area was found, and divided by five to give an average layer cross-sectional area. This was compared with theoretical cross-sectional areas included in Table 5.1 to give a percentage of nominal cross-sectional area. This was expected to be close to or slightly less than 100% in most cases. The total height of all five layers was again captured and divided by five to calculate an average layer height. The maximum filament width and bond width for each layer was found, and averaged across all layers as shown in Figure 5.3. The outermost filament was considered to form the theoretical geometry boundary, and then each layer's deviation to this was calculated (with a minimum of one layer necessarily have a deviation of zero by definition), and then averaged.

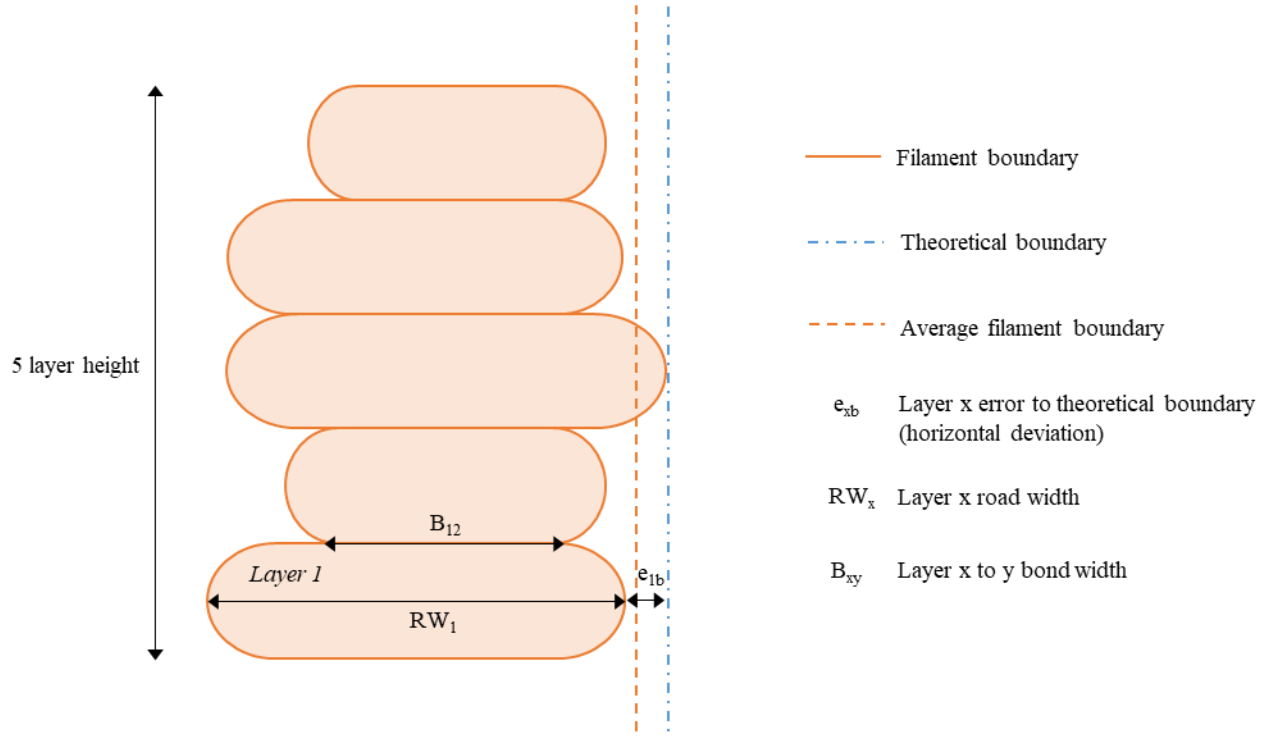

Figure 5.3 *Measured filament morphology errors*

Finally, the outer surface was converted to XY coordinates for surface metric analysis in *Microsoft Excel*. A workbook was created to calculate Rz, Ra and Rq according to the equations shown below.

$$Rz = Rp + Rv$$

Equation 4 *Calculation for maximum peak to valley height across a single sampling length where Rp = peak height and Rv = valley depth below the mean line*

$$Ra = \frac{1}{l}\int_0^l |z(x)|dx$$

Equation 5 *Calculation for surface roughness (arithmetic average) across a sampling length where l= sampling length and z(x) is the height profile relative to the mean*

$$Rq = \sqrt{\frac{1}{l}\int_0^l |z(x)^2|dx}$$

Equation 6 *Calculation for surface roughness (root mean square) across a sampling length*

The rate limit experimentation was conducted with a similar methodology, although in this case samples were removed on their acrylic slides and road widths measured manually with a calibrated Vernier calipers rather than being set in resin and processed as described above.

5.3. RESULTS

The filament morphology for single, double and triple perimeters is shown in this section. In all cases, the leftmost perimeter represents the outer perimeter, which is deposited after any inner perimeters in line with *CURA*'s default perimeter order. Full numerical results may be found in the Appendix.

5.3.1. EXPERIMENTAL MEASUREMENT VALIDATION

In order to validate the experimental measurement methodology, a cross check was performed against identical samples. For this, the single perimeter sample number 7 from Table 5.1 was used (i.e. the default *CURA* setting with a layer height of 0.2mm, road width of 0.4mm, temperature of 200°C and print speed of 1800 mm/min). As was noted previously, it is relatively common practice to encase samples in resin, then cut and polish to reveal the cross-section of interest. To ensure that this process did not adversely affect the morphological integrity of the sample, a check was made between two samples set in resin against two which were cut with a craft knife directly after production, and two which were not cut at all but could be viewed from the side only. In additional to validation of the morphology, there was a possibility that simply cutting the sample without the use of resin may allow for an accurate cross-sectional image, though likely not for the more fragile samples with only a single perimeter and low road widths.

The samples are shown below in Figure 5.4, with two samples viewed from the side, two cross-sections with no resin, and two samples that have been set in resin, cut and polished.

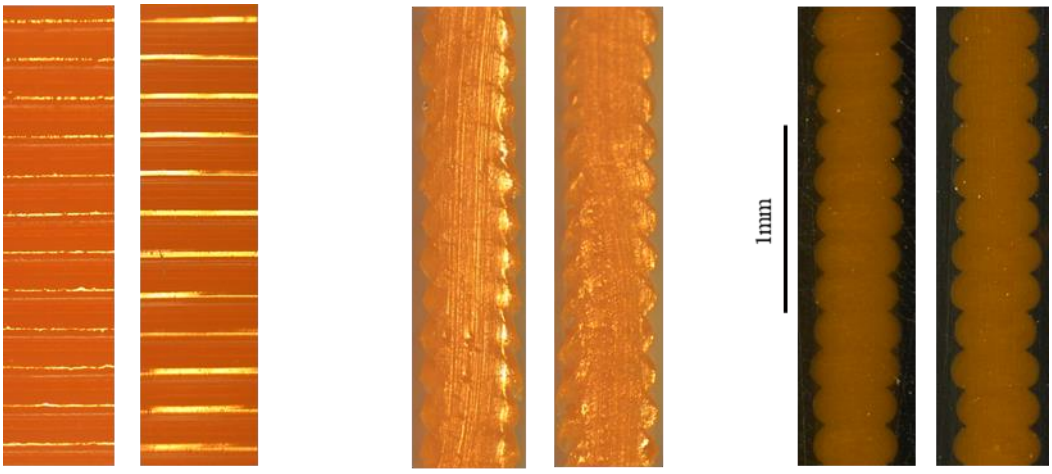

Figure 5.4 *Deposition dimensions: (a) No resin preparation, side view, (b) No resin preparation, cross-sectional view, (c) Resin preparation and polish, cross-sectional view*

A height measurement was taken over 12 layers for each sample. This gave an average layer height of 0.1992mm for both the non-resin samples and 0.1987mm for the resin methodology. This suggests that the resin setting process has very little effect on the dimensional integrity of the samples. As can be seen in the figure above, the manual cutting process on the samples in (b) locally deforms the

deposited filament relative to the resin sample. In order to properly characterise the filament morphology it is therefore necessary to conduct the resin-setting process as in doing so, the morphology of the sample is maintained.

5.3.2. SINGLE PERIMETER

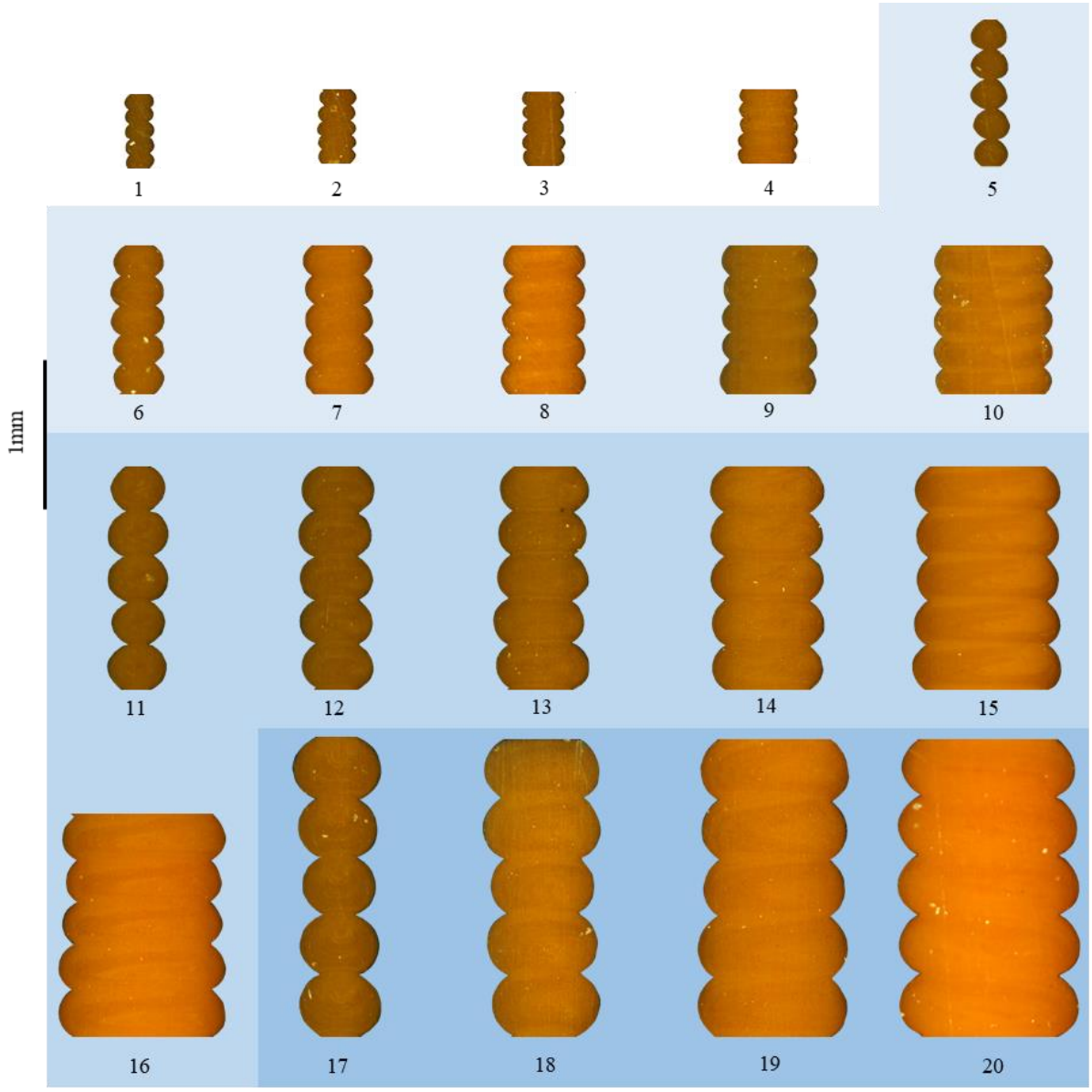

Figure 5.5 *Single perimeter steady state filament morphology images*

5.3.3. DOUBLE PERIMETER

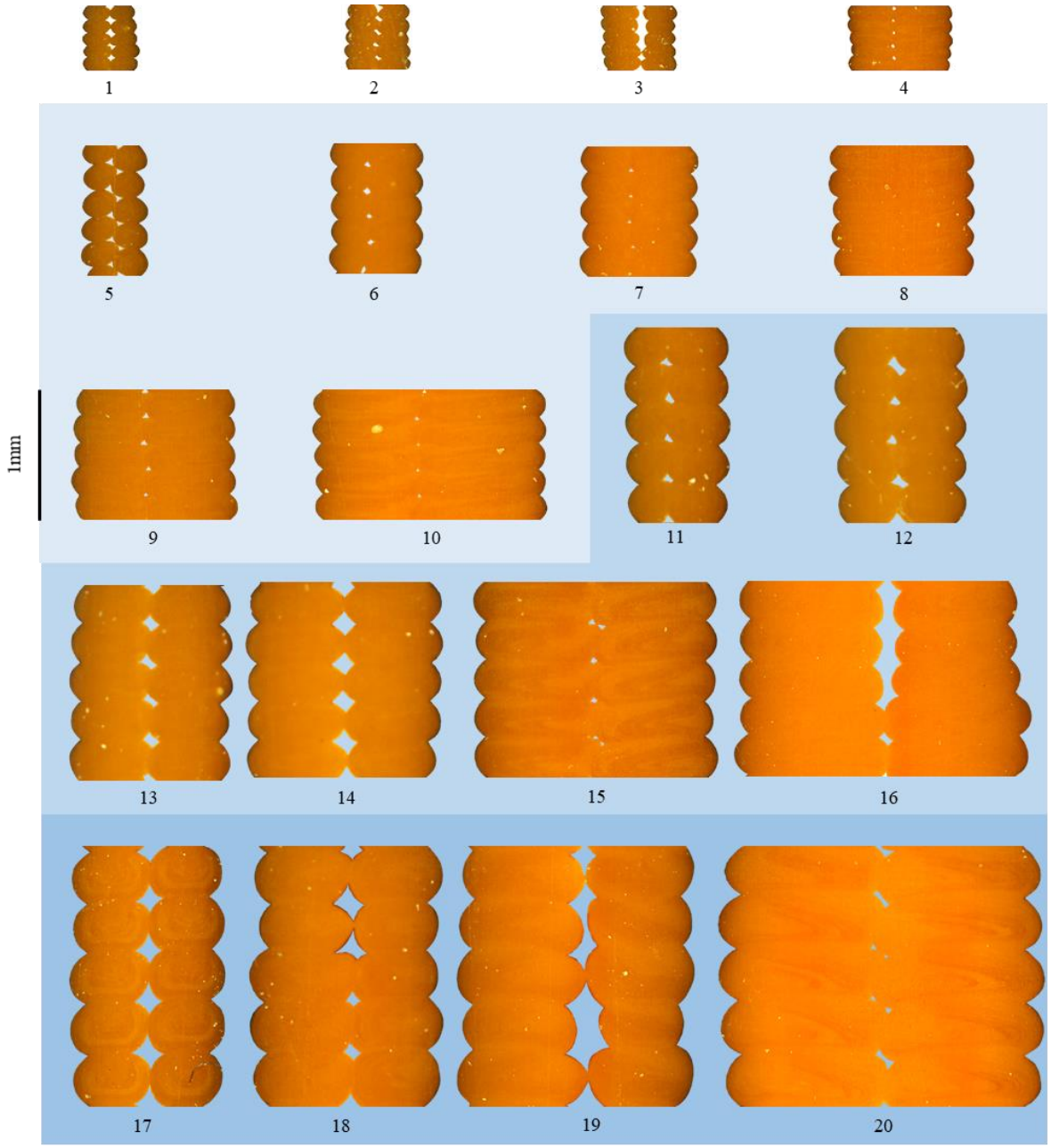

Figure 5.6 *Double perimeter steady state filament morphology images*

5.3.4. TRIPLE PERIMETER

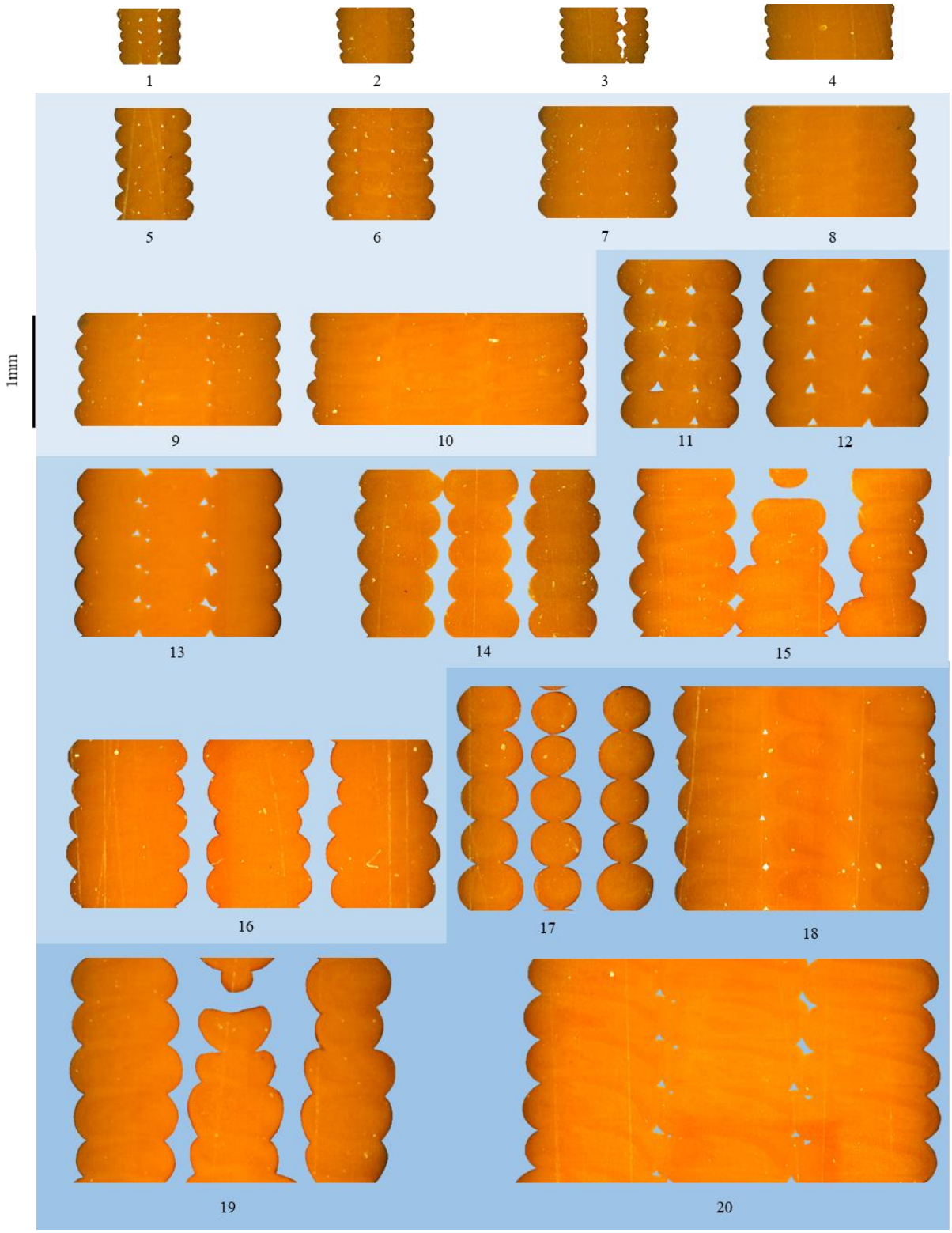

Figure 5.7 *Triple perimeter steady state filament morphology images*

5.3.5. OTHER MATERIALS

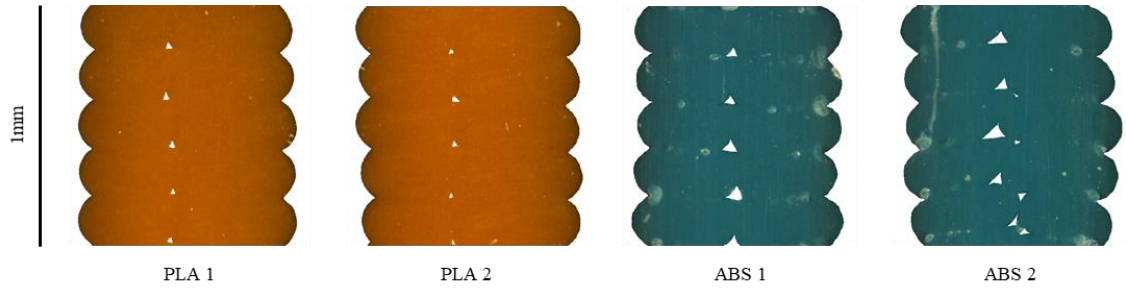

Figure 5.8 *PLA and ABS double perimeter default print parameters comparison images*

5.3.6. RATE LIMITS

As was discussed in earlier in Section 5.1.3, there exist upper limits in the rate of material flow for the ME AM process arising from limited compressive force to overcome the pressure drop across the nozzle. The experimentation included in this subsection provides empirical data for this limit on the ANet A8 ME AM desktop machine using PLA filament.

To investigate the actual material flow rate (i.e. the volume of material extruded through the nozzle per unit time, also equal to the volume of unmelted filament fed into the top of the liquefier if volume is conserved) there are two main approaches. In order to vary volumetric flow rates one can either increase the cross-sectional area of the deposited filament for a given print speed or increase the speed for a set cross-sectional area. In the first case, the volumetric flow rate with respect to position (mm^3 per mm travelled) is increased, which therefore translates to an increased volumetric flow rate with respect to time. In the latter case, the speed increase directly contributes to the increased volumetric flow rate with respect to time.

Figure 5.9 shows the relationship between the extrusion rate and the measured deposited road width. These have been produced with a temperature of 200ºC and a print speed of 1800mmmin^{-1} (30mms^{-1}). The default EF is 1, which represents the *CURA* expected road width of 0.4mm and layer height of 0.4mm. With an EF of 1, the deposition cross-sectional area should therefore be 0.16mm^2 with volumetric flow rates of 0.16mm^3mm^{-1} and 4.8 mm^3s^{-1}.

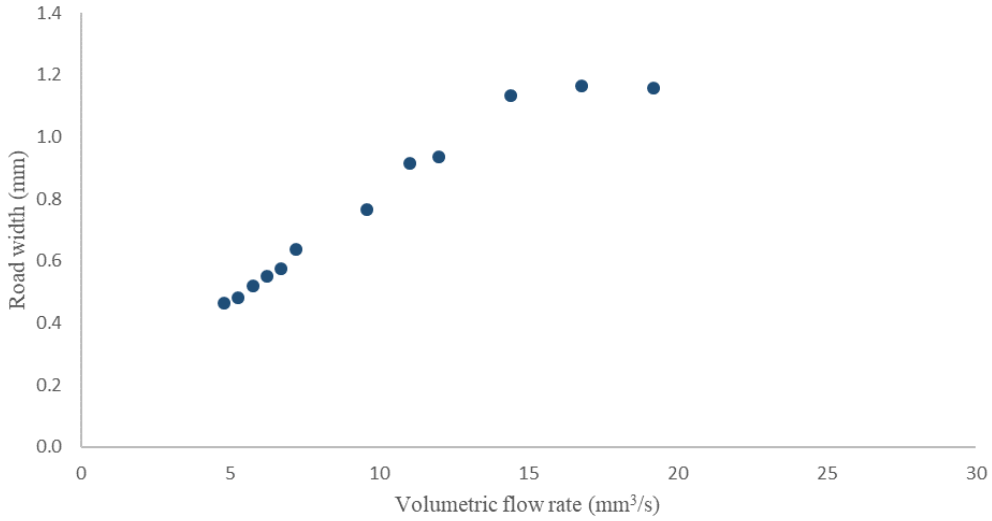

Figure 5.9 *Effect of changing extrusion rate on measured road width*

Figure 5.10 demonstrates the relationship between print speed and the measured deposited road width. Again, a temperature of 200ºC was used throughout, with an EF of 1.5. In this scenario, the expected road width is therefore 0.6mm and the layer height 0.4mm.

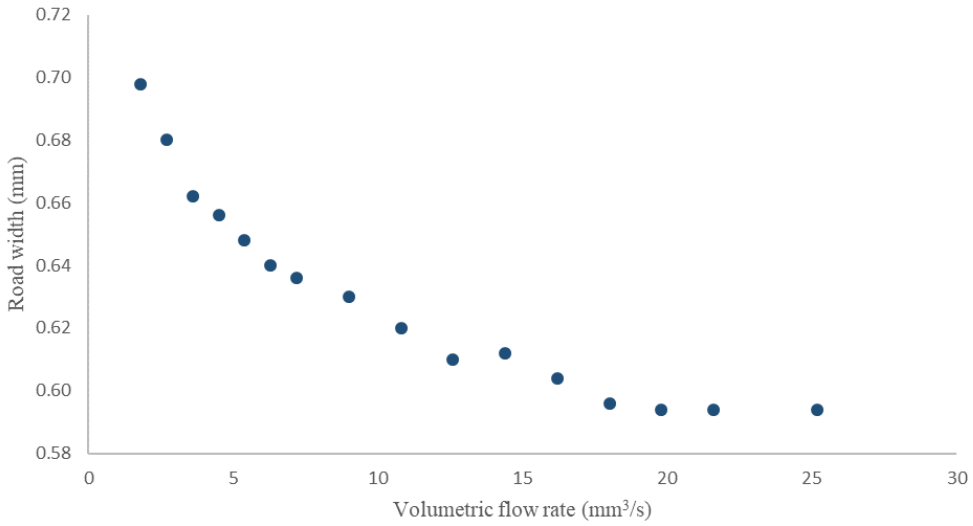

Figure 5.10 *Effect of changing print speed on measured road width*

5.4. DISCUSSION

This section discusses the data presented in the previous subsection. It covers analysis of the single, double and triple perimeter steady state experimentation and presents an empirical model of the single filament morphology and outer surface profile. It also covers the rate limit aspects of the perimeter experimentation and rate limit-specific work. The focus of this experimental work is towards dimensional accuracy rather than precision, which has been investigated in particular by Golab et al. [360].

5.4.1. PERIMETER EXPERIMENTATION

The single perimeter stacked filaments in Figure 5.5 demonstrate a good degree of uniformity between layers regardless of the layer height or extrusion rate used. It is evident that the morphology changes significantly from near-circular cross-sections for nominal aspect ratio (i.e. nominal width with respect to layer height) values of close to 1 to far more elongated oblongs at higher extrusion rates. Since these are a single perimeter, they are the outermost perimeter by definition and are therefore printed at the lower print speeds indicated in Table 5.1. From the earlier modelling discussion, these lower speeds aid heat transfer into the melt within the liquefier and the reduced velocity also reduces the overall force required to extrude, leading to high quality steady extrusion profiles.

The cross-sectional area observed directly corresponds to the volume, and therefore flow rate, of material extruded. For the single perimeter prints, cross-sectional values are in the range of 80-100% of the expected area. In cases where this value is much less than 100%, this suggests that the force required to reach that extrusion rate cannot be applied and that there must be some slippage between the drive wheels and the incoming filament or missed stepper motor steps. The lowest values for cross-sectional area are mainly observed on prints with a layer height of 0.1mm and 0.4mm. The first two 0.1mm layer height prints were conducted with a 0.2mm nozzle, the smallest of any run. Previous discussion noted that nozzle diameter significantly affects the pressure drop across the nozzle and therefore force required to extrude, which explains these low values. Indeed, Figure 5.11 demonstrates that as the nozzle diameter increases, the cross-sectional area as a percentage of the nominal value also increases although the effect of flow rates within each nozzle diameter must also be considered.

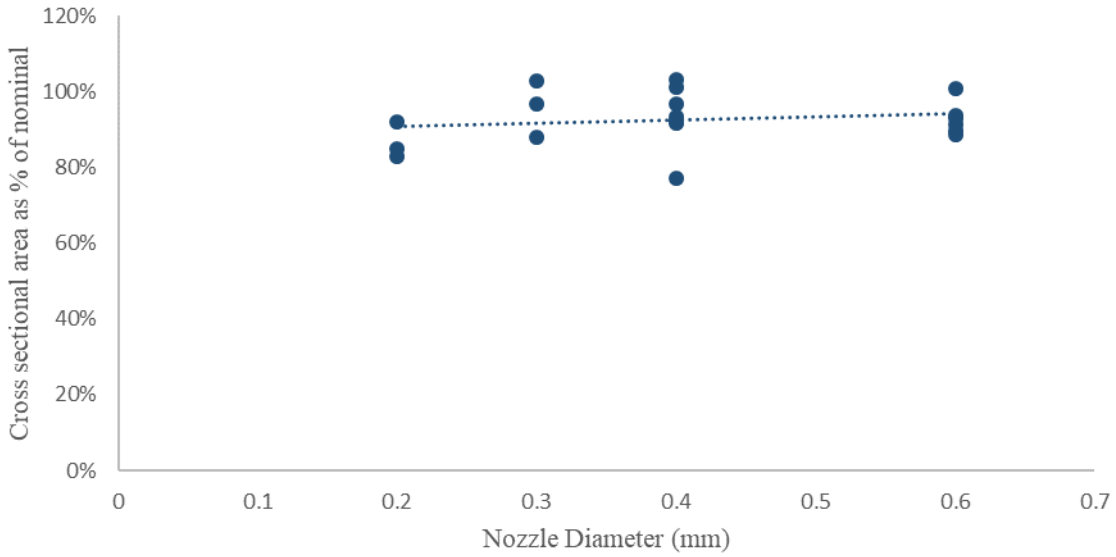

Figure 5.11 *Relationship between nozzle diameter and cross-sectional area as a percentage of the nominal value*

Considering each nozzle diameter separately, as in Figure 5.12, reveals a peak extrusion rate at a mid-range value for all 4 nozzle diameters.

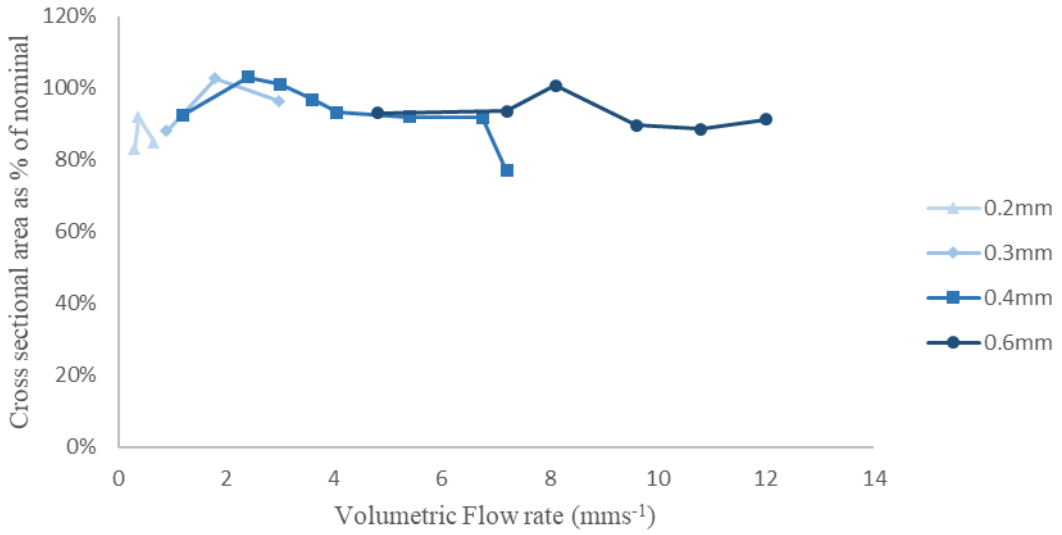

Figure 5.12 *Relationship between volumetric flow rate and cross-sectional area as a percentage of the nominal value for 0.2-0.6mm nozzles*

This suggests that insufficient force is applied to reach the desired volumetric flow rates for both high and low values. The drop at higher flow rates may be explained by insufficient thermal transfer to the melt at high rates leading to higher viscosity material and higher pressure drop and required extrusion force. At lower flow rates, this again suggests that insufficient force is being generated. This could be due to the lower shear rates experienced in such flow and therefore increased viscosity of the melt.

There appears to be a ‘sweet spot’ where the flow rate is very close to that expected between experiments 6 and 9, all of which are printed at a layer height of 0.2mm. For these parameters, it is clear that the melt is receiving sufficient thermal energy within the liquefier and that the extrusion force provided by the stepper motor and the drive wheels is sufficient for the flow rates and 0.4mm nozzle.

The inner perimeters in the double and triple perimeter experimentation often suffer from severe under-extrusion. This means that adjacent perimeters exhibit no inter-perimeter bonding, which would lead to significantly reduced component strength. This is due to the increased print speed and hence increased flow rate required, as this is the only variable that differs with the slower outer perimeter. In some examples, the inner perimeters could not be printed at twice the outer perimeter speed without complete fabrication failure (i.e. the rate limit was being exceeded). Where the print speed for all perimeters were equal, such as experiments 1, 2, 5 and 20, there is very strong uniformity between the perimeters as would be expected. However, for large volumetric flow rates with differential print speeds such as those in 14, 15, 16, 17 and 19, the inner perimeters exhibit significantly lower cross-sectional areas than dictated by the G-code (although in most cases, not outright print failure).

Between experiments 14 to 20, only experiments 18 and 20 show good rates of extrusion. This is likely because 18 is the lowest flow rate for the larger 0.6mm nozzle, which reduces the force required for extrusion. This suggests that the outer perimeter was not close to the rate limit of the process, unlike for the other combinations of flow rate, layer height and nozzle diameter. Similarly, the print speed was necessarily reduced to 900mmmin^{-1} for experiment 20 for both outer and inner perimeters, as the print suffered complete failure at the speeds used for the other experimental runs.

Layer heights are in all cases very close to the nominal value for all perimeters. This is unsurprising, as this is over a small length scale and all movements in the Z direction are without backlash since there are no direction changes.

Horizontal deviations against the nominal outer surface are small in all cases, never exceeding 0.04mm. The value of these deviations increases as layer height increases. The source of these deviations must be either from positional error or extrusion rate irregularities. The fact that they increase with increasing layer height (and therefore volumetric flow rate) suggest that the extrusion rate is the dominant factor. Another observation is that the highest values tend to occur for low aspect ratios. This is likely due to post-deposition movement owing to low bond widths between layers.

Bond widths can be seen to be highly dependent on the predicted road width as is expected. The bond widths are therefore proportional to the volumetric flow rate (or cross-sectional area) divided by the layer height, as shown below in Figure 5.13.

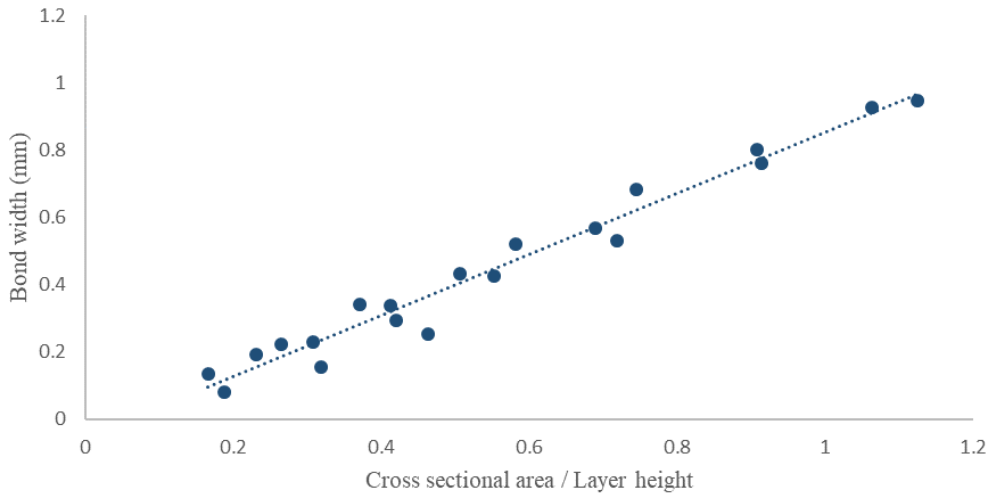

Figure 5.13 *Relationship between cross-sectional area/layer height and bond width*

A model is developed in the following subsection to describe this relationship in greater detail. As with bond widths, road widths also scale in proportion to the extruded area and layer height. This behaviour is captured by the same model.

The surface roughness measurements outlined in Section 5.2 increase with increasing layer height. Given that the outer perimeter is often modelled as an arc or semicircle, it is congruent with these models to find this relationship. Values of Ra/Rq range from approximately 0.007-0.010mm for the 0.1mm layer height to 0.030-0.045mm for a layer height of 0.4mm. Within fixed layer heights, these measurements tend to slightly decrease with increasing volumetric flow rate. This is shown in Figure 5.14 for Rq.

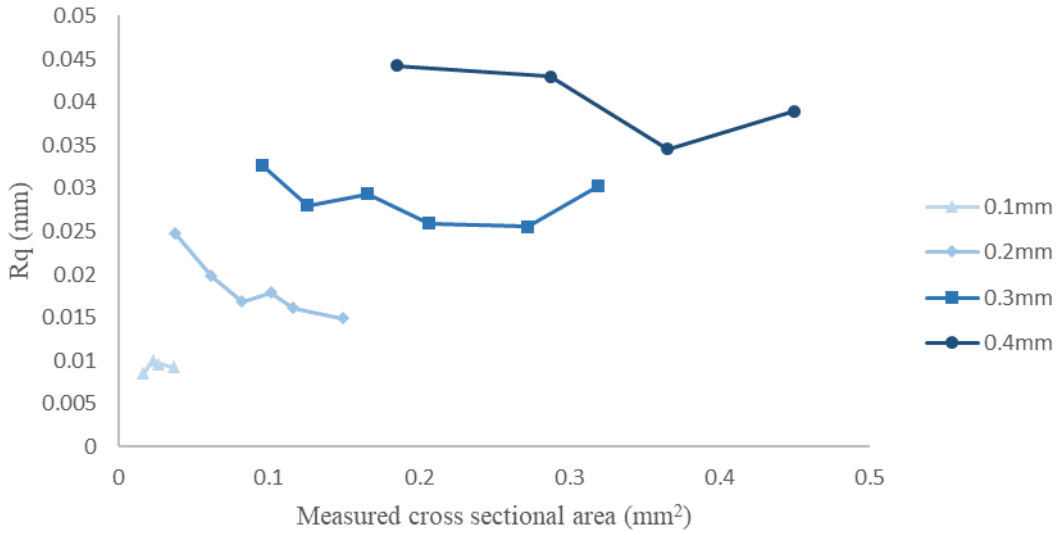

Figure 5.14 *Relationship between cross-sectional area and Rq*

This also suggests that for interacting filaments, the surface roughness should be slightly improved on the outer perimeter as an inner perimeter is similar to the melt flow of a deposition with a higher aspect ratio. This will be explored in the filament geometry models in the next sub section.

Figure 5.8 and Table 12.7 in the Appendix show a comparison between the PLA used throughout the rest of this experimentation and another popular ME AM material, ABS. For this, the default *CURA* settings were used for ABS. The only changes versus PLA in this regard are the temperatures, where a bed temperature of 80°C and print temperature of 240°C were used instead. The dual perimeter experiment number 7 was selected for comparison, which corresponds to the default layer height and road width assumptions included in the slicer. Comparing the two materials, it is clear that the extrusion rate is slightly lower for the ABS, despite its nominal value being the same. This results in slight reductions in road and bond width and inferior surface roughness. Given this, it is likely that a higher print temperature than the default value would yield improved results for ABS. Nonetheless, the deposited morphology appears very similar, suggesting the steady state analysis conducted in this section would be applicable to ABS as well as PLA, especially if compared to measured volumetric flow rates rather than nominal.

Where the measured extrusion rate is high enough for the inner perimeters, a good degree of bonding between perimeters is observed. In some cases, there are little or no voids between the perimeters, such as in the double and triple perimeter experiment numbers 7, 8, 9, 10 and 15. In order for this to be the case, the inner perimeter volumetric flow rate must be close to the expected value to give a road width wide enough for inter-perimeter interaction.

For more limited bonding, the void shapes are diamond in nature as in, for example, experiments 14 and 17. However, as the inner and outer perimeters have cross-sectional areas closer to the nominal value, the degree of bonding increases. This phenomenon is described by Gleadall et al. [352], Serdeczny et al. [306] and Kasim et al [373]. In such bonding, the upper half of the filament which is deposited second is deformed into the adjacent layer. In more extreme examples, this changes the diamond-shaped voids to triangular as displayed in experiments such as 7, 9 and 11. For low aspect ratios, this has the effect of distorting the subsequent filament significantly, such as in experiment 5, where the outer perimeter appears rotated.

Where a single colour of filament is used it is difficult to detect the boundaries between perimeters. Specific experimentation was therefore undertaken using multiple colours of filament. Initial attempts at creating a multi-coloured filament via thermal or adhesive joins of short sections of filament proved problematic, where the joins often interacted with the drive wheel mechanism leading to print failures. Instead, short sections of 41mm were manually fed into the drive mechanism as deposition was taking place. Between layers, a sacrificial geometry was produced to allow for colour changes away from the region of interest. The manual interaction with the gantry and filament extrusion mechanism was expected to lead to extrusion and layer height variability, but in the context of this experimentation this was considered beneficial as it would provide a range of filament interaction scenarios. The results from this experimentation are shown in Figure 5.15.

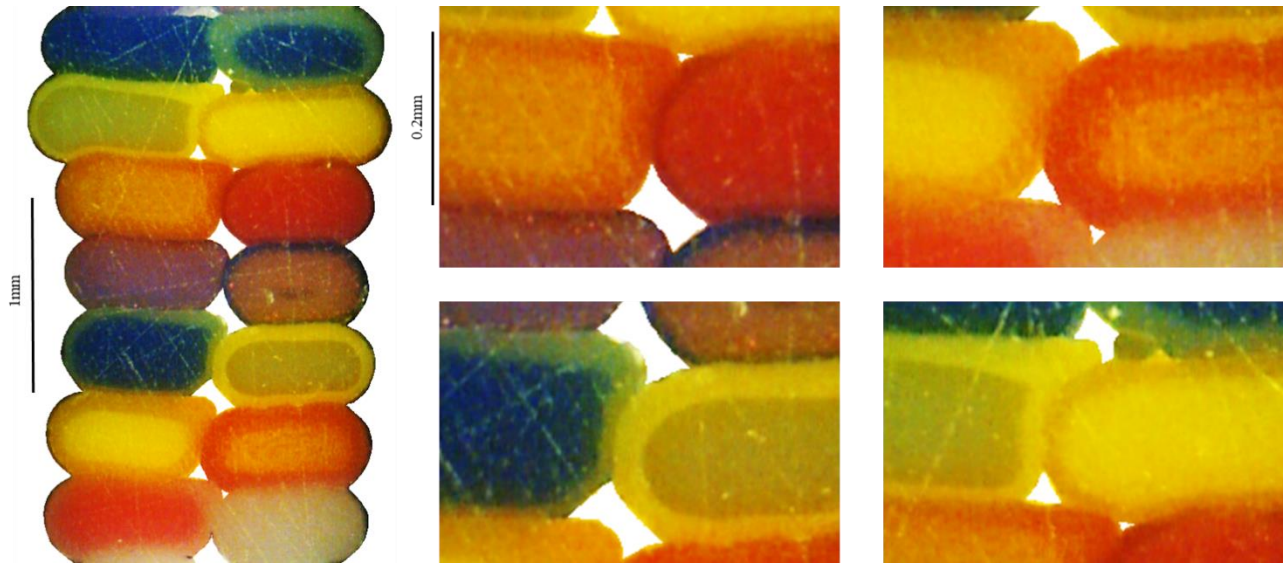

Figure 5.15 *Dual perimeter morphology*

This clearly shows that where filaments in adjacent perimeters interact, the filament which is deposited second deforms around the first. Where the layer height is reduced or the extrusion rate is slightly higher, the filament interaction is more marked such as layers 2 and 6. This manifests as a greater deformation in the upper half of the layer and a full transformation from diamond to triangular void morphologies. This figure also suggests that there is limited melt flow between strands both between layers and perimeters.

An interesting feature observed in the multicolour image is the variable colour gradient within the strand cross-section. The colour order of deposition was: red, orange, yellow, green, blue, purple. As a result, it can be seen that the earliest deposition of each colour is at the centre of the strand, with the final elements of that colour section then deposited around the outside of the next strand. Bellini et al. [309] noted that melt adheres to the walls, which is what gives rise to the shear deformation during the flow which was discussed earlier in Section 5.1.3. Zhou et al. [329] assumed a uniform temperature across the extruded cross-section. However the outer colour ring demonstrated above suggests this is not the case because the latest-deposited filament has spent longer in the melt chamber and is therefore likely to be hotter, especially when close to process rate limits at higher extrusion rates.

Heller et al. [374] used a non-uniform velocity profile with a no-slip condition at the walls in their modelling of fibre reinforcement alignment, which would be consistent with the observations made here. Similarly, Peng et al. [316] introduced die markers to show the filament flow within the liquefier. They concluded that the velocity profile is far from an isothermal power law solution and presented results congruent with those above.

5.4.2. Single Filament and Outer Surface Models

There have been a large number of models to empirically describe a single deposited strand shape or the outer surface of a ME AM component. It is common for these to consider either semi-circular elements or arcs as the outer face of each layer. From observations of the cross-sections taken in Figures 5.5 to 5.7, it is clear that an arc-based model is most suitable. Prior models have not distinguished between single and multiple adjacent perimeters, nor have they considered a wide range of layer heights and volumetric flow rates. The models developed here shown general applicability for layer heights of between 0.1 and 0.4mm and nominal road widths from 0.2 to 1.2mm. The proposed filament morphology model is shown below in Figure 5.16.

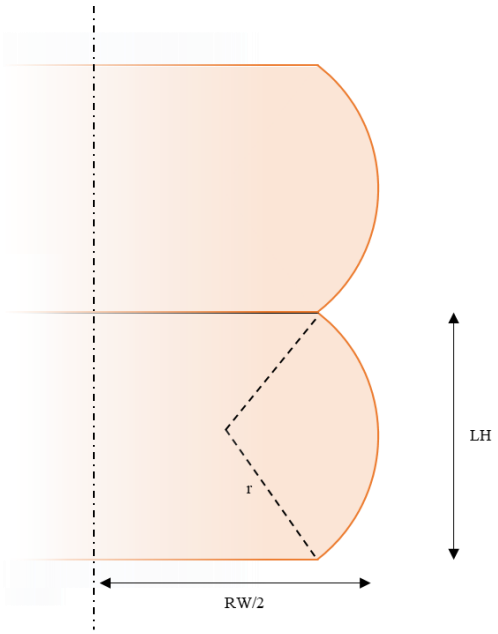

Figure 5.16 *Proposed filament morphology model*

This describes each layer as having a road width, *RW* (to be calculated later), an arc of radius *r*, and a layer height *LH*.

5.4.2.1. SINGLE PERIMETER

For the single perimeter case, the average distance between the five measured road widths and four measured bond widths was calculated for each experimental run. This gives the arc height, which can then be converted to an arc radius r given it is modelled as producing a segment equal to the layer height, LH. Normalising this value of r against the LH and plotting against the aspect ratio gives the relationship shown in Figure 5.17 and Equation 7.

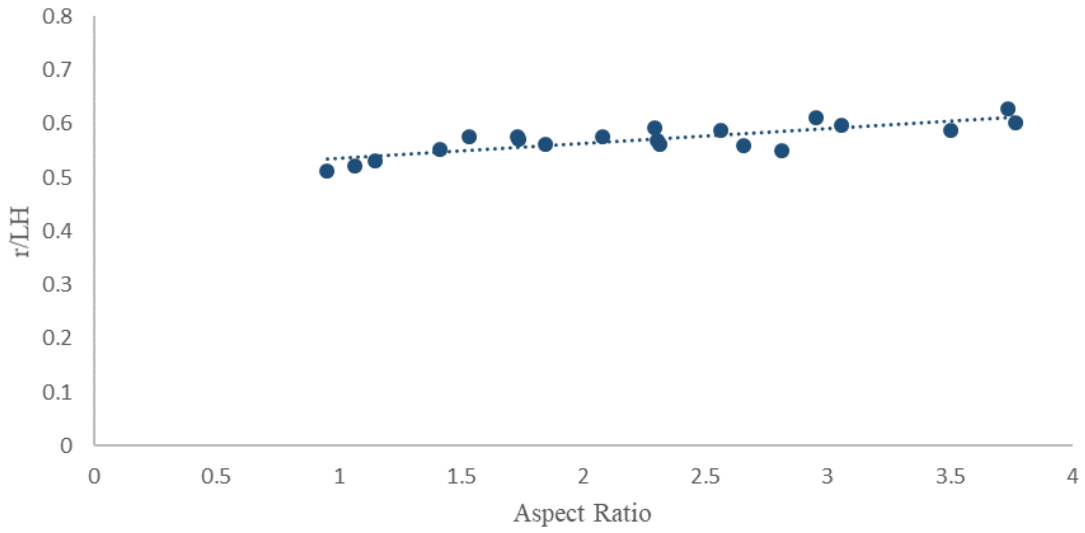

Figure 5.17 *Relationship between aspect ratio and radius of curvature divided by layer height for a single perimeter*

$$r = LH[(0.0273 \times AR) + 0.5091]$$

Equation 7 *Radius of curvature for single perimeter*

Where; r is the arc radius of curvature, LH is the nominal layer height, assumed to also be deposited layer height and AR is the Aspect ratio, defined as nominal road width divided by layer height, assuming 100% flow rate. Through geometrical analysis, it can be shown that the resulting road width is given by Equation 8.

$$\boldsymbol{RW = \frac{1}{LH}\left[(LH \times RW_{nom}) - \left(r^2\left(cos^{-1}\left(1 - \frac{LH^2}{2r^2}\right) - sin\left(cos^{-1}\left(1 - \frac{LH^2}{2r^2}\right)\right)\right)\right] + 2\left(r^2 + \sqrt{r^2 - \frac{LH^2}{4}}\right)}$$

Equation 8 *Single perimeter road width calculation*

Where *RW* is the actual deposited road width, RW_{nom} is the nominal road width (usually an input in slicer). Note that $LH \times RW_{nom}$ = cross-sectional area according to the basic rectangular model. Equation 8 can therefore also be rewritten in terms of the volumetric flow rate through the replacement of the $LH \times RW_{nom}$ term with the volumetric flow rate (units: mm^2 per mm of travel). The actual road width is therefor considered to depend on the layer height, volumetric flow rate and nominal aspect ratio only.

5.4.2.1. DOUBLE AND TRIPLE PERIMETERS

Repeating the approach taken for the single perimeter, but this time calculating the side segment height from a vertical reference plane aligned with the outer perimeter gives the results shown in Figure 5.18 and Equation 9. To calculate these, only experimental runs with significant inter-perimeter interaction were included.

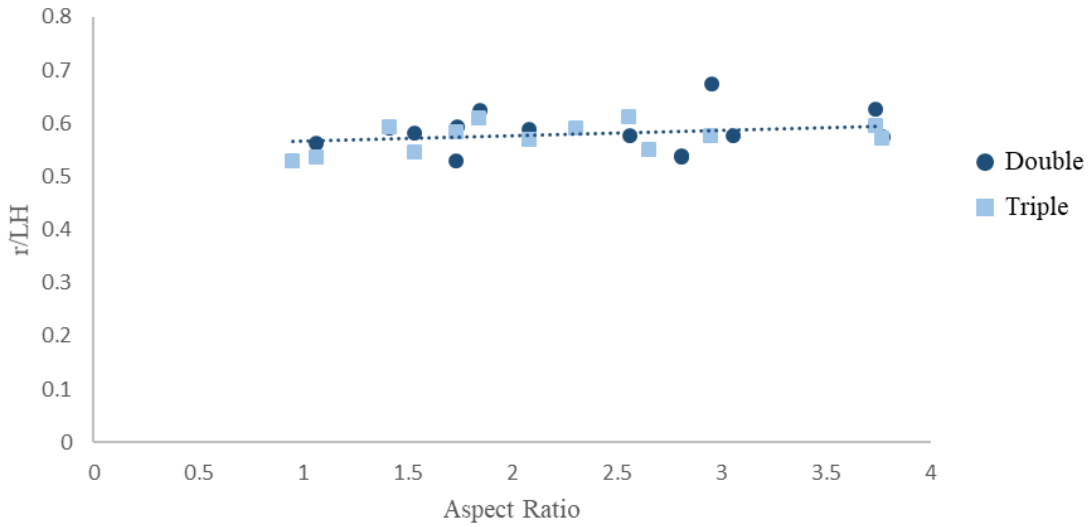

Figure 5.18 *Relationship between aspect ratio and radius of curvature divided by layer height for a double and triple perimeters*

$$r_{multi} = LH[(0.0106 \times AR) + 0.5549]$$

Equation 9 *Radius of curvature for multiple perimeters.*

As was hypothesised earlier, this does indeed give a higher arc radius and therefore slightly improved surface roughness metrics. The individual equations governing both double and triple perimeters are shown below, and show a good degree of agreement with each other.

$$r_{double} = LH[(0.011 \times AR) + 0.5613]$$

Equation 10 *Radius of curvature for double perimeter*

$$r_{triple} = LH[(0.009 \times AR) + 0.5518]$$

Equation 11 *Radius of curvature for triple perimeter*

5.4.3. RATE LIMITS

What exactly constitutes a rate limit of the process depends on the metric considered. In the literature discussed in Section 5.1.3, the term is usually applied to the maximum volumetric flow possible for a specific set of parameters. However, if this simply results in filament slippage or missed stepper motor increments it is possible that for high nominal volumetric flow values, a component is nonetheless 'successfully' fabricated. Previous sections have shown that actual volumetric flow rates for the ME AM machine used in this section are consistently below the nominal value, and so with respect to the perimeter experimentation a rate limit is considered the rate at which complete print failure occurs (i.e. deposition is so unstable as to not produce a useful component). Nevertheless, it is noted that rate limits as defined by the nominal volumetric flow values are reached before this point in most cases.

An initial observation of rate limits is possible from the single and double perimeter experimentation. Where the print speed had to be reduced to avoid complete print failure, it can be assumed that the process rate limits were reached. In these cases, the layer height does not appear the most important factor, but rather nozzle diameter and volumetric flow rate. For the 0.2mm nozzle, print failure were observed if any layer height and road width combination was attempted at a print speed of 1800mmmin^{-1}. This translates to a volumetric flow rate limit of approximately 0.66mm^{3}s^{-1}, above which the rate limit is reached. No 0.3 or 0.4mm nozzle speed reductions were required, though observation of the multi-perimeter images in Figures 5.6 and 5.7 suggest that the limit is close to being reached in some experimentation where poor inter-perimeter bonding is observed. In the worst case for the 0.4mm nozzle, a nominal flow rate of 7.2mm^{3}s^{-1} for the outer perimeter was possible in experiment number 17, though the measured flow rate via the actual cross-sectional area was some 25% lower suggesting close proximity to print failure. Indeed, the multi-perimeter examples for this experiment show no real inter-perimeter interaction. For the 0.6mm nozzle, the rate limit was reached only on the final experimental run. This run corresponded to a volumetric flow rate of 14.4mm^{3}s^{-1} with a speed of 1800mmmin^{-1}. The highest volumetric flow rate for this nozzle diameter which did not result in complete deposition failure was 12.0mm^{3}s^{-1}, though this did result in a 10% reduction in measured cross-sectional area versus the nominal value, corresponding to an actual flow rate of approximately 10.8mm^{3}s^{-1}.

The two-part experimentation included in Section 5.4.3 demonstrates that a nominal rate limit is reached after which prints remain successful but at a constant actual volumetric flow rate. Where the extrusion rate is increased at a constant speed, the measured road width (a proxy for actual volumetric flow rate and calculable via the model presented in the previous sub section) increases linearly up to a nominal volumetric flow rate of approximately 15mm^{3}s^{-1}. Above this rate, the road width no longer increases, suggesting that a maximum physical volumetric flow rate is achieved. In the scenario where speed is changed rather than the nominal cross-sectional area the measured road with displays a slight decay for all nominal volumetric flow rates. It again reaches a plateau at approximately 18 mm^{3}s^{-1}. This higher value is likely due to the lower counter-pressure from the deposited filament, as described by Percoco et al. [364]. If there are identical conditions within the liquefier itself (i.e. regardless of how the volumetric flow rate is desired – to achieve a large deposited cross-section at slow speed or smaller cross-section at high speed), the feeding rate and thermal history of the filament should be the same. It is instead hypothesised that at increasing print travel speeds, the initial extrusion process has not reached a steady state by the position of measurement which gives rise to lower observed road widths. This is further evidenced by the fact that of the three measurements taken across the sample, the measurement furthest from the beginning of the deposited strand was usually the largest. This same delay would occur before the period of measurement in the first experimental approach.

5.4.4. COMPONENT ACCURACY IMPLICATIONS

As discussed at the beginning of this section, the outer perimeter toolpath is created by offsetting from the nominal perimeter by half of the predicted road width and therefore road width deviation will directly translate to dimensional and geometrical error. The experimentation in this section suggests two major sources of error. First, for a given volumetric flow rate there may be a difference between the actual deposition morphology/road width and that assumed in the slicer. Second, differences between the nominal and actual volumetric flow rates will lead to road width errors of the deposited strand.

For the former, a model was proposed and experimentally validated for both single and multiple perimeters. If it is assumed that the lateral positioning of the outer perimeter is unaffected by the presence of inner perimeter(s) (likely valid if some internal voids remain), then both surface models can be directly compared with the slicer assumptions. For the default *CURA* parameters with a layer height of 0.2mm and road width of 0.4mm the expected road widths according to the models developed in Section 5.4.2 are 0.435mm and 0.434mm for single and multiple perimeters respectively. This translates to an oversize error of approximately 0.035mm across a component (half the road width error, encountered once on each surface) when compared to the *CURA* filament model, although this will of course be a much less significant error if compared to the semi-circular side profile model used by some other slicer.

Under-extrusions of up to approximately 20% were observed during the perimeter experimentation when operating at or close to process rate limits. However, to again consider the default *CURA* settings, an oxer-extrusion was in fact observed. Any extrusion deviation may be translated to road width error via the filament model. This suggests that the 3% over-extrusion under default conditions leads to a total error of approximately 0.012mm (neglecting the minor effect of a changed aspect ratio).

Combining these two errors gives a total error of approximately 0.047mm for default printing conditions. However, it should be noted that this error is likely to be larger for higher layer heights and volumetric flow rates, should these be selected.

Precision performance was not explicitly addressed in this experimentation. As with the accuracy errors presented above, variability can also arise from either volumetric flow rate or strand morphology for the same. The low deviation of data points against the developed linear equation in Figure 5.17 suggests very low variability of shape for the same cross-sectional area. Instead, any road width precision error is more likely to arise from volumetric flow rate variability. Golab et al. [360] investigated the repeatability of strand cross-sectional areas and road widths for single strand depositions at standard print parameters. This demonstrated that under steady state conditions, variability was minimal but that at the beginning end of depositions the precision error was increased.

6. XY PLANE GEOMETRICAL PERFORMANCE

As previously mentioned, component dimensional error can be considered to arise directly from errors in the outer perimeter. In Section 3, potential sources of error that affect the outer perimeter were hypothesised. Broadly, these were those related to positional error as investigated in Section 4 and extrusion-related errors. The previous section investigated steady-state deposition error for a wide range of printing conditions. This section covers in-layer XY plane deposition errors through corner and weld experimentation.

The use of machine code within the ME AM process was outlined in Section 5. This described that the nozzle is moved in XYZ space in conjunction with extrusion length commands. Implicit in this process is a nominal outer perimeter of each layer, produced by the combination of the toolpath and extrusion width for the external perimeter. This section therefore explores this combination and compares the results to the desired nominal geometry.

Whereas previously layer heights and volumetric flow rates were varied between experimental runs, this experimentation focuses on the errors arising under standard printing parameters in line with the errors experienced in the components fabricated in Section 3.

6.1. XY PLANE DEPOSITION

Slicers assume a constant road width and therefore constant volumetric flow rate regardless of printing conditions. As an example, a straight movement of 10mm at a print speed of $10mms^{-1}$ with an extrusion rate of $10mm^3s^{-1}$ would yield a total extruded volume of $10mm^3$. For simplicity, assuming a layer height of 1mm and the standard rectangular strand morphology model would yield a nominal constant road width of 1mm. A hypothetical 10mm square perimeter with the same parameters would theoretically yield a hollow square section with a wall thickness of 1mm in all locations, although the toolpath would be a 9mm square to ensure the outer perimeter maintains dimensional performance. The previous steady-state experimentation explored the validity of this under consistent movement conditions. However, in order to complete a closed perimeter, direction and therefore speed changes must occur. Any mismatch between the extrusion profile and movement will directly lead to error. Every point of over-extrusion must necessarily be matched by underextrusion elsewhere assuming the entire nominal volume is deposited across the toolpath. Similarly, deviations between the nominal nozzle path and actual path will also contribute to error. Extant literature regarding direction change error and movement-extrusion errors are included within this subsection.

Yardimci [368] conceptually divided the deposition process into five separate segments. These were: pre-movement, start-up, steady-state, slow-down and exit-move. As mentioned above, previous experimentation in Section 5 explored performance in the middle, steady-state region. Bellini et al.

[309] developed a detailed fluid and melting model within the liquefier. They added further detail to the five stage model;

I. Pre-movement: a prescribed volumetric flow rate is started before the deposition begins. A glob of certain size is generated to compensate for the intrinsic deposition delay, due to the internal length of the liquefier, which is the distance between the point of application of the pressure and the point of the material delivery.

II. Start-up: as soon as the motion starts, an absolute flow-rate, higher than the steady state flow rate, is established and maintained throughout the acceleration phase;

III. Steady-state: once the acceleration phase is complete, a constant flow rate is specified;

IV. Slow-down: the main flow rate is stopped and a certain amount of material ~empirically determinated [sic] and dependent on the deceleration constant and the steady state flow rate is brought back revolving the motion of the rollers;

V. Exit-move: the flow control is turned off and the nozzle is moved to a pre-specified distance from the last point of the toolpath in order to avoid any further interferences.

They showed that this process led to irregularities in a typically deposited strand. Specifically, they noted a zone of under-extrusion at the beginning, in the acceleration phase and over-extrusion at the end during deceleration. They stated that in order to overcome these effects, better correlation between the deposition speed and volumetric flow rate must be achieved. Given the need to understand the dynamics of the extrusion process in order to control it, they then developed a transfer function approach to be integrated as part of improved flow control and therefore improved part quality.

Ravi et al. [375] undertook experimental investigations of strand width using a variety of layer heights and temperatures. Prior to the measurement of the strand of interest, they included ‘initialization’ and ‘transition’ regions. These clearly displayed the non-linearity of volumetric flow rate and road width with position, though the authors did not investigate the phenomenon further instead concentrating on the steady state region that followed. Similarly, the over-extrusion at corners was observed by Mohamed et al. [376] and Galantucci et al. [19], though not explicitly addressed. García Plaza et al. [377] investigated corner swell at 90^{o} corners, and reported geometrical errors of approximately 0.15mm though did not state the machine or slicer used. Han et al. [378] considered the interaction between the position of the nozzle and the material deposition process, using a toolpath-based approach to plan extrusion commands. In this study, extrusion rates are assigned to each group with similar vector length sections by using grouping and mapping algorithms. They demonstrated the feasibility of the approach through experimentation on an ME AM machine. In a subsequent study, Han and Jafari [379] also explored this behaviour and investigated another potential solution. They

proposed a coordination controller which tracks the movement speed within the XY plane in real time and regulates the volumetric flow rate accordingly. They conducted simulations of this proposed approach which suggested significant improvement in the layer quality of fabricated components. Ertay et al. [380] presented an integrated methodology for the planning of path velocity volumetric flow rate and temperature control along curved paths. The volumetric flow rate is controlled proportionally to the path velocity whilst maintaining temperature constant via adaptive control of the liquefier. This was experimentally verified to show more uniform deposition at sharp curvatures thus directly leading to improved dimensional accuracy. Pollard et al. [381] showed overshoots of liquefier temperature for both PLA and ABS when dealing with step changes in extrusion rate and around retractions, suggesting that for their experimental setup the process was not well controlled.

Tronvoll et al. [382] investigated the use of pressure advance algorithms to compensate for the under and over extrusion known to occur during the acceleration and deceleration phases. The algorithms presented were first simulated then tested on a Prusa i3 desktop ME AM machine. It was demonstrated that such algorithms have the potential to substantially increase the dimensional accuracy of the ME AM process but that if not properly configured, they may affect performance negatively. They investigated the effect of layer height and found significant differences meaning optimal parameters would need to be found for each. They also stated that there remains uncertainty as to how the algorithms presented are affected by common process parameters including material, print temperature and nozzle geometry. While such approaches show promise, they remain unused by many popular ME AM machines today and would require further work to be effective across a wide variety of print conditions.

Comminal et al. [383] used computational fluid dynamics to simulate material deposition at 30^{o} and 90^{o} sharp corners. They considered modification of the toolpath itself by rounding corners subject to a maximum acceleration. The internal and external corner under and over extrusions were quantified, including those arising from double deposition with an implied uniform road width. With suitable toolpath changes, significant improvements were predicted leading to constant extrusion rates and road widths. Gilberti et al. [384] also presented a technique based on Bézier curves to ensure constant feed rates for direction changes. They proposed combinations of straight lines and parabolas to guarantee uniform material deposition, effectively introducing rounded corners to reduce the acceleration and deceleration effects associated with sharp corners. It was found that this would have general applicability to other extrusion-based processes, and was experimentally validated with a gluing deposition system.

Friedrich and Begley [385] investigated these same behaviours in the direct ink writing process. They similarly noted the presence of corner swelling (i.e. over-extrusion), but also discussed the geometry

of these areas. In particular, they highlighted that the internal area tends to produce a radius which increases due to the Laplace pressure differential between the inner and outer surfaces.

Weiss et al. [294] demonstrated deviations between the nominal and actual toolpath of up to 1mm and showed significant improvements were possible through the use of closed loop control. Jin et al. [386] demonstrated three separate models for the filament deposition and nozzle trajectory. A tractrix, parabola and catenary model were compared with experimental results and it was found that the tractrix model showed the greatest agreement. They then modelled the nozzle path for three depositions; a straight line, circle and arbitrary curve. This showed an offset between the nozzle path and the actual point of material deposition. Although a discrete corner was not modelled, this same offset would be present. Bouhal et al. [387] developed a tracking-control and trajectory-planning model which looked ahead to reduce path errors and under and over fills. However, their model assumed a constant volumetric flow rate with respect to travel speed and therefore ignored motion-extrusion related errors. Prša et al. [388] proposed a positional algorithm to improve areas which exhibited under-extrusion such as narrow edges and sharp corners through the optimisation of the toolpath whilst holding the extrusion rate constant. Kuipers et al. [389] developed a framework for adaptive width control to aid the fabrication of contour-parallel extrusion paths. Under standard extrusion methods, the presence of over and under-filled regions are detrimental to the mechanical performance of components. In this study, they proposed a novel scheme to produce superior density parts and physically validated the approach through the development of a technique called ‘back pressure compensation’. Similarly, Eiliat and Urbanic [390] demonstrated the formation of voids within the layer and suggested methods to modify the deposition sequence and toolpath to minimise these.

There has been very little attention given to perimeter welds, despite their inherent presence in the process. Taşdemir [190] identified the presence of welds at sharp corners or on the perimeter of cylinders and ellipses. They determined that the weld had a significant impact on dimensional accuracy and is of importance for assembled components. They also determined that these ‘seam marks’ become more pronounced as wall thickness was increased (i.e. the volumetric flow rate increased). However, their exact deviation values were not isolated from other geometrical error around the perimeter.

6.2. METHODOLOGY

Despite the studies identified above covering the errors which occur at corners, the majority have dealt with theoretical modelling and simulations for improvement solutions. In addition, only continuous corners are considered, whereas it is common practice for slicers to place the perimeter weld (i.e. the start and stop locations) at sharp corners to avoid over-extrusion on other flat surfaces. Finally, single deposited strands have been considered in isolation, although this is relatively rare in

practice due to the reduced component strength that it causes. The experimentation in this section therefore addresses these shortcomings. It covers angles of between 15° and 165° for double perimeters, varying the perimeter order of deposition and presence of corner welds. The effect of print speed and component orientation are also investigated. Non-corner welds are also produced and analysed, to understand the feasibility of changing the location away from sharp corners.

Solid components manufactured via ME AM consists of perimeters and infill. As has been established, the outer perimeter is critical in defining the overall accuracy of the printed part. By default, *CURA* uses two perimeters each with a nominal layer height of 0.2mm and a road width of 0.4mm, according to their standard rectangular strand morphology model (and therefore a nominal cross-sectional area of 0.16mm^2). The use of two perimeters is also supported by default in other popular slicers such as *Slic3r*, *KISS* and *MakerBot Print*.

As was mentioned in Section 5, traditional slicers is poorly suited to producing the custom artefacts needed to investigate the perimeter accuracy in isolation. As such, a custom G-code generator was again produced in *Microsoft Excel* to mimic only the outer perimeter of various slicers in terms of the toolpath, road widths and perimeter spacing, as demonstrated in Figure 12.5 in the Appendix. This custom G-code generator also allows the selection of multiple print parameters including print temperature, bed temperature, print speeds, layer heights, road width (i.e. volumetric flow rate), side length and perimeter order.

Artefacts were produced on a low cost ANet A8 desktop ME AM machine with a v1.7 motherboard running *Marlin* firmware. This is the same machine design as has been employed in previous experimentation for continuity. As was explained in Section 5.2, to aid the removal and subsequent analysis of the corner a removable acrylic slide was incorporated into a custom aluminium print bed. This experimental setup is shown below in Figure 6.1, demonstrating the fabrication of a 60° corner using a 40mm side length, as was used throughout the experimentation in this section. All prints were conducted at a print temperature of 200°C and a bed temperature of 60°C. Orange Velleman PLA filament was used in line with other experimental work in this thesis.

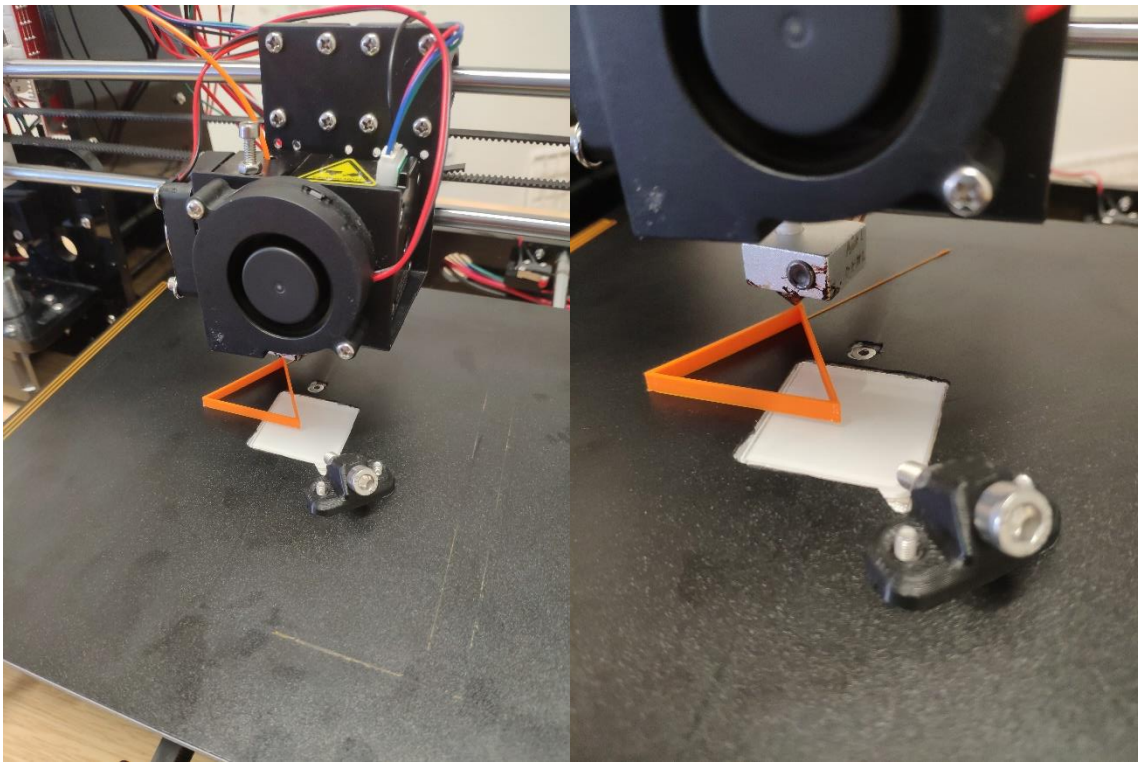

Figure 6.1 *Experimental machine setup utilising a modified print bed with removable slide on ANet A8 ME AM Desktop printer for XY plane experimentation*

In contrast to the steady state cross-sectional measurements, no cutting was required to reveal the geometry of interest. As a result it was not necessary to replicate the resin setting, cutting and polishing preparation prior to measurement. Samples were removed from the print bed and excess deposited material beyond the acrylic slide manually removed. The corner geometry was then measured using a *Zeiss Olympus BX51 TRF-6* Optical Microscope with 5x magnification.

The images were imported in *ImageJ* software, where the corner outline was detected. Reference lines were constructed using a best fit with the perimeter side away from the corner. The angle between these reference lines was checked, and found to be within 0.1^{o} in all cases. Any excess material beyond this theoretical geometrical boundary was identified, as outlined in Figure 6.2.

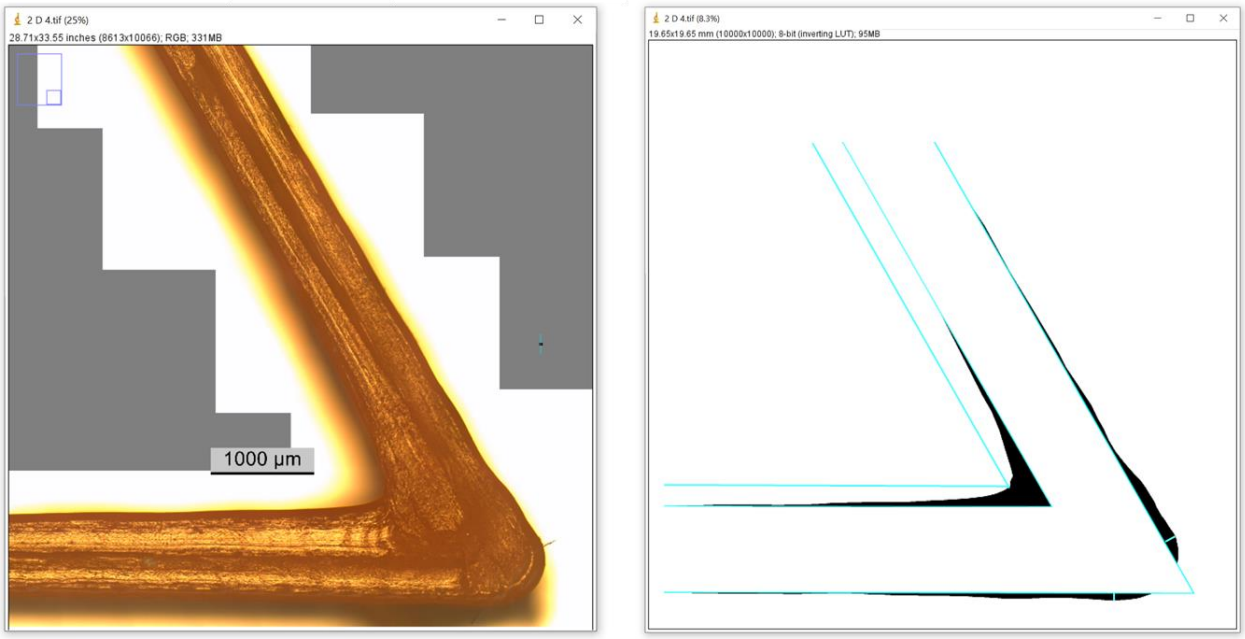

Figure 6.2 *Identification of overextruded XY material*

Figure 6.3 shows the metrics taken from the experiments for analysis. The total internal and external over-extrusion areas as viewed from above were calculated using *ImageJ*'s area calculation function. In addition, the maximum deviations perpendicular to the direction of travel were taken for the corner exterior, and maximum boundary that would fit internally as demonstrated in the figure below. In all experimental runs, the direction of travel is as indicated here (i.e. left to right in the X axis on the corner entry).

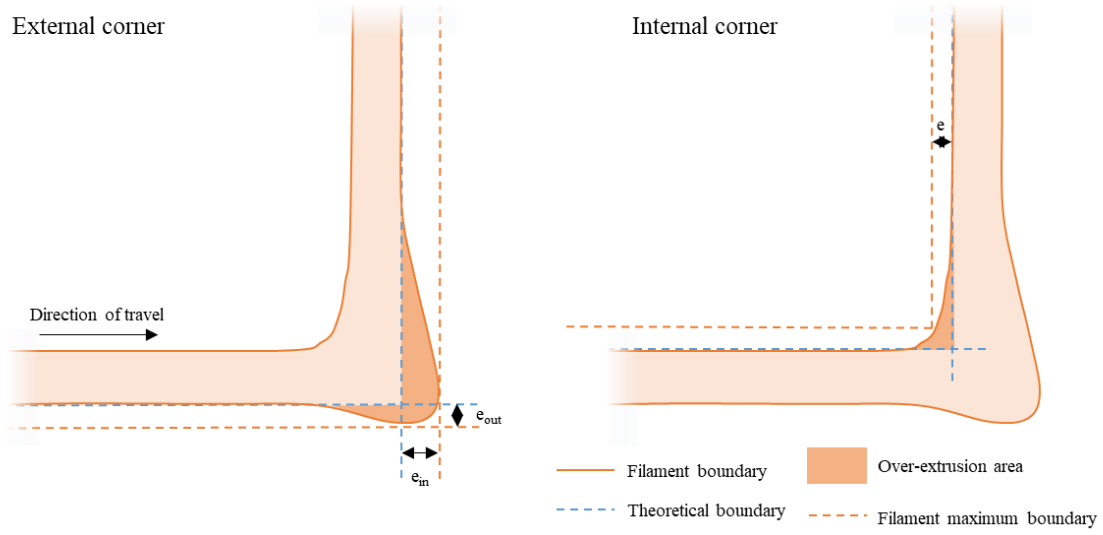

Figure 6.3 *Measured XY Plane errors*

These areas and dimensions directly inform the accuracy of the component and have implications for mating parts. The over-extrusion area cannot be converted to a volume without considering the

filament morphology as explored in the previous section, though it does help inform the nature of the error and draw comparisons between experimental runs. The internal and external metrics are captured for every experiment. In the context of this experimental work, the 'internal' corners refer to corners where the uppermost (i.e. above and to the left, as presented in the following figures) perimeter is printed last and 'external' the reverse. This is therefore effectively also a proxy term for perimeter order. The internal and external errors are quantified for both 'internal' and 'external' corners.

In addition to flow rate, print speed and perimeter spacing, the weld location and perimeter order can also be selected within the slicers. It is important to be able to quantify errors for both internal and external corners as components may exhibit a mixture of these features and where components are to be assembled, their internal and external features come into directly contact. Noriega et al. [281] measured hollow components to enable measurement of both these aspects. However, with two perimeters and a single corner feature this would not be representative in a single component perimeter as utilised in this study. By default *CURA* deposits the perimeters from internal to external in order. It uses a print speed of 3600 $mmmin^{-1}$ for internal perimeters and 1800$mmmin^{-1}$ for external perimeters. The sharpest corner is selected for the weld location although this may be changed by the user. The experimentation included in this section therefore reflects these settings. 11 angles at 15^{o} increments from 15^{o} to 165^{o} with and without welds and with alternate perimeter orders were produced giving a total of 44 unique corner parameter combinations.

Slicers enable the exact location of a weld on a perimeter to be selected, although sharp corners are used as a default to avoid unsightly vertical weld lines forming across multiple layers. Experimentation to determine the error of weld on straight sections was therefore also undertaken. The toolpaths and movement speeds for these were taken directly from *CURA*, whereby all perimeter welds are directly linked to component infill at the beginning and end of perimeters. In general terms, the first perimeter is started, then once the nozzle returns to that position, a fast perpendicular movement is made toward the next perimeter and so on.

6.3. RESULTS

Microscope images and figures that summarise the key results are included in this section. As before, full numerical results can be found in the Appendix. For each corner specimen in each array of eleven images, the deposition movement was from left to right with the bottom horizontal feature produced first, then a further straight feature at the specific angle. In most cases, the weld between the two perimeters can also be observed. These corners would typically form a section of a closed outer perimeter used to construct each layer of a three-dimensional component.

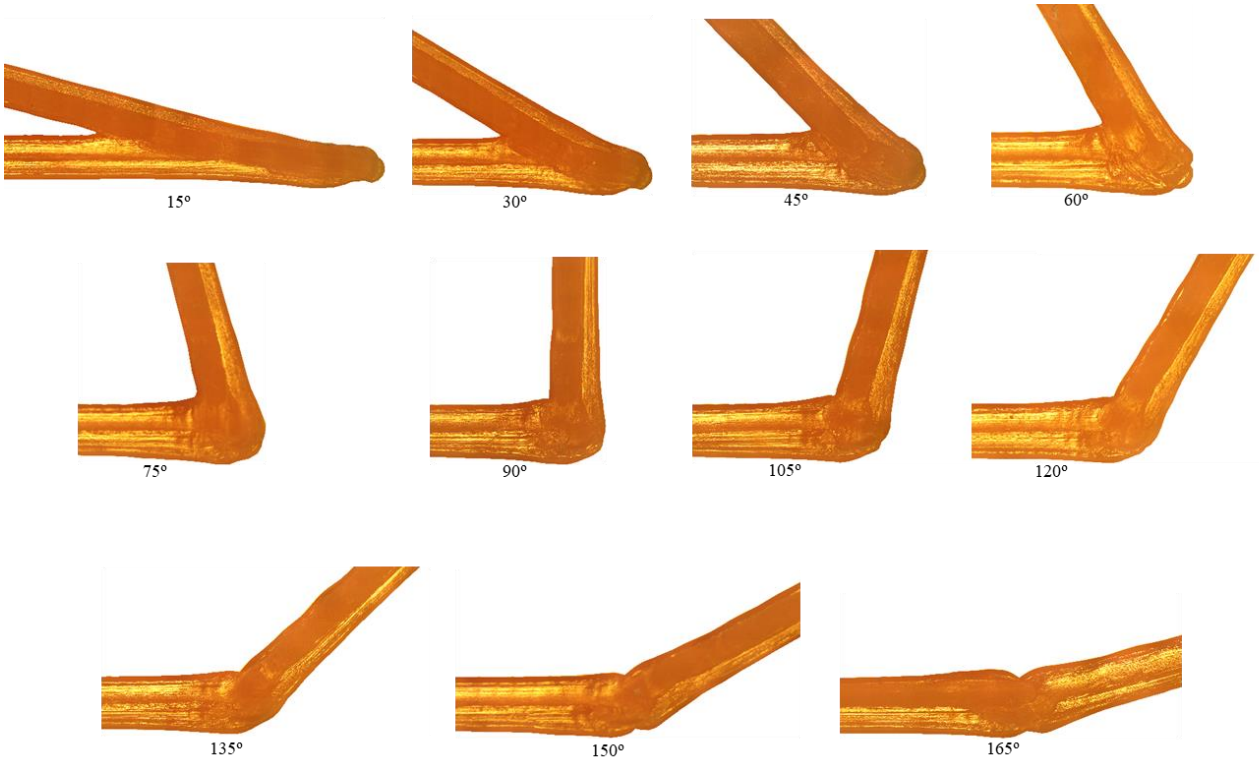

Figure 6.4 *XY Plane internal corners with weld images*

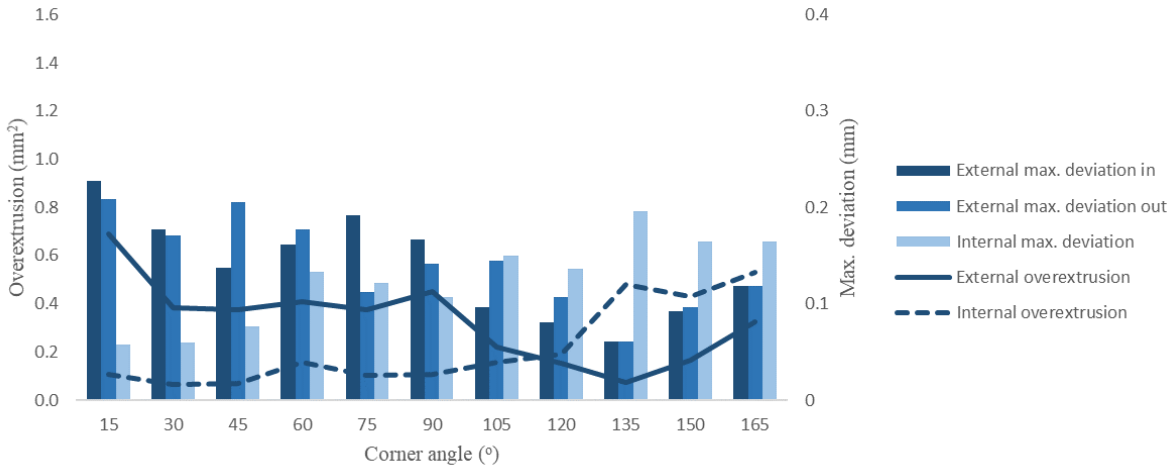

Figure 6.5 *XY Plane internal corners with weld relationship between corner angle and error values*

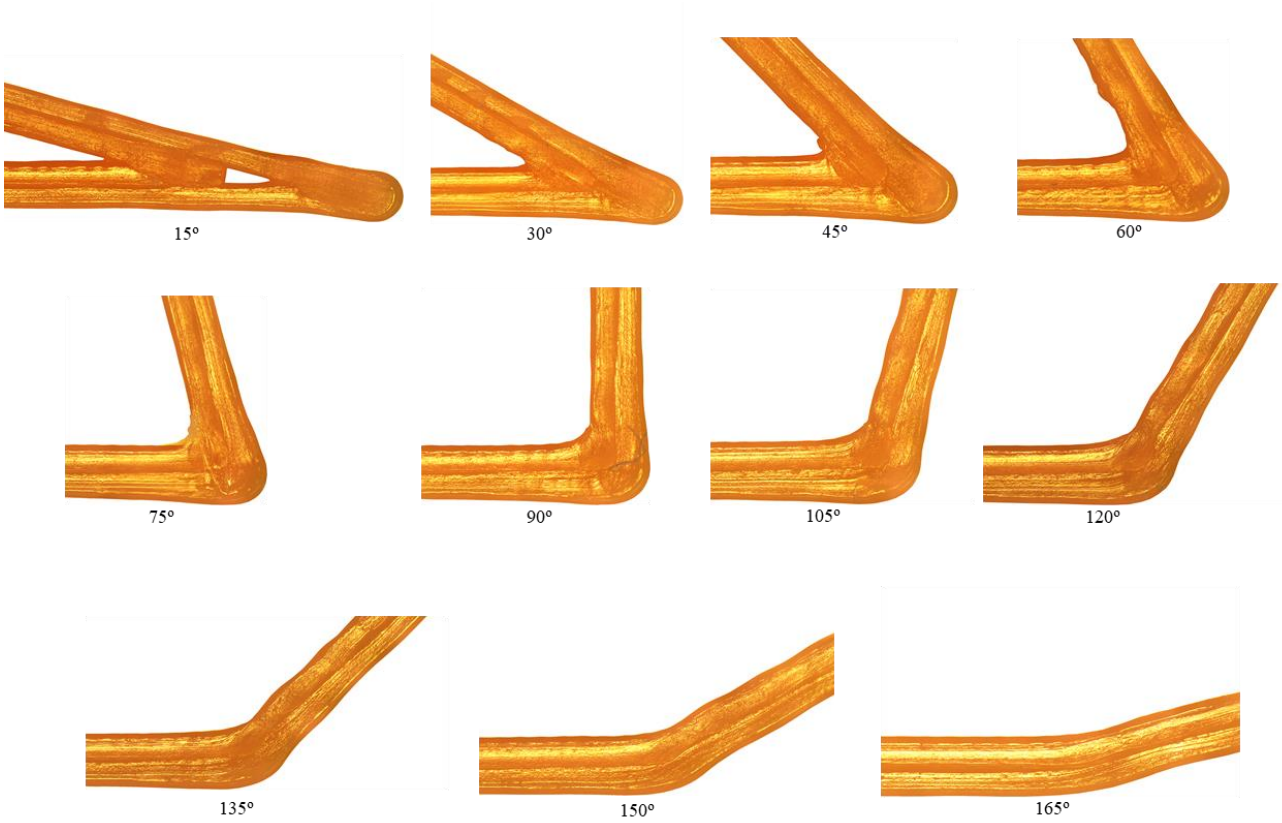

Figure 6.6 *XY Plane internal corners without weld*

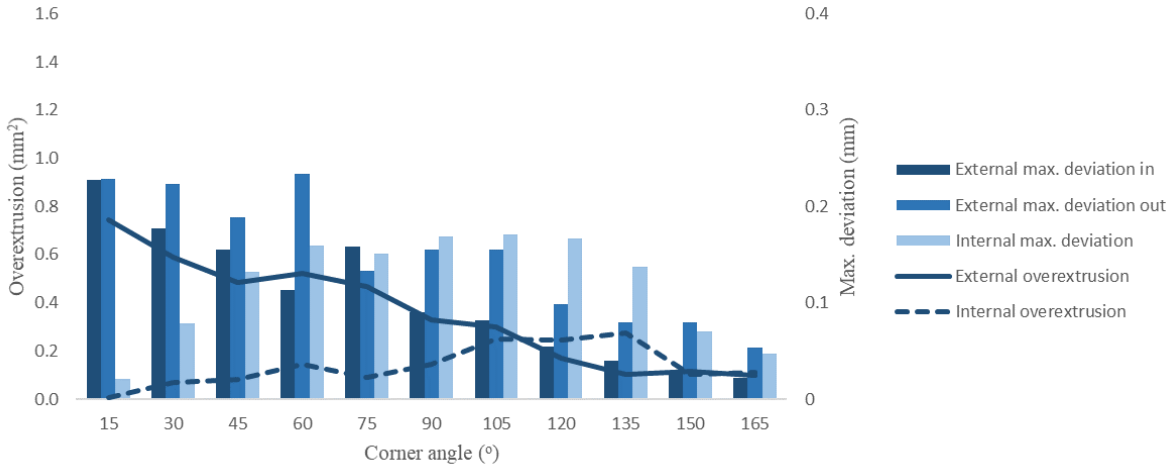

Figure 6.7 *XY Plane internal corners without weld relationship between corner angle and error values*

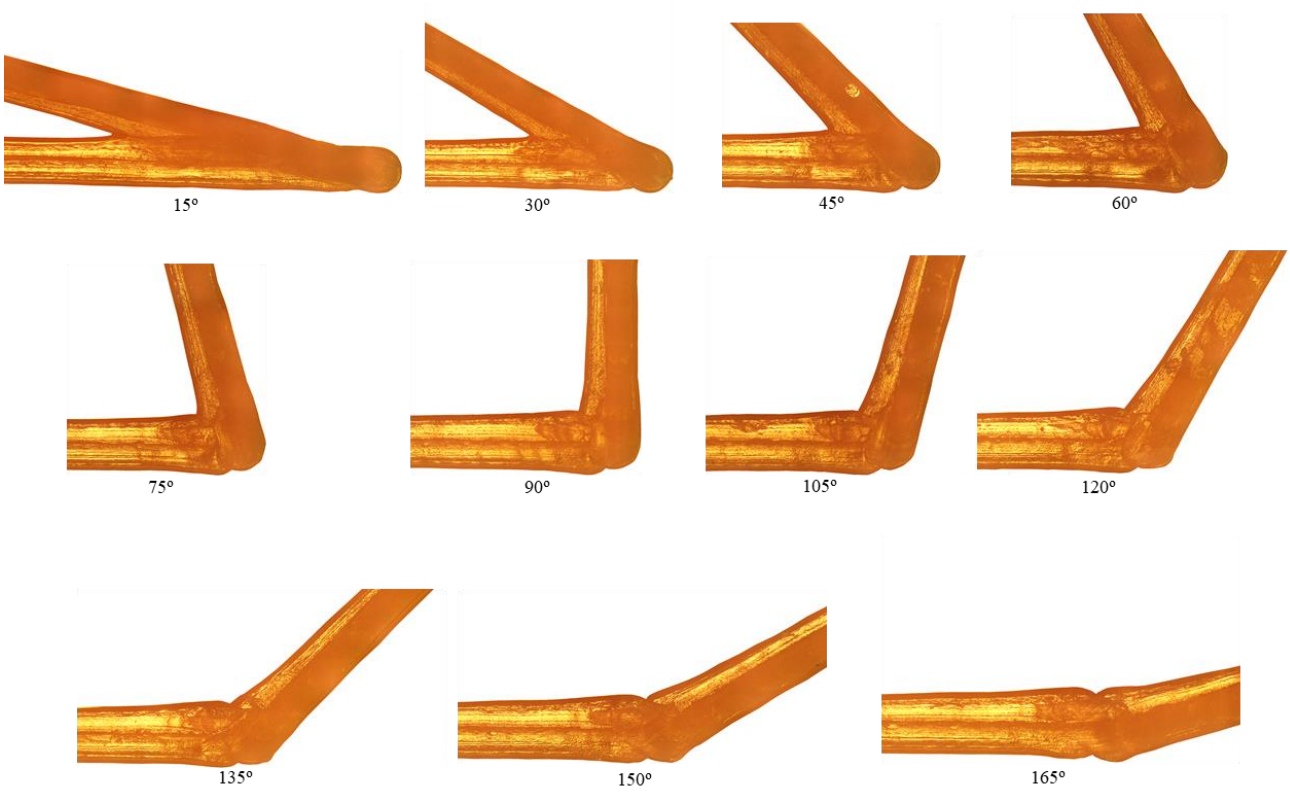

Figure 6.8 *XY Plane external corners with weld*

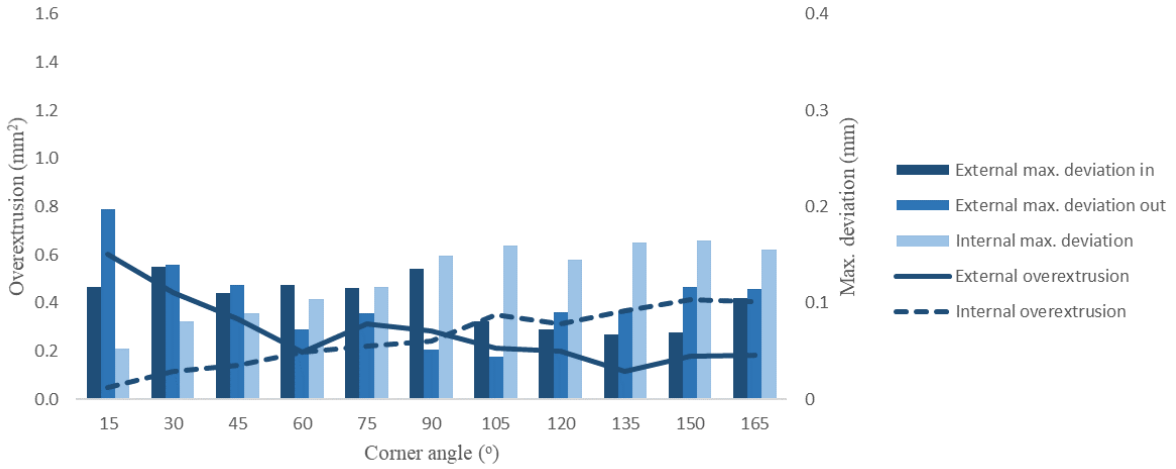

Figure 6.9 *XY Plane external corners with weld relationship between corner angle and error values*

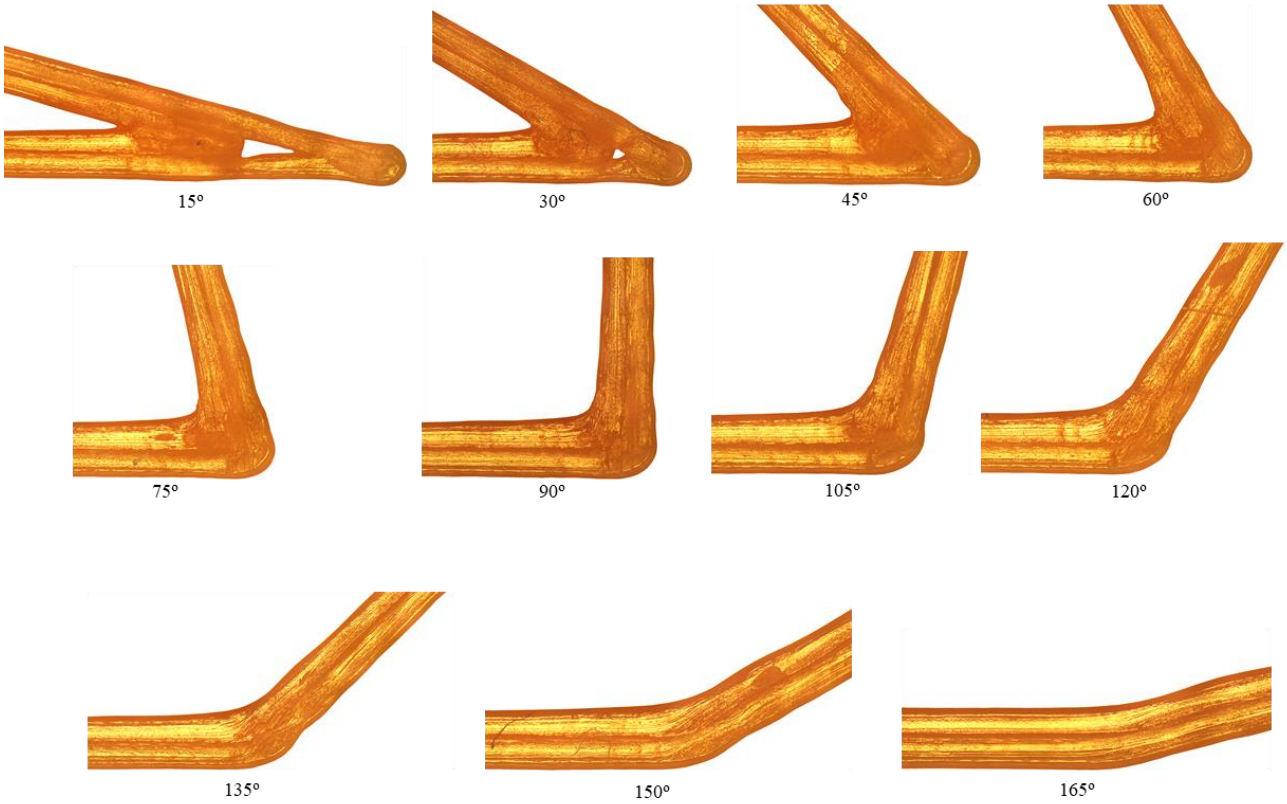

Figure 6.10 *XY Plane external corners without weld*

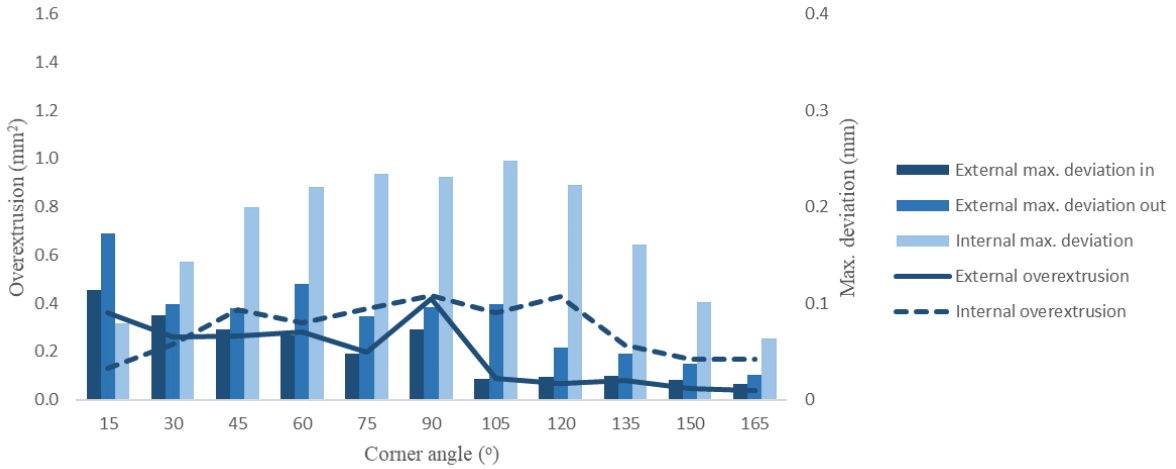

Figure 6.11 *XY Plane external corners without weld relationship between corner angle and error values*

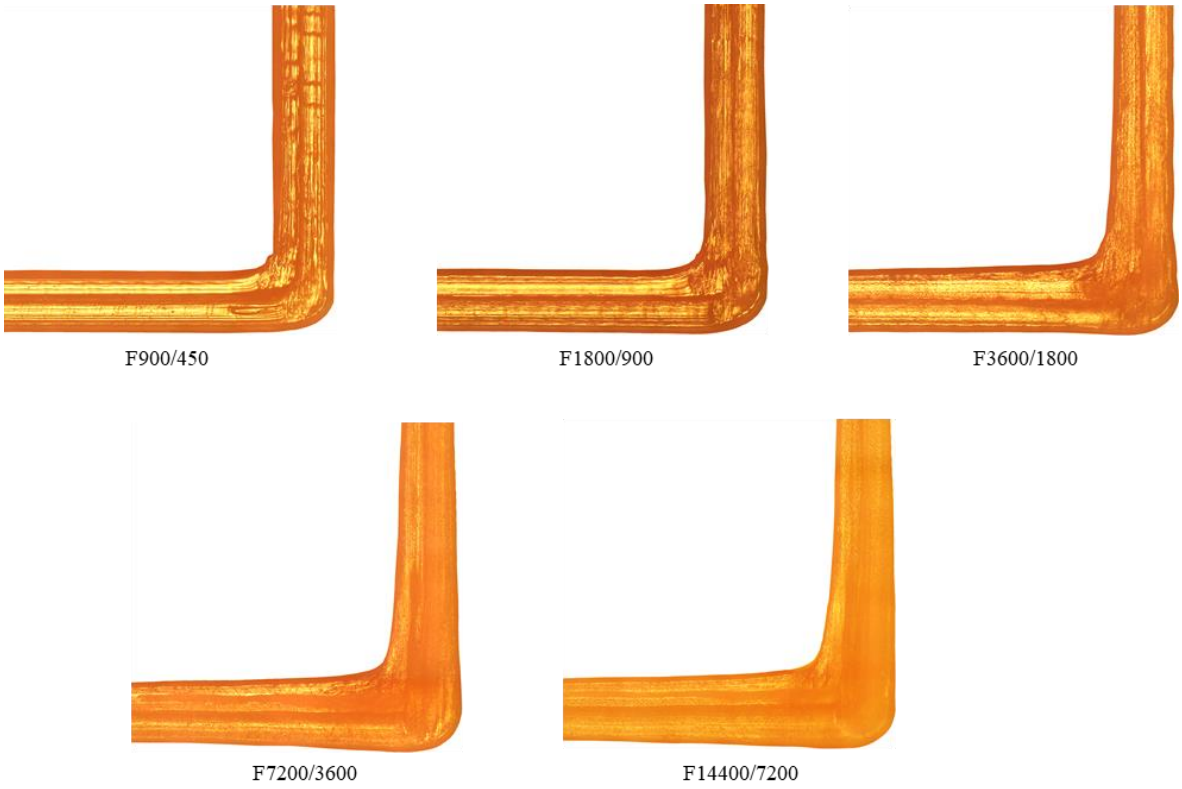

Figure 6.12 *XY Plane external corners with print speed variation*

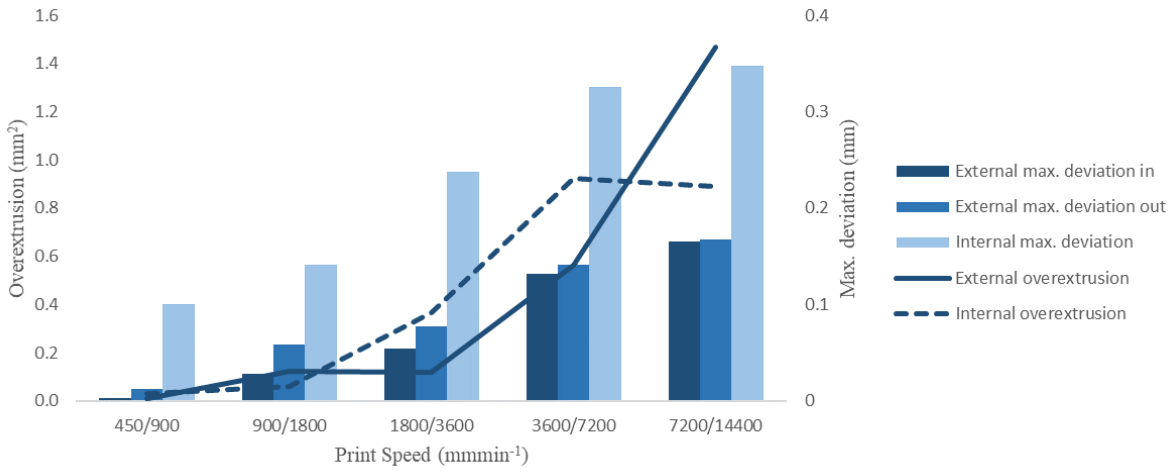

Figure 6.13 *XY Plane relationship between print speed and error values*

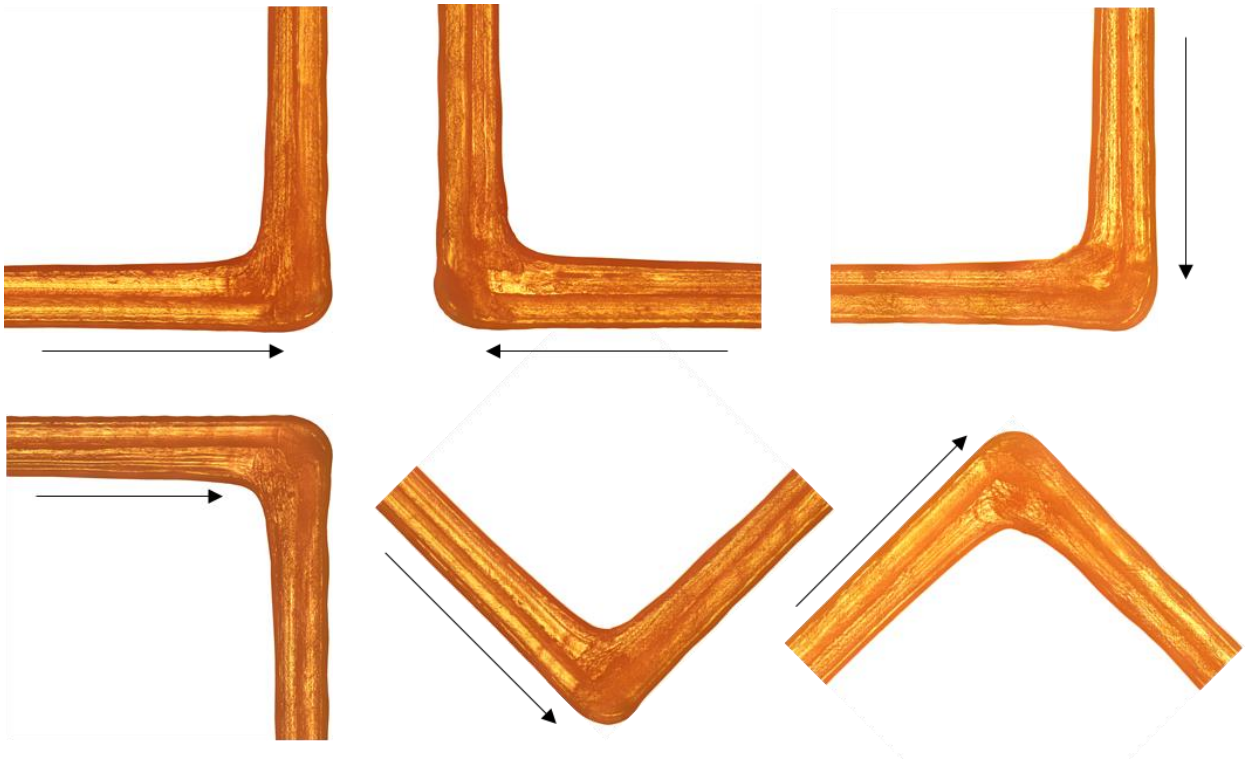

Figure 6.14 *XY Plane external corners with orientation and direction variation*

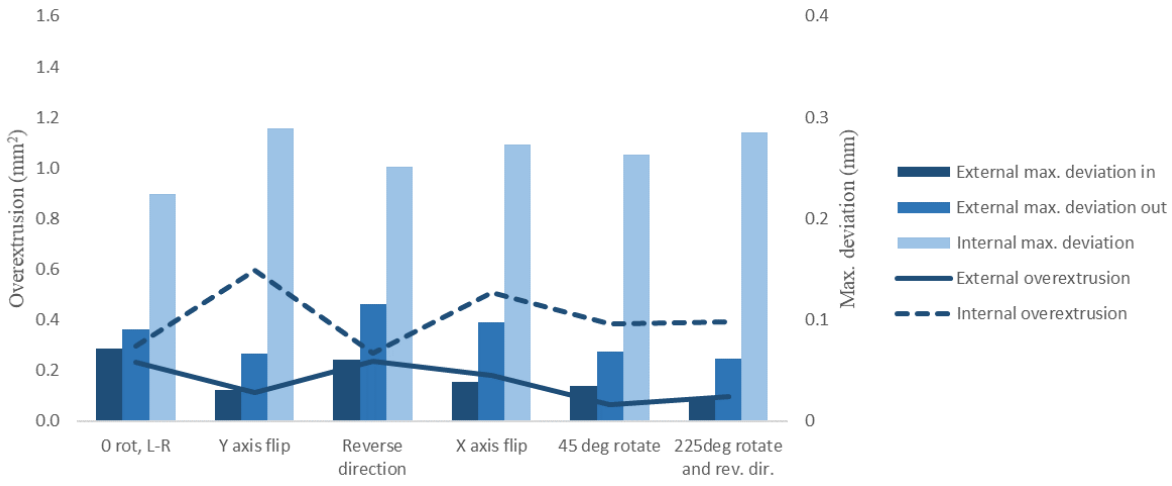

Figure 6.15 *XY Plane relationship between orientation/direction and error values*

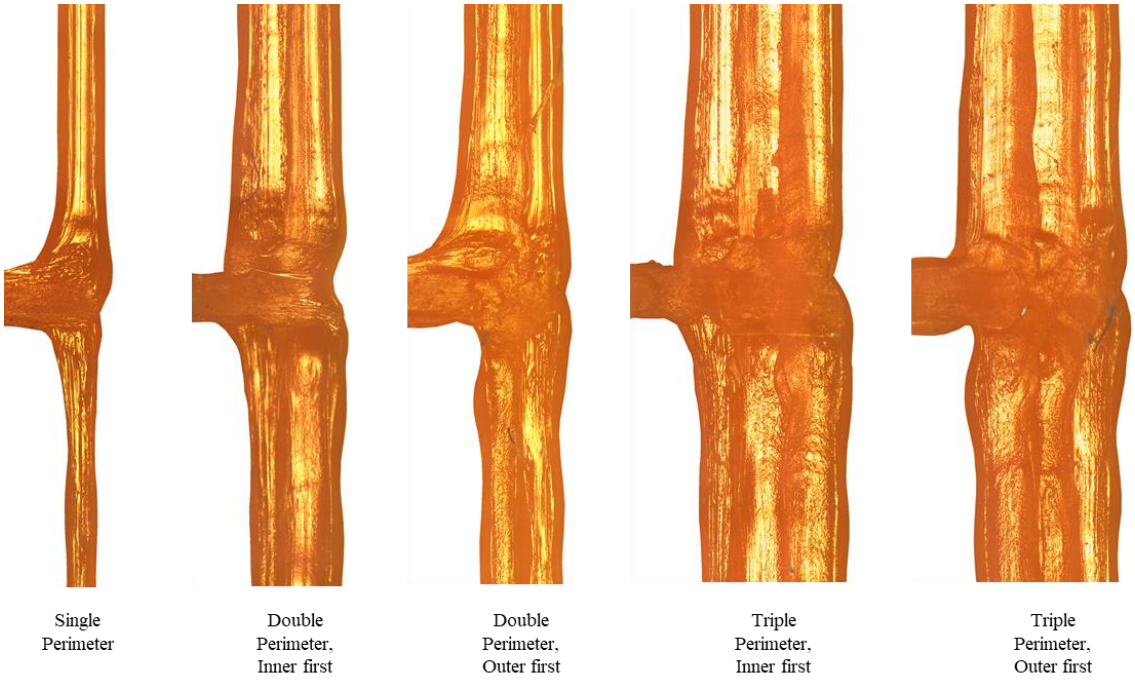

Figure 6.16 *XY Plane non-corner weld*

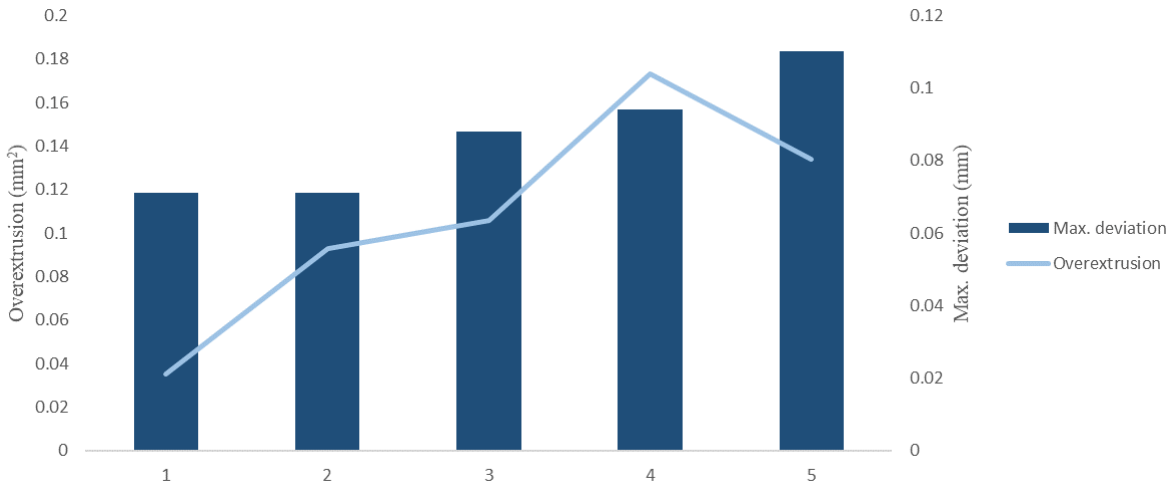

Figure 6.17 *XY Plane non-corner weld errors*

6.4. DISCUSSION

In this section, the results presented previously are descriptively analysed and the underlying behaviour discussed. This covers the influence of corner angle, presence of a weld, perimeter order, print speed and orientation for the corner geometries measured. The performance of welds on straight sections are then discussed as a possible alternative to corner welds.

6.4.1. CORNER ANGLE

Two primary sources of error were identified by Comminal et al. [383]. The first arises from a duplication of material via double extrusion. Given the assumption of a constant road width regardless of the geometry, material on the inside of direction changes overlaps with previously deposited material and due to conservation of volume this must manifest as over-extrusion. This area increases with reducing corner angle as the overlap becomes more pronounced. Clearly at extreme angles this ranges between 100% of the material for a corner angle of 0^o (i.e. a retracing of the previous path) and 0% for a corner of 180^o (i.e. a straight deposition road). Second, a mismatch between the movement of the nozzle and the extrusion mechanism as noted in detail in Section 6.1, produces over-extrusions at corners. It is expected that the acceleration and deceleration effect would be more significant for tighter corners, and therefore the error would be larger for these too. It is not possible to isolate these effects from each other with this experimental setup, so the combined effect is analysed and discussed here.

As predicted, all four experimental setups exhibit a strong negative relationship between corner angle and the external over-extrusion area (Figures 6.4 to 6.11). For the 15^o angle, this shows an area of between 0.4 and 0.7mm^2 of total external over-extrusion reducing to minimum values of approximately 0.1mm^2 at the higher angles. This is in line with the reasons given above, where both an increased theoretical double extrusion and larger acceleration and decelerations lead to a greater error.

However, the relationship for internal over-extrusion is far less consistent. In most cases, it is lower than the external over-extrusion area with values of approximately 0.1 to 0.4$mm^{2.}$. Rather than decreasing with increasing corner angle as per the outer area, the internal area often increases. This may be due to the previously-deposited filament on the entrance to the corner interacting with the filament deposited on the exit. If the entrance deposition ‘blocks’ the exit deposition, this will instead manifest as an external deviation. At higher angles, this blocking behaviour will be reduced and hence internal extrusion can increase. In an extreme case of a 180^o corner (i.e. a straight line), it would be expected that the deposition would be symmetrical and therefore the internal and external over-extrusions would be equal. The internal maximum deviation shows strong correlation with the internal over-extrusion area. These values range between 0.05mm and 0.25mm depending on the experimental setup. These values are significantly higher than for the external maximum deviations, as these are much less concentrated at the corner. The internal over extrusion tends to manifest as an internal radius, especially at higher corner angles. This phenomenon was noted by Friedrich and Begley [385] and is less prevalent at tighter corners where the previously deposited filament has had a longer cooling time. The maximum deviation is therefore concentrated very close to the corner rather than the extended over-extrusion areas found on the external perimeter.

The results presented in the previous section show the external maximum deviation on the way in and way out of the corner separately. Both these external maximum deviation measurements tend to decrease with an increase in corner angle as the total outer over-extrusion also did. The entrance maximum deviation is almost always smaller than the exit deviation. This suggests that the interaction of the exit deposition with the entrance deposition does indeed lead to increased external over-extrusion, which would manifest on the exit more than the entrance due to the direction of travel and cooling history. This is in contrast to the simulation work undertaken by Comminal et al. [383] which suggests far more equal over-extrusion at both the entrance and exit.

The external non-weld corner is likely the most representative of standard outer perimeter geometry changes as the weld only occurs once per layer and the perimeter angle must sum to 360°. Figure 6.18 shows the total over-extrusion as a function of corner angle.

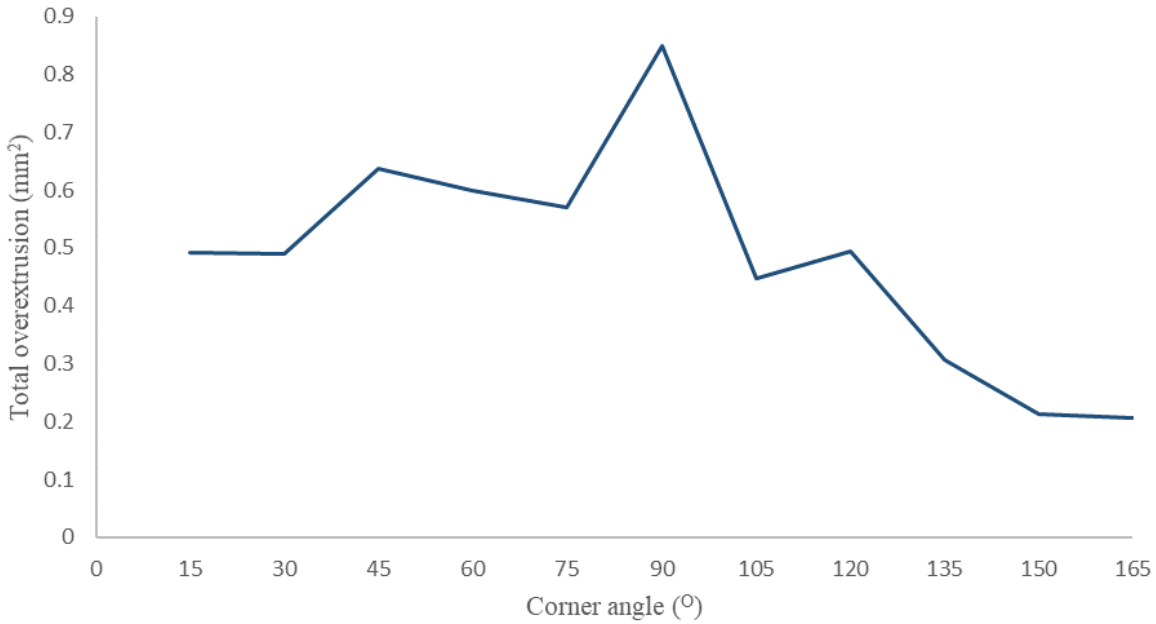

Figure 6.18 *XY Plane external corners without weld total over extrusion*

This demonstrates a general decreasing trend, although also displays a maximum value at a corner angle of 90°. Observation of the deposition morphology shown in Figure 6.10 suggests that the road width deviation occurs over a longer deposition length (i.e. it is less concentrated at the corner). This then leads to a larger overall over-extrusion value. It is not clear exactly why this occurs, though it is most likely due to the acceleration algorithm contained within the *Marlin* firmware causing a more gradual deceleration for this specific geometry.

6.4.1.1. WELD VS. NON-WELD

The comparison of weld with non-weld corners is complex. The physical XY location of the start and end of strands are identical, as per the toolpath algorithm contained within *CURA*. As was discussed

earlier, if a constant road width is assumed, then the double extrusion problem exists regardless of whether a weld occurs. However, at a weld location a layer height change occurs for each of the two perimeters. The first perimeter begins directly after a layer change, whilst the second perimeter ends with a layer change. In addition, a small movement equal to the perimeter spacing width must also be performed. This movement results in a small pause, and since the pressure drop across the nozzle does not instantaneously fall to zero [309], some degree of over-extrusion will occur. In combination with this, the slight pause will lead to greater solidification of the deposited strand at the entrance to the corner.

From the results presented in the previous subsection, it is clear that corners which feature a weld do exhibit differing geometry to those without. One notable feature is that for the 15º and 30º angles without a weld, a central void is often visible. However, this is not the case for weld examples, suggesting a higher extrusion rate local to the corner in line with the reasoning above, likely in combination with the inter-perimeter and inter-layer moves.

The relationship between corner angle and maximum deviations for non-weld versus weld and the internal corner deposition sequence is shown in Figure 6.19. For example, this shows that for a 90 degree corner where the outer perimeter is deposited first, the internal and maximum deviations on the way out are both larger when no weld is present compared to when there is a weld, and the reverse is true for maximum deviation on the way in to the corner.

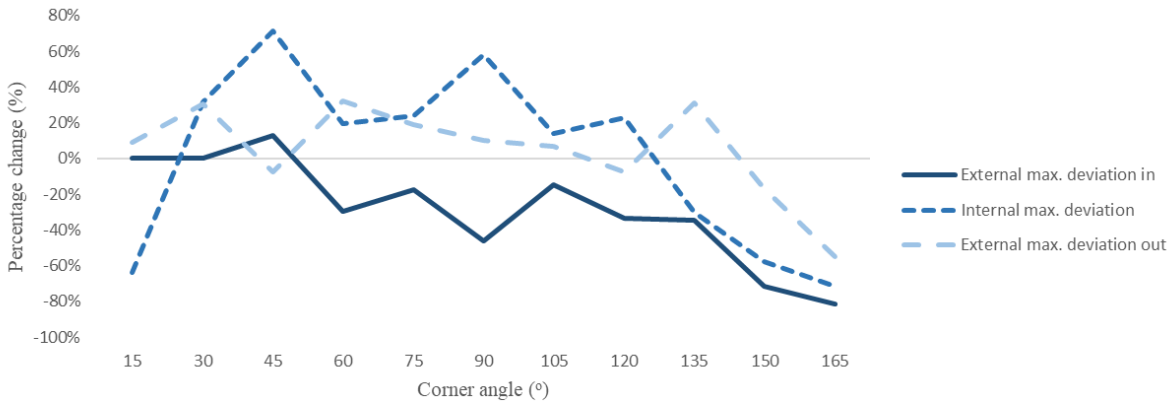

Figure 6.19 *Comparison of non-weld versus weld maximum geometrical deviations for internal perimeter order*

Figure 6.19 shows that the internal maximum deviation is lower for the non-weld condition at both high and low angles, otherwise it is higher. At both small and large angles, this may be explained by the weld over-extrusion caused by the additional moves. However, at intermediate angle values, the internal maximum deviation is higher when there is no weld. Observation of the samples shows the presence of internal radii features for the non-weld samples. This significantly contributes to maximum internal deviation, and is likely caused as the continuous corner path is followed rather than a perpendicular path to start the next perimeter.

External maximum deviations are generally similar, though are much lower for the non-weld samples at angles above 135º. This is due to the much lower over-extrusion resulting from reduced speed changes at shallower corners versus the weld corners that must make sharp changes in direction to either the next perimeter or layer.

Figure 6.20 shows the same metrics for the external corner deposition order (i.e. the outer perimeter is deposited second).

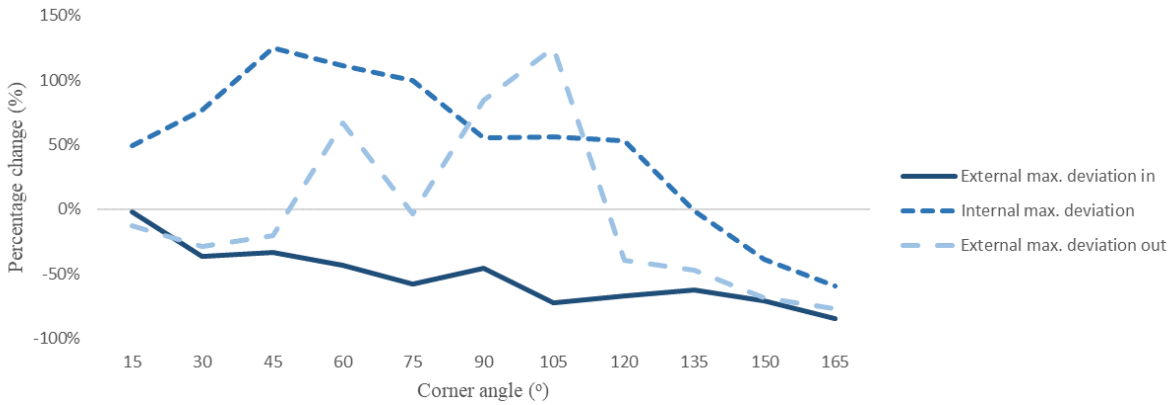

Figure 6.20 *Comparison of non-weld versus weld maximum geometrical deviations for external perimeter order*

This demonstrates that the internal maximum deviation for the non-weld against weld reduces with increasing angle over 45º. The absolute value is higher up to 135º owing to the same rounded internal geometry mentioned previously. The reducing trend is likely due to the lower acceleration and deceleration associated with smaller direction changes. For small angles, the rounded internal perimeter geometry is less marked as the velocity decreases to a greater degree at these sharp corners.

External maximum deviations are generally smaller for the non-weld corner due to the reduced over-extrusion. However it is higher for the non-weld case on the corner exit for intermediate angles since the outer corner contains no move inwards to change perimeters.

Internal, external and total and over-extrusions are shown for both perimeter orders in Figures 6.21 and 6.22.

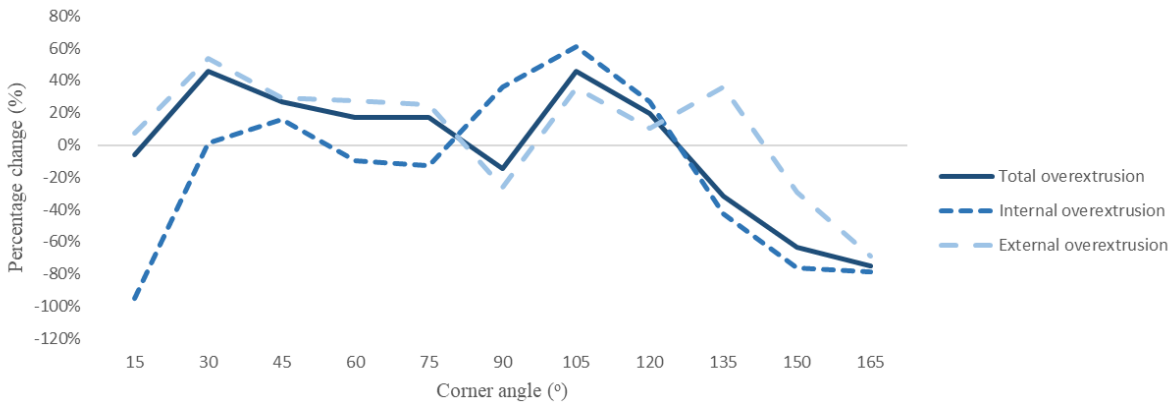

Figure 6.21 *Comparison of non-weld versus weld over-extrusion error for internal perimeter order*

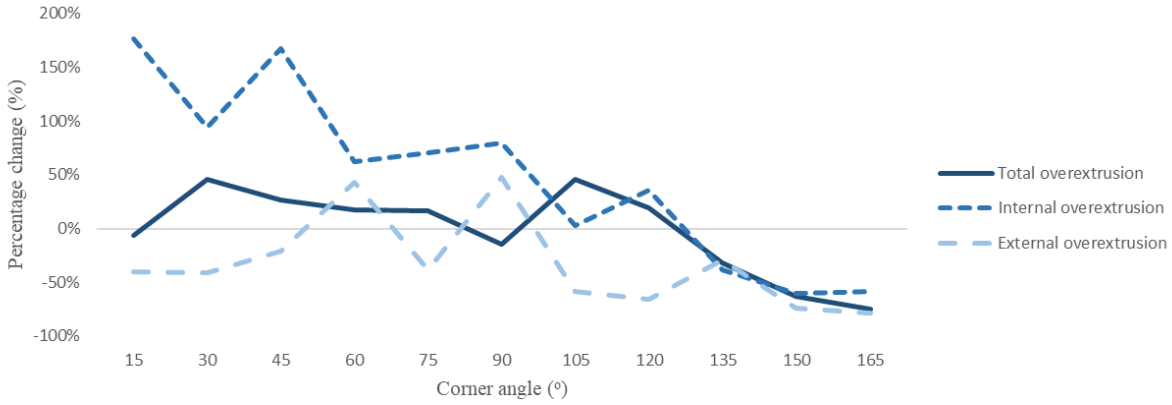

Figure 6.22 *Comparison of non-weld versus weld over-extrusion error for external perimeter order*

For the internal corner perimeter order, the internal over-extrusion is much lower at smaller angles for the non-weld corner. This is likely due to the lack of over-extrusion arising from perimeter and layer changes and lack of curved over-extrusion at higher speeds and angles. At high angles, the extrusion is again lower due to the lack of pause. The external over-extrusion and total over-extrusion show strong correlation since the external value is much larger than the internal. This trend can once more be explained by the lack of pause and faster movement in the non-weld case for higher angles.

For the external corner perimeter order, all three extrusion metrics show generally decreasing trends with increasing corner angle. These are again explained by the lower acceleration and deceleration at increasing angles in the non-weld case versus the pause over-extrusion for the weld corners. Initially, the internal over-extrusion is higher for the non-weld case in particular due to increased over-extrusion on the entrance to the corner where motion is continued within the same perimeter instead of switching to the outer perimeter.

6.4.1.2. PERIMETER ORDER

There are two primary factors to consider regarding the choice of perimeter order. Firstly, as was discussed previously the second perimeter is deposited at half the speed of the first, giving

significantly lower over-extrusion. Secondly, the second perimeter interacts with the first such that any over-extrusion will be forced outwards. These two effects counteract each other and the overall behaviour arises from the interaction of these.

Regarding the latter effect, whilst it may seem that an over-extrusion on the first perimeter will simply push the second further outwards, it is observed that the road width is actually reduced locally in these cases. For example, the 15º and 30º examples in Figure 6.10 clearly show this behaviour. Nonetheless, some outwards deviation is still observed.

Figure 6.23 shows the relationship between corner angle and percentage change of maximum deviations for the external versus internal perimeter orders with a weld present.

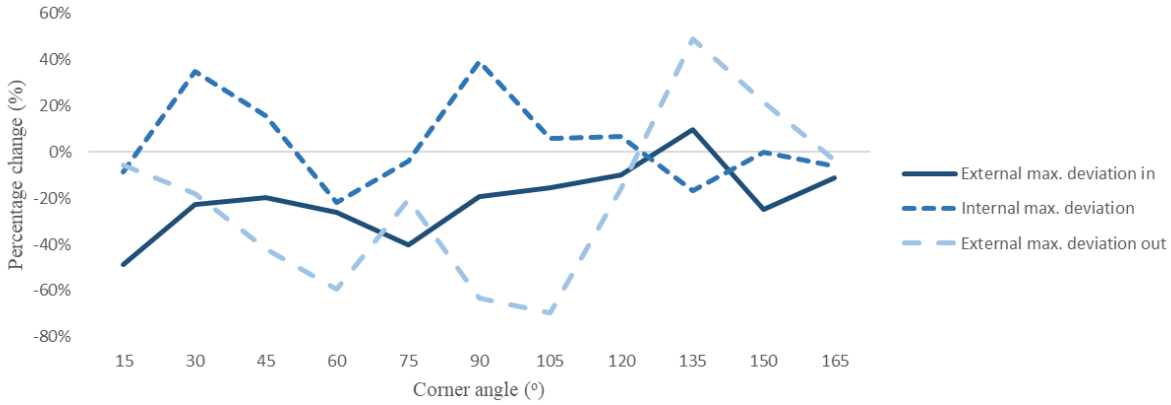

Figure 6.23 *Comparison of internal perimeter first with external perimeter first for maximum geometrical deviations with weld*

This shows that the internal maximum deviations are not that dissimilar regardless of corner angle and there is no strong overall trend. This suggests that the perimeter order is not especially important for internal geometry accuracy. It is possible that the presence of a weld offsets the perimeter speed differences as a pause is required regardless of speed. In general, the faster internal perimeter would give higher internal over-extrusion but because it is deposited first, any over extrusion is not forced inwards. External maximum deviations are generally lower where that perimeter is deposited second. The reduced print speed for the outer perimeter gives lower over-extrusion which therefore more than counteracts the internal perimeter pushing over-extruded material outwards. All deviations show similar values for angles above 135º where the print speed effects and level of over-extrusion are mitigated.

Figure 6.24 shows the same metrics for corners without a weld. This data appears much clearer than with the weld, suggesting the welding process itself leads to either more complex behaviour or is inherently less predictable.

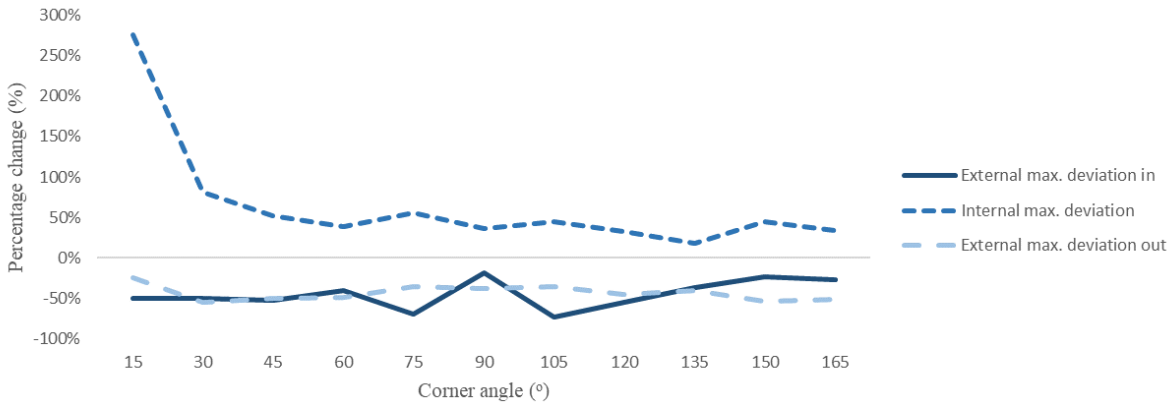

Figure 6.24 *Comparison of internal perimeter first with external perimeter first for maximum geometrical deviations without weld*

The internal maximum deviation is much higher in all cases and lower for the external maximum because the inner perimeter has a higher print speed and therefore higher over-extrusion. This indicates a strong dependency on print speed. In both cases, this suggests that the reduced over-extrusion for the slower perimeter overcomes the perimeter interaction effects.

Figures 6.25 and 6.26 show the same relationships (with a weld and without respectively) but for over-extruded areas.

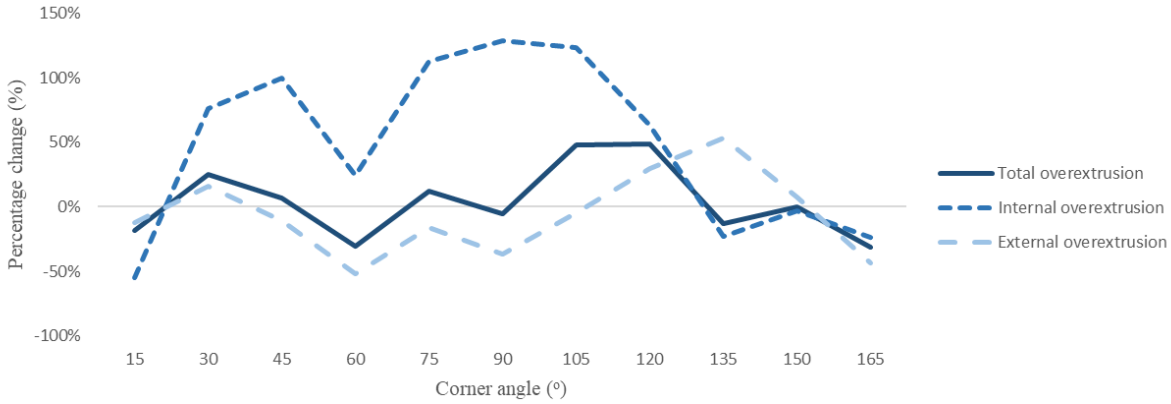

Figure 6.25 *Comparison of internal perimeter first with external perimeter first for over-extrusion error with weld*

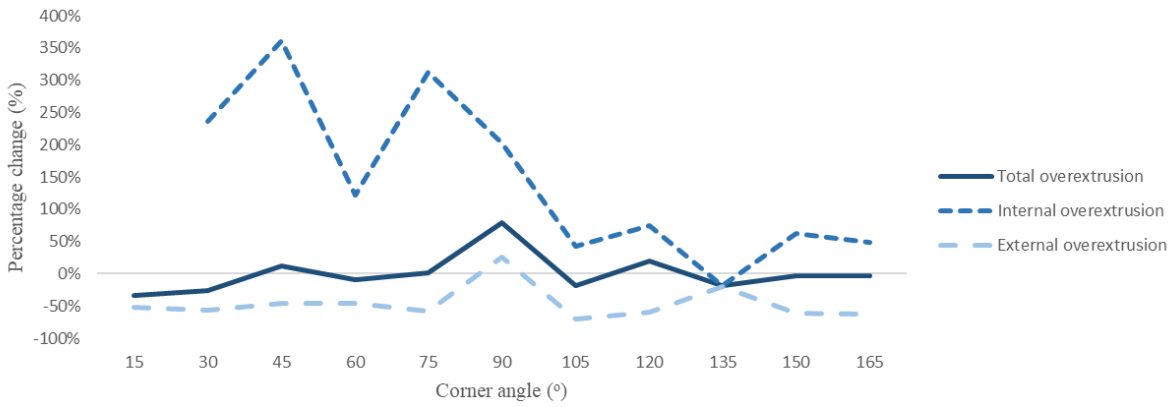

Figure 6.26 *Comparison of internal perimeter first with external perimeter first for over-extrusion error without weld*

This shows similar trends to those observed for the maximum deviations. With the presence of a weld, the internal over-extrusion is higher when the external perimeter is deposited second for intermediate angles only. At low and high angles, the reverse is true. This suggests that despite the faster internal perimeter, the movement inwards to change perimeter counteracts the error. The relative values for internal and external values remain the same when extrusion area rather than maximum deviation are considered without a weld. However, in this case, the external and therefore total over-extrusion values are sometimes higher, despite the maximum deviations always being lower. This is particularly true for the 90° corner, where the external over-extrusion is slightly larger. This is because despite not deviating further at any given point when the outer perimeter is deposited second, the (smaller) deviation continues for a longer distance. This may be due to the interaction with the inner perimeter, but would require further investigation for this specific geometry.

6.4.1.3. COMPONENT FIT

Ultimately, the accuracy of internal and external corners is especially important in the context of mating components. Errors in one or both of these aspects could directly result in components not fitting as intended or large tolerances being required, which can then lead to issues of increased wear. Figure 6.27 shows the fit for the non-weld cases of 15°, 90° and 165°.

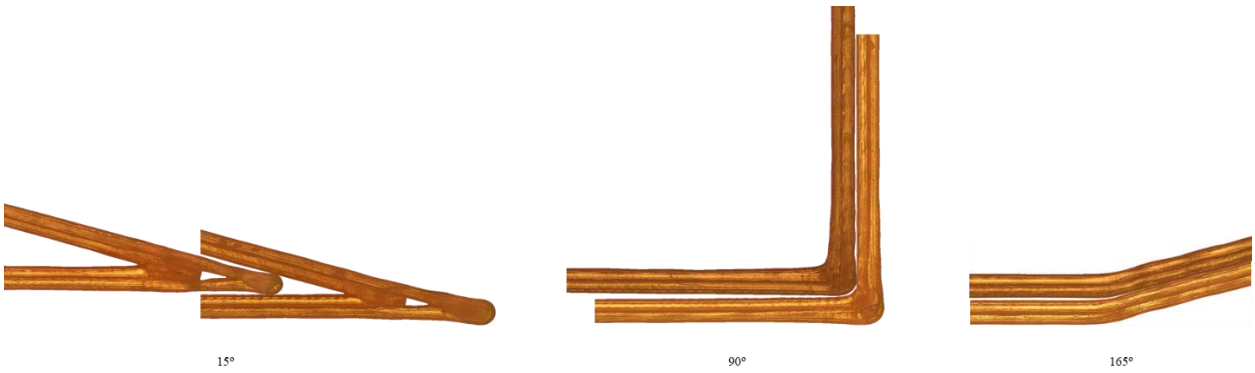

Figure 6.27 *Representative fit of corners for 15°, 90° and 165° angles*

It can be seen that the internal radius is not a significant factor in mating components given the external corner radius and deviations also present. Instead, the dominant over-extrusion error for fit cases it the external over-extrusion. This results in required tolerances of approximately 0.15mm for smaller angles, though it is of course preferable to reduce the error source or perhaps design around it with the use of rounded or chamfered corners in component design.

6.4.2. PRINT SPEED

Figure 6.13 shows the relationship of print speed to maximum deviations and over-extrusions for a 90^{o} non-weld corner. This shows a very strong positive relationship between errors and print speed. At a print speed of 450 and 900mmmin^{-1} for the inner and outer perimeters respectively, there is very low error for all metrics except internal maximum deviation. This error arises from a rounded internal corner, which is unlikely to cause significant problems for fit as demonstrated above. However, a low print speed naturally increases the build time in a relationship approximately proportional to the print speed. As the print speed is increased, all errors increase. At a print speed of 7200 and 14400mmmin^{-1}, the external maximum deviation increases to approximately 0.15mm, with an associated significant increase in over-extrusion area. The internal over-extrusion and maximum deviation do not significantly increase between the two highest printer speeds, suggesting that after 3600/7200mmmin^{-1} the internal geometry does not change significantly and errors are concentrated on the exterior perimeter. In light of the experimentation in the previous section, it may be that rate limits are reached above this speed and filament slippage occurs, reducing the actual deposition volume. For the default print conditions with an inner perimeter speed of 3600mmmin^{-1} and outer perimeter speed of 1800mmmin^{-1}, the outer perimeter maximum deviations are approximately 0.06mm.

6.4.3. ORIENTATION AND DIRECTION

90^{o} corners were printed in a variety of directions and orientations, as displayed in Figure 6.14. The results from this experimentation show very little change in the internal maximum deviation, although there is some variation in the internal area error of between 0.3mm^{2} and 0.6mm^{2}. All external errors fall between 0.02 and 0.12mm. The largest errors are observed for the reverse direction (i.e. negative Y followed by negative X). In all cases, the maximum deviation is highest on the exit of the corner. This is likely the result of much of the over-extrusion occurring just after then corner has been reached and any effects of double extrusion being realised only after the direction change has occurred.

A summary of the results is also shown below in Table 6.1 for comparison between experimental runs.

Print	Axis in	Direction	Axis out	Direction	Summary	Total over-extrusion (mm^2)	Square perimeter corner
1	X	+	Y	+	X+Y+	0.529	Bottom right
2	X	-	Y	+	X-Y+	0.705	Bottom left
3	Y	-	X	-	Y-X-	0.506	Bottom right
4	X	+	Y	-	X+Y-	0.691	Top right
5	XY	+-	XY	++	XY+-XY++	0.449	Bottom
6	XY	++	XY	+-	XY++XY+-	0.489	Top

Table 6.1 *90^o corner orientation and direction summary*

The two samples that would represent the bottom right of a square perimeter show very similar over-extrusion amounts. These utilise the same two axes but in opposite directions of motion. This confirms that the perimeter direction does not affect the level of error, though it does change the region of maximum error as the exit position of the corner changes. The total over-extrusion appears lower for the two 45^o orientations. The print speed experimentation shows non-linear relationships between speed and extrusion error. Utilising both axes equally therefore reduces the speed of both and therefore potentially benefits from this non-linearity if these effects arise from axis dynamics.

6.4.4. STRAIGHT SECTION WELD

Straight section welds are shown in Figure 6.16. The perpendicular extrusion at the midpoint is part of the simulated infill, which would necessarily meet the perimeter at this point unless no infill is selected. This is an alternative to placing a weld at the corner, as *CURA* does by default. Between the five experiments, the number of perimeters and perimeter order were changed. Again, the outermost perimeter (i.e. the final deposition) was deposited at a speed of $1800mmmin^{-1}$ at half the speed of other perimeters. As with the corner experimentation, the behaviour is explained by the combination of reduced extrusion error from the reduced print speed and increased extrusion from the restriction of previous perimeters. The results show that where the outer perimeter is deposited first, the maximum deviation increases. This suggests that in the case of straight section welds, the increased speed error outweighs the perimeter order interaction error. This order also gives superior geometrical performance in most corner scenarios, so if a straight section weld is utilised this perimeter order is suggested.

6.4.5. COMPONENT ACCURACY IMPLICATIONS

The experimentation undertaken in Section 3 produced square-section components. The relevant corner for error implication analysis is therefore the 90^o corner. It was shown that the maximum outer perimeter error is dominant, and that the error on the entrance and exit of the corner differed. Regardless, the components produced in Section 3 exhibit only external corners. Assuming a single weld corner and three non-weld corners with the external perimeter printed second at a speed of $1800mmmin^{-1}$, the relevant errors for the entrance and exit of corners are 0.135mm and 0.052mm for the weld corner and 0.073 and 0.096mm for the non-weld corners. The maximum side length requires an entrance and exit error to be included giving a side length error of between 0.125mm and

0.208mm. This error is relative to the straight and flat side rather than an absolute error, but is nevertheless useful to consider.

Precision performance was not explicitly investigated in the experimental work included in this section, with greater focus instead being given to the influence of corner angle, weld and perimeter deposition order on accuracy. However, the repeatability measures included in Section 3 do provide an indication of representative error. In the macro experimentation presented there, the underlying precision performance was demonstrated to be approximately ±0.2mm. This value consists of the positional and extrusion errors as discussed previously. However, steady state and strand morphology precision error is thought to be low, so a direct comparison may be made between the macro precision and positional variability where any difference is likely to be representative of corner deposition variation. Position precision for a nominal 15mm dimension was determined to be approximately ±0.1mm for most XY axes. This suggests a similar precision error of ±0.1mm may be applicable to corner fabrication. Although a limited sample size of two, identical 90^{o} corners were fabricated with no weld and the outer perimeter printed last. These demonstrate a difference (if applied across a component) of approximately 0.04mm, which would appear to support this level of precision. However, this would benefit from additional experimental work to validate.

7. IMPROVING DIMENSIONAL AND GEOMETRICAL PERFORMANCE

Noriega et al. [281] stated that studies of the ME AM process can be broadly placed into two categories. Firstly, *error analysis*, or understanding the current level of performance. Second, *error improvement*, or actively seeking to improve the process capability in some way. Tong et al. [391] noted that error improvement can be further categorised as one of; *error avoidance*, *error compensation* or *post-processing*.

Error analysis involves investigating the current performance of the process without actively seeking improvement. For example, in Section 3 the dimensional and geometrical performance of three desktop ME AM machines was investigated and tolerances suggested. This focused on the errors present in the process rather than providing any detailed and direct means of improvement. Sections 5 and 6 also investigated the nature of current errors, though owing to their more targeted nature direct improvements were possible (e.g. new road width assumptions or perimeter order selection).

This section provides a discussion of potential approaches to mitigate the errors identified in order to improve the process. It covers the three main groups of error improvement identified above. In general, the following options are available to improve the process outcomes: altering the virtual part, altering the machine code, changes to the hardware or utilising additional processes post-production. Figure 7.1 provides a summary of errors and their constituent elements, which represents the framework for the discussion in this section.

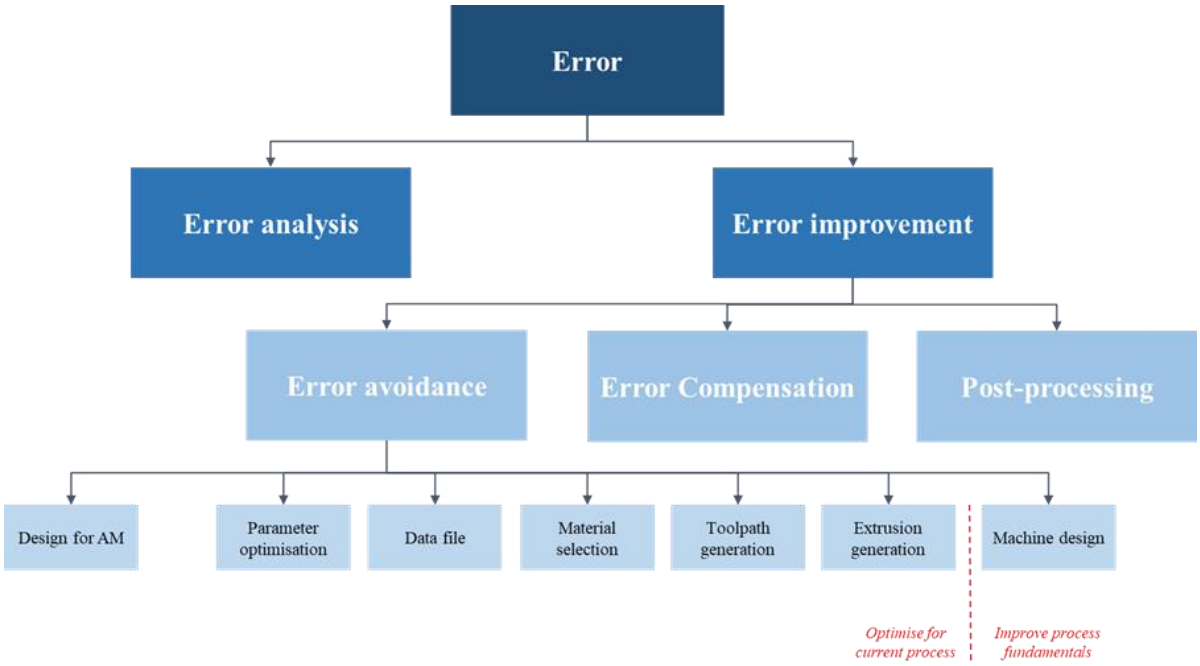

Figure 7.1 *ME AM error framework*

Some of these approaches are preferable to others in terms of their ease of use from the perspective of the operator. Avoiding the need for a user to make complicated decisions or conduct additional

processes reduces the cost and increases the likelihood of improved performance. Consider a consistent length error present across multiple components of the same design. One potential way to improve this is for the user to redesign the component, perhaps with a new nominal value or different feature. However, this is time consuming and a first revision may not yield the desired results. Instead, it would be preferable for the process itself to achieve the desired performance independent of the user. As shown in Figure 7.1 there are many ways of achieving this. One is to simply optimise the current process (in an ideal case, automatically for the given geometry, machine and material combination). Alternatively, the machine design itself can be altered to improve fundamental errors in the process which are not easily addressed via optimisation alone. Otherwise, machine-specific compensation or automated post-processing may also be applied.

7.1. ERROR AVOIDANCE

There are three main approaches to avoiding the sources of error. The first is to understand the current capabilities of the process and design with these specifically in mind in a methodology commonly referred to as Design for Manufacturing (DfM). The second is to optimise the current process as far as possible, either by altering slicer algorithms (including slicing strategies, toolpath generation and extrusion profiles), or by optimising print parameters to maximise certain dependent variables. Finally, the process can be fundamentally altered with changes to the design of ME AM machines which may directly reduce error (e.g. through superior quality machine components) or enable new print strategies.

7.1.1. DESIGN FOR MANUFACTURING

DfM is a set of methods and methodologies that ensure the designer understands any constraints imposed by the existing manufacturing process in order to provide the best outcome for the manufactured product [62]. Whilst this generalised approach is highly applicable to ME AM, it is not specific to it. In addition, the majority of ME AM DfM recommendations are focused on avoiding outright fabrication failures rather than the improvement of accuracy or precision performance.

Designers may be unaware of specific manufacturing details or rules, potentially resulting in ‘non-manufacturable’ designs and ultimately contributing to time-consuming and costly iterations between the design and final manufacturing stages [392]. The Manufacturability Analysis System (MAS) was developed to allow manufacturability aspects to be considered at the design stage in order to ensure an error-free transition from design to manufacturing. Shukor and Axinte [392] provide a basic methodology for developing an MAS. This consists of an input stage, where the CAD model and manufacturing method information is collated. The second stage analyses manufacturability aspects, whereby data and rules pertaining to the manufacturing process are checked against the proposed design. The final output stage gives (reiterated) design suggestions, process sequencing and material suggestions.

In the specific context of ME AM, a number of ‘design rules’ exist which should considered when designing components. The original developer of FDM (ME AM), Stratasys, have published a Design Guidelines Document [70]. This details the limitations of the ME AM process with regards to wall thicknesses, threads, feature size, fillets, size, orientation and clearance. Pascu et al. [393] have also provided design rules specific to plastics and ME AM. They suggest a number of general rules regarding feature orientation, though once again offered little specific detail. Simion and Arion [394] have given dimensioning rules for ME AM components. They fabricated a variety of geometries on a desktop machine, and noted many tradeoffs between parameters and performance goals. Their major contribution was proposed dimensioning formats to communicate the various features common in ME AM production. Urbanic and Hendrick [395] have presented a series of modelling design rules for building large, complex components via ME AM. They noted size, surface finish and accuracy limitations of the process, and suggest avoiding these during design by carefully considering orientation, building in tolerances and aligning certain features such as holes with the build direction. In total, 23 separate recommendations were made, though these were rarely quantitative in nature. Zeimian and Crawn [396] explored the use of computer aided decision support specifically for ME AM. This aided the user in setting process variables to achieve specific performance goals by providing the quantification of trade-offs among conflicting goals such as build time versus part accuracy and resolution.

Hague et al. [397] provided a general overview of the implications of rapid manufacturing technologies on the design process. In this, they noted that AM technologies removed a number of constraints typically present in conventional processes such as mould considerations, wall thicknesses and other manufacturability factors. Similarly, they suggested that the use of AM made the iterative prototyping process typically associated with conventional technologies redundant.

Multiple studies have presented a decision support system to select the most suitable rapid prototyping technology. These considered factors such as build time, cost, accuracy, surface roughness, wall thickness, materials and mechanical performance [398-402]. Many others have provided generalised support systems to aid process parameter selection common to all AM technologies. Mahesh et al. [403] proposed a decision making system using Integrated Rapid Prototyping Decision Making System (IRPDMS) fuzzy decision methodology to find an optimal solution. Ransikarbum and Kim [404] also provided a method for multi-criteria decision making, though this focused on orientation selection. Similarly, Hur and Lee [405] developed a CAD environment to determine the optimal build direction. Wang et al. [406] developed a knowledge management system using Bayesian networks to model AM knowledge and identify causal relationships. This provides the user with suggested parameter settings, though does not directly address component dimension and feature design choices. Ahsan and Khoda [407] provided an

integrated framework for both part and process attributes for AM technologies. This algorithm simultaneously controls build orientation and toolpath direction for an optimal solution.

Hague et al. [397] stated that additive manufacturing processes enable complexity of geometry at no extra cost as the main determinant of cost was simply build time, which is only dependent on orientation. Wang et al. [406] supported this notion. Many other publications have also alluded to the increased freedom for designers [393,395]. However, Pradel et al. [408,409] explored these claims in two separate studies and concluded that shape complexity impacts both build time and material consumption for ME AM, demonstrating that the simple notion of 'complexity for free' is not the case in practice.

7.1.2. PROCESS OPTIMISATION

There have been a wide variety of methodologies employed to understand the ME AM process and yield performance improvements. These are summarised in Table 7.1 below.

Improvement methodology	Studies
Neural networks	[281,410-420]
Taguchi experimental design / ANOVA	[181,202,421-430]
Response surface	[178,373,431-435]
Evolutionary computation	[436]
Teaching-learning-based algorithm	[437,438]
I-optimality	[376]
Expert system	[439]
Fuzzy logic	[440,441]
Finite element analysis	[187,271,442-445]
Machine learning	[446-448]
Spectral graph theory	[264,449]
Artificial intelligence	[450]
Particle swarm	[433,451]
Symbiotic Organism search	[433]
Support vector regression	[416]
Group method	[420]
Genetic algorithm	[452,454]
Analytic hierarchy	[455]

Table 7.1 *Summary of methodologies applied to the ME AM process*

As can be seen, the most common methodologies are the use of neural networks to compute large and complicated datasets, finite element analysis of the material flow during heating and deposition and Taguchi experimental design combined with analysis of variance (ANOVA) to optimise print parameters.

7.1.2.1. PARAMETER OPTIMISATION

There is a large body of literature focused on parameter optimisation. In the related experimentation, one or more independent variables are changed and one or more dependent output variables measured. The effects of changing print parameter settings are investigated and their values optimised for superior dimensional performance or other quality metrics.

A summary of these parameter optimisation studies is included in Table 7.2 below. As demonstrated, a variety of process parameters have been investigated to understand their relation to dimensional accuracy.

Process parameter	Studies
Layer Height	[19,68,177,179,181,182,184,188,194,208,212,216,245,246,267,279,342,343,347,359,372,376, 421,423,425,427,428,430,431,434,456-487]
Feed rate	[430,462,475,478,482,487-490]
Print speed	[184,194,208,216,245,246,267,332,372,427,458,460,464,467,474,475,480,485-487,490,491]
Air gap	[181,182,268,376,428,431,434,465,492-494]
Raster angle	[181,182,268,376,421,428,431,434,461,467,479,84,492-495]
Road width	[19,181,182,184,245,268,359,376,421,428,431,434,457,460,464,481,492-496]
Number of perimeters	[268,376,423-425,427,429,434,460,463,466,488,495,497]
Print temperature	[194,208,264,267,279,327,332,347,348,359,372,424,425,429,430,458,460,467,471,477,482,487,488,490,491]
Nozzle diameter	[19,481,498]
Bed temperature	[194,208,267,490]
Build orientation	[68,177,181,212,246,253,266,342,376,421,423,428,431,434,459,461,463,466,475,476,483-486,499-503]
Infill pattern	[212,372,425,427,471,479,488,496,497]
Infill density	[68,179,194,208,264,266,267,279,343,424,427,460,467,471,472,474,479,483,489,491,501,502,504]
Build envelope position	[212,211]

Table 7.2 *Summary dimensional error parameter optimisation studies*

These studies typically employ either full factorial or Taguchi experimental design to vary multiple parameters at various levels in an experimental approach. Analysis of variance (ANOVA) is used to understand which parameters have an influence on the selected performance characteristics. Then, main effect plots either of the raw output data or of signal-to-noise ratios are presented to determine which combination of parameters is optimal. This is then often then experimentally validated, particularly where a Taguchi experimental design was used.

Despite the existence of extensive research on parameter optimisation, this has not typically informed parameter settings in the most popular slicers. Equally, the majority of users are not aware of their findings and do not consult studies prior to component production. One of the major drawbacks of these approaches is that there are additional parameters that are not held constant between studies and are often not even specified in the study. In particular, the machine, material, component geometry and slicer selected are rarely the same between any two studies.

The machine used, even for the same print parameters and component geometry, was demonstrated to affect dimensional and geometrical accuracy and precision in Section 3. Similarly, the material [505] (see also: Section 5) and component design [278,497] (see also: Section 6) are both known to affect performance. Finally, as noted previously, and as explored by Baumann et al. [57], Šljivic et al. [58] and Torok et al. [59], the slicer used can also have a significant impact on dimensional performance. Failure to account for these additional effects means that outcomes cannot be properly generalised and therefore each study provides only a specific solution for its experimental setup.

7.1.2.2. DATA FILES

Potential sources of error in the production of data files were discussed in Section 3.4.1. This highlighted the approximation of curved geometry to a series of straight lines as the primary source of error within digital file creation. There has been a limited amount of attention given to this error source in existing literature. Ledalla et al. [506] investigated various STL file mesh refining algorithms as applied to the ME AM process. They identified the chordal error arising from the mismatch between the straight line geometry of the STL model and a curved design surface. They concluded that subdivision techniques could improve the component surface roughness, volume accuracy and build time. Hällgren et al. [507] investigated the export of 3D data between CAD systems. They noted that poor tessellation accuracy in the digital file directly translated to component errors for the printed product. They proposed a data exchange method using STEP – ISO10303 standards to produce mathematically exact data rather than the STL approximation to improve geometric accuracy. Zha and Anand [53] developed a STL production technique that increased resolution locally to more complex features. Qu and Stucker [508] provided a surface offset methodology based on vertices rather than facets. This allowed inward or outward offsets for STL models against the nominal geometry to be produced, allowing for the control of chord and volumetric error.

The effect of data file errors are ultimately relatively small, and only arise with more complex curved geometry. In most cases, selecting a reasonable resolution in the STL production produces a file that gives a very close approximation of the nominal geometry.

7.1.2.3. MATERIAL SELECTION

Thermoplastic polymers have typically been used in the ME AM process, with ABS and PLA being by far the most popular. Whilst not strictly a means of reducing error in all cases, the correct selection of material ensures high quality parts and the development for new materials allows the possibility of novel applications. A summary of non-polymeric materials explored in existing literature is provided in Table 7.3.

Material	Studies
Metals	[47,509-518]
Composites	[44-46,352,374,519-541]
Biomaterials	[30,48,252,465,523,542-551]

Table 7.3 *Summary of novel materials covered in extant literature*

These studies have performed a variety of functions. In some cases, the use of the materials within the current process is investigated to understand the level of performance possible. In other cases, changes have been made to the software or hardware to specifically address limitations of the current process and its historical focus on polymer feedstock.

Duty et al. [552] investigated the main factors that influence the printability of polymers in ME AM. They developed a viscoelastic model which identified flow through the nozzle, strand morphology, mechanical strength and overall stability to be important factors. Their framework showed the suitability of and provided guidance for the use of more unusual polymers such as high temperature thermoplastics, fibre-reinforcements, low-viscosity thermosets and high coefficient of thermal expansion thermoplastics. Wittbrodt and Pearce [553] showed the effect of PLA material colour on the properties of ME AM components. They demonstrated differing levels of crystallinity in different colours, which led to changes in tensile strength. Similarly, Hanon et al. [28] showed that PLA colour affects the part weight and dimensional accuracy. Many studies have commented on the propensity for ABS to warp post-deposition [180,273] and slicer generally includes higher bed temperatures to try to overcome this effect. Fitzharris et al. [274] commented on the degree of crystallinity again being a key driver for warpage behaviour. In order to provide the best dimensional performance for a given material, the flow and deposition characteristics must be properly understood. For the most popular thermoplastics this has been modelled in some detail, such as by Bellini et al [309]. However, for more novel materials the exact characteristics would benefit from further research.

7.1.2.4. TOOLPATH GENERATION

The toolpath is generated by the slicer according to its own toolpath algorithm, print parameters and the component geometry. The standard approach is to build a component layer-by-layer. Whilst there has been much work covering the optimal orientation of the component, this nonetheless usually requires that a two-dimensional toolpath is generated for each slice. Existing literature therefore covers both the toolpath within the slice as well as generation of slice height and therefore consecutive layers to produce three-dimensional components with optimal quality characteristics. In terms of toolpath optimisation, the two most prominent output metrics that have been identified are accuracy and build time. These factors are therefore considered in turn in this subsection.

XY plane deposition methodologies were introduced in Section 6.1 in the context of perimeter corner deposition. This section presented viable approaches for toolpaths at corners and also some methods to limit under-fill and over-fill errors within the interior. Jin et al. [554] presented an adaptive tool path generation method. This considered both surface quality and build time to produce contours. They then developed a hybrid tool path to improve both of these metrics whilst exploring contour parallel and direction parallel infill. Jin et al. [555] modelled the outer contours using Non-Uniform Rational Basis Splines (NURBS) and developed hybrid toolpaths to produce both the boundary and zigzag infill. They additionally considered an adapted travel speed approach to reduce build time whilst maintaining component quality. Han et al. [556] developed a deposition planning approach based on a grouping and mapping algorithm in order to improve the quality of functional parts, particularly reducing over- and under-fill within the layer. Volpato and Zanotto [557] explored the impact of deposition sequence for low cost ME AM. This work mainly focused on the resulting

mechanical performance, but found that deposition sequence strongly impacted this. Cao and Miyamoto [558] described a method for directly slicing from CAD files using lines, arcs and circles, to improve the slicing speed and accuracy. Simsek and Yaman [559] demonstrated the impact of infill around holes. They suggested that the use of symmetric depositions and control of the order could yield improved dimensional accuracy. Yaman [560] later refined this proposal further. Jin et al. [561] developed a toolpath algorithm to reduce the need for inter-deposition moves with their associated retractions. It has been noted in previous sections that the start and end of strands provide significant impediments to dimensional accuracy, so this approach may help improve component quality even though the study focused on reducing build time. Guerrero-De-Mier et al. [562] proposed a novel slicing methodology to reduce component warpage. In this approach, the component was broken up into blocks in a process referred to as 'bricking' to minimise the presence of long uninterrupted sections perpendicular to the build direction known to contribute to warping. Ghazanfari et al. [563] developed an adaptive raster pattern to reduce infill errors at the boundary, though this did not acknowledge the presence of contour parallel perimeters which usually mitigate these errors. Jin et al. [564] provided a novel path planning approach specific to thin-walled parts, though for sufficient part mechanical performance such features are often avoided. Jensen et al. [565] provided toolpath strategies for novel 5- and 6-axis AM machines.

The concept of cusp height tolerance was first introduced by Dolenc and Makela [340]. If a maximum allowable cusp height error is determined in advance, then suitable layer thicknesses and outer perimeter position can be generated. Boschetto and Bottini [62] analysed the virtual surface of components to be manufactured via ME AM to assess its suitability for production. This work focused on the error generated on slopes as a result of the layer-by-layer nature of the process. Anisotropic offsets are applied across the virtual model surfaces prior to manufacturing, and show a good level of improvement even when thermal and kinetic effects were not explicitly considered in the modelling. Mohan Pandey et al. [566] described the possibility of all slicing sitting either within the nominal outer surface, all outside the surface, or some combination of the two depending on whether cusp heights or volumetric errors are deemed more important. Kulkarni and Dutta [337] also studied the interaction of slice heights with the outer surface. They provided a detailed slicing method to reduce volumetric error again based on a prescribed cusp height. Chui et al. [567] developed a new slicing method to ensure unilateral tolerance. This selected slicing rules based on the working direction and outer surface normal vector. As with other studies, they identified that certain geometries are more prone to error; for example peaks, valleys and fine features.

Much of the literature regarding toolpath generation has focused on reducing build times. As with the accuracy-related studies outlined above, these again address the two primary aspects of XY plane deposition and (vertical) slicing procedures. Slicers typically allow the user to select infill proportions, print speeds and number of perimeters. Some guidance is given when the user interacts with these and

an estimated print time is calculated. In order to improve the build time, it is most common to reduce the infill (at the cost of mechanical performance) and increase print speed (at the cost of dimensional accuracy).

Sabourin et al. [339] proposed toolpath generation whereby the exterior was deposited more slowly for maximum accuracy, whilst a more rapid infill reduced build time. As noted in Section 6, current popular slicing software utilises this approach. Shoji et al. [568] also investigated high speed deposition techniques, by introducing variable nozzle feed speed depending on toolpath. Brooks et al. [569] explored the concept of variable deposition. They noted that a small nozzle is essential for fine details whilst leading to long build times. They developed a variable diameter nozzle and new toolpaths to demonstrate the validity of their approach. Kuipers et al. [570] and Xiong et al. [571] also dealt with variable width deposition via contour parallel toolpaths and variable extrusion rates, though they did not propose hardware revisions. The resulting method claimed improved build times as well as reduced dimensional error and voids. Papacharalampopoulos et al. [572] developed an infill-specific path planning approach based on Hilbert curves to reduce idle time associated with grid-based patterns. Shaikh et al. [573] also used Hilbert curves in their toolpath generation method and demonstrated the same improvements. Wang et al. [574] developed multiple print heads working at once with their own toolpaths. They identified regions of potential conflict and introduced algorithms to allow simultaneous deposition and reduce build times. Han et al [575] developed a build time analysis method to assess the most important parameters and their effect on other output characteristics with respect to build time. Lensgraf and Mettu [576] proposed an algorithm to print complex features in their entirety before moving elsewhere on the component. This vastly reduced build time for components where there were many closed geometries in a single layer, but also led to some printing inaccuracies from excessive heat build-up.

The analysis of cusp height error leads to the concept of adaptive slicing, whereby layer heights vary at the local level whilst maintaining cusp height limits. Tyberg and Bohn [577] first introduced this technique, though it has since been studied by many others [338,341,578-590]. This allows much faster build times by increasing height around more simple geometries. However, it should be noted that this reduces surface roughness as demonstrated in detail in Section 5 for vertical walls and on sloped walls due to the more prominent staircase effect.

In a departure from the common sequential deposition of two-dimensional layers, a number of studies have considered alternative approaches. The most common of these is known as curved layer deposition, or curved layer slicing [591-599]. In this process, the three-dimensional component is decomposed not into a series of parallel planes but rather curved planes which are usually defined relative to an upper surface. This reduces the presence of the staircase error on inclined surfaces and

can reduce component anisotropy. Similarly, Zhao et al. [600] developed a solution for inclined layer printing to reduce the need for support structures and improve surface roughness.

Whilst there has clearly been significant attention given to the generation of toolpaths within the ME AM process both to reduce build times and fabrication errors, these approaches have gained little traction in popular slicers. In many cases, the proposed solutions are highly complex or are not applicable to the grid-like infill patterns most commonly used in modern slicers. As a result, the toolpath for most components and most slicers remains relatively basic, consisting of contour parallel perimeters and porous grid infill.

7.1.2.5. *Extrusion Generation*

It has previously been discussed that the G-code assumes constant extrusion along the toolpath, but that in reality this is not achieved. Section 6.1 covered this phenomenon in some detail as well as the existing approaches to produce more uniform material flow. Whilst these will not be repeated here, it is worth reiterating that the improvements could be divided into two broad approaches. The first was to control the extrusion itself as a function of nozzle position and velocity. This involved matching the flow rate to the actually nozzle dynamics rather than the nominal uniform motion. The second was to alter the toolpath to ensure that current extrusion generation methods yielded improved performance. This usually resulted in more rounded toolpaths to reduce velocity changes at sharp corners in the XY plane.

7.1.2.6. *Novel Machine Design*

Improvement approaches presented in the previous subsections involve optimising the current process hardware. This has revealed significant research across component design and software aspects including process parameters, data file aspects and toolpath and extrusion generation. This subsection presents existing studies which have developed novel machine design elements in order to change the traditional ME AM process and yield performance improvement. These approaches can be grouped into the following categories, which are explored in turn: machine motion, extrusion/heating mechanism, nozzle design, deposition assistance and sensing/failure monitoring. Machines which integrate a further processing step are discussed separately in Section 7.3.

Kampker et al. [601] noted four main printer designs: Cartesian, polar, delta and robot arm. Park et al. [35] developed a 4-axis machine, where material was deposited around a rotating cylinder in order to fabricate an artificial trachea. There are numerous examples of the development of 5-axis machines. This motion has been achieved in different ways, but the most common purpose has been to remove the need for support structure on overhangs. Gilberti et al. [518] developed a 5-axis parallel kinematics machine to enable improved surface quality and remove the need for supports. Wang et al. [391] provide an implementation of a 5-axis dynamic slice algorithm to reduce the need for support generation. They used a rotating build plate to enable an additional two degrees of freedom and

demonstrated the validity of the approach on various complex geometries. Khan and Ademujimi [602] modified a 5-axis Cartesian CNC machine to produce complex components without support structures. Zhang et al. [603] undertook a very similar study, again demonstrating a reduced need for support material. Asif et al. [604] designed a 5-axis machine to reduce the need for support material in combination with a photocurable filament material. Isa and Lazoglu [605] developed a 5-axis machine based on the delta design to enable novel curved deposition paths. Finally, Lee et al. [298] also modified a 5-axis machine to combine ME AM with a CNC machining process.

Zhao et al. [599] developed a 4-axis rotary printer with dual extruders to enable curved layer deposition. They noted that this brought improvements in surface finish, geometrical accuracy and mechanical performance. Zhang et al. [22] developed a 6-axis machine to aid with the deposition of continuous fibre strands. This was based on a Cartesian system with three additional axes of rotation.

Wulle et al. [606] identified the requirements and capabilities of multi-axis ME AM systems. They again identified improved surface finish and the lack of support structures as benefits. They noted increased complexity of hardware and software, including avoiding collisions with the component as it is being fabricated. Minetola and Glati [41] investigated the use of self-replicated components on a low cost desktop machine to improve performance, including tensioners, rigid supports, anti-vibration support and bed levelling mechanisms. Hu et al. [607] utilised a two degree of freedom fixing mechanism for the bed enabling better dimensional integrity at high temperatures.

Hu et al. [607] added a heat collector module to the extrusion mechanism to enable the printing of high melting temperature materials such as PEEK. Bezukladnikov et al. [608] noted that once major disadvantage of the standard induction heating method is the unevenness of the heat distribution. They therefore presented an optimisation of the heating process via mathematical modelling and suggested improvements for more linear temperature distribution. Sukindar et al. [609] developed a design for a cylindrical heating block rather than the more traditional square section, which they demonstrated was better able to maintain temperature.

Gilberti et al. [518] developed a novel extrusion mechanism to deal with high viscosity mixtures with low polymeric content. Leng et al. [610] developed a conical screw-based extrusion mechanism. This was combined with a precise positioning and control system and yielded improved extrusion performance for soft materials such as TPU, which the traditional extrusion mechanism can have difficulties with owing to the increased elasticity. Hou [516] presented analysis of three separate extrusion mechanisms. They simulated the behaviour of piston and slide pump-based extruders to improve flow control and overall part quality. Netto and Silveira [611] developed a new print head incorporating a twin-screw extrusion mechanism. This enabled material mixing and demonstrated the potential for improved flow control. Han et al. [612] also developed a colour mixing extrusion mechanism based on two conventional extrusion mechanisms arranged in a Y-shaped geometry.

Similarly, Prusinowski et al [536] developed a mixing extruder to enable control of the polymer filling proportion for fibre reinforced composites. Klar et al. [613] presented a syringe-based extrusion mechanism based on an open source design. This was combined with a load cell to measure piston force and control material flow and was suggested as a viable solution for paste extrusion. Durna and Fries [614] provided a modification of the nozzle assembly to aid heat transfer and print materials with higher melting temperatures.

Sukindar et al. [615] investigated the effect of nozzle diameter on the extrusion of PLA during the ME AM process. They used FEA to model the pressure drop, concluding that a 0.2mm nozzle created a larger pressure drop and was therefore not optimal when compared to the more standard 0.4mm diameter. In their study of extrusion mechanisms, Hou [516] also investigated a design with reduced nozzle diameter which they found improved printing precision and did not lead to printability issues. Shaw et al [616] investigated the use of high aspect ratio nozzle to achieve high speed ME AM. This work focused on the deposition of pastes, but showed the potential for higher rates to be reached. Gao et al. [617] demonstrated that the angle within the nozzle and the radius of the transition arc and length of the extrusion section are important factors which affect output flow. Sukindar et al. [618] undertook analysis of the mechanical properties of components produced in PLA using a novel 3D printer nozzle. They altered die angle and nozzle diameter in order to improve strength. In a separate study [619], they also investigate the effect of die angle when printing polymethylmethacrylate (PMMA). They varied the angle from 80^{o} to 170^{o} and determined 130^{o} to be the optimal angle for consistent extrusion rate. Min et al. [620] proposed a lengthening of the nozzle flow passage in order to increase adhesive force against the melt and reduce over extrusion between depositions due to residual pressure. Li et al. [621] studied the die geometry of the nozzle against the non-Newtonian fluid flow in the ME AM process. They explored the use of different materials and geometries to improve the fluid flow and concluded that a non-parallel final passage improved fluid flow. Comminal et al. [356] conducted a detailed study of nozzle geometry on the deposited strand cross-section. They tested a cylindrical, square and side plate extension nozzle and found that the side plate improved compactness of the outer surface but that the square orifice offered no significant benefits over the standard cylindrical design. Tsao et al. [622] developed a novel nozzle design to allow vari-directional and vari-dimensional deposition. This design consisted of a controllable gate and flow channel together with additional axes of motion to perform freeform shapes and variable deposition. However, this design produced poor results when operating at a scale of below 1mm. Nienhaus et al. [623] tested a range of commercially available and custom-made nozzles to investigate the effect of various diameters and conical angles. They concluded that 56^{o} gave the lowest extrusion force, though noted that between 30^{o} and 118^{o} the contribution to overall forces was low. They also concluded that the effect of nozzle materials and the use of coatings has a negligible effect, but two entry channels had the possibility to increase maximum feed velocities. Despite this, Liu et al. [624] proposed to

change the nozzle material from the common aluminium bronze to beryllium bronze to reduce the likelihood of nozzle blockages.

Wei et al. [625] developed a nozzle cleaning mechanism to prevent damage to the nozzle and reduce error defects from total and partial blockages. Kłodowski [626] developed a novel nozzle assembly to eliminate the problem of melt leakage, which can lead to flow rate errors that in turn contribute directly to dimensional inaccuracy.

There have been some isolated studies which have combined additional processes with deposition to improve performance. Ravi et al. [627] integrated a laser ahead of the deposition path to improve interlayer bond strength. Wjesundera et al. [628] integrated the use of acetone vapour between layers to achieve similar improvements in strength, was well as noting improved surface finish and reduced porosity. Similarly, Maidin et al. [629] investigated vacuum assistance in the printing of ABS microstructure to improve tensile strength.

Wu et al. [630] developed a method for monitoring process failures via the analysis of acoustic emissions (AE). The found that nozzle blockages or lack of material feed could be analysed acoustically with an accuracy rate of over 90%, allowing corrective measures to be taken prior to complete failure. Liu et al. [631] also presented an acoustic-based solution, which they demonstrated to be effective for detecting relatively minor nozzle blockages. Yang et al. [632] utilised AE monitoring to target filament breakage in particular and demonstrated feasibility and effectiveness of their proposed system. Tlegenov et al. [633,634] presented a system for nozzle condition monitoring in ME AM. This approach focused on identifying nozzle clogging errors using a vibration sensor mounted to the chassis. Kim et al. [635] developed an in-situ motoring and diagnostic system based on a support vector machine (SVM) algorithm utilising both an accelerometer and AE sensor. This demonstrated fault detection accuracy of 87.5%.

A large number of studies proposed the use of optical systems to generate process performance data. Baumann and Roller [636] developed a vision based error detection system. This checked for component detachment, missing material flow and part deformation and allowed remote monitoring and alarms where these were detected. Wu et al. [637] developed a machine vision-based statistical process control of ME AM. This involved taking an image of each layer, extracting the contour and comparison with the nominal geometry. This was shown to be able to detect errors with an accuracy of 0.5mm, and was therefore not suitable for micro-geometrical errors. He et al. [638] monitored the geometric quality of components using a non-contact machine vision technique. The applied a statistical process control method which generated geometrical deviation data to detect layer shifts in particular. This approach was experimentally validated and shown to be effective. Preissler et al. [639] evaluated the effectiveness of a single camera mounted above the build plate versus stereoscopic vision systems. They concluded that both approaches were viable, though the 3D system

was preferable as it provided more detailed data. Preissler et al. [640] developed this approach further, integrating a three-dimensional hardware platform to capture point cloud data and identify errors such as warpage, blobbing, weak infill and poor bed adhesion. Liu et al. [641] demonstrated the feasibility of image analysis-based closed loop control. This combined the collation of image data with real time parameter control to improve component quality. Park et al. [642] measured axis deflection in real time using an optical sensor and corrected for the error. Nuchitprasitchai et al. [643] presented a method for 360 degree monitoring of the ME AM process using two cameras integrated with a low cost open source printer. They developed an algorithm in Python run on a *Raspberry Pi* computer to detect print failures in real time. Shen et al. [644] proposed an online vision detection system. This process collected image data, applied and combined multiple image processing techniques and showed a strong ability to identify layer defects. The majority of previous vision based systems were demonstrated to deliver improvements targeted against specific error modes, though were not generalisable to alternative component designs, machines, materials or parameters. However, recently Brion and Pattinson [645] presented an approach utilising deep learning with the capability to provide real time process improvement, particularly for novel materials or unknown parameters. Whilst all of the techniques outlined above rely on additional hardware and processing, it may not be necessary to include a full installation on all ME AM machines. Instead, it may be possible for manufacturers to utilise these approaches and the findings be integrated into suggested parameters or even into the physical design of the machine itself.

Lianghua [646] developed the concept of a ‘digital twin’ component in ME AM. Sensing data was used to create a digital copy of the component under production, which could then be analysed for contour errors. Rao et al. [647,648] proposed an online quality monitoring system using heterogeneous sensors to monitor ME AM in real-time. This involved the use of a complete range of thermocouples, accelerometers, IR sensors and a miniature borescope to detect errors. The authors showed that this set up was able to detect any error with an accuracy of approximately 85%. They noted this was superior to existing approaches for monitoring which were typically capable of between 55 and 75%. Moretti et al. [649] similarly proposed the development of a ‘smart’ ME AM system which used multi-sensor data fusion for in-situ monitoring. They noted that multiple sensors enabled detection of faults that single-sensor based solutions would miss.

Kousiata and Karalekas [650] monitored strain and temperature distribution during the deposition process. They integrated optical Fiber Bragg Grating (FBG) sensors for continual in-situ real-time monitoring and demonstrated that recorded strains were significant and temperature gradients were found across the build envelope, both of which can negatively affect dimensional performance. He et al. [651] developed an approach to error monitoring by measuring the temperature field of a component during deposition. This allowed the identification of the component geometry as well as deposition start and end points.

Coogan and Kazmer [652] proposed a solution for in-line rheological monitoring. This involved the measurement of volumetric flow and shear rates in combination with temperature to improve fluid flow accuracy. Similarly, Anderegg et al. [653] developed an in-situ flow temperature and pressure monitoring solution.

Tlegenov et al [654] proposed a nozzle condition monitoring solution based on current of the extruding motor, rather than vibration sensors as had previously been demonstrated. Similarly, Kim et al. [655] presented a study where the pressure was monitored within the melt chamber to detect material deposition errors. This was experimentally validated and showed that flow rate changes directly fed back to current levels supplied to the feeding motor.

Moretti and Senin [272] developed a solution to detect part warpage through analysis of the repulsive force acting on the extruder during subsequent layers. This approach showed warpage detection accuracy of over 90%, though did not seek to improve performance.

7.2. Error Compensation

In the context of ME AM, error compensation is considered to be machine-specific offsets given known (measured) errors. The application of compensation factors can then be added to the original virtual component to produce final dimensions closer to the nominal values. Alternative methods often referred to as compensation, such as generalised techniques to minimise feature-based errors or generic process offsets are considered elsewhere.

Before discussing existing work on error compensation, it should be noted that manual error compensation, specific to a machine, material and component is often the approach taken in practice by a user. This trial-and-error approach was outlined in Section 2 and was noted to mitigate many of the potential benefits of the ME AM process. The studies outlined here instead suggest the application of automatic compensation factors, which can either be applied to the input file or accounted for in the machine firmware.

In a 1995 publication, Sartori and Zhang [656] outlined methods for measuring geometric error of machines and applying software compensation. This provided generic approaches regardless of the exact process by developing a vectorial equation to describe errors, including highlighting 18 error modes. They recommended application at the production rather than machine level to improve errors.

Tong et al. [657] developed an error compensation method inspired by parametric evaluation of CMM and machine tool systems. They later updated this approach [183], where they proposed an error compensation technique which involved the production and measurement of reference geometry, comparison between actual and nominal values and the development of a virtual parametric error model. They noted that this could be applied either to the virtual part (STL) or in the slice file (machine code) and that in practice given machine resolution limits, it was not important which was

used. Cajal et al. [658] simplified the kinematic model of a Cartesian AM machine to 18 independent error functions. Reference artefacts containing various geometries were produced, and each was measured using a CMM. The 18 error modes were then quantified and compensated for, yielding an improvement of 70% in global error. Keaveney et al. [296] provided methodologies associated with CNC machining systems. They utilised an ISO230-4 standardised test and a Renishaw ballbar QC10 to populate an error model. Post-processing of the printing code yielded a 58% improvement in circularity error and a 90% reduction in squareness error. Song et al. [51] printed small cross-shaped components across the build envelope to measure error prior to error compensation. They determined that errors varied in their direction and magnitude depending on build plate position. Huang [659] provided an analytical framework for compensation of components produced on AM machines. They used a minimum area deviation criterion to offset two-dimensional shapes and covert this to three-dimensional components as produced in ME AM. Li et al. [660] determined error compensation values for a fabricated bracket for use with printed circuit boards. They produced an error model and calculated adjustment factors, which yielded significant improvement in the function of the component.

Rahman et al. [661] investigated scale errors in the fabrication of ABS components. They altered six processing parameters and measured scale errors. They found that these varied significantly with changing input parameters, which makes simple error compensation somewhat unsuitable. Boschetto and Bottini [662] proposed the use of a triangular mesh offset approach to improve dimensional accuracy. They noted errors of the order of tenths of a millimetre depending on the geometry, and demonstrated improved performance on both simple and complex geometries by applying their mesh offset. Stopp et al. [663] developed a novel method for machine calibration. They produced a series of test cubes across the build area which were then measured and compared against the nominal values. They found machine error to vary significantly depending on position. Through suitable calibration, they noted error improvement from 0.4mm±0.2mm to 0.04mm±0.03mm. Lyu and Manoochehri [664] provided an integrated error model with compensation to improve performance. They fabricated a reference artefact and measured it using a CMM to calculate coefficients for the error model.

Many studies have investigated shrinkage error, primarily of ABS which shrinks during solidification due to its high degree of crystallinity. Dao et al. [195] calculated a shrinkage compensation factor (SCF) using the ‘Christmas-tree’ test procedure. They found a SCF of 1.010 reduced mean error by over 50% for a component manufactured in ABS. Manmadhachary et al. [207] found correction factors for a bio-AM model produced via ME AM. They fabricated and measured a mandible using ABS and found a correction factor of 1.003, which they noted gave a dimensional error of within 0.3%. Dilberoglu et al. [196] calculated SCFs for ABS. They used FEA to predict shrinkage behaviour and applied correction factors after fabricating and measuring a component with a CMM. Ranganathan et al. [25] analysed SCFs of a part manufactured from ABS. They produced a

component and measured it via a CMM, finding a uniform SCF of 1.068. Bahnini et al. [230] calculated SCFs for circular and square shapes via modelling and measurement of fabricated components. They then modified the CAD file directly and demonstrated superior dimensional performance.

Sbaglia et al. [665] provided a simplified methodology for the calibration of a linear delta ME AM machine. They measured nine error modes and multiple positions using a dial gauge to produce a kinematic error model against which offsets could be generated.

7.3. POST-PROCESSING

Post-processing refers to the addition of a separate process after the production of an ME AM component to improve quality characteristics. Such processes can be categorised in terms of their physical mechanism; chemical, mechanical and heat. Studies which have proposed and demonstrated the use of each of these are provided in this subsection.

There have been a large number of studies which have investigated the use of chemical treatments to improve the performance of the ME AM process. These have generally focused on improving surface roughness by removal of the staircase or vertical layer effects and have overwhelmingly used ABS.

Kuo and Mao [666] and Kuo et al. [667] developed a precision surface polishing machine for ME AM components. They used an acetone vapour system to smooth ABS parts and reduce the surface roughness whilst maintaining dimensional accuracy. Nsengimana et al. [668] investigated mechanical post-processing on other AM technologies and vapour smoothing of an ME AM ABS component. They reported dimensional accuracy of approximately ±0.1mm after the vapour treatment. Galantucci et al. [669] provided a quantitative study of dimethylketone–water solution dipping to reduce the surface roughness of ABS components. They demonstrated improved surface roughness with no loss of mechanical performance, though sharp corners exhibited significant rounding. Jayanth et al. [670] investigated the application of acetone and 1, 2 dichloroethane chemical treatments on ABS components. They showed that the dichloroethane game the biggest improvement in surface finish and dimensional accuracy, but that tensile strength was reduced. Chohan et al. [234] investigated the use of vapour smoothing on dimensional accuracy and surface finish using ABS. They found that surface finish was improved but linear and radial dimensions both reduced after the smoothing process. Jo et al. [671] introduced two possible techniques to improve the surface finish of ABS parts. They provided experimental examples of an acetone fumigation/dipping and resin infiltration. They concluded that resin infiltration was the most promising method. Haidiezul et al. [672] demonstrated significant improvements in the surface finish of ME AM components through the use of *XTC-3D* chemical coating on ABS. In the interests of brevity, in addition to the above studies it is noted that many others have specifically addressed vapour smoothing of ABS components to improve surface finish [499,502,673-683].

Nguyen and Lee [684] proposed a methodology consisting of chemical treatment, and aluminium coating to produce improved surfaces suitable for high temperature applications. This process reduced surface roughness to approximately 2µm. Krishna et al. [685] investigated acetone vapour smoothing, shot blasting and laser assisted finishing of ME AM components. They concluded that vapour smoothing performed the best, whereas shot blasting led to loss of surface features and laser processing burned the surface leading to discolouration. Dixit et al. [686] explored the effect of electroless metallic coating on ABS to improve surface roughness. They investigated the deposition of copper and aluminium and found reductions in surface roughness of approximately 30%.

Jin et al. [687] have highlighted that chemical treatment of PLA has received little attention in existing literature. They therefore proposed a theoretical model and used dichloromethane to improve the surface roughness of components. The concluded that this process both improved surface finish and toughness of PLA specimens.

The most common mechanical process proposed in the literature is the use of CNC machining together with ME AM in a process commonly referred to as ‘hybrid AM’. There are many studies that have combined machining with other AM techniques such as SLA, SLS and metal welding processes, though only ME AM solutions are presented here.

Tomal et al. [469] noted two main issues with integrating CNC machining; running two separate control systems and alignment of the two toolpieces. Printing and machining components at layer heights of between 0.1mm and 0.2mm showed that the addition of a machining process improved dimensional accuracy by between 66% and 80%. Hu et al. [688] explored the optimal build orientation for components subject to CNC machining post-fabrication. They provided an algorithm to optimise for build time, machining accuracy and to allow tool access to surface features. Lee at al. [298] designed an integrated ME AM and machining 5-axis machine. This allowed the extruder and spindle to be interchanged with no reduction in build envelope. They noted improved dimensional accuracy and surface finish. Similarly, Amanullah et al. [689] proposed a CNC machining and ME AM hybrid machine which uses a rotary stage to eliminate misalignment errors. Boschetto et al. [690] applied CNC machining with variable cutting depths to reduce surface error without introducing inner defects. They developed a method of varying cutting depth with cutting angle to reduce average roughness and increase uniformity. Del-sol et al. [691] studied the surface quality of ABS components following machining. They discussed that vapour-based treatments are costly and can have a significant environmental impact. By using various milling path strategies, they demonstrated improvements in dimensional accuracy of 50% and surface roughness measurements by up to 90%. Kale et al. [692] optimised a CNC machining and ME AM hybrid process. They demonstrated that for similar performance to conventional machining, less material wastage was observed. Parenti et al.

[693] combined the extrusion of metals and ceramics with a green component milling operation. They showed that this allowed significant improvements in accuracy and surface quality.

Limited alternative mechanical operations have been added as a post-process. Pandey et al. [55] developed a hybrid system which utilised Hot Cutter Machining (HCM). They provided an adaptive slicing algorithm prior to machining, and demonstrated that in combination with machining this allowed lower build times and superior surface finish. This approach was later improved upon [694]. Grguraš and Kramar [695] utilised a CNC machining process after deposition with a much larger nozzle than standard. They demonstrated significantly reduced overall build times without detrimental effects on surface finish. Boschetto and Bottini modelled [696] and investigated [697] surface improvement via barrel finishing. They found that the deposition angle during fabrication significantly affected the rate of material removal and that surface profile height was reduced from approximately 60µm to 15 µm.

Some studies have utilised heat-based processes to improve the characteristics of ME AM components. Taufik and Jain [698] proposed a selective melting process to improve surface finish. They mounted a heated ball nose tool at 200^{o}C to the machine and melted the peaks of the layer-based surface profile. This reduced the surface roughness Ra value from approximately 16µm to 3µm. Chen et al. [699] presented a method of improving surface reflectivity. After production, a surface was pressed into glass and heated to produce significantly lower surface roughness. However, the authors noted significant shrinkage and dimensional fidelity loss of the component, and the proposed approach was limited to flat surfaces. Taufik and Jain [700] proposed a laser-assisted finishing process. This demonstrated complete removal of the visible surface roughness. Adel et al. [701] explored the use of hot air jets to improve surface finish. They demonstrated that this process was capable of reducing surface roughness from approximately 9 µm to less than 1µm. Thermal annealing of ME AM components has also been investigated, though this has focused exclusively on improving mechanical performance [702-704].

7.4. Proposed Process Improvement Approach

7.4.1. Limitations of existing proposals

The previous three subsections have collated existing methods of improving the ME AM process. However, whilst a significant amount of literature has been generated, the majority has not been adopted by popular machines or software and so has thus far had little impact for the typical user. These solutions often add complexity and cost, do not properly address the types of error investigated in the earlier sections and lack general applicability to the range of scenarios that an ME AM user might experience. This subsection provides a brief explanation of these shortcomings.

7.4.1.1. ERROR AVOIDANCE

Many studies have suggested disparate approaches for rules and support systems to help the user make design decision specific to ME AM, though these have typically addressed the use of print parameters rather than component design. Some publications have also included component design rules, but these have been quite general in nature. There are many further support systems which aid process attributes common between AM technologies such as layer geometry. It is evident that there is no single recognised set of rules for ME AM, and that users still lack clear and concise information, as Wang et al. [406] have noted. This is validated by the trial-and-error approach which is commonly adopted by users.

Whilst parameter optimisation studies have been widespread, their findings have not been adopted by popular slicers. A wide variety of print parameters have been investigated and their effects on output characteristics measured but because other factors are rarely constant, such as component design, slicer and material, generalisable rules cannot be gained. There is relatively little scope for improvement in data file handling, and such factors become less relevant if geometry isn't highly complex. Toolpath generation approaches have largely focused on speed and surface roughness rather than dimensional error, and as such have limited applicability. Extrusion generation has often also not focused on macro dimensionally performance and where it has, relatively complex systems to control fluid flow have been proposed. These also lack general applicability to specific materials, machine design and geometry and undoubtedly add cost and complexity to the process. Materials research has tended to concentrate on achieving printability for novel materials rather than dimensional error of the most popular polymers. Finally, novel machine designs have also rarely focused on increasing accuracy. More complex motion systems primarily address support reduction. Other machine design elements improve the process slightly, but leave the same fundamental problems of fluid flow control and subsequent deposition errors. Monitoring systems mainly aim to avoid outright failure and lack the resolution to detect the smaller dimensional errors demonstrated in previous sections, and in any case once more add significant cost and complexity.

7.4.1.2. ERROR COMPENSATION

To produce error compensation metrics for a specific machine necessarily requires the fabrication of test components then accurate measurement of various features. Clearly, for the typical user access to and knowledge of such measurement systems is not likely to be feasible. It is possible that machine manufacturers could calibrate machines prior to distribution, however many popular desktop machines require self-assembly which would make this approach impossible.

Regardless, because the performance of the process is known to vary with component design, print parameters, material and even environmental factors, any attempt to quantify and correct for errors is necessarily narrow and could yield worse results in certain circumstances. Efforts are likely best

placed in reducing machine error and variability through high quality machine design and components.

7.4.1.3. POST-PROCESSING

Effective post-processing techniques were shown to mainly consist of chemical, mechanical and heat-based approaches. However, the addition of separate processes to ME AM requires new hardware and software to be integrated and therefore also adds complexity, time and cost. The extant literature has also revealed that the processes themselves have limitations both in application and output characteristics. For example, chemical processes have almost exclusively been applied to ABS, whereas PLA has been an increasingly important material for safe and cheap ME AM production. Similarly, heat-based processes are not applicable to certain materials such as composites and pastes and mechanical approaches cannot be applied to all component geometries. In terms of improved performance, the vast majority of these post-processes deal with improvements in surface finish rather than component dimensional accuracy. In some cases, the improved surface finish is to the detriment of other quality characteristics such as mechanical performance or dimensional error, particularly of sharp corners or small features. As a result, they have limited applicability to improve the accuracy and precision errors outlined in the previous four sections.

7.4.2. HARDWARE VERSUS SOFTWARE

The modes of error improvement presented in this section have variously been applied at the hardware or software level. For example, extrusion flow control methods, new toolpath approaches and parameter optimisation studies all utilise the current process and modify software to achieve improvements. Conversely, novel machine motion systems, nozzle designs and post-processing techniques all require hardware revision.

Regardless of the approach taken, it is clearly preferable for process improvements to be realised independently of user interaction wherever possible to remove the possibility of human error, streamline the process and remove the need for extensive user experience. The ME AM process has shown to be complex, consisting of the heating and extrusion of non-Newtonian polymers through a sub-millimetre scale nozzle into fine deposited strands. Although in specific circumstances, the software approaches have been demonstrated to yield improved results these are often highly complex solutions and have yet to be implemented on desktop ME AM machines. The process is highly sensitive to the selection of process parameters, material, machine design and component geometry. Given there are a great number of possible combinations of these, delivering improved performance in all situations is therefore a very difficult task.

In contrast, hardware solutions aim to alter the process in some fundamental manner for all situations. As an example, improvements in machine motion through the addition of axes of rotation or the application of CNC machining post-process produces improvements impossible via software

modulation alone. In the case of CNC machine, the sensitivity to print parameters is reduced such that the complexity of processing may be reduced for the end user. Although many hardware solutions add some processing complexity, they nonetheless present an opportunity to radically improve the fundamental performance of the ME AM process.

7.4.3. PROPOSED HARDWARE APPROACH

Despite the numerous examples of potential solutions outlined in this section, these have not been incorporated into popular machines or slicers today. The proposed approach investigates a new nozzle and machine design and associated slicing parameters which can be taken together with the aim of yielding immediate improvements.

Comminal et al. [356] conducted a numerical study of three different nozzle designs. The first two designs were the standard circular orifice versus a square section. Whilst the square section has a different geometry and a slightly higher throughput, it was demonstrated that following the deposition and solidification of molten material the final strand morphology was unaffected. In this same study, a novel nozzle design incorporating a side plate extension was also modelled. The presence of this plate marginally increased printing forces (though less than for the square section nozzle) and suggested a significant improvement in the outer deposition surface. This study was limited to numerical modelling and so did not demonstrate the practical feasibility of the design. It is proposed that physical experimentation utilising this design is undertaken to demonstrate the validity of the model.

The design with a side piece theoretically enables a consistent vertical side geometry to be realised despite flow irregularities. Previous experimentation has shown significant changes in strand morphology and outer perimeter geometrical accuracy both for changing print parameters and at direction changes. Such a design therefore has significant potential for rectifying these errors and reducing the sensitivity of the process to changing parameters, materials and geometry. In addition to improved dimensional accuracy, the proposed design may have other benefits. Surface finish was shown to deteriorate with increasing layer height, whereas theoretically a uniform vertical edge would be unaffected and so would enable lower build times. The altered strand morphology may also enable larger inter-strand bonding areas and lower bulk porosity leading to improved component mechanical performance.

The previous numerical study considered only steady state straight depositions. Clearly, to deposit a closed outer perimeter the nozzle must also rotate such that the side piece is always parallel to the instantaneous direction of travel and is on the outer edge of the perimeter. This requires the addition of a fourth axis for the rotation of the nozzle relative to the build plate.

The experimentation of this new design consists of two aspects. First, the steady state performance of the novel nozzle design is determined. Second, the most promising design and print parameters are translated to XY performance in combination with a modified ME AM machine allowing rotation.

8. MODIFIED NOZZLE GEOMETRY STEADY-STATE FILAMENT MORPHOLOGY

This section describes the experimental work undertaken with novel nozzle designs which incorporate an additional side piece to guide material extrusion and deposition, hence improving the uniformity and surface profile of strands. First, preliminary studies are undertaken of a number of modified nozzle designs to understand the impact of various design parameters and machine setup factors. This is necessary as this work is completely novel, with a modified nozzle of this nature and scale only having been explored in the theoretical modelling approach used by Comminal et al. [356]. Following these qualitative investigations, the most promising modified nozzle design and experimental setup is selected for a quantitative study, whereby the optimum print parameters are selected with the newly-modified nozzle via a parameter optimisation study. The results from this are then used to inform the inputs for the XY plane experimentation in the next section.

The morphology of filament cross-sections for the current ME AM process was explored in detail in Section 5. This experimentation specifically covered the steady-state behaviour of the standard process, removing the variability associated with the acceleration and decelerations necessary for direction changes. This demonstrated a relationship between surface roughness and both layer height and aspect ratio (i.e. volumetric flow rate). Notwithstanding the additional flow rate variability around corners, it is expected that the addition of a nozzle side piece has the potential to produce lower sensitivity to these factors and an improved overall surface roughness and geometrical accuracy as any extrusion related errors primarily manifest on the internal perimeter surface.

8.1. METHODOLOGY

This subsection presents both the experimental procedure and design of the modified nozzles used first in the preliminary study and later in the parameter optimisation experimentation.

8.1.1. EXPERIMENTAL DESIGN

Throughout the experimentation in this section, low-cost ANet A8 desktop ME AM machines are used as were utilised in the entirety of the unmodified process experimentation (current performance, positional performance, steady state morphology and XY plane geometrical performance). This enables continuity of results and also allows for direct comparison of the results in this section with those of the unmodified process in Section 5. Both nozzle designs 3 and 4 and the parameter optimisation study contain repeated experimental runs using a separate but identical machine with a newly-fabricated nozzle.

As was discussed in Section 5, experimentation of the external perimeters in isolation requires the use of custom G-code. The G-code generator used in the standard nozzle steady state study was re-used. This approach was demonstrated in Figure 12.4 in the Appendix, with the only modification made to

layer height. Whereas with a standard nozzle, the initial layer height requires a gap between the nozzle and the bed, the first layer with a side piece present has no gap between the lowest part of the nozzle and the bed. Each layer was therefore printed at a layer height of *LH*(n-1)* where n is the layer number currently being deposited.

Prints were conducted with the modified nozzle fixed in position. The side piece was located on the right hand side of the machine as viewed from the front, with Y motion again occurring from the rear to the front of the build plate for strand deposition. Machine calibration in terms of build plate and gantry axis alignments were again conducted using the standard manufacturer's recommended approaches.

Sample production and preparation for measurement were conducted in line with the previous steady state experimentation. As before, this involved printing on a removable acrylic slide as part of a modified build plate, setting this in resin, cutting and polishing, then measurement using a *Zeiss Olympus BX51 TRF-6* Optical Microscope with 5x magnification. Analysis of the strand morphology was conducted using a mix of *ImageJ* and *Microsoft Excel*. In all presented examples, the modified surface is on the left-hand side of strand cross-sections and the print direction was into the page.

Following the initial measurement of earlier nozzle designs, it became clear that nozzle side piece alignment was an important factor in determining the outer surface morphology. Experimental runs were therefore conducted to specifically address this, utilising nozzle sidepieces at 5 angles between significantly trailing and significantly leading (i.e. whether the trailing or leading edge were inboard of the direction of motion). This was conducted for single and double perimeters, and for 0.2mm and 0.4mm step height designs. A new alignment methodology was introduced to measure this. First, a marker pen was mounted the gantry and the Y axis moved to draw a line on the print bed. A piece of adhesive putty was placed next to the line, and the nozzle moved above that position on the build plate. The Z axis position was reduced until a semi-circular imprint was left in the putty. A 45x magnifier was used to manually judge alignment, and adjustments made as necessary. This approach was then applied to the experimental runs presented in this section, as demonstrated in Figure 12.6 in the Appendix.

8.1.2. MODIFIED NOZZLE DESIGN

There are various aspects of the modified nozzle which can be changed and which may affect the morphology of deposited strands. In this section, four separate designs are presented and their potential merits discussed. These are modified from standard brass 0.4mm diameter nozzles on a CNC milling machine. Since most popular slicers and the previous XY plane experimentation utilised a 0.2mm layer height, three of the four nozzle designs contain a side piece step height of 0.2mm. The fourth design uses 0.4mm to explore the possibility of improved surface finish with the combined benefit of increased build speed.

The four designs are as follows:

- Design 1 - Simple modification to the standard nozzle with a 0.2mm step height. This gives a trapezoidal side piece of a maximum length.
- Design 2 - As per design 1 but with leading and trailing edges square.
- Design 3 - Full bespoke nozzle design consisting of 0.2mm step height and long side piece
- Design 4 - As per design 2 with a 0.4mm step height

Photographs of each of these nozzle designs are included in Figure 12.7 in the Appendix.

8.1.2.1. *Modified Nozzle Design 1*

The geometry if this nozzle is shown in Figure 8.1. This was produced via a straightforward milling operation of a 0.2mm depth on a standard 0.4mm diameter nozzle.

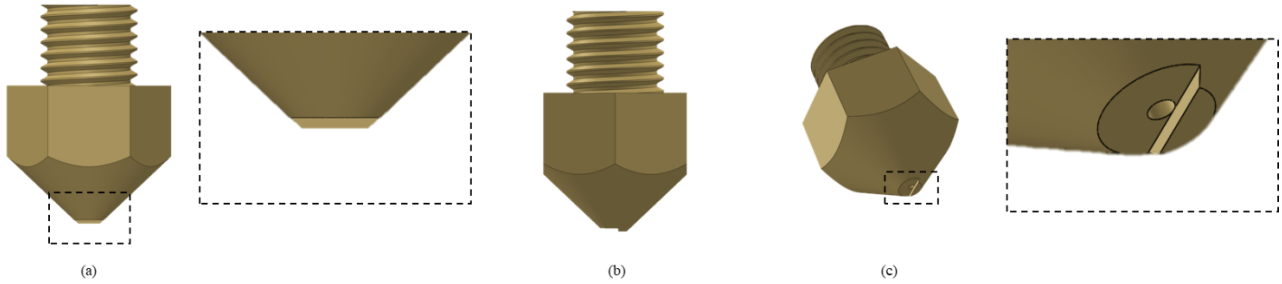

Figure 8.1 *Modified nozzle design 1*

This design maximises the side piece length without a custom nozzle being fabricated. This reduces the likelihood of the extruded material moving beyond the side piece under high extrusion rates. However, interactions between the deposited material and the trailing edge of the side piece is likely to be uneven due to the trapezoidal geometry. The experimental runs used in conjunction with this nozzle are listed in Table 8.1.

Number(s)	Purpose	Print Speed (mm/min)	Temperature (ºC)	Extrusion Factor	Other
1,2	Default parameters - baseline test	1800	200	1	-
3	Lower print speed	450	200	1	-
4	Higher print speed	3600	200	1	-
5	Increased EF	1800	200	1.2	-
6,7	Increased EF	1800	200	1.5	-
8	Increased EF	1800	200	2	
9	Lower temperature	1800	170	1.2	-
10	Lower temperature	1800	170	1.5	-
11	Higher temperature	1800	230	1	-
12	Higher temperature	1800	230	1.2	-
13	Higher temperature	1800	230	1.5	-
14	Wipe	1800	200	1.5	Wipe, no offset
15	Specific layer behaviour	1800	230	1/1.5	16th layer EF 1.5, all other layers EF 1

Table 8.1 *Modified Nozzle Design 1 Experimental Plan*

Two baseline runs are conducted with standard printing conditions. An extrusion factor of 1 is related to the volumetric flow of a 0.2mm and a width of 0.4mm (i.e. a nominal cross-sectional area of 0.08mm^2). An EF of 1.5 represents a 50% increase in this nominal area. Next, the effect of speed changes are explored and then changes in volumetric flow rate via the change in EF. Lower and elevated temperatures are then explored in combination with changing flow rates to understand the material-side piece integration. A zero offset wipe (i.e. the deposition path is repeated without deposition for every layer) is introduced to determine any potential improvement. Finally, a single high extrusion rate layer is isolated for characterisation.

8.1.2.2. *Modified Nozzle Design 2*

This nozzle design takes the previous geometry and adds square leading and trailing edges. The main potential benefit of this approach is hypothesised to be that interactions with the trailing edge would not be affected by asymmetrical geometry as in the first design. However, the shortened length (to approximately 0.98mm) may mean a greater propensity for over-extrusion beyond the side piece. In addition to a side piece aligned with the nozzle orifice edge, a side piece with an offset of 0.1mm inboard was also produced. It was expected that this would enable a greater degree of interaction with the side piece and therefore potentially a more well-defined square outer geometry. These designs are shown in Figure 8.2.

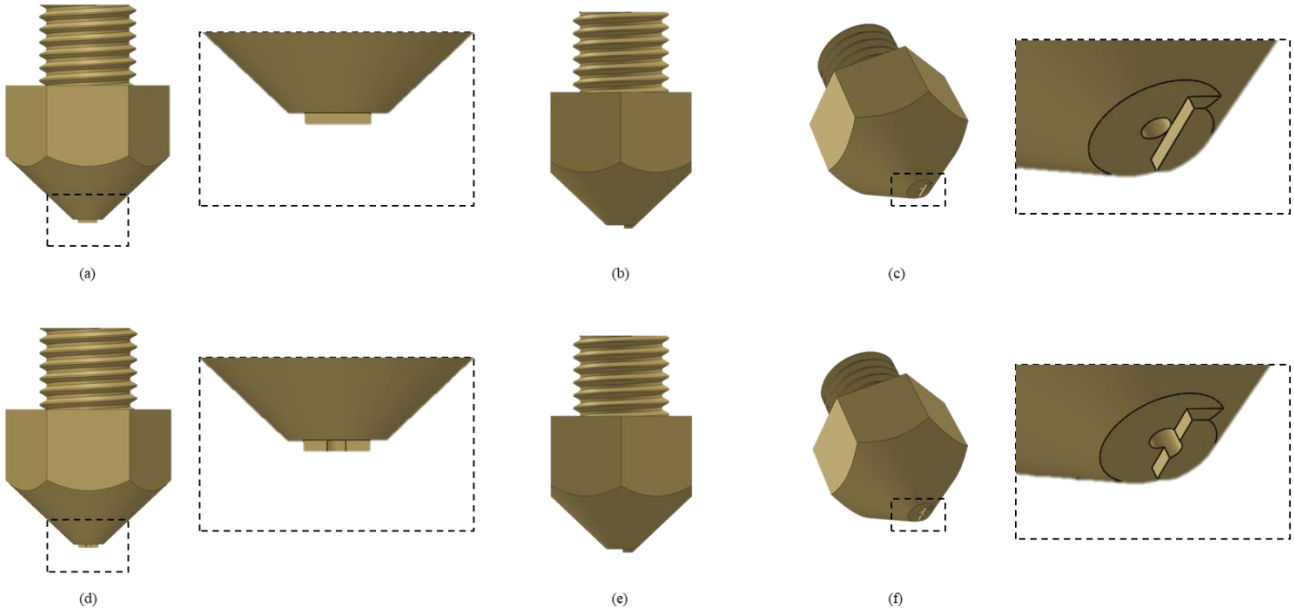

Figure 8.2 *Modified nozzle design 2 with no shoulder offset ((a)-(c)) and 0.1mm offset ((d)-(f))*

The experimental runs used in conjunction with this nozzle are listed in Table 8.2.

Number(s)	Purpose	Print Speed (mm/min)	Temperature (ºC)	Extrusion Factor	Other
1,2,3,4	Default parameters - baseline test	1800	200	1	First two nozzle 1, second 2 nozzle 2
5	Increased EF	1800	200	1.1	-
6	Increased EF	1800	200	1.2	-
7	Higher print speed	3600	200	0.9	-
8	Higher print speed	3600	200	1	-
9	Higher print speed	3600	200	1.2	-
10	Higher print speed	3600	200	1.5	-
11	Lower print speed	900	200	0.85	-
12	Lower print speed	900	200	1.5	-
13	Lower temperature, low EF	1800	170	0.85	-
14	Lower temperature, low EF	1800	170	0.9	-
15	Higher temperature, higher print speed	7200	230	1	-
16	Higher temperature, higher print speed	7200	230	1.5	-
17	Reduced layer height	1800	200	1	Layer Height 0.1mm, Road Width 0.4mm
18	Reduced layer height	3600	200	1.5	Layer Height 0.15mm, Road Width 0.3mm
19	Reduced layer height	3600	200	1.2	Layer Height 0.18mm, Road Width 0.36mm
20	Increased layer height	3600	200	1	Layer Height 0.3mm, Road Width 0.6mm
21	Wipe	3600	200	1	Wipe, no offset
22	First layer only	1800	200	5	Only initial layer printed
23	Offset side piece	1800	200	1	Change to modified nozzle design, side piece 0.1mm offset inboard of nozzle diameter
24	Offset side piece	1800	200	1.2	Change to modified nozzle design, side piece 0.1mm offset inboard of nozzle diameter
25	2 Perimeters	1800/3600	200	1.3	Inner perimeter F3600, Outer Perimeter F1800
26	2 Perimeters	1800/3600	200	1.6	Inner perimeter F3600, Outer Perimeter F1800

Table 8.2 *Modified Nozzle Design 2 Experimental Plan*

In addition to the experimental runs outlines for nozzle design 1, a greater range of print speeds are explored. As was mentioned previously, a 0.1mm offset side piece nozzle is also used for two separate extrusion rates. Alternative layer heights are also tested to understand the interaction with previous layers where the side piece extends beyond the bottom of the current layer. The first layer is also isolated in an experimental run which uses the acrylic slide as a fixed previous layer. Finally, double perimeters are tested to understand the interaction of neighbouring depositions with the modified nozzle.

8.1.2.3. MODIFIED NOZZLE DESIGN 3

The third nozzle design involves a 0.2mm step height with a long side piece. This ensures that over-extrusion beyond the side piece is very unlikely and so helps inform any outer surface deviations. This design entails a bespoke nozzle to be fabricated, again manufactured from brass using a CNC machining operation.

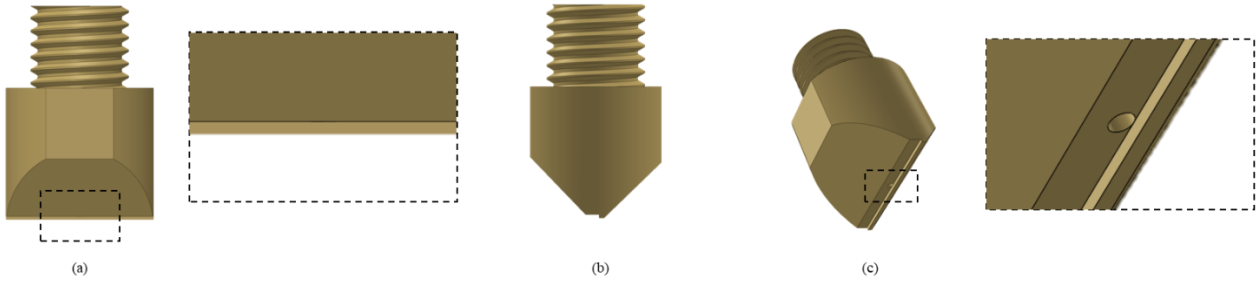

Figure 8.3 *Modified nozzle design 3*

Whilst the longer side piece ensures that in-layer over-extrusion is unlikely, this geometry does mean that isolated fine features may not be possible without clashing with previous depositions. In addition, it is likely that this design may apply more heat to previous layers which could both improve bonding and reduce dimensional performance. The experimental runs used in conjunction with this nozzle are listed in Table 8.3.

Number(s)	Purpose	Print Speed (mm/min)	Temperature (ºC)	Extrusion Factor	Other
1	Default parameters - baseline test	1800	200	1	-
2	Increased EF	1800	200	1.1	-
3	Increased EF	1800	200	1.2	-
4	Increased EF	1800	200	1.3	-
5	Increased EF	1800	200	1.4	-
6	Increased EF	1800	200	1.5	-
7	Increased EF	1800	200	1.75	-
8	Increased EF	1800	200	2	-
9	Lower temperature, slower print speed	900	170	1.2	-
10	Higher temperature	1800	230	1.2	-
11	Multiple EFs	1800	200	1/2/3	Layers alternately EF 1,2,3
12	First layer only	1800	200	2	Only initial layer printed
13	2 Perimeters	1800	200	1	-
14	2 Perimeters	1800	200	1.2	-

Table 8.3 *Modified Nozzle Design 3 Experimental Plan*

In addition to the experimental runs undertaken for the previous nozzle designs, a run where the EF is alternated between 1, 2 and 3 on alternating layers is included. This helps identify where the additional material is deposited in higher extrusion rate cases.

8.1.2.4. MODIFIED NOZZLE DESIGN 4

The final nozzle design repeats design 4 with a 0.4mm layer height.

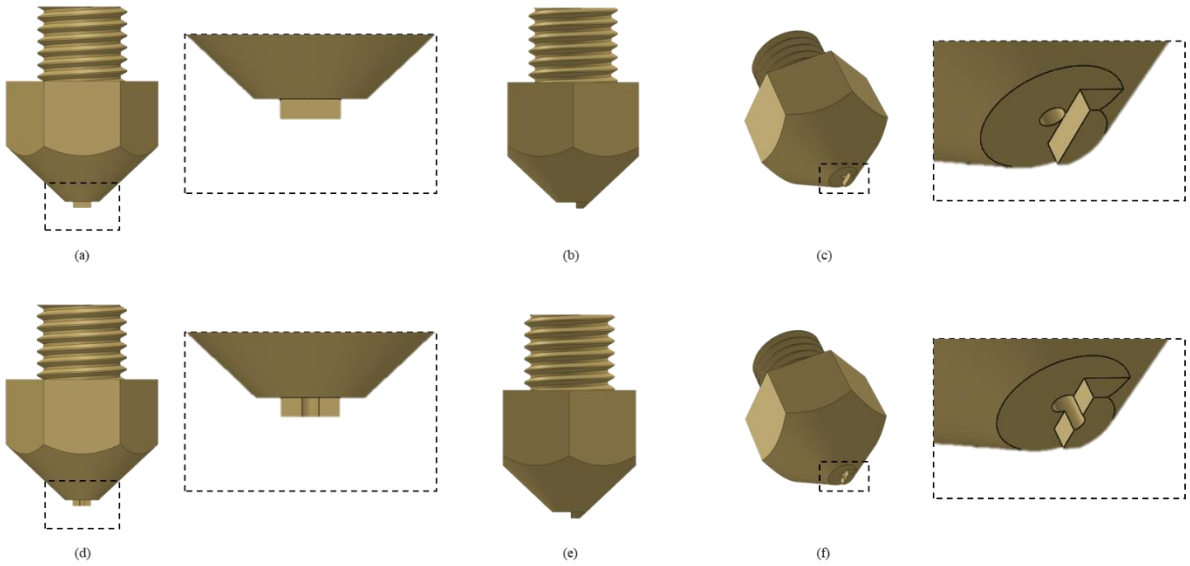

Figure 8.4 *Modified nozzle design 4 with no shoulder offset ((a)-(c)) and 0.1mm offset ((d)-(f))*

This design requires increased volumetric flow rates. In this case, the standard EF value of 1 represents a layer height of 0.4mm and a road width of 0.4mm, giving a cross-sectional area of 0.16mm^2. Whilst this layer height is larger than is typically used in the ME AM process, modified machine-based processes have often used layer heights in excess of the standard. For example, in a hybrid CNC process a layer height of 1mm was used [298]. The increased step height will reduce the heating of the previous layers and allows for a greater range of volumetric flow rates, though proximity to process rate limits may lead to less stable extrusion. The experimental runs used in conjunction with this nozzle are listed in Table 8.4.

Number(s)	Purpose	Print Speed (mm/min)	Temperature (ºC)	Extrusion Factor	Other
1	Default parameters - baseline test	1800	200	1	-
2	Increased EF	1800	200	1.1	-
3	Increased EF	1800	200	1.2	-
4	Increased EF	1800	200	1.3	-
5	Increased EF	1800	200	1.4	-
6	Increased EF	1800	200	1.5	-
7	Increased EF	1800	200	1.75	-
8	Increased EF	1800	200	2	-
9	Lower Temperature, increased EF	1800	170	1.5	-
10	Higher Temperature, increased EF	1800	230	1.5	-
11	Reduced layer height	1800	200	1.5	Layer Height 0.3mm, Road Width 0.6mm
12	Multiple EFs	1800	200	1.1/1.2/1.3/1.4/1.5	Layers alternately EF 1.1,1.2,1.3,1.4,1.5
13	Multiple EFs	1800	200	1/2/3	Layers alternately EF 1,2,3
14	Wipe	1800	200	1.5	Wipe, no offset
15	Wipe	1800	200	1.5	Wipe, offset of 0.05mm
16	Multiple Filament Colours	1800	200	1.75	Change of filament colour between certain layers
17	Offset side piece	1800	200	1	Change to modified nozzle design, side piece 0.1mm offset inboard of nozzle diameter
18	2 Perimeters	1800	200	1	Inner perimeter F3600, Outer Perimeter F1800

Table 8.4 *Modified Nozzle Design 4 Experimental Plan*

As previously, baseline tests, changing EFs, temperature changes, wipes, offset designs and double perimeters are all investigated. In addition to these, alternative colours are investigated since previous studies [28,553] have suggested PLA colour can affect performance. Additional colours have also been used in alternate layers in a process the same as that demonstrated in Section 5 with the multicolour filament experimentation. This enables the visualisation of inter-layer and material-nozzle side piece interactions.

8.1.2.5. PARAMETER OPTIMISATION

The use of parameter optimisation studies was discussed in Section 7.1.2.1. These were found to be limited in their general applicability because machines, materials and components vary between studies. Regardless, with the presence of a specific modified design such an approach has greater relevance in this case to understand the general behaviour. In addition, the parameter optimisation will enable the determination of factors which influence the output performance characteristics and what combination gives the best performance. As with the standard nozzle design, cross-sectional area, bond width, horizontal deviations and the surface roughness metrics of Rz, Ra and Rq are presented in the results. Calculations for these were outlined in Section 5.2 and are not repeated here.

As was noted previously in the discussion of parameter optimisation studies, it is common practice to calculate signal-to-noise (S/N) ratios to investigate the optimal print parameters. The relevant formula

for this depends on whether values are required to be minimised (such as errors) or maximised (such as bonding widths). The formulae for these two cases are demonstrated below in Equation 12 and Equation 13.

$$S/N = -10\log_{10}\left(\frac{\sum(Y^2)}{n}\right)$$

Equation 12 *Smaller-the-better SN ratio calculation*

$$S/N = -10\log_{10}\left(\frac{\sum\left(\frac{1}{Y^2}\right)}{n}\right)$$

Equation 13 *Larger-the-better SN ratio calculation*

where; Y = responses for a given factor level and n = number of responses.

In addition, ANOVA analysis has been undertaken in order to understand which of the selected print parameters have a significant effect on the output. Calculations required for ANOVA are shown in Equations 14 to 17.

$$S_T = \sum_{i=1}^{N}(n_i - \bar{n})^2$$

Equation 14 *Total sum of squares calculation*

where; S_T = total sum of square, N = total number of observations and $\bar{n}$ = overall mean of the S/N ratio

$$SS_j = \sum_{i=1}^{l}\left(n_{ji} - \bar{n}\right)^2$$

Equation 15 *Sum of squares calculation*

where; SS_j = sum of square deviation of *j*th factor and l = level of *j*th factor

$$V_j = \frac{SS_j}{f_j}$$

Equation 16 *Variance calculation*

where; Vj = variance of *j*th factor and f_j = degrees of freedom of *j*th factor

$$F_j = \frac{V_j}{V_e}$$

Equation 17 *F-ratio calculation*

where; F_j = F-ratio of the jth factor and V_e = variance of error

From the F-ratio and the degrees of freedom, a p-value is then calculated. This is the probability of rejecting the null hypothesis (i.e. that an offset occurs purely as a result of randomness rather than as a result of the control factors). This is considered valid if it is below 5% as is standard practice.

Three factors each of three levels (see Figure 8.5) were selected for the parameter optimisation study based on the findings from the preliminary studies.

Factor	Units	Levels
Temperature, *T*	^{o}C	170 200 230
Print Speed, *v*	mm/min	900 1800 3600
Extrusion Factor, *e*	-	1 1.2 1.5

Figure 8.5 *Parameter optimisation factors and levels selected for experimentation*

Given the relatively low number of factors and levels, a full factorial experimental design was selected, which with repeats gives 54 separate experimental runs. In Figure 8.11, the 27 unique parameter settings are displayed with a -1 and -2 identifier for experimental runs one and two.

8.2. RESULTS

These results are divided into two main sections. The first is preliminary studies, where detailed images for each of the modified nozzle designs were obtained and the behaviour of the deposited filament were investigated as a function of changing parameters and nozzle design. These studies were then used to select the relevant modified nozzle design to progress to more formalised studies, both for steady-state parameter optimisation (in this section) and then subsequent experimentation of the XY plane performance (in the next section). This was found to be design 4 (i.e. a step height of 0.4mm), for which dimensional results, main effect plots and ANOVA analysis are then presented.

8.2.1. PRELIMINARY STUDIES

8.2.1.1. SENSITIVITY TO NOZZLE ALIGNMENT

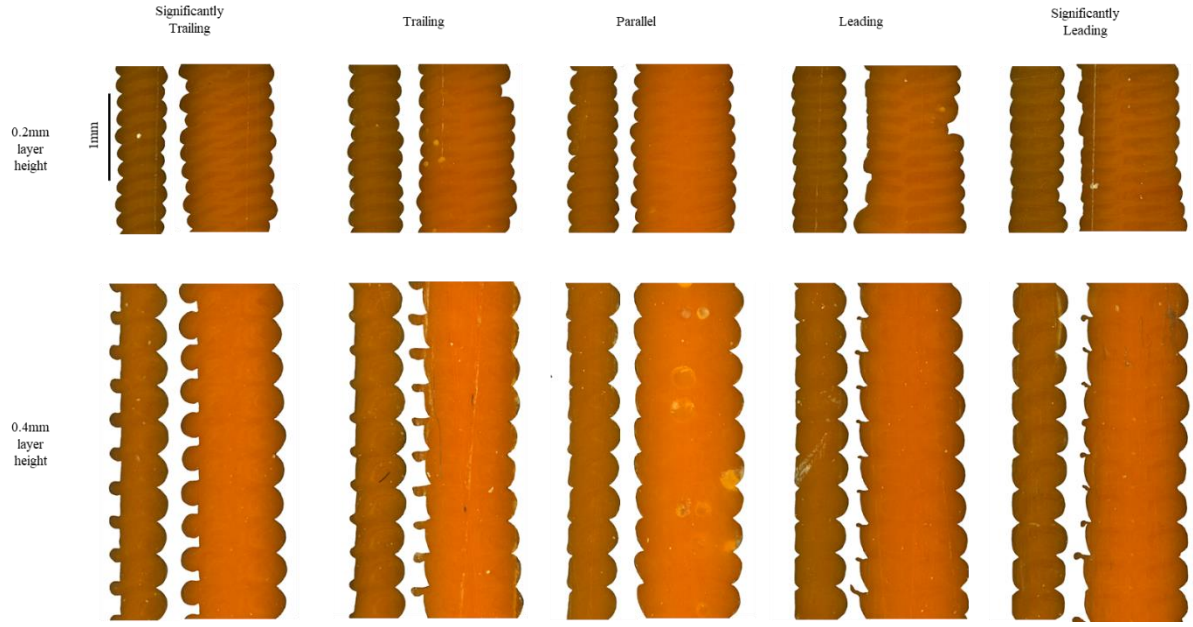

Figure 8.6 *Alignment tests for 0.2mm (design 2) and 0.4mm (design 4) modified nozzles using a temperature of 200°C, EF of 1.5 and outer perimeter print speed of 1800mmmin^{-1}*

8.2.1.2. MODIFIED NOZZLE DESIGN 1

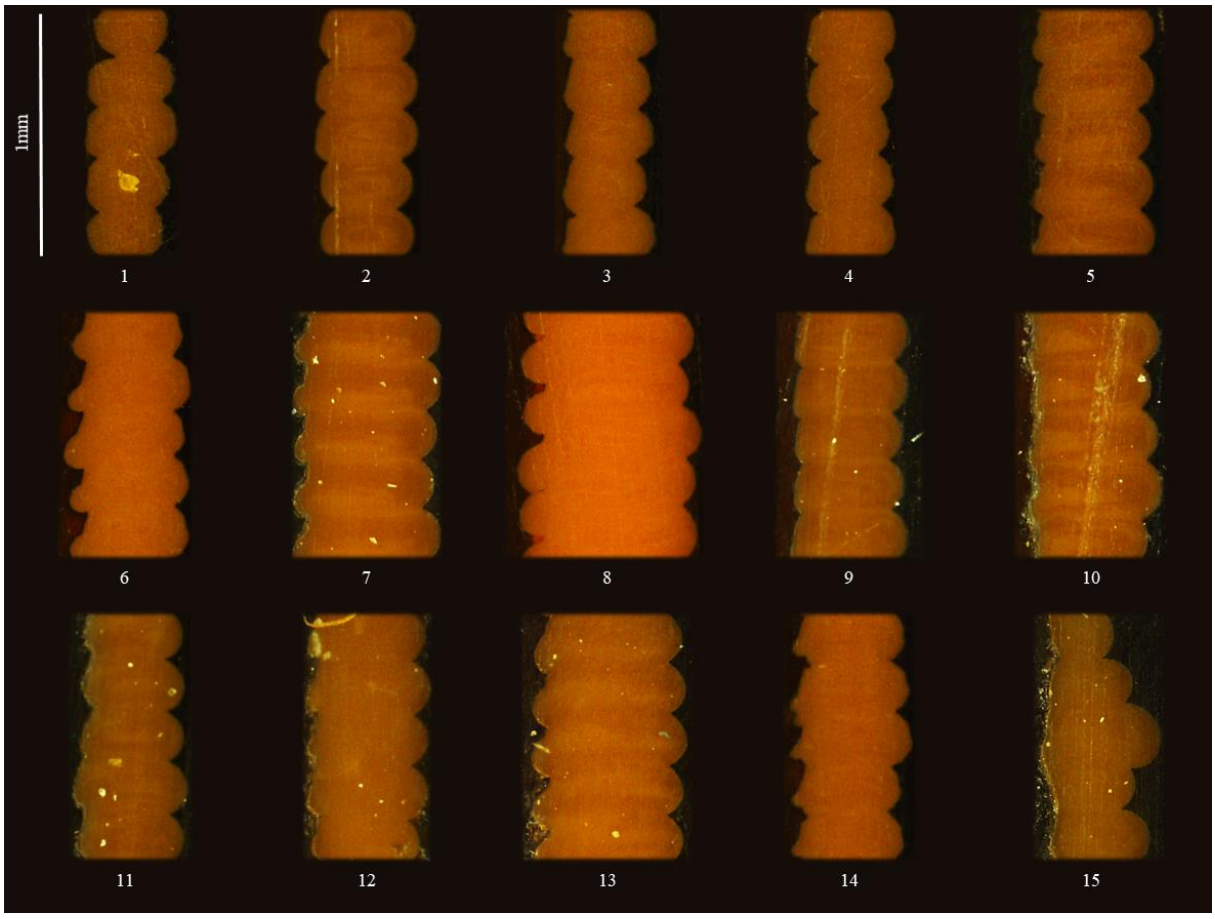

Figure 8.7 *Cross-sectional images Modified Nozzle Design 1*

8.2.1.3. MODIFIED NOZZLE DESIGN 2

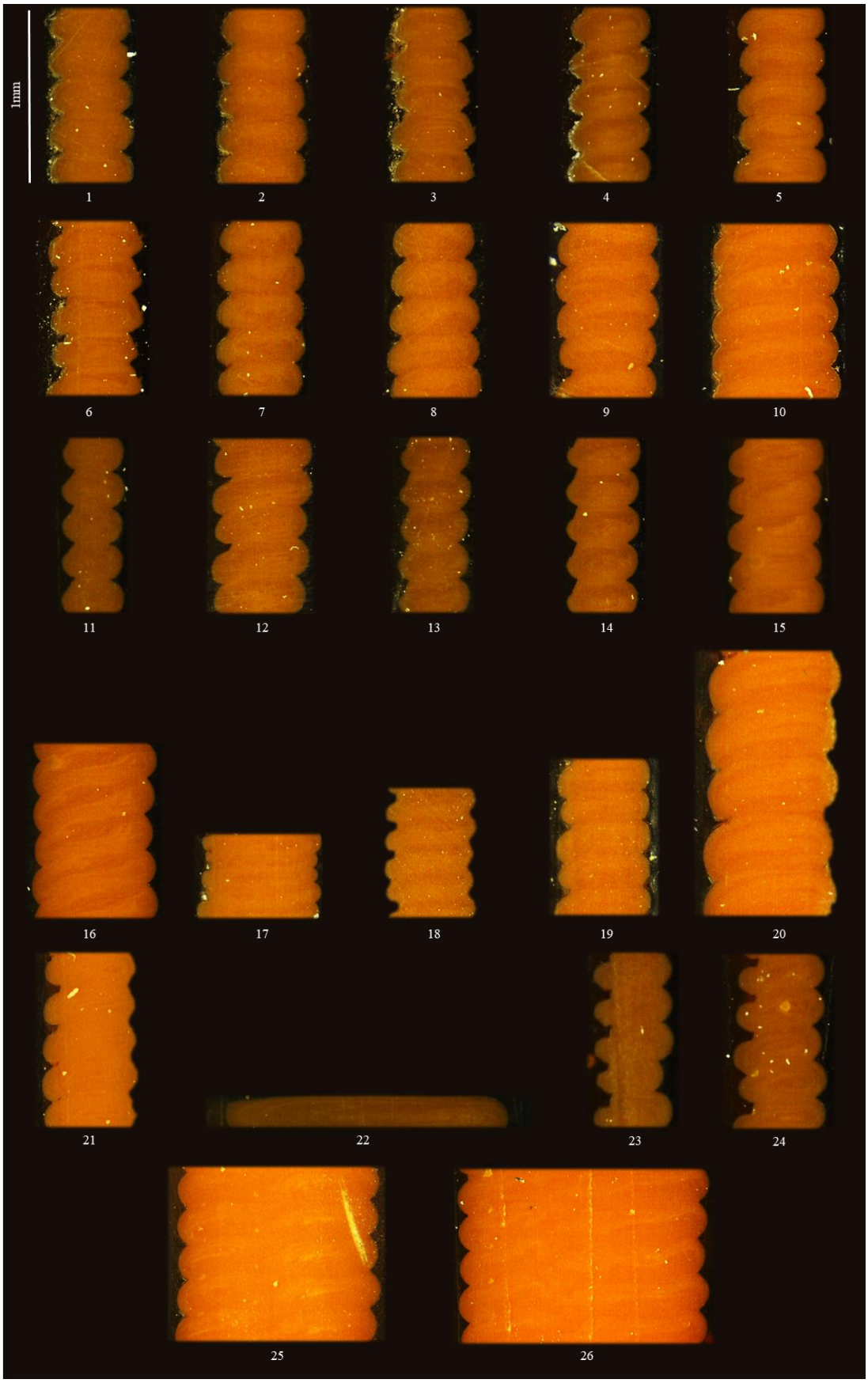

Figure 8.8 *Cross-sectional images Modified Nozzle Design 2*

8.2.1.4. MODIFIED NOZZLE DESIGN 3

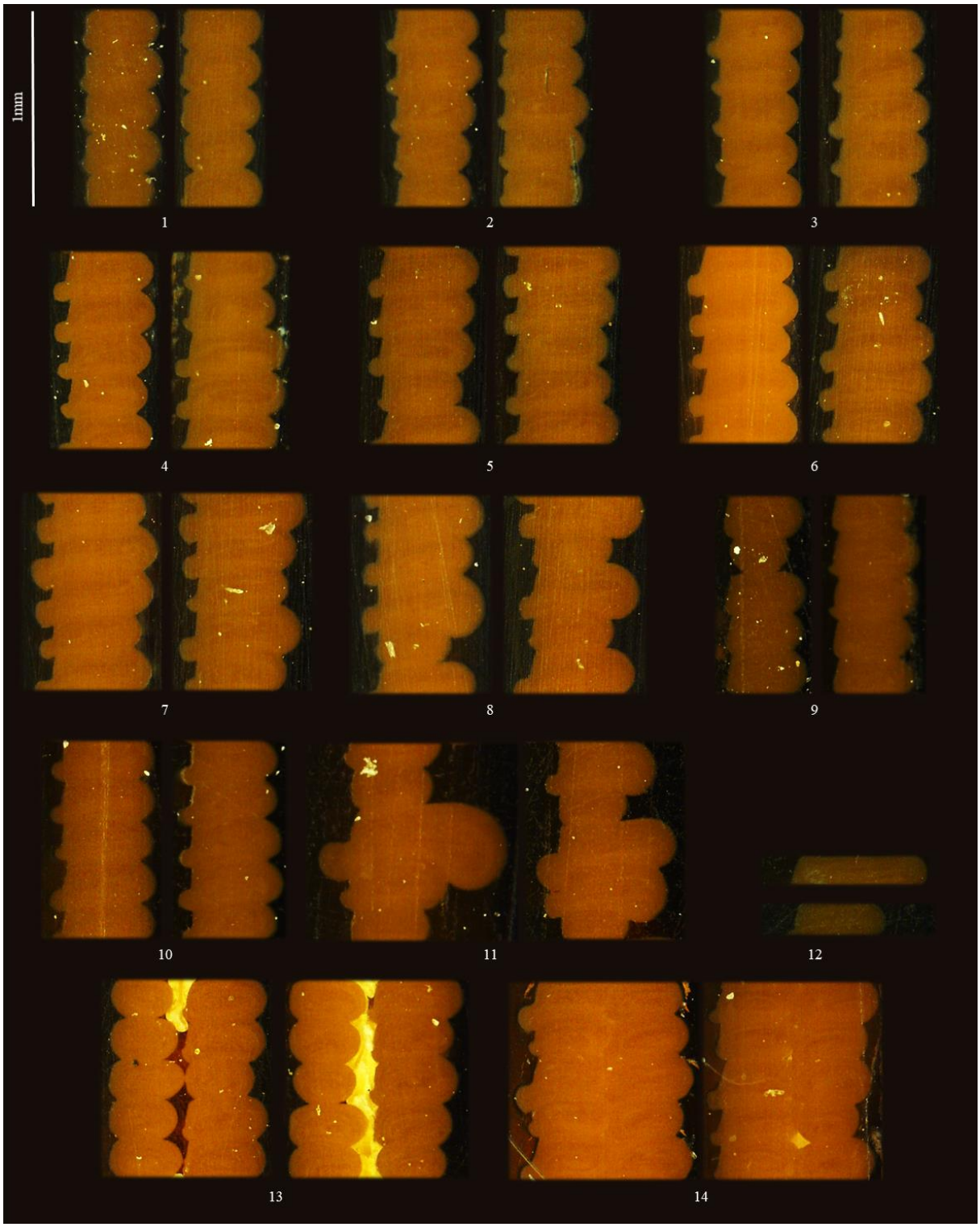

Figure 8.9 *Cross-sectional images Modified Nozzle Design 3*

8.2.1.5. MODIFIED NOZZLE DESIGN 4

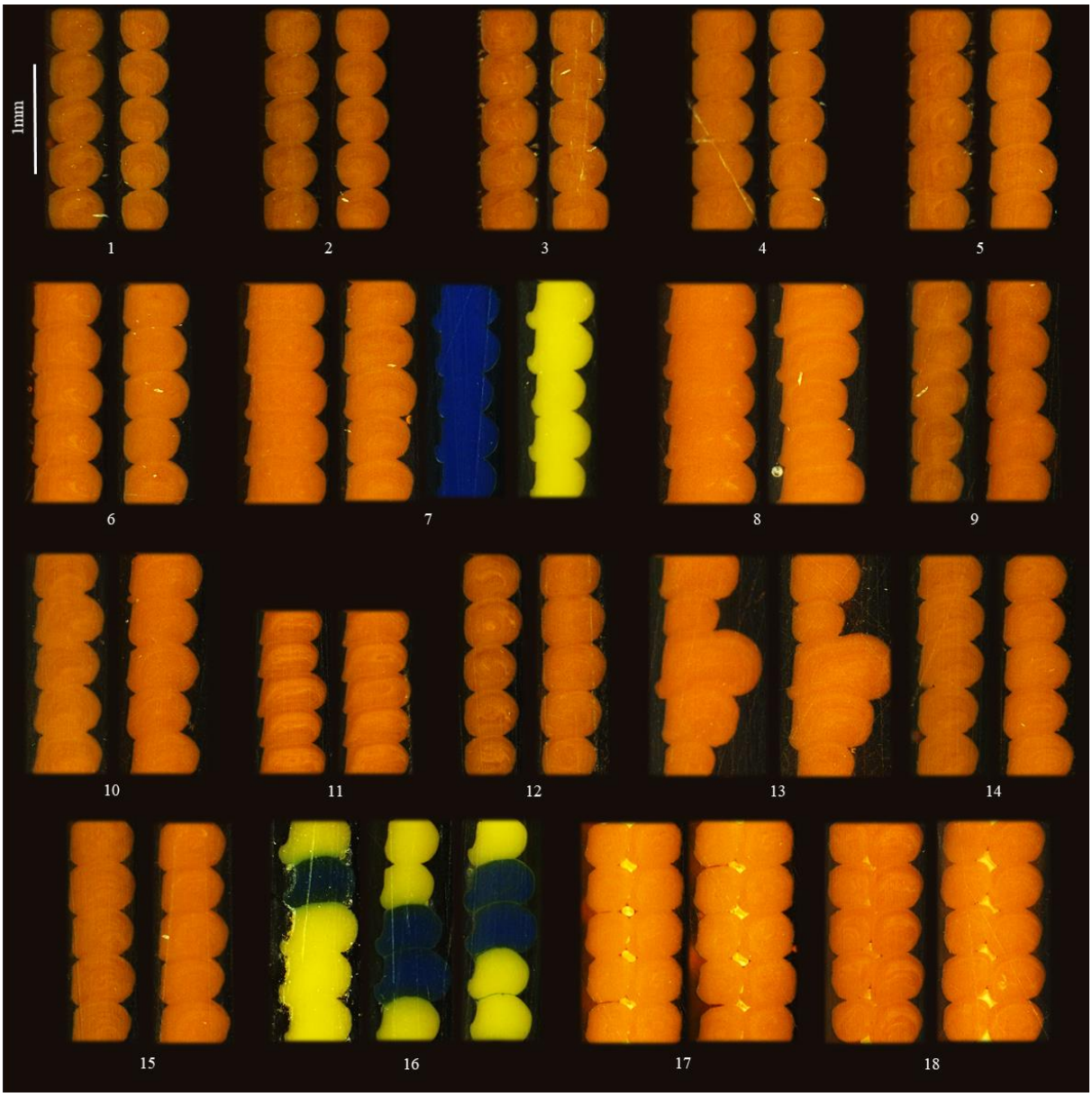

Figure 8.10 *Cross-sectional images Modified Nozzle Design 4*

8.2.2. MODIFIED NOZZLE PARAMETER OPTIMISATION STUDY

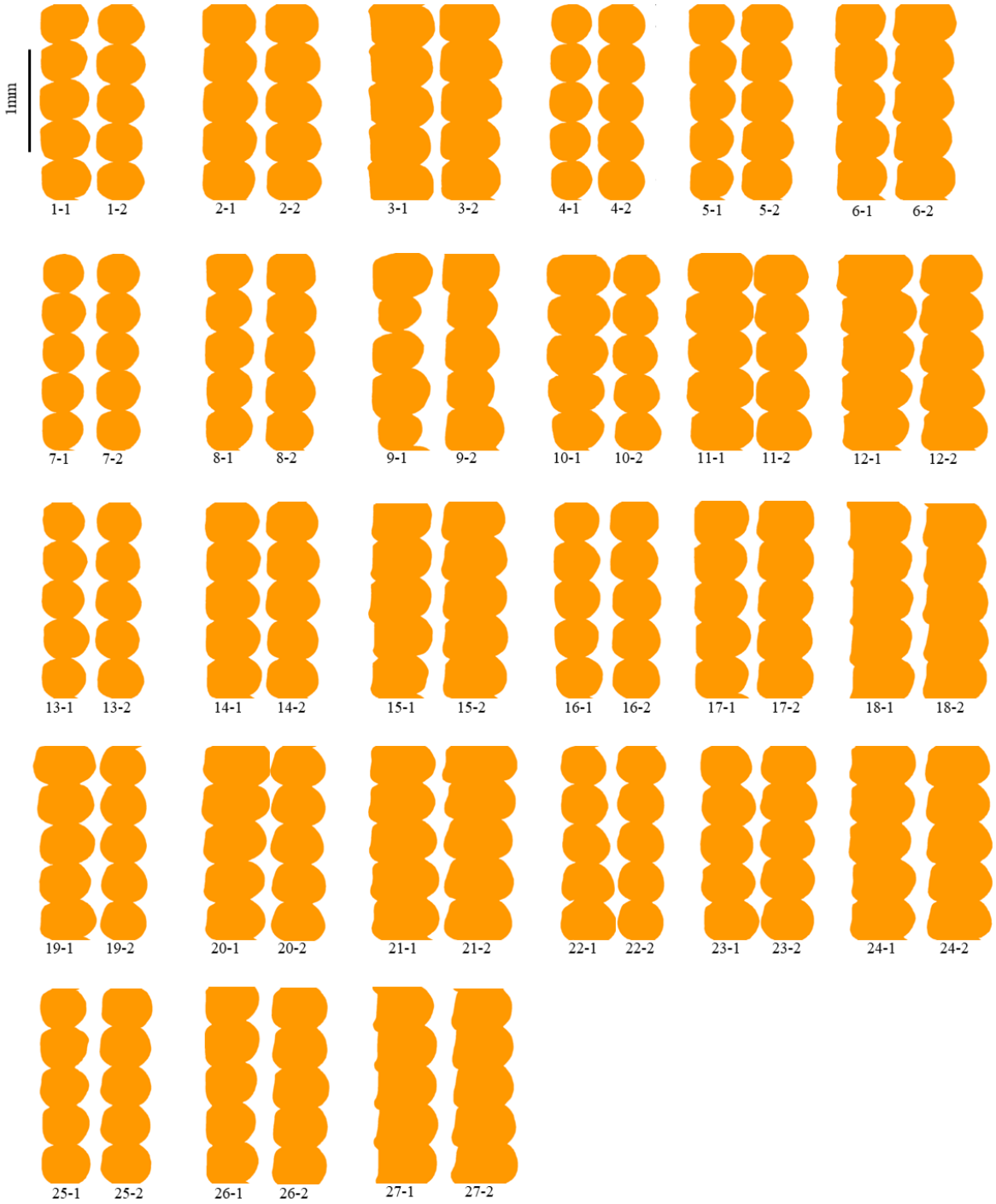

Figure 8.11 *Cross-sectional morphology for design 4 parameter optimisation study*

8.2.2.1. EXTRUSION AND BONDING

Run	*T* (ºC)	*v* (mm/min)	*e*	Cross-sectional area (%)		Bond width (mm)	
1	170	900	1	97.5	92.6	0.178	0.164
2	170	900	1.2	98.9	97.6	0.342	0.283
3	170	900	1.5	96.6	90.1	0.462	0.390
4	170	1800	1	84.5	102.9	0.095	0.217
5	170	1800	1.2	86.4	94.5	0.222	0.285
6	170	1800	1.5	81.8	92.2	0.344	0.420
7	170	3600	1	87.6	94.4	0.115	0.151
8	170	3600	1.2	85.9	92.7	0.241	0.281
9	170	3600	1.5	95.4	77.5	0.253	0.336
10	200	900	1	124.6	93.9	0.320	0.182
11	200	900	1.2	123.1	95.7	0.418	0.275
12	200	900	1.5	114.3	97.1	0.535	0.430
13	200	1800	1	93.4	91.0	0.165	0.177
14	200	1800	1.2	104.8	95.8	0.333	0.290
15	200	1800	1.5	92.6	95.6	0.437	0.451
16	200	3600	1	101.0	102.4	0.216	0.236
17	200	3600	1.2	97.0	97.7	0.333	0.359
18	200	3600	1.5	95.8	96.2	0.487	0.506
19	230	900	1	107.9	96.9	0.271	0.212
20	230	900	1.2	111.0	95.9	0.378	0.288
21	230	900	1.5	102.1	99.3	0.470	0.460
22	230	1800	1	106.0	98.5	0.239	0.224
23	230	1800	1.2	95.7	94.0	0.311	0.317
24	230	1800	1.5	97.5	101.9	0.465	0.452
25	230	3600	1	101.3	105.0	0.244	0.270
26	230	3600	1.2	97.8	99.3	0.330	0.357
27	230	3600	1.5	95.8	93.5	0.499	0.479

Table 8.5 *Modified nozzle parameter optimisation measured cross-sectional area as a proportion of expected area and bond width results*

Source	DoF	Sum of squares (SS)	Mean square (MS)	F	p	Effect	Contribution
T	2	0.09142	0.04571	6.97	0.004	Significant	24.4%
v	2	0.05583	0.02792	4.26	0.025	Significant	14.9%
e	2	0.01304	0.00652	0.99	0.383	Insignificant	3.5%
*T * v*	4	0.01567	0.00392	0.60	0.667	Insignificant	4.2%
*T * e*	4	0.00425	0.00106	0.16	0.956	Insignificant	1.1%
*v * e*	4	0.00499	0.00125	0.19	0.941	Insignificant	1.3%
*T * v * e*	8	0.01303	0.00163	0.25	0.977	Insignificant	3.5%
Error	27	0.17700	0.00656				47.2%
Total	53	0.37525					

Table 8.6 *Modified nozzle parameter optimisation measured cross-sectional area as a proportion of expected area ANOVA analysis*

Source	DoF	Sum of squares (SS)	Mean square (MS)	F	p	Effect	Contribution
T	2	0.07594	0.03797	18.36	0.000	Significant	11.4%
v	2	0.01064	0.00532	2.57	0.095	Insignificant	1.6%
e	2	0.49169	0.24585	118.87	0.000	Significant	73.7%
T * *v*	4	0.01781	0.00445	2.15	0.102	Insignificant	2.7%
T * *e*	4	0.00674	0.00169	0.81	0.527	Insignificant	1.0%
v * *e*	4	0.00114	0.00029	0.14	0.967	Insignificant	0.2%
T * *v* * *e*	8	0.00763	0.00095	0.46	0.873	Insignificant	1.1%
Error	27	0.05584	0.00207				8.4%
Total	53	0.66743					

Table 8.7 *Modified nozzle parameter optimisation bond width ANOVA analysis*

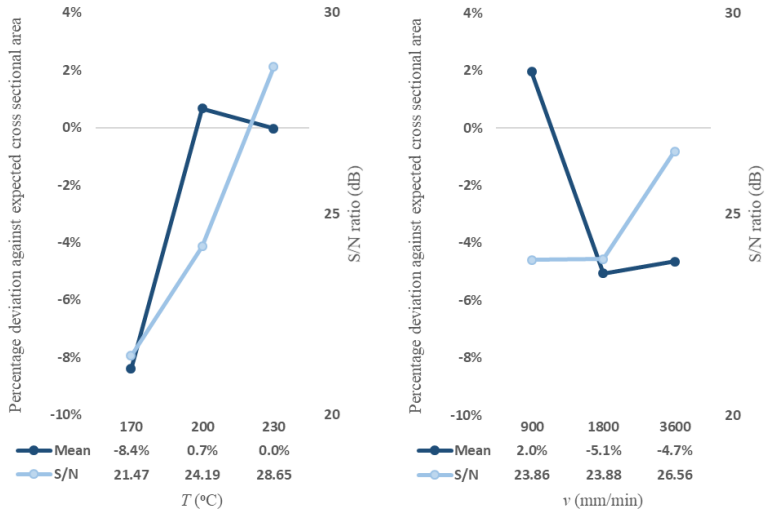

Figure 8.12 *Main effect plots for temperature and print speed with respect to measured cross-sectional area as a proportion of expected area*

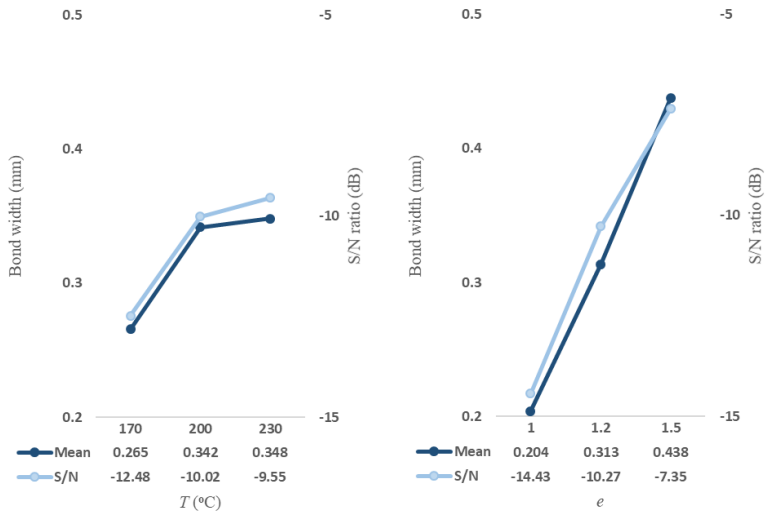

Figure 8.13 *Main effect plots for temperature and extrusion factor with respect to bond width*

8.2.2.1. SURFACE QUALITY

Run	*T* (ºC)	*v* (mm/min)	*e*	Horizontal deviation (mm)		Rz (mm)		Ra (mm)		Rq (mm)	
1	170	900	1	0.007	0.008	0.153	0.171	0.031	0.035	0.037	0.042
2	170	900	1.2	0.005	0.009	0.106	0.135	0.023	0.029	0.027	0.034
3	170	900	1.5	0.010	0.010	0.084	0.108	0.017	0.023	0.020	0.027
4	170	1800	1	0.011	0.005	0.185	0.130	0.034	0.030	0.042	0.035
5	170	1800	1.2	0.008	0.006	0.137	0.128	0.025	0.027	0.031	0.032
6	170	1800	1.5	0.013	0.009	0.084	0.108	0.017	0.021	0.021	0.025
7	170	3600	1	0.007	0.004	0.196	0.159	0.035	0.034	0.043	0.040
8	170	3600	1.2	0.010	0.010	0.120	0.114	0.025	0.024	0.030	0.028
9	170	3600	1.5	0.028	0.030	0.198	0.126	0.035	0.023	0.045	0.029
10	200	900	1	0.016	0.009	0.151	0.153	0.033	0.032	0.039	0.038
11	200	900	1.2	0.024	0.015	0.143	0.161	0.029	0.031	0.035	0.037
12	200	900	1.5	0.043	0.010	0.139	0.112	0.024	0.024	0.031	0.028
13	200	1800	1	0.009	0.009	0.155	0.153	0.031	0.032	0.037	0.038
14	200	1800	1.2	0.010	0.008	0.104	0.137	0.022	0.028	0.026	0.033
15	200	1800	1.5	0.026	0.010	0.102	0.090	0.019	0.019	0.023	0.022
16	200	3600	1	0.009	0.016	0.145	0.149	0.029	0.031	0.034	0.037
17	200	3600	1.2	0.007	0.006	0.088	0.096	0.018	0.020	0.022	0.023
18	200	3600	1.5	0.021	0.006	0.079	0.069	0.014	0.014	0.017	0.016
19	230	900	1	0.048	0.007	0.189	0.145	0.034	0.030	0.042	0.035
20	230	900	1.2	0.018	0.008	0.139	0.139	0.026	0.030	0.031	0.036
21	230	900	1.5	0.017	0.016	0.102	0.141	0.020	0.027	0.024	0.032
22	230	1800	1	0.007	0.012	0.149	0.149	0.031	0.030	0.037	0.036
23	230	1800	1.2	0.013	0.004	0.122	0.126	0.026	0.026	0.031	0.031
24	230	1800	1.5	0.014	0.015	0.088	0.122	0.019	0.024	0.022	0.028
25	230	3600	1	0.010	0.009	0.137	0.130	0.027	0.028	0.032	0.033
26	230	3600	1.2	0.007	0.006	0.079	0.104	0.017	0.022	0.020	0.025
27	230	3600	1.5	0.009	0.010	0.071	0.079	0.013	0.016	0.016	0.019

Table 8.8 *Modified nozzle parameter optimisation surface quality metric results*

Source	DoF	Sum of squares (SS)	Mean square (MS)	F	p	Effect	Contribution
T	2	0.00013	0.00006	0.93	0.409	Insignificant	3.1%
v	2	0.00027	0.00013	1.94	0.163	Insignificant	6.6%
e	2	0.00043	0.00022	3.14	0.060	Insignificant	10.6%
*T * v*	4	0.00053	0.00013	1.90	0.139	Insignificant	12.9%
*T * e*	4	0.00024	0.00006	0.88	0.488	Insignificant	6.0%
*v * e*	4	0.00007	0.00002	0.26	0.901	Insignificant	1.8%
*T * v * e*	8	0.00054	0.00007	0.98	0.472	Insignificant	13.3%
Error	27	0.00186	0.00007				45.7%
Total	53	0.00408					

Table 8.9 *Modified nozzle parameter optimisation horizontal deviation ANOVA analysis*

Source	DoF	Sum of squares (SS)	Mean square (MS)	F	p	Effect	Contribution
T	2	0.00185	0.00092	2.50	0.101	Insignificant	3.4%
v	2	0.00318	0.00159	4.31	0.024	Significant	5.8%
e	2	0.02346	0.01173	31.78	0.000	Significant	43.1%
*T * v*	4	0.00943	0.00236	6.39	0.001	Significant	17.3%
*T * e*	4	0.00055	0.00014	0.37	0.825	Insignificant	1.0%
*v * e*	4	0.00215	0.00054	1.46	0.243	Insignificant	3.9%
*T * v * e*	8	0.00391	0.00049	1.32	0.274	Insignificant	7.2%
Error	27	0.00997	0.00037				18.3%
Total	53	0.05450					

Table 8.10 *Modified nozzle parameter optimisation Rz ANOVA analysis*

Source	DoF	Sum of squares (SS)	Mean square (MS)	F	p	Effect	Contribution
T	2	0.00007	0.00003	3.97	0.031	Significant	3.3%
v	2	0.00015	0.00007	8.94	0.001	Significant	7.5%
e	2	0.00111	0.00055	66.95	0.000	Significant	56.1%
*T * v*	4	0.00027	0.00007	8.02	0.000	Significant	13.4%
*T * e*	4	0.00002	0.00001	0.68	0.615	Insignificant	1.1%
*v * e*	4	0.00005	0.00001	1.64	0.192	Insignificant	2.8%
*T * v * e*	8	0.00009	0.00001	1.32	0.275	Insignificant	4.4%
Error	27	0.00022	0.00001				11.3%
Total	53	0.00198					

Table 8.11 *Modified nozzle parameter optimisation Ra ANOVA analysis*

Source	DoF	Sum of squares (SS)	Mean square (MS)	F	p	Effect	Contribution
T	2	0.00011	0.00005	3.93	0.032	Significant	3.7%
v	2	0.00021	0.00011	7.74	0.002	Significant	7.2%
e	2	0.00152	0.00076	56.03	0.000	Significant	52.2%
*T * v*	4	0.00043	0.00011	7.96	0.000	Significant	14.8%
*T * e*	4	0.00003	0.00001	0.57	0.689	Insignificant	1.1%
*v * e*	4	0.00009	0.00002	1.63	0.196	Insignificant	3.0%
*T * v * e*	8	0.00016	0.00002	1.43	0.228	Insignificant	5.3%
Error	27	0.00037	0.00001				12.6%
Total	53	0.00292					

Table 8.12 *Modified nozzle parameter optimisation Rq ANOVA analysis*

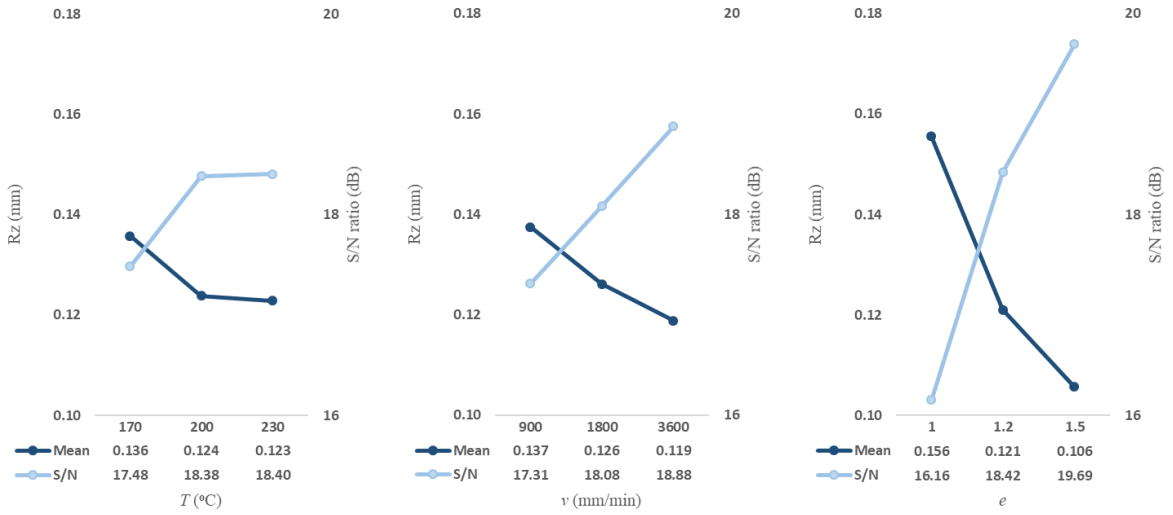

Figure 8.14 *Main effect plots for print speed and extrusion factor with respect to Rz*

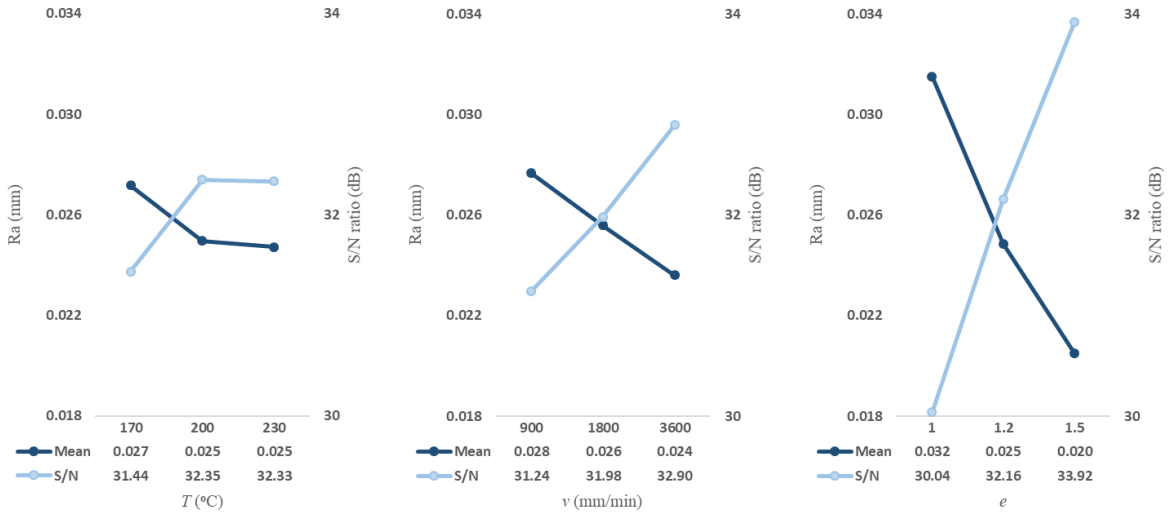

Figure 8.15 *Main effect plots for print speed and extrusion factor with respect to Ra*

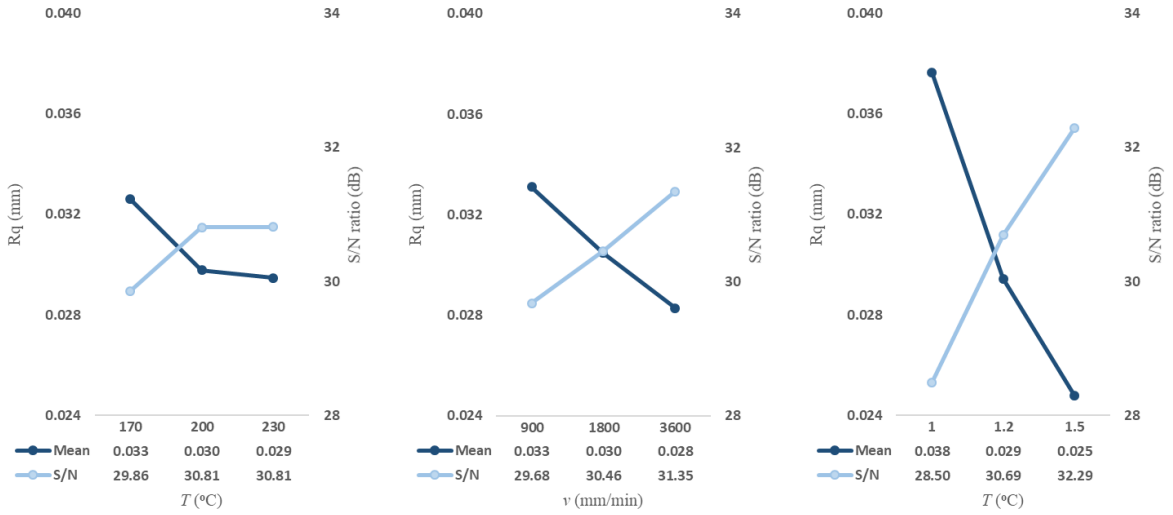

Figure 8.16 *Main effect plots for print speed and extrusion factor with respect to Rq*

8.3. DISCUSSION

8.3.1. PRELIMINARY STUDIES

8.3.1.1. SENSITIVITY TO NOZZLE ALIGNMENT

During initial testing with the 0.2mm nozzle designs, cross-sectional profiles were observed using a 45x magnifying glass on a manually cut profile (as per the example in Figure 5.4 with no resin processing). This revealed that in many cases, significant over-extrusion was occurring beyond the boundary of the nozzle side piece. It was similarly observed that this over-extrusion was offset towards the bottom of the layer, suggesting that molten material was escaping between the bottom of the nozzle side piece and the top of the previous layer. In these initial experimental runs, the alignment of the modified nozzle was conducted by eye, with a slight tendency to place the side piece trailing edge inboard of the outer perimeter vector. This would ensure strong interaction with the deposited material, whereas extrusion rate variabilities would theoretically yield outer perimeter irregularities if the nozzle were instead leading. Figure 8.17 demonstrates the theoretical effect of parallel, leading and trailing nozzle alignments.

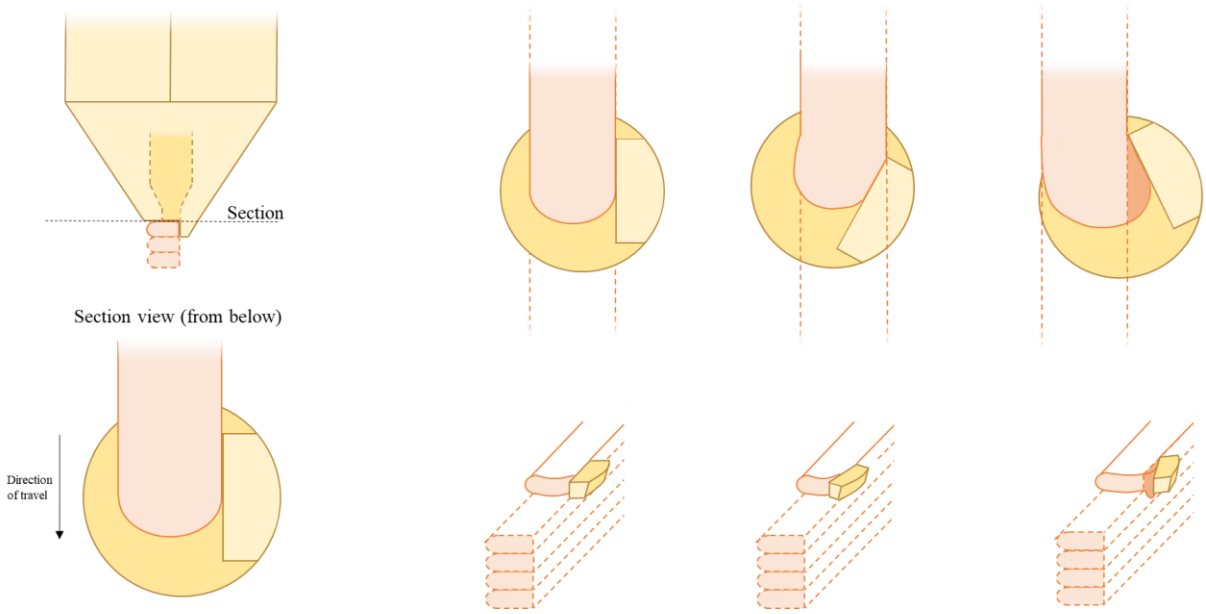

Figure 8.17 *Effect of modified nozzle rotational alignment*

In the trailing example on the far right, it can clearly be seen that a gap is produced relative to the layer below through which molten material can flow. This is obvious from the trailing examples for both nozzle heights in Figure 8.6 and becomes more apparent when the nozzle angle is more strongly trailing. For the leading alignment, curved outer geometry remains as the deposited material does not fully interact with the trailing edge. The single perimeter examples appear to give improved outer geometry as the addition of an inner perimeter forces material in the outer perimeter outwards beyond the nozzle side piece. Whilst this could be controlled by volumetric flow rates or a reversal in perimeter order, doing so would reintroduce much of the process sensitivity to input parameters that the novel nozzle design seeks to remove. It is also observed that the 0.4mm step height nozzle produced a much more pronounced straight vertical outer surface. As a result of these tests, the single perimeter parallel alignment is selected for the subsequent nozzle design and parameter optimisation tests (except for a few limited double perimeter tests).

8.3.1.2. MODIFIED NOZZLE DESIGN 1

The first two cross-sections with default parameters with an EF of 1, temperature of 200°C and print speed of 1800mmmin^{-1} shows some change to outer perimeter morphology (Figure 8.7). However, the volumetric flow rate is highly variable between layers and between the two experimental runs, which has a significant effect on the morphology. The outer edge still shows strong evidence of a layer-based morphology as the material is not fully interacting with the nozzle side piece, so this is a minor improvement over a standard nozzle.

Increasing and decreasing the print speed to 450 and 3600mmmin^{-1} respectively is observed to have some effect on the outer perimeter geometry. At the slower print speed, the volumetric flow rate is slightly increased and therefore also interaction with the side piece. However, the outer edge layer

morphology appears skewed, with the lower half of the layer protruding beyond the upper half. This could be due to the non-square trailing edge geometry as the over-extrusion appears limited to within the deposition layer or other more complex interaction effects.

Increasing the EF from 1.2 to 2 shows increasing over-extrusion beyond the outer perimeter. For the higher EF values, there is a clear offset between the over-extruded material and the current layer of deposition. This suggests that the material flows between the bottom of the nozzle side piece and the previous layer as demonstrated in Figure 8.18.

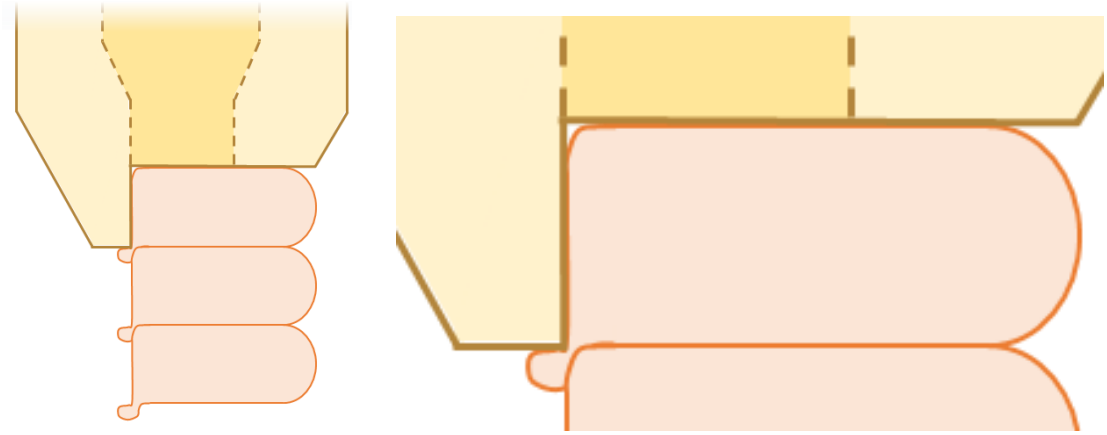

Figure 8.18 *Over-extrusion below the nozzle side piece*

The presence of interaction with the side piece is clearly visible, especially for the EF of 1.5. As such, the majority of the molten material does indeed flow inwards (and away from the side piece) but a significant amount does still flow beyond the side piece.

A number of studies have demonstrated the reheating of previous layers. If enough heat is transferred to the layer below, the sharp upper 90^{o} corner may re-melt and allow material from the current layer to flow past. This may be especially likely given the increased proximity of the previous layer to the heated nozzle side piece. Vanaei et al. [325] showed that the temperature of previously-deposited layers is increased for the subsequent five depositions in a single-walled setup very similar to the experimentation undertaken within this section. However, the peak temperature is vastly reduced with each newly deposited layer, and the crystallisation temperature is not exceeded on any previous layers. This is based on a standard nozzle, so it is likely that in the case of the modified nozzle some local deformation close to the nozzle side piece can occur, which would directly affect the ability to limit over extrusion in subsequent layers. Seppala et al. [326] undertook IR thermography of the deposition process. This also showed some reheating of the two prior layers, for a period of approximately four seconds with a print speed of 100mms^{-1}. Wolszczak et al. [327] and Wijnen at al. [61] also demonstrated that significant reheating of the layers below occurs whilst Ravoori et al. [705] showed that these layers cool significantly not long after deposition. The shape and stability of the

previous layer is key to achieving strong surface quality and as such, minimising the heat transfer to this corner can be important.

Lowering the temperature from 200ºC to 170ºC in experimental runs 9 and 10 yields improved outer perimeter geometry. The increased material viscosity and decreased solidification time in combination with lower heat transfer to the previous layer and hence increased stability may explain this as well as the lower apparent volumetric flow rate. However, a temperature of 170ºC combined with an EF of 1 led to complete print failure. Increasing the temperature in the experimental runs 11 to 13 gave less distinctive layer-based morphology, in particular with less sharp inter-layer under-extrusion features. However, a greater over-extrusion is observed at an EF of 1.5 compared to the 200ºC example. The molten material viscosity falls with increasing temperature as was discussed in Section 5.1.1. This reduced viscosity therefore enables greater flow beyond the nozzle side piece as well as transferring more heat to the previous layer.

The addition of a second toolpath pass without extrusion (i.e. a wipe) in experimental run 14 reveals an exaggerated over-extrusion morphology on the outer perimeter. This suggests a small amount of local re-melting during the wipe and leads to highly asymmetric outer surface layer morphology. Finally, an isolated increase in EF of 1.5 for the middle layer in experimental run 15 shows that the EF strongly affects the outer perimeter over-extrusion feature as was experienced in the earlier experimental runs.

The main conclusion from this nozzle design is that there remains a significant amount of sensitivity to print parameters. At low extrusion rates, straight and vertical outer surfaces are not realised due to insufficient interaction with the nozzle side piece. However, at increased extrusion rates some of the additional material extends beyond the nozzle either underneath at very high extrusion rates, or within the layer for more intermediate values. It is likely that a good vertical surface could be achieved but it would require an exact set of parameters.

8.3.1.3. MODIFIED NOZZLE DESIGN 2

Modified nozzle design 2 is as per design 1 but with vertical leading and trailing edges on the nozzle side piece. In general, this has yielded little improvement in the outer perimeter morphology suggesting limited interaction with the trailing edge of the nozzle side piece (Figure 8.8).

Experimental runs 1 to 4 show multiple repeats of the default parameters and demonstrate reasonable repeatability although limited interaction with the nozzle side piece and so the rounded outer edge morphology remains. Run 5 with a slightly increased EF of 1.1 retains this behaviour.

Increased print speed to 3600mmmin^{-1} with various EF values in runs 7 to 10 were investigated in order to reduce the heat placed into the layer below and thus potentially reduce the over-extrusion on the outer perimeter, though the increased rate may have negative effects on the flow rate stability.

This shows over-extrusion for all EF settings and improved surface finish for the higher EF, though a layer offset is introduced whereby the layer based geometry is lower down on the external surface again suggesting over-extrusion below the nozzle side piece. The lower print speeds in runs 11 and 12 with an EF of 0.85 and 1.5 respectively both show poor surface finish. For the low extrusion rate, there is little interaction with the side piece meaning that the morphology remains similar to the standard nozzle. With the higher EF of 1.5, significant over-extrusion is then observed despite the reduced temperature.

The lowered temperature to 170ºC in runs 13 and 14 shows similar morphology to the same parameters with design 1. This suggests that the asymmetrical layer geometry is not a direct result of the trapezoidal side piece in design 1, but is due to other effects perhaps including increased heat in the deposited layer and gravity. Higher temperatures with higher print speeds were expected to put less heat into the previous layer as a result of the increased speed, whilst the increased temperature aids steadier material flow. However, these also exhibited significant over-extrusion suggesting that the side piece is not able to form a seal against the top corner of the previous layer even with the increased print speed.

Experimental runs 17 to 20 investigated the effect of changing layer heights. For layer heights lower than the nozzle step height, it was expected that this would help reduce the over-extrusion of material beyond the side piece. This is because contact between the bottom of the nozzle side piece and the previous layer would be more certain, effectively closing the potential route for material over-extrusion. Conversely, for layer heights greater than the nozzle side piece step height, very significant over-extrusion would be observed as the gap between the side piece and previous layer becomes much larger. For reduced layer heights, the layer morphology remains observable in the outer perimeter. This suggests that the layer below is subject to local re-melting which leads to the over-extrusion beyond the nozzle side piece. As expected, the increased layer height reveals significant over-extrusion.

Run 22 involved a single layer deposition with a very high EF of 5. This was undertaken to utilise the solid acrylic print base to understand where the material flows if the previous layer was not re-melted. This showed that with the stable previous layer, the over-extrusion no longer occurs and the entire additional volume is directed inwards by the nozzle side piece. This confirms that over-extrusion is below the bottom of the nozzle side piece and not within the current deposition layer. As with the previous nozzle design, the addition of a wipe movement gave more pronounced over-extrusion geometry. The alternative nozzle design where the side piece is offset from the nozzle outer diameter by 0.1mm was explored in runs 23 and 24. This modification gave even more significant over-extrusion and so does not appear to be a useful design modification with the parameters selected.

Finally, double perimeters were shown in runs 25 and 26. As previously demonstrated in the alignment experimentation, the addition of an inner perimeter leads to worsened outer perimeter quality, especially at higher extrusion rates. This is again shown to be the case, where the over-extrusion is so prevalent that the outer perimeter appears as per the standard nozzle arc morphology, offset by approximately half the layer height (i.e. the straight section from the side piece is completely lost).

8.3.1.4. MODIFIED NOZZLE DESIGN 3

The third nozzle design consisted of a significantly longer side piece to remove the effects of trailing edge interaction and enable improved alignment. In addition, repeats of each parameter combination were conducted to assess the repeatability of the process. As with the previous two designs a default parameters print, various increased EFs, changes in temperature and double perimeters were investigated.

The default print conditions show slightly improved morphology (Figure 8.9). This is likely due to the increased heat transfer from the larger nozzle design and increased heat transfer during deposition from the longer side piece. As the EF factor is raised from 1 to 2 increased over-extrusion is observed, where in all cases this is below of the bottom edge of the nozzle side piece. This shows that the in-layer over-extrusion is not significant to the observed error, but rather the lack of seal with the previous layer is the primary cause. Experimental run 11 shows EFs of 1, 2 and 3 between layers. This clearly shows that the over-extrusion beyond the side piece is strongly linked to the volumetric flow rate.

Both the lower and higher temperature in runs 9 and 10 with an EF of 1.2 do not show significant improvements. The main difference between these is the lowered actual flow rate (and lower cross-sectional area) with the lower temperature which yields a smaller volume of over-extrusion, though this is not strictly related to the material temperature.

Experimental run 12 demonstrates only the first layer utilising the acrylic slide as a stable and fixed substrate. As with the previous example, this removes the over-extrusion though there is a significant difference in the flow rates between the two examples. Finally the presence of a second, inner perimeter leads to increased over-extrusion in the outer perimeter as the material is blocked from flowing inwards in the second double perimeter example.

8.3.1.5. MODIFIED NOZZLE DESIGN 4

This nozzle design replicates design 2 but with an increased step height of 0.4mm. The main benefits of this design are that there is less heat transferred to previous layers, the volumetric flow rate is higher and build time is reduced. It may also be easier to observe and understand the material behaviour given the slightly larger scale.

The baseline test for this nozzle design is a nominal layer height of 0.4mm and road width of 0.4mm according to the *CURA* rectangular model. There is therefore relatively little interaction with the side piece as shown in the cross-sections from experimental run 1 as the aspect ratio is lower than for the 0.2mm examples (Figure 8.10). Subsequent increasing EFs show an increased interaction with the side piece, though at these higher layer heights the prominence of the over-extruded region is significantly reduced compared to previous designs.

A major proposed benefit of introducing a novel nozzle design with a side piece was to control over-extrusion beyond the theoretical external perimeter. Experimental runs 12 and 13 show layers with increasing EFs of between 1 and 1.5 and 1 and 3 respectively. This demonstrates that for higher extrusion rates, an increasing volume of molten material protrudes below the lower surface of the side piece. However, as Figure 8.19 shows, this effect is significantly reduced compared to a standard nozzle arrangement with the same print parameters.

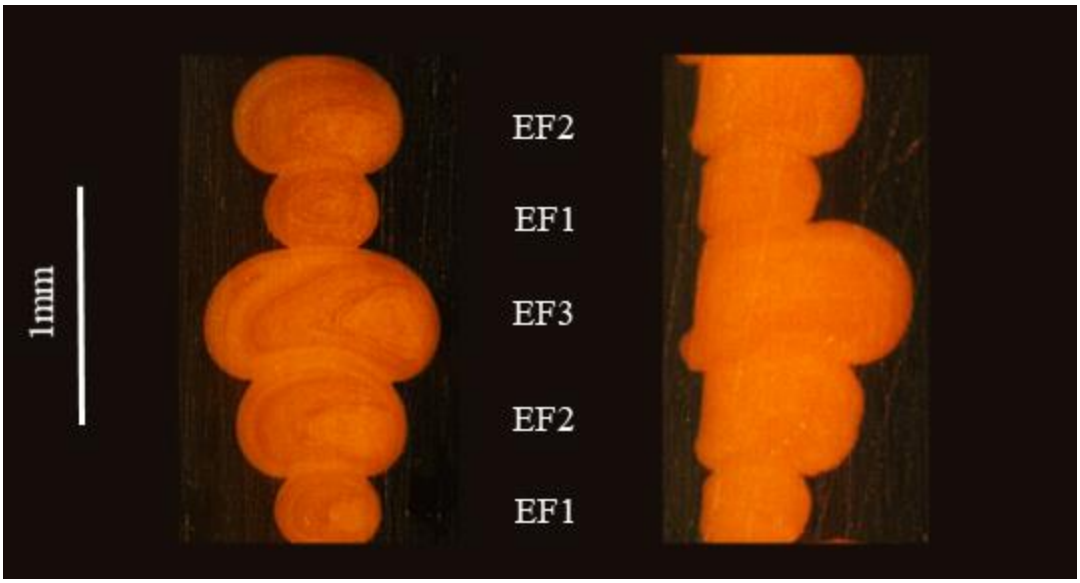

Figure 8.19 *Comparison of standard nozzle (left) with modified nozzle design 4 (right) for EFs of 1, 2 and 3 on alternating layers.*

The lowered and increased temperatures have similar effects to the other nozzle designs, where the reduced temperature gives a lower actual flow rate and therefore reduced interaction with the side piece. As previously, the increased temperature gives slightly more pronounced over-extrusion owing to higher flow rates and lower material viscosity. The reduced layer height experimental example leads to over-extrusion, suggesting that the top corner of the previous layer is again not the sole cause of over-extrusion.

Experimental run 7 was repeated with blue and yellow PLA material, both produced by the same manufacturer as the orange filament used throughout the rest of the experimentation. These show significantly reduced actual volumetric flow rates despite having identical nominal values and print parameters. This suggests that filament colour can have a significant effect on the deposited strands,

though both colours still exhibit the same local over-extrusion at the bottom of the side piece. Previous studies which have assessed the effect of PLA colour were noted earlier in Section 8.1.2.4. Run 16 used these blue and yellow filaments in alternating layers. This showed that the over-extrusion does indeed originate from the layer above, and also that the bond between the two layers exhibits significant curvature. Jang et al. [358] noted a flat top and wide strands for lower layer heights but a more curved interface at higher layer heights. This is also likely to be less significant at higher extrusion rates, though it can also be observed for the standard nozzle example in Figure 8.19 above.

The use of a wipe, a wipe with an offset, and a 0.1mm offset side piece nozzle again demonstrate no significant improvement in performance. Double perimeters show reduced surface quality for the same reason of inner perimeter interaction as was outlined previously.

8.3.1.1. SUMMARY

Extrusion factor

The EF (and therefore volumetric flow rate) is the most important factor in determining the morphology of the outer perimeter. At lower EFs, the material does not significantly interact with the nozzle side piece but where there is some contact, the surface finish is slightly improved. However, as the EF is increased, whilst an increasing amount of molten material is indeed pushed inwards some escapes below the side piece and appears as a region of over-extrusion at the top of the previous layer. The 0.4mm nozzle is less sensitive to extrusion factor changes and so represents a more promising design.

Temperature

Increased temperature reduces the viscosity of the molten material and reduces the stability of the previous layer, leading to increased over-extrusion. Lower temperatures have the opposite effect, though this is in part due to the lowered effective volumetric flow rates observed at 170^{o}C.

Print speed

Increased print speeds give improved results where significant over-extrusion has already been observed for a particular nominal volumetric flow rate. However, much of this benefit is likely to be due to the lowered effective flow rate rather than reduced heat transfer to the previous layer, and at higher flow rates the increased speed can lead to deposition instability.

Wipe

The addition of a wipe move does not improve surface finish, but rather has the opposite effect. This approach was always applied to cases where some over-extrusion had already been observed and a second non-extrusion pass made the morphology more pronounced.

Other approaches

Double perimeters where the inner perimeter is deposited first and the extrusion rates were high enough for significant inter-perimeter interaction gave worsened surface finish. This is because the inner perimeter blocks the inward flow of the material in the outer perimeter, forcing it instead past the nozzle side piece. Reduced layer heights do not give improved performance, suggesting it is not the top corner of the previous layer alone that allows over-extrusion below and beyond the nozzle side piece. Finally, the addition of a 0.1mm offset side piece as part of the nozzle design gives slightly worse surface finish as it acts analogous to higher extrusion rates, with greater interaction between the molten material and the side piece.

Nozzle design selection and parameter optimisation factors

The primary cause of over-extrusion error is shown to be due to the actual volumetric flow rate (i.e. cross-sectional area as shown in the actual deposition). The preliminary experimentation has demonstrated that nozzle design 4 with the increased step height of 0.4mm is clearly superior in maintaining good surface finish with changing flow rate. This nozzle was therefore selected for the identification of optimal parameters in the subsequent parameter optimisation study.

Double perimeters have been demonstrated to reduce surface quality and give greater sensitivity to varying volumetric flow rates. The main factors which affect the process can be seen as temperature, print speed and extrusion factor, and the values selected in the preliminary studies also appear valid. As a result, the factors for a single perimeter deposition are used for the parameter optimisation study.

8.3.2. PARAMETER OPTIMISATION

As noted previously, EF, temperature and print speed are explored in the parameter optimisation study. Extrusion factor theoretically controls only the nominal cross-section of the deposited strand. Temperature effects are more complex. A higher temperature reduces the viscosity of the material and so enables increased flow, whilst also generating additional heat in the previous layer. However, it can be beneficial to improve flow stability if close to process rate limits. Print speed affects heat transfer to the layer below, though higher speeds may also lead to rate limit issues.

From the previous experimentation, a low, middle and high level for each of the three factors can be determined. This previous experimentation is important to inform this selection, as the parameter optimisation study relies on the valid selection of level values in order to find an optimal solution. Temperature was already bounded by recommended print temperatures for the PLA material used. The manufacturer suggests a range of 180ºC to 210ºC, but this is narrower than many other sources would suggest. A low value which nonetheless is above the melting temperature was selected as the lower bound (170 ºC), whilst a recommended value of 200 ºC was used as the mid value and a high value of 230 ºC in line with slicers and existing literature. Print speed has been selected based on the

previous experimentation and guidelines given in the slicer. Therefore a mid-level speed of F1800 (i.e. 1800 mmmin^{-1} or 30mms^{-1}) was used. The lower speed was taken as half this, and the upper as double. Slicers rarely utilise extrusion movement speeds outside of this range. Extrusion factor has been heavily influenced by the previous experimentation. Given the selection of a layer height of 0.4mm, a minimum road width of 0.4mm has been selected as going below an aspect ratio of 1 is known to lead to print errors (and indeed, some slicers will not allow an aspect ratio of below 1 to be used). The mid value is selected based on the previous experimentation, where increased interaction with the modified nozzle side piece is demonstrated and then an upper level where significant over extrusion beyond the outer boundary was observed.

8.3.2.1. EXTRUSION AND BONDING

The volumetric flow rates in the parameter optimisation study were controlled via changing EFs. An EF of 1 corresponded to a layer height of 0.4mm and road width of 0.4mm with the standard rectangular filament model. The expected cross-sectional area for an EF of 1 is therefore 0.160mm^2 and 0.192mm^2 and 0.240mm^2 for EFs of 1.2 and 1.5 respectively.

Table 8.5 displays actual cross-sectional area as a proportion of the expected values outlined above. These values are expected not to exceed 100%, as to do so suggests greater extrusion of material than the G-code dictates. It can be seen that in many cases, this value is between 80% and 100% of the expected as was also found for the standard nozzle experimentation in Section 5. In general, the first experimental example of each parameter combination undertaken on machine 1 shows higher extrusion values, suggesting a systematic greater extrusion rate associated with that machine perhaps arising from the filament feed system itself. There are some examples where the cross-sectional area significantly exceeds the nominal value. In particular, these high values were observed for the lowest print speeds and temperatures of 200^{o}C and 230^{o}C and only on machine 1. The total volume deposited is determined by the G-code. As a result, the increased rates observed in these runs should be matched by under-extrusion elsewhere within the deposited road. It is therefore possible that at higher temperatures and lower speeds, the material flows through the nozzle at a higher rate in the first half of deposition with lower extrusion towards the end of the road.

The ANOVA analysis shows that the only two factors which have a significant impact on the cross-sectional area as a proportion of the nominal value are temperature and print speed. Figure 8.12 demonstrates that a temperature of 230^{o}C and print speed of 3600mmmin^{-1} are both optimal parameter settings. The higher temperature has previously been noted to reduce material viscosity and increase the rate limit of the process, thereby improving cross-sectional area conformity. The increased print speed involved a faster rate of filament feed for the same nominal cross-sectional area, which increases the pressure across the nozzle and therefore improves the cross-sectional area percentage.

Figure 8.20 shows the relationship between temperature and cross-sectional area as a proportion of the nominal value. This shows that machine 1 is more sensitive to temperature, which is surprising given identical experimental procedure and machine design. It also clearly demonstrates the increased variability for machine 1, particularly at a print temperature of 200°C.

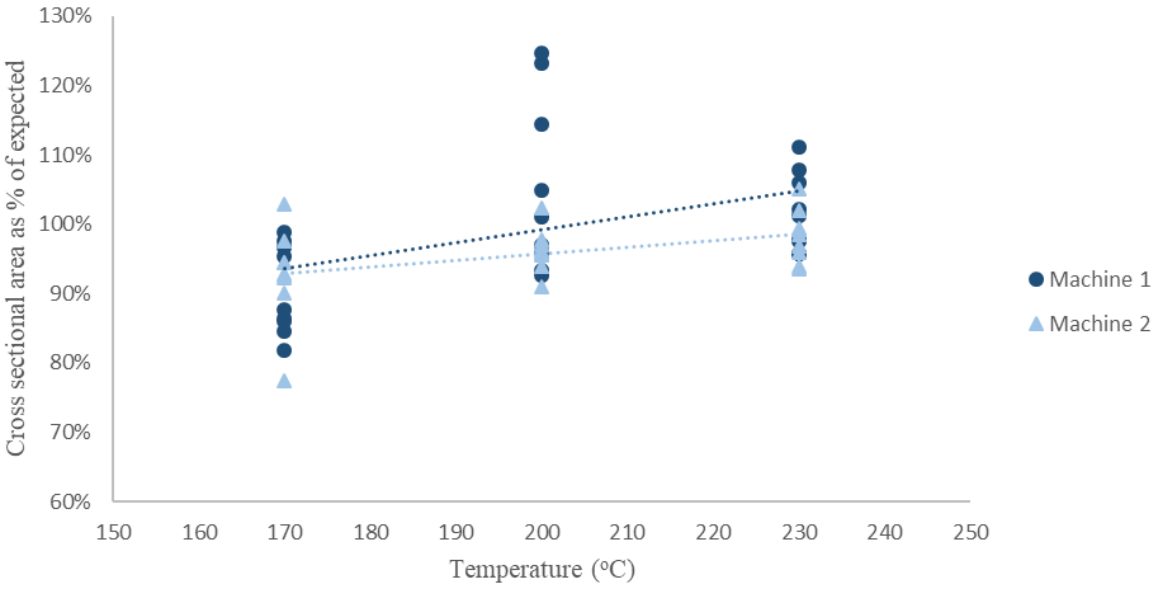

Figure 8.20 *Relationship between print temperature and cross-sectional area as a proportion of the nominal value*

Figure 8.21 shows the relationship between print speed and cross-sectional area. Again, machine 1 is more sensitive to the changing print speed and appears to be the main contributor to the ANOVA result showing significance of print speed. For machine 2, there is little difference between print speeds whereas for machine 1, the area reduces with increased speed. This is likely due to the increased volumetric flow rate required with increasing speed (for fixed EF and T) which requires higher pressure for the nominal extrusion as was noted by Coogan and Kazmer [706] for standard nozzles. This then results either in filament slippage or missed steps on the filament drive stepper motor.

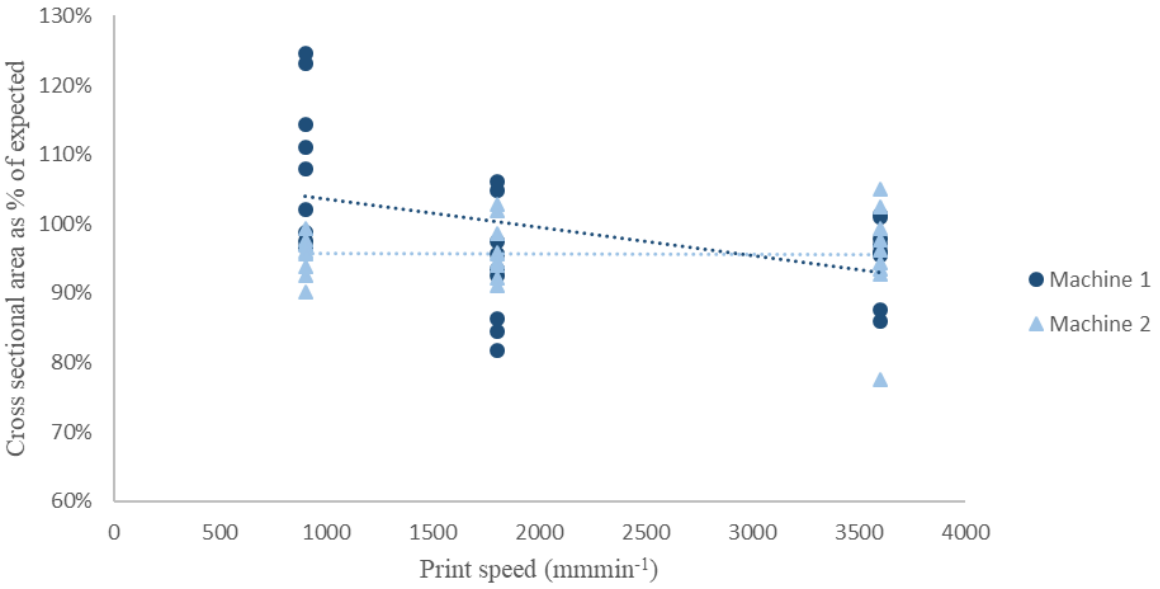

Figure 8.21 *Relationship between print speed and cross-sectional area as a proportion of the nominal value*

Existing literature has identified bond width to be a key determinant of bonding strength and therefore overall mechanical performance. Li et al. [707] developed a model for mechanical strength of polymer ME AM components. In this, they first presented a general model that assumed bonding between neighbouring layers to be perfect and therefore the behaviour of the bonded materials was identical to the input feedstock. The internal geometry, similar to those demonstrated in the multiple perimeter experiments in Section 5, are treated as internal cavities. However, they noted that this assumption is not valid for the ME AM process. They conducted a series of mechanical strength experiments which demonstrated non-perfect bonding. They demonstrated that reductions in void density (and therefore increased bonding areas) strongly influence the overall component mechanical performance. Similarly, Serdeczny et al. [355] stated that the cross-section of a deposited strand is an important parameter for bonding strength between layers as it determines the bonding area, which itself is a direct contributor to part strength.

Many studies have investigated the formation of bond morphology, typically finding that increased temperatures enable greater coalescence and inter-diffusion. Bellehumeur et al. [708] modelled the bond formation between ABS strands in the ME AM process. They determined that the most suitable measure of bonding quality was bond width, and that the deposition cooling conditions had a strong effect on coalescence. Kaveh et al. [359] found that the presence of internal cavities depended on print temperature. In their experimentation, they found greater evidence of cavities at a print temperature of 230ºC compared to 210º-C for HIPS material. Shahriar et al. [709] investigated the coalescence phenomenon of PLA and PEEK. They found that the bonding length was maximised at a temperature of 167ºC for PLA. Sun et al. [13] investigated the effect of processing conditions on the bonding quality of polymer ME AM components. They considered the mesostructure of the strands post-

deposition, and found that fabrication strategy, envelope temperature and convection coefficients arising from build plate location all had significant effects. They noted the sintering phenomenon as being primarily responsible for the bond structure, but only for a short time after deposition before solidification. Gurrala and Regalla [710] presented mathematical modelling and experimentation to understand the contribution of coalescence to the strength of ME AM components. The model considered sintering between cylindrical filaments, and the resulting bond width shown to directly contribute to component tensile strength. They concluded that under standard conditions, some coalescence does occur but that the process is not complete. Davis et al. [711] also explored the effect of print parameters on bonding strength. They specifically considered print speed and temperature, concluding that high speed ($100mms^{-1}$) and high temperature $250^{o}C$ for ABS) gave optimal bonding. Coogan and Kazmer [706] conducted experimentation to understand the effect of other print parameters on bond strengths. They found that high bed temperatures, print temperatures, higher road widths and smaller layer heights give the best bonding performance. Zhang et al. [712] also found that component strength decreased with increasing layer height and print speeds. Yin et al. [713] investigated bonding strength between TPU and ABS in a multi-material ME AM process. They found increased bed temperature to give the biggest improvement in strength and suggested thermal diffusion between depositions to be of significant importance. McIlroy and Olmsted [714] stated that the strength of welds between strands is controlled by the inter-diffusion and entanglement across the boundary. They noted that high shear rates (associated with higher volumetric flow rates) during the extrusion process led to disentanglement and lowered bond strength.

Given the demonstrated importance of bonding width on component strength, Figure 8.22 shows the relationship between the measured cross-sectional area and bond width. The outlier results from experimental run 9 on machine 1. This showed significant flow rate variability between layers, likely due to the low print temperature, which gives rise to low bonding areas. Nevertheless, this demonstrates strong positive correlation between the cross-sectional area and bond width. As a result, for maximum bond width high EFs are combined with a high temperature. This is supported by the ANOVA analysis, which demonstrates both of these factors to be statistically significant and that increasing both factors gives the optimal response.

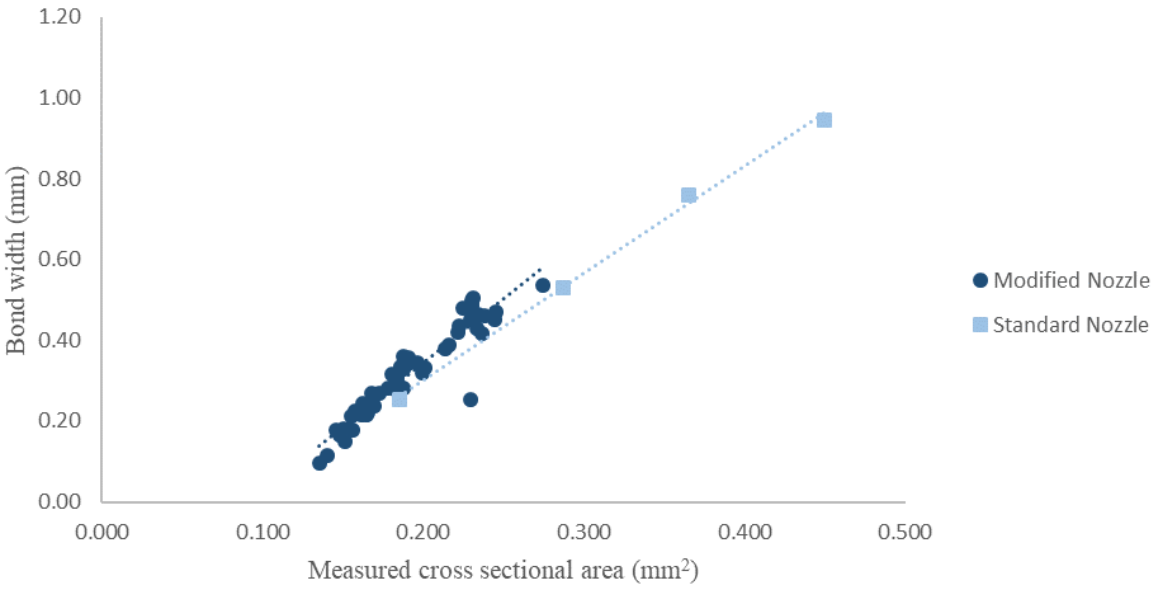

Figure 8.22 *Relationship between measured cross-sectional area and bond width*

This also suggests that for the same cross-sectional area, the bond width is increased as a result of the modified nozzle. According to the relationship discussed previously, this also indicates that the modified nozzle will create single perimeter walls with improved part strength.

8.3.2.2. SURFACE QUALITY

ANOVA analysis of the average horizontal deviations between the furthest point on the perimeter of each layer relative the furthest point of any perimeter shows no significant factors. These deviations are therefore likely due to other aspects of process variability such as inherent flow instability and positional repeatability. In any case, these values are small in all cases, rarely exceeding 0.02mm. Additionally, the measure of deviation with varying extrusion rates such as those present around direction changes is arguably a more important measure, for which the modified nozzle was shown to be significantly stronger.

Comparison with the standard nozzle horizontal deviation values is shown in Figure 8.23. This shows a reduced average deviation for the modified nozzle with a layer height of 0.4mm. Horizontal deviations are also lower for the optimum parameters and 0.4mm LH modified nozzle than for the standard nozzle with a LH of 0.2mm, despite the finer resolution of deposited strands.

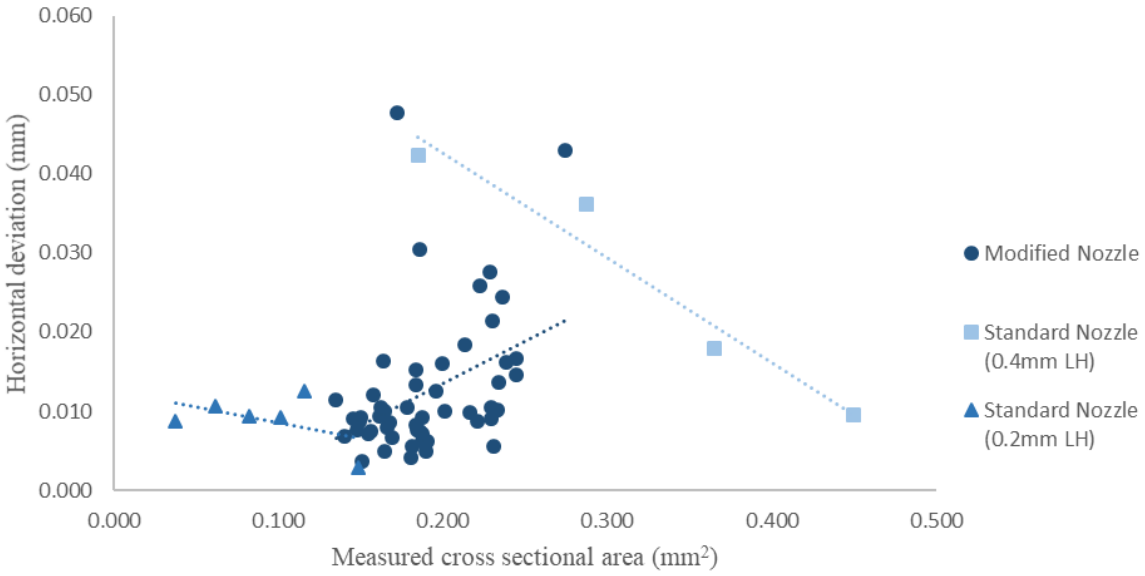

Figure 8.23 *Relationship between measured cross-sectional area and average horizontal deviation*

ANOVA analysis of the three surface quality metrics, *Rz*, *Ra* and *Rq* show that temperature, EF and print speed all have a significant influence on the output, except for temperature with *Rz*. In addition, the interaction of temperature and velocity are demonstrated to be statistically significant in all cases. Across these surface quality metrics, EF is consistently the most important factor, with around half of the total contribution. The combination of temperature and velocity being significant may be interpreted in two different ways. The first concerns actual volumetric flow rate, where this combination determines the feed rate (and therefore pressure applied to the molten material) and viscosity of the material. The other possibility is that it affects the heat applied to the previous layer. Faster and higher temperatures combined may produce both more stable and higher volumetric flow whilst reducing previous layer deformation and therefore lower over-extrusion beyond the modified nozzle side piece.

Figure 8.24 shows the relationship between the measured cross-sectional area and *Rq*. It demonstrates a negative correlation, where increased extrusion rates and cross-sectional areas give increased interaction with the nozzle side piece and therefore improved surface finish. Also compared is the standard nozzle for the 0.4mm layer height experimentation undertaken in Section 5. This shows that the modified nozzle clearly produced lower surface roughness for all parameters. Alternatively, the optimised parameters show a surface roughness similar to that with a 0.2mm layer height. This is of course particularly significant for the optimal parameter settings, shown by the lowest *Rq* values on the figure.

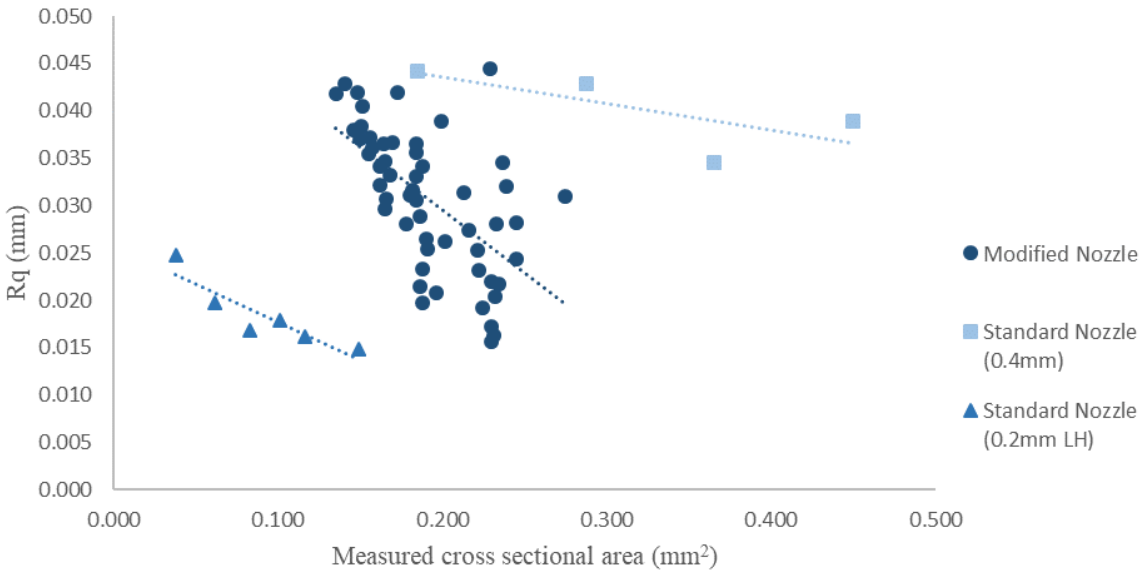

Figure 8.24 *Relationship between measured cross-sectional area and Rq*

Rz, *Ra* and *Rq* are all shown to improve with increasing temperature, increased print speed and increased extrusion rate, although the improvement between 200ºC and 230ºC is small.

The optimal parameters across all output metrics are demonstrated to be an EF of 1.5, a temperature of 230ºC and a print speed of 3600mmmin^{-1}. This can be validated by the strand cross-sections displayed in Figure 8.11. These also clearly show that the EF of 1.5 is the most significant factor.

8.3.2.3. PERFORMANCE IMPLICATIONS

As a result of using the modified nozzle for steady state deposition, it has been demonstrated that bond area, horizontal deviation and surface roughness characteristics have all been improved versus a standard nozzle. In addition, it has enabled a layer height of 0.4mm with similar surface roughness to a standard nozzle 0.2mm layer height and significantly improved bond width and improved horizontal deviation. This theoretically enables stronger, more accurate components with shorter build times to be produced.

9. MODIFIED NOZZLE XY PLANE GEOMETRICAL PERFORMANCE

The experimentation presented in this section builds upon the modified nozzle studies conducted on steady state straight depositions in the previous section to understand XY plane behaviour. In particular, the ability to translate the improved nozzle performance observed for steady state to the variable speed and extrusion conditions known to occur at corners is explored. This serves as a direct comparison to the XY plane experimentation conducted in Section 6, where a standard nozzle was used to quantify corner and non-corner weld errors. The use of a 4-axis machine with a modified stepped nozzle is unique. As such, the experimentation in this section provides an initial investigation of the behaviour of this machine and an exploration of which factors influence its performance.

9.1. METHODOLOGY

This section presents the methodology for XY corner error experimentation utilising a novel machine design and straight section weld errors using the same experimental setup as in the previous steady state experimentation.

9.1.1. CORNER ERRORS

Whereas previous steady state experimentation featured a fixed modified nozzle, to conduct corner experimentation the nozzle side piece must remain parallel to the direction of motion at all points. This necessitates the development of a fourth axis of rotation, enabling rotation of the nozzle relative to the build plate.

There are some limited examples where extrusion-based deposition has been combined with a rotational axis in addition to the standard three linear axes of motion. The most prominent example is the development of Contour Crafting (CC) - a technique for automated construction using concrete. This was developed almost 25 years ago [715] and has received some attention since. Khoshnevis [716] detailed the process, where an adjustable side piece is combined with an extrusion mechanism to produce smoothed outer surfaces. Other studies have explored CC further to develop modelling [718-719], new materials [720-722], or various modifications and improvements to the original process [716,723,724-734]. Although similar to the proposed modified experimentation, CC is conducted on a significantly larger scale, with layer heights typically many tens of millimetres rather than sub-millimetre. In addition, the materials used are not subject to melting and reheating. Other examples of rotational extrusion processes include adding rotation to enable multi-axis deposition [735], high speed rotational printing to enable fibre alignment in composites [736] and creating variable width paths with a slotted nozzle [345].

For ease of manufacturing and simplicity of operation, an existing 3-axis ME AM machine was selected for modification. This was the dual extrusion derivative of the ANet A8 used throughout the rest of the experimentation, the ANet A8-M. It features a dual extrusion mechanism with separate

stepper motors controlling each feed. The orientation of one of these motors was therefore changed and then used to enable rotation of the remaining nozzle assembly. In simple terms, this gives a machine with three Cartesian axes of motion and an additional rotary axis according to the machine motion specifications presented by Kampker et al. [601]. The arrangement of the two stepper motors and modified spindle are shown in Figure 12.8 in the Appendix. The second stepper motor and the rotating spindle were connected via a belt drive. The rotating drive gear had 60 teeth whilst the spindle gear has 20, giving a reduction ratio of 3:1. A major benefit of modifying the existing dual extrusion setup was that it negated the need for firmware or mainboard modifications. Instead, the extrusion command (i.e. a length of extruded filament) could be converted to a rotation. This value was calibrated over 50 full rotations, with the start and end point noted. This process showed that an extrusion value of 11.230mm corresponded to a full 360º rotation.

The experimental procedure was very similar to that employed in Section 6. This involved the use of a removable acrylic slide in a modified aluminium print bed. A bespoke gantry mounting solution and spindle assembly was fabricated from aluminium, and the central spindle from steel. 12mm outer and 6mm inner bearings were used at a spacing of 85mm, with the belt drive gear between these to prevent a bending force being introduced. A brass locking ring was used below the lower bearing to prevent movement upwards, whilst a top hat arrangement at the top of the steel spindle prevented movement downwards. The experimental machine setup is shown in Figure 9.1.

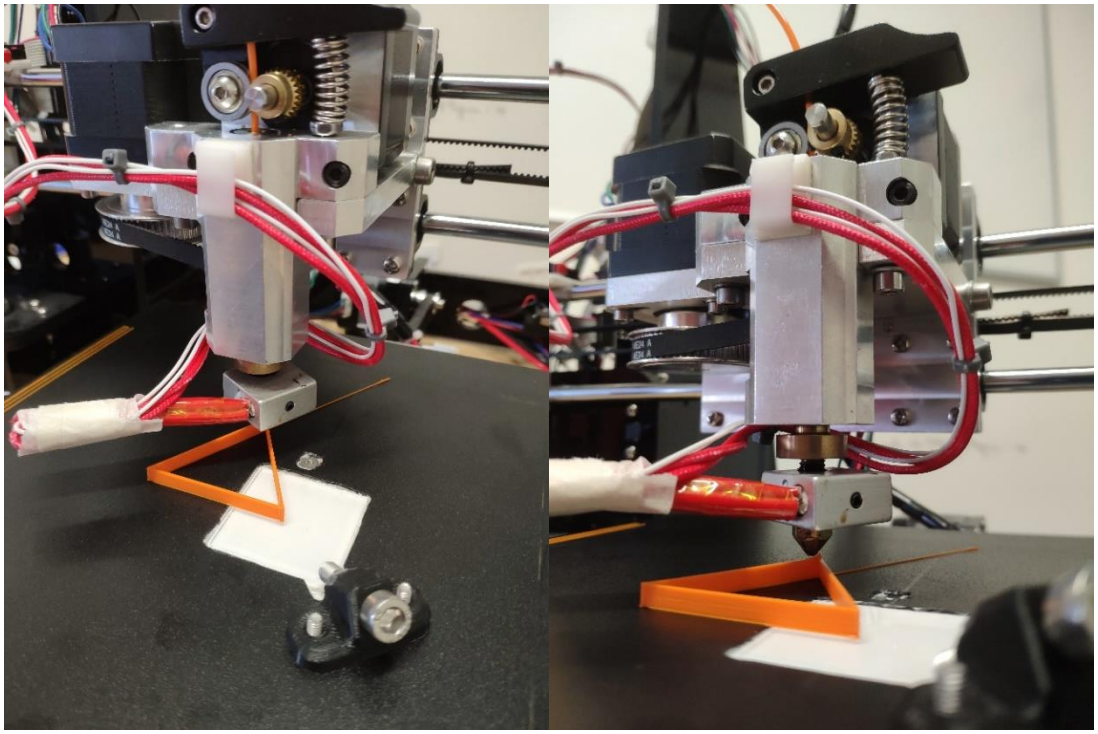

Figure 9.1 *Experimental machine setup utilising a modified print bed with removable slide on a modified ANet A8M ME AM desktop printer for XY plane with a modified nozzle experimentation*

As before, a custom G-code generator was developed to enable selection of toolpath, rotation, print speeds, rotation speeds, volumetric flow rate, print temperature and bed temperature. The acrylic slide was removed after deposition and measured using a *Zeiss Olympus BX51 TRF-6* Optical Microscope with 5x magnification. Analysis of the strand morphology was conducted *ImageJ*. An interesting effect of the increased print temperature versus the standard nozzle XY study is that the top surface was observed to be far smoother. The stitching algorithm used by the microscope software subsequently had difficulty in recognising position. Black marker pen features were therefore added, which are evident throughout the images in this section.

The previous steady state experimentation with the modified nozzle demonstrated optimal parameters of 230^{o}C, 3600mmmin^{-1} and EF of 1.5 (i.e. nominal cross-sectional area of 0.24mm^{2}). However, it has been demonstrated that the extrusion rate is non-linear at direction changes, whereby the effective extrusion rate is increased as motion slows towards corners. Given this, the increased extrusion rate at a corner must become the dimensioning factor for the outer surface and so a lower nominal extrusion factor was selected. Otherwise, the higher extrusion rate at the corner is beyond the optimal extrusion rate identified in the parameter optimisation and significant dimensional error would be expected. Similarly, initial experimentation showed that a print speed of 3600mmmin^{-1} produced significant deposition errors under acceleration so this was reduced to 1800mmmin^{-1}. As such, initial experimentation was conducted at a temperature of 230^{o}C, print speed of 1800mmmin^{-1} and EF of 1.2. In subsequent experimentation, the effects of extrusion rate, print temperature, corner angle, rotation speed, retractions and single layer depositions were explored, all for a single perimeter.

Preliminary experimentation revealed pauses at corners associated with the rotational motion of the nozzle. As a result, the standard XY plane experimental equipment and design used in Section 6 was utilised to measure the effects of corner delays and retraction experiments conducted to counter this phenomenon.

9.1.2. NON-CORNER WELD

Non-corner welds were fabricated using the modified 0.4mm step height nozzle. This does not require rotation, so the standard ANet A8 machine setup as used in Section 8 was utilised. A custom G-code generator was produced, which mimics the weld algorithm contained in *CURA*. This approach was almost identical to the experimental design in Section 6 but instead with the modified nozzle. This enabled the use of wipes past the weld to improve geometrical accuracy. Otherwise, the experimental procedure was identical using the removable acrylic slide, measurement at 5x magnification and measurement and analysis in *ImageJ*.

9.2. RESULTS

9.2.1. CORNER EXPERIMENTATION

The preliminary experiment with an EF of 1.2, temperature of 230ºC and print speed of 1800mmmin^{-1} is shown in Figure 9.2. This shows over-extrusion beyond the nozzle side piece. This feature is highlighted in black below and is also highlighted in subsequent microscope images.

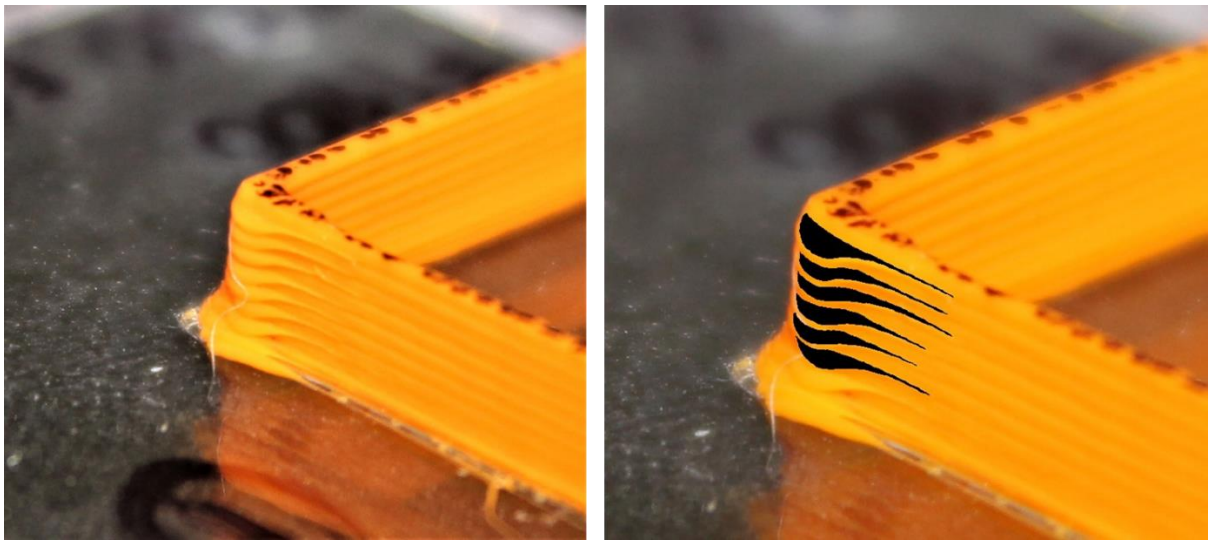

Figure 9.2 *Initial 90 degree corner over-extrusion (corner over-extrusion highlighted, right)*

9.2.1.1. PRELIMINARY EXPERIMENTATION

The images shown here are preliminary studies of the rotating modified nozzle behaviour with the expected optimal steady state parameters (Figure 9.3) and with reduced temperature and extrusion rate (Figure 9.4).

Figure 9.3 *Initial 90 degree corner result*

Figure 9.4 *90 degree corner with reduced temperature (200°C) and extrusion factor (1)*

9.2.1.2. SINGLE LAYER EXPERIMENTATION

The images shown here are for the first layer only, deposited directly on the removable acrylic slide.

Figure 9.5 *Single layer 90 degree corner using modified nozzle on 4-axis machine*

Figure 9.6 *Single layer 90 degree corner using modified nozzle on 4-axis machine with wipe (F1800, left and F450, right)*

Figure 9.7 *Single layer 90 degree corner using modified nozzle on 4-axis machine with straight wipe beyond corner (F450)*

9.2.1.3. CORNER ROTATION DELAYS

The need to rotate the nozzle assembly at corners led to corner delays. The experimental results presented in this subsection show the decrease in rotation time per layer with increasing rotation speed (Figure 9.8), the effect of corner pause on a standard nozzle non-rotational example (Figure 9.9) and the application of the minimised corner delay (i.e. maximised rotational speed) for 90 degree (Figure 9.10) and other corner angles (Figure 9.11).

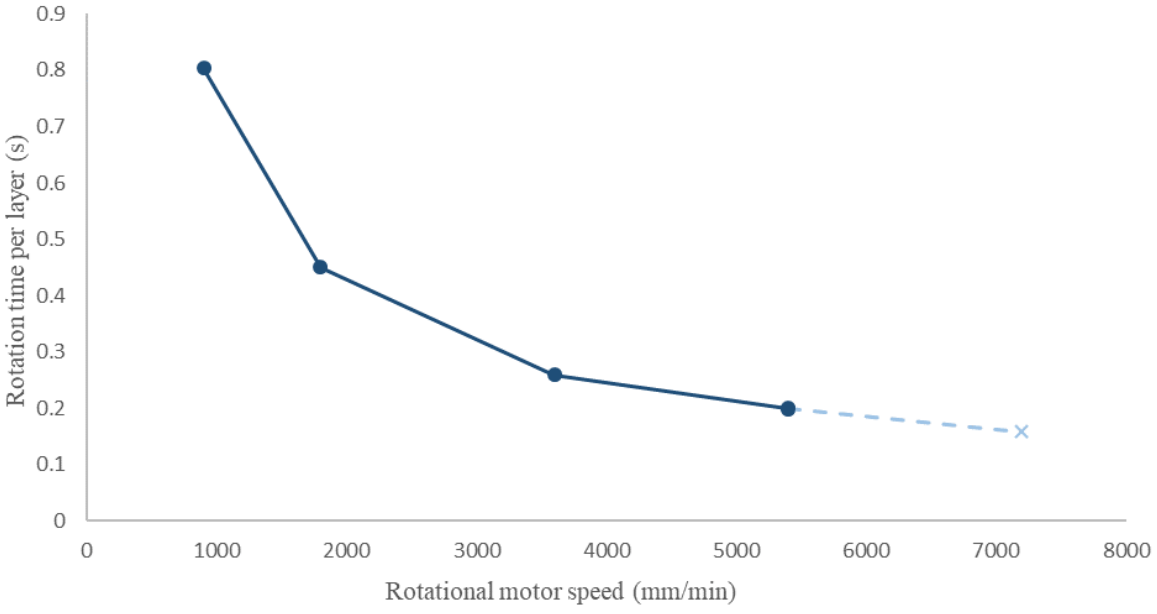

Figure 9.8 *Nozzle rotation time per layer*

Figure 9.9 *Effect of corner pause using standard machine and nozzle*

Figure 9.10 *90 degree corner with rotational modified nozzle and optimised corner delay time*

Figure 9.11 *45 degree corner (left) and 135 degree corner (right) with rotational modified nozzle and optimised corner delay time*

9.2.1.4. USE OF RETRACTION DURING ROTATION

The use of retractions during the rotational corner pause is demonstrated for the standard nozzle first (Figure 9.12) and is then applied to the rotating modified nozzle (Figure 9.13).

Figure 9.12 *Effect of adding filament retraction during corner pauses*

Figure 9.13 *Effect of adding 5mm F10800 filament retraction during corner rotation*

9.2.1.1. EFFECT OF TEMPERATURE

The effect of temperature is shown for the standard nozzle with pause (Figure 9.14) and both a pause and retraction (Figure 9.15) and for the modified nozzle with a pause and retraction (Figure 9.16).

Figure 9.14 *200°C and 230°C 90 degree corners using standard nozzle and machine with 49ms pause at corner*

Figure 9.15 *200°C and 10mm retraction with 49ms pause at corner*

Figure 9.16 *200°C, 10mm retraction results*

9.2.2. SUMMARY OF CORNER EXTRUSION ERRORS

Number	Figure	Print Speed	Rotation speed	Temperature	Other changes	Over-extruded area (mm^2)	Max over-extrusion deviation (mm)
1	Figure 9.3	3600	3600	230	-	0.659	0.361
2	Figure 9.4	3600	3600	200	EF 1	0.350	0.181
3	Figure 9.10	3600	5400	230	-	0.419	0.230
4	Figure 9.11	3600	5400	230	45º angle	0.940	0.342
5	Figure 9.11	3600	5400	230	135º angle	0.376	0.165
6	Figure 9.11	3600	5400	230	165º angle	0.092	0.084
7	Figure 9.13	3600	5400	230	5mm retraction	0.304	0.213
8	Figure 9.16	3600	5400	200	10mm retraction	0.256	-

Table 9.1 *Summary of corner over-extrusion errors in corner experimentation with rotational modified nozzle*

Number	Figure	Print Speed	Temperature	Other changes	Over-extruded area (mm^2)	Max over-extrusion deviation (mm)
1	Figure 9.9	3600	230	No pause	0.224	0.171
2	Figure 9.9, Figure 9.12, Figure 9.14	3600	230	49ms pause	0.633	0.348
3	Figure 9.12	3600	230	49mm pause, 5mm retraction	0.317	0.157
4	Figure 9.12	3600	230	49mm pause, 10mm retraction	0.477	0.157
5	Figure 9.12	3600	230	49mm pause, 20mm retraction	0.364	0.167
6	Figure 9.14	3600	200	49ms pause	0.559	0.303
7	Figure 9.15	3600	200	49mm pause, 10mm retraction	0.212	0.084

Table 9.2 *Summary of corner over-extrusion errors in corner experimentation with non-rotational standard nozzle*

9.2.3. NON-CORNER WELD

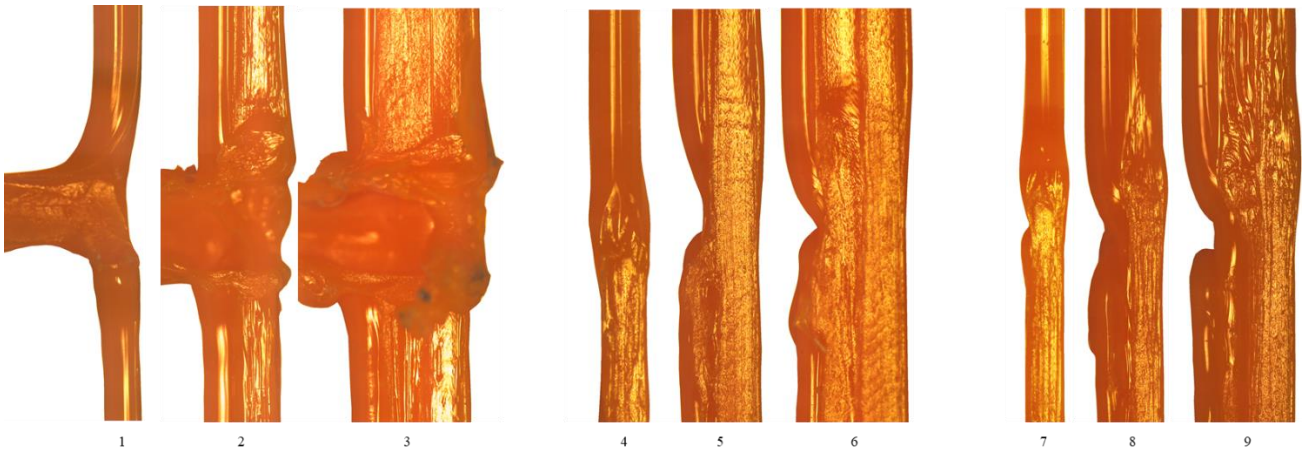

Figure 9.17 *XY plane non-corner weld with modified nozzle. Left: EF1.2, no move. Middle: EF1.2, 50mm final move. Right: EF1, 50mm final move.*

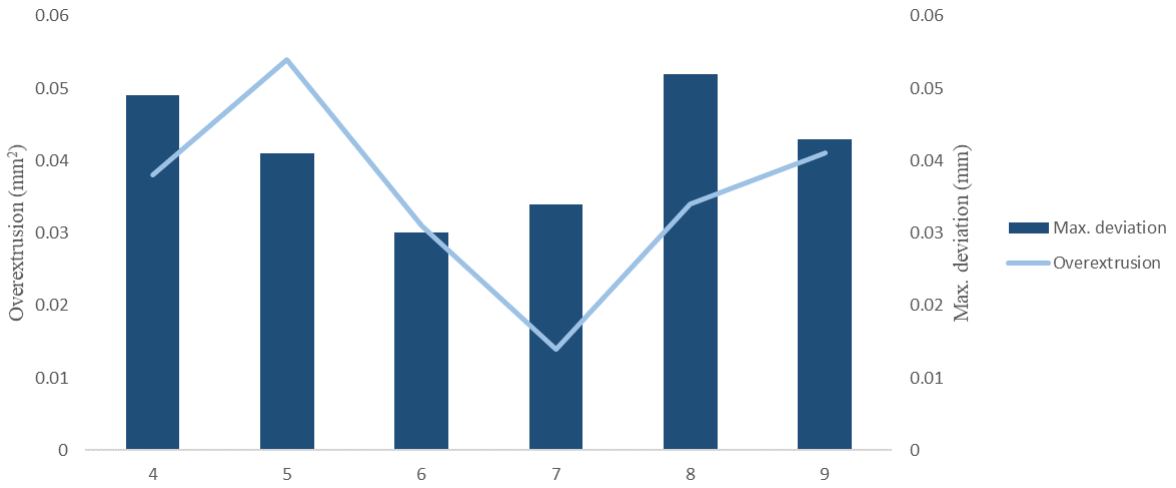

Figure 9.18 *XY Plane non-corner weld with modified nozzle errors*

9.3. DISCUSSION

9.3.1. CORNER PERFORMANCE

9.3.1.1. PRELIMINARY EXPERIMENTATION

The first fabrication in Figure 9.3 shows a preliminary test using the optimal parameters as informed by the steady state experimentation. This shows that whilst the nozzle side piece does clearly interact with the deposited filament, significant over-extrusion is observed on the corner exit. The specific area measured 0.659mm^2 with a maximum deviation of 0.361mm. This is significantly worse than the non-weld standard nozzle 90^o corner example with a LH of 0.2mm, where the maximum deviation was less than 0.1mm and the area approximately 35% lower. As was the case with the steady state study, this clearly occurs at the top of the previous layer. The over-extruded material is therefore being pushed below the nozzle side piece. The larger increase in effective volumetric flow rate at the corner likely pushes the behaviour beyond the highest EFs used in the steady state experimentation, where the same result of significant over-extrusion was also seen. In addition to the steady state over-extrusion, it is likely that the rotation itself contributes to this geometry. When approaching the corner, the side piece is parallel to the entry direction. At the corner, the over-extrusion begins (as was demonstrated in detail in Section 6). This additional material is likely to be deposited ahead of the nozzle as it is blocked by the solidifying strand. It is posited that the rotation then directs this further around the corner and below the nozzle as the additional material volume can no longer be contained. It was noted that the morphology in the straight regions away from the corners remained as per the results presented in the previous section.

Reducing the temperature to 200^{o}C and the EF to 1 shows a reduction in the over-extrusion (Figure 9.4). The total over-extrusion area is almost halved to 0.350mm^2 and the maximum deviation halved to 0.181mm, though this remains almost double that of the standard nozzle example. With a reduced

temperature, the lower viscosity of the extruded material likely reduces flow beyond the side piece and the reduced EF clearly reduces the overall volumetric flow rate leading to smaller error.

9.3.1.2. *Single Layer Experimentation*

As was tested in isolated experimentation runs during the steady state experimentation, single layers were deposited on the acrylic slide in order to understand the deposition behaviour with a solid and stable previous layer. In this case, the area of over-extrusion changes from the exit of corners to the entrance. This suggests that there is indeed some degree of interaction with the nozzle side piece during the rotation phase. This behaviour is outlined in Figure 9.19.

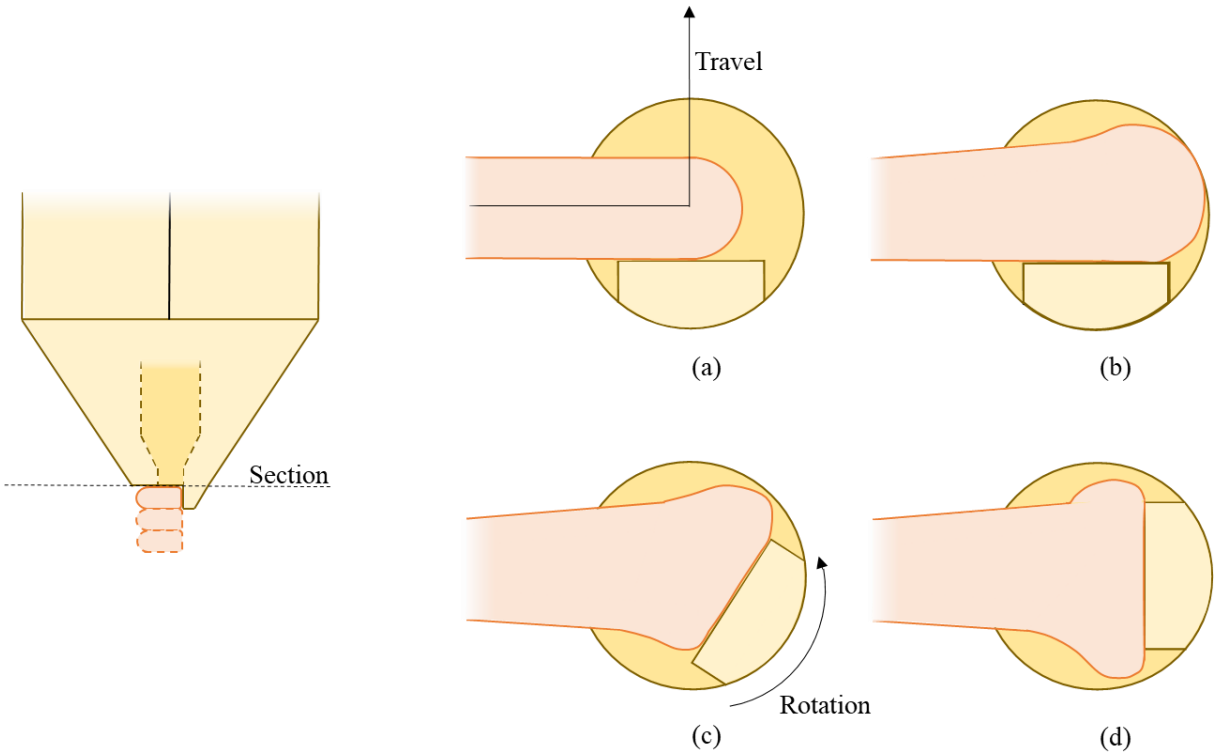

Figure 9.19: *Over-extrusion process on first layer experimentation; (a) steady state, straight, (b)increasing extrusion rate as speed reduced on entrance to corner, (c) beginning of corner rotation, (d) rotation complete*

The addition of a wipe at a speed of 1800mmmin^{-1} slightly modifies this area, and doing so at a slower speed of 450mmmin^{-1} modifies it still further. This appears to maintain the same over-extrusion area but reduce the maximum deviation by distributing the material further from the corner. Finally, continuing with a wipe past the corner without rotation removes most of the over-extruded area, although some remains even at a low speed of 450mmmin^{-1}.

9.3.1.3. *Corner Rotation Delays*

It was hypothesised that delays at the corner required to allow the rotation of the modified nozzle leads to significant over-extrusion, beyond what the nozzle side piece is able to mitigate against. In addition, the pause at the corner leads to greater heat transfer to the previous layer, which could further increase errors through reduced material stability.

The initial rotational motor was set at an (implied extrusion) speed of 3600mmmin^{-1}. Experiments were conducted to understand the relationship between changing rotation speeds and in particular, to compare these against a non-rotational perimeter example. Figure 9.8 shows the difference between the non-rotational and rotational perimeters for varying rotational speeds. This demonstrates that the rate of improvement falls. The maximum speed possible before missed steps and therefore rotational position was found to be 5400mmmin^{-1}. Assuming this delay is purely a function of corner angle, this suggests the minimum corner delay for a 90^{o} corner is 49ms.

Pausing at the corner produces significant over-extrusion as the material continues to flow during the pause, since the pressure remains within the melt chamber. This is then matched by a period of under-extrusion on the corner exit. Figure 9.9 shows this over-extrusion behaviour clearly, introducing significant additional perimeter dimensional error. Including the 49ms delay on a standard nozzle 90^{o} corner approximately triples the over-extrusion area and doubles the maximum deviation.

Appling the increased rotational speed with the original temperature of 230^{o}C and EF of 1.2, shows a significant reduction in geometrical error. Both the over-extruded area and maximum deviation are reduced by 36%. This is purely as a result of the reduced corner pause.

Other corner angles are presented in Figure 9.11. Smaller angles (i.e. sharper corners) have required greater reductions in speed and so produce higher over-extrusion. In addition, the smaller angle leads to a higher double extrusion area as was discussed in detail in Section 6. As expected, this shows that the over-extruded area and maximum deviation are highest for the smaller angle and are significantly reduced for larger angles.

9.3.1.4. Corner Retraction

A usual source of pause in extrusion is the change between sections within a layer or moves between layers. Slicing software commonly applies a retraction move, whereby the filament is driven upwards to reduce the pressure within the liquefier and reduce unwanted extrusion. Figure 9.12 shows the effect of adding various retraction distances, all conducted at the standard extrusion retraction speed of 10800mmmin^{-1}. This suggests that the retraction length has little effect, but that adding a retraction at all improves the maximum deviation from 0.348mm to approximately 0.16mm.

Adding the retraction slightly increases the pause time, but the reduction in pressure overcomes this effect. The 5mm retraction was integrated into the default rotational 90^{o} experimentation. This reduced the over-extruded area and maximum deviation to slightly but had the effect of introducing inwards corner deflection. It appears that the corner was dragged inwards as a result of the retraction and rotation combination, which was observed to become more pronounced with an increased number of layers as demonstrated in Figure 9.20.

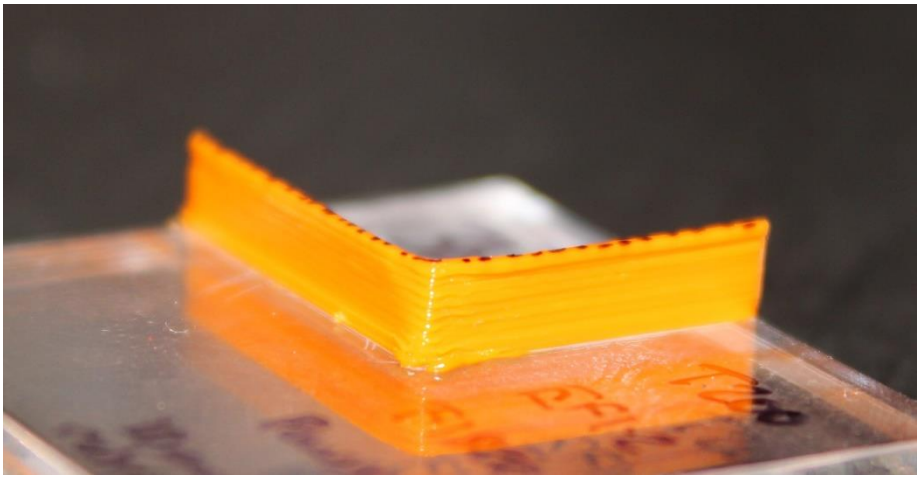

Figure 9.20 *Corner error increasing with layer number*

9.3.1.5. EFFECT OF TEMPERATURE

Finally, reductions in temperature were investigated. Any improvements as a result of this will have a negative effect on the steady state performance as was demonstrated in Section 8. Figure 9.14 shows some reduction in over-extrusion where a temperature of 200ºC was used together with the 49ms pause. This is due to the increased material viscosity which reduces over-extrusion from the latent liquefier pressure. Combining the lowered temperature with a 10mm retraction with the standard nozzle shows very significant improvement. This performs very similarly to the original standard nozzle experiments with no pause. Finally, these parameters were applied to the rotational approach with a temperature of 200ºC, an EF of 1.2, print speed of 1800mmmin^{-1} and retraction of 10mm at 10800mmmin^{-1}. Whilst this results in decreased over-extrusion, as shown in Figure 9.16, the corner is again deformed inwards very significantly losing corner geometrical accuracy.

9.3.1.1. SUMMARY OF PERFORMANCE

The rotational experimentation has shown that the induced pause leads to higher over-extrusion, particularly on the exit of the corner. Reducing temperature, optimising the corner pause and adding a retraction theoretically reduces this. However, the greatest improvement is given by the retraction although this instead directly leads to a loss of corner geometry inwards.

9.3.2. NON-CORNER WELD

Previous experimentation in Section 6 showed that welds at corners gave increased error, though placing welds on continuous perimeters also introduced error. The addition of a modified nozzle with a side piece has the ability to guide the material at the weld to improve both the bonding and reduce the error.

The first approach utilised the same toolpath and extrusion conditions as was conducted for the standard nozzle previously. This gave significant errors as the nozzle side piece moved between perimeters and clashed with previously-deposited material.

The second approach utilised a 50mm movement past the weld on the outer perimeter for an EF of 1.2 and 1, and single, double and triple perimeters. The number of perimeters did not have a significant effect on the error, nor did the extrusion factor. With the addition of the 50mm wipe, the maximum deviation was reduced to approximately 0.04-0.05mm from 0.07-0.11mm without the modified nozzle as presented in Section 6.3.

10. DISCUSSION

This section provides a discussion of the work conducted in this thesis. Section 3 focused on understanding the current level of performance achievable, whilst Sections 4, 5 and 6 further explored the source of demonstrated errors. A novel nozzle design was then proposed and fabricated to investigate potential steady state (Section 8) and XY plane improvements (Section 9).

10.1. CURRENT ME AM PROCESS PERFORMANCE

Sections 3 to 6 presented experimental work to improve understanding of the current performance and the nature of process errors. Prior to this, existing experimental literature was reviewed. This demonstrated that more than 300 macro experimental studies have been conducted, covering both error characterisation and error improvement work. However, it has proven to be difficult to draw generalisable conclusions which explains the apparent disconnect between academic work and the ME AM process in practice. Although AM technologies are commonly used to produce one-off prototypes as a result of their reduced setup costs, small batch processes are becoming increasingly attractive via AM. It was demonstrated that work reflecting this was lacking in the existing literature, where a comparison of the process performance between prints or between machines for identical components was rare.

The first experimental work presented in Section 3 therefore sought to understand the dimensional and geometrical accuracy and precision performance for a square-section component fabricated at multiple locations within a print, across multiple prints and different ME AM machines. In doing so, it directly addressed a key gap identified in the literature as part of Section 2. This experimental work shows that accuracy errors were highly dependent on the axis direction being measured and the machine used, but were typically less than 0.25mm. There was no clear relationship between machine design or cost, and accuracy performance. Three measures of precision were introduced, demonstrating that the more expensive machine achieved superior precision, likely due to the use of higher quality components. Underlying precision, where each measurement position was normalised against the average of values at that position, revealed a ‘best case’ precision of approximately ±0.2mm. As a result of the combined accuracy and precision errors, it was found that a tolerance of 1.2mm would be required to ensure that assembled components would fit according to a C_{pk} value of 1.33 (or 99.99% of components falling within the range). It was similarly demonstrated that significant improvements to this could be realised with immediate blanket scale error compensation factors. Geometrical error was observed to be concentrated at the 90^{o} corners, where these tended to deviate outwards relative to the straight side sections. Finally, a basic model was presented to classify macro component errors as a direct result of errors in the outer perimeter. The source of these errors was hypothesised as arising from either nozzle position (i.e. *toolpath*) or extrusion (i.e. *volumetric*

flow and *deposition morphology*) deviations. These two aspects were therefore investigated in the subsequent experimental sections.

A review of the existing literature revealed that little attention has been given to the accuracy of the ME AM machine itself, decoupled from the extrusion aspect of the process. Similarly, experimental data relating to the dimensional accuracy and precision of the filament feedstock was demonstrated to be lacking. To address these gaps, machine positional performance was investigated on two ME AM machines with different chassis mechanics and filament-related dimensional errors were investigated. Filament manufacturers typically claim a diameter tolerance of ±0.03mm or better. This was confirmed via the measurement of ten different filaments from a variety of manufacturers and materials. Extrusion length error was also determined using a cold extrusion with no nozzle present. This showed a difference in performance between the two machines used, with a maximum accuracy scale error of approximately 3% and a variability of ±1%. The combination of filament diameter error and extrusion length corresponds to a modest final XY error of approximately 0.012mm.

XYZ position error was modelled in terms of its scale and backlash components. Backlash errors were demonstrated to be highly dependent on the motion mechanism. Both machines utilised a lead screw mechanism for the Z axis, which showed much lower backlash error than most of the belt-driven X and Y axes. Increased tensioning of the belt mechanism or gantry guide wheels appears to significantly reduce backlash errors and therefore should be applied to current machines if not done already. Scale errors were found to be significant on all axes on all machines. In all cases, the actual movement was smaller than the nominal distance. Although a relatively small sample size, this does suggest that significant dimensional improvement could be made through machine and axis-specific compensation factors or improved calibration by machine manufacturers. The errors arising from backlash and scale were significantly larger than the filament-related error at approximately 0.1mm for the X and Y axes and 0.05mm for the Z axis based on a 15mm nominal component dimension. However, these errors may be less significant in practice if mating components are fabricated using the same machine, where both sets of measured dimensions will naturally exhibit the same error.

Steady state morphology experimentation investigated the dimensions and shape of the deposited strand for a wide variety of layer height and volumetric flow rate combinations. Two principle existing models were presented, as used by current popular slicers. These were the rectangular model and semi-circular model, where for the same cross-sectional area (i.e. volumetric flow rate with respect to movement speed) the semi-circular model predicts a greater road width. Cross-sectional characterisation was conducted for single, double and triple perimeters, with double and triple the most common slicer default settings. This showed that the presence of an inner perimeter slightly altered the outer surface resulting in a marginally improved surface roughness. A new model was developed consisting of arc segments rather than semi-circles. This morphology was found to vary

with nominal cross-sectional aspect ratio and layer height, as well as with the aforementioned number of perimeters. Versus the standard rectangular model, this new model predicts an increased road width of approximately 0.035mm and therefore suggests existing components fabricated using the rectangular model have an oversized error contribution of this value.

Finally, XY plane errors were investigated. 11 corner angles between 15^{o} and 165^{o} were fabricated with a double perimeter, varying the presence or absence of a weld joint and perimeter deposition order. The presence of corner error was noted to be caused by two main factors: theoretical double-extrusion and a mismatch of extrusion and print head velocity profiles. In line with typical slicer settings, the outer (i.e. second deposited) filament was deposited at half the speed of the inner. This reduced corner deviation, though to some degree the improvement was offset by the error of the adjacent perimeter blocking material flow in that direction. Internal corner deviations were shown to have little significance versus the rounded external geometry and external over-extrusion errors for cases of assembled components. Maximum geometric deviation relative to the straight and flat sections away from the corner was typically of the order of 0.1mm and was generally worse for smaller angles, with the weld present and where the outer perimeter was deposited first at the doubled print speed. Tests were conducted at different orientations and by reversing the print direction, which showed little difference in the errors present. The effect of print speeds was also investigated. This showed that a lower sprint speed of 450mmmin^{-1} reduced the errors significantly, though this would result in a large increase in build time. Finally, non-corner welds were produced on a representative straight section. This showed a deviation of approximately 0.1mm, similar to those observed at the corner outer perimeters. Given that the weld corners exhibited slightly increased corner error compared to the non-weld examples, this suggests moving the weld away from distinct corners can slightly improve tolerancing. However, this weld would then likely become far more visually distinctive which is often the rationale for the current placement at the sharpest corner.

In addition to the experimentation discussed above, Section 7 presented existing approaches to improve the performance of the ME AM process. Improvement methods were classified into three categories: error avoidance, error compensation and post-processing. Existing studies have demonstrated that significant effort has been made in these areas, but that nonetheless the majority of the findings have not been incorporated into current slicers or the ME AM process as a whole.

Being a relatively new technology, designers are still learning about the limitations of ME AM and how to design components to best harness its performance capability. Detailed dimensional performance data is still lacking and most users instead rely on a trial-and-error approach. Individual parameter optimisation studies have considered only isolated combinations of machine, material, component and slicer. This makes their general applicability difficult, such that the findings of any one study applied to an alternative experimental setup may not yield the expected impact or could

even worsen performance rather than optimising it. The generation of new toolpaths has tended to focus on reducing theoretical staircase errors or voids within the layer and as a result have not led to improvement in dimensional or geometrical performance. Extrusion generation approaches have reported improved continuity of material flow at direction changes. However, such approaches require more complex control and potentially higher quality components to be used and have yet to be adopted by slicers. Novel machine designs have addressed both XYZ motion and nozzle design. Alternative machine motion designs have failed to demonstrate improved dimensional performance and have instead focused on reducing the need for support or improving very specific component types. Nozzle designs have typically focused on internal geometry to ensure steady material deposition, with only one theoretical example presented to physically alter the deposition morphology.

Error compensation at the machine level is demonstrated to be effective for scale errors, but requires a relatively intensive experimental procedure which cannot reasonably be performed by a typical user. Post-processing techniques have usually focused on improving surface roughness rather than dimensional accuracy. In addition, these are limited in their applicability to various component designs and materials, and necessarily introduce time and cost penalties.

10.2. NOVEL NOZZLE DESIGN AND 4-AXIS MACHINE

Based on the surface profile and XY errors demonstrated on a standard ME AM machine, a novel nozzle design was proposed featuring a side piece, similar to that proposed in a previous numerical study which suggested promising results. This design theoretically prevents XY plane deviation by directing excess material resulting from increased effective extrusion rates away from the external perimeter. In addition, for vertical walls the interaction of the deposited material with the side piece gives a theoretical improvement in surface quality. It is important to state that the experimental investigation of a nozzle of this design is entirely novel, and builds on only a significantly limited amount of theoretical modelling conducted previously.

Steady state experimentation, similar to that conducted with a standard nozzle, was performed. Initial experimentation using four separate nozzle designs showed that a 0.4mm layer height was required to achieve suitable morphological control. The stability of the previous layer was found to be a very important factor and at lower layer heights, it was hypothesised that increased heat transfer resulted in some local re-melting and therefore over-extrusion beyond the nozzle side piece.

Using a 0.4mm step height modified nozzle, improved surface finish and deviation was demonstrated combined with theoretical improvements in build time owing to the increased layer height. A parameter optimisation study was then conducted to determine the optimal values of print speed, extrusion rate and print temperature. All three factors were demonstrated to be statistically significant, as well as the interaction of temperature and print speed. Optimal print parameters were found to be a

print temperature of 230ºC, print speed of 3600mmmin^{-1} and an extrusion factor of 1.5 (i.e. a theoretical cross-sectional area of 0.24mm^2).

Various alternative approaches were tested to improve performance including wipe movements, reduced layer heights and multiple perimeters. However, these did not yield any significant improvements and instead introduced further error. Beyond cross-sectional areas of between 0.192 mm^2 and 0.240mm^2, over-extrusion beyond the side piece was observed. For variable extrusion rates such as those in poorly-controlled deposition, variability was demonstrated to be significantly reduced compared to a standard nozzle with no side piece.

In contrast to the improved performance demonstrated for straight steady state depositions, preliminary experimentation utilising the modified nozzle on a modified 4-axis machine in the XY plane revealed significant limitations. As discussed previously, the effective extrusion rate increases at corners due to a mismatch between extrusion rate and print speed. Initial tests demonstrated that there was an additional corner delay of approximately 0.5ms per degree of direction change for an optimum rotational speed. Given that the pressure within the melt chamber cannot instantaneously be reduced to zero, this pause introduces additional over-extrusion. As was demonstrated both in the modified nozzle steady state experimentation and the standard nozzle XY tests, this manifests as over-extrusion on the exit of the corner and below the nozzle side piece. The inclusion of corner retractions and lower temperatures reduces pause over-extrusion, but deviates from the optimal parameters generated via steady state deposition and introduces additional inwards corner geometry error.

10.3. CONCLUSIONS AND CONTRIBUTIONS

The research questions in Section 1.4.1 focused on characterisation of the existing process, immediate improvements and potential modifications to the process. This thesis has made both theoretical and practical contributions in each of these areas through detailed experimentation.

Directly comparable dimensional accuracy and precision data for identical components between different ME AM machines was an area that was shown to be lacking in the current literature and in part contributed to the limited generalisability of findings. The experimentation undertaken to address this demonstrated that the current process accuracy error is highly axis and machine specific but was less than 0.25mm in all cases. Precision errors were typically of the order of ±0.2mm. Geometrical errors were demonstrated to be concentrated at corners. The combined effects of these suggested that the process tolerance required is significantly higher than other manufacturing processes. Given the current performance of the process, a tolerance of approximately 1.2mm is appropriate to ensure 99.99% of fabricated components can be assembled. This initial experimentation is useful in immediately providing direct information for those seeking to set up batch production using low-cost ME AM machines, as has been shown to be increasingly the case. This experimental work addresses a key research question, where it was noted that it was not clear what the magnitude and nature of errors

are between multiple components, prints and machines. In addition, the apparent disconnect between the large number of parameter optimisation studies conducted and their influence on current ME AM performance was highlighted as a notable issue. It was discussed that this was primarily due to their lack of generalisability, a major aspect of which is the applicability of findings between different machines. The experimentation in Section 3 is therefore incredibly useful, in that it directly compares results between machines of differing designs and thus provides results where this crucial yet often overlooked element of variability is included.

The subsequent experimentation addressed the major gap in the literature identified in Section 2 regarding the lack of detailed knowledge of errors in terms of their influencing factors and where and in what way they manifest. Macro errors on a fabricated component were categorised in terms of positional and extrusion errors of the outer perimeter. A summary of these errors is included in Figure 10.1, in an 'error budget' approach for both steady state sections and corners. The data presented here is based on a nominal 15mm component dimension featuring a 90^{o} corner in the XY plane on the ANet A8 desktop machine used throughout Sections 4 to 6. Accuracy data was captured for every error source, whilst precision data was generated for positional error only.

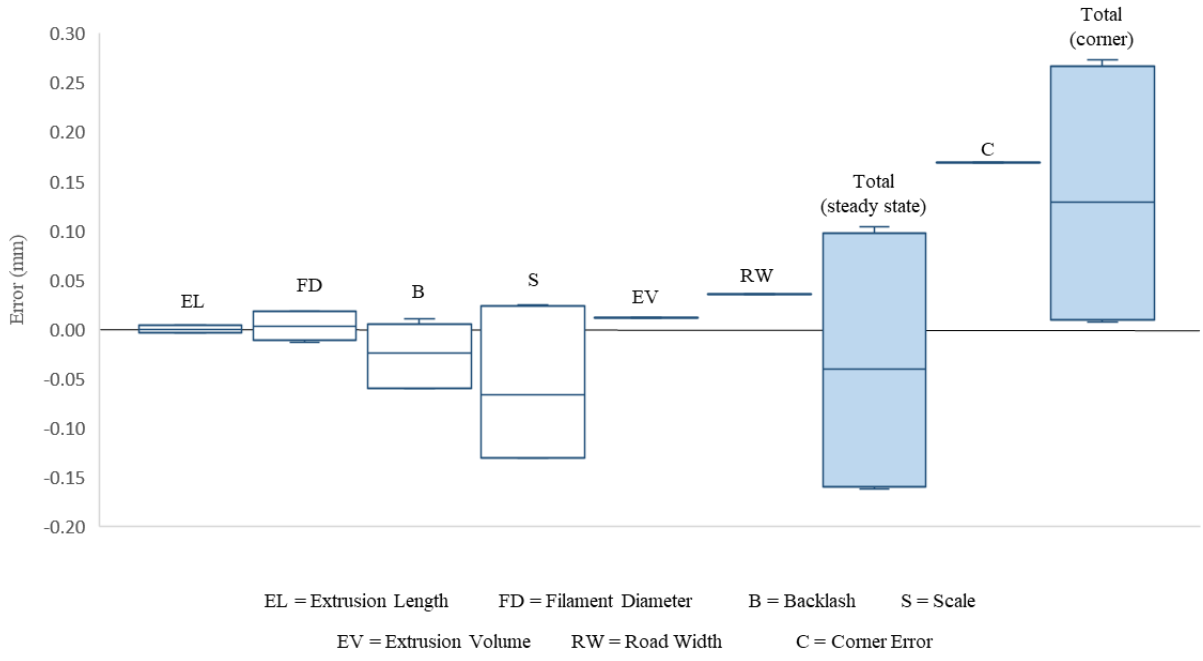

Figure 10.1 *Summary of error sources in the existing ME AM process. Based on combined XY errors for ANet A8 machine, 90 degree corner and default RW and LH (0.4mm and 0.2mm respectively).*

This shows that the extrusion length and filament diameter accuracy and precision errors are small. From a positional perspective, the backlash and scale errors dominate. Clearly, for larger nominal dimensions the scale error will contribute to an even greater degree. Default layer heights and extrusion rates are not close to process limits and as such, the extrusion volume accuracy error is modest. However, if closer to rate limits through reduced temperature or increased volumetric flow

rate the contribution is likely to be more significant. In addition, although not quantified in this study, the variable behaviour of unsteady extrusion when at rate limits suggest a potentially significant contribution. The accuracy error between the rectangular cross-sectional model and the model developed in Section 5 was demonstrated to be relatively modest, and given this models the road width for a specified cross-sectional area, has very little theoretical precision error. Finally, corner errors were demonstrated to significantly contribute to geometrical error and represent the single largest contribution to accuracy error on a component. However, precision errors relating to variability at corners were not actively investigated in this study. As the original machine used in Section 3 was not available for subsequent experimentation, it is difficult to directly compare these accuracy and precision errors with those determined in the original component study. Whilst the errors presented above are similar to those of the three machines presented in Section 3, it should be noted that other machine and axis-specific scale errors in particular could have a strong impact on the measured dimensions.

Immediate improvements are possible for the existing process. It was first suggested that blanket X, Y and Z scale correction factors could be applied, which could reduce the required tolerance from 1.2mm to 0.8mm. Further, machine-specific correction of backlash and scale error would yield the most significant improvements, as demonstrated in Figure 10.1. In addition, small improvements of approximately 0.03mm are possible by incorporating the filament geometry model developed in Section 5 directly into slicers. However, the corner-based accuracy error is a more complex problem for which a unique modification to the process was proposed and investigated.

The modified nozzle shows significant improvement in steady state performance, reducing dimensional error and improving surface finish whilst also reducing the build time of vertical walls. The use of this modified nozzle to produce physical artefacts is entirely novel, and provides a clear basis for future work to build upon the findings included in this thesis. Whilst the modified nozzle design used was shown to have performance issues in XY deposition due to additional over-extrusion and the escape of deposited material below the modified nozzle side piece, the overall approach nonetheless represents an exciting contribution which, subject to further development, may provide a marked improvement in the performance of the ME AM process.

Scale, backlash and extrusion errors can be dealt with by manufacturers and slicing software producers, though machine-level calibration remains relatively time consuming and difficult to perform for the average user. The updated filament morphology model may be adopted immediately as part of the existing toolpath strategy, where the outer perimeter toolpath is offset by half the road width from the nominal layer boundary. Filament diameter errors are small for all manufacturers, and do not significantly contribute to dimensional or precision error. Corner errors are shown to dominate geometrical error, where the mismatch of the extrusion and movement gives over-extrusion at corners.

Whilst this can be mitigated by reducing print speed, this has an associated increased build time. Instead, it is important to properly control extrusion through improved flow control, or potentially refine the modified nozzle with the 4-axis machine to reduce the effect of this.

In parallel, efforts to gather process performance knowledge to better inform users of ME AM at the component design stage could reduce error. Precision performance data would reduce reliance on the trial-and-error approach and knowledge of the corner error outlined above could potentially be reduced through modifications to component design. However, it remains preferable for the process itself to gain robustness and improved performance, such that it is more capable of manufacturing to the nominal dimensions and geometry as designed by the user.

The knowledge of the source, magnitude and behaviour of errors presented in this thesis can be immediately used to inform the most suitable improvement approaches. The application of these will ultimately provide a more capable technology that is better able to fulfil its promise as a widespread manufacturing process.

10.4. RESEARCH LIMITATIONS AND FUTURE WORK

As was first discussed in Section 3.1.4, the experimental work contained within this thesis was conducted without direct measurement or control of the physical environment surrounding the print process. In particular, neither the ambient temperature nor the humidity levels were controlled for, though neither extreme temperature nor humidity were expected in the air conditioned and heated laboratory facilities used. Although it was noted that it is rare for ME AM experimental studies to record these environmental factors, it remains a limitation of this research and as such would benefit from direct exploration, potentially through the replication of one chapter's experimental results with varying environmental parameters to understand their impact.

Similarly, the elapsed time between component fabrication and measurement was not recorded, although it was never an extended period beyond approximately one month. This was also discussed in Section 3.1.4, where it was noted that the near exclusive use of PLA in this thesis is expected to mitigate against post-deposition dimensional changes to a large degree. However, once again this may be considered a limitation whose impact could also be determined through the replication of measurements for a specific experiment within this thesis at designated time periods following production of the test artefacts.

Throughout the experimental work contained within this thesis, PLA feedstock material was used almost exclusively with the exception of the direct comparison between PLA and ABS in Section 5. This was justified by the increasingly dominant selection of PLA in experimental work identified in Section 3. However, the analysis contained within that section shows that ABS remains in use in many studies and that in addition, other materials (including other thermoplastics, ceramic pastes or

biomaterials) are also gaining popularity. The exclusive use of the popular PLA is therefore a limitation of the experimental work, which once more would benefit from further detailed experimentation to address. In particular, non-thermal materials (i.e. pastes, gels) may be particularly suitable to the modified nozzle experimentation in Sections 8 and 9, where the morphology of the previously deposited layer will not be affected by heat from either the nozzle or the current layer.

The nozzle material also remained unchanged throughout experimental runs, where brass nozzles were used in all cases. For standard (i.e. unmodified) nozzles, stainless or hardened steel nozzles are commercially available and specifically recommended for use with composite or fibre-reinforced polymers where nozzle wear is of greater concern. In addition, some coatings have been applied, though again this has principally been aimed at reducing wear. As with alternative feedstock materials, the modified nozzle experimentation in Sections 8 and 9 may particularly benefit from further work centred on the combination of nozzle material and coatings.

As has been mentioned previously, the overall generalisability (or lack thereof) of previous experimental work is a source of significant interest. Whilst the experimental work contained in Section 3 is more generalisable than many of the experimental studies identified in the review since multiple machines are utilised, the selection of constant parameter values remains a limitation. Similarly, the use of two machines in the positional experimentation in Section 4 with a good degree of alignment between them suggests a reasonable likelihood of the findings being generalisable. The strand morphology and XY geometry experimental work utilising the existing nozzle design may be generalisable in that cross-sectional areas were measured directly, and inferences for flow rates were made from this. However, it would remain the case that there will be different alignments between slicer (i.e. theoretical) flow rate and the actual flow rate on any given machine, which may limit the generalisability of findings. The relatively close results from the prior two experimental sections nonetheless suggest that some degree of applicability across the ME AM process should be expected. The use of the modified nozzle design in the final two experimental sections may be expected to increase the level of generalisability, since if the modified nozzle were placed on an alternative machine or with different parameters, any strand deviation would be reduced as the side piece directs excess material inwards. As was mentioned above, the applicability of the findings in this thesis have not been demonstrated to extend to alternative feedstock materials and as such, further work in this specific area would prove highly beneficial. Other future work would be well placed to support and further develop the experimental results of this thesis. First, it was identified that scale errors significantly contribute to the overall process inaccuracy. Whilst the error compensation process to account for this is well understood, applying this to individual machines and axes requires time consuming measurements using highly precise equipment. Efforts to reduce the difficulty of applying this approach and limiting the need for user interaction should be explored, perhaps via the development of standard protocols or cheaper and simpler measurement and error analysis processes.

Corner errors were demonstrated to be prevalent in the XY plane regardless of the machine selected throughout Section 6. Improvement to extrusion flow control methods that can be integrated into existing slicers and used with existing desktop machines would be very productive, potentially in combination with further exploration of the modified nozzle approach investigated in this thesis.

Further development of the XY modified nozzle may yield performance improvements. In particular, additional techniques to overcome the over-extrusion errors at the corner should reduce the errors determined in this study, potentially covering nozzle geometry changes, slicing algorithm advances as well as investigations surrounding the effects of alternative materials mentioned above. Provided the XY errors determined in this study can be overcome, attention should then be given to the demonstration of modified nozzle performance on non-vertical walls and integration with infill deposition. This would require experimentation similar to that conducted in Sections 8 and 9, with careful consideration of approaches to develop the limited experimental work contained in this thesis to bridge the gap between two-dimensional samples and full three-dimensional components with improved properties.

Finally, there have been recent and significant advances in the use of new techniques surrounding in-process error detection and correction. It was noted in Section 7.1.2 that many novel approaches had been suggested to improve the ME AM process, though many of these relied on components being manufactured, with measurement and analysis then taking place to inform future production. However, the use of real time control using advanced techniques enables faster and more direct improvements to be made, such as those suggested in Section 7.1.2.6. For example, the recently-presented work by Brion and Pattinson [645] suggests exciting possibilities for process improvement in a wider range of fabrication scenarios through the use of deep learning utilising neural networks. Whilst such improvements would still be somewhat limited by the performance of conventional hardware, it may be possible to combine this with the modified nozzle approach to enable the potential benefits of this step change in process capability to be fully realised.

11. BIBLIOGRAPHY

[1] Kai, C.C. Three-dimensional rapid prototyping technologies and key development areas, Computing and Control Engineering Journal, 5(4), (1994) 200-206 https://doi.org/10.1049/cce:19940407

[2] Wohlers, T. Wohlers Report 2020: Global Reports, Wohlers Associates, Belgium. (2020)

[3] Berman, B. 3-D printing: The new industrial revolution, Business Horizons, 55(2), (2012) 155-162 https://doi.org/10.1016/j.bushor.2011.11.003

[4] Byun, H.-S., Lee, K.H. Determination of the optimal build direction for different rapid prototyping processes using multi-criterion decision making, Robotics and Computer-Integrated Manufacturing, 22 (1), (2006) 69-80. https://doi.org/10.1016/j.rcim.2005.03.001

[5] Sinnreich, A. 3D Printing: hype, hope or threat, Giga Omni Media, United States (2014).

[6] Mohamed, O.A., Masood, S.H., Bhowmik, J.L. Investigation of dimensional variation in parts manufactured by fused deposition modeling using Gauge Repeatability and Reproducibility, IOP Conference Series: Materials Science and Engineering, 310(1), (2018) 012090 (2018). https://doi.org/10.1088/1757-899X/310/1/012090

[7] ASTM F2792-12a Standard Terminology for Additive Manufacturing Technologies, ASTM (2012).

[8] Rupal, B.S., Ahmad, R., Qureshi, A.J. Feature-Based Methodology for Design of Geometric Benchmark Test Artifacts for Additive Manufacturing Processes, Procedia CIRP, 70, (2018) 84-89 https://doi.org/10.1016/j.procir.2018.02.012

[9] Thompson, M.K., Moroni, G., Vaneker, T., Fadel, G., Campbell, R.I., Gibson, I., Bernard, A., Schulz, J., Graf, P., Ahuja, B., Martina, F. Design for Additive Manufacturing: Trends, opportunities, considerations, and constraints, CIRP Annals, Volume 65, Issue 2, (2016) 737-760 https://doi.org/10.1016/j.cirp.2016.05.004

[10] Leutenecker-Twelsiek, B., Klahn, C., Meboldt, M. Considering Part Orientation in Design for Additive Manufacturing, Procedia CIRP, Volume 50, 2016, (2016) 408-413 https://doi.org/10.1016/j.procir.2016.05.016

[11] Melenka, G.W., Schofield, J.S., Dawson, M.R., Carey, J.P. Evaluation of dimensional accuracy and material properties of the MakerBot 3D desktop printer, Rapid Prototyping Journal, 21(5), (2015) 618-627 https://doi.org/10.1108/RPJ-09-2013-0093

[12] Whitney, T.S. A structured look at performance capability and machine design of fused deposition modeling machines, Masters Thesis, Institute for Manufacturing, University of Cambridge, United Kingdom. (2016).

[13] Sun, Q., Rizvi, G.M., Bellehumeur, C.T., Gu, P. Effect of processing conditions on the bonding quality of FDM polymer filaments, Rapid Prototyping Journal, 14 (2), (2008) 72-80 https://doi.org/10.1108/13552540810862028

[14] Garg, H.K., Singh, R. Pattern development for manufacturing applications with fused deposition modelling-a case study, International Journal of Automotive and Mechanical Engineering 7(1), (2013) 981-992 https://doi.org/10.15282/ijame.7.2012.14.0079

[15] Jyothish Kumar, L., Pandey, P.M., Wimpenny, D.I. 3D printing and additive manufacturing technologies, 3D Printing and Additive Manufacturing Technologies, (2018) 1-311 https://doi.org/10.1007/978-981-13-0305-0

[16] Mahamood, R. M., Akinlabi, E. T., Shukla, M., Pityana, S. Revolutionary Additive Manufacturing: An Overview, Lasers in Engineering, 27(3-4), (2014) 161-178

[17] Whitney, T.S., Moultrie, J. A structured look at new design possibilities for additive manufacturing machines, Proceedings of International Design Conference, DESIGN, DS 84, (2016) 561-570

[18] Huang, S.H., Liu, P., Mokasdar, A., Hou, L. Additive manufacturing and its societal impact: A literature review, International Journal of Advanced Manufacturing Technology, 67(5-8), (2013) 1191-1203 https://doi.org/10.1007/s00170-012-4558-5

[19] Galantucci, L.M., Bodi, I., Kacani, J., Lavecchia, F. Analysis of dimensional performance for a 3D open-source printer based on fused deposition modeling technique, Procedia CIRP, 28, (2015) 82-87 https://doi.org/10.1016/j.procir.2015.04.014

[20] Wang, X., Jiang, M., Zhou, Z., Gou, J., Hui, D. 3D printing of polymer matrix composites: A review and prospective, Composites Part B: Engineering, 110, (2017) 442-458 https://doi.org/10.1016/j.compositesb.2016.11.034

[21] Dey, A., Yodo, N. A Systematic Survey of FDM Process Parameter Optimization and Their Influence on Part Characteristics, Journal of Manufacturing and Materials Processing, 3(3), 64 (2019). https://doi.org/10.3390/jmmp3030064

[22] Zhang, K., Zhang, W., Ding, X. Multi-axis manufacturing process for continuous fibre reinforced composite parts, Procedia CIRP 85, (2019) 113-117 https://doi.org/10.1016/j.procir.2019.09.022

[23] Gulanová, J., Kister, I., Káčer, N., Gulan, L. A Comparative Study of various AM Technologies Based on Their Accuracy, Procedia CIRP, 67, (2018) 238-243 https://doi.org/10.1016/j.procir.2017.12.206

[24] Kim, G.D., Oh, Y.T. A benchmark study on rapid prototyping processes and machines: Quantitative comparisons of mechanical properties, accuracy, roughness, speed, and material cost, Proceedings of the Institution of Mechanical Engineers, Part B: Journal of Engineering Manufacture, 222(2), (2008) 201-215 https://doi.org/10.1243/09544054JEM724

[25] Ranganathan, R., Ravi, T., Pugalendhi, A. Analysis of shrinkage compensation factor (SCF) of FDM uPrint SE for accuracy enhancement, International Journal of Integrated Engineering, 11(1), (2019) 207-216 https://doi.org/10.30880/ijie.2019.11.01.022

[26] Bellini A., Güçeri S. Mechanical characterization of parts fabricated using fused deposition modeling, Rapid Prototyping Journal, 9 (4), (2003) 252-264. https://doi.org/10.1016/s0261-3069(99)00059-x

[27] Stansbury, J.W., Idacavage, M.J. 3D printing with polymers: Challenges among expanding options and opportunities, Dental Materials, 32(1), (2016) 54-64 https://doi.org/10.1016/j.dental.2015.09.018

[28] Hanon, M.M., Zsidai, L., Ma, Q. Accuracy investigation of 3D printed PLA with various process parameters and different colors, Materials Today: Proceedings, 42, (2021) 3089-3096 https://doi.org/10.1016/j.matpr.2020.12.1246

[29] Upcraft, S., Fletcher, R. The rapid prototyping technologies, Assembly Automation, 23 (4), (2003) 318-330 https://doi.org/10.1108/01445150310698634

[30] Do, A.-V., Khorsand, B., Geary, S.M., Salem, A.K. 3D Printing of Scaffolds for Tissue Regeneration Applications, Advanced Healthcare Materials, 4(12), (2015) 1742-1762 https://doi.org/10.1002/adhm.201500168

[31] Li, J., Li, H.-B., Dong, J.-C., Wang, T.-Y., Zhang, H.-T. The investigation of the effect caused by deposition velocity on bonding degree within the structure of FDM, Key Engineering Materials, 764, (2018) 142-155 https://doi.org/10.4028/www.scientific.net/KEM.764.142

[32] Wohlers, T. Wohlers Report 2020: Global Reports, Wohlers Associates, Belgium. (2021)

[33] Additive Manufacturing UK National Strategy 2018-25: Leading Additive Manufacturing in the UK, Additive Manufacturing UK, United Kindom (2018)

[34] Schirmeister, C.G., Hees, T., Licht, E.H., Mülhaupt, R. 3D printing of high density polyethylene by fused filament fabrication, Additive Manufacturing, 28, (2019) 152-159 https://doi.org/10.1016/j.addma.2019.05.003

[35] Park, H.S., Park, H.J., Lee, J., Kim, P., Lee, J.S., Lee, Y.J., Seo, Y.B., Kim, D.Y., Ajiteru, O., Lee, O.J., Park, C.H. A 4-Axis Technique for Three-Dimensional Printing of an Artificial Trachea, Tissue Engineering and Regenerative Medicine, 15(4), (2018) 415-425 https://doi.org/10.1007/s13770-018-0136-8

[36] Additive manufacturing and 3D printing - statistics & facts. [online] Available at: <https://www.statista.com/topics/1969/additive-manufacturing-and-3d-printing/#dossierKeyfigures>, Statista (2022)

[37] Polymer Material Extrusion Market Poses $2.2B Revenue Opportunity. [online] Available at: <https://www.smartechanalysis.com/news/polymer-material-extrusion-market/>, SmarTech Analysis (2022)

[38] Crump, S. Apparatus and method for creating three-dimensional objects, (US5121329A) (1992).

[39] Vyavahare, S., Teraiya, S., Panghal, D., Kumar, S. Fused deposition modelling: a review, Rapid Prototyping Journal, 26(1), (2020) 176-201 https://doi.org/10.1108/RPJ-04-2019-0106

[40] Sonsalla, T., Moore, A.L., Meng, W.J., Radadia, A.D., Weiss, L. 3-D printer settings effects on the thermal conductivity of acrylonitrile butadiene styrene (ABS), Polymer Testing, 70, (2018) 389-395 https://doi.org/10.1016/j.polymertesting.2018.07.018

[41] Minetola, P., Galati, M. A challenge for enhancing the dimensional accuracy of a low-cost 3D printer by means of self-replicated parts, Additive Manufacturing, 22, (2018) 256-264 https://doi.org/10.1016/j.addma.2018.05.028

[42] Ford, S., Despeisse, M. Additive manufacturing and sustainability: an exploratory study of the advantages and challenges, Journal of Cleaner Production, 137, (2016) 1573-1587 https://doi.org/10.1016/j.jclepro.2016.04.150

[43] Giberti H., Sbaglia L., Urgo M. A path planning algorithm for industrial processes under velocity constraints with an application to additive manufacturing, Journal of Manufacturing Systems, Part 1 43, (2017) 160-167. https://doi.org/10.1016/j.jmsy.2017.03.003

[44] Singh, S., Ramakrishna, S., Berto, F. 3D Printing of Polymer Composites: A Short Review, Material Design and Processing Communications, 2(2), e97 (2019). https://doi.org/10.1002/mdp2.97

[45] Tay, B.Y., Evans, J.R.G., Edirisinghe, M.J. Solid freeform fabrication of ceramics, International Materials Reviews, 48(6), (2003) 341-370 https://doi.org/10.1179/095066003225010263

[46] Bettini, P., Alitta, G., Sala, G., Di Landro, L. Fused Deposition Technique for Continuous Fiber Reinforced Thermoplastic, Journal of Materials Engineering and Performance, 26(2), (2017) 843-848 https://doi.org/10.1007/s11665-016-2459-8

[47] Mireles, J., Espalin, D., Roberson, D., Zinniel, B., Medina, F., Wicker, R. Fused deposition modeling of metals, 23rd Annual International Solid Freeform Fabrication Symposium - An Additive Manufacturing Conference, SFF 2012, (2012) 836-845

[48] Chia, H.N., Wu, B.M. Recent advances in 3D printing of biomaterials, Journal of Biological Engineering, 9(1), (2015) 4 (2015). https://doi.org/10.1186/s13036-015-0001-4

[49] Bikas, H., Stavropoulos, P., Chryssolouris, G. Additive manufacturing methods and modeling approaches: A critical review, International Journal of Advanced Manufacturing Technology, 83(1-4), (2016) 389-405 https://doi.org/10.1007/s00170-015-7576-2

[50] McIlroy, C., Olmsted, P.D. Deformation of an amorphous polymer during the fused-filament-fabrication method for additive manufacturing, Journal of Rheology, 61(2), (2017) 379-397 https://doi.org/10.1122/1.4976839

[51] Song, S., Wang, A., Huang, Q., Tsung, F. Shape deviation modeling for fused deposition modeling processes, IEEE International Conference on Automation Science and Engineering, 2014-January,6899411, (2014) 758-763 https://doi.org/10.1109/CoASE.2014.6899411

[52] Hager, I., Golonka, A., Putanowicz, R. 3D Printing of Buildings and Building Components as the Future of Sustainable Construction? Procedia Engineering, 151, (2016) 292-299 https://doi.org/10.1016/j.proeng.2016.07.357

[53] Zha, W., Anand, S. Geometric approaches to input file modification for part quality improvement in additive manufacturing, Journal of Manufacturing Processes 20, (2015) 465-477 https://doi.org/10.1016/j.jmapro.2015.06.021

[54] Gilmer, E.L., Miller, D., Chatham, C.A., Zawaski, C., Fallon, J.J., Pekkanen, A., Long, T.E., Williams, C.B., Bortner, M.J. Model analysis of feedstock behavior in fused filament fabrication: Enabling rapid materials screening, Polymer, 152, (2018) 51-61 https://doi.org/10.1016/j.polymer.2017.11.068

[55] Pandey, P.M., Reddy, N., Dhande, S.G. Improvement of surface finish by staircase machining in fused deposition modelling, Journal of Materials Processing Technology, 132(1-3), (2003) 323-331 https://doi.org/10.1016/S0924-0136(02)00953-6

[56] Thrimurthulu, K., Pandey, P.M., Reddy, N.V. Optimum part deposition orientation in fused deposition modeling, International Journal of Machine Tools and Manufacture, 44(6), (2004) 585-594 https://doi.org/10.1016/j.ijmachtools.2003.12.004

[57] Baumann, F., Bugdayci, H., Grunert, J., Keller, F., Roller, D. Influence of slicing tools on quality of 3D printed parts, Computer-Aided Design and Applications, 13 (1), (2016) 14-31. https://doi.org/10.1080/16864360.2015.1059184

[58] Šljivic, M., Pavlovic, A., Kraišnik, M., Ilić, J. Comparing the accuracy of 3D slicer software in printed enduse parts, IOP Conference Series: Materials Science and Engineering, 659(1), 012082 (2019). https://doi.org/10.1088/1757-899X/659/1/012082

[59] Torok, J., Kocisko, M., Teliskova, M., Petrus, J., Paulisin, D. Quality of 3D printed surface based on selected post processor, MM Science Journal, 2018(June), (2018) 2346-2349 https://doi.org/10.17973/MMSJ.2018_06_201745

[60] Budzik, G., Burek, J., Bazan, A., Turek, P. Analysis of the accuracy of reconstructed two teeth models manufactured using the 3DP and FDM technologies, Strojniski Vestnik/Journal of Mechanical Engineering, 62(1), (2016) 11-20 https://doi.org/10.5545/sv-jme.2015.2699

[61] Wijnen, B., Sanders, P., Pearce, J.M. Improved Model and Experimental Validation of Deformation in Fused Filament Fabrication of Poly Lactic Acid, Progress in Additive Manufacturing, 3(4), (2018) 193-203 https://doi.org/10.1007/s40964-018-0052-4

[62] Boschetto, A., Bottini, L. Design for manufacturing of surfaces to improve accuracy in Fused Deposition Modeling, Robotics and Computer-Integrated Manufacturing, 37,1357, (2016) 103-114 https://doi.org/10.1016/j.rcim.2015.07.005

[63] Bayley, C., Bockmann, L., Hurlbut, C., Helu, M., Transchel, R., Dornfeld, D., , Understanding Error Generation in Fused Deposition Modeling, Proceedings - ASPE 2014 Spring Topical Meeting: Dimensional Accuracy and Surface Finish in Additive Manufacturing, (2014) 98-103 ISBN: 978-188770664-3

[64] Mahesh, M., Wong, Y.S., Fuh, J.Y.H., Loh, H.T. Benchmarking for comparative evaluation of RP systems and processes, Rapid Prototyping Journal, 10(2), (2004) 123-135 https://doi.org/10.1108/13552540410526999

[65] Huang, Y., Leu, M.C., Mazumder, J., Donmez, A. Additive manufacturing: Current state, future potential, gaps and needs, and recommendations, Journal of Manufacturing Science and Engineering, Transactions of the ASME, 137(1), (2015) 014001 (2015). https://doi.org/10.1115/1.4028725

[66] El-Katatny, I., Masood, S.H., Morsi, Y.S. Error analysis of FDM fabricated medical replicas, Rapid Prototyping Journal, 16(1), (2010) 36-43 https://doi.org/10.1108/13552541011011695

[67] Paul, R., Anand, S. Optimization of Layered manufacturing process for reducing form errors with minimal support structures, Journal of Manufacturing Systems, 36, (2014) 231–243 https://doi.org/10.1016/j.jmsy.2014.06.014

[68] Haghighi, A., Li, L. Study of the relationship between dimensional performance and manufacturing cost in fused deposition modeling, Rapid Prototyping Journal, 24(2), (2018) 395-408 https://doi.org/10.1108/RPJ-11-2016-0177

[69] Bochmann, L., Bayley, C., Helu, M., Transchel, R., Wegener, K., Dornfeld, D. Understanding error generation in fused deposition modeling, Surface Topography: Metrology and Properties 3(1), (2015) e014002 (2015). https://doi.org/10.1088/2051-672X/3/1/014002

[70] Resource Guides: Fused Deposition Modeling. [online] Available at: <https://www.stratasysdirect.com/resources/design-guidelines/fused-deposition-modeling-old>, Stratasys (2022)

[71] Relvas, C., Ramos, A., Completo, A., Simões, J.A. A systematic approach for an accuracy level using rapid prototyping technologies, Proceedings of the Institution of Mechanical Engineers, Part B: Journal of Engineering Manufacture, 226(12), (2012) 2023-2034 https://doi.org/10.1177/0954405412461865

[72] Moher, D., Liberati, A., Tetzlaff, J., Altman, D.G. Preferred Reporting Items for Systematic Reviews and Meta-Analyses: The PRISMA Statement, Journal of clinical epidemiology 62(10), (2009) 1006-1012 https://doi.org/10.1016/j.jclinepi.2009.06.005"

[73] Cruz Sanchez, F.A., Boudaoud, H., Camargo, M., Pearce, J.M. Plastic recycling in additive manufacturing: A systematic literature review and opportunities for the circular economy, Journal of Cleaner Production 264,121602 (2020). https://doi.org/10.1016/j.jclepro.2020.121602

[74] Ai, J.-R., Peng, F., Joo, P., Vogt, B.D. Enhanced Dimensional Accuracy of Material Extrusion 3D-Printed Plastics through Filament Architecture, ACS Applied Polymer Materials, 3(5), (2021) 2518-2528 10.1021/acsapm.1c00110

[75] Akbaş, O.E., Hıra, O., Hervan, S.Z., Samankan, S., Altınkaynak, A. Dimensional accuracy of FDM-printed polymer parts, Rapid Prototyping Journal, 26(2), (2019) 288-298 10.1108/RPJ-04-2019-0115

[76] Alhijjaj, M., Nasereddin, J., Belton, P., Qi, S. Impact of processing parameters on the quality of pharmaceutical solid dosage forms produced by fused deposition modeling (FDM), Pharmaceutics, 11(12),633 (2019). 10.3390/pharmaceutics11120633

[77] Ansari, A.A., Kamil, M. Analysis of dimensional quality in 3D printed polylactic acid parts fabricated by fused deposition modeling, Materials Today: Proceedings, 47, (2021) 2281-2287 10.1016/j.matpr.2021.04.219

[78] Antony Samy, A., Golbang, A., Harkin-Jones, E., Archer, E., McIlhagger, A. Prediction of part distortion in Fused Deposition Modelling (FDM) of semi-crystalline polymers via COMSOL: Effect of printing conditions, CIRP Journal of Manufacturing Science and Technology, 33, (2021) 443-453 10.1016/j.cirpj.2021.04.012

[79] Azli, A.A., Muhammad, N., Abdullah Albakri, M.M., Ghazali, M.F., Abd Rahim, S.Z., Saleh, M.S., Victor, S.A. Printing parameter optimization of stent length accuracy by using Response Surface Methodology (RSM), AIP Conference Proceedings, 2339,020242 (2021). 10.1063/5.0044535

[80] Basile, S., Mathew, E., Genta, I., Conti, B., Dorati, R., Lamprou, D.A. Optimization of FDM 3D printing process parameters to produce haemodialysis curcumin-loaded vascular grafts, Drug Delivery and Translational Research (2021). 10.1007/s13346-021-01078-2

[81] Bergweiler, G., Fiedler, F., Shaukat, A., Löffler, B. Experimental investigation of dimensional precision of deep drawn cups using direct polymer additive tooling, Journal of Manufacturing and Materials Processing, 5(1),3 (2021). 10.3390/jmmp5010003

[82] Bhowmik, S., Jagadish, Gupta, K. Modeling and optimization of rapid prototyping process, SpringerBriefs in Applied Sciences and Technology, (2019) 59-74 10.1007/978-3-030-00036-3_5

[83] Biglete, E.R., Dela Cruz, J.C., Verdadero, M.S., Christian E. Manuel, M., Altea, A.R., Joseph O. Lubi, A., Gatpayat, A.G.R., Dale B. Santos, C. Dimensional Accuracy Evaluation of 3D - Printed Parts Using a 3D Scanning Surface Metrology Technique, 2020 11th IEEE Control and System Graduate Research Colloquium, ICSGRC 2020 - Proceedings, 9232583, (2020) 185-190 10.1109/ICSGRC49013.2020.9232583

[84] Boca, M.A., Sover, A., Slătineanu, L. The dimensional accuracy of plastic parts made by the fused filament fabrication, IOP Conference Series: Materials Science and Engineering, 997(1), 012021 (2020). 10.1088/1757-899X/997/1/012021

[85] Bodaghi, M., Ban, D., Mobin, M., Park, C.H., Lomov, S.V., Nikzad, M. Additively manufactured three dimensional reference porous media for the calibration of permeability measurement set-ups, Composites Part A: Applied Science and Manufacturing, 139,106119 (2020). 10.1016/j.compositesa.2020.106119

[86] Buonamici, F., Carfagni, M., Furferi, R., Governi, L., Saccardi, M., Volpe, Y. Optimizing fabrication outcome in low-cost FDM machines. Part 2-Tests, Manufacturing Technology, 18(4), (2018) 552-558 10.21062/ujep/152.2018/a/1213-2489/MT/18/4/552

[87] Butt, J., Bhaskar, R., Mohaghegh, V. Investigating the effects of extrusion temperatures and material extrusion rates on FFF-printed thermoplastics, International Journal of Advanced Manufacturing Technology, 117(9-10), (2021) 2679-2699 10.1007/s00170-021-07850-5

[88] Camposeco-Negrete, C., Varela-Soriano, J., Rojas-Carreón, J.J. The effects of printing parameters on quality, strength, mass, and processing time of polylactic acid specimens produced by additive manufacturing, Progress in Additive Manufacturing (2021). 10.1007/s40964-021-00198-y

[89] Cardoso, P.H.M., Teixeira, B.N., Calado, V.M.D.A., de Oliveira, M.G., Mendonça, T.D.S., Mendonça, R.H., de Almeida, H.R.O., Cunha, M.S., Thiré, R.M.D.S.M. Mechanical and dimensional performance of poly(lactic acid) 3D-printed parts using thin plate spline interpolation, Journal of Applied Polymer Science, 137(39),49171 (2020). 10.1002/app.49171

[90] Cekic, A., Begic-Hajdarevic, D., Cohodar, M., Muhamedagic, K., Osmanlic, M. Optimization of stereolithography and fused deposition modeling process parameters, Annals of DAAAM and Proceedings of the International DAAAM Symposium, 30(1), (2019) 681-687 10.2507/30th.daaam.proceedings.093

[91] Cekic, A., Muhamedagic, K., Begic-Hajdarevic, D., Djuzo, N. Effect of process parameters on dimensional accuracy and tensile strength of FDM printed parts, Annals of DAAAM and Proceedings of the International DAAAM Symposium, 31(1), (2020) 66-71 10.2507/31st.daaam.proceedings.009

[92] Chae, M.P., Chung, R.D., Smith, J.A., Hunter-Smith, D.J., Rozen, W.M. The accuracy of clinical 3D printing in reconstructive surgery: literature review and in vivo validation study, Gland Surgery, 10(7), (2021) 2293-2303 10.21037/gs-21-264

[93] Chamo, D., Msallem, B., Sharma, N., Aghlmandi, S., Kunz, C., Thieringer, F.M. Accuracy assessment of molded, patient-specific polymethylmethacrylate craniofacial implants compared to their 3D printed originals, Journal of Clinical Medicine, 9(3),832 (2020). 10.3390/jcm9030832

[94] Cheng, L., Wang, A., Tsung, F. A prediction and compensation scheme for in-plane shape deviation of additive manufacturing with information on process parameters, IISE Transactions, 50(5), (2018) 394-406 10.1080/24725854.2017.1402224

[95] Dardzinska, A., Fiedorczuk, K. Geometric accuracy of rapid prototyping technologies using laser scanner and coordinate measurement machine, IOP Conference Series: Materials Science and Engineering, 770(1),012086 (2020). 10.1088/1757-899X/770/1/012086

[96] Decker, N., Lyu, M., Wang, Y., Huang, Q. Geometric Accuracy Prediction and Improvement for Additive Manufacturing Using Triangular Mesh Shape Data, Journal of Manufacturing Science and Engineering, Transactions of the ASME, 143(6),061006 (2021). 10.1115/1.4049089

[97] Deng, K., Chen, H., Zhao, Y., Zhou, Y., Wang, Y., Sun, Y. Evaluation of adaptation of the polylactic acid pattern of maxillary complete dentures fabricated by fused deposition modelling technology: A pilot study, PLoS ONE, 13(8),e0201777 (2018). 10.1371/journal.pone.0201777

[98] Dikova, T.D., Dzhendov, D.A., Ivanov, D., Bliznakova, K. Dimensional accuracy and surface roughness of polymeric dental bridges produced by different 3D printing processes, Archives of Materials Science and Engineering, 94(2), (2018) 65-75 10.5604/01.3001.0012.8660

[99] Dixit, N.K., Srivastava, R., Narain, R. Dimensional accuracy improvement of part fabricated by low cost 3D open source printer for industrial application, Proceedings of the 10th International

Conference on Intelligent Systems and Control, ISCO 2016, 7726882 (2016). https://doi.org/10.1109/ISCO.2016.7726882

[100] Dong, H., Gao, X., Wei, M. Quality Prediction of Fused Deposition Molding Parts Based on Improved Deep Belief Network, Computational Intelligence and Neuroscience, 2021,8100371 (2021). 10.1155/2021/8100371

[101] Dorweiler, B., Baqué, P.E., Chaban, R., Ghazy, A., Salem, O. Quality control in 3D printing: Accuracy analysis of 3D-printed models of patient-specific anatomy, Materials, 14(4), 1021, (2021) 1-13 10.3390/ma14041021

[102] Dyrbuś, G. The study on the model orientation angle for accuracy of elements made with rapid prototyping fdm method, International Journal of Modern Manufacturing Technologies, 12(2), (2020) 29-34 20673604

[103] Edoimioya, N., Ramani, K.S., Okwudire, C.E. Software compensation of undesirable racking motion of H-frame 3D printers using filtered B-splines, Additive Manufacturing, 47,102290 (2021). 10.1016/j.addma.2021.102290

[104] Elkaseer, A., Schneider, S., Scholz, S.G. Experiment-based process modeling and optimization for high-quality and resource-efficient FFF 3D printing, Applied Sciences (Switzerland), 10(8), 2899 (2020). 10.3390/APP10082899

[105] Eltes, P.E., Kiss, L., Bartos, M., Gyorgy, Z.M., Csakany, T., Bereczki, F., Lesko, V., Puhl, M., Varga, P.P., Lazary, A. Geometrical accuracy evaluation of an affordable 3D printing technology for spine physical models, Journal of Clinical Neuroscience, 72, (2020) 438-446 10.1016/j.jocn.2019.12.027

[106] Enemuoh, E.U., Duginski, S., Feyen, C., Menta, V.G. Effect of process parameters on energy consumption, physical, and mechanical properties of fused deposition modeling, Polymers, 13(15),2406 (2021). 10.3390/polym13152406

[107] Fountas, N.A., Vaxevanidis, N.M. Optimization of fused deposition modeling process using a virus-evolutionary genetic algorithm, Computers in Industry, 125,103371 (2021). 10.1016/j.compind.2020.103371

[108] Fuhrmann, M., Falk, B., Schmitt, R. Model-based parameter optimization of a fused deposition modelling process, IEEE International Symposium on Intelligent Control - Proceedings, (2016) 7579992 (2016). 10.1109/ISIC.2016.7579992

[109] Galetto, M., Verna, E., Genta, G. Effect of process parameters on parts quality and process efficiency of fused deposition modeling, Computers and Industrial Engineering, 156,107238 (2021). 10.1016/j.cie.2021.107238

[110] Gapiński, B., Wieczorowski, M., Bak, A., Domínguez, A.P., Mathia, T. The assessment of accuracy of inner shapes manufactured by FDM, AIP Conference Proceedings, 1960,140009 (2018). 10.1063/1.5035001

[111] Gill, D.K., Bajaj, D., Rawat, A., Mittal, Y.G., Juneja, M., Jindal, P. Dimensional Accuracy of Surgical Guides Fabricated from Different Materials Using 3D Printer, Lecture Notes in Networks and Systems, 46, (2019) 805-813 10.1007/978-981-13-1217-5_80

[112] Gómez-Gras, G., Pérez, M.A., Fábregas-Moreno, J., Reyes-Pozo, G. Experimental study on the accuracy and surface quality of printed versus machined holes in PEI Ultem 9085 FDM specimens, Rapid Prototyping Journal, 27(11), (2021) 1-12 10.1108/RPJ-12-2019-0306

[113] Goo, B., Kim, J.-B., Ahn, D.-G., Park, K. Irreversible and repeatable shape transformation of additively manufactured annular composite structures, Materials, 14(6),1383, (2021) 1-18 10.3390/ma14061383

[114] Hafsa, M.N., Ibrahim, M., Wahab, M.S., Zahid, M.S. Evaluation of FDM pattern with ABS and PLA material, Applied Mechanics and Materials, 465-466, (2014) 55-59 10.4028/www.scientific.net/AMM.465-466.55

[115] Haidiezul, A.H.M., Hazwan, M.H.M., Lee, W.S., Gunalan, Najihah, N.F., Fadhli, I. Shrinkage optimisation on the 3D printed part using Full Factorial Design (FFD) optimisation approach, IOP Conference Series: Materials Science and Engineering, 932(1),012109 (2020). 10.1088/1757-899X/932/1/012109

[116] Haidiezul, A.H.M., Hazwan, M.H.M., Soon Lee, W., Gunalan, Fatin Najihah, N., Fadhli, I. Full Factorial Design Exploration Approach for Multi-Objective Optimization on the (FDM) 3D Printed Part, IOP Conference Series: Materials Science and Engineering, 917(1), 012029 (2020). 10.1088/1757-899X/917/1/012029

[117] Holzmond, O., Li, X. In situ real time defect detection of 3D printed parts, Additive Manufacturing, 17, (2017) 135-142 10.1016/j.addma.2017.08.003

[118] Hriţuc, A., Slătineanu, L., Mihalache, A., Dodun, O., Coteaţă, M., Nagîţ, G. Accuracy of Polylactide Parts Made by 3D Printing, Macromolecular Symposia, 389(1), 1900064 (2020). 10.1002/masy.201900064

[119] Hriţuc, A., Slătineanu, L., Mihalache, A., Dodun, O., Coteaţă, M., Nagîţ, G. Accuracy of Polylactide Parts Made by 3D Printing, Macromolecular Symposia, 389(1), 1900064 (2020). 10.1002/masy.201900064

[120] Hsu, C.-P., Lin, C.-S., Fan, C.-H., Chiang, N.-Y., Tsai, C.-W., Chang, C.-M., Liu, I.-L. Geometric accuracy of an acrylonitrile butadiene styrene canine tibia model fabricated using fused deposition modelling and the effects of hydrogen peroxide gas plasma sterilisation, BMC Veterinary Research, 16(1),478 (2020). 10.1186/s12917-020-02691-y

[121] Im, C.-H., Park, J.-M., Kim, J.-H., Kang, Y.-J., Kim, J.-H. Assessment of compatibility between various intraoral scanners and 3D printers through an accuracy analysis of 3D printed models, Materials, 13(19), 4419, (2020) 1-16 10.3390/ma13194419

[122] Ishida, Y., Miura, D., Miyasaka, T., Shinya, A. Dimensional accuracy of dental casting patterns fabricated using consumer 3d printers, Polymers, 12(10), 2244, (2020) 1-9 10.3390/polym12102244

[123] Johnson, A., Jani, G., Carew, R., Pandey, A. Assessment of the accuracy of 3D printed teeth by various 3D printers in forensic odontology, Forensic Science International, 328,111044 (2021). 10.1016/j.forsciint.2021.111044

[124] Juneja, M., Thakur, N., Kumar, D., Gupta, A., Bajwa, B., Jindal, P. Accuracy in dental surgical guide fabrication using different 3-D printing techniques, Additive Manufacturing, 22, (2018) 243-255 10.1016/j.addma.2018.05.012

[125] Kitsakis, K., Alabey, P., Kechagias, J., Vaxevanidis, N. A Study of the dimensional accuracy obtained by low cost 3D printing for possible application in medicine, IOP Conference Series: Materials Science and Engineering, 161(1), (2016) 012025 (2016). 10.1088/1757-899X/161/1/012025

[126] Kuczko, W., Hamrol, A., Wichniarek, R., Gorski, F., Rogalewicz, M. Mechanical properties and geometric accuracy of angle-shaped parts manufactured using the FFF method, Bulletin of the

Polish Academy of Sciences: Technical Sciences, 69(3),e137387 (2021). 10.24425/bpasts.2021.137387

[127] Kumar, V.V., Tagore, G.R.N., Venugopal, A. Some investigations on geometric conformity analysis of a 3-D freeform objects produced by rapid prototyping (FDM) process, International Journal of Applied Research In Mechanical Engineering, 1, (2011) 2 (2011). 10.47893/IJARME.2012.1036

[128] Lee, K.-Y., Cho, J.-W., Chang, N.-Y., Chae, J.-M., Kang, K.-H., Kim, S.-C., Cho, J.-H. Accuracy of three-dimensional printing for manufacturing replica teeth, Korean Journal of Orthodontics, 45(5), (2015) 217-225 10.4041/kjod.2015.45.5.217

[129] Lee, S., Squelch, A., Sun, Z. Quantitative assessment of 3d printed model accuracy in delineating congenital heart disease, Biomolecules, 11(2),270, (2021) 1-11 10.3390/biom11020270

[130] Li, F., Liu, C., Song, X., Huan, Y., Gao, S., Jiang, Z. Production of accurate skeletal models of domestic animals using three-dimensional scanning and printing technology, Anatomical Sciences Education, 11(1), (2018) 73-80 10.1002/ase.1725

[131] Li, H., Wang, T., Li, Q., Yu, Z., Wang, N. A quantitative investigation of distortion of polylactic acid/PLA) part in FDM from the point of interface residual stress, International Journal of Advanced Manufacturing Technology, 94(1-4), (2018) 381-395 https://doi.org/10.1007/s00170-017-0820-1

[132] Luis Pérez, C.J. Analysis of the surface roughness and dimensional accuracy capability of fused deposition modelling processes, International Journal of Production Research, 40(12), (2002) 2865-2881 https://doi.org/10.1080/00207540210146099

[133] Macatangay, I.O.D., Malipot, J.J.C., Lopez, A.M.M., Mabulay, R.E.C., Magpantay, R.A.K.O., Malecdan, L.S., Malingan, J.L.M., Malolos, G.Z.C., Mamaril, P.A.A., Mananghaya, A.N.M., Bundoc, R.C. Dimensional accuracy of 3d-printed models of the right first metacarpal bones of cadavers, Acta Medica Philippina, 54(5), (2020) 454-461 10.47895/AMP.V54I5.2212

[134] Maidin, N.A., Rahman, M.H.A., Ahmad, M.N., Salahuddin, M.B.M., Mazlan, S.N.H., Wahid, M.K., Osman, M.H., Jumaidin, R. Design for manufacturability (DFM) of 3D printed parts fabricated using open source 3D printer, International Journal of Integrated Engineering, 12(5), (2020) 203-209 10.30880/ijie.2020.12.05.025

[135] Mejia, S., Stewart, N., Miller, A., Savicky, R., Monarski, C., Moore, G.E., Keith, D. Accuracy of external measurements of 3-dimensional (3D) printed biomodels of the canine radius used in an in-hospital setting, Canadian Journal of Veterinary Research, 83(3), (2019) 181-186 8309000

[136] Mendricky, R., Fris, D. Analysis of the accuracy and the surface roughness of fdm/fff technology and optimisation of process parameters, Tehnicki Vjesnik, 27(4), (2020) 1166-1173 10.17559/TV-20190320142210

[137] Messimer, S.L., Pereira, T.R., Patterson, A.E., Lubna, M., Drozda, F.O. Full-density fused deposition modeling dimensional error as a function of raster angle and build orientation: Large dataset for eleven materials, Journal of Manufacturing and Materials Processing, 3(1),6 (2019). 10.3390/jmmp3010006

[138] Milde, J., Jurina, F. Comparison of selected thermoplastic materials in the fused deposition modeling process and their influence on the dimensional accuracy of an orthodontic upper teeth model, Materials Science Forum, 952, (2019) 143-152 10.4028/www.scientific.net/MSF.952.143

[139] Milovanović, A., Milošević, M., Mladenović, G., Likozar, B., Čolić, K., Mitrović, N. Experimental dimensional accuracy analysis of reformer prototype model produced by FDM and SLA 3D printing technology, Lecture Notes in Networks and Systems, 54, (2019) 84-95 10.1007/978-3-319-99620-2_7

[140] Molnár, I., Hrušecký, R., Morovič, L., Görög, A. Observation of shape and dimensional accuracy changing of parts in time intervals manufactured by additive method fused deposition modeling, Materials Science Forum, 919, (2018) 182-189 10.4028/www.scientific.net/MSF.919.182

[141] Murugesan, K., Anandapandian, P.A., Sharma, S.K., Vasantha Kumar, M. Comparative evaluation of dimension and surface detail accuracy of models produced by three different rapid prototype techniques, Journal of Indian Prosthodontist Society, 12(1), (2012) 16-20 https://doi.org/10.1007/s13191-011-0103-8

[142] Muta, S., Ikeda, M., Nikaido, T., Sayed, M., Sadr, A., Suzuki, T., Tagami, J. Chairside fabrication of provisional crowns on FDM 3D-printed PVA model, Journal of Prosthodontic Research, 64(4), (2020) 401-407 10.1016/j.jpor.2019.11.004

[143] Nath, P., Olson, J.D., Mahadevan, S., Lee, Y.-T.T. Optimization of fused filament fabrication process parameters under uncertainty to maximize part geometry accuracy, Additive Manufacturing, 35,101331 (2020). 10.1016/j.addma.2020.101331

[144] Nestler, N., Wesemann, C., Spies, B.C., Beuer, F., Bumann, A. Dimensional accuracy of extrusion- and photopolymerization-based 3D printers: In vitro study comparing printed casts, Journal of Prosthetic Dentistry, 125(1), (2021) 103-110 10.1016/j.prosdent.2019.11.011

[145] Park, J.-M., Jeon, J., Koak, J.-Y., Kim, S.-K., Heo, S.-J. Dimensional accuracy and surface characteristics of 3D-printed dental casts, Journal of Prosthetic Dentistry, 126(3), (2021) 427-437 10.1016/j.prosdent.2020.07.008

[146] Park, K., Kim, G., No, H., Jeon, H.W., Kremer, G.E.O. Identification of optimal process parameter settings based on manufacturing performance for fused filament fabrication of CFR-PEEK, Applied Sciences (Switzerland), 10(13),4630 (2020). 10.3390/app10134630

[147] Park, S.-I., Rosen, D.W., Choi, S.-K., Duty, C.E. Effective mechanical properties of lattice material fabricated by material extrusion additive manufacturing, Additive Manufacturing Volume 1, 1 October 2014, (2014) 12-23 https://doi.org/10.1016/j.addma.2014.07.002

[148] Pepliński, K., Czyzewski, P., Górecki, D., Sykutera, D., Bieliński, M. Selected geometrical features and strength indicators of elements manufactured by fused deposition modeling technology [Wybrane cechy geometryczne i wskaźniki wytrzymałościowe elementów wykonanych metod\ą modelowania uplastycznionym tworzywem], Polimery/Polymers, 62(3), (2017) 198-207 10.14314/polimery.2017.198

[149] Pooladvand, K., Furlong, C. Computational and experimental characterization of 3D printed components by fused deposition modeling, Conference Proceedings of the Society for Experimental Mechanics Series, (2019) 87-95 10.1007/978-3-319-95083-9_16

[150] Ramos-Lozano, S., Molina-Salazar, J., Rico-Pérez, L., Atayde-Campos, D. Performance evaluation of a commercial 3d printer that uses fused filament deposition technology, Best Practices in Manufacturing Processes: Experiences from Latin America, (2018) 389-410 https://doi.org/10.1007/978-3-319-99190-0_18

[151] Rebong, R.E., Stewart, K.T., Utreja, A., Ghoneima, A.A. Accuracy of three-dimensional dental resin models created by fused deposition modeling, stereolithography, and Polyjet prototype technologies: A comparative study, Angle Orthodontist, 88(3), (2018) 363-369 https://doi.org/10.2319/071117-460.1

[152] Reddy, M.V., Eachempati, K., Gurava Reddy, A.V., Mugalur, A. Error analysis: How precise is fused deposition modeling in fabrication of bone models in comparison to the parent bones? Indian Journal of Orthopaedics, 52(2), (2018) 196-201 10.4103/ortho.IJOrtho_312_16

[153] Ribeiro, M., Sousa Carneiro, O., Ferreira da Silva, A. Interface geometries in 3D multi-material prints by fused filament fabrication, Rapid Prototyping Journal, 25(1), (2018) 38-46 10.1108/RPJ-05-2017-0107

[154] Rivas Santos, V.M., Maskery, I., Sims-Waterhouse, D., Thompson, A., Leach, R., Ellis, A., Woolliams, P. Benchmarking of an additive manufacturing process, Proceedings - 2018 ASPE and euspen Summer Topical Meeting: Advancing Precision in Additive Manufacturing, (2018) 138-142 978-188770676-6

[155] Saqib, S., Urbanic, R.J. An experimental study to determine geometric and dimensional accuracy impact factors for fused deposition modelled parts, 4th International Conference on Changeable, Agile, Reconfigurable and Virtual Production (CARV2011), Montreal, Canada, (2011) 293-298 https://doi.org/10.1007/978-3-642-23860-4_48

[156] Savitri, I.T., Badri, C., Sulistyani, L.D. The accuracy of three-dimensional fused deposition modeling (FDM) compared with three-dimensional CT-Scans on the measurement of the mandibular ramus vertical length, gonion-menton length, and gonial angle, Journal of Physics: Conference Series, 884(1), (2017) 012050 (2017). 10.1088/1742-6596/884/1/012050

[157] Singh, G., Singh, R., Bal, S.S. Investigations for partial denture casting by fused deposition modelling-assisted chemical vapour smoothing, Assembly Automation, 40(5), (2020) 745-754 10.1108/AA-03-2020-0048

[158] Song, D., Baek, A.M.C., Koo, J., Busogi, M., Kim, N. Forecasting warping deformation using multivariate thermal time series and k-nearest neighbors in fused deposition modeling, Applied Sciences (Switzerland), 10(24),8951, (2020) 1-11 10.3390/app10248951

[159] Sun, H., Rao, P.K., Kong, Z.J., Deng, X., Jin, R. Functional Quantitative and Qualitative Models for Quality Modeling in a Fused Deposition Modeling Process, IEEE Transactions on Automation Science and Engineering 15(1),8103913, (2018) 393-403 https://doi.org/10.1109/tase.2017.2763609

[160] Thompson, A., White, C., Sreebhashyam, S.K. Evaluation of the performance and capability of a 3-dimensional part printer and its fused deposition modeling process, 61st Annual IIE Conference and Expo Proceedings, (2011) (2011).

[161] Unkovskiy, A., Spintzyk, S., Axmann, D., Engel, E.-M., Weber, H., Huettig, F. Additive Manufacturing: A Comparative Analysis of Dimensional Accuracy and Skin Texture Reproduction of Auricular Prostheses Replicas, Journal of Prosthodontics, 28(2), (2019) e460-e468 10.1111/jopr.12681

[162] Valerga Puerta, A.P., Sanchez, D.M., Batista, M., Salguero, J. Criteria selection for a comparative study of functional performance of Fused Deposition Modelling and Vacuum Casting processes, Journal of Manufacturing Processes, 35, (2018) 721-727 10.1016/j.jmapro.2018.08.033

[163] Volpato, N., Foggiatto, J.A., Schwarz, D.C. The influence of support base on FDM accuracy in Z, Rapid Prototyping Journal, 20(3),17111230, (2014) 182-191 10.1108/RPJ-12-2012-0116

[164] Vyavahare, S., Kumar, S., Panghal, D. Experimental study of surface roughness, dimensional accuracy and time of fabrication of parts produced by fused deposition modelling, Rapid Prototyping Journal, 26(9), (2020) 1535-1554 10.1108/RPJ-12-2019-0315

[165] Wang, A., Song, S., Huang, Q., Tsung, F. In-Plane Shape-Deviation Modeling and Compensation for Fused Deposition Modeling Processes, IEEE Transactions on Automation Science and Engineering, 14(2),7460927, (2017) 968-976 https://doi.org/10.1109/TASE.2016.2544941

[166] Wang, T., Xi, J., Jin, Y. Prototype warp deformation in the FDM process, Jixie Gongcheng Xuebao/Chinese Journal of Mechanical Engineering, 42(3), (2006) 233-238 10.3901/JME.2006.03.233

[167] Weiß, M., Maurath, J., Willenbacher, N., Koos, E. Shrinkage and dimensional accuracy of porous ceramics derived from capillary suspensions, Journal of the European Ceramic Society, 39(5), (2019) 1887-1892 10.1016/j.jeurceramsoc.2019.01.011

[168] Wilza, R., Iskandar, Seprianto, D., Adesta, E.Y.T. Optimization of parameters in three-dimensional printing objects with fused deposition modeling technology against geometry accuracy, International Journal of Recent Technology and Engineering, 7(6), (2019) 175-179 22773878

[169] Xinhua, L., Shengpeng, L., Zhou, L., Xianhua, Z., Xiaohu, C., Zhongbin, W. An investigation on distortion of PLA thin-plate part in the FDM process, International Journal of Advanced Manufacturing Technology, 79(5-8), (2015) 1117-1126 10.1007/s00170-015-6893-9

[170] Xu, F., Wong, Y.S., Loh, H.T. , Toward generic models for comparative evaluation and process selection in rapid prototyping and manufacturing, Journal of Manufacturing Systems, 19(5), (2001) 283-296 https://doi.org/10.1016/S0278-6125(01)89001-4

[171] Yousefi, F., Shokri, A., Farhadian, M., Vafaei, F., Forutan, F. Accuracy of maxillofacial prototypes fabricated by different 3-dimensional printing technologies using multi-slice and cone-beam computed tomography, Imaging Science in Dentistry, 51, (2021) 1-7 10.5624/isd.20200175

[172] Žarko, J., Vladić, G., Pál, M., Dedijer, S. Influence of printing speed on production of embossing tools using FDM 3D printing technology, Journal of Graphic Engineering and Design, 8 (1),(2017) 19 http://doi.org/10.24867/JGED-2017-1-019

[173] Zeller, A.-N., Neuhaus, M.-T., Fresenborg, S., Zimmerer, R.M., Jehn, P., Spalthoff, S., Gellrich, N.-C., Dittmann, J.A. Accurate and cost-effective mandibular biomodels: a standardized evaluation of 3D-Printing via fused layer deposition modeling on soluble support structures, Journal of Stomatology, Oral and Maxillofacial Surgery (2020). 10.1016/j.jormas.2020.09.018

[174] Zhai, W., Hu, B., Li, M., Jiang, J., Zhou, M. Dimensional Accuracy Control and Compressive Property of Microcellular Polyetherimide Honeycomb Foams Manufactured by an In Situ Foaming Fused Deposition Modeling Technology, Advanced Engineering Materials, 23(7),2001449 (2021). 10.1002/adem.202001449

[175] Zhang, Y., Chou, K. A parametric study of part distortions in fused deposition modelling using three-dimensional finite element analysis, Proceedings of the Institution of Mechanical Engineers, Part B: Journal of Engineering Manufacture, 222 (8), (2008) 959-967. https://doi.org/10.1243/09544054JEM990

[176] Ippolito, R., Iuliano, L., Gatto, A. Benchmarking of Rapid Prototyping Techniques in Terms of Dimensional Accuracy and Surface Finish, CIRP Annals - Manufacturing Technology, 44(1), (1995) 157-160 https://doi.org/10.1016/S0007-8506(07)62296-3

[177] Boschetto, A., Bottini, L. Accuracy prediction in fused deposition modeling, International Journal of Advanced Manufacturing Technology, 73(5-8), (2014) 913-928 https://doi.org/10.1007/s00170-014-5886-4

[178] Peng, A., Xiao, X., Yue, R. Process parameter optimization for fused deposition modeling using response surface methodology combined with fuzzy inference system, International Journal of Advanced Manufacturing Technology, 73(1-4), (2014) 87-100 https://doi.org/10.1007/s00170-014-5796-5

[179] Nuñez, P.J., Rivas, A., García-Plaza, E., Beamud, E., Sanz-Lobera, A. Dimensional and Surface Texture Characterization in Fused Deposition Modelling (FDM) with ABS plus, Procedia Engineering, 132, (2015) 856-863 https://doi.org/10.1016/j.proeng.2015.12.570

[180] Wang, T.-M., Xi, J.-T., Jin, Y. A model research for prototype warp deformation in the FDM process, International Journal of Advanced Manufacturing Technology, 33 (11-12), (2007) 1087-1096 https://doi.org/10.1007/s00170-006-0556-9

[181] Sood, A.K., Ohdar, R.K., Mahapatra, S.S. Improving dimensional accuracy of Fused Deposition Modelling processed part using grey Taguchi method, Materials and Design 30(10), (2009) 4243-4252 https://doi.org/10.1016/j.matdes.2009.04.030

[182] Nancharaiah, T., Ranga Raju, D., Ramachandra Raju, V. An experimental investigation on surface quality and dimensional accuracy of FDM components, International Journal on Emerging Technologies 1(2): 106-111 (2010). 0975-8364

[183] Tong, K., Joshi, S., Lehtihet, E.A. Error compensation for fused deposition modeling (FDM) machine by correcting slice files, Rapid Prototyping Journal, 14(1), (2008) 4-14 https://doi.org/10.1108/13552540810841517

[184] Anitha, R., Arunachalam, S., Radhakrishnan, P. Critical parameters influencing the quality of prototypes in fused deposition modelling, Journal of Materials Processing Technology, 118(1-3), (2001) 385-388 https://doi.org/10.1016/S0924-0136(01)00980-3

[185] Lee, B.H., Abdullah, J., Khan, Z.A. Optimization of rapid prototyping parameters for production of flexible ABS object, Journal of Materials Processing Technology, 169(1), (2005) 54-61 https://doi.org/10.1016/j.jmatprotec.2005.02.259

[186] Ahn, S.-H., Montero, M., Odell, D., Roundy, S., Wright, P.K. Anisotropic material properties of fused deposition modeling ABS, Rapid Prototyping Journal, 8(4), (2002) 248-257 https://doi.org/10.1108/13552540210441166

[187] Samy, A.A., Golbang, A., Harkin-Jones, E., Archer, E., Tormey, D., McIlhagger, A. Finite element analysis of residual stress and warpage in a 3D printed semi-crystalline polymer: Effect of ambient temperature and nozzle speed, Journal of Manufacturing Processes, 70, (2021) 389-399 https://doi.org/10.1016/j.jmapro.2021.08.054

[188] Petropolis, C., Kozan, D., Sigurdson, L. Accuracy of medical models made by consumer-grade fused deposition modelling printers, Canadian Journal of Plastic Surgery, 23(2), (2015) 91-94 https://doi.org/10.1177/229255031502300201

[189] Sudin, M.N., Shamsudin, S.A., Abdullah, M.A. Effect of part features on dimensional accuracy of fdm model, ARPN Journal of Engineering and Applied Sciences, 11(13), (2016) 8067-8072

[190] Taşdemir, V. Investigation of Dimensional Integrity and Surface Quality of Different Thin-Walled Geometric Parts Produced via Fused Deposition Modeling 3D Printing, Journal of Materials Engineering and Performance, 30(5), (2021) 3381-3387 https://doi.org/10.1007/s11665-021-05809-x

[191] Schumacher, C., Schöppner, V., Fels, C. A method to evaluate the process-specific warpage for different polymers in the FDM process, AIP Conference Proceedings, 2065,030057 (2019). https://doi.org/10.1063/1.5088315

[192] Gurrala, P.K., Regalla, S.P. Multi-objective optimisation of strength and volumetric shrinkage of FDM parts: A multi-objective optimization scheme is used to optimize the strength and volumetric shrinkage of FDM parts considering different process parameters, Virtual and Physical Prototyping, 9(2), (2014) 127-138 https://doi.org/10.1080/17452759.2014.898851

[193] Gregorian, A., Elliott, B., Navarro, R., Ochoa, F., Singh, H., Monge, E., Foyos, J., Noorani, R., Fritz, B., Jayanthi, S. Accuracy improvement in rapid prototyping machine (FDM-1650), Solid Freeform Fabrication Proceedings,, 2001, (2001) 77–84 http://doi.org/10.26153/tsw/3239

[194] Marwah, O.M.F., Yahaya, N.F., Darsani, A., Mohamad, E.J., Haq, R.H.A., Johar, M.A., Othman, M.H. Investigation for Shrinkage Deformation in the Desktop 3D Printer Process by Using DOE Approach of the ABS Materials, Journal of Physics: Conference Series, 1150(1),012038 (2019). https://doi.org/10.1088/1742-6596/1150/1/012038

[195] Dao, Q., Frimodig, J.C., Le, H.N., Li, X.-Z., Putnam, S.B., Golda, K., Foyos, J., Noorani, R., Fritz, B. Calculation of Shrinkage Compensation Factors for Rapid Prototyping (FDM 1650), Computer Applications in Engineering Education, 7(3), (1999) 186-195 https://doi.org/10.1002/(SICI)1099-0542(1999)7:3<186::AID-CAE7>3.0.CO;2-Q

[196] Dilberoglu, U.M., Simsek, S., Yaman, U. Shrinkage compensation approach proposed for ABS material in FDM process, Materials and Manufacturing Processes, 34(9), (2019) 993-998 https://doi.org/10.1080/10426914.2019.1594252

[197] Sljivic, M., Pavlovic, A., Ilic, J., Stanojevic, M., Todorovic, S. Comparing the accuracy of professional and consumer grade 3D printers in complex models production, FME Transactions, 45(3), (2017) 348-353 https://doi.org/10.5937/fmet1703348S

[198] Clemon, L., Sudradjat, A., Jaquez, M., Krishna, A., Rammah, M., Dornfeld, D. Precision and energy usage for additive manufacturing, ASME International Mechanical Engineering Congress and Exposition, Proceedings, (2013) 2 A (2013). https://doi.org/10.1115/IMECE2013-65688

[199] Shahrain, M., Didier, T., Lim, G.K., Qureshi, A.J. Fast Deviation Simulation for 'Fused Deposition Modeling' Process, Procedia CIRP, 43, (2016) 327-332 https://doi.org/10.1016/j.procir.2016.02.004

[200] Al-Ahmari, A., Ashfaq, M., Mian, S.H., Ameen, W. Evaluation of additive manufacturing technologies for dimensional and geometric accuracy, International Journal of Materials and Product Technology, 58(2-3), (2019) 129-154 https://doi.org/10.1504/IJMPT.2019.097665

[201] Taczała, J., Czepułkowska, W., Konieczny, B., Sokołowski, J., Kozakiewicz, M., Szymor, P. Comparison of 3d printing mjp and fdm technology in dentistry, Archives of Materials Science and Engineering, 101(1), (2020) 32-40 https://doi.org/10.5604/01.3001.0013.9504

[202] Aslani, K.-E., Kitsakis, K., Kechagias, J.D., Vaxevanidis, N.M., Manolakos, D.E. On the application of grey Taguchi method for benchmarking the dimensional accuracy of the PLA fused filament fabrication process, SN Applied Sciences, 2(6),1016 (2020). https://doi.org/10.1007/s42452-020-2823-z

[203] Caminero, M.Á., Chacón, J.M., García-Plaza, E., Núñez, P.J., Reverte, J.M., Becar, J.P. Additive manufacturing of PLA-based composites using fused filament fabrication: Effect of graphene nanoplatelet reinforcement on mechanical properties, dimensional accuracy and texture, Polymers, 11(5),799 (2019). https://doi.org/10.3390/polym11050799

[204] Pieralli, S., Spies, B.C., Hromadnik, V., Nicic, R., Beuer, F., Wesemann, C. How accurate is oral implant installation using surgical guides printed from a degradable and steam-sterilized biopolymer?, Journal of Clinical Medicine, 9(8),2322, (2020) 1-12 https://doi.org/10.3390/jcm9082322

[205] Zhou, C., Han, T. Research on the Influencing Factors of FDM 3D Printing Accuracy, Journal of Physics: Conference Series, 1838(1), 012027 (2021). https://doi.org/10.1088/1742-6596/1838/1/012027

[206] Syrlybayev, D., Perveen, A., Talamona, D. Fused deposition modelling: Effect of extrusion temperature on the accuracy of print, Materials Today: Proceedings, 44, (2021) 832-837 https://doi.org/10.1016/j.matpr.2020.10.716

[207] Manmadhachary, A., Ravi Kumar, Y., Krishnanand, L. Finding of Correction Factor and Dimensional Error in Bio-AM Model by FDM Technique, Journal of The Institution of Engineers (India): Series C, 99(3), (2018) 293-300 https://doi.org/10.1007/s40032-016-0294-1

[208] Rahman, H., John, T.D., Sivadasan, M., Singh, N.K. Investigation on the Scale Factor applicable to ABS based FDM Additive Manufacturing, Materials Today: Proceedings, 5(1), (2018) 1640-1648 https://doi.org/10.1016/j.matpr.2017.11.258

[209] Knoop, F., Schoeppner, V. Geometrical accuracy of holes and cylinders manufactured with fused deposition modeling, Solid Freeform Fabrication 2017: Proceedings of the 28th Annual International Solid Freeform Fabrication Symposium - An Additive Manufacturing Conference, SFF 2017, (2020) 2757-2776

[210] Reverte, J.M., Caminero, M.A., Chacón, J.M., García-Plaza, E., Núñez, P.J., Becar, J.P. Mechanical and geometric performance of PLA-based polymer composites processed by the fused filament fabrication additive manufacturing technique, Materials, 13(8),1924 (2020). https://doi.org/10.3390/MA13081924

[211] Pennington, R.C., Hoekstra, N.L., Newcomer, J.L. Significant factors in the dimensional accuracy of fused deposition modelling, Proceedings of the Institution of Mechanical Engineers, Part E: Journal of Process Mechanical Engineering, 219(1), (2005) 89-92 https://doi.org/10.1243/095440805X6964

[212] Camposeco-Negrete, C. Optimization of FDM parameters for improving part quality, productivity and sustainability of the process using Taguchi methodology and desirability approach, Progress in Additive Manufacturing, 5(1), (2020) 59-65 https://doi.org/10.1007/s40964-020-00115-9

[213] Camposeco-Negrete, C. Optimization of printing parameters in fused deposition modeling for improving part quality and process sustainability, International Journal of Advanced Manufacturing Technology, 108(7-8), (2020) 2131-2147 https://doi.org/10.1007/s00170-020-05555-9

[214] Pennington, R.C., Hoekstra, N.L., Newcomer, J.L. Significant factors on the dimensional accuracy of fused deposition modeling, Annual Technical Conference - ANTEC, Conference Proceedings, 1, (2003) 880-883 https://doi.org/10.1243/095440805X6964

[215] Vitolo, F., Martorelli, M., Gerbino, S., Patalano, S., Lanzotti, A. Controlling form errors in 3D printed models associated to size and position on the working plane, International Journal on Interactive Design and Manufacturing, 12(3), (2018) 969-977 https://doi.org/10.1007/s12008-017-0441-9

[216] Velineni, A., Günay, E.E., Park, K., Okudan Kremer, G.E., Schnieders, T.M., Stone, R.T. An investigation on selected factors that cause variability in additive manufacturing, IISE Annual Conference and Expo 2018, (2018) 983-988

[217] Bottini, L., Boschetto, A. Interference fit of material extrusion parts, Additive Manufacturing, 25, (2019) 335-346 https://doi.org/10.1016/j.addma.2018.11.025

[218] Lieneke, T., Denzer, V., Adam, G.A.O., Zimmer, D. Dimensional Tolerances for Additive Manufacturing: Experimental Investigation for Fused Deposition Modeling, Procedia CIRP, 43, (2016) 286-291 https://doi.org/10.1016/j.procir.2016.02.361

[219] Jaber, S.T., Hajeer, M.Y., Khattab, T.Z., Mahaini, L. Evaluation of the fused deposition modeling and the digital light processing techniques in terms of dimensional accuracy of printing dental models used for the fabrication of clear aligners, Clinical and Experimental Dental Research, 7(4), (2021) 591-600 https://doi.org/10.1002/cre2.366

[220] Bazan, A., Turek, P., Przeszłowski, Ł. Assessment of InfiniteFocus system measurement errors in testing the accuracy of crown and tooth body model, Journal of Mechanical Science and Technology, 35(3), (2021) 1167-1176 https://doi.org/10.1007/s12206-021-0230-z

[221] Boursier J.-F., Fournet A., Bassanino J., Manassero M., Bedu A.-S., Leperlier D. Reproducibility, Accuracy and Effect of Autoclave Sterilization on a Thermoplastic Three-Dimensional Model Printed by a Desktop Fused Deposition Modelling Three-Dimensional Printer, Veterinary and Comparative Orthopaedics and Traumatology, 31(6), (2018) 422-430 https://doi.org/10.1055/s-0038-1668113

[222] Górski F., Kuczko W., Wichniarek R. Influence of process parameters on dimensional accuracy of parts manufactured using fused deposition modelling technology, Advances in Science and Technology Research Journal, 7 (19), (2013) 27-35 https://doi.org/10.5604/20804075.1062340

[223] Johnson, W.M., Rowell, M., Deason, B., Eubanks, M. Comparative evaluation of an open-source FDM system, Rapid Prototyping Journal, 20(3),17111232, (2014) 205-214 https://doi.org/10.1108/RPJ-06-2012-0058

[224] Kim, S.-Y., Shin, Y.-S., Jung, H.-D., Hwang, C.-J., Baik, H.-S., Cha, J.-Y. Precision and trueness of dental models manufactured with different 3-dimensional printing techniques, American Journal of Orthodontics and Dentofacial Orthopedics, 153(1), (2018) 144-153 https://doi.org/10.1016/j.ajodo.2017.05.025

[225] Turek, P., Budzik, G. Estimating the accuracy of mandible anatomical models manufactured using material extrusion methods, Polymers, 13(14),2271 (2021). https://doi.org/10.3390/polym13142271

[226] Drozda, F.O., Pereira, T.R., Patterson, A.E. End-user manufacturing with FDM/FFF: Interfaces, tolerances, repeatability, and dimensional accuracy, Proceedings of the 2020 IISE Annual Conference, (2020) 513-518 ISBN: 978-171382781-8

[227] Wegmüller, L., Halbeisen, F., Sharma, N., Kühl, S., Thieringer, F.M. Consumer vs. High-end 3D printers for guided implant surgery—An in vitro accuracy assessment study of different 3D printing technologies, Journal of Clinical Medicine, 10(21),4894 (2021). https://doi.org/10.3390/jcm10214894

[228] Msallem, B., Sharma, N., Cao, S., Halbeisen, F.S., Zeilhofer, H.-F., Thieringer, F.M. Evaluation of the dimensional accuracy of 3D-printed anatomical mandibular models using FFF, SLA, SLS, MJ, and BJ printing technology, Journal of Clinical Medicine, 9(3),817 (2020). https://doi.org/10.3390/jcm9030817

[229] Abduo, J., Lau, D. Effect of Manufacturing Technique on the Accuracy of Guides for Static Computer-Aided Implant Surgery, International Journal of Oral and Maxillofacial Implants, 35(5), (2020) 931-938 https://doi.org/10.11607/jomi.8186

[230] Bahnini, I., uz Zaman, U.K., Rivette, M., Bonnet, N., Siadat, A. Computer-aided design (CAD) compensation through modeling of shrinkage in additively manufactured parts, International Journal of Advanced Manufacturing Technology, 106(9-10), (2020) 3999-4009 https://doi.org/10.1007/s00170-020-04924-8

[231] Zhou, J., Chen, X. Analysis of the difference in forming precision of different non-metallic additive manufacturing antennas, Lecture Notes in Electrical Engineering, 588, (2020) 952-961 https://doi.org/10.1007/978-981-32-9437-0_98

[232] Johnson, W.M., Rowell, M., Deason, B., Eubanks, M. Benchmarking evaluation of an open source fused deposition modeling additive manufacturing system, 22nd Annual International Solid Freeform Fabrication Symposium - An Additive Manufacturing Conference, SFF 2011, (2011) 197-211

[233] El-Katatny, I., Masood, S.H., Morsi, Y.S. Evaluation and validation of the shape accuracy of FDM fabricated medical models, Advanced Materials Research, 83-86, (2010) 275-280 https://doi.org/10.4028/www.scientific.net/AMR.83-86.275

[234] Chohan, J.S., Singh, R., Boparai, K.S., Penna, R., Fraternali, F. Dimensional accuracy analysis of coupled fused deposition modeling and vapour smoothing operations for biomedical applications, Composites Part B: Engineering, 117, (2017) 138-149 https://doi.org/10.1016/j.compositesb.2017.02.045

[235] Ide, Y., Nayar, S., Logan, H., Gallagher, B., Wolfaardt, J. The effect of the angle of acuteness of additive manufactured models and the direction of printing on the dimensional fidelity: clinical implications, Odontology, 105(1), (2017) 108-115 https://doi.org/10.1007/s10266-016-0239-4

[236] Alsoufi, M.S., Elsayed, A.E. Warping deformation of desktop 3D printed parts manufactured by open source fused deposition modeling (FDM) system, International Journal of Mechanical and Mechatronics Engineering, 17(4), (2017) 7-16

[237] Budzik, G., Turek, P., Dziubek, T., Gdula, M. Elaboration of the measuring procedure facilitating precision assessment of the geometry of mandible anatomical model manufactured using additive methods, Measurement and Control (United Kingdom), 53(1-2), (2020) 181-191 https://doi.org/10.1177/0020294019881708

[238] Hatz, C.R., Msallem, B., Aghlmandi, S., Brantner, P., Thieringer, F.M. Can an entry-level 3D printer create high-quality anatomical models? Accuracy assessment of mandibular models printed by a desktop 3D printer and a professional device, International Journal of Oral and Maxillofacial Surgery, 49(1), (2020) 143-148 https://doi.org/10.1016/j.ijom.2019.03.962

[239] Lo Russo, L., Lo Muzio, E., Troiano, G., Salamini, A., Zhurakivska, K., Guida, L. Accuracy of trial complete dentures fabricated by using fused deposition modeling 3-dimensional printing: An in vitro study, Journal of Prosthetic Dentistry (2021). https://doi.org/10.1016/j.prosdent.2021.07.021

[240] Lanzotti, A., Martorelli, M., Staiano, G. Understanding process parameter effects of reprap open-source three-dimensional printers through a design of experiments approach, Journal of Manufacturing Science and Engineering, Transactions of the ASME, 137 (1), art. no. 011017. (2015). https://doi.org/10.1115/1.4029045

[241] Queral, V., Rincón, E., Mirones, V., Rios, L., Cabrera, S. Dimensional accuracy of additively manufactured structures for modular coil windings of stellarators, Fusion Engineering and Design, 124, (2017) 173-178 https://doi.org/10.1016/j.fusengdes.2016.12.014

[242] Queral, V., Cabrera, S., Rincon, E., Mirones, V. Prospects for Stellarators Based on Additive Manufacturing: Coil Frame Accuracy and Vacuum Vessels, IEEE Transactions on Plasma Science, 46(5), (2018) 1173-1179 https://doi.org/10.1109/TPS.2018.2790168

[243] ISO 286–1:2010, Geometrical product specifications (GPS) ISO code system for tolerances on linear sizes–part 1: basis of tolerances, deviations and fits, ISO, Geneva, Switzerland. (2010)

[244] Minetola, P., Iuliano, L., Marchiandi, G. Benchmarking of FDM machines through part quality using IT grades, Procedia CIRP, 41, (2015) 1027-1032 https://doi.org/10.1016/j.procir.2015.12.075

[245] Cruz Sanchez, F.A., Boudaoud, H., Muller, L., Camargo, M. Towards a standard experimental protocol for open source additive manufacturing: This paper proposes a benchmarking model for evaluating accuracy performance of 3D printers, Virtual and Physical Prototyping, 9(3), (2014) 151-167 https://doi.org/10.1080/17452759.2014.919553

[246] Günay, E.E., Velineni, A., Park, K., Okudan Kremer, G.E. An Investigation on Process Capability Analysis for Fused Filament Fabrication, International Journal of Precision Engineering and Manufacturing, 21(4), (2020) 759-774 https://doi.org/10.1007/s12541-019-00298-4

[247] Maurya, N.K., Rastogi, V., Singh, P. Comparative study and measurement of form errors for the component printed by FDM and polyjet process, Instrumentation Mesure Metrologie, 18(4), (2019) 353-359 https://doi.org/10.18280/i2m.180404

[248] Minetola, P., Calignano, F., Galati, M. Comparing geometric tolerance capabilities of additive manufacturing systems for polymers, Additive Manufacturing, 32,101103 (2020). https://doi.org/10.1016/j.addma.2020.101103

[249] Maurya, N.K., Rastogi, V., Singh, P. Fabrication of prototype connecting rod of PLA plastic material using FDM prototype technology, Indian Journal of Engineering and Materials Sciences, 27(2), (2020) 333-343 9714588

[250] Dimitrov, D., Van Wijck, W., Schreve, K., De Beer, N. Investigating the achievable accuracy of three dimensional printing, Rapid Prototyping Journal, 12 (1), (2006) 42-52. https://doi.org/10.1108/13552540610637264

[251] Maurya, N.K., Rastogi, V., Singh, P. Investigation of dimensional accuracy and international tolerance grades of 3D printed polycarbonate parts, Materials Today: Proceedings, 25, (2019) 537-543 https://doi.org/10.1016/j.matpr.2019.06.007

[252] Singh, J., Singh, R., Singh, H. Repeatability of linear and radial dimension of ABS replicas fabricated by fused deposition modelling and chemical vapor smoothing process: A case study, Measurement: Journal of the International Measurement Confederation, 94, (2016) 5-11 https://doi.org/10.1016/j.measurement.2016.07.064

[253] Singh, R. Some investigations for small-sized product fabrication with FDM for plastic components, Rapid Prototyping Journal, 19(1), (2013) 58-63 https://doi.org/10.1108/13552541311292745

[254] Singh, R. Process capability analysis of fused deposition modelling for plastic components, Rapid Prototyping Journal, 20(1), (2014) 69-76 https://doi.org/10.1108/RPJ-02-2012-0018

[255] Huang, Z., Dantan, J.-Y., Etienne, A., Rivette, M., Bonnet, N. Geometrical deviation identification and prediction method for additive manufacturing, Rapid Prototyping Journal, 24(9), (2018) 1524-1538 https://doi.org/10.1108/RPJ-07-2017-0137

[256] Bodur, O., Stepanek, V., Walcher, E.M., Durakbasa, N. Precision in additive manufacturing, optimization and evaluation of the accuracy of 3D printer based on GPS system, Annals of DAAAM and Proceedings of the International DAAAM Symposium, 31(1), (2020) 963-972 https://doi.org/10.2507/31st.daaam.proceedings.134

[257] ASME Y14.5-2009, Dimensioning and Tolerancing, ASME, New York. (2009)

[258] ISO 1101:2012, Geometrical Product Specifications (GPS)—Geometrical Tolerancing—Tolerances of Form, Orientation, Location and Run-Out, ISO, Geneva, Switzerland. (2012)

[259] Fahad, M., Khalid, M., Nauman, M., Khan, M.A. Effect of deposition speed on the flatness and cylindricity of parts produced by three dimensional printing process, Journal of Physics: Conference Series, 885(1), (2017) 012012 (2017). https://doi.org/10.1088/1742-6596/885/1/012012

[260] Chandrashekarappa, M.P.G., Chate, G.R., Parashivamurthy, V., Kumar, B.S., Bandukwala, M.A.N., Kaisar, A., Giasin, K., Pimenov, D.Y., Wojciechowski, S. Analysis and optimization of dimensional accuracy and porosity of high impact polystyrene material printed by FDM process: PSO, JAYA, Rao, and bald eagle search algorithms, Materials, 14(23),7479 (2021). https://doi.org/10.3390/ma14237479

[261] Kumar, Y.R. An application of Taguchi's technique to improve the accuracy of rapid prototyped FDM parts, International Journal of Materials Engineering Innovation, 3(3-4), (2012) 228-246 https://doi.org/10.1504/IJMATEI.2012.049263

[262] Aboutaleb, A.M., Tschopp, M.A., Rao, P.K., Bian, L. Multi-Objective Accelerated Process Optimization of Part Geometric Accuracy in Additive Manufacturing, Journal of Manufacturing Science and Engineering, Transactions of the ASME, 139(10), (2017) 101001 (2017). https://doi.org/10.1115/1.4037319

[263] Aboutaleb, A.M., Bian, L., Rao, P.K., Tschopp, M.A. Accelerated geometry accuracy optimization of additive manufacturing parts, ASME 2017 12th International Manufacturing Science and Engineering Conference, (2017) 2 (2017). https://doi.org/10.1115/MSEC2017-2892

[264] Tootooni, M.S., Dsouza, A., Donovan, R., Rao, P.K., Kong, Z., Borgesen, P. Assessing the geometric integrity of additive manufactured parts from point cloud data using spectral graph theoretic sparse representation-based classification, ASME 2017 12th International Manufacturing Science and Engineering Conference, (2017) 2 (2017). https://doi.org/10.1115/MSEC2017-2794

[265] Das, P., Mhapsekar, K., Chowdhury, S., Samant, R., Anand, S. Selection of build orientation for optimal support structures and minimum part errors in additive manufacturing, Computer-Aided Design and Applications, 14, (2017) 1-13 https://doi.org/10.1080/16864360.2017.1308074

[266] Eswaran, P., Sivakumar, K., Subramaniyan, M. Minimizing error on circularity of FDM manufactured part, Materials Today: Proceedings, 5(2), (2018) 6675-6683 https://doi.org/10.1016/j.matpr.2017.11.324

[267] Sajan, N., John, T.D., Sivadasan, M., Singh, N.K. An investigation on circularity error of components processed on Fused Deposition Modeling (FDM), Materials Today: Proceedings 5(1), (2018) 1327-1334 https://doi.org/10.1016/j.matpr.2017.11.218

[268] Kumar, Y.R., Rao, C.S.P., Reddy, T.A.J. A robust process optimisation for fused deposition modelling, International Journal of Manufacturing Technology and Management, 14(1-2), (2008) 228-245 https://doi.org/10.1504/IJMTM.2008.017497

[269] Etesami, F., Griffin, T. Characterizing the accuracy of FDM rapid prototyping machines for machine design applications, ASME International Mechanical Engineering Congress and Exposition, Proceedings, (2013) 12 (2013). https://doi.org/10.1115/IMECE2013-64972

[270] Arni, R., Gupta, S. Manufacturability analysis of flatness tolerances in solid freeform fabrication, Journal Of Mechanical Design, 123(1), (2001) 148–156. https://doi.org/10.1115/1.1326439

[271] Syrlybayev, D., Zharylkassyn, B., Seisekulova, A., Perveen, A., Talamona, D. Optimization of the warpage of fused deposition modeling parts using finite element method, Polymers, 13(21),3849 (2021). https://doi.org/10.3390/polym13213849

[272] Moretti, M., Senin, N. In-process monitoring of part warpage in fused filament fabrication through the analysis of the repulsive force acting on the extruder, Additive Manufacturing, 102505 (2021). https://doi.org/10.1016/j.addma.2021.102505

[273] Armillotta, A., Bellotti, M., Cavallaro, M. Warpage of FDM parts: Experimental tests and analytic model, Robotics and Computer-Integrated Manufacturing 50, (2018) 140-152 https://doi.org/10.1016/j.rcim.2017.09.007

[274] Fitzharris, E.R., Watanabe, N., Rosen, D.W., Shofner, M.L. Effects of material properties on warpage in fused deposition modeling parts, International Journal of Advanced Manufacturing Technology, 95(5-8), (2018) 2059-2070 https://doi.org/10.1007/s00170-017-1340-8

[275] Peng, A. Research on the interlayer stress and warpage deformation in FDM, Advanced Materials Research, 538-541, (2012) 1564-1567 https://doi.org/10.4028/www.scientific.net/AMR.538-541.1564

[276] Liu, L., Wan, C., Li, K., Wu, J. Research on warpage deformation mechanism & control method of fused deposition parts, Lecture Notes in Electrical Engineering, 417, (2017) 729-737 https://doi.org/10.1007/978-981-10-3530-2_91

[277] Kuo, C.-C., Wu, Y.-R., Li, M.-H., Wu, H.-W. Minimizing warpage of ABS prototypes built with low-cost fused deposition modeling machine using developed closed-chamber and optimal process parameters, International Journal of Advanced Manufacturing Technology, 101(1-4), (2019) 593-602 https://doi.org/10.1007/s00170-018-2969-7

[278] Spoerk, M., Holzer, C., Gonzalez-Gutierrez, J. Material extrusion-based additive manufacturing of polypropylene: A review on how to improve dimensional inaccuracy and warpage, Journal of Applied Polymer Science, 137(12), 48545 (2020). https://doi.org/10.1002/app.48545

[279] Lyu, J., Manoochehri, S. Modeling machine motion and process parameter errors for improving dimensional accuracy of fused deposition modeling machines, Journal of Manufacturing Science and Engineering, Transactions of the ASME, 140(12), (2018) 121012 (2018). https://doi.org/10.1115/1.4041328

[280] Pisula, J. The geometric accuracy analysis of polymer spiral bevel gears carried out in a measurement system based on the Industry 4.0 structure, Polimery/Polymers, 64(5), (2019) 353-360 https://doi.org/10.14314/polimery.2019.5.6

[281] Noriega, A., Blanco, D., Alvarez, B.J., Garcia, A. Dimensional accuracy improvement of FDM square cross-section parts using artificial neural networks and an optimization algorithm, International Journal of Advanced Manufacturing Technology, 69(9-12), (2013) 2301-2313 https://doi.org/10.1007/s00170-013-5196-2

[282] Moylan, S., Slotwinski, J., Cooke, A., Jurrens, K., Donmez, M.A. Proposal for a standardized test artifact for additive manufacturing machines and processes, 23rd Annual International Solid Freeform Fabrication Symposium - An Additive Manufacturing Conference, (2012) 902-920

[283] Kacmarcik, J., Spahic, D., Varda, K., Porca, E., Zaimovic-Uzunovic, N. An investigation of geometrical accuracy of desktop 3D printers using CMM, IOP Conference Series: Materials Science and Engineering, 393(1), (2018) 012085 (2018). https://doi.org/10.1088/1757-899X/393/1/012085

[284] Chua, C.K., Leong, K.F., Lim, C.S. Rapid prototyping: Principles and applications, third edition, World Scientific Publishing Co. Pte. Ltd., (2010) 1-512 https://doi.org/10.1142/6665

[285] Bouyssié, J.F., Bouyssié, S., Sharrock, P., Duran, D. Stereolithographic models derived from X-ray computed tomography reproduction accuracy, Surgical and Radiologic Anatomy, 19(3), (1997) 193-199 https://doi.org/10.1007/bf01627975

[286] Choi J.-Y., Choi J.-H., Kim N.-K., Kim Y., Lee J.-K., Kim M.-K., Lee J.-H., Kim M.-J. Analysis of errors in medical rapid prototyping models, International Journal of Oral and Maxillofacial Surgery, 31(1), (2002) 23-32 https://doi.org/10.1054/ijom.2000.0135

[287] Agarwala, M.K., Jamalabad, V.R., Langrana, N.A., Safari, A., Whalen, P.J., Danforth, S.C. Structural quality of parts processed by fused deposition, Rapid Prototyping Journal, 2(4), (1996) 4-19 https://doi.org/10.1108/13552549610732034

[288] Kulkarni, P., Dutta, D. Deposition strategies and resulting part stiffnesses in fused deposition modeling, Journal of Manufacturing Science and Engineering, Transactions of the ASME, 121 (1), (1999) 93-103. https://doi.org/10.1115/1.2830582

[289] Turner, B.N., Gold, S.A. A review of melt extrusion additive manufacturing processes: II. Materials, dimensional accuracy, and surface roughness, Rapid Prototyping Journal, 21(3), (2015) 250-261 https://doi.org/10.1108/RPJ-02-2013-0017

[290] Kłodowski, A. Planar four-link mechanism analysis for application in 3D printing machines, Mechanisms and Machine Science 24, (2015) 99-108 https://doi.org/10.1007/978-3-319-09411-3_11

[291] Kun, K. Reconstruction and development of a 3D printer using FDM technology, International Conference on Manufacturing Engineering and Materials, (2016) (2016). https://doi.org/10.1016/j.proeng.2016.06.657

[292] Wesley Machado Cunico, M., de Carvalho, J. Optimization of positioning system of FDM machine design using analytical approach, Rapid Prototyping Journal 19(3), (2013) 144-152 https://doi.org/10.1108/13552541311312139

[293] Cunico, M.W.M., De Carvalho, J. Design of an FDM positioning system and application of an error-cost multiobjective optimization approach, Rapid Prototyping Journal, 19(5),17093923, (2013) 344-352 https://doi.org/10.1108/RPJ-11-2011-0117

[294] Weiss, B., Storti, D., Ganter, M. Low-cost closed-loop control of a 3D printer gantry, Rapid Prototyping Journal 21(5), (2015) 482-490 https://doi.org/10.1108/RPJ-09-2014-0108

[295] Feuerbach, T., Kock, S., Thommes, M. Characterisation of fused deposition modeling 3D printers for pharmaceutical and medical applications, Pharmaceutical Development and Technology, 23(10), (2018) 1136-1145 https://doi.org/10.1080/10837450.2018.1492618

[296] Shane, K., Pat, C., Eoin, D. Kinematic error modeling and error compensation of desktop 3D printer, Nami Jishu yu Jingmi Gongcheng/Nanotechnology and Precision Engineering, 1(3), (2018) 180-186 https://doi.org/10.1016/j.npe.2018.09.002

[297] Heras, E.S., Haro, F.B., María, J., Del Burgo, A., Marcos, M.E.I. Plate auto-level system for fused deposition modelling (FDM) 3D printers, Rapid Prototyping Journal 23(2), (2017) 401-413 https://doi.org/10.1108/RPJ-06-2015-0065

[298] Lee, W.-C., Wei, C.-C., Chung, S.-C. Development of a hybrid rapid prototyping system using low-cost fused deposition modeling and five-axis machining, Journal of Materials Processing Technology, 214(11), (2014) 2366-2374 https://doi.org/10.1016/j.jmatprotec.2014.05.004

[299] Marchewka, J., Laska, J. Processing of poly-l-lactide and poly(l-lactide-co-trimethylene carbonate) blends by fused filament fabrication and fused granulate fabrication using RepRap 3D printer, International Journal of Advanced Manufacturing Technology, 106(11-12), (2020) 4933-4944 https://doi.org/10.1007/s00170-020-04981-z

[300] Santana, L., Ahrens, C.H., Da Costa Sabino Netto, A., Bonin, C. Evaluating the deposition quality of parts produced by an open-source 3D printer, Rapid Prototyping Journal, 23(4), (2017) 796-803 https://doi.org/10.1108/RPJ-05-2016-0078

[301] Evans, B. Practical 3D printers: the science and art of 3D printing, (2012) p. 321 New York, NY: Apress. ISBN: 978-1-4302-4393-9

[302] Elshennawy, A.K.M. Performance evaluation of coordinate measuring machines, PhD thesis, The Pennsylvania State University, University Park, PA. (1987).

[303] Alvarez C., K.L., Lagos C., R.F., Aizpun, M. Investigating the influence of infill percentage on the mechanical properties of fused deposition modelled ABS parts [Investigando la influencia del porcentaje de relleno en las propiedades mecánicas, de elementos impresos con ABS por el método de modelado por deposición fundida], Ingenieria e Investigacion, 36(3), (2016) 110-116 https://doi.org/10.15446/ing.investig.v36n3.56610

[304] Lubombo, C., Huneault, M.A. Effect of infill patterns on the mechanical performance of lightweight 3D-printed cellular PLA parts, Materials Today Communications, 17, (2018) 214-228 https://doi.org/10.1016/j.mtcomm.2018.09.017

[305] Harpool, T.D., Alamir, M., Asmatulu, R. Effects of infill shapes on mechanical behaviors of 3D printed plastics, CAMX 2017 - Composites and Advanced Materials Expo, (2017) (2017).

[306] Serdeczny M.P., Comminal R., Pedersen D.B., Spangenberg J. Numerical simulations of the mesostructure formation in material extrusion additive manufacturing, Additive Manufacturing, 28, (2019) 419-429 https://doi.org/10.1016/j.addma.2019.05.024

[307] Yardimci, M.A., Hattori, T., Guceri, S.I., Danforth, S.C. Thermal analysis of fused deposition, Solid Freeform Fabrication Proceedings. University of Texas at Austin, Austin (1997).

[308] Ramanath, H.S., Chua, C.K., Leong, K.F., Shah, K.D. Melt flow behaviour of poly-ε-caprolactone in fused deposition modelling, Journal of Materials Science: Materials in Medicine, 19(7), (2008) 2541-2550 https://doi.org/10.1007/s10856-007-3203-6

[309] Bellini, A., Güçeri, S., Bertoldi, M. Liquefier dynamics in fused deposition, Journal of Manufacturing Science and Engineering, Transactions of the ASME, 126 (2), (2004) 237-246. https://doi.org/10.1115/1.1688377

[310] Pandey, A., Pradhan, S.K. Investigations into Complete Liquefier Dynamics and Optimization of Process Parameters for Fused Deposition Modeling, Materials Today: Proceedings, 5(5), (2018) 12940-12955 https://doi.org/10.1016/j.matpr.2018.02.279

[311] Venkataraman N., Rangarajan S., Matthewson M.J., Harper B., Safari A., Danforth S.C., Wu G., Langrana N., Guceri S., Yardimci A. Feedstock material property - Process relationships in fused deposition of ceramics (FDC), Rapid Prototyping Journal, 6 (4), (2000) 244-252. https://doi.org/10.1108/13552540010373344

[312] Jerez-Mesa, R., Travieso-Rodriguez, J.A., Corbella, X., Busqué, R., Gomez-Gras, G. Finite element analysis of the thermal behavior of a RepRap 3D printer liquefier, Mechatronics, 36, (2016) 119-126 https://doi.org/10.1016/j.mechatronics.2016.04.007

[313] Ouballouch, A., Elalaiji, R., Ouahmane, I., Lasri, L., Sallaou, M. Finite element analysis of a FDM 3D printer liquefier, Key Engineering Materials, 820, (2019) 173-178 https://doi.org/10.4028/www.scientific.net/KEM.820.173

[314] Jerez-Mesa, R., Gomez-Gras, G., Travieso-Rodriguez, J.A., Garcia-Plana, V. A comparative study of the thermal behavior of three different 3D printer liquefiers, Mechatronics, 56, (2017) 297-305 https://doi.org/10.1016/j.mechatronics.2017.06.008

[315] Mackay, M.E., Swain, Z.R., Banbury, C.R., Phan, D.D., Edwards, D.A. The performance of the hot end in a plasticating 3D printer, Journal of Rheology, 61(2), (2017) 229-236 https://doi.org/10.1122/1.4973852

[316] Peng, F., Vogt, B.D., Cakmak, M. Complex flow and temperature history during melt extrusion in material extrusion additive manufacturing, Additive Manufacturing, 22, (2018) 197-206 https://doi.org/10.1016/j.addma.2018.05.015

[317] Pigeonneau, F., Xu, D., Vincent, M., Agassant, J.-F. Heating and flow computations of an amorphous polymer in the liquefier of a material extrusion 3D printer, Additive Manufacturing, 32,101001 (2020). https://doi.org/10.1016/j.addma.2019.101001

[318] Serdeczny, M.P., Comminal, R., Pedersen, D.B., Spangenberg, J. Experimental and analytical study of the polymer melt flow through the hot-end in material extrusion additive manufacturing, Additive Manufacturing, 32,100997 (2020). https://doi.org/10.1016/j.addma.2019.100997

[319] Phan, D.D., Swain, Z.R., MacKay, M.E. Rheological and heat transfer effects in fused filament fabrication, Journal of Rheology, 62(5), (2018) 1097-1107 https://doi.org/10.1122/1.5022982

[320] Serdeczny, M.P., Comminal, R., Mollah, M.T., Pedersen, D.B., Spangenberg, J. Numerical modeling of the polymer flow through the hot-end in filament-based material extrusion additive manufacturing, Additive Manufacturing, 36,10145 (2020). https://doi.org/10.1016/j.addma.2020.101454

[321] Stewart, S.R., Wentz, J.E., Allison, J.T. Experimental and computational fluid dynamic analysis of melt flow behavior in fused deposition modelling of poly(lactic) acid, ASME International Mechanical Engineering Congress and Exposition, Proceedings (2015) (2015). https://doi.org/10.1115/IMECE2015-52261

[322] Phan, D.D., Horner, J.S., Swain, Z.R., Beris, A.N., Mackay, M.E. Computational fluid dynamics simulation of the melting process in the fused filament fabrication additive manufacturing technique, Additive Manufacturing, 33,101161 (2020). https://doi.org/10.1016/j.addma.2020.101161

[323] Osswald, T.A., Puentes, J., Kattinger, J. Fused filament fabrication melting model, Additive Manufacturing, 22, (2018) 51-59 https://doi.org/10.1016/j.addma.2018.04.030

[324] Mostafa, N., Syed, H.M., Igor, S., Andrew, G. A study of melt flow analysis of an ABS-iron composite in fused deposition modelling process, Tsinghua Science and Technology, 14(SUPPL. 1), (2009) 29-37 https://doi.org/10.1016/S1007-0214(09)70063-X

[325] Vanaei, H.R., Shirinbayan, M., Costa, S.F., Duarte, F.M., Covas, J.A, Deligant, M., Khelladi, S., Tcharkhtchi, A. Experimental study of PLA thermal behavior during fused filament fabrication, Journal of Applied Polymer Science, 138(4),49747 (2020). https://doi.org/10.1002/app.49747

[326] Seppala, J.E., Migler, K.D. Infrared thermography of welding zones produced by polymer extrusion additive manufacturing, Additive Manufacturing, Part A 12, (2016) 71-76. https://doi.org/10.1016/j.addma.2016.06.007

[327] Wolszczak, P., Lygas, K., Paszko, M., Wach, R.A. Heat distribution in material during fused deposition modelling, Rapid Prototyping Journal, 24(3), (2018) 615-622 https://doi.org/10.1108/RPJ-04-2017-0062

[328] Xia H., Lu J., Dabiri S., Tryggvason G. Fully resolved numerical simulations of fused deposition modeling. Part I: fluid flow, Rapid Prototyping Journal, 24(2), (2018) 463-476 https://doi.org/10.1108/RPJ-12-2016-0217

[329] Zhou, Y., Nyberg, T., Xiong, G., Liu, D. Temperature Analysis in the Fused Deposition Modeling Process, Proceedings - 2016 3rd International Conference on Information Science and Control Engineering, ICISCE 2016, 7726247, (2016) 678-682 https://doi.org/10.1109/ICISCE.2016.150

[330] Zhou, X., Hsieh, S.-J., Sun, Y. Experimental and numerical investigation of the thermal behaviour of polylactic acid during the fused deposition process, Virtual and Physical Prototyping, 12(3), (2017) 221-233 https://doi.org/10.1080/17452759.2017.1317214

[331] Zhou, X., Hsieh, S.-J. Thermal analysis of fused deposition modeling process using infrared thermography imaging and finite element modeling, Proceedings of SPIE - The International Society for Optical Engineering, 10214, (2017) 1021409 (2017). https://doi.org/10.1117/12.2262796

[332] Zhou, Y., Lu, H., Wang, G., Wang, J., Li, W. Voxelization modelling based finite element simulation and process parameter optimization for Fused Filament Fabrication, Materials and Design, 187,108409 (2020). https://doi.org/10.1016/j.matdes.2019.108409

[333] Costa, S.F., Duarte, F.M., Covas, J.A. Estimation of filament temperature and adhesion development in fused deposition techniques, Journal of Materials Processing Technology, 245, (2017) 167-179 https://doi.org/10.1016/j.jmatprotec.2017.02.026

[334] Costa, S.F., Duarte, F.M., Covas, J.A. Thermal conditions affecting heat transfer in FDM/FFE: a contribution towards the numerical modelling of the process: This paper investigates convection, conduction and radiation phenomena in the filament deposition process, Virtual and Physical Prototyping, 10(1), (2015) 35-46 https://doi.org/10.1080/17452759.2014.984042

[335] Prajapati, H., Ravoori, D., Jain, A. Measurement and modeling of filament temperature distribution in the standoff gap between nozzle and bed in polymer-based additive manufacturing, Additive Manufacturing, 24, (2019) 224-231 https://doi.org/10.1016/j.addma.2018.09.030

[336] D'Amico, T., Peterson, A.M. Bead parameterization of desktop and room-scale material extrusion additive manufacturing: How print speed and thermal properties affect heat transfer, Additive Manufacturing, 34,101239 (2020). https://doi.org/10.1016/j.addma.2020.101239

[337] Kulkarni, P., Dutta, D. An accurate slicing procedure for layered manufacturing, CAD Computer Aided Design, 28(9), (1996) 683-697 https://doi.org/10.1016/0010-4485(95)00083-6

[338] Sabourin, E., Houser, S.A., Bøhn, J.H. Adaptive slicing using stepwise uniform refinement, Rapid Prototyping Journal, 2(4), (1996) 20-26 https://doi.org/10.1108/13552549610153370

[339] Sabourin, E., Houser, S.A., Bøhn, J.H. Accurate exterior, fast interior layered manufacturing, Rapid Prototyping Journal, 3 (2), (1997) 44-52. https://doi.org/10.1108/13552549710176662

[340] Dolenc, A., Mäkelä, I. Slicing procedures for layered manufacturing techniques, Computer-Aided Design, 26 (2), (1994) 119-126. https://doi.org/10.1016/0010-4485(94)90032-9

[341] Pandey, P.M., Reddy, N.V., Dhande, S.G. Real time adaptive slicing for fused deposition modelling, International Journal of Machine Tools and Manufacture, 43(1), (2003) 61-71 https://doi.org/10.1016/S0890-6955(02)00164-5

[342] Vasudevarao, B., Natarajan, D.P., Razdan, A., Henderson, M. Sensitivity of RP surface finish to process parameters variation, Solid Freeform Fabrication Proceedings, (2000) 251-258.

[343] Boschetto, A., Giordano, V., Veniali, F. Modelling micro geometrical profile in fused deposition process, International Journal of Advanced Manufacturing Technology, 61(9-12), (2012) 945-956 https://doi.org/10.1007/s00170-011-3744-1

[344] Boschetto, A., Giordano, V., Veniali, F. 3D roughness profile model in fused deposition modelling, Rapid Prototyping Journal, 19(4), 17088799, (2013) 240-252 https://doi.org/10.1108/13552541311323254

[345] Gharehpapagh, B., Dolen, M., Yaman, U. Investigation of variable bead widths in FFF process, Procedia Manufacturing, 38, (2019) 52-59 https://doi.org/10.1016/j.promfg.2020.01.007

[346] Bakrani Balani, S., Chabert, F., Nassiet, V., Cantarel, A. Influence of printing parameters on the stability of deposited beads in fused filament fabrication of poly(lactic) acid, Additive Manufacturing, 25, (2019) 112-121. https://doi.org/10.1016/j.addma.2018.10.012

[347] Ma, W., But, W.-C., He, P. NURBS-based adaptive slicing for efficient rapid prototyping, CAD Computer Aided Design, 36(13), (2004) 1309-1325 https://doi.org/10.1016/j.cad.2004.02.001

[348] Vega, G., Paz, R., Gleadall, A., Monzón, M., Alemán-Domínguez, M.E. Comparison of cad and voxel-based modelling methodologies for the mechanical simulation of extrusion-based 3d printed scaffolds, Materials, 14(19),5670 (2021). https://doi.org/10.3390/ma14195670

[349] Aksoy, D., Balta, E.C., Tilbury, D.M., Barton, K. A Control-Oriented Model for Bead Cross-Sectional Geometry in Fused Deposition Modeling, Proceedings of the American Control Conference, 2020-July, 9147769, (2020) 474-480 https://doi.org/10.23919/ACC45564.2020.9147769

[350] Dabiri, S., Schmid, S., Tryggvason, G. Fully resolved numerical simulations of fused deposition modeling, ASME 2014 International Manufacturing Science and Engineering Conference, 2, (2014) V002T02A045 (2014). https://doi.org/10.1115/MSEC2014-4107

[351] Gleadall, A., Ashcroft, I., Segal, J. VOLCO: A predictive model for 3D printed microarchitecture, Additive Manufacturing 21, (2018) 605-618 https://doi.org/10.1016/j.addma.2018.04.004

[352] Macedo, R.Q.D., Ferreira, R.T.L., Gleadall, A., Ashcroft, I. VOLCO-X: Numerical simulation of material distribution and voids in extrusion additive manufacturing, Additive Manufacturing, 40,101900 (2021). https://doi.org/10.1016/j.addma.2021.101900

[353] Comminal, R., Serdeczny, M.P., Pedersen, D.B., Spangenberg, J. Numerical modeling of the strand deposition flow in extrusion-based additive manufacturing, Additive Manufacturing, 20, (2018) 68-76 https://doi.org/10.1016/j.addma.2017.12.013

[354] Du, J., Wei, Z., Wang, X., Wang, J., Chen, Z. An improved fused deposition modeling process for forming large-size thin-walled parts, Journal of Materials Processing Technology, 234, (2016) 332-341 https://doi.org/10.1016/j.jmatprotec.2016.04.005

[355] Serdeczny, M.P., Comminal, R., Pedersen, D.B., Spangenberg, J. Experimental validation of a numerical model for the strand shape in material extrusion additive manufacturing, Additive Manufacturing, 24, (2018) 145-153 https://doi.org/10.1016/j.addma.2018.09.022

[356] Comminal, R., Serdeczny, M.P., Pedersen, D.B., Spangenberg, J. Numerical simulation of extrusion-based additive manufacturing - Effect of the nozzle geometry on the strand cross-section, European Society for Precision Engineering and Nanotechnology, Conference Proceedings - 18th International Conference and Exhibition, EUSPEN 2018, (2018) 285-286

[357] Rodriguez, J.F., Thomas, J.P., Renaud, J.E. Characterization of the mesostructure of fused-deposition acrylonitrile-butadiene-styrene materials, Rapid Prototyping Journal, 6(3), (2000) 175-185 https://doi.org/10.1108/13552540010337056

[358] Jang, S., Boddorff, A., Jang, D.J., Lloyd, J., Wagner, K., Thadhani, N., Brettmann, B. Effect of material extrusion process parameters on filament geometry and inter-filament voids in as-fabricated high solids loaded polymer composites, Additive Manufacturing, 47,102313 (2021). https://doi.org/10.1016/j.addma.2021.102313

[359] Kaveh, M., Badrossamay, M., Foroozmehr, E., Hemasian Etefagh, A. Optimization of the printing parameters affecting dimensional accuracy and internal cavity for HIPS material used in fused deposition modeling processes, Journal of Materials Processing Technology, 226, (2015) 280-286 https://doi.org/10.1016/j.jmatprotec.2015.07.012

[360] Golab, M., Massey, S., Moultrie, J. Experimental Investigation of Filament Behaviour in Material Extrusion Additive Manufacturing, In: Meboldt, M., Klahn, C. (eds) Industrializing Additive Manufacturing. AMPA 2020. Springer, Cham. (2020). https://doi.org/10.1007/978-3-030-54334-1_20

[361] Michaeli, W. Extrusion Dies for Plastics and Rubber: Design and Engineering Computation—Second Edition, Hanser ed., New York, ISBN 3-446-16190-2 (1992).

[362] Osswald, T.A., Menges, G. Materials Science of Polymers for Engineers, Carl Hanser Verlag, Kempten. (2003).

[363] Liang, J.Z., Chan, J.S.F., Wong, E.T.T. Effects of operation conditions and die angles on the pressure losses in capillary flow of polystyrene melt, Journal of Materials Processing Technology 114(2), (2001) 118-121 https://doi.org/10.1016/S0924-0136(01)00731-2

[364] Percoco, G., Arleo, L., Stano, G., Bottiglione, F. Analytical model to predict the extrusion force as a function of the layer height, in extrusion based 3D printing, Additive Manufacturing, 38,101791 (2021). https://doi.org/10.1016/j.addma.2020.101791

[365] Go, J., Schiffres, S.N., Stevens, A.G., Hart, A.J. Rate limits of additive manufacturing by fused filament fabrication and guidelines for high-throughput system design, Additive Manufacturing, 16, (2017) 1-11 https://doi.org/10.1016/j.addma.2017.03.007

[366] Luo, C., Wang, X., Migler, K.B., Seppala, J.E. Upper bound of feed rates in thermoplastic material extrusion additive manufacturing, Additive Manufacturing, 32,101019 (2020). https://doi.org/10.1016/j.addma.2019.101019

[367] Gutowski, T., Jiang, S., Cooper, D., Corman, G., Hausmann, M., Manson, J-A., Schudeleit, T., Wegener, K., Sabelle, M., Ramos-Grez, J., Sekulic, D.P. Note on the Rate and Energy Efficiency

Limits for Additive Manufacturing, Journal of Industrial Ecology, 21, (2017) S69-S79 https://doi.org/10.1111/jiec.12664

[368] Yardimci, M.A. Process Analysis and Development for Fused Deposition, PhD Thesis, University of Illinois at Chicago, Chicago (1999).

[369] Wang, J., Xie, H., Weng, Z., Senthil, T., Wu, L. A novel approach to improve mechanical properties of parts fabricated by fused deposition modeling, Materials and Design, 105, (2016) 152-159 https://doi.org/10.1016/j.matdes.2016.05.078

[370] Takagishi, K., Umezu, S. Development of the Improving Process for the 3D Printed Structure, Scientific Reports, 7, (2017) 39852 (2017). https://doi.org/10.1038/srep39852

[371] Wang, J.Y., Xu, D.D., Sun, W., Du, S.M., Guo, J.J., Xu, G.J. Effects of nozzle-bed distance on the surface quality and mechanical properties of fused filament fabrication parts, IOP Conference Series: Materials Science and Engineering, 479(1), (2019) 012094 (2019). https://doi.org/10.1088/1757-899X/479/1/012094

[372] Alafaghani, A., Qattawi, A., Alrawi, B., Guzman, A. Experimental Optimization of Fused Deposition Modelling Processing Parameters: A Design-for-Manufacturing Approach, Procedia Manufacturing, 10, (2017) 791-803 https://doi.org/10.1016/j.promfg.2017.07.079

[373] Kasim, M.S., Harun, N.H., Hafiz, M.S.A., Mohamed, S.B., Mohamad, W.N.F.W. Multi-response optimization of process parameter in fused deposition modelling by response surface methodology, International Journal of Recent Technology and Engineering, 8(3), (2019) 327-338 https://doi.org/10.35940/ijrte.C4152.098319

[374] Heller, B.P., Smith, D.E., Jack, D.A. Effects of extrudate swell and nozzle geometry on fiber orientation in Fused Filament Fabrication nozzle flow, Additive Manufacturing, 12, (2016) 252-264 https://doi.org/10.1016/j.addma.2016.06.005

[375] Ravi, P., Shiakolas, P.S., Thorat, A.D. Analyzing the Effects of Temperature, Nozzle-Bed Distance, and Their Interactions on the Width of Fused Deposition Modeled Struts Using Statistical Techniques Toward Precision Scaffold Fabrication, Journal of Manufacturing Science and Engineering, Transactions of the ASME, 139(7), (2017) 071007 (2017). https://doi.org/10.1115/1.4035963

[376] Mohamed, O.A., Masood, S.H., Bhowmik, J.L. Optimization of fused deposition modeling process parameters for dimensional accuracy using I-optimality criterion, Measurement, Volume 81, (2016) 174-196 https://doi.org/10.1016/j.measurement.2015.12.011

[377] García Plaza, E., Núñez López, P.J., Caminero Torija, M.Á., Chacón Muñoz, J.M. Analysis of PLA geometric properties processed by FFF additive manufacturing: Effects of process parameters and plate-extruder precision motion, Polymers, 11(10),1581 (2019). https://doi.org/10.3390/polym11101581

[378] Han, W., Jafari, M.A., Danforth, S.C., Safari, A. Tool path based deposition planning in fused deposition processes, Journal of Manufacturing Science and Engineering 124(2), (2002) 462-472 https://doi.org/10.1115/1.1455026

[379] Han, W., Jafari, M.A. Coordination control of positioning and deposition in layered manufacturing, IEEE Transactions on Industrial Electronics, 54(1), (2007) 651-659 https://doi.org/10.1109/TIE.2006.885468

[380] Ertay, D.S., Yuen, A., Altintas, Y. Synchronized material deposition rate control with path velocity on fused filament fabrication machines, Additive Manufacturing, 19, (2018) 205-213 https://doi.org/10.1016/j.addma.2017.05.011

[381] Pollard, D., Ward, C., Herrmann, G., Etches, J. Filament Temperature Dynamics in Fused Deposition Modelling and Outlook for Control, Procedia Manufacturing, 11, (2017) 536-544 https://doi.org/10.1016/j.promfg.2017.07.147

[382] Tronvoll, S.A., Popp, S., Elverum, C.W., Welo, T. Investigating pressure advance algorithms for filament-based melt extrusion additive manufacturing: theory, practice and simulations, Rapid Prototyping Journal, 25(5), (2019) 830-839 https://doi.org/10.1108/RPJ-10-2018-0275

[383] Comminal, R., Serdeczny, M.P., Pedersen, D.B., Spangenberg, J. Motion planning and numerical simulation of material deposition at corners in extrusion additive manufacturing, Additive Manufacturing, 29, 100753 (2019). https://doi.org/10.1016/j.addma.2019.06.005

[384] Giberti H., Sbaglia L., Parabiaghi M. Trajectories generation with constant extrusion rate for experimentations on am techniques and extrusion based technologies, Mechanisms and Machine Science, 47, (2017) 153-160. https://doi.org/10.1007/978-3-319-48375-7_17

[385] Friedrich, L., Begley, M. Corner accuracy in direct ink writing with support material, Bioprinting, 19, e00086 (2020). https://doi.org/10.1016/j.bprint.2020.e00086

[386] Jin, Y.-Z., Zhang, J.-F., Wang, Y., Zhu, Z.-C. Filament geometrical model and nozzle trajectory analysis in the fused deposition modeling process, Journal of Zhejiang University: Science A, 10(3), (2009) 370-376 https://doi.org/10.1631/jzus.A0820346

[387] Bouhal A. Tracking control and trajectory planning in layered manufacturing applications, IEEE Transactions on Industrial Electronics, 46(2), (1999) 445-451 https://doi.org/10.1109/41.753784

[388] Prša, J., Irlinger, F., Lueth, T.C. Algorithm for detecting and solving the problemof under-filled pointed ends based on 3D printing plastic droplet generation, ASME International Mechanical Engineering Congress and Exposition, Proceedings (IMECE) 2A (2014). https://doi.org/10.1115/IMECE2014-36573

[389] Kuipers, T., Doubrovski, E.L., Wu, J., Wang, C.C.L. A Framework for Adaptive Width Control of Dense Contour-Parallel Toolpaths in Fused Deposition Modeling, CAD Computer Aided Design, 128,102907 (2020). https://doi.org/10.1016/j.cad.2020.102907

[390] Eiliat, H., Urbanic, J. Visualizing, analyzing, and managing voids in the material extrusion process, International Journal of Advanced Manufacturing Technology, 96(9-12), (2018) 4095-4109 https://doi.org/10.1007/s00170-018-1820-5

[391] Wang, M., Zhang, H., Hu, Q., Liu, D., Lammer, H. Research and implementation of a non-supporting 3D printing method based on 5-axis dynamic slice algorithm, Robotics and Computer-Integrated Manufacturing, 57, (2019) 496-505 https://doi.org/10.1016/j.rcim.2019.01.007

[392] Shukor, S.A., Axinte, D.A. Manufacturability analysis system: issues and future trends, International Journal of Production Research, 47(5), (2009) 1369-1390 https://doi.org/10.1080/00207540701589398

[393] Pascu, N.E., Arion, A.F., Dobrescu, T., Carutasu, N.L. Fused Deposition Modeling design rules for plastics, Materiale Plastice, 52(2), (2015) 141-143 0255289

[394] Simion, I., Arion, A.F. Dimensioning rules for 3D printed parts using additive technologies (FDM), UPB Scientific Bulletin, Series D: Mechanical Engineering, 78(2), (2016) 79-92

[395] Urbanic, R.J., Hedrick, R. , Fused Deposition Modeling Design Rules for Building Large, Complex Components, Computer-Aided Design and Applications, 13(3), (2016) 348-368 https://doi.org/10.1080/16864360.2015.1114393

[396] Ziemian, C.W., Crawn III, P.M. Computer aided decision support for fused deposition modeling, Rapid Prototyping Journal, 7(3), (2001) 138-147 https://doi.org/10.1108/13552540110395538

[397] Hague, R., Campbell, I., Dickens, P. Implications on design of rapid manufacturing, Proceedings of the Institution of Mechanical Engineers, Part C: Journal of Mechanical Engineering Science, 217 (1), (2003) 25-30. https://doi.org/10.1243/095440603762554587

[398] Byun, H.S., Lee, K.H. A decision support system for the selection of a rapid prototyping process using the modified TOPSIS method, International Journal of Advanced Manufacturing Technology, 26(11-12), (2005) 1338-1347 https://doi.org/10.1007/s00170-004-2099-2

[399] Phillipson, D.K. Rapid prototyping machine selection program, The 6th European conference on rapid prototyping and manufacturing, Nottingham, UK, 1997, pp 292–303 (1997).

[400] Bibb, R. The development of a rapid prototyping selection system for small companies, Thesis, School of Product Design and Engineering,

University of Wales Institute, Cardiff (1999). http://hdl.handle.net/10369/6518"

[401] Bauer, J., Klingenberg, H.H., Müller, H. Computer based rapid prototyping system selection and support, Proceedings of time compression technologies conference, The Heritage Motor Center, Gaydon, UK, 1996, pp 241–250 (1996). "

[402] Masood, S.H., Soo, A. A rule based expert system for rapid prototyping system selection, Robotics and Computer-Integrated Manufacturing 18(3-4), (2002) 267-274 https://doi.org/10.1016/S0736-5845(02)00017-0

[403] Mahesh, M., Fuh, J.Y.H., Wong, Y.S., Loh, H.T. Benchmarking for decision making in rapid prototyping systems, Proceedings of the 2005 IEEE Conference on Automation Science and Engineering, IEEE-CASE 2005, 2005,1506739, (2005) 19-24 https://doi.org/10.1109/COASE.2005.1506739

[404] Ransikarbum, K., Kim, N. Data envelopment analysis-based multi-criteria decision making for part orientation selection in fused deposition modeling, 2017 4th International Conference on Industrial Engineering and Applications, ICIEA 2017, 7939183, (2017) 81-85 https://doi.org/10.1109/IEA.2017.7939183

[405] Hur, J., Lee, K. The development of a CAD environment to determine the preferred build-up direction for layered manufacturing, International Journal of Advanced Manufacturing Technology, 14(4), (1998) 247-254 https://doi.org/10.1007/BF01199879

[406] Wang, Y., Blache, R., Zheng, P., Xu, X. A Knowledge Management System to Support Design for Additive Manufacturing Using Bayesian Networks, Journal of Mechanical Design, Transactions of the ASME, 140(5), (2018) 051701 (2018). https://doi.org/10.1115/1.4039201

[407] Ahsan, N., Khoda, B. AM optimization framework for part and process attributes through geometric analysis, Additive Manufacturing, 11, (2016) 85-96 https://doi.org/10.1016/j.addma.2016.05.013

[408] Pradel, P., Bibb, R., Zhu, Z., Moultrie, J. Exploring the Impact of Shape Complexity on Build Time for Material Extrusion and Material Jetting, International Conference on Additive Manufacturing in Products and Applications, (2018) (2018). https://doi.org/10.1007/978-3-319-66866-6_3

[409] Pradel, P., Bibb, R., Zhu, Z., Moultrie, J. Complexity is not For free: The impact of component complexity on additive manufacturing build time, Rapid Design, Prototyping & Manufacturing, Newcastle, UK, (2017) (2018).

[410] Boschetto, A., Giordano, V., Veniali, F. Surface roughness prediction in fused deposition modelling by neural networks, International Journal of Advanced Manufacturing Technology, 67(9-12), (2013) 2727-2742 https://doi.org/10.1007/s00170-012-4687-x

[411] Bayraktar, Ö., Uzun, G., Çakiroğlu, R., Guldas, A. Experimental study on the 3D-printed plastic parts and predicting the mechanical properties using artificial neural networks, Polymers for Advanced Technologies, 28(8), (2017) 1044-1051 https://doi.org/10.1002/pat.3960

[412] Vahabli, E., Rahmati, S. Improvement of FDM parts' surface quality using optimized neural networks - Medical case studies, Rapid Prototyping Journal, 23(4), (2017) 825-842 https://doi.org/10.1108/RPJ-06-2015-0075

[413] Vahabli, E., Rahmati, S. Application of an RBF neural network for FDM parts' surface roughness prediction for enhancing surface quality, International Journal of Precision Engineering and Manufacturing, 17(12), (2016) 1589-1603 https://doi.org/10.1007/s12541-016-0185-7

[414] Zhang, S.-U. Degradation classification of 3D printing thermoplastics using fourier transform infrared spectroscopy and artificial neural networks, Applied Sciences (Switzerland), 8(8), (2018) 1224 (2018). https://doi.org/10.3390/app8081224

[415] Munteanu, A., Chitariu, D.-F. The neural networks used in FDM printing study, MATEC Web of Conferences, 178, (2018) 02002 (2018). https://doi.org/10.1051/matecconf/201817802002

[416] Lyu, J., Manoochehri, S. Dimensional prediction for FDM machines using artificial neural network and support vector regression, Proceedings of the ASME Design Engineering Technical Conference 1 (2019). https://doi.org/10.1115/DETC2019-97963

[417] Mohamed, O.A., Masood, S.H., Bhowmik, J.L. Modeling, analysis, and optimization of dimensional accuracy of FDM-fabricated parts using definitive screening design and deep learning feedforward artificial neural network, Advances in Manufacturing, 9(1), (2021) 115-129 https://doi.org/10.1007/s40436-020-00336-9

[418] Meißner, P., Watschke, H., Winter, J., Vietor, T. Artificial neural networks-based material parameter identification for numerical simulations of additively manufactured parts by material extrusion, Polymers, 12(12), 2949, (2020) 1-28 https://doi.org/10.3390/polym12122949

[419] Meiabadi, M.S., Moradi, M., Karamimoghadam, M., Ardabili, S., Bodaghi, M., Shokri, M., Mosavi, A.H. Modeling the producibility of 3d printing in polylactic acid using artificial neural networks and fused filament fabrication, Polymers, 13(19),3219 (2021). https://doi.org/10.3390/polym13193219

[420] Shang, G.Q., Sun, C.H., Chen, X.F., Du, J.H. Precision model of predicting FDM rapid prototype based on BP neural network, Key Engineering Materials, 392-394, (2009) 891-897 10139826

[421] Sood, A.K., Ohdar, R.K., Mahapatra, S.S. Parametric appraisal of fused deposition modelling process using the grey Taguchi method, Proceedings of the Institution of Mechanical Engineers, Part

B: Journal of Engineering Manufacture, 224(1), (2010) 135-145 https://doi.org/10.1243/09544054JEM1565

[422] Wang, C.C., Lin, T., Hu, S. Optimizing the rapid prototyping process by integrating the Taguchi method with the Gray relational analysis, Rapid Prototyping Journal, 13(5), (2007) 304-315 https://doi.org/10.1108/13552540710824814

[423] Vishwas, M., Basavaraj, C.K., Vinyas, M. Experimental Investigation using Taguchi Method to Optimize Process Parameters of Fused Deposition Modeling for ABS and Nylon Materials, Materials Today: Proceedings, 5(2), (2018) 7106-7114 https://doi.org/10.1016/j.matpr.2017.11.375

[424] Mahmood, S., Qureshi, A.J., Talamona, D. Taguchi based process optimization for dimension and tolerance control for fused deposition modelling, Additive Manufacturing, 21, (2018) 183-190 https://doi.org/10.1016/j.addma.2018.03.009

[425] Hamza, I., Abdellah, E.G., Mohamed, O. Experimental optimization of fused deposition modeling process parameters: A Taguchi process approach for dimension and tolerance control, Proceedings of the International Conference on Industrial Engineering and Operations Management, 2018(JUL), (2018) 2992-2993 21698767

[426] Venkata Narayana, Y., Pruthvi Reddy, N. Influence of process parameters on tensile strength of additive manufactured pla parts using taguchi method, International Journal of Recent Technology and Engineering, 8(3), (2019) 7635-7639 https://doi.org/10.35940/ijrte.C6191.098319

[427] Huynh, H.N., Nguyen, A.T., Ha, N.L., Ha Thai, T.T. Application of fuzzy Taguchi method to improve the dimensional accuracy of Fused Deposition Modeling processed product, Proceedings - 2017 International Conference on System Science and Engineering, ICSSE 2017, 8030847, (2017) 107-112 https://doi.org/10.1109/ICSSE.2017.8030847

[428] Padhi S.K., Sahu R.K., Mahapatra S.S., Das H.C., Sood A.K., Patro B., Mondal A.K. Optimization of fused deposition modeling process parameters using a fuzzy inference system coupled with Taguchi philosophy, Advances in Manufacturing, 5(3), (2017) 231-242 https://doi.org/10.1007/s40436-017-0187-4

[429] Aslani, K-E., Chaidas, D., Kechagias, J., Kyratsis, P., Salonitis, K. Quality Performance Evaluation of Thin Walled PLA 3D Printed Parts Using the Taguchi Method and Grey Relational Analysis, Journal of Manufacturing Material Processing, 4(2), 47 (2020). https://doi.org/10.3390/jmmp4020047

[430] Herianto, Arifsa, F.B., Prastowo, A. Application of taguchi method in the optimization of 3D-printer process parameters for dimensional accuracy and surface roughness, Journal of Manufacturing Technology Research, 11(1-2), (2019) 55-69 19438095

[431] Devika, D., Gupta, N.S. Modeling the process parameters of RP-FDM using ANOVA and RESPONSE SURFACE METHODOLOGY for PC-ABS materials, International Conference on Electrical, Electronics, and Optimization Techniques, ICEEOT 2016, 7755051, (2016) 2059-2062 https://doi.org/10.1109/ICEEOT.2016.7755051

[432] Mohamed, O.A., Masood, S.H., Bhowmik, J.L. Mathematical modeling and FDM process parameters optimization using response surface methodology based on Q-optimal design, Applied Mathematical Modelling, 40(23-24), (2016) 10052-10073 https://doi.org/10.1016/j.apm.2016.06.055

[433] Saad, M.S., Nor, A.M., Baharudin, M.E., Zakaria, M.Z., Aiman, A.F. Optimization of surface roughness in FDM 3D printer using response surface methodology, particle swarm optimization, and symbiotic organism search algorithms, International Journal of Advanced Manufacturing Technology, 105(12), (2019) 5121-5137 https://doi.org/10.1007/s00170-019-04568-3

[434] Mohamed O.A., Masood S.H., Bhowmik J.L. Experimental investigation for dynamic stiffness and dimensional accuracy of FDM manufactured part using IV-Optimal response surface design, Rapid Prototyping Journal, 23(4), (2017) 736-749 https://doi.org/10.1108/RPJ-10-2015-0137

[435] Maurya, N.K., Maurya, M., Dwivedi, S.P., Srivastava, A.K., Saxena, A., Chahuan, S., Tiwari, A., Mishra, A. Investigation of effect of process variable on dimensional accuracy of FDM component using response surface methodology, World Journal of Engineering, 18(5), (2021) 710-719 https://doi.org/10.1108/WJE-08-2020-0347

[436] Vijayaraghavan, V., Garg, A., Lam, J.S.L., Panda, B., Mahapatra, S.S. Process characterisation of 3D-printed FDM components using improved evolutionary computational approach, International Journal of Advanced Manufacturing Technology, 78(5-8), (2015) 781-793 https://doi.org/10.1007/s00170-014-6679-5

[437] Rao, R.V., Rai, D.P. Optimization of fused deposition modeling process using teaching-learning-based optimization algorithm, Engineering Science and Technology, an International Journal, Volume 19, Issue 1, (2016) 587-603 https://doi.org/10.1016/j.jestch.2015.09.008

[438] Chohan, J.S., Mittal, N., Kumar, R. Parametric optimization of fused deposition modeling using learning enthusiasm enabled teaching learning based algorithm, SN Applied Sciences, 2(12),1978 (2020). https://doi.org/10.1007/s42452-020-03818-4

[439] Frank, D., Fadel, G. Expert system-based selection of the preferred direction of build for rapid prototyping processes, Journal of Intelligent Manufacturing, 6 (5), (1995) 339-345. https://doi.org/10.1007/BF00124677

[440] Equbal, A., Sood, A.K., Ohdar, R.K., Mahapatra, S.S. Prediction of dimensional accuracy in fused deposition modelling: A fuzzy logic approach, International Journal of Productivity and Quality Management, 7(1), (2011) 22-43 https://doi.org/10.1504/IJPQM.2011.037730

[441] Li, C., Fu, G., Guo, K. Study on forecast of forming temperature of ABS resin during fused deposition manufacturing by fuzzy comprehensive evaluation, Key Engineering Materials, 464, (2011) 264-267 https://doi.org/10.4028/www.scientific.net/KEM.464.264

[442] Hambali, R.H., Smith, P., Rennie, A.E.W. Determination of the effect of part orientation to the strength value on additive manufacturing FDM for end-use parts by physical testing and validation via three-dimensional finite element analysis, International Journal of Materials Engineering Innovation, 3(3-4), (2012) 269-281 https://doi.org/10.1504/IJMATEI.2012.049266

[443] Zhang, Y., Chou, Y. Three-dimensional finite element analysis simulations of the fused deposition modelling process, Proceedings of the Institution of Mechanical Engineers, Part B: Journal of Engineering Manufacture, 220(10), (2006) 1663-1671 https://doi.org/10.1243/09544054JEM572

[444] Zhang, Y., Kevin Chou, Y. 3D fea simulations of fused deposition modeling process, Proceedings of the International Conference on Manufacturing Science and Engineering, (2006) (2006).

[445] Baoqing, Z., Farid, M.I., Shuo, Y., Cong, C., Zhang, S. Finite element simulation, analysis and research on the influence of 3D printing parameters on forming precision, Recent Patents on Engineering, 13(4), (2019) 448-454 https://doi.org/10.2174/1872212112666181002101151

[446] Khanzadeh, M., Rao, P., Jafari-Marandi, R., Smith, B.K., Tschopp, M.A., Bian, L. Quantifying Geometric Accuracy with Unsupervised Machine Learning: Using Self-Organizing Map on Fused Filament Fabrication Additive Manufacturing Parts, Journal of Manufacturing Science and Engineering, Transactions of the ASME, 140(3), (2018) 0310111 (2018). https://doi.org/10.1115/1.4038598

[447] Tootooni, M.S., Dsouza, A., Donovan, R., Rao, P.K., Kong, Z.J., Borgesen, P. Classifying the Dimensional Variation in Additive Manufactured Parts from Laser-Scanned Three-Dimensional Point Cloud Data Using Machine Learning Approaches, Journal of Manufacturing Science and Engineering, Transactions of the ASME, 139(9), (2017) 091005 (2017). https://doi.org/10.1115/1.4036641

[448] Hooda, N., Chohan, J.S., Gupta, R., Kumar, R. Deposition angle prediction of Fused Deposition Modeling process using ensemble machine learning, ISA Transactions, 116, (2021) 121-128 https://doi.org/10.1016/j.isatra.2021.01.035

[449] Rao, P.K., Kong, Z., Duty, C.E., Smith, R.J., Kunc, V., Love, L.J. Assessment of dimensional integrity and spatial defect localization in additive manufacturing using spectral graph theory, Journal of Manufacturing Science and Engineering, Transactions of the ASME, 138(5), (2016) 051007 (2016). https://doi.org/10.1115/1.4031574

[450] Stavroulakis, P., Sims-Waterhouse, D., Shaheen, A., Catalucci, S., Bointon, P., Doyen, E., Kong, Y.B., Tzimiropoulos, Y., Leach, R. External shape measurement for industrial applications using artificial intelligence and optimised data fusion, Advances in Intelligent Systems and Computing, 869, (2018) 1273-1281 https://doi.org/10.1007/978-3-030-01057-7_96

[451] Liu, X., Liu, L., Zhao, Y., Ma, J., Li, M., Mao, L. Optimization of forming accuracy of additive manufacturing complex parts based on PSO, Proceedings of the 14th IEEE Conference on Industrial Electronics and Applications, ICIEA 2019, 8833732, (2019) 339-344 https://doi.org/10.1109/ICIEA.2019.8833732

[452] Phatak, A.M., Pande, S.S. Optimum part orientation in Rapid Prototyping using genetic algorithm, Journal of Manufacturing Systems, Volume 31, Issue 4, 2012, (2012) 395-402 https://doi.org/10.1016/j.jmsy.2012.07.001

[453] Pandey, P.M., Thrimurthulu, K., Reddy, N.V. Optimal part deposition orientation in FDM by using a multicriteria genetic algorithm, International Journal of Production Research, 42 (19), (2004) 4069-4089. https://doi.org/10.1080/00207540410001708470

[454] Weidong, Y. Optimal path planning in rapid prototyping based on genetic algorithm, Chinese Control and Decision Conference, CCDC 2009, art. no. 5194966, (2009) 5068-5072. https://doi.org/10.1109/CCDC.2009.5194966

[455] Peko, I., Gjeldum, N., Bilić, B. Application of AHP, fuzzy AHP and PROMETHEE method in solving additive manufacturing process selection problem, Tehnicki Vjesnik, 25(2), (2018) 453-461 https://doi.org/10.17559/TV-20170124092906

[456] Ahn, D., Kweon, J.-H., Kwon, S., Song, J., Lee, S. Representation of surface roughness in fused deposition modeling, Journal of Materials Processing Technology, 209(15-16), (2009) 5593-5600 https://doi.org/10.1016/j.jmatprotec.2009.05.016

[457] Galantucci, L.M., Lavecchia, F., Percoco, G. Experimental study aiming to enhance the surface finish of fused deposition modeled parts, CIRP Annals - Manufacturing Technology, 58(1), (2009) 189-192 https://doi.org/10.1016/j.cirp.2009.03.071

[458] Ouballouch, A., Alaiji, R.E., Ettaqi, S., Bouayad, A., Sallaou, M., Lasri, L. Evaluation of dimensional accuracy and mechanical behavior of 3D printed reinforced polyamide parts, Procedia Structural Integrity, 19, (2019) 433-441 https://doi.org/10.1016/j.prostr.2019.12.047

[459] Castelão, A., Soares, B.A.R., Machado, C.M., Leite, M., Mourão, A.J.M. Design for AM: Contributions from surface finish, part geometry and part positioning, Procedia CIRP, 84, (2019) 491-495 https://doi.org/10.1016/j.procir.2019.04.247

[460] Durão, L.F.C.S., Barkoczy, R., Zancul, E., Lee Ho, L., Bonnard, R. Optimizing additive manufacturing parameters for the fused deposition modeling technology using a design of experiments, Progress in Additive Manufacturing, 4(3), (2019) 291-313 https://doi.org/10.1007/s40964-019-00075-9

[461] Nidagundi, V.B., Keshavamurthy, R., Prakash, C.P.S. Studies on Parametric Optimization for Fused Deposition Modelling Process, Materials Today: Proceedings, 2(4-5), (2015) 1691-1699 https://doi.org/10.1016/j.matpr.2015.07.097

[462] Jin, Y.-A., Li, H., He, Y., Fu, J.-Z. Quantitative analysis of surface profile in fused deposition modelling, Additive Manufacturing, 8, (2015) 142-148 https://doi.org/10.1016/j.addma.2015.10.001

[463] Basavaraj, C.K., Vishwas, M. Studies on Effect of Fused Deposition Modelling Process Parameters on Ultimate Tensile Strength and Dimensional Accuracy of Nylon, IOP Conference Series: Materials Science and Engineering, 149 012035 (2016). https://doi.org/10.1088/1757-899X/149/1/012035

[464] Anusree, T.G., Nair, A.R., Sivadasan, M., John, T.D. Process Parameter Optimization of Fused Deposition Modeling for Helical Surfaces Using Grey Relational Analysis, Materials Science Forum, 879, (2017) 861-866 https://doi.org/10.4028/www.scientific.net/MSF.879.861

[465] Ceretti, E., Ginestra, P., Neto, P.I., Fiorentino, A., Da Silva, J.V.L. Multi-layered Scaffolds Production via Fused Deposition Modeling (FDM) Using an Open Source 3D Printer: Process Parameters Optimization for Dimensional Accuracy and Design Reproducibility, Procedia CIRP, 65, (2017) 13-18 https://doi.org/10.1016/j.procir.2017.04.042

[466] Vishwas M., Basavaraj C.K. Studies on Optimizing Process Parameters of Fused Deposition Modelling Technology for ABS, Materials Today: Proceedings, 4(10), (2017) 10994-11003 https://doi.org/10.1016/j.matpr.2017.08.057

[467] Sukindar, N.A., Ariffin, M.K.A.M., Baharudin, B.T.H.T., Jaafar, C.N.A., Ismail, M.I.S. Optimization of the parameters for surface quality of the open-source 3D printing, Journal of Mechanical Engineering, SI 3(1), (2017) 33-43

[468] Ingrassia, T., Nigrelli, V., Ricotta, V., Tartamella, C. Process parameters influence in additive manufacturing, Lecture Notes in Mechanical Engineering, (2017) 261-270 https://doi.org/10.1007/978-3-319-45781-9_27

[469] Tomal, A.N.M.A., Saleh, T., Khan, M.R. Improvement of Dimensional Accuracy of 3-D Printed Parts using an Additive/Subtractive Based Hybrid Prototyping Approach, IOP Conference Series: Materials Science and Engineering, 260(1), 012031 (2017). https://doi.org/10.1088/1757-899X/260/1/012031

[470] Tronvoll, S.A., Elverum, C.W., Welo, T. Dimensional accuracy of threads manufactured by fused deposition modeling, Procedia Manufacturing, 26, (2018) 763-773 https://doi.org/10.1016/j.promfg.2018.07.088

[471] Alafaghani, A., Qattawi, A. Investigating the effect of fused deposition modeling processing parameters using Taguchi design of experiment method, Journal of Manufacturing Processes, 36, (2018) 164-174 https://doi.org/10.1016/j.jmapro.2018.09.025

[472] Ramli, F.R., Faudzie, M.S.M., Nazan, M.A., Alkahari, M.R., Sudin, M.N., Mat, S., Khalil, S.N. Dimensional accuracy and surface roughness of part features manufactured by open source 3D printer, ARPN Journal of Engineering and Applied Sciences, 13(3), (2018) 1139-1144

[473] Wu, J. Study on optimization of 3D printing parameters, IOP Conference Series: Materials Science and Engineering, 392(6), (2018) 062050 (2018). https://doi.org/10.1088/1757-899X/392/6/062050

[474] Peng, T., Yan, F. Dual-objective Analysis for Desktop FDM Printers: Energy Consumption and Surface Roughness, Procedia CIRP, 69, (2018) 106-111 https://doi.org/10.1016/j.procir.2017.11.084

[475] Papazetis, G., Vosniakos, G.-C. Mapping of deposition-stable and defect-free additive manufacturing via material extrusion from minimal experiments, International Journal of Advanced Manufacturing Technology, 100(9-12), (2018) 2207-2219 https://doi.org/10.1007/s00170-018-2820-1

[476] Dambatta, Y.S., Diaa Sarhan, A.A., Maher, I., Hourmand, M. Volumetric shrinkage prediction in fused deposition modelling process – ANFIS modelling approach, International Journal of Materials and Product Technology, 59(4), (2019) 347-365 https://doi.org/10.1504/IJMPT.2019.104568

[477] Beniak, J., Križan, P., Šooš, Ľ., Matuš, M. Research on Shape and Dimensional Accuracy of FDM Produced Parts, IOP Conference Series: Materials Science and Engineering, 501(1), 012030 (2019). https://doi.org/10.1088/1757-899X/501/1/012030

[478] Mora, S.M., Gil, J.C., López, A.M.C. Influence of manufacturing parameters in the dimensional characteristics of ABS parts obtained by FDM using reverse engineering techniques, Procedia Manufacturing, 41, (2019) 968-975 23519789

[479] Tsiolikas, A., Mikrou, T., Vakouftsi, F., Aslani, K.E., Kechagias, J. Robust design application for optimizing ABS fused filament fabrication process: A case study, IOP Conference Series: Materials Science and Engineering, 564(1), 12021 (2019). https://doi.org/10.1088/1757-899X/564/1/012021

[480] Eswaran, P., Subramaniyan, M., Appusamy, A., Annakalyani, N.S., Pusapati, S.R. Investigations on acute angle parts fabricated fusion deposition modelling parts volumetric shrinkage and surface roughness, Materials Today: Proceedings, 45, (2020) 930-935 https://doi.org/10.1016/j.matpr.2020.02.945

[481] Dixit, N.K., Srivastava,R., Narain, R. Comparison of Two Different Rapid Prototyping System Based on Dimensional Performance Using Grey Relational Grade Method, Procedia Technology, Volume 25, 2016, Pages 908-915 (2016). https://doi.org/10.1016/j.protcy.2016.08.178

[482] Buonamici, F., Carfagni, M., Furferi, R., Governi, L., Saccardi, M., Volpe, Y. Optimizing fabrication outcome in low-cost FDM machines. Part 1-Metrics, Manufacturing Technology, 18(3), (2018) 372-378 https://doi.org/10.21062/ujep/108.2018/a/1213-2489/MT/18/3/372

[483] Chaudhari, M., Jogi, B.F., Pawade, R.S. Comparative Study of Part Characteristics Built Using Additive Manufacturing (FDM), Procedia Manufacturing, 20, (2018) 73-78 https://doi.org/10.1016/j.promfg.2018.02.010

[484] Hyndhavi, D., Babu, G.R., Murthy, S.B. Investigation of Dimensional Accuracy and Material Performance in Fused Deposition Modeling, Materials Today: Proceedings, 5(11), (2018) 23508-23517 https://doi.org/10.1016/j.matpr.2018.10.138

[485] Yadav, A.C., Navin Kumar, N., Raja, K., Naiju, C.D. Investigations on Dimensional Analysis of Fused Filament Fabrication of Wax Filament by Taguchi Design, SAE Technical Papers (October) (2019). https://doi.org/10.4271/2019-28-0133

[486] Sandhu, K., Singh, S., Prakash, C. Analysis of angular shrinkage of fused filament fabricated poly-lactic-acid prints and its relationship with other process parameters, IOP Conference Series:

Materials Science and Engineering, 561(1), 012058 (2019). https://doi.org/10.1088/1757-899X/561/1/012058

[487] Abdul Haq, R.H., Faizan Marwah, O.M., Abdol Rahman, M.N., Haw, H.F., Abdullah, H., Ahmad, S. 3D Printer parameters analysis for PCL/PLA filament wire using Design of Experiment (DOE), IOP Conference Series: Materials Science and Engineering, 607(1),012001 (2019). https://doi.org/10.1088/1757-899X/607/1/012001

[488] Herath, H.M.D.B., Thalagala, S., Gamage, P. Enhancing the Dimensional Accuracy of Components Fabricated Using Rapid Prototyping Technique by Optimizing Machine Parameters of a 3D Printer, IEEE International Conference on Industrial Engineering and Engineering Management, 8978854, (2019) 1379-1383 https://doi.org/10.1109/IEEM44572.2019.8978854

[489] Santana, L., Lino Alves, J., da Costa Sabino Netto, A. A study of parametric calibration for low cost 3D printing: Seeking improvement in dimensional quality, Materials and Design, 135, (2017) 159-172 https://doi.org/10.1016/j.matdes.2017.09.020

[490] Kuo, C.-C., You, Z.-Y. A cost-effective approach for rapid fabricating cooling channels with smooth surface, International Journal of Advanced Manufacturing Technology. 95(1-4), (2018) 1135-1141 https://doi.org/10.1007/s00170-017-1328-4

[491] Chung, M., Radacsi, N., Robert, C., McCarthy, E.D., Callanan, A., Conlisk, N., Hoskins, P.R., Vasileios, K. On the optimization of low-cost FDM 3D printers for accurate replication of patient-specific abdominal aortic aneurysm geometry, 3D Printing in Medicine, 4(2) (2018). https://doi.org/10.1186/s41205-017-0023-2

[492] Khan, M.S., Mishra, S.B. Minimizing surface roughness of ABS-FDM build parts: An experimental approach, Materials Today: Proceedings. 26, (2019) 1557-1566 https://doi.org/10.1016/j.matpr.2020.02.320

[493] Equbal, A., Sood, A.K., Ansari, A.R., Equbal, M.A. Optimization of process parameters of FDM part for minimiizing its dimensional inaccuracy, International Journal of Mechanical and Production Engineering Research and Development, 7(2), IJMPERDAPR20176, (2017) 57-66 22496890

[494] Equbal, A., Equbal, M.I., Sood, A.K. PCA-based desirability method for dimensional improvement of part extruded by fused deposition modelling technology, Progress in Additive Manufacturing, 4(3), (2019) 269-280 https://doi.org/10.1007/s40964-018-00072-4

[495] Chang, D.-Y., Huang, B.-H. Studies on profile error and extruding aperture for the RP parts using the fused deposition modeling process, International Journal of Advanced Manufacturing Technology, 53(9-12), (2011) 1027-1037 https://doi.org/10.1007/s00170-010-2882-1

[496] Pérez, M., Medina-Sánchez, G., García-Collado, A., Gupta, M., Carou, D. Surface quality enhancement of fused deposition modeling (FDM) printed samples based on the selection of critical printing parameters, Materials, 11(8), (2018) 1382 (2018). https://doi.org/10.3390/ma11081382

[497] Bakar, N.S.A., Alkahari, M.R., Boejang, H. Analysis on fused deposition modelling performance, Journal of Zhejiang University: Science A, 11(12), (2010) 972-977 https://doi.org/10.1631/jzus.A1001365

[498] Reyes-Rodríguez, A., Dorado-Vicente, R., Mayor-Vicario, R. Dimensional and form errors of PC parts printed via Fused Deposition Modelling, Procedia Manufacturing, 13, (2017) 880-887 https://doi.org/10.1016/j.promfg.2017.09.149

[499] Garg, A., Bhattacharya, A., Batish, A. Chemical vapor treatment of ABS parts built by FDM: Analysis of surface finish and mechanical strength, International Journal of Advanced Manufacturing Technology, 89(5-8), (2017) 2175-2191 https://doi.org/10.1007/s00170-016-9257-1

[500] Tiwari, K., Kumar, S. Analysis of the factors affecting the dimensional accuracy of 3D printed products, Materials Today: Proceedings, 5(9), (2018) 18674-18680 https://doi.org/10.1016/j.matpr.2018.06.213

[501] Latiff, Z.A., Rahman, M.R.A., Saad, F. Dimensional Accuracy Evaluation of Rapid Prototyping Fused Deposition Modeling Process of FDM200mc Machine on Basic Engineering Profiles, Applied Mechanics and Materials, 465-466, (2014) 96-100 https://doi.org/10.4028/www.scientific.net/AMM.465-466.96

[502] Kalyan K., Singh J., Phull G.S., Soni S., Singh H., Kaur G. Integration of FDM and vapor smoothing process: Analyzing properties of fabricated ABS replicas, Materials Today: Proceedings, 5(14), (2018) 27902-27911 https://doi.org/10.1016/j.matpr.2018.10.029

[503] Abdelrhman, A.M., Wei Gan, W., Kurniawan, D. Effect of part orientation on dimensional accuracy, part strength, and surface quality of three dimensional printed part, IOP Conference Series: Materials Science and Engineering, 694(1),012048 (2019). https://doi.org/10.1088/1757-899X/694/1/012048

[504] Bedi, P., Singh, R., Ahuja, I.P.S. Multifactor optimization of FDM process parameters for development of rapid tooling using SiC/Al2O3-reinforced LDPE filament, Journal of Thermoplastic Composite Materials, 33(5), (2020) 581-598 https://doi.org/10.1177/0892705718808572

[505] Mašović, R., Jagarčec, V., Miler, D., Domitran, Z., Bojčetić, N., Žeželj, D. Analysis of printing direction impact on dimensional accuracy of spur gears, Mechanisms and Machine Science, 73, (2019) 1111-1120 https://doi.org/10.1007/978-3-030-20131-9_110

[506] Ledalla, S.R.K., Tirupathi, B., Sriram, V. Performance Evaluation of Various STL File Mesh Refining Algorithms Applied for FDM-RP Process, Journal of The Institution of Engineers (India): Series C, 99(3), (2018) 339-346 https://doi.org/10.1007/s40032-016-0303-4

[507] Hällgren, S., Pejryd, L., Ekengren, J. 3D Data Export for Additive Manufacturing-Improving Geometric Accuracy, Procedia CIRP, 50, (2016) 518-523 https://doi.org/10.1016/j.procir.2016.05.046

[508] Qu, X., Stucker, B. A 3D surface offset method for STL-format models, Rapid Prototyping Journal, 9(3), (2003) 133-141 https://doi.org/10.1108/13552540310477436

[509] Wu, G., Langrana, N.A., Sadanji, R., Danforth, S. Solid freeform fabrication of metal components using fused deposition of metals, Materials and Design, 23(1), (2002) 97-105 https://doi.org/10.1016/S0261-3069(01)00079-6

[510] Ding, D., Pan, Z., Cuiuri, D., Li, H. Wire-feed additive manufacturing of metal components: technologies, developments and future interests, International Journal of Advanced Manufacturing Technology, 81(1-4), (2015) 465-481 https://doi.org/10.1007/s00170-015-7077-3

[511] Masood, S.H., Song, W.Q. Development of new metal/polymer materials for rapid tooling using Fused deposition modelling, Materials and Design, 25(7), (2004) 587-594 https://doi.org/10.1016/j.matdes.2004.02.009

[512] Gibson, M.A., Mykulowycz, N.M., Shim, J., Fontana, R., Schmitt, P., Roberts, A., Ketkaew, J., Shao, L., Chen, W., Bordeenithikasem, P., Myerberg, J.S., Fulop, R., Verminski, M.D., Sachs, E.M., Chiang, Y.-M., Schuh, C.A., John Hart, A., Schroers, J. 3D printing metals like thermoplastics: Fused

filament fabrication of metallic glasses, Materials Today, 21(7), (2018) 697-702 https://doi.org/10.1016/j.mattod.2018.07.001

[513] Butt, J., Shirvani, H. Experimental analysis of metal/plastic composites made by a new hybrid method, Additive Manufacturing, 22, (2018) 216-222 https://doi.org/10.1016/j.addma.2018.05.029

[514] Nilsiam, Y., Sanders, P., Pearce, J.M. Slicer and process improvements for open-source GMAW-based metal 3-D printing, Additive Manufacturing, 18, (2017) 110-120 https://doi.org/10.1016/j.addma.2017.10.007

[515] Venkataraman, N., Rangarajan, S., Matthewson, M.J., Safari, A., Danforth, S.C., Yardimci, A. Mechanical and rheological properties of feedstock material for fused deposition of ceramics and metals (FDC and FDMet) and their relationship to process performance, Solid Freeform Fabrication Proceedings, (1999) 351-360.

[516] Hou, F. Design of 3D metal FDM printing nozzle based on melt forming, Journal of Advanced Oxidation Technologies, 21(2), 201803615 (2018). https://doi.org/10.26802/jaots.2018.03615

[517] Zhao, J. Design of 3D metal FDM printing nozzle based on melt forming, Chemical Engineering Transactions, 59, (2017) 73-78 https://doi.org/10.3303/CET1759013

[518] Giberti, H., Strano, M., Annoni, M. An innovative machine for Fused Deposition Modeling of metals and advanced ceramics, MATEC Web of Conferences, 43, 03003 (2016). https://doi.org/10.1051/mateccont/20164303003

[519] Tekinalp, H.L., Kunc, V., Velez-Garcia, G.M., Duty, C.E., Love, L.J., Naskar, A.K., Blue, C.A., Ozcan, S. Highly oriented carbon fiber-polymer composites via additive manufacturing, Composites Science and Technology, 105, (2014) 144-150 https://doi.org/10.1016/j.compscitech.2014.10.009

[520] Kalita, S.J., Bose, S., Hosick, H.L., Bandyopadhyay, A. Development of controlled porosity polymer-ceramic composite scaffolds via fused deposition modeling, Materials Science and Engineering C, 23(5), (2003) 611-620 https://doi.org/10.1016/S0928-4931(03)00052-3

[521] Zhong, W., Li, F., Zhang, Z., Song, L., Li, Z. Short fiber reinforced composites for fused deposition modeling, Materials Science and Engineering A, 301(2), (2001) 125-130 https://doi.org/10.1016/S0921-5093(00)01810-4

[522] Ferreira, R.T.L., Amatte, I.C., Dutra, T.A., Bürger, D. Experimental characterization and micrography of 3D printed PLA and PLA reinforced with short carbon fibers, Composites Part B: Engineering, 124, (2017) 88-100 https://doi.org/10.1016/j.compositesb.2017.05.013

[523] Ramanath, H.S., Chandrasekaran, M., Chua, C.K., Leong, K.F., Shah, K.D. Modeling of extrusion behavior of biopolymer and composites in fused deposition modeling, Key Engineering Materials, 334-335 II, (2007) 1241-1244 https://doi.org/10.4028/www.scientific.net/KEM.334-335.1241

[524] Young, D., Wetmore, N., Czabaj, M. Interlayer fracture toughness of additively manufactured unreinforced and carbon-fiber-reinforced acrylonitrile butadiene styrene, Additive Manufacturing, 22, (2018) 508-515 https://doi.org/10.1016/j.addma.2018.02.023

[525] Kukla, C., Gonzalez-Gutierrez, J., Duretek, I., Schuschnigg, S., Holzer, C. Effect of particle size on the properties of highly-filled polymers for fused filament fabrication, AIP Conference Proceedings, 1914, (2017) 190006 (2017). https://doi.org/10.1063/1.5016795

[526] Weidenmann, K.A., Baumann, S., Pinter, P., Elsner, P. Analysis of fiber orientation, microstructure and mechanical properties of specimens made from fiber-reinforced ABS

manufactured by Fused Filament Fabrication (FFF), Proceeding of the 17th European Conference on Composite Materials, (2016) (2016).

[527] Lebedev, S.M., Gefle, O.S., Amitov, E.T., Zhuravlev, D.V., Berchuk, D.Y., Mikutskiy, E.A. Mechanical properties of PLA-based composites for fused deposition modeling technology, International Journal of Advanced Manufacturing Technology, 97(1-4), (2018) 511-518 https://doi.org/10.1007/s00170-018-1953-6

[528] Nötzel, D., Eickhoff, R., Hanemann, T. Fused filament fabrication of small ceramic components, Materials, 11(8), (2018) 1463 (2018). https://doi.org/10.3390/ma11081463

[529] Liu, H., He, H., Peng, X., Huang, B., Li, J. Three-dimensional printing of poly(lactic acid) bio-based composites with sugarcane bagasse fiber: Effect of printing orientation on tensile performance, Polymers for Advanced Technologies, 30(4), (2019) 910-922 https://doi.org/10.1002/pat.4524

[530] Khatri, B., Lappe, K., Habedank, M., Mueller, T., Megnin, C., Hanemann, T. Fused deposition modeling of ABS-barium titanate composites: A simple route towards tailored dielectric devices, Polymers, 10(6), (2018) 666 (2018). https://doi.org/10.3390/polym10060666

[531] Chen, Q., Mangadlao, J.D., Wallat, J., De Leon, A., Pokorski, J.K., Advincula, R.C. 3D printing biocompatible polyurethane/poly(lactic acid)/graphene oxide nanocomposites: Anisotropic properties, ACS Applied Materials and Interfaces, 9(4), (2017) 4015-4023 https://doi.org/10.1021/acsami.6b11793

[532] Weng, Z., Wang, J., Senthil, T., Wu, L. Mechanical and thermal properties of ABS/montmorillonite nanocomposites for fused deposition modeling 3D printing, Materials and Design, 102, (2016) 276-283 https://doi.org/10.1016/j.matdes.2016.04.045

[533] Ning, F., Cong, W., Qiu, J., Wei, J., Wang, S. Additive manufacturing of carbon fiber reinforced thermoplastic composites using fused deposition modeling, Composites Part B: Engineering, 80, (2015) 369-378 https://doi.org/10.1016/j.compositesb.2015.06.013

[534] Brenken, B., Barocio, E., Favaloro, A., Kunc, V., Pipes, R.B. Fused filament fabrication of fiber-reinforced polymers: A review, Additive Manufacturing, 21, (2018) 1-16 https://doi.org/10.1016/j.addma.2018.01.002

[535] Backes, E.H., Pires, L.D.N., Beatrice, C.A.G., Costa, L.C., Passador, F.R., Pessan, L.A. Fabrication of Biocompatible Composites of Poly(lactic acid)/Hydroxyapatite Envisioning Medical Applications, Polymer Engineering and Science, 60(3), (2020) 636-644 https://doi.org/10.1002/pen.25322

[536] Prusinowski, A., Kaczyński, R., Motyl, P. Analysis of FDM extrusion head design as application reinforced composite materials productions, Mechanisms and Machine Science, 73, (2019) 2769-2778 https://doi.org/10.1007/978-3-030-20131-9_274

[537] Yasa, E., Ersoy, K. Dimensional accuracy and mechanical properties of chopped carbon reinforced polymers produced by material extrusion additive manufacturing, Materials, 12(23),3885 (2019). https://doi.org/10.3390/ma122333885

[538] Hamidi, F., Aslani, F. Additive manufacturing of cementitious composites: Materials, methods, potentials, and challenges, Construction and Building Materials, 218, (2019) 582-609 https://doi.org/10.1016/j.conbuildmat.2019.05.140

[539] de Toro, E.V., Sobrino, J.C., Martínez, A.M., Eguía, V.M., Pérez, J.A. Investigation of a short carbon fibre-reinforced polyamide and comparison of two manufacturing processes: Fused Deposition

Modelling (FDM) and polymer injection moulding (PIM), Materials, 13(3),672 (2020). https://doi.org/10.3390/ma13030672

[540] García, E., Núñez, P.J., Chacón, J.M., Caminero, M.A., Kamarthi, S. Comparative study of geometric properties of unreinforced PLA and PLA-Graphene composite materials applied to additive manufacturing using FFF technology, Polymer Testing, 91,106860 (2020). https://doi.org/10.1016/j.polymertesting.2020.106860

[541] Wu, D., Spanou, A., Diez-Escudero, A., Persson, C. 3D-printed PLA/HA composite structures as synthetic trabecular bone: A feasibility study using fused deposition modeling, Journal of the Mechanical Behavior of Biomedical Materials, 103,103608 (2020). https://doi.org/10.1016/j.jmbbm.2019.103608

[542] Leong, K.F., Cheah, C.M., Chua, C.K. Solid freeform fabrication of three-dimensional scaffolds for engineering replacement tissues and organs, Biomaterials, 24(13), (2003) 2363-2378 https://doi.org/10.1016/S0142-9612(03)00030-9

[543] Sachlos, E., Czernuszka, J.T., Gogolewski, S., Dalby, M. Making tissue engineering scaffolds work. Review on the application ofsolid freeform fabrication technology to the production of tissue engineeringscaffolds, European Cells and Materials, 5, (2003) 29-40 14732262

[544] Zein, I., Hutmacher, D.W., Tan, K.C., Teoh, S.H. Fused deposition modeling of novel scaffold architectures for tissue engineering applications, Biomaterials, 23(4), (2002) 1169-1185 https://doi.org/10.1016/S0142-9612(01)00232-0

[545] Loh, Q.L., Choong, C. Three-dimensional scaffolds for tissue engineering applications: Role of porosity and pore size, Tissue Engineering - Part B: Reviews, 19(6), (2013) 485-502 https://doi.org/10.1089/ten.teb.2012.0437

[546] Peltola, S.M., Melchels, F.P.W., Grijpma, D.W., Kellomäki, M. A review of rapid prototyping techniques for tissue engineering purposes, Annals of Medicine, 40(4), (2008) 268-280 https://doi.org/10.1080/07853890701881788

[547] Pfister, A., Landers, R., Laib, A., Hübner, U., Schmelzeisen, R., Mülhaupt, R. Biofunctional Rapid Prototyping for Tissue-Engineering Applications: 3D Bioplotting versus 3D Printing, Journal of Polymer Science, Part A: Polymer Chemistry, 42(3), (2004) 624-638 https://doi.org/10.1002/pola.10807

[548] Kyle, S., Jessop, Z.M., Al-Sabah, A., Whitaker, I.S. 'Printability' of Candidate Biomaterials for Extrusion Based 3D Printing: State-of-the-Art, Advanced Healthcare Materials, 6(16), 1700264 (2017). https://doi.org/10.1002/adhm.201700264

[549] Guerra Silva, R., Torres, M.J., Zahr Viñuela, J. A comparison of miniature lattice structures produced by material extrusion and vat photopolymerization additive manufacturing, Polymers, 13(13), 2163 (2021). https://doi.org/10.3390/polym13132163

[550] Kladovasilakis, N., Charalampous, P., Tsongas, K., Kostavelis, I., Tzetzis, D., Tzovaras, D. Experimental and computational investigation of lattice sandwich structures constructed by additive manufacturing technologies, Journal of Manufacturing and Materials Processing, 5(3),95 (2021). https://doi.org/10.3390/JMMP5030095

[551] Azdast, T., Hasanzadeh, R. Polylactide scaffold fabrication using a novel combination technique of fused deposition modeling and batch foaming: dimensional accuracy and structural properties, International Journal of Advanced Manufacturing Technology (2021). https://doi.org/10.1007/s00170-021-06915-9

[552] Duty, C., Ajinjeru, C., Kishore, V., Compton, B., Hmeidat, N., Chen, X., Liu, P., Hassen, A.A., Lindahl, J., Kunc, V. What makes a material printable? A viscoelastic model for extrusion-based 3D printing of polymers, Journal of Manufacturing Processes, 35, (2018) 526-537 https://doi.org/10.1016/j.jmapro.2018.08.008

[553] Wittbrodt, B., Pearce, J.M. The Effects of PLA Color on Material Properties of 3-D Printed Components, Additive Manufacturing, 8, (2015) 110-116 https://doi.org/10.1016/j.addma.2015.09.006

[554] Jin, Y.A., He, Y., Fu, J.Z. An adaptive tool path generation for Fused Deposition Modeling, Advanced Materials Research, 819, (2013) 7-12 https://doi.org/10.4028/www.scientific.net/AMR.819.7

[555] Jin, G.Q., Li, W.D., Gao, L., Popplewell, K. A hybrid and adaptive tool-path generation approach of rapid prototyping and manufacturing for biomedical models, Computers in Industry, 64(3), (2013) 336-349 https://doi.org/10.1016/j.compind.2012.12.003

[556] Han W., Jafari M.A., Danforth S.C., Safari A. Tool path-based deposition planning in fused deposition processes, Journal of Manufacturing Science and Engineering, Transactions of the ASME, 124 (2), (2002) 462-472. https://doi.org/10.1115/1.1455026

[557] Volpato, N., Zanotto, T.T. Analysis of deposition sequence in tool-path optimization for low-cost material extrusion additive manufacturing, International Journal of Advanced Manufacturing Technology, 101(5-8), (2019) 1855-1863 https://doi.org/10.1007/s00170-018-3108-1

[558] Cao, W., Miyamoto, Y. Direct Slicing from AutoCAD Solid Models for Rapid Prototyping, International Journal of Advanced Manufacturing Technology, 21(10-11), (2003) 739-742 https://doi.org/10.1007/s00170-002-1316-0

[559] Simsek, S., Yaman, U. Dimensional accuracy improvement of fused filament fabrication holes utilizing modified interior, 19th International Conference on Electrical Machines and Systems, (2016) 7837103 (2017).

[560] Yaman, U. Shrinkage compensation of holes via shrinkage of interior structure in FDM process, International Journal of Advanced Manufacturing Technology 94(5-8), (2018) 2187-2197 https://doi.org/10.1007/s00170-017-1018-2

[561] Jin, Y., He, Y., Fu, G., Zhang, A., Du, J. A non-retraction path planning approach for extrusion-based additive manufacturing, Robotics and Computer-Integrated Manufacturing, 48, (2017) 132-144. https://doi.org/10.1016/j.rcim.2017.03.008

[562] Guerrero-De-Mier, A., Espinosa, M.M., Domínguez, M. Bricking: A New Slicing Method to Reduce Warping, Procedia Engineering, 132, (2015) 126-131 https://doi.org/10.1016/j.proeng.2015.12.488

[563] Ghazanfari, A., Li, W., Leu, M.C. Adaptive rastering algorithm for freeform extrusion fabrication processes, Virtual and Physical Prototyping, 10(3), (2015) 163-172 https://doi.org/10.1080/17452759.2015.1096798

[564] Jin, Y., He, Y., Du, J. A novel path planning methodology for extrusion-based additive manufacturing of thin-walled parts, International Journal of Computer Integrated Manufacturing, 30(12), (2017) 1301-1315 https://doi.org/10.1080/0951192X.2017.1307526

[565] Jensen, M.L., Mahshid, R., D'Angelo, G., Walther, J.U., Kiewning, M.K., Spangenberg, J., Hansen, H.N., Pedersen, D.B. Toolpath strategies for 5DOF and 6DOF extrusion-based additive

manufacturing, Applied Sciences (Switzerland), 9(19),4168 (2019). https://doi.org/10.3390/app9194168

[566] Mohan Pandey, P., Venkata Reddy, N., Dhande, S.G. Slicing procedures in layered manufacturing: A review, Rapid Prototyping Journal, 9 (5), (2003) 274-288. https://doi.org/10.1108/13552540310502185

[567] Chiu, Y.Y., Liao, Y.S., Lee, S.C. Slicing strategies to obtain accuracy of feature relation in rapidly prototyped parts, International Journal of Machine Tools and Manufacture, 44(7-8), (2004) 797-806 https://doi.org/10.1016/j.ijmachtools.2004.01.008

[568] Shoji, A., Tasaki, R., Terashima, K. High-Speed Additive Manufacturing Process Using Variable Motion Trajectory, 2018 IEEE Conference on Control Technology and Applications, CCTA 2018, 8511574, (2018) 483-488 https://doi.org/10.1109/CCTA.2018.8511574

[569] Brooks, H.L., Rennie, A.E.W., Abram, T.N., McGovern, J., Caron, F. Variable Fused Deposition Modelling - Analysis of benefits, concept design and tool path generation, Innovative Developments in Virtual and Physical Prototyping - Proceedings of the 5th International Conference on Advanced Research and Rapid Prototyping, (2012) 511-517

[570] Kuipers, T., Doubrovski, E.L., Wu, J., Wang, C.C.L. A Framework for Adaptive Width Control of Dense Contour-Parallel Toolpaths in Fused Deposition Modeling, CAD Computer Aided Design, 128,102907 (2020). https://doi.org/10.1016/j.cad.2020.102907

[571] Xiong, Y., Park, S.-I., Padmanathan, S., Dharmawan, A. G., Foong, S., Rosen, D.W., Soh, G.S. Process planning for adaptive contour parallel toolpath in additive manufacturing with variable bead width, International Journal of Advanced Manufacturing Technology, 105(10), (2019) 4159-4170 https://doi.org/10.1007/s00170-019-03954-1

[572] Papacharalampopoulos, A., Bikas, H., Stavropoulos, P. Path planning for the infill of 3D printed parts utilizing Hilbert curves, Procedia Manufacturing, 21, (2018) 757-764 https://doi.org/10.1016/j.promfg.2018.02.181

[573] Shaikh, S., Kumar, N., Jain, P.K., Tandon, P. Hilbert curve based toolpath for fdm process, Lecture Notes in Mechanical Engineering, (2016) 751-759 https://doi.org/10.1007/978-81-322-2740-3_72

[574] Wang, Y., Gu, Z., Song, L., Li, T., Cui, H., Lau, F.C.M. Speeding up 3D Printing Using Multi-Head Slicing Algorithms, Proceedings - 2017 5th International Conference on Enterprise Systems: Industrial Digitalization by Enterprise Systems, ES 2017, 8119374, (2017) 99-106 https://doi.org/10.1109/ES.2017.23

[575] Han, W., Jafari, M.A., Seyed, K. Process speeding up via deposition planning in fused deposition-based layered manufacturing processes, Rapid Prototyping Journal, 9 (4), (2003) 212-218. https://doi.org/10.1108/13552540310489596

[576] Lensgraf, S., Mettu, R.R. An improved toolpath generation algorithm for fused filament fabrication, Proceedings - IEEE International Conference on Robotics and Automation, 7989141, (2017) 1181-1187 https://doi.org/10.1109/ICRA.2017.7989141

[577] Tyberg, J., Bøhn, J.H. Local adaptive slicing, Rapid Prototyping Journal, 4 (3), (1998) 118-127. https://doi.org/10.1108/13552549810222993

[578] Hope, R.L., Roth, R.N., Jacobs, P.A. Adaptive slicing with sloping layer surfaces, Rapid Prototyping Journal, 3 (3), (1997) 89-98. https://doi.org/10.1108/13552549710185662

[579] Sreeram, P.N., Dutta, D. Determination of optimal orientation based on variable slicing thickness in layered manufacturing, Technical Report UM-MEAM-94-14, The University of Michigan, Ann Arbor, MI, (1994) (1994).

[580] Byun, H.S., Lee, K.H. Determination of optimal build direction in rapid prototyping with variable slicing, International Journal of Advanced Manufacturing Technology, 28 (3-4), (2006) 307-313. https://doi.org/10.1007/s00170-004-2355-5

[581] Tyberg, J., Bøhn, J.H. FDM systems and local adaptive slicing, Materials and Design, 20(2-3), (1999) 77-82 https://doi.org/10.1016/s0261-3069(99)00012-6

[582] Nadiyapara, H.H., Pande, S. A Review of Variable Slicing in Fused Deposition Modeling, Journal of The Institution of Engineers (India): Series C, 98(3), (2017) 387-393 https://doi.org/10.1007/s40032-016-0272-7

[583] Li, H., Wang, T., Sun, J., Yu, Z. The adaptive slicing algorithm and its impact on the mechanical property and surface roughness of freeform extrusion parts, Virtual and Physical Prototyping, 11(1), (2016) 27-39 https://doi.org/10.1080/17452759.2015.1136868

[584] Singamneni, S., Joe, R.A., Huang, B. Adaptive slicing for Fused Deposition Modeling and practical implementation schemes, Advanced Materials Research, 428, (2012) 137-140 https://doi.org/10.4028/www.scientific.net/AMR.428.137

[585] Deng, A., Badr, Y., Gupta, P. Dynamic programming approach to adaptive slicing for optimization under a global volumetric error constraint, Proceedings of SPIE - The International Society for Optical Engineering, 10523, (2018) 105230B (2018). https://doi.org/10.1117/12.2287944

[586] Fu, G., Fu, J., Lin, Z., Shen, H., Jin, Y. A polygons Boolean operations-based adaptive slicing with sliced data for additive manufacturing, Proceedings of the Institution of Mechanical Engineers, Part C: Journal of Mechanical Engineering Science, 231(15), (2017) 2783-2799 https://doi.org/10.1177/0954406216640576

[587] Mao, H., Kwok, T.-H., Chen, Y., Wang, C.C.L. Adaptive slicing based on efficient profile analysis, CAD Computer Aided Design, 107, (2019) 89-101 https://doi.org/10.1016/j.cad.2018.09.006

[588] Hayasi, M.T., Asiabanpour, B. A new adaptive slicing approach for the fully dense freeform fabrication (FDFF) process, Journal of Intelligent Manufacturing, 24(4), (2013) 683-694 https://doi.org/10.1007/s10845-011-0615-4

[589] Mani, K., Kulkarni, P., Dutta, D. Region-based adaptive slicing, CAD Computer Aided Design, 31 (5), (1999) 317-333. https://doi.org/10.1016/S0010-4485(99)00033-0

[590] Huang, B., Singamneni, S. Adaptive slicing and speed-and time-dependent consolidation mechanisms in fused deposition modeling, Proceedings of the Institution of Mechanical Engineers, Part B: Journal of Engineering Manufacture, 228 (1), (2014) 111-126. https://doi.org/10.1177/0954405413497474

[591] Jin, Y., Du, J., He, Y., Fu, G. Modeling and process planning for curved layer fused deposition, International Journal of Advanced Manufacturing Technology, 91(1-4), (2017) 273-285 https://doi.org/10.1007/s00170-016-9743-5

[592] Huang, B., Singamneni, S.B. Curved layer adaptive slicing (CLAS) for fused deposition modelling, Rapid Prototyping Journal, 21(4), (2015) 354-367 https://doi.org/10.1108/RPJ-06-2013-0059

[593] Singamneni, S., Roychoudhury, A., Diegel, O., Huang, B. Modeling and evaluation of curved layer fused deposition, Journal of Materials Processing Technology, 212(1), (2012) 27-35 https://doi.org/10.1016/j.jmatprotec.2011.08.001

[594] Diegel, O., Singamneni, S., Huang, B., Gibson, I. Curved layer fused deposition modeling in conductive polymer additive manufacturing, Advanced Materials Research, 199-200, (2011) 1984-1987 https://doi.org/10.4028/www.scientific.net/AMR.199-200.1984

[595] Chakraborty, D., Aneesh Reddy, B., Roy Choudhury, A. Extruder path generation for Curved Layer Fused Deposition Modeling, CAD Computer Aided Design, 40(2), (2008) 235-243 https://doi.org/10.1016/j.cad.2007.10.014

[596] Lensgraf, S., Mettu, R.R. Beyond layers: A 3D-aware toolpath algorithm for fused filament fabrication, Proceedings - IEEE International Conference on Robotics and Automation, 2016-June, 7487546, (2016) 3625-3631 https://doi.org/10.1109/ICRA.2016.7487546

[597] Allen, R.J.A., Trask, R.S. An experimental demonstration of effective Curved Layer Fused Filament Fabrication utilising a parallel deposition robot, Additive Manufacturing, 8, (2015) 78-87 https://doi.org/10.1016/j.addma.2015.09.001

[598] Llewellyn-Jones, T., Allen, R., Trask, R. Curved Layer Fused Filament Fabrication Using Automated Toolpath Generation, 3D Printing and Additive Manufacturing, 3(4), (2016) 236-243 https://doi.org/10.1089/3dp.2016.0033

[599] Zhao, D., Li, T., Shen, B., Jiang, Y., Guo, W., Gao, F. A multi-DOF rotary 3D printer: machine design, performance analysis and process planning of curved layer fused deposition modeling (CLFDM), Rapid Prototyping Journal, 26(6), (2020) 1079-1093 https://doi.org/10.1108/RPJ-06-2019-0160

[600] Zhao, H.-M., He, Y., Fu, J.-Z., Qiu, J.-J. Inclined layer printing for fused deposition modeling without assisted supporting structure, Robotics and Computer-Integrated Manufacturing, 51, (2018) 1-13 https://doi.org/10.1016/j.rcim.2017.11.011

[601] Kampker, A., Triebs, J., Kawollek, S., Ayvaz, P., Hohenstein, S. Review on machine designs of material extrusion based additive manufacturing (AM) systems - Status-Quo and potential analysis for future AM systems, Procedia CIRP, 81, (2020) 815-819 https://doi.org/10.1016/j.procir.2019.03.205

[602] Khan, H.A., Ademujimi, T. Development of novel hybrid manufacturing technique for manufacturing support structures free complex parts, ASME 2019 14th International Manufacturing Science and Engineering Conference, MSEC 2019, 1 (2019). https://doi.org/10.1115/MSEC2019-2928

[603] Zhang, H., Sun, Z., Hu, Q., Lammer, H. Research and implementation of integrated methods of unsupported printing and five-axis CNC machining technology, Tehnicki Vjesnik, 26(5), (2019) 1267-1274 https://doi.org/10.17559/TV-20180313125041

[604] Asif, M., Lee, J.H., Lin-Yip, M.J., Chiang, S., Levaslot, A., Giffney, T., Ramezani, M., Aw, K.C. A new photopolymer extrusion 5-axis 3D printer, Additive Manufacturing, 23, (2018) 355-361 https://doi.org/10.1016/j.addma.2018.08.026

[605] Isa, M.A., Lazoglu, I. Five-axis additive manufacturing of freeform models through buildup of transition layers, Journal of Manufacturing Systems, 50, (2019) 69-80 https://doi.org/10.1016/j.jmsy.2018.12.002

[606] Wulle, F., Coupek, D., Schäffner, F., Verl, A., Oberhofer, F., Maier, T. Workpiece and Machine Design in Additive Manufacturing for Multi-Axis Fused Deposition Modeling, Procedia CIRP, 60, (2017) 229-234 https://doi.org/10.1016/j.procir.2017.01.046

[607] Hu, B., Duan, X., Xing, Z., Xu, Z., Du, C., Zhou, H., Chen, R., Shan, B. Improved design of fused deposition modeling equipment for 3D printing of high-performance PEEK parts, Mechanics of Materials, 137,103139 (2019). https://doi.org/10.1016/j.mechmat.2019.103139

[608] Bezukladnikov, I.I., Trushnikov, D.N., Shilova, Y.A., Yuzhakov, A.A., Oskolkov, A.A., Matveev, E.V. Study the possibility of improving induction heating of fdm 3d printer nozzle, International Journal of Mechanical Engineering and Technology, 9(9), (2018) 1463-1474 9766340

[609] Sukindar, N.A., Mohd Ariffin M.K.A., Bin Baharudin B.T.H.T. Comparison on dimensional accuracy using a newly developed nozzle for open-source 3D printer, Applied Mechanics and Materials 859:15-19 (2016). https://doi.org/10.4028/www.scientific.net/AMM.859.15"

[610] Leng, J., Wu, J., Chen, N., Xu, X., Zhang, J. The development of a conical screw-based extrusion deposition system and its application in fused deposition modeling with thermoplastic polyurethane, Rapid Prototyping Journal, 26(2), (2019) 409-417 https://doi.org/10.1108/RPJ-05-2019-0139

[611] Netto, J.M.J., Silveira, Z.D.C. Design of an innovative three-dimensional print head based on twin-screw extrusion, Journal of Mechanical Design, Transactions of the ASME, 140(12), (2018) 125002 (2018). https://doi.org/10.1115/1.4041175

[612] Han, S., Xiao, Y., Qi, T., Li, Z., Zeng, Q. Design and Analysis of Fused Deposition Modeling 3D Printer Nozzle for Color Mixing, Advances in Materials Science and Engineering, 2017,2095137 (2017). https://doi.org/10.1155/2017/2095137

[613] Klar, V., Pearce, J.M., Kärki, P., Kuosmanen, P. Ystruder: Open source multifunction extruder with sensing and monitoring capabilities, HardwareX, 6, e00080 (2019). https://doi.org/10.1016/j.ohx.2019.e00080

[614] Durna, A., Fries, J. Modification of the nozzle assembly in a 3D printer for printing materials with higher melting temperatures, International Multidisciplinary Scientific GeoConference Surveying Geology and Mining Ecology Management, SGEM, 17(62), (2017) 923-930 https://doi.org/10.5593/sgem2017/62/S28.118

[615] Sukindar, N.A., Ariffin, M.K.A., Hang Tuah Baharudin, B.T., Jaafar, C.N.A., Ismail, M.I.S. Analyzing the effect of nozzle diameter in fused deposition modeling for extruding polylactic acid using open source 3D printing, Jurnal Teknologi, 78(10), (2016) 7-15 https://doi.org/10.11113/jt.v78.6265

[616] Shaw, L., Islam, M., Li, J., Li, L., Ayub, S.M.I. High-Speed Additive Manufacturing Through High-Aspect-Ratio Nozzles, JOM, 70(3), (2018) 284-291 https://doi.org/10.1007/s11837-017-2729-4

[617] Gao, Q., Zhou, M., Zhu, L.L. Flow field analysis and structure optimization of the nozzle of FDM 3D printer, Comb Mach Tool Autom Process Technol 537(11):39–42+52 (2018).

[618] Sukindar, N.A., Ariffin, M.K.A.M., Baharudin, B.T.H.T., Jaafar, C.N.A., Ismail, M.I.S. Analysis of mechanical properties of polylactic acid using a new 3D printer nozzle, Journal of Computational and Theoretical Nanoscience, 15(2), (2018) 666-675 https://doi.org/10.1166/jctn.2018.7142

[619] Sukindar, N.A., Ariffin, M.K.A.M., Baharudin, B.T.H.T., Jaafar, C.N.A., Ismail, M.I.S. Effects of nozzle die angle on extruding polymethylmethacrylate in open-source 3D printing, Journal of

Computational and Theoretical Nanoscience, 15(2), (2018) 663-665 https://doi.org/10.1166/jctn.2018.7141

[620] Li, M., Jiang, J., Hu, B., Zhai, W. Fused deposition modeling of hierarchical porous polyetherimide assisted by an in-situ CO2 foaming technology, Composites Science and Technology, 200,108454 (2020). https://doi.org/10.1016/j.compscitech.2020.108454

[621] Li, H.-Y., Lin, Z.-H., Li, B.-L., Chang, C.-L. The study of the die geometry and the characteristics of a non-Newtonian viscoelastic fluid during extrusion, Proceedings of the 2017 IEEE International Conference on Applied System Innovation: Applied System Innovation for Modern Technology, ICASI 2017, 7988236, (2017) 1595-1598 https://doi.org/10.1109/ICASI.2017.7988236

[622] Tsao, C.-C., Chang, H.-H., Liu, M.-H., Chen, H.-C., Hsu, Y.-T., Lin, P.-Y., Chou, Y.-L., Chao, Y.-C., Shen, Y.-H., Huang, C.-Y., Chan, K.-C., Chen, Y.-H. Freeform additive manufacturing by vari-directional vari-dimensional material deposition, Rapid Prototyping Journal, 24(2), (2018) 379-394 https://doi.org/10.1108/RPJ-01-2017-0014

[623] Nienhaus, V., Smith, K., Spiehl, D., Dörsam, E. Investigations on nozzle geometry in fused filament fabrication, Additive Manufacturing, 28, (2019) 711-718 https://doi.org/10.1016/j.addma.2019.06.019

[624] Liu X.J., Wang C.S., Chi B.H. Optimum design of heat transfer structure for grained 3D printer head wood, Plastics 4:113–116 (2018).

[625] Wei, W., Chen, N., Zhang, J., Zhang, X. Design of an intelligent rapid nozzle cleaning control system for fused deposition modelling 3D printers, International Journal of Heat and Technology, 36(2), (2018) 704-708 https://doi.org/10.18280/ijht.360236

[626] Kłodowski, A., Eskelinen, H., Semken, S. Leakage-proof nozzle design for RepRap community 3D printer, Robotica,l 33(4), (2015) 721-746 https://doi.org/10.1017/S0263574714000502

[627] Ravi, A.K., Deshpande, A., Hsu, K.H. An in-process laser localized pre-deposition heating approach to inter-layer bond strengthening in extrusion based polymer additive manufacturing, Journal of Manufacturing Processes, 24, (2016) 179-185 https://doi.org/10.1016/j.jmapro.2016.08.007

[628] Wjesundera, P., Schutte, J., Potgieter, J. The effects of acetone vapour inter-layer processing on fused deposition modelling 3D printed acrylonitrile butadiene styrene, 2017 24th International Conference on Mechatronics and Machine Vision in Practice, M2VIP 2017, 2017-December, (2017) 1-8 https://doi.org/10.1109/M2VIP.2017.8211520

[629] Maidin, S., Wong, J.H.U., Mohamed, A.S., Mohamed, S.B. Effect of vacuum assisted fused deposition modeling on 3D printed ABS microstructure, International Journal of Applied Engineering Research, 12(15), (2017) 4877-4881

[630] Wu, H.-X., Yu, Z.-H., Zhang, H., Yang, Z.-S., Wang, Y. Method for monitoring of FDM 3D printer failure based on acoustic emission, Zhejiang Daxue Xuebao (Gongxue Ban)/Journal of Zhejiang University (Engineering Science), 50(1), (2016) 78-84 https://doi.org/10.3785/j.issn.1008-973X.2016.01.012

[631] Liu, J., Hu, Y., Wu, B., Wang, Y. An improved fault diagnosis approach for FDM process with acoustic emission, Journal of Manufacturing Processes, 35, (2018) 570-579 https://doi.org/10.1016/j.jmapro.2018.08.038

[632] Yang, Z., Jin, L., Yan, Y., Mei, Y. Filament breakage monitoring in fused deposition modeling using acoustic emission technique, Sensors (Switzerland), 18(3), (2018) 749 (2018). https://doi.org/10.3390/s18030749

[633] Tlegenov, Y., Hong, G.S., Lu, W.F. Nozzle condition monitoring in 3D printing, Robotics and Computer-Integrated Manufacturing, 54, (2018) 45-55 https://doi.org/10.1016/j.rcim.2018.05.010

[634] Tlegenov, Y., Wong, Y.S., Hong, G.S. A dynamic model for nozzle clog monitoring in fused deposition modelling, Rapid Prototyping Journal, 23(2), (2017) 391-400 https://doi.org/10.1108/RPJ-04-2016-0054

[635] Kim, J.S., Lee, C.S., Kim, S.-M., Lee, S.W. Development of Data-Driven In-Situ Monitoring and Diagnosis System of Fused Deposition Modeling (FDM) Process Based on Support Vector Machine Algorithm, International Journal of Precision Engineering and Manufacturing - Green Technology, 5(4), (2018) 479-486 https://doi.org/10.1007/s40684-018-0051-4

[636] Baumann, F., Roller, D. Vision based error detection for 3D printing processes, MATEC Web of Conferences, 59, (2016) 06003 (2016). https://doi.org/10.1051/matecconf/20165906003

[637] Wu, Y., He, K., Zhou, X., DIng, W. Machine vision based statistical process control in fused deposition modeling, Proceedings of the 2017 12th IEEE Conference on Industrial Electronics and Applications, ICIEA 2017, 2018-February, (2018) 936-941 https://doi.org/10.1109/ICIEA.2017.8282973

[638] He, K., Zhang, Q., Hong, Y. Profile monitoring based quality control method for fused deposition modeling process, Journal of Intelligent Manufacturing, 30(2), (2018) 947-958 https://doi.org/10.1007/s10845-018-1424-9

[639] Preissler, M., Zhang, C., Rosenberger, M., Notni, G. Platform for 3D inline process control in additive manufacturing, Proceedings of SPIE - The International Society for Optical Engineering, 10329, (2017) 103290R (2017). https://doi.org/10.1117/12.2270493

[640] Preissler, M., Broghammer, J., Rosenberger, M., Notni, G. Inline process monitoring method for geometrical characteristics in additive manufacturing, Journal of Physics: Conference Series, 1044(1), (2018) 012035 (2018). https://doi.org/10.1088/1742-6596/1044/1/012035

[641] Liu, C., Law, A.C.C., Roberson, D., Kong, Z.J. Image analysis-based closed loop quality control for additive manufacturing with fused filament fabrication, Journal of Manufacturing Systems, 51, (2019) 75-86 https://doi.org/10.1016/j.jmsy.2019.04.002

[642] Park, T.J., Go, D.H., Choi, M.S., Kim, B.C., Lee, W.S., Park, S.J. Development of high-precision 3D printers using optics, World Congress on Recent Advances in Nanotechnology, 130 (2018). https://doi.org/10.11159/icnnfc18.130

[643] Nuchitprasitchai, S., Roggeman, M.C., Pearce, J.M. Three Hundred and Sixty Degree Real-Time Monitoring of 3-D Printing Using Computer Analysis of Two Camera Views, Journal of Manufacturing and Materials Processing, 1(1), 2 (2017). https://doi.org/10.3390/jmmp1010002

[644] Shen, H., Sun, W., Fu, J. Multi-view online vision detection based on robot fused deposit modeling 3D printing technology, Rapid Prototyping Journal, 25(2), (2019) 343-355 https://doi.org/10.1108/RPJ-03-2018-0052

[645] Brion, D.A.J., Pattinson, S.W Quantitative and Real-Time Control of 3D Printing Material Flow Through Deep Learning, Advanced Intelligent Systems. 4(11), 2200153 (2022). https://doi.org/10.1002/aisy.202200153

[646] Lianghua, Z. Research on Error Analysis and Online Recognition Method of Contour in 3D Printing, Journal of Physics: Conference Series, 1605(1), 012031 (2020). https://doi.org/10.1088/1742-6596/1605/1/012031

[647] Rao, P.K., Liu, J., Roberson, D., Kong, Z., Williams, C. Online Real-Time Quality Monitoring in Additive Manufacturing Processes Using Heterogeneous Sensors, Journal of Manufacturing Science and Engineering, Transactions of the ASME, 137(6), (2015) 061007 (2015). https://doi.org/10.1115/1.4029823

[648] Rao, P.K., Roberson, D., Liu, J.P., Kong, Z.J. Sensor-based online process fault detection in additive manufacturing, ASME 2015 International Manufacturing Science and Engineering Conference, (2015) 2 (2015). https://doi.org/10.1115/MSEC20159389

[649] Moretti, M., Bianchi, F., Senin, N. Towards the development of a smart fused filament fabrication system using multi-sensor data fusion for in-process monitoring, Rapid Prototyping Journal, 26(7), (2020) 1249-1261 https://doi.org/10.1108/RPJ-06-2019-0167

[650] Kousiatza, C., Karalekas, D. In-situ monitoring of strain and temperature distribution during fused deposition modeling process, Materials and Design, 97, (2016) 400-406 https://doi.org/10.1016/j.matdes.2016.02.099

[651] He, K., Wang, H., Hu, H. Approach to online defect monitoring in fused deposition modeling based on the variation of the temperature field, Complexity, 2018,3426928 (2018). https://doi.org/10.1155/2018/3426928

[652] Coogan, T.J., Kazmer, D.O. In-line rheological monitoring of fused deposition modeling, Journal of Rheology, 63(1), (2019) 141-155 https://doi.org/10.1122/1.5054648

[653] Anderegg, D.A., Bryant, H.A., Ruffin, D.C., Skrip, S.M., Fallon, J.J., Gilmer, E.L., Bortner, M.J. In-situ monitoring of polymer flow temperature and pressure in extrusion based additive manufacturing, Additive Manufacturing, 26, (2019) 76-83 https://doi.org/10.1016/j.addma.2019.01.002

[654] Tlegenov, Y., Lu, W.F., Hong, G.S. A dynamic model for current-based nozzle condition monitoring in fused deposition modelling, Progress in Additive Manufacturing, 4(3), (2019) 211-223 https://doi.org/10.1007/s40964-019-00089-3

[655] Kim, C., Espalin, D., Cuaron, A., Perez, M.A., Macdonald, E., Wicker, R.B. A study to detect a material deposition status in fused deposition modeling technology, IEEE/ASME International Conference on Advanced Intelligent Mechatronics, AIM, 2015-August,7222632, (2015) 779-783 https://doi.org/10.1109/AIM.2015.7222632

[656] Sartori, S., Zhang, G.X. Geometric Error Measurement and Compensation of Machines, CIRP Annals - Manufacturing Technology, 44(2), (1995) 599-609 https://doi.org/10.1016/S0007-8506(07)60507-1

[657] Tong, K., Lehtihet, E.A., Joshi, S. Software compensation of rapid prototyping machines, Precision Engineering, 28(3), (2004) 280-292 https://doi.org/10.1016/j.precisioneng.2003.11.003

[658] Cajal, C., Santolaria, J., Samper, D., Velazquez, J. Efficient volumetric error compensation technique for additive manufacturing machines, Rapid Prototyping Journal 22(1), (2016) 2-19 https://doi.org/10.1108/RPJ-05-2014-0061

[659] Huang, Q. An Analytical Foundation for Optimal Compensation of Three-Dimensional Shape Deformation in Additive Manufacturing, Journal of Manufacturing Science and Engineering, Transactions of the ASME, 138(6), 061010 (2016). https://doi.org/10.1115/1.4032220

[660] Li, S., Liu, T., Xiao, X., Hu, W., Liao, W. Study on Size Error Compensation of Connecting Bracket Based on Fused Deposition Modeling, IOP Conference Series: Materials Science and Engineering, 686(1),012013 (2019). https://doi.org/10.1088/1757-899X/686/1/012013

[661] Rahman, H., John, T.D., Sivadasan, M., Singh, N.K. Investigation on the Scale Factor applicable to ABS based FDM Additive Manufacturing, Materials Today: Proceedings 5(1), (2018) 1640-1648 https://doi.org/10.1016/j.matpr.2017.11.258

[662] Boschetto, A., Bottini, L. Triangular mesh offset aiming to enhance Fused Deposition Modeling accuracy, International Journal of Advanced Manufacturing Technology, 80(1-4), (2015) 99-111 https://doi.org/10.1007/s00170-015-6992-7

[663] Stopp, S., Wolff, T., Irlinger, F., Lueth, T. A new method for printer calibration and contour accuracy manufacturing with 3D-print technology, Rapid Prototyping Journal, 14 (3), (2008) 167-172. https://doi.org/10.1108/13552540810878030

[664] Lyu, J., Manoochehri, S. Error modeling and compensation for FDM machines, Rapid Prototyping Journal, 25(10), (2019) 1565-1574 https://doi.org/10.1108/RPJ-04-2017-0068

[665] Sbaglia, L., Giberti, H., Castelli, K. A simplified approach to the calibration of extrusion based am systems, Mechanisms and Machine Science, 68, (2019) 432-440 https://doi.org/10.1007/978-3-030-03320-0_47

[666] Kuo, C.-C., Mao, R.-C. Development of a Precision Surface Polishing System for Parts Fabricated by Fused Deposition Modeling, Materials and Manufacturing Processes, 31(8), (2016) 1113-1118 https://doi.org/10.1080/10426914.2015.1090594

[667] Kuo, C.-C., Chen, C.-M., Chang, S.-X. Polishing mechanism for ABS parts fabricated by additive manufacturing, International Journal of Advanced Manufacturing Technology, 91(5-8), (2017) 1473-1479 https://doi.org/10.1007/s00170-016-9845-0

[668] Nsengimana, J., Van der Walt, J., Pei, E., Miah, M. Effect of post-processing on the dimensional accuracy of small plastic additive manufactured parts, Rapid Prototyping Journal, 25(1), (2019) 1-12 https://doi.org/10.1108/RPJ-09-2016-0153

[669] Galantucci, L.M., Lavecchia, F., Percoco, G. Quantitative analysis of a chemical treatment to reduce roughness of parts fabricated using fused deposition modeling, CIRP Annals - Manufacturing Technology, 59(1), (2010) 247-250 https://doi.org/10.1016/j.cirp.2010.03.074

[670] Jayanth, N., Senthil, P., Prakash, C. Effect of chemical treatment on tensile strength and surface roughness of 3D-printed ABS using the FDM process, Virtual and Physical Prototyping, 13(3), (2018) 155-163 https://doi.org/10.1080/17452759.2018.1449565

[671] Jo, K.-H., Jeong, Y.-S., Lee, J.-H., Lee, S.-H. A study of post-processing methods for improving the tightness of a part fabricated by fused deposition modeling, International Journal of Precision Engineering and Manufacturing, 17(11), (2016) 1541-1546 https://doi.org/10.1007/s12541-016-0180-z

[672] Haidiezul, A.H.M., Aiman, A.F., Bakar, B. Surface Finish Effects Using Coating Method on 3D Printing (FDM) Parts, IOP Conference Series: Materials Science and Engineering, 318(1), (2018) 012065 (2018). https://doi.org/10.1088/1757-899X/318/1/012065

[673] Garg, A., Bhattacharya, A., Batish, A. On Surface Finish and Dimensional Accuracy of FDM Parts after Cold Vapor Treatment, Materials and Manufacturing Processes, 31(4), (2016) 522-529 https://doi.org/10.1080/10426914.2015.1070425

[674] Mazlan, S.N.H., Alkahari, M.R., Ramli, F.R., Maidin, N.A., Sudin, M.N., Zolkaply, A.R. Surface finish and mechanical properties of FDM part after blow cold vapor treatment, Journal of Advanced Research in Fluid Mechanics and Thermal Sciences, 48(2), (2018) 148-155

[675] Singh, R., Singh, S., Singh, I.P., Fabbrocino, F., Fraternali, F. Investigation for surface finish improvement of FDM parts by vapor smoothing process, Composites Part B: Engineering, 111, (2017) 228-234 https://doi.org/10.1016/j.compositesb.2016.11.062

[676] Singh, J., Singh, R., Singh, H. Investigations for improving the surface finish of FDM based ABS replicas by chemical vapor smoothing process: A case study, Assembly Automation, 37(1), (2017) 13-21 https://doi.org/10.1108/AA-12-2015-127

[677] Chohan, J.S., Singh, R., Boparai, K.S. Parametric optimization of fused deposition modeling and vapour smoothing processes for surface finishing of biomedical implant replicas, Measurement: Journal of the International Measurement Confederation, 94, (2016) 602-613 https://doi.org/10.1016/j.measurement.2016.09.001

[678] Chohan, J.S., Singh, R., Boparai, K.S. Mathematical modelling of surface roughness for vapour processing of ABS parts fabricated with fused deposition modelling, Journal of Manufacturing Processes, 24, (2016) 161-169 https://doi.org/10.1016/j.jmapro.2016.09.002

[679] Lalehpour, A., Barari, A. Post processing for Fused Deposition Modeling Parts with Acetone Vapour Bath, IFAC-PapersOnLine, 49(31), (2016) 42-48 https://doi.org/10.1016/j.ifacol.2016.12.159

[680] Lalehpour, A., Janeteas, C., Barari, A. Surface roughness of FDM parts after post-processing with acetone vapor bath smoothing process, International Journal of Advanced Manufacturing Technology, 95(1-4), (2018) 1505-1520 https://doi.org/10.1007/s00170-017-1165-5

[681] Beniak, J., Križan, P., Šooš, Ľ., Matuš, M. Roughness and compressive strength of FDM 3D printed specimens affected by acetone vapour treatment, IOP Conference Series: Materials Science and Engineering, 297(1), (2018) 012018 (2018). https://doi.org/10.1088/1757-899X/297/1/012018

[682] Coppola, A., Impero, F., Ruggiero, C., Scala, F., Squillace, A. Set-up of an experimental procedure for the surface smoothing of FDM parts through acetone vapor, Key Engineering Materials, 813 KEM, (2019) 447-452 https://doi.org/10.4028/www.scientific.net/KEM.813.447

[683] Chohan, J.S., Singh, R., Boparai, K.S. Multi response optimization and process capability analysis of fused filament fabrication and chemical vapor smoothing operations for rapid casting of biomedical implants, ASME 2019 14th International Manufacturing Science and Engineering Conference, MSEC 2019 1 (2019). https://doi.org/10.1115/MSEC2019-2739

[684] Nguyen, T.K., Lee, B.-K. Post-processing of FDM parts to improve surface and thermal properties, Rapid Prototyping Journal, 24(7), (2018) 1091-1100 https://doi.org/10.1108/RPJ-12-2016-0207

[685] Krishna, A.V., Faulcon, M., Timmers, B., Reddy, V.V., Barth, H., Nilsson, G., Rosén, B.G. Influence of different post-processing methods on surface topography of fused deposition modelling samples, Surface Topography: Metrology and Properties, 8(1),014001 (2020). https://doi.org/10.1088/2051-672X/ab77d7

[686] Dixit, N.K., Srivastava, R., Narain, R. Improving surface roughness of the 3D printed part using electroless plating, Proceedings of the Institution of Mechanical Engineers, Part L: Journal of Materials: Design and Applications, (2017) (2017). https://doi.org/10.1177/1464420717719920

[687] Jin, Y., Wan, Y., Zhang, B., Liu, Z. Modeling of the chemical finishing process for polylactic acid parts in fused deposition modeling and investigation of its tensile properties, Journal of Materials Processing Technology, 240, (2017) 233-239 https://doi.org/10.1016/j.jmatprotec.2016.10.003

[688] Hu, Z., Lee, K., Hur, J. Determination of optimal build orientation for hybrid rapid-prototyping, Journal of Materials Processing Technology, 130-131, (2002) 378-383. https://doi.org/10.1016/S0924-0136(02)00727-6

[689] Amanullah, A.N.M., Murshiduzzaman, Saleh, T., Khan, R. Design and Development of a Hybrid Machine Combining Rapid Prototyping and CNC Milling Operation, Procedia Engineering 184, (2017) 163-170 https://doi.org/10.1016/j.proeng.2017.04.081

[690] Boschetto, A., Bottini, L., Veniali, F. Finishing of Fused Deposition Modeling parts by CNC machining, Robotics and Computer-Integrated Manufacturing, 41, (2016) 92-101 https://doi.org/10.1016/j.rcim.2016.03.004

[691] Del-Sol, I., Domínguez-Calvo, A., Piñero, D., Salguero, J., Batista, M. Study of the FDM parameters of the ABS parts in the surface quality after machining operations, Key Engineering Materials, 813 KEM, (2019) 203-208 https://doi.org/10.4028/www.scientific.net/KEM.813.203

[692] Kale, A., Kumar, A.L., Murali Krishna Kumar, M., Prakasah, M. Optimization of hybrid manufacturing process parameters by using FDM in CNC machine, IOP Conference Series: Materials Science and Engineering, 402(1), 012088 (2018). https://doi.org/10.1088/1757-899X/402/1/012088

[693] Parenti, P., Cataldo, S., Grigis, A., Covelli, M., Annoni, M. Implementation of hybrid additive manufacturing based on extrusion of feedstock and milling, 47th SME North American Manufacturing Research Conference, Penn State Behrend Erie, Pennsylvania (2019). https://doi.org/10.1016/j.promfg.2019.06.230

[694] Pandey, P.M., Reddy, N.V., Dhande, S.G. Virtual hybrid-FDM system to enhance surface finish, Virtual and Physical Prototyping, 1(2), (2006) 101-116 https://doi.org/10.1080/17452750600763905

[695] Grguraš, D., Kramar, D. Optimization of hybrid manufacturing for surface quality, material consumption and productivity improvement, Strojniski Vestnik/Journal of Mechanical Engineering, 63(10), (2017) 567-576 https://doi.org/10.5545/sv-jme.2017.4396

[696] Boschetto, A., Bottini, L. Roughness prediction in coupled operations of fused deposition modeling and barrel finishing, Journal of Materials Processing Technology, 219, (2015) 181-192 https://doi.org/10.1016/j.jmatprotec.2014.12.021

[697] Boschetto, A., Bottini, L. Surface improvement of fused deposition modeling parts by barrel finishing, Rapid Prototyping Journal, 21(6), (2015) 686-696 https://doi.org/10.1108/RPJ-10-2013-0105

[698] Taufik, M., Jain, P.K. Development and analysis of accurate and adaptive FDM post-finishing approach, 3D Printing and Additive Manufacturing Technologies, (2018) 59-71 https://doi.org/10.1007/978-981-13-0305-0_6

[699] Chen, Y.-F., Wang, Y.-H., Tsai, J.-C. Enhancement of surface reflectivity of fused deposition modeling parts by post-processing, Optics Communications, 430, (2019) 479-485 https://doi.org/10.1016/j.optcom.2018.07.011

[700] Taufik, M., Jain, P.K. Laser assisted finishing process for improved surface finish of fused deposition modelled parts, Journal of Manufacturing Processes, 30, (2017) 161-177 https://doi.org/10.1016/j.jmapro.2017.09.020

[701] Adel, M., Abdelaal, O., Gad, A., Nasr, A.B., Khalil, A. Polishing of fused deposition modeling products by hot air jet: Evaluation of surface roughness, Journal of Materials Processing Technology, 251, (2018) 73-82 https://doi.org/10.1016/j.jmatprotec.2017.07.019

[702] Wach, R.A., Wolszczak, P., Adamus-Wlodarczyk, A. Enhancement of Mechanical Properties of FDM-PLA Parts via Thermal Annealing, Macromolecular Materials and Engineering, 303(9), (2018) 1800169 (2018). https://doi.org/10.1002/mame.201800169

[703] Rangisetty, S., Peel, L.D. The effect of infill patterns and annealing on mechanical properties of additively manufactured thermoplastic composites, ASME 2017 Conference on Smart Materials, Adaptive Structures and Intelligent Systems, (2017) 1 (2017). https://doi.org/10.1115/SMASIS2017-4011

[704] Hart, K.R., Dunn, R.M., Sietins, J.M., Hofmeister Mock, C.M., Mackay, M.E., Wetzel, E.D. Increased fracture toughness of additively manufactured amorphous thermoplastics via thermal annealing, Polymer, 144, (2018) 192-204 https://doi.org/10.1016/j.polymer.2018.04.024

[705] Ravoori, D., Lowery, C., Prajapati, H., Jain, A. Experimental and theoretical investigation of heat transfer in platform bed during polymer extrusion based additive manufacturing, Polymer Testing, 73, (2019) 439-446 https://doi.org/10.1016/j.polymertesting.2018.11.025

[706] Coogan, T.J., Kazmer, D.O. Bond and part strength in fused deposition modeling, Rapid Prototyping Journal, 23(2), (2017) 414-422 https://doi.org/10.1108/RPJ-03-2016-0050

[707] Li, L., Sun, Q., Bellehumeur, C., Gu, P. Composite Modeling and Analysis for Fabrication of FDM Prototypes with Locally Controlled Properties, Journal of Manufacturing Processes, 4(2), (2002) 129-141 https://doi.org/10.1016/S1526-6125(02)70139-4

[708] Bellehumeur, C., Li, L., Sun, Q., Gu, P. Modeling of bond formation between polymer filaments in the fused deposition modeling process, Journal of Manufacturing Processes, 6 (2), (2004) 170-178 https://doi.org/10.1016/S1526-6125(04)70071-7

[709] Shahriar, B.B., France, C., Valerie, N., Arthur, C., Christian, G. Toward improvement of the properties of parts manufactured by FFF (fused filament fabrication) through understanding the influence of temperature and rheological behaviour on the coalescence phenomenon, AIP Conference Proceedings, 1896, (2017) 040008 (2017). https://doi.org/10.1063/1.5008034

[710] Gurrala, P.K., Regalla, S.P. Part strength evolution with bonding between filaments in fused deposition modelling: This paper studies how coalescence of filaments contributes to the strength of final FDM part, Virtual and Physical Prototyping, 9(3), (2014) 141-149 https://doi.org/10.1080/17452759.2014.913400

[711] Davis, C.S., Hillgartner, K.E., Han, S.H., Seppala, J.E. Mechanical strength of welding zones produced by polymer extrusion additive manufacturing, Additive Manufacturing, 16, (2017) 162-166. https://doi.org/10.1016/j.addma.2017.06.006

[712] Zhang, W., Cotton, C., Sun, J., Heider, D., Gu, B., Sun, B., Chou, T.-W. Interfacial bonding strength of short carbon fiber/acrylonitrile-butadiene-styrene composites fabricated by fused deposition modeling, Composites Part B: Engineering, 137, (2018) 51-59 https://doi.org/10.1016/j.compositesb.2017.11.018

[713] Yin, J., Lu, C., Fu, J., Huang, Y., Zheng, Y. Interfacial bonding during multi-material fused deposition modeling (FDM) process due to inter-molecular diffusion, Materials and Design, 150, (2018) 104-112 https://doi.org/10.1016/j.matdes.2018.04.029

[714] McIlroy, C., Olmsted, P.D. Disentanglement effects on welding behaviour of polymer melts during the fused-filament-fabrication method for additive manufacturing, Polymer, 123, (2017) 376-391 https://doi.org/10.1016/j.polymer.2017.06.051

[715] Khoshnevis, B., Dutton, R. Innovative rapid prototyping process makes large sized, smooth surfaced complex shapes in a wide variety of materials, Materials Technology, 13(2), (1998) 53-56 https://doi.org/10.1080/10667857.1998.11752766

[716] Khoshnevis, B. Automated construction by contour crafting - Related robotics and information technologies, Automation in Construction, 13(1), (2004) 5-19 https://doi.org/10.1016/j.autcon.2003.08.012

[717] Bukkanatnam, S., Clark, B. Dynamic modeling and monitoring of contour crafting - An extrusion-based layered manufacturing process, Journal of Manufacturing Science and Engineering, Transactions of the ASME, 129 (1), (2007) 135-142. https://doi.org/10.1115/1.2375137

[718] Kwon, H.-K., Kim, K.-S. Effect of orifice shape in contour crafting with ceramic material: a simulation for extrusion and deposition mechanism, Advanced Materials Research, 24-25, (2007) 953-956 https://doi.org/10.4028/0-87849-463-4.953

[719] Liu, Z., Li, M., Tay, Y.W.D., Weng, Y., Wong, T.N., Tan, M.J. Rotation nozzle and numerical simulation of mass distribution at corners in 3D cementitious material printing, Additive Manufacturing, 34,101190 (2020). https://doi.org/10.1016/j.addma.2020.101190

[720] Khoshnevis, B., Bukkapatnam, S., Kwon, H., Saito, J. Experimental investigation of contour crafting using ceramics materials, Rapid Prototyping Journal, 7(1), (2001) 32-41 https://doi.org/10.1108/13552540110365144

[721] Khoshnevis, B., Yuan, X., Zahiri, B., Zhang, J., Xia, B. Construction by contour crafting using sulfur concrete with planetary applications, Rapid Prototyping Journal, 22(5), (2016) 848-856 https://doi.org/10.1108/RPJ-11-2015-0165

[722] Shirooyeh, M., Vali, M., Shackleford, D., Torabi, P., Rehrig, P.W., Kwon, O.-H., Khoshnevis, B. Contour crafting of advanced ceramic materials, Ceramic Engineering and Science Proceedings, 36(6), (2016) 159-168 ISBN: 978-111904043-9

[723] Lao, W., Tay, Y.W.D., Quirin, D., Tan, M.J. The effect of nozzle shapes on the compactness and strength of structures printed by additive manufacturing of concrete, Proceedings of the International Conference on Progress in Additive Manufacturing, 2018-May, (2018) 80-86 https://doi.org/10.25341/D4V01X

[724] Lao, W., Li, M., Wong, T.N., Tan, M.J., Tjahjowidodo, T. Improving surface finish quality in extrusion-based 3D concrete printing using machine learning-based extrudate geometry control, Virtual and Physical Prototyping, 15(2), (2020) 178-193 https://doi.org/10.1080/17452759.2020.1713580

[725] Khoshnevis, B., Hwang, D., Yao, K.-T., Yeh, Z. Mega-scale fabrication by Contour Crafting, International Journal of Industrial and Systems Engineering, 1(3), (2006) 301-320 https://doi.org/10.1504/IJISE.2006.009791

[726] Bosscher, P., Williams II, R.L., Bryson, L.S., Castro-Lacouture, D. Cable-suspended robotic contour crafting system, Automation in Construction, 17(1), (2007) 45-55 https://doi.org/10.1016/j.autcon.2007.02.011

[727] Zareiyan, B., Khoshnevis, B. Interlayer adhesion and strength of structures in Contour Crafting - Effects of aggregate size, extrusion rate, and layer thickness, Automation in Construction, 81, (2017) 112-121 https://doi.org/10.1016/j.autcon.2017.06.013

[728] Zhang, J., Khoshnevis, B. Optimal machine operation planning for construction by Contour Crafting, Automation in Construction, 29, (2013) 50-67 https://doi.org/10.1016/j.autcon.2012.08.006

[729] Davtalab, O., Kazemian, A., Khoshnevis, B. Perspectives on a BIM-integrated software platform for robotic construction through Contour Crafting, Automation in Construction, 89, (2018) 13-23 https://doi.org/10.1016/j.autcon.2018.01.006

[730] Williams II, R.L., Xin, M., Bosscher, P. Contour-crafting-cartesian-cable robot system concepts: Workspace and stiffness comparisons, Proceedings of the ASME Design Engineering Technical Conference, 2(PARTS A AND B), (2008) 31-38 https://doi.org/10.1115/DETC2008-49478

[731] Kwon, H., Bukkapatnam, S., Khoshnevis, B., Saito, J. Effects of orifice shape in contour crafting of ceramic materials, Rapid Prototyping Journal, 8(3), (2002) 147-160 https://doi.org/10.1108/13552540210430988

[732] Yeh, Z., Khoshnevis, B. Geometric conformity analysis for automated fabrication processes generating ruled surfaces: Demonstration for contour crafting, Rapid Prototyping Journal, 15(5), (2009) 361-369 https://doi.org/10.1108/13552540910993897

[733] Kwon, H.-K., Jang, M.-K. 3D free form fabrication using the pivoting side trowel with ceramic material, Materials Science Forum, 658, (2010) 268-271 https://doi.org/10.4028/www.scientific.net/MSF.658.268

[734] Zhang, J., Khoshnevis, B. Contour crafting process planning and optimization, 2009 26th International Symposium on Automation and Robotics in Construction, ISARC 2009, (2009) 576-583 https://doi.org/10.22260/isarc2009/0028

[735] Wüthrich, M., Gubser, M., Elspass, W.J., Jaeger, C. Novel 4-Axis 3D printing process to print overhangs without support material, Applied Sciences (Switzerland). 11(18), 8760 (2021). https://doi.org/10.3390/app11188760

[736] Raney, J.R., Compton, B.G., Mueller, J., Ober, T.J., Shea, K., Lewis, J.A. , Rotational 3D printing of damage-tolerant composites with programmable mechanics, Proceedings of the National Academy of Sciences of the United States of America 115(6), (2018) 1198-1203 https://doi.org/10.1073/pnas.1715157115

12. APPENDIX

12.1. MATERIAL EXTRUSION ADDITIVE MANUFACTURING ACCURACY AND PRECISION

GD&T definitions;

Cylindricity – measure of roundness and straightness along a cyclinder's axis

Circularity – a 2D slice measure similar to cyclindricity without the straightness along the axis measure. A measure of how closely the shape of an object approaches that of a mathematically perfect circle, within two circular boundaries

Concentricity/Coaxiality - deviation of feature axis against a datum axis

Flatness - straightness in multiple dimensions, measured between the highest and lowest points on a surface representing upper and lower planes

Parallelism - straightness at a distance, the degree of deviation between two line or planar features

Straightness – deviation from a single dimensional datum

Perpendicularity – flatness perpendicular to a datum plane or line, defined between two planes

Angle deviation – also called angularity, flatness at an angle to a datum utilising an upper and lower plane

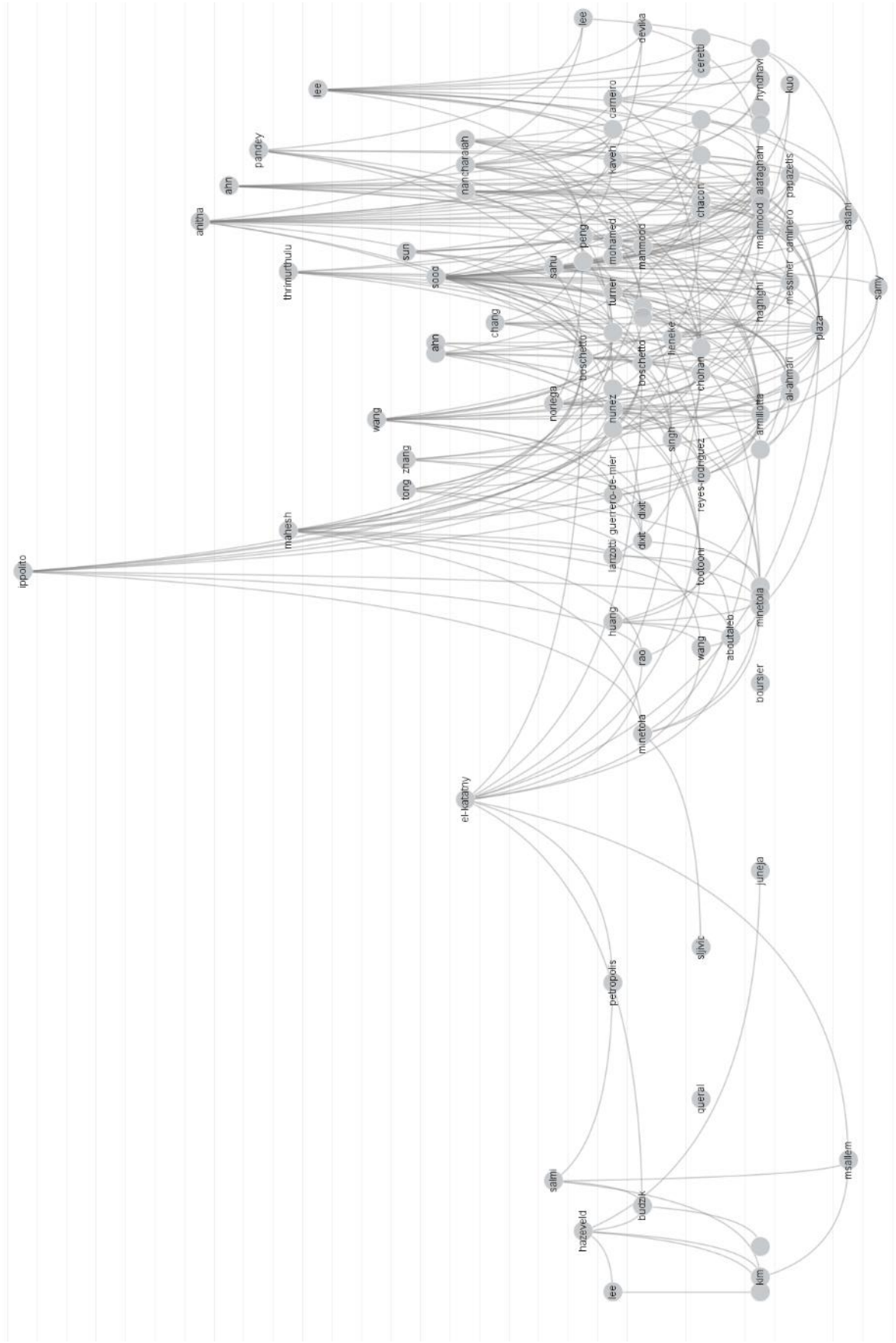

Figure 12.1: *Citation network of key publications*

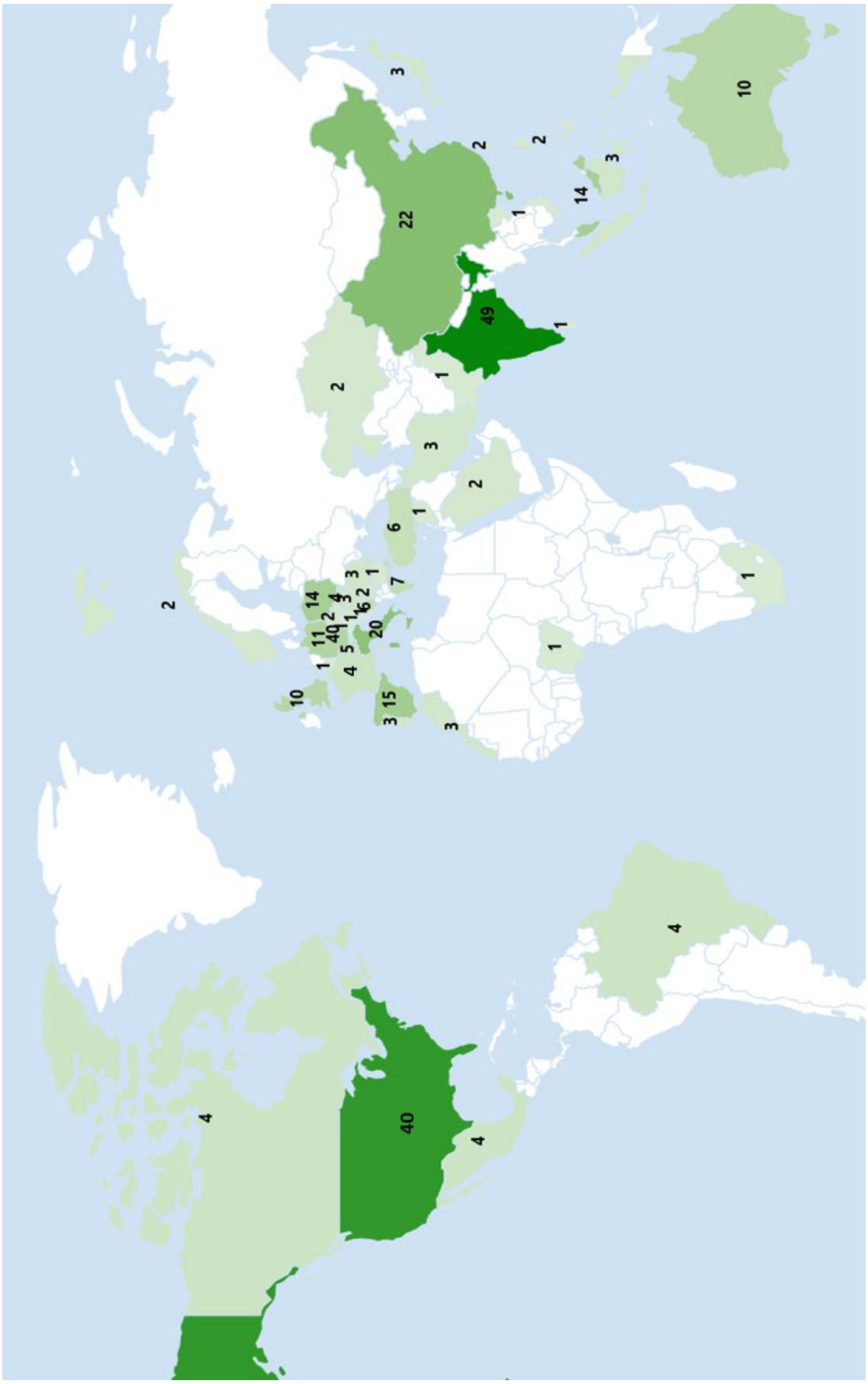

Figure 12.2: *Experimental study geographic distribution (Worldwide)*

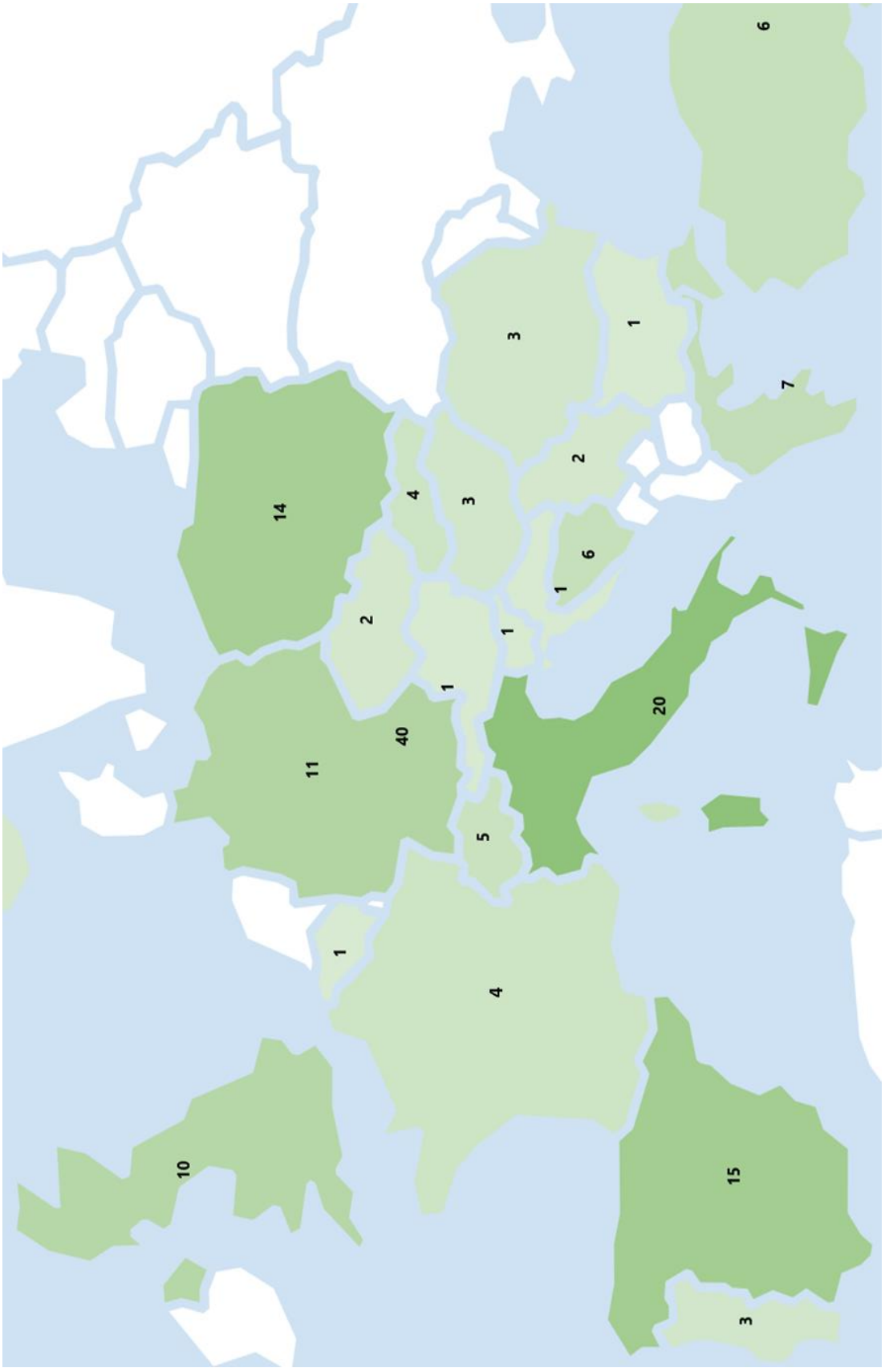

Figure 12.3: *Experimental study geographic distribution (Europe)*

12.2. CURRENT ME AM PERFORMANCE

X axis	Overall	Level 1	Level 2	Level 3	Level 4	Level 5	Centre	Corner
Mean	-0.006	-0.185	-0.094	0.030	0.095	0.124	-0.011	-0.001
Max.	0.480	0.400	0.280	0.210	0.340	0.480	0.480	0.380
Min.	-0.390	-0.390	-0.280	-0.160	-0.330	-0.180	-0.390	-0.330
SD	0.152	0.114	0.082	0.069	0.112	0.102	0.167	0.136
Y axis	**Overall**	**Level 1**	**Level 2**	**Level 3**	**Level 4**	**Level 5**	**Centre**	**Corner**
Mean	0.111	0.045	0.160	0.159	0.138	0.052	0.064	0.158
Max.	0.620	0.380	0.530	0.460	0.620	0.220	0.620	0.380
Min.	-0.260	-0.200	-0.030	-0.040	-0.130	-0.260	-0.260	-0.160
SD	0.112	0.136	0.094	0.080	0.093	0.084	0.113	0.089
Z axis	**Overall**	**Level 1**	**Level 2**	**Level 3**	**Level 4**	**Level 5**	**Centre**	**Corner**
Mean	-0.045	-0.025	-0.047	-0.054	-0.052	-0.047	-0.042	-0.049
Max.	0.210	0.140	0.160	0.130	0.210	0.160	0.210	0.160
Min.	-0.240	-0.200	-0.200	-0.220	-0.240	-0.230	-0.160	-0.240
SD	0.069	0.068	0.062	0.065	0.074	0.073	0.052	0.083

Table 12.1 *ANet A8 summary table of dimensional accuracy and precision (all measurements in mm)*

X axis	Overall	Level 1	Level 2	Level 3	Level 4	Level 5	Centre	Corner
Mean	0.032	-0.078	-0.055	0.029	0.144	0.122	0.057	0.008
Max.	0.510	0.200	0.200	0.380	0.430	0.510	0.510	0.430
Min.	-0.300	-0.300	-0.290	-0.190	-0.150	-0.140	-0.210	-0.300
SD	0.128	0.096	0.097	0.091	0.083	0.092	0.117	0.134
Y axis	**Overall**	**Level 1**	**Level 2**	**Level 3**	**Level 4**	**Level 5**	**Centre**	**Corner**
Mean	0.132	0.030	0.055	0.102	0.231	0.240	0.108	0.155
Max.	0.680	0.240	0.360	0.370	0.680	0.450	0.680	0.610
Min.	-0.240	-0.240	-0.190	-0.150	0.040	-0.020	-0.240	-0.180
SD	0.144	0.118	0.122	0.122	0.114	0.092	0.144	0.140
Z axis	**Overall**	**Level 1**	**Level 2**	**Level 3**	**Level 4**	**Level 5**	**Centre**	**Corner**
Mean	-0.065	-0.038	-0.044	-0.055	-0.077	-0.106	-0.039	-0.091
Max.	0.120	0.120	0.100	0.090	0.060	0.090	0.120	0.110
Min.	-0.260	-0.240	-0.250	-0.250	-0.230	-0.260	-0.210	-0.260
SD	0.068	0.068	0.062	0.066	0.059	0.063	0.057	0.069

Table 12.2 *MakerBot Replicator summary table of dimensional accuracy and precision (all measurements in mm)*

X axis	Overall	Level 1	Level 2	Level 3	Level 4	Level 5	Centre	Corner
Mean	0.150	0.124	0.153	0.160	0.152	0.160	0.138	0.162
Max.	0.510	0.230	0.360	0.340	0.430	0.510	0.510	0.430
Min.	-0.090	-0.090	-0.080	0.020	0.000	-0.080	-0.080	-0.090
SD	0.072	0.057	0.059	0.058	0.073	0.099	0.069	0.073
Y axis	**Overall**	**Level 1**	**Level 2**	**Level 3**	**Level 4**	**Level 5**	**Centre**	**Corner**
Mean	0.159	0.122	0.169	0.173	0.180	0.149	0.173	0.144
Max.	0.540	0.220	0.350	0.340	0.290	0.540	0.290	0.540
Min.	-0.100	-0.060	-0.010	0.000	0.040	-0.100	-0.100	-0.060
SD	0.063	0.050	0.061	0.053	0.041	0.082	0.057	0.065
Z axis	**Overall**	**Level 1**	**Level 2**	**Level 3**	**Level 4**	**Level 5**	**Centre**	**Corner**
Mean	-0.188	-0.087	-0.179	-0.203	-0.221	-0.242	-0.193	-0.183
Max.	0.040	0.040	0.000	-0.040	-0.060	-0.060	0.030	0.040
Min.	-0.390	-0.180	-0.300	-0.330	-0.350	-0.390	-0.310	-0.390
SD	0.084	0.042	0.064	0.068	0.068	0.074	0.067	0.098

Table 12.3 *Ultimaker 3 summary table of dimensional accuracy and precision (all measurements in mm)*

12.3. MACHINE POSITIONAL PERFORMANCE

12.3.1. EXTRUSION MECHANISM ERROR

Nominal distance (mm)	Measurement 1 (mm)	Measurement 2 (mm)	Measurement 3 (mm)	Measurement 1 (%)	Measurement 2 (%)	Measurement 3 (%)
50	-0.50	0.50	0.00	-1.0%	1.0%	0.0%
100	-1.00	1.00	0.00	-1.0%	1.0%	0.0%
150	-0.50	0.50	0.50	-0.3%	0.3%	0.3%
200	-1.00	0.00	0.50	-0.5%	0.0%	0.3%
250	-1.50	0.00	0.50	-0.6%	0.0%	0.2%
300	-1.50	0.50	0.50	-0.5%	0.2%	0.2%
350	-1.50	1.00	0.00	-0.4%	0.3%	0.0%
400	-1.50	1.00	-0.50	-0.4%	0.3%	-0.1%
450	-1.00	1.00	-1.00	-0.2%	0.2%	-0.2%
500	-0.50	1.50	-0.50	-0.1%	0.3%	-0.1%

Table 12.4 *ANet A8 extrusion length error*

Nominal distance (mm)	Measurement 1 (mm)	Measurement 2 (mm)	Measurement 3 (mm)	Measurement 1 (%)	Measurement 2 (%)	Measurement 3 (%)
50	-2.00	-2.00	-2.00	-4.0%	-4.0%	-4.0%
100	-3.00	-3.00	-2.50	-3.0%	-3.0%	-2.5%
150	-5.00	-5.50	-5.00	-3.3%	-3.7%	-3.3%
200	-7.00	-7.00	-7.00	-3.5%	-3.5%	-3.5%
250	-8.00	-8.00	-7.50	-3.2%	-3.2%	-3.0%
300	-9.00	-9.50	-9.00	-3.0%	-3.2%	-3.0%
350	-10.50	-10.50	-10.00	-3.0%	-3.0%	-2.9%
400	-12.00	-12.50	-12.00	-3.0%	-3.1%	-3.0%
450	-13.50	-14.00	-13.50	-3.0%	-3.1%	-3.0%
500	-14.50	-15.00	-14.50	-2.9%	-3.0%	-2.9%

Table 12.5 *Creality Ender-5 Pro extrusion length error*

12.3.2. MEASURED FILAMENT DIAMETER DIMENSIONAL ERRORS

Measurement No.	Vellemann PLA Orange 1	Vellemann PLA Orange 2	Vellemann PLA Yellow 1	Vellemann PLA Dark Blue 1	Vellemann PLA Natural 1	Vellemann PLA Light Blue 1	Vellemann PLA Light Blue 2	Vellemann PET Natural 1	Multicomp TPU-95A Black 1	Polymaker PLA Red 1
1	-0.02	0.00	-0.02	-0.02	0.01	0.02	0.03	0.00	0.03	0.01
2	-0.02	0.01	-0.02	0.01	0.02	0.03	0.00	0.01	0.02	0.00
3	0.02	0.02	0.01	-0.01	0.02	0.05	-0.03	-0.01	0.01	0.00
4	0.01	0.03	0.02	0.00	0.04	0.05	0.00	0.01	0.02	0.00
5	0.03	0.03	-0.01	-0.03	0.03	0.04	0.01	0.00	0.01	0.01
6	-0.03	0.02	0.00	-0.02	0.02	0.04	0.02	0.00	0.01	0.00
7	0.01	0.02	0.01	-0.01	0.02	0.06	0.02	0.01	0.02	0.00
8	0.03	0.00	0.01	0.01	0.00	0.03	0.03	0.00	0.01	-0.01
9	0.02	0.02	0.01	-0.02	0.02	0.04	0.00	0.00	0.02	0.00
10	0.01	-0.01	0.02	-0.02	0.00	0.04	0.01	0.01	0.02	0.00
11	0.00	-0.01	0.01	-0.01	0.02	0.06	0.00	0.00	0.02	0.01
12	0.01	0.00	0.00	-0.03	-0.01	0.05	0.01	0.00	0.02	0.01
13	0.03	-0.01	0.00	0.00	0.02	0.05	0.02	0.00	0.01	0.00
14	0.02	0.01	-0.01	-0.03	0.02	0.01	0.02	0.01	0.00	-0.01
15	0.02	0.02	-0.01	0.00	0.03	0.02	0.00	0.00	0.02	0.00
16	0.00	0.02	0.00	0.00	0.00	0.04	0.01	0.00	0.00	0.00
17	-0.01	0.00	0.01	0.00	0.00	0.00	0.00	0.01	0.00	0.02
18	-0.01	-0.01	0.00	0.01	0.02	0.03	-0.02	0.01	0.02	-0.01
19	-0.02	0.01	-0.01	0.00	0.02	0.01	0.01	0.00	0.02	-0.01
20	-0.01	0.02	0.00	0.01	0.01	0.02	-0.01	-0.01	0.01	-0.01
21	0.01	0.00	0.00	0.00	0.03	0.02	0.03	0.01	0.04	0.02
22	0.01	-0.01	0.00	-0.02	0.04	0.02	0.03	0.01	0.03	0.00
23	0.01	0.03	0.00	-0.01	0.02	0.04	-0.01	0.02	0.04	0.00
24	0.00	0.01	0.01	0.00	0.04	0.02	0.00	0.01	0.03	-0.02
25	0.00	-0.01	-0.01	0.00	0.03	0.03	-0.03	0.01	0.04	0.01
26	-0.01	0.01	-0.02	0.00	0.04	0.01	0.00	0.00	0.04	0.02
27	-0.01	0.02	-0.01	-0.01	0.04	0.02	-0.04	0.00	0.03	0.00
28	-0.01	0.00	-0.01	0.01	0.03	0.02	-0.02	0.01	0.03	-0.01
29	-0.02	0.01	-0.03	-0.02	0.04	0.04	-0.03	0.01	0.04	0.01
30	0.00	0.01	0.01	0.01	0.01	0.03	-0.04	0.01	0.04	0.01
31	0.02	0.03	0.02	0.01	0.02	0.01	0.02	0.01	0.01	0.01
32	0.02	-0.01	0.01	0.02	0.03	0.04	-0.03	0.01	0.04	-0.01
33	0.02	0.00	0.01	0.00	0.04	0.05	-0.02	0.00	0.02	0.01
34	0.01	-0.02	0.01	0.01	0.03	0.05	-0.01	0.00	0.01	-0.01
35	0.02	0.03	0.01	-0.01	0.02	0.04	-0.01	0.01	0.01	0.02
36	0.01	-0.02	0.00	-0.01	0.03	0.04	-0.02	0.01	0.03	0.01
37	0.02	-0.01	0.01	0.02	0.03	0.02	-0.02	0.01	0.03	0.02
38	0.03	0.01	0.01	0.02	0.02	-0.01	0.01	-0.01	0.02	0.01
39	0.01	0.00	0.01	0.00	0.02	0.02	-0.01	0.00	0.03	0.03
40	0.01	0.00	0.02	-0.01	0.03	0.04	0.01	-0.02	0.02	0.02
41	0.01	0.01	0.00	0.00	0.04	0.03	-0.03	-0.01	0.00	0.02
42	-0.01	0.02	0.00	0.02	0.03	0.01	0.01	-0.01	0.01	0.01
43	-0.01	0.01	-0.01	-0.02	0.04	0.03	0.03	0.00	0.03	0.00
44	-0.01	-0.01	0.02	0.01	0.04	0.01	-0.03	-0.01	0.00	0.00
45	0.01	0.01	0.01	-0.01	0.01	0.04	0.02	0.00	0.01	-0.01
46	0.02	0.01	0.01	0.02	0.04	0.00	0.01	0.00	0.00	0.01
47	0.03	0.00	0.00	-0.02	0.04	0.02	0.00	0.00	-0.01	0.01
48	-0.02	-0.01	-0.01	-0.01	0.00	0.02	0.00	-0.01	0.02	0.00
49	0.01	0.02	-0.01	-0.02	0.01	0.01	-0.01	0.00	0.02	0.01
50	0.01	0.00	-0.01	-0.02	-0.01	-0.02	0.03	-0.01	0.03	-0.02

Table 12.6 *Measured Filament Diameter Errors (mm)*

12.4. STEADY-STATE FILAMENT MORPHOLOGY

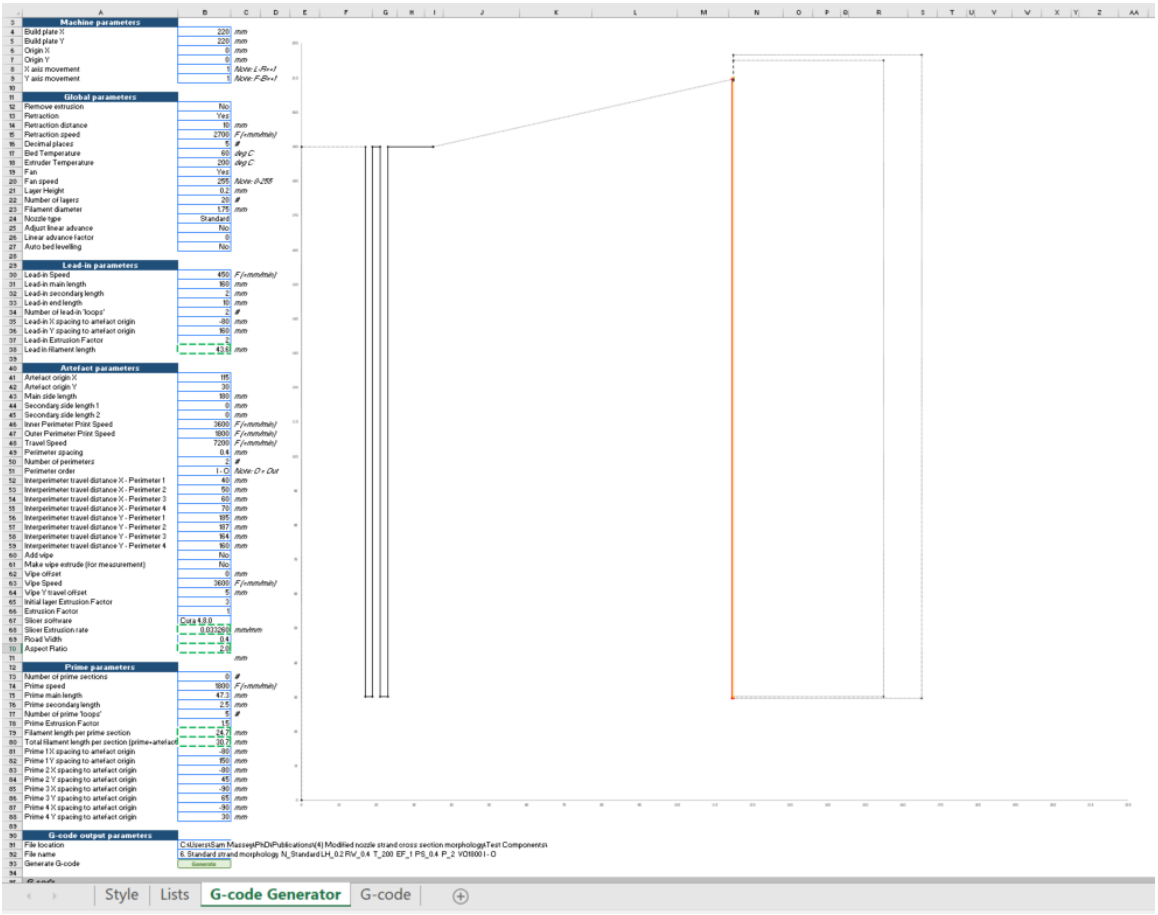

Figure 12.4: *Custom G-code generator for steady state filament morphology*

Number	Cross-sectional area (%)	Layer height (mm)	Road width (mm)	Bond width (mm)	Horizontal deviations (mm)	Rz (mm)	Ra (mm)	Rq (mm)
1	83.0	0.096	0.192	0.136	0.005	0.035	0.007	0.009
2	92.0	0.100	0.251	0.191	0.006	0.045	0.008	0.010
3	88.0	0.099	0.286	0.224	0.003	0.039	0.008	0.010
4	92.5	0.099	0.389	0.340	0.006	0.039	0.008	0.009
5	85.0	0.196	0.240	0.081	0.009	0.108	0.021	0.025
6	102.7	0.201	0.346	0.230	0.011	0.098	0.016	0.020
7	103.0	0.198	0.453	0.338	0.009	0.075	0.014	0.017
8	101.2	0.198	0.544	0.434	0.009	0.083	0.015	0.018
9	96.8	0.197	0.622	0.520	0.013	0.075	0.013	0.016
10	93.1	0.198	0.789	0.684	0.003	0.059	0.013	0.015
11	96.6	0.299	0.379	0.157	0.012	0.139	0.028	0.033
12	93.2	0.297	0.482	0.294	0.013	0.114	0.024	0.028
13	92.0	0.299	0.608	0.425	0.027	0.136	0.024	0.029
14	91.8	0.298	0.752	0.569	0.008	0.102	0.022	0.026
15	100.8	0.297	0.961	0.800	0.019	0.110	0.022	0.026
16	88.6	0.303	1.095	0.926	0.020	0.128	0.025	0.030
17	77.1	0.402	0.537	0.255	0.042	0.206	0.036	0.044
18	89.8	0.413	0.776	0.531	0.036	0.204	0.035	0.043
19	91.4	0.398	0.980	0.761	0.018	0.143	0.029	0.035
20	93.7	0.400	1.203	0.946	0.010	0.161	0.033	0.039

Table 12.7 *Single perimeter steady state filament morphology results*

Number	Cross-sectional area (%)	Layer height (mm)	Road width (mm)	Bond width (mm)	Horizontal deviations (mm)	Rz (mm)	Ra (mm)	Rq (mm)
1	89.5	0.097	0.403	0.141	0.002	0.043	0.009	0.010
2	107.6	0.099	0.483	0.189	0.010	0.047	0.009	0.011
3	84.7	0.100	0.574	0.238	0.012	0.055	0.010	0.012
4	99.8	0.102	0.805	0.314	0.009	0.047	0.010	0.012
5	95.5	0.196	0.482	0.089	0.007	0.112	0.021	0.025
6	111.3	0.201	0.705	0.211	0.011	0.073	0.014	0.017
7	109.5	0.202	0.905	0.318	0.008	0.075	0.014	0.017
8	108.6	0.203	1.115	0.997	0.023	0.092	0.018	0.022
9	101.5	0.201	1.246	0.490	0.024	0.086	0.015	0.019
10	109.2	0.200	1.782	0.730	0.013	0.079	0.016	0.019
11	110.2	0.299	0.802	0.201	0.015	0.118	0.024	0.028
12	99.2	0.294	0.983	0.322	0.011	0.114	0.022	0.026
13	95.7	0.299	1.223	0.474	0.011	0.112	0.021	0.025
14	91.1	0.298	1.483	0.568	0.015	0.110	0.021	0.025
15	98.9	0.298	1.842	0.803	0.009	0.098	0.021	0.025
16	85.8	0.301	2.165	0.962	0.036	0.136	0.024	0.029
17	91.5	0.410	1.202	0.373	0.017	0.159	0.032	0.038
18	90.7	0.417	1.498	0.580	0.034	0.165	0.033	0.039
19	85.0	0.410	1.812	0.711	0.022	0.138	0.028	0.033
20	98.7	0.401	2.466	1.023	0.028	0.185	0.037	0.044

Table 12.8 *Double perimeter steady state filament morphology results*

Number	Cross-sectional area (%)	Layer height (mm)	Road width (mm)	Bond width (mm)	Horizontal deviations (mm)	Rz (mm)	Ra (mm)	Rq (mm)
1	88.0	0.100	0.556	0.194	0.015	0.057	0.011	0.013
2	96.5	0.105	0.721	0.656	0.020	0.071	0.015	0.018
3	90.4	0.099	0.777	0.473	0.006	0.061	0.010	0.012
4	94.8	0.101	1.147	1.102	0.011	0.053	0.011	0.013
5	98.8	0.202	0.687	0.133	0.010	0.094	0.018	0.022
6	100.2	0.200	0.936	0.177	0.013	0.092	0.017	0.020
7	98.8	0.200	1.215	0.309	0.019	0.084	0.017	0.020
8	98.1	0.198	1.521	1.417	0.008	0.075	0.015	0.017
9	99.7	0.200	1.823	0.497	0.022	0.090	0.017	0.021
10	100.2	0.199	2.454	2.341	0.032	0.106	0.020	0.025
11	101.9	0.302	1.082	0.180	0.043	0.167	0.029	0.036
12	100.7	0.297	1.452	0.282	0.024	0.126	0.023	0.028
13	99.6	0.302	1.858	0.456	0.012	0.118	0.021	0.025
14	79.4	0.299	2.145	0.531	0.035	0.136	0.024	0.030
15	72.9	0.289	2.500	0.708	0.043	0.141	0.027	0.033
16	83.1	0.312	3.401	0.914	0.026	0.145	0.026	0.031
17	63.1	0.391	1.678	0.255	0.016	0.169	0.033	0.040
18	95.3	0.403	2.351	0.670	0.021	0.147	0.028	0.033
19	70.9	0.395	2.810	0.725	0.026	0.151	0.028	0.033
20	95.7	0.391	3.618	1.014	0.083	0.226	0.036	0.045

Table 12.9 *Triple perimeter steady state filament morphology results*

Number	Layer height (mm)	Road width (mm)	Bond width (mm)	Horizontal deviations (mm)	Rz (mm)	Ra (mm)	Rq (mm)
PLA 1	0.200	0.896	0.785	0.004	0.069	0.014	0.016
PLA 2	0.198	0.913	0.803	0.011	0.081	0.015	0.018
ABS 1	0.202	0.872	0.748	0.011	0.088	0.017	0.020
ABS 2	0.197	0.860	0.736	0.019	0.100	0.018	0.022

Table 12.10 *PLA and ABS double perimeter default print parameters comparison results*

12.5. XY PLANE GEOMETRICAL PERFORMANCE

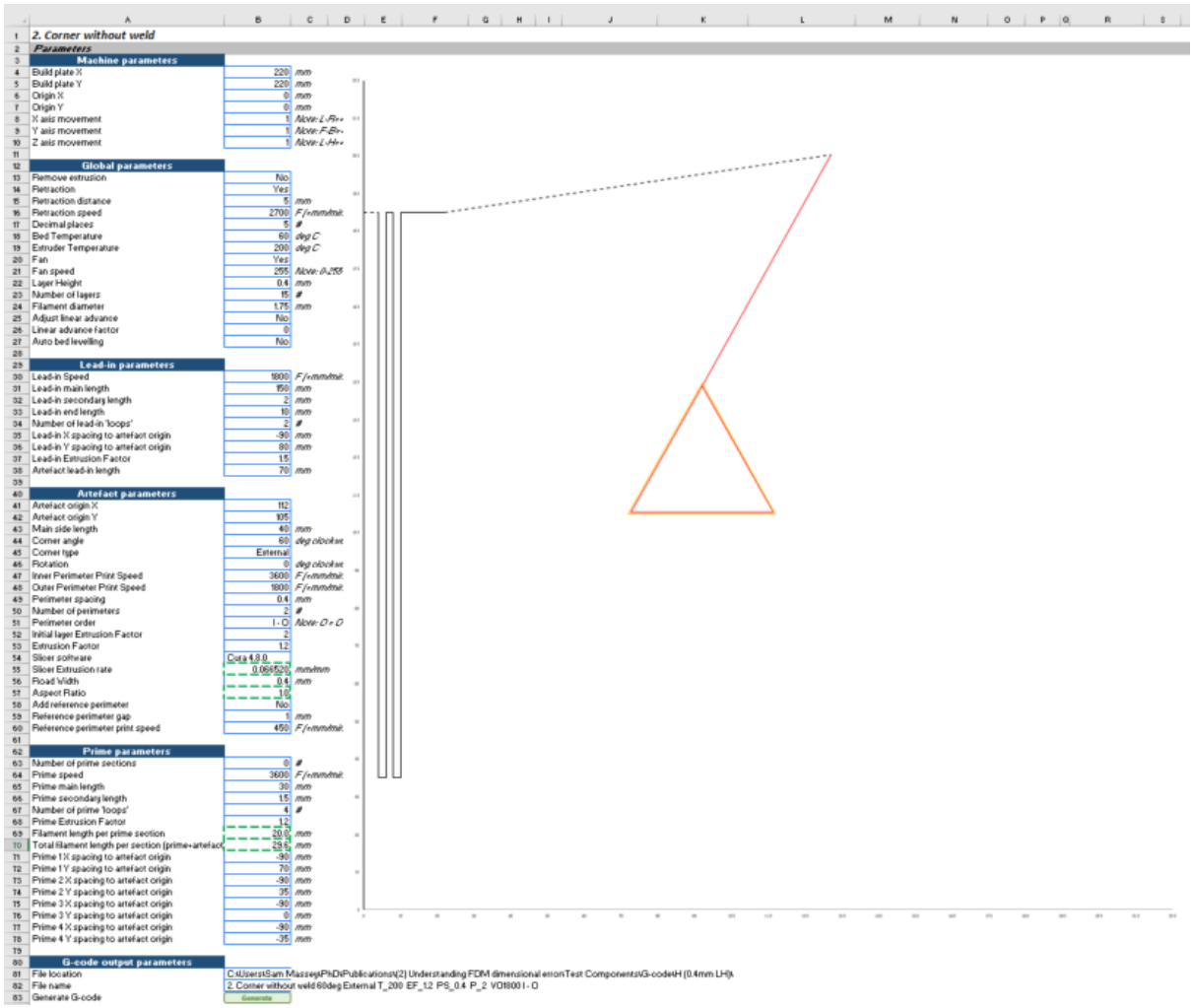

Figure 12.5: *Custom G-code generator for XY plane geometrical performance*

Angle (º)	Internal over-extrusion (mm^2)	External over-extrusion (mm^2)	Internal max. deviation (mm)	External max. deviation in (mm)	External max. deviation out (mm)
15	0.105	0.691	0.058	0.227	0.209
30	0.067	0.384	0.06	0.177	0.171
45	0.07	0.375	0.077	0.137	0.205
60	0.158	0.409	0.133	0.161	0.177
75	0.104	0.375	0.122	0.192	0.112
90	0.105	0.449	0.107	0.167	0.141
105	0.156	0.222	0.15	0.096	0.145
120	0.192	0.155	0.136	0.081	0.107
135	0.48	0.075	0.196	0.061	0.061
150	0.428	0.166	0.165	0.092	0.096
165	0.532	0.324	0.165	0.118	0.118

Table 12.11 *XY Plane internal corners with weld table of results*

Angle (º)	Internal over-extrusion (mm^2)	External over-extrusion (mm^2)	Internal max. deviation (mm)	External max. deviation in (mm)	External max. deviation out (mm)
15	0.005	0.742	0.021	0.227	0.228
30	0.068	0.589	0.079	0.177	0.223
45	0.081	0.484	0.132	0.155	0.189
60	0.143	0.521	0.159	0.113	0.234
75	0.091	0.469	0.151	0.158	0.133
90	0.143	0.331	0.169	0.090	0.155
105	0.251	0.300	0.171	0.082	0.155
120	0.244	0.171	0.167	0.054	0.099
135	0.276	0.102	0.137	0.040	0.080
150	0.102	0.117	0.070	0.026	0.080
165	0.113	0.100	0.047	0.022	0.053

Table 12.12 *XY Plane internal corners without weld table of results*

Angle (º)	Internal over-extrusion (mm^2)	External over-extrusion (mm^2)	Internal max. deviation (mm)	External max. deviation in (mm)	External max. deviation out (mm)
15	0.047	0.604	0.053	0.116	0.197
30	0.118	0.445	0.081	0.137	0.140
45	0.140	0.336	0.089	0.110	0.119
60	0.196	0.197	0.104	0.119	0.072
75	0.221	0.315	0.117	0.115	0.089
90	0.240	0.284	0.149	0.135	0.052
105	0.349	0.211	0.159	0.081	0.044
120	0.314	0.201	0.145	0.073	0.090
135	0.369	0.115	0.163	0.067	0.091
150	0.415	0.179	0.165	0.069	0.117
165	0.405	0.182	0.155	0.105	0.114

Table 12.13 *XY Plane external corners with weld table of results*

Angle (º)	Internal over-extrusion (mm^2)	External over-extrusion (mm^2)	Internal max. deviation (mm)	External max. deviation in (mm)	External max. deviation out (mm)
15	0.130	0.361	0.079	0.114	0.172
30	0.229	0.260	0.143	0.087	0.099
45	0.374	0.264	0.200	0.073	0.095
60	0.318	0.281	0.220	0.067	0.120
75	0.376	0.195	0.234	0.048	0.086
90	0.432	0.418	0.231	0.073	0.096
105	0.360	0.088	0.248	0.022	0.099
120	0.426	0.068	0.222	0.024	0.054
135	0.226	0.081	0.161	0.025	0.048
150	0.166	0.046	0.101	0.02	0.037
165	0.168	0.038	0.063	0.016	0.026

Table 12.14 *XY Plane external corners without weld table of results*

Print speed (inner/outer, $mmmin^{-1}$)	Internal over-extrusion (mm^2)	External over-extrusion (mm^2)	Internal max. deviation (mm)	External max. deviation in (mm)	External max. deviation out (mm)
F900/450	0.031	0.009	0.100	0.003	0.012
F1800/900	0.059	0.122	0.141	0.028	0.058
F3600/1800	0.364	0.119	0.238	0.054	0.077
F7200/3600	0.925	0.563	0.326	0.132	0.141
F14400/7200	0.889	1.467	0.348	0.165	0.167

Table 12.15 *XY Plane external corners with print speed variation table of results*

Print	Internal over-extrusion (mm^2)	External over-extrusion (mm^2)	Internal max. deviation (mm)	External max. deviation in (mm)	External max. deviation out (mm)
1	0.298	0.231	0.224	0.072	0.091
2	0.594	0.111	0.289	0.031	0.067
3	0.269	0.237	0.251	0.061	0.116
4	0.510	0.181	0.273	0.039	0.098
5	0.383	0.066	0.263	0.035	0.069
6	0.394	0.095	0.285	0.021	0.062

Table 12.16 *XY Plane external corners with orientation and direction variation table of results*

12.6. MODIFIED NOZZLE GEOMETRY STEADY-STATE FILAMENT MORPHOLOGY

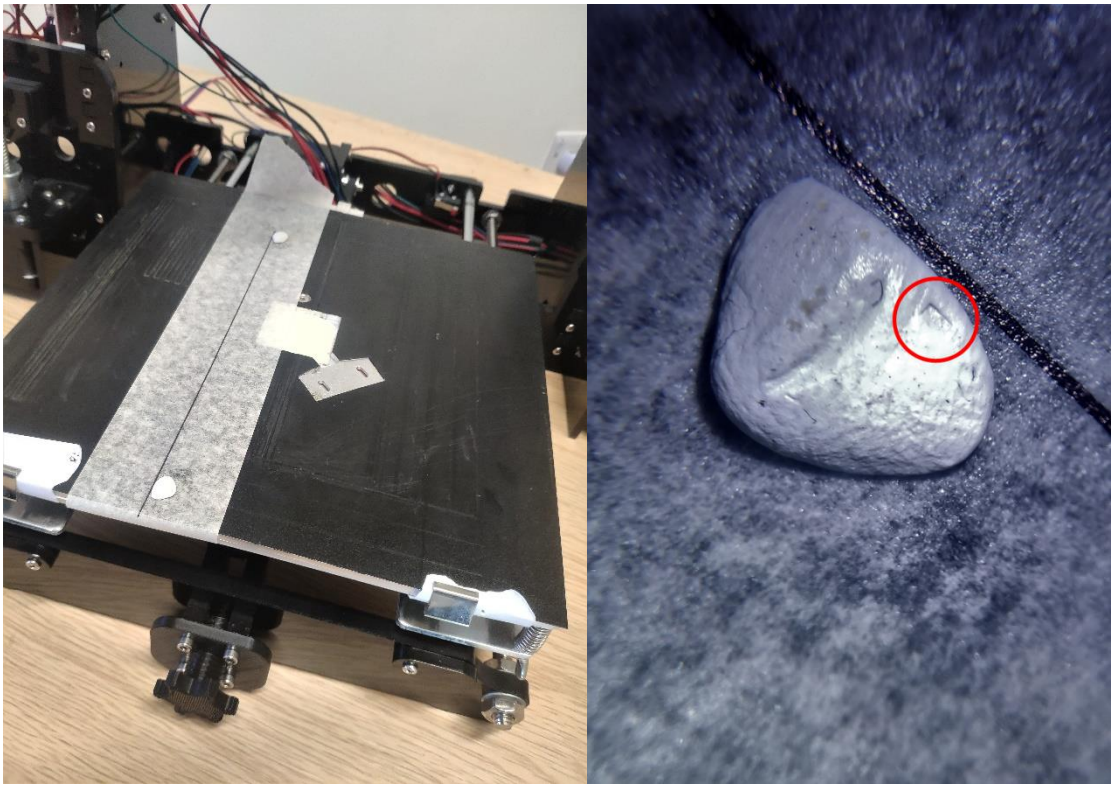

Figure 12.6 *Nozzle side piece parallel alignment process*

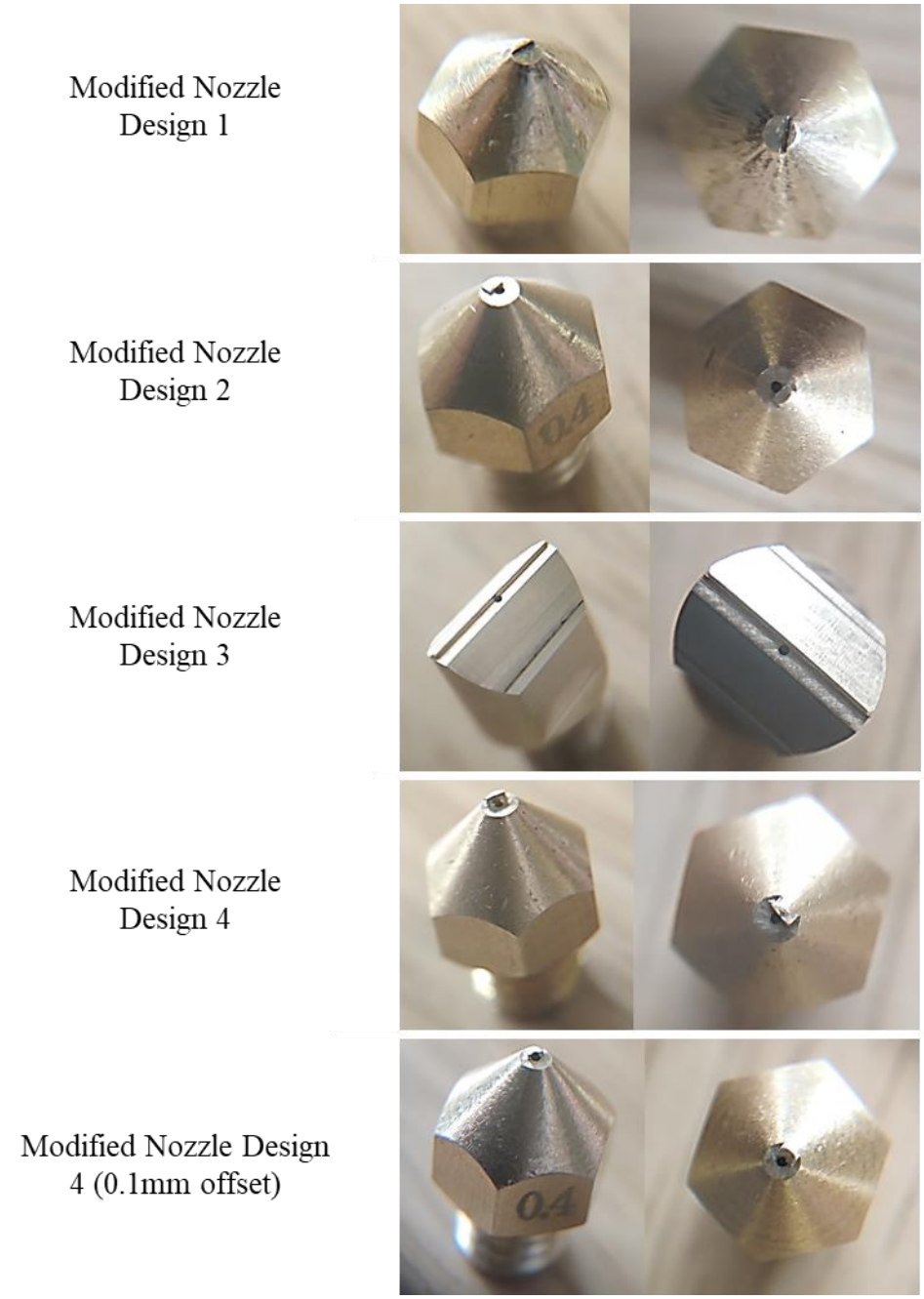

Figure 12.7 *Modified nozzle photographs*

12.7. MODIFIED NOZZLE XY PLANE GEOMETRICAL PERFORMANCE

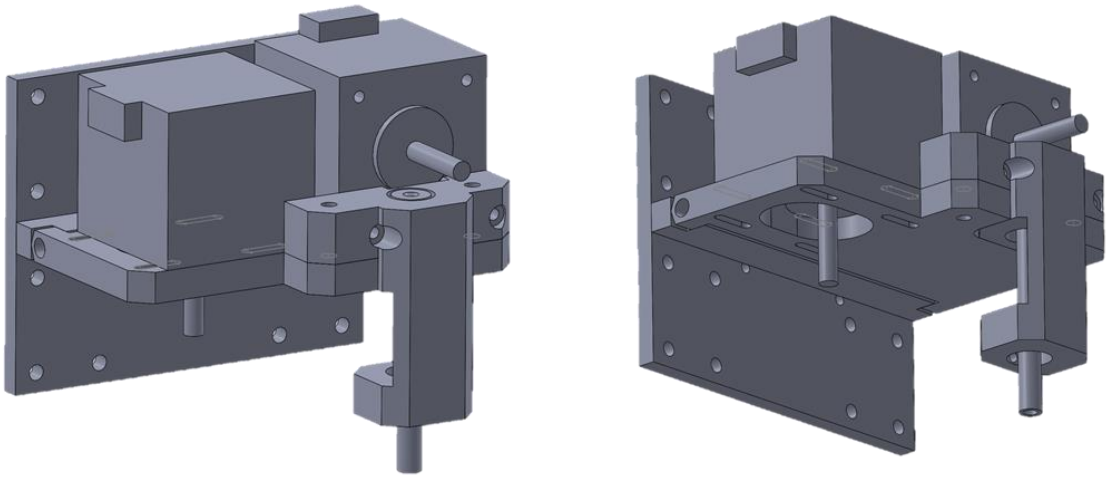

Figure 12.8 *Modification of ANet A8-M gantry to provide rotation via second stepper motor reorientation*